

## Special Collection on Alzheimer's Disease

Imaging of control mice showed microglia that were characterized by a small cell body and highly elaborated thin processes, see Koukouli et al. - "Early and progressive deficit of neuronal activity patterns in a model of local amyloid pathology in mouse prefrontal cortex"

**Alzheimer's  
Disease**

**AGING**

## **Editorial and Publishing Office Aging (Albany NY)**

6666 E. Quaker Str., Suite 1B

Orchard Park, NY 14127

Phone: 1-800-922-0957, option 1

Fax: 1-716-508-8254

e-Fax: 1-716-608-1380

### **Submission**

Please submit your manuscript on-line at <http://aging.msubmit.net>

### **Editorial**

For editorial inquiries, please call us or email [editors@impactaging.com](mailto:editors@impactaging.com)

### **Production**

For questions related to preparation of your article for publication, please call us or email [krasnova@impactaging.com](mailto:krasnova@impactaging.com)

### **Indexing**

If you have questions about the indexing status of your paper, please email [kurenova@impactaging.com](mailto:kurenova@impactaging.com)

### **Printing**

Each issue or paper can be printed on demand. To make a printing request, please call us or email [krasnova@impactaging.com](mailto:krasnova@impactaging.com).

### **Billing/Payments**

If you have questions about billing/invoicing or would like to make a payment, please call us or email [payment@impactaging.com](mailto:payment@impactaging.com)

### **Publisher's Office**

Aging is published by Impact Journals, LLC

To contact the Publisher's Office, please email: [publisher@impactjournals.com](mailto:publisher@impactjournals.com), visit [www.impactjournals.com](http://www.impactjournals.com), or call 1-800-922-0957, option 5

# AGING

(Albany NY)

## EDITORIAL BOARD

### EDITORS-IN-CHIEF

[Jan Vijg](#) - Albert Einstein College of Medicine, Bronx, NY, USA

[David A. Sinclair](#) - Harvard Medical School, Boston, MA, USA

[Vera Gorbunova](#) - University of Rochester, Rochester, NY, USA

[Judith Campisi](#) - The Buck Institute for Research on Aging, Novato, CA, USA

[Mikhail V. Blagosklonny](#) - Roswell Park Cancer Institute, Buffalo, NY, USA

### EDITORIAL BOARD

[Frederick Alt](#) - Harvard Medical School, Boston, MA, USA

[Vladimir Anisimov](#) - Petrov Institute of Oncology, St.Petersburg, Russia

[Johan Auwerx](#) - Ecole Polytechnique Fédérale de Lausanne, Switzerland

[Andrzej Bartke](#) - Southern Illinois University, Springfield, IL, USA

[Nir Barzilai](#) - Albert Einstein College of Medicine, Bronx, NY, USA

[Elizabeth H. Blackburn](#) - University of California, San Francisco, CA, USA

[Maria Blasco](#) - Spanish National Cancer Center, Madrid, Spain

[Vilhelm A. Bohr](#) - National Institute on Aging, NIH, Baltimore, MD, USA

[William M. Bonner](#) - National Cancer Institute, NIH, Bethesda, MD, USA

[Robert M. Brosh, Jr.](#) - National Institute on Aging, NIH, Baltimore, MD, USA

[Anne Brunet](#) - Stanford University, Stanford, CA, USA

[Rafael de Cabo](#) - NIA, NIH, Baltimore, MD, USA

[Ronald A. DePinho](#) - Dana-Farber Cancer Institute, Boston, MA, USA

[Jan van Deursen](#) - Mayo Clinic, Rochester, MN, USA

[Lawrence A. Donehower](#) - Baylor College of Medicine, Houston, TX, USA

[Caleb E. Finch](#) - University of Southern California, Los Angeles, CA, USA

[Toren Finkel](#) - National Institutes of Health, Bethesda, MD, USA

[Luigi Fontana](#) - Washington University, St. Louis, MO, USA

[Claudio Franceschi](#) - University of Bologna, Bologna, Italy

[David Gems](#) - Inst. of Healthy Ageing, Univ. College London, UK

[Myriam Gorospe](#) - National Institute on Aging, NIH, Baltimore, MD, USA

[Leonard Guarente](#) - MIT, Cambridge, MA, USA

[Andrei Gudkov](#) - Roswell Park Cancer Institute, Buffalo, NY, USA

[Michael Hall](#) - University of Basel, Basel, Switzerland

[Philip Hanawalt](#) - Stanford University, CA, USA

[Nissim Hay](#) - University of Illinois at Chicago, Chicago, IL, USA

[Siegfried Hekimi](#) - McGill University, Montreal, Canada

---

## EDITORIAL BOARD

[Stephen L. Helfand](#) - Brown University, Providence, RI, USA

[Jan H.J. Hoeijmakers](#) - Erasmus MC, Rotterdam, The Netherlands

[John O. Holloszy](#) - Washington University, St. Louis, MO, USA

[Stephen P. Jackson](#) - University of Cambridge, Cambridge, UK

[Heinrich Jasper](#) - The Buck Institute for Research on Aging, Novato, CA, USA

[Pankaj Kapahi](#) - The Buck Institute for Research on Aging, Novato, CA, USA

[Jan Karlseder](#) - The Salk Institute, La Jolla, CA, USA

[Cynthia Kenyon](#) - University of California San Francisco, San Francisco, CA, USA

[James L. Kirkland](#) - Mayo Clinic, Rochester, MN, USA

[Guido Kroemer](#) - INSERM, Paris, France

[Titia de Lange](#) - Rockefeller University, New York, NY, USA

[Arnold Levine](#) - The Institute for Advanced Study, Princeton, NJ, USA

[Michael P. Lisanti](#) - University of Salford, Salford, UK

[Lawrence A. Loeb](#) - University of Washington, Seattle, WA, USA

[Valter Longo](#) - University of Southern California, Los Angeles, CA, USA

[Gerry Melino](#) - University of Rome, Rome, Italy

[Simon Melov](#) - The Buck Institute for Research on Aging, Novato, CA, USA

[Alexey Moskalev](#) - Komi Science Center of RAS, Syktyvkar, Russia

[Masashi Narita](#) - University of Cambridge, Cambridge, UK

[Andre Nussenzweig](#) - National Cancer Institute, NIH, Bethesda, MD, USA

[William C. Orr](#) - Southern Methodist University, Dallas, TX, USA

[Daniel S. Peeper](#) - The Netherlands Cancer Institute, Amsterdam, The Netherlands

[Thomas Rando](#) - Stanford University School of Medicine, Stanford, CA, USA

[Michael Ristow](#) - Swiss Federal Institute of Technology, Zurich, Switzerland

[Igor B. Roninson](#) - Ordway Research Institute, Albany, NY, USA

[Michael R. Rose](#) - University of California, Irvine, CA, USA

[K Lenhard Rudolph](#) - Hannover Medical School, Hannover, Germany

[Paolo Sassone-Corsi](#) - University of California, Irvine, CA, USA

[John Sedivy](#) - Brown University, Providence, RI, USA

[Manuel Serrano](#) - Spanish National Cancer Research Center, Madrid, Spain

[Gerald S. Shadel](#) - Yale University School of Medicine, New Haven, CT, USA

[Norman E. Sharpless](#) - University of North Carolina, Chapel Hill, NC, USA

[Vladimir P. Skulachev](#) - Moscow State University, Moscow, Russia

[Sally Temple](#) - NY Neural Stem Cell Institute, Albany, NY, USA

[George Thomas](#) - University of Cincinnati, Cincinnati, OH, USA

[Jonathan L. Tilly](#) - Massachusetts General Hospital, Boston, MA, USA

[John Tower](#) - University of Southern California, LA, CA, USA

[Eric Verdin](#) - University of California, San Francisco, CA, USA

[Thomas von Zglinicki](#) - Newcastle University, Newcastle, UK

[Alex Zhavoronkov](#) - Insilico Medicine, Baltimore, MD, USA

---

# Table of Contents

Serum protein mediators of dementia and aging proper .....	1
<a href="#">Originally published in Volume 8, Issue 12 pp 3241—3254</a>	
Early and progressive deficit of neuronal activity patterns in a model of local amyloid pathology in mouse prefrontal cortex .....	15
<a href="#">Originally published Volume 8, Issue 12 pp 3430—3449</a>	
Long-term caloric restriction in ApoE-deficient mice results in neuroprotection via Fgf21-induced AMPK/mTOR pathway .....	35
<a href="#">Originally published Volume 8, Issue 11 pp 2777—2789</a>	
An antioxidant specifically targeting mitochondria delays progression of Alzheimer’s disease-like pathology.....	48
<a href="#">Originally published Volume 8, Issue 11 pp 2713—2733</a>	
Targeting therapy for homocysteic acid in the blood represents a potential recovery treatment for cognition in Alzheimer’s disease patients.....	69
<a href="#">Originally published Volume 8, Issue 9 pp 1838—1843</a>	
Biological and biophysics aspects of metformin-induced effects: cortex mitochondrial dysfunction and promotion of toxic amyloid pre-fibrillar aggregates.....	75
<a href="#">Originally published Volume 8, Issue 8 pp 1718—1734</a>	
Reversal of cognitive decline in Alzheimer's disease .....	92
<a href="#">Originally published Volume 8, Issue 6 pp 1250—1258</a>	
Epigenetic mechanisms underlying cognitive impairment and Alzheimer disease hallmarks in 5XFAD mice.....	101
<a href="#">Originally published Volume 8, Issue 4 pp 664—684</a>	
Inhalational Alzheimer's disease: an unrecognized—and treatable—epidemic .....	122
<a href="#">Originally published Volume 8, Issue 2 pp 304—313</a>	
Epigenetic age of the pre-frontal cortex is associated with neuritic plaques, amyloid load, and Alzheimer’s disease related cognitive functioning.....	132
<a href="#">Originally published Volume 7, Issue 12 pp 1198—1211</a>	
A comprehensive multiomics approach toward understanding the relationship between aging and dementia.....	146
<a href="#">Originally published Volume 7, Issue 11 pp 937—952</a>	
Defective mitochondrial respiration, altered dNTP pools and reduced AP endonuclease 1 activity in peripheral blood mononuclear cells of Alzheimer's disease patients.....	162
<a href="#">Originally published Volume 7, Issue 10 pp 793—810</a>	
Metabolic profiling distinguishes three subtypes of Alzheimer's disease.....	180
<a href="#">Originally published Volume 7, Issue 8 pp 595—600</a>	
Reversal of cognitive decline: A novel therapeutic program .....	186
<a href="#">Originally published Volume 6, Issue 9 pp 707—717</a>	

## Serum protein mediators of dementia and aging proper

Donald R. Royall<sup>1,2,3,4</sup>, Safa Al-Rubaye<sup>1</sup>, Ram Bishnoi<sup>5</sup>, Raymond F. Palmer<sup>3</sup>

<sup>1</sup>Department of Psychiatry, University of Texas Health Science Center at San Antonio, San Antonio, TX 78229, USA

<sup>2</sup>Department of Medicine, University of Texas Health Science Center at San Antonio, San Antonio, TX 78229, USA

<sup>3</sup>Department of Family and Community Medicine, University of Texas Health Science Center at San Antonio, San Antonio, TX 78229, USA

<sup>4</sup>South Texas Veterans' Health System Audie L. Murphy Division GRECC, San Antonio, TX 78229, USA

<sup>5</sup>Department of Psychiatry, The Medical College of Georgia, Augusta, GA 30912, USA

**Correspondence to:** Donald R. Royall; email: [royall@uthscsa.edu](mailto:royall@uthscsa.edu)

**Keywords:** aging, cognition, dementia, functional status, *g*, intelligence

**Received:** August 31, 2016 **Accepted:** November 17, 2016 **Published:** December 3, 2016 **doi:** [10.18632/aging.101091](https://doi.org/10.18632/aging.101091)

### ABSTRACT

The latent variable “ $\delta$ ” (for “dementia”) appears to be uniquely responsible for the dementing aspects of cognitive impairment. Age, depressive symptoms, gender and the apolipoprotein E (APOE)  $\epsilon 4$  allele are independently associated with  $\delta$ . In this analysis, we explore serum proteins as potential mediators of age’s specific association with  $\delta$  in a large, ethnically diverse longitudinal cohort, the Texas Alzheimer’s Research and Care Consortium (TARCC). 22 serum proteins were recognized as partial mediators of age’s association with  $\delta$ . These include Insulin-like Growth Factor-Binding Protein 2 (IGF-BP2), which we had previously associated with age-specific cognitive change, and both Pancreatic Polypeptide (PP) and von Willebrand Factor (vWF), previously associated with  $\delta$ . Nine other  $\delta$ -related proteins were not confirmed by this ethnicity adjusted analysis. Our findings suggest that age’s association with the disabling fraction of cognitive performance is partially mediated by serum proteins, somatomedins and hormones. Those proteins may offer targets for the specific treatment of age-related effects on dementia severity and conversion risk.

### INTRODUCTION

Age, depression, and the apolipoprotein E (APOE)  $\epsilon 4$  allele are independently associated with the latent dementia phenotype “ $\delta$ ” (for “dementia”) [1]. Their associations with dementia do not necessarily involve neurodegeneration. Depression’s association with cognitive decline in older persons is not mediated by neurodegenerative changes [2], while age’s association with  $\delta$  has been shown to be fully mediated by a paucity of neurodegenerative changes in pathologically confirmed Alzheimer’s Disease (AD) cases [3]. Brain aging is therefore not AD [4].

On the other hand, clinical “AD” may very well have an aging component. Since  $\delta$  is essentially the sole cognitive determinant of dementia severity, clinical dementia must arise from the sum of all independent  $\delta$ -related processes. Age’s small independent effect appears to be linear over the lifespan, and cumulative

[5]. Over a 50 year age range, aging might account for up to a standard deviation change in composite “d-scores”. That is not trivial.  $\delta$ ’s intercept and slope are uniquely strong determinants of future dementia status [6-7]. Each quintile in the d-score distribution of non-demented persons increases conversion to clinical “AD” by 50% [three-fold among “Mild Cognitive Impairment (MCI)” cases] [8].

In the “oldest old”, aging alone might sum with comorbid neurodegenerative processes to push d-scores into their demented range. This should effectively reduce the amount of neuropathology required to make the diagnosis of dementia in centenarians, and modulate the apparent associations between various neuropathologies and clinical dementia. In fact, dementia at advanced age is associated with lower levels of AD-specific neuropathology [9], and less widely spread pathology [10].

**Table 1. Descriptive Statistics.**

Variable	N	Mean (SD)
Age (observed)	3381	70.88 (9.48)
APOE e4 alleles (1 = e4+, n = 1223)	3154	0.39 (0.49)
CDR (Sum of Boxes)	3306	2.42 (3.35)
COWA	3381	8.41 (3.49)
DIS	3381	8.89 (3.01)
EDUC (observed)	3381	13.24 (4.25)
Ethnicity (1 = MA, n = 1189)	3381	0.36 (0.47)
GDS <sub>30</sub> (observed)	3005	5.60 (5.25)
Gender (♂ = 1, n = 1281)	3312	0.39 (0.49)
IADL (Summed)	3381	10.48 (4.52)
MMSE	3311	25.52 (4.76)
WMS LM II	3381	8.05 (4.30)
WMS VR I	3381	7.88 (3.68)
Complete Cases	2861	

CDR = Clinical Dementia Rating scale; COWA = Controlled Oral Word Association Test; DIS = Digit Span Test; GDS = Geriatric Depression Scale [66]; IADL = Instrumental Activities of Daily Living; MMSE = Mini-Mental State Exam [67]; SD = standard deviation; WMS LM II = Weschler Memory Scale: Delayed Logical Memory; WMS VR I = Weschler Memory Scale: Immediate Visual Reproduction.

Even in their aggregate, demographic-specific dementia risks explain a minority of  $\delta$ 's variance [1]. Thus, regardless of whether age's effect is mediated by neurodegeneration, observed dementia status must be largely determined by age-independent factors. In Age, depression and APOE adjusted models, we have found the majority of  $\delta$ 's remaining variance to be associated with a large number of pro- and anti-inflammatory serum protein biomarkers [1, 11-13].

On the other hand, we have reported serum Insulin-like Binding Protein 2 (IGF-BP2) to be a strong correlate of age's specific cognitive effects [14]. However, age has both direct ( $\delta$ -independent) and indirect ( $\delta$ -related) effects on cognition. It has yet to be determined whether IGF-BP2 mediates age's association with  $\delta$ , or its  $\delta$ -independent direct effects instead.

In this analysis, we combine structural equation models (SEM) with longitudinal data from the Texas Alzheimer's Research and Care Consortium (TARCC) to explore more than 100 serum proteins as potential mediators of age's specific association with  $\delta$ . Our models are constructed such that the significant mediators of age's effect on prospective  $\delta$  scores can be interpreted causally. The mediators should offer both insights into the pathophysiology of Aging Proper, and potential targets for the remediation of age-specific cognitive impairments.

## RESULTS

The demographic characteristics of our sample are presented in Table 1. The ethnicity equivalent unadjusted Visit 2  $\delta$  homolog composite score (i.e.,

**Table 2. Potential Mediators of Age’s-Specific Dementing Effect.**

Adiponectin (APN)  
Angiopoetin-2N (ANG-2)  
Compliment 3 (C3)  
Creatinine Kinase-MB (CK-MB)  
Epidermal Growth Factor Receptor 1 (EGFR)  
FAS  
Follicle stimulating hormone (FSH)  
Glutathione S-Transferase (GST)  
granulocyte colony stimulating factor (G-CSF)  
Insulin-like Growth Factor-1 (IGF-I)  
Insulin-like Growth Factor-Binding Protein 2 (IGF-BP2)\*  
Interleukin 5 (IL-5)  
Myoglobin (MyG)  
Pancreatic Polypeptide (PP)†  
Plasminogen Activator Inhibitor type 1(PAI-1)  
Platelet-Derived Growth Factor (PDGF)  
Progesterone  
Resistin  
S100b  
Serum Amyloid P (SAP)  
Thyroxine Binding Globulin (TBG)  
von Willebrand Factor (vWF)†

\*Previously recognized aging biomarker [14]. †Previously recognized biomarker of  $\delta$  [13].

“dEQ”) achieved a high Area Under the Receiver Operating Characteristic curve (AUC/ROC) for the discrimination between AD cases and normal controls (NC) (AUC = 0.953; CI: 0.946-0.960). “g”’s (i.e.,  $\delta$ ’s residual in Spearman’s general intelligence factor “g”) AUC for the same discrimination was at a near chance level [AUC = 0.536 (CI: 0.514-0.558)]. This is consistent with past findings, across batteries, in this and other cohorts.

The Base Model had excellent fit [ $\chi^2 = 5.59$  (13),  $p = 0.960$ ; CFI = 1.00; RMSEA = 0.00]. Independently of the covariates [i.e., APOE  $\epsilon 4$  allelic burden, depressive symptoms, education, ethnicity, gender, homocysteine (HCY), and hemoglobin A1c (HgbA1c)], baseline age was significantly directly associated with Visit 2 dEQ ( $r = -0.25$ ,  $p < 0.001$ ), and weakly with the Visit 2 g’ composite ( $r = -0.11$ ,  $p \leq 0.001$ ). Age’s significant association with Visit 2 dEQ scores was in a negative direction suggesting an adverse effect on observed cognitive performance.

The mediation models all had acceptable fit [e.g., IGF-BP2:  $\chi^2 = 387.90$  (17),  $p < 0.001$ ; CFI = 0.927; RMSEA = 0.044 (Figure 1)]. 22 proteins achieved statistically significant mediation effects after Bonferroni correction

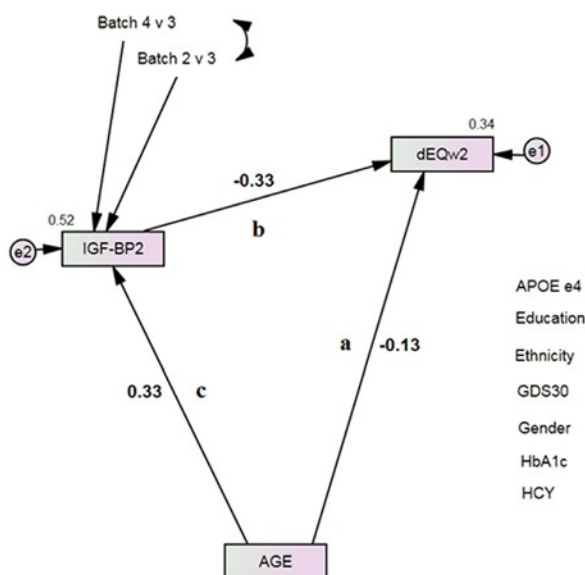
for multiple comparisons (Table 2). IGF-BP2 had previously been recognized as an age-specific serum protein biomarker [14]. Pancreatic Polypeptide (PP) and von Willebrand Factor (vWF) had previously been recognized as  $\delta$ -related serum protein biomarkers [13]. Table 3 presents the mediation effects. All the identified proteins were partial mediators, but several had relatively large effects (range 9.9 – 45.2%). We did not test multivariate mediations or interactions.

Table 4 presents other age-related proteins, unrelated to  $\delta$  by path b (Figure 1). Alpha2-macroglobulin ( $\alpha 2M$ ), Interferon-gamma (IFN- $\gamma$ ), Interleukin 10 (IL-10), Interleukin 12-p40 (IL-12p40), Interleukin 15 (IL-15), Prolactin (PRL), Stem Cell Factor (SCF), Thrombopoietin (THPO), and Tumor Necrosis Factor alpha (TNF- $\alpha$ ) had previously been associated with  $\delta$  in non-Hispanic White (NHW) TARCC participants [1, 13]. None were associated with  $\delta$  in these ethnicity adjusted models.

Table 5 presents  $\delta$ -related proteins unrelated to age by path c (Figure 1). Beta2-Microglobulin ( $\beta 2M$ ) was the only previously recognized  $\delta$  biomarker [13]. The remainders are newly recognized as such. Table 6 lists biomarkers that were related neither to age nor to  $\delta$ .

**Table 3. Mediation Effects (Class 1).**

Mediating Biomarkers	Adjusted Path a (Figure 1)	Z (p)	Effect (%)
Adiponectin (APN)	-0.22, p < 0.001	-4.26 (<0.001)	11.7
Angiopoetin-2 (ANG-2)	-0.20, p < 0.001	-4.72 (<0.001)	13.8
Compliment 3 (C3)	-0.27, p < 0.001	4.46 (<0.001)	11.9
Creatinine Kinase-MB (CK-MB)	-0.21, p < 0.001	-5.50 (<0.001)	13.1
Epidermal Growth Factor Receptor 1 (EGFR)	-0.19, p < 0.001	-6.15 (<0.001)	22.5
Fatty Acid Synthase (FAS)	-0.22, p < 0.001	-2.65 (0.004)	14.1
Follicle stimulating hormone (FSH)	-0.20, p < 0.001	-5.27 (<0.001)	14.0
Glutathione S-Transferase (GST)	-0.28, p < 0.001	3.80 (<0.001)	17.2
granulocyte colony stimulating factor (G-CSF)	-0.21, p < 0.001	-5.22 (<0.001)	12.6
Insulin-like Growth Factor-1 (IGF-I)	-0.25, p < 0.001	1.83 (0.03)	9.9
Insulin-like Growth Factor-Binding Protein 2 (IGF-BP2)	-0.13, p < 0.001	-8.85 (<0.001)	45.2
Interleukin 5 (IL-5)	-0.27, p < 0.001	2.57 (0.005)	17.6
Myoglobin (MyG)	-0.30, p < 0.001	4.87 (<0.001)	21.6
Pancreatic Polypeptide (PP)	-0.21, p < 0.001	-4.71 (<0.001)	14.1
Plasminogen Activator Inhibitor type 1(PAI-1)	-0.21, p < 0.001	-5.50 (<0.001)	15.0
Platelet-Derived Growth Factor (PDGF)	-0.29, p < 0.001	4.22 (<0.001)	17.8
Progesterone	-0.27, p < 0.001	2.56 (0.005)	12.2
Resistin	-0.20, p < 0.001	-4.39 (<0.001)	13.8
S100b	-0.28, p < 0.001	4.97 (<0.001)	18.1
Serum Amyloid P (SAP)	-0.21, p < 0.001	-5.66 (<0.001)	13.5
Thyroxine Binding Globulin (TBG)	-0.22, p < 0.001	-4.60 (<0.001)	9.9
von Willebrand Factor (vWF)	-0.22, p < 0.001	-3.92 (<0.001)	11.0



**Figure 1. IGF-BP2 Mediates Age’s Direct Association with Future Dementia Severity, as measured by dEQ.** APOE = apolipoprotein e4 status; CFI = Comparative Fit Index; GDS = Geriatric Depression Scale; HCY = serum homocysteine; HgbA1c = serum hemoglobin A1c; IGF-BP2 = Insulin-like Growth Factor Binding Protein 2; RMSEA = Root Mean Square Error of Association.

\*All observed variables except AGE are adjusted for APOE, education, ethnicity, gender, GDS, HCY, and HgbA1c (paths not shown for clarity). The covariates are densely intercorrelated.

**Table Other Age-Related Biomarkers (unrelated to the dEQ by Path b).**

Adrenocorticotrophic Hormone (ACTH)  
alpha1-antitrypsin (A1AT)  
alpha2-macroglobulin ( $\alpha$ 2M)\*  
alpha-Fetoprotein ( $\alpha$ -FP)  
Amphiregulin (AREG)  
Angiotensinogen  
AXL  
Betacellulin  
Bone Morphogenic Protein 6 (BMP6)  
Cortisol  
Eotaxin-3  
Epiregulin (EREG)  
FAS-Ligand (FAS-L)  
Heparin-binding EGF-like growth factor (HB-EGF)  
Hepatocyte Growth Factor (HGF)  
Interferon-gamma (IFN- $\gamma$ )\*  
Interleukin 1 receptor (IL-1r)  
Interleukin 3 (IL-3)  
Interleukin 7 (IL-7)  
Interleukin 10 (IL-10)\*  
Interleukin 12-p40 (IL-12p40)\*  
Interleukin 13 (IL-13)  
Interleukin 15 (IL-15)<sup>††</sup>  
Interleukin 16 (IL-16)  
Lipoprotein a  
Luteinizing Hormone (LH)  
Matrix Metalloproteinase type 3 (MMP-3)  
Prolactin (PRL)\*  
Prostatic Acid Phosphatase (PAP)  
Pulmonary and Activation-Regulated Chemokine (PARC)  
Serum Glutamic Oxaloacetic Transaminase (SGOT)  
Stem Cell Factor (SCF) \*  
Thrombopoietin (THPO)\*<sup>†</sup>  
Thrombospondin-1 (THBS1)  
Thymus-Expressed Chemokine (TECK)  
Tissue Factor (TF)  
Tissue Growth Factor alpha (TGF- $\alpha$ )  
Tissue Inhibitor of Metalloproteinase type 1 (TIMP-1)  
Tumor Necrosis Factor alpha (TNF- $\alpha$ )\*  
Tumor Necrosis Factor-Related Apoptosis-Inducing Ligand Receptor 3 (TRAIL-R3)  
Vascular Endothelial Growth Factor (VEGF)<sup>‡</sup>

\*Previously recognized  $\delta$  biomarkers in non-Hispanic Whites (NHW) only [13],<sup>†</sup> [1] (i.e., unconfirmed as a biomarker of dEQ in this ethnicity adjusted analysis). <sup>††</sup> Previously recognized ethnicity adjusted  $\delta$  biomarker [11]. <sup>‡</sup> $\delta$ -related trend, p = 0.002.

**Table 5. Age-independent dEQ Biomarkers (unrelated to Age by Path c).**

beta2-Microglobulin ( $\beta$ 2M)\*  
Brain-Derived Neurotrophic Factor (BDNF)  
Carcinoembryonic antigen (CEA)  
CD40  
Chromogranin A  
Fatty Acid Binding Protein (FABP)  
Growth Hormone  
Immunoglobulin M (IgM)  
Insulin  
Interleukin 8 (IL-8)  
Interleukin 18 (IL-18)  
Macrophage Inflammatory Protein type 1 alpha (MIP-1 $\alpha$ )  
RANTES  
Sex Hormone Binding Globulin (SHBG)  
Tenascin C  
Testosterone  
Tumor Necrosis Factor receptor type II (TNF-RII)  
Vascular Cell Adhesion Molecule type 1 (VCAM-1)

\*Previously recognized  $\delta$  biomarker [13].

## DISCUSSION

We have surveyed more than 100 potential mediators of age's specific and significant association with the latent dementia phenotype,  $\delta$ . Our sample size was large, and we were powered to detect even statistically weak effects. All our findings have been replicated in random subsets of TARCC's data. We have replicated our previously reported association between age and IGF-BP2, and three of our previously observed age-independent associations with  $\delta$ , even though 1) TARCC's sample size has increased over time, 2) we are using a new  $\delta$  homolog, 3) the biomarkers are being used here to predict future cognitive performance, and 4) the prior associations were obtained using raw biomarker data, while these employ normalized variables.

We have identified four classes of proteins: 1) potential mediators of age's significant direct effect on  $\delta$ , 2)  $\delta$ -independent age-related proteins, 3) age-independent predictors of  $\delta$ , and 4) proteins related neither to age nor to  $\delta$ .

While many proteins were related to age, only a subset was also associated with  $\delta$  (Class 1, Table 2).  $\delta$  in turn has been associated with atrophy in the Default Mode Network (DMN) [15]. This suggests that the mediators in Table 2 may effect aging-specific changes to the structure or function of the DMN.

The DMN is a network of interconnected brain regions that are particularly active in the resting state [16]. Functional connectivity studies in older subjects have shown decreased DMN connectivity [17-20] and less deactivation during task performance [21-22]. The impact of aging-related serum biomarkers on the integrity and functioning of the DMN is not well-studied. However, Thompson et al. [23] found that elevated Serum protein S100B levels significantly correlated with DMN activity. S100B has been confirmed by this analysis to mediate age's specific-effect on a DMN-related cognitive construct (i.e.,  $\delta$ ).

Our observations may help further clarify age's specific effects on cognitive function. First, although age has both direct and indirect effects on observed cognitive performance [5], only its indirect effects, mediated by  $\delta$ , are functionally salient, and thus "dementing." This constrains "senility" and its biology to an effect on intelligence.

Second,  $\delta$  has been shown to be "agnostic" to dementia's etiology [6]. Age's association with  $\delta$  suggests that it too may have a role in determining *all cause* dementia risk, not just AD risk. This risk may not be conveyed through neurodegeneration. Age's specific association with  $\delta$  is characterized by lesser levels of AD-specific lesions [3].

Age accounts for only 5% of  $\delta$ 's variance in this sample (per the base model). Regardless, correcting any  $\delta$ -

**Table 6. Unrelated Biomarkers.**

Angiotensin Converting Enzyme (ACE)  
Agouti-Related Protein (AgRP)  
Apolipoprotein A1 (APOA1)  
Apolipoprotein CIII (APOCIII)  
Apolipoprotein H (apoH)  
B Lymphocyte Chemoattractant (BLC)  
Cancer Antigen 125 (CA 125)  
Cancer Antigen 19-9 (CA 19-9)  
CD40 Ligand  
Connective Tissue Growth Factor (CTGF)  
C Reactive Protein (CRP)  
ENA-78 (ENA-78)  
EN-RAGE (EN-RAGE)  
Epidermal Growth Factor (EGF)  
Eotaxin  
Factor VII  
Ferritin  
Fibrinogen  
GRO alpha (GROa)  
Haptoglobin  
Human CC Cytokine (HCC-4)  
I-309  
Immunoglobulin A (IgA)  
Immunoglobulin E (IgE)  
Intercellular Adhesion Molecule, type 1 (ICAM-1)  
Interleukin 1 receptor antagonist (IL-1ra)  
Leptin  
Macrophage Inflammatory Protein type 1 beta (MIP-1b)  
Macrophage Derived Chemokine (MDC)  
Macrophage Migration Inhibitory Factor (MMIF)  
Monocyte Chemotactic Protein type 1 (MCP-1)  
Prostate Specific Antigen (PSA)  
Serum Amyloid P (SAP)  
Soluble Advanced Glycosylation End Product-Specific Receptor (sRAGE)  
Sortilin  
Thyroid Stimulating Hormone (TSH)  
Tumor Necrosis Factor beta (TNFb)  
Vitamin D Binding Protein (VDBP)<sup>†</sup>

<sup>†</sup> Previously recognized  $\delta$  biomarker (Bishnoi, Palmer & Royall, 2015).

related pathology might improve dementia status, including age's small effect. The mediators identified in Table 2 then, may offer targets for the remediation of age's specific contribution.

Each Class 1 protein is a partial mediator of age's contribution, ranging from Thyroxine Binding Globulin (TBG) (9.9%) to IGF-BP2 (45.2%) (Table 3). In their aggregate, they may have interacting effects. For example, S100b is elevated after cardiac surgery and

correlated with post-operative cognitive impairments [24]. It binds to the receptor for advanced glycation end products (RAGE), which induces nuclear factor kappa-B (NF-kappaB)-regulated cytokines, including Complement 3 (C3) [25]. However, we did not test multivariate interactions.

We note that not all of the mediators attenuate age's direct effect. C3, Glutathione S-Transferase (GST), Interleukin 5 (IL-5), Myoglobin (MyG), Platelet-

Derived Growth Factor (PDGF), Progesterone, and S100b accentuated age's adverse effect on  $\delta$ .

We had previously identified IGF-BP2 as a strong predictor of a  $\delta$  ortholog targeting age itself instead of IADL [14]. That ortholog was significantly associated with  $\delta$ , suggesting overlap between  $\delta$  and Aging Proper. It has since been shown that  $\delta$  mediates the majority of age's effect on cognition, but not all [5]. IGF-BP2's appearance in Class 1 confirms its contribution to age's dementing aspect (i.e., "Senility").

Class 1 also contains Insulin-like Growth Factor-1 (IGF-1). The appearance of both IGF-1 and IGF-BP2 among the Class 1 mediators strongly implicates the insulin-like growth factor (IGF) system in Aging Proper. The IGF system is comprised of two growth factors (IGF-I and 2), six high affinity binding proteins (IGF-BP 1 to 6) and four receptors [26-27]. Most of these are not available in TARCC.

Serum levels of IGFs I and II appear to mediate growth hormone (GH)-related somatotrophic changes in humans. These "somatomedins" circulate in non-covalent associations with IGF-BP2. It has been suggested that decreased function of the GH-somatomedin axis is responsible for age-specific anabolic changes (e.g., the "somatopause") [28]. Interestingly, GH itself appears to be an age-independent  $\delta$ -related protein (Class 3) (Table 5).

Serum IGF-BP2 increases with age, and high serum levels have been associated with greater disability, poorer physical performance, reduced muscle strength and lower mineral bone density [29]. Serum IGF-I declines with age [30-31]. Consistent with those findings, IGF-BP2's association with age was positive (Figure 1) while IGF-I's association with age was inverse. Insulin itself is related to  $\delta$ , but not to age (in this HgbA1c adjusted analysis) (Table 5).

MyG and Creatinine Kinase-MB (CK-MB)'s appearance among the Class 1 mediators, recent associations between simple motor tasks and dementia risk [32], and the age-related somatomedins in Classes 1 and 2 lend credence to the hypothesis that there is a cognitive ortholog of somatic "frailty" [33].

IGF-I had an inverse adverse effect on dEQ. Other adverse mediators were Adiponectin (APN), Angiopoietin-2N (ANG-2), C3, CK-MB, Fatty Acid Synthase (FAS), Follicle stimulating hormone (FSH), Glutathione S-Transferase (GST), IGF-BP2, PP, PDGF, Progesterone, Resistin, and vWF. Like IGF-1, C3, GST, PDGF, and Progesterone declined with age [while also

accentuating age's effect on dEQ (see above)]. The others increased significantly with age. Thus all might contribute to age's adverse effect on  $\delta$ .

Epidermal Growth Factor Receptor 1 (EGFR), granulocyte colony stimulating factor (G-CSF), IL-5, MyG, Plasminogen Activator Inhibitor type 1 (PAI-1), S100b, Serum Amyloid P (SAP) and Thyroxine Binding Globulin (TBG) had positive associations with  $\delta$  and might offer some protection from age's otherwise adverse effects.

The mechanism(s) by which the other Class 1 proteins affect  $\delta$  remain to be elucidated. However, aging's pathophysiology will be necessarily constrained, by  $\delta$ 's mediation of its dementing effects, to the physiological processes that mediate intelligence. Two candidate processes might be synaptogenesis and network connectivity. C3, IGF-I, Progesterone, PAI-1, and S100b, all Class 1 mediators, are modulators of synaptic structure and function [34-38].

Class 2 (Table 4) comprises proteins that although age-related, never the less fail to contribute to dementia via  $\delta$  scores. They may mediate non-dementing age-related cognitive changes via  $g$ 's "domain-specific" residuals (e.g., memory, etc.). Alternatively, they may contribute to Aging Proper's manifestation in other tissues or organs.

Notable among these are multiple EGFR agonist ligands, including Amphiregulin (AREG), Betacellulin, Epiregulin (EREG), Heparin-binding EGF-like growth factor (HB-EGF), and Tissue Growth Factor alpha (TGF- $\alpha$ ) [39]. Epidermal Growth Factor (EGF), another EGFR agonist ligand, showed statistically insignificant trends as a potential mediator. The EGFR itself is a Class 1 Mediator (Table 2). These findings suggest the EGFR family of agonist ligands may have potential roles as therapeutic agents for age-specific cognitive and /or somatic decline.

On the other hand, several EGFR antagonists are approved by the Federal Drug Administration (FDA) for the treatment of certain cancers. These might be expected to have adverse effects, according to our findings. Chemotherapy has been noted to adversely impact connectivity in the DMN [40]. Such effects might explain reports of disability due to "chemobrain" in the literature [41]. They also illustrate the potential for reciprocal relationships between cognitive performance and cancer risks. It has been suggested both that chemotherapy is a risk factor for cognitive decline in late life [42], and that AD cases are relatively protected from cancer [43].

Class 2 also includes almost all of TARCC's interleukin panel. The interleukins' appearance in Table 4 suggests that inflammatory mechanisms may mediate age-specific changes outside the brain (and /or non-dementing aspects of cognition). IL-6 has been reported to protect cognition in centenarians [44], but is not in TARCC's biomarker panel. The interleukin 1 receptor antagonist is related neither to age nor to  $\delta$  (Table 6).

Eight of the eleven proteins we previously associated with  $\delta$  in TARCC [13] are also in Class 2 (Table 5), including IFN- $\gamma$ , Interleukins 10, 15, 12p40, and the Interleukin 1 receptor (IL-1r). Five of those eight [i.e., alpha2-macroglobulin ( $\alpha$ 2M), IFN- $\gamma$ , IL-10, IL-12-p40 (IL-12p40), and SCF], exhibited otherwise significant trends in their associations with  $\delta$ , which could not survive Bonferroni correction. Their previously reported associations were specific to NHW, while the current models were ethnicity adjusted. It remains to be seen whether ethnicity-specific effects on  $\delta$  can be confirmed for any of the Class 2 proteins in Table 4.

Table 5 identifies many newly recognized age-independent determinants of dEQ (Class 3). Their relationships with  $\delta$  are beyond the scope of this manuscript. However, GH's appearance on this list is of interest given the prominence of other somatomedins among the Class 1 and 2 proteins (Tables 2 and 4).

In summary, we have surveyed over 100 serum proteins for their possible roles as mediators of age's specific association with a latent dementia phenotype. 22 potential mediators were identified. These may offer targets for the disabling aspects of Aging Proper. An additional 41 age-related proteins were identified. These may mediate age's effects on other organs. Notable among them are the EGFR and many of its ligands. Some EGFR ligands may protect the brain and other organs from age-related changes. However, this may occur at a risk of incurring cancer. Conversely, the use of EGFR antagonists in cancer treatment may accelerate the effects of Aging Proper in the brain and other organs.

## METHODS

### Subjects

Subjects included  $n = 3385$  TARCC participants, including 1240 cases of AD, 688 MCI cases, and 1384 NC. Each underwent serial annual standardized clinical examinations, culminating in a consensus clinical diagnosis of NC, MCI or AD. Institutional Review Board approval was obtained at each site and written informed consent was obtained from all participants.

$\delta$ 's Indicators included Logical Memory II (LMII) [45], Visual Reproduction I (VRI) [45], the Controlled Oral Word Association (COWA) [46], Digit Span Test (DST) [45] and Instrumental Activities of Daily Living (IADL) [47]. All tests were available in Spanish translation. The indicators were not adjusted for this analysis. The resulting unadjusted  $\delta$  homolog was validated by its association with dementia severity, as measured by the Clinical Dementia Rating Scale sum of boxes (CDR) [48] and by ROC analysis.

TARCC's methodology has been described elsewhere [49]. Serum samples were sent frozen to Rules-Based Medicine (RBM) in Austin, TX. There they were assayed without additional freeze-thaw cycles. RBM conducted multiplexed immunoassay via their human multi-analyte profile (human MAP). A complete listing of the biomarker panel we employed is available at <http://www.rulesbasedmedicine.com>.

Raw biomarker data were inspected to ascertain their normality. Data points beyond 3.0 standard deviations (SD) about the mean were labeled as "outliers" and deleted. Logarithmic transformation was used to normalize highly skewed distributions. The data were then standardized to a mean of zero and unit variance.

### Covariates

All observed measures in the structural models were adjusted for APOE  $\epsilon$ 4 burden, education, ethnicity, gender, HCY, and HgbA1c. Measurements of HCY, HgbA1c and APOE  $\epsilon$ 4 genotyping were performed in the Ballantyne laboratory at the Baylor College of Medicine. HgbA1c was measured in whole blood by the turbidimetric inhibition immunoassay (TINIA). HCY was measured in serum using the recombinant enzymatic cycling assay (i.e., Roche Hitachi911).

### APOE genotyping

APOE genotyping was conducted using standard polymerase chain reaction (PCR) methods [50]. APOE $\epsilon$ 4 status was coded dichotomously based on the presence of one or more  $\epsilon$ 4 alleles. TARCC's RBM biomarkers exhibit significant batch effects. Therefore, each biomarker was additionally adjusted for dichotomous dummy variables coding batch.

### Statistical analysis

#### Analysis Sequence

This analysis was performed using Analysis of Moment Structures (AMOS) software [51]. The maximum likelihood estimator was chosen. All observed

indicators were adjusted for age, education, ethnicity and gender. Co-variances between the residuals were estimated if they were significant and improved fit.

We used the ethnicity equivalent  $\delta$  homolog (“dEQ”) as previously described [1]. That homolog has been reported to 1) have excellent fit (i.e.,  $\chi^2/df = 181/24$ ,  $p < 0.001$ ; CFI = 0.97; RMSEA = 0.05), 2) have acceptable factor determinacy by Grice’s Method [52], 3) exhibit factor equivalence across ethnicity, 4) to be strongly correlated with dementia severity as measured by the CDR ( $r = 0.99$ ,  $p < 0.001$ ) and 5) to exhibit an AUC of 0.97 (CI: 0.97-0.98) for the discrimination between AD cases and controls (in Visit 2 TARCC data). For the purposes of this analysis, dEQ was again constructed in Visit 2 data, but without any covariates, specifically age, ethnicity, GDS, gender, HCY, HGBA1c and APOE  $\epsilon 4$  status.

dEQ and  $g'$  factor weights were applied to Visit 2 observed data to generate Visit 2 dEQ and  $g'$  composite scores (i.e., dEQ v2 and  $g'$  v2, respectively).  $g'$  is dEQ’s residual in Spearman’s  $g$  [53]. The composite scores were used as observed dependent variables in multiple regression models of age’s direct association with covariate adjusted Visit 2  $g'$  and dEQ.

Next, we constructed a longitudinal mediation model in SEM (Figure 1). Such models can arguably be interpreted causally [54]. Path “a” represents age’s direct association with Visit 2 dEQ scores. Path “b” represents the Visit 1 biomarker’s independent effect on dEQ. Bonferroni correction to  $p < 0.001$  was used to offset the potential for Type 2 error after multiple comparisons. When both paths were significant, we considered path “c”. The biomarker’s mediation effect on age’s direct association can then be calculated by MaKinnon’s method [55].

The mediation models were constructed in a randomly selected subset of TARCC participants, comprising approximately 50% of the subjects (i.e., Class 1:  $n = 1691$ ). As a test of each model’s generalizability to the remainder ( $n = 1694$ ), each mediation path’s significant direct association was constrained across the two groups, and model fit compared across constrained and unconstrained conditions [56-57]. Mediation effects were calculated in the constrained models.

### Missing data

We used the newest instance of TARCC’s dataset (circa 2016). The entire dataset was employed. Clinical diagnoses were available on 3385 subjects, 2861 of whom had complete data for  $\delta$ ’s cognitive indicators and covariates. Modern Missing Data Methods were

automatically applied by the AMOS software [58]. AMOS employs Full information Maximum Likelihood (FIML) [59-60]. Only the ROC analyses, performed in Statistical Package for the Social Sciences (SPSS) [61], were limited to complete cases.

### Fit indices

Fit was assessed using four common test statistics: chi-square, the ratio of the chi-square to the degrees of freedom in the model (CMIN /DF), the comparative fit index (CFI), and the root mean square error of approximation (RMSEA). A non-significant chi-square signifies that the data are consistent with the model [62]. However, in large samples, this metric conflicts with other fit indices (insensitive to sample size) show that the model fits the data very well. A CMIN/DF ratio  $< 5.0$  suggests an adequate fit to the data [63]. The CFI statistic compares the specified model with a null model [64]. CFI values range from 0 to 1.0. Values below 0.90 suggest model misspecification. Values approaching 1.0 indicate adequate to excellent fit. An RMSEA of 0.05 or less indicates a close fit to the data, with models below 0.05 considered “good” fit, and up to 0.08 as “acceptable” [65]. All fit statistics should be simultaneously considered when assessing the adequacy of the models to the data.

### ACKNOWLEDGEMENTS

Investigators from the Texas Alzheimer’s Research and Care Consortium: Baylor College of Medicine: Rachele Doody MD, PhD, Mimi M. Dang MD, Valory Pavlik PhD, Wen Chan PhD, Paul Massman PhD, Eveleen Darby, Monica Rodrigue RN, Aisha Khaleeq; Texas Tech University Health Sciences Center: Chuang-Kuo Wu MD, PhD, Matthew Lambert PhD, Victoria Perez, Michelle Hernandez; University of North Texas Health Science Center: Thomas Fairchild PhD, Janice Knebl DO, Sid E. O’Bryant PhD, James R. Hall PhD, Leigh Johnson PhD, Robert C. Barber PhD, Douglas Mains, Lisa Alvarez, Rosemary McCallum; University of Texas Southwestern Medical Center: Perrie Adams PhD, Munro Cullum PhD, Roger Rosenberg MD, Benjamin Williams MD, PhD, Mary Quiceno MD, Joan Reisch PhD, Ryan Huebinger PhD, Natalie Martinez, Janet Smith; University of Texas Health Science Center – San Antonio: Donald Royall MD, Raymond Palmer PhD, Marsha Polk; Texas A&M University Health Science Center: Farida Sohrabji PhD, Steve Balsis PhD, Rajesh Miranda, PhD; Essentia Institute of Rural Health: Stephen C. Waring DVM, PhD; University of North Carolina: Kirk C. Wilhelmsen MD, PhD, Jeffrey L. Tilson PhD, Scott Chasse PhD.

## CONFLICTS OF INTEREST

DRR and RFP have disclosed the results of these analyses to the University of Texas Health Science Center at San Antonio (UTHSCSA), which has filed patent application 2012.039.US1.HSCS and provisional patents 61/603,226 and 61/671,858 relating to the latent variable  $\delta$ 's construction and biomarkers.

## FUNDING

This study was made possible by the Texas Alzheimer's Research and Care Consortium (TARCC) funded by the state of Texas through the Texas Council on Alzheimer's Disease and Related Disorders.

## REFERENCES

1. Royall DR, Palmer RF. Thrombopoietin is associated with  $\delta$ 's intercept, and only in Non-Hispanic Whites. *Alzheimers Dement (Amst)*. 2016;3:35–42. doi: 10.1016/j.dadm.2016.02.003.
2. Royall DR, Palmer RF. Alzheimer's disease pathology does not mediate the association between depressive symptoms and subsequent cognitive decline. *Alzheimers Dement*. 2013; 9:318–25. doi: 10.1016/j.jalz.2011.11.009
3. Gavett BE, John SE, Gurnani AS, Bussell CA, Saurman JL. The role of Alzheimer's and cerebrovascular pathology in mediating the effects of age, race, and apolipoprotein E genotype on dementia severity in pathologically confirmed Alzheimer's disease. *J Alzheimers Dis*. 2016; 49:531–45. doi: 10.3233/JAD-150252
4. Nelson PT, Head E, Schmitt FA, Davis PR, Neltner JH, Jicha GA, Abner EL, Smith CD, Van Eldik LJ, Kryscio RJ, Scheff SW. Alzheimer's disease is not "brain aging": neuropathological, genetic, and epidemiological human studies. *Acta Neuropathol*. 2011; 121:571–87. doi:10.1007/s00401-011-0826-y
5. Royall DR, Palmer RF. Aging is a weak but relentless determinant of dementia severity. *Oncotarget*. 2016; 7:13307–18. doi:10.18632/oncotarget.7759.
6. Gavett BE, Vudy V, Jeffrey M, John SE, Gurnani AS, Adams JW. The  $\delta$  latent dementia phenotype in the uniform data set: cross-validation and extension. *Neuropsychology*. 2015; 29:344–52. doi: 10.1037/neu0000128
7. Palmer RF, Royall DR. Future dementia status is almost entirely explained by the latent variable  $\delta$ 's intercept and slope. *J Alzheimers Dis*. 2016; 49:521–29. doi: 10.3233/JAD-150254
8. Royall DR, Palmer RF.  $\delta$  scores predict MCI and AD conversions from non-demented states. *J Prev Alzheimers Dis*. 2015a; 2:337–38. Abstract
9. von Guten A, Ebbing K, Imhof A, Giannakopoulos P, Kövari E. Brain aging in the oldest-old. *Curr Gerontol Geriatr Res*. 2010. pii:358531. doi: 10.1155/2010/358531
10. Cray JF, Trojanowski JQ, Schneider JA, Abisambra JF, Abner EL, Alafuzoff I, Arnold SE, Attems J, Beach TG, Bigio EH, Cairns NJ, Dickson DW, Gearing M, et al. Primary age-related tauopathy (PART): a common pathology associated with human aging. *Acta Neuropathol*. 2014; 128:755–66. doi: 10.1007/s00401-014-1349-0
11. Bishnoi R, Palmer RF, Royall DR. Serum interleukin (IL) -15 as a biomarker of Alzheimer's disease. *PLoS One*. 2015; 10:e0117282. doi: 10.1371/journal.pone.0117282
12. Bishnoi RJ, Palmer RF, Royall DR. Vitamin D binding protein as a serum biomarker of Alzheimer's disease. *J Alzheimers Dis*. 2015; 43:37–45. doi: 10.3233/JAD-140042
13. Royall DR, Palmer RF. Ethnicity moderates dementia's biomarkers. *J Alzheimers Dis*. 2015; 43:275–87. doi: 10.3233/JAD-140264
14. Royall DR, Bishnoi RJ, Palmer RF. Serum IGF-BP2 strongly moderates age's effect on cognition: a MIMIC analysis. *Neurobiol Aging*. 2015; 36:2232–40. doi: 10.1016/j.neurobiolaging.2015.04.003
15. Royall DR, Palmer RF, Vidoni ED, Honea RA, Burns JM. The default mode network and related right hemisphere structures may be the key substrates of dementia. *J Alzheimers Dis*. 2012; 32:467–78. doi: 10.3233/JAD-2012-120424
16. Raichle ME, MacLeod AM, Snyder AZ, Powers WJ, Gusnard DA, Shulman GL. A default mode of brain function. *Proc Natl Acad Sci USA*. 2001; 98:676–82. doi: 10.1073/pnas.98.2.676
17. Andrews-Hanna JR, Snyder AZ, Vincent JL, Lustig C, Head D, Raichle ME, Buckner RL. Disruption of large-scale brain systems in advanced aging. *Neuron*. 2007; 56:924–35. doi:10.1016/j.neuron.2007.10.038
18. Damoiseaux JS, Beckmann CF, Arigita EJ, Barkhof F, Scheltens P, Stam CJ, Smith SM, Rombouts SA. Reduced resting-state brain activity in the "default network" in normal aging. *Cereb Cortex*. 2008; 18:1856–64. doi: 10.1093/cercor/bhm207
19. Biswal BB, Mennes M, Zuo XN, Gohel S, Kelly C, Smith SM, Beckmann CF, Adelstein JS, Buckner RL, Colcombe S, Dogonowski AM, Ernst M, Fair D, et al.

- Toward discovery science of human brain function. *Proc Natl Acad Sci USA*. 2010; 107:4734–39. doi: 10.1073/pnas.0911855107
20. Koch W, Teipel S, Mueller S, Buerger K, Bokde AL, Hampel H, Coates U, Reiser M, Meindl T. Effects of aging on default mode network activity in resting state fMRI: does the method of analysis matter? *Neuroimage*. 2010; 51:280–87. doi: 10.1016/j.neuroimage.2009.12.008
  21. Lustig C, Snyder AZ, Bhakta M, O'Brien KC, McAvoy M, Raichle ME, Morris JC, Buckner RL. Functional deactivations: change with age and dementia of the Alzheimer type. *Proc Natl Acad Sci USA*. 2003; 100:14504–09. doi:10.1073/pnas.2235925100
  22. Grady CL, Springer MV, Hongwanishkul D, McIntosh AR, Winocur G. Age-related changes in brain activity across the adult lifespan. *J Cogn Neurosci*. 2006; 18:227–41. doi:10.1162/jocn.2006.18.2.227
  23. Thompson WH, Thelin EP, Lilja A, Bellander BM, Fransson P. Functional resting-state fMRI connectivity correlates with serum levels of the S100B protein in the acute phase of traumatic brain injury. *Neuroimage Clin*. Epub ahead of print.
  24. Ali MS, Harmer M, Vaughan R. Serum S100 protein as a marker of cerebral damage during cardiac surgery. *Br J Anaesth*. 2000; 85:287–98. doi: 10.1093/bja/85.2.287
  25. Lian H, Yang L, Cole A, Sun L, Chiang AC, Fowler SW, Shim DJ, Rodriguez-Rivera J, Tagliatalata G, Jankowsky JL, Lu HC, Zheng H. NFκB-activated astroglial release of complement C3 compromises neuronal morphology and function associated with Alzheimer's disease. *Neuron*. 2015; 85:101–15. doi: 10.1016/j.neuron.2014.11.018
  26. Le Roith D. The insulin-like growth factor system. *Exp Diabesity Res*. 2003; 4:205–12. doi: 10.1155/EDR.2003.205
  27. Berryman DE, Christiansen JS, Johannsson G, Thorner MO, Kopchick JJ. Role of the GH/IGF-1 axis in lifespan and healthspan: lessons from animal models. *Growth Horm IGF Res*. 2008; 18:455–71. doi: 10.1016/j.ghir.2008.05.005
  28. Hoffman AR, Pyka G, Lieberman SA, Ceda GP, Marcus R. The somatopause. In: Muller EE, Cocchi D, Locatelli V, eds. *Growth hormone and somatomedins during lifespan*. Berlin: Springer Verlag, 1993.
  29. Hu D, Pawlikowska L, Kanaya A, Hsueh WC, Colbert L, Newman AB, Satterfield S, Rosen C, Cummings SR, Harris TB, Ziv E, and Health, Aging, and Body Composition Study. Serum insulin-like growth factor-1 binding proteins 1 and 2 and mortality in older adults: the Health, Aging, and Body Composition Study. *J Am Geriatr Soc*. 2009; 57:1213–18. doi: 10.1111/j.1532-5415.2009.02318.x
  30. Aleman A, Verhaar HJ, De Haan EH, De Vries WR, Samson MM, Drent ML, Van der Veen EA, Koppeschaar HP. Insulin-like growth factor-I and cognitive function in healthy older men. *J Clin Endocrinol Metab*. 1999; 84:471–75. doi: 10.1210/jcem.84.2.5455
  31. Aleman A, Torres-Alemán I. Circulating insulin-like growth factor I and cognitive function: neuromodulation throughout the lifespan. *Prog Neurobiol*. 2009; 89:256–65. doi: 10.1016/j.pneurobio.2009.07.008
  32. Camargo EC, Weinstein G, Beiser AS, Tan ZS, DeCarli C, Kelly-Hayes M, Kase C, Murabito JM, Seshadri S. Association of physical function with clinical and subclinical brain disease: The Framingham Offspring Study. *J Alzheimers Dis*. 2016; 53:1597–608. doi: 10.3233/JAD-160229
  33. Panza F, Solfrizzi V, Barulli MR, Santamato A, Seripa D, Pilotto A, Logroscino G. Cognitive Frailty: A systematic review of epidemiological and neurobiological evidence of an age-related clinical condition. *Rejuvenation Res*. 2015; 18:389–412. doi: 10.1089/rej.2014.1637
  34. McAdory BS, Van Eldik LJ, Norden JJ. S100B, a neurotropic protein that modulates neuronal protein phosphorylation, is upregulated during lesion-induced collateral sprouting and reactive synaptogenesis. *Brain Res*. 1998; 813:211–17. doi: 10.1016/S0006-8993(98)01014-2
  35. Tournell CE, Bergstrom RA, Ferreira A. Progesterone-induced agrin expression in astrocytes modulates glia-neuron interactions leading to synapse formation. *Neuroscience*. 2006; 141:1327–38. doi: 10.1016/j.neuroscience.2006.05.004
  36. Deak F, Sonntag WE. Aging, synaptic dysfunction, and insulin-like growth factor (IGF)-1. *J Gerontol A Biol Sci Med Sci*. 2012; 67:611–25. doi: 10.1093/gerona/gls118
  37. Cho H, Joo Y, Kim S, Woo RS, Lee SH, Kim HS. Plasminogen activator inhibitor-1 promotes synaptogenesis and protects against aβ(1-42)-induced neurotoxicity in primary cultured hippocampal neurons. *Int J Neurosci*. 2013; 123:42–49. doi:10.3109/00207454.2012.724127
  38. Mastellos DC. Complement emerges as a masterful regulator of CNS homeostasis, neural synaptic plasticity and cognitive function. *Exp Neurol*. 2014; 261:469–74. doi:10.1016/j.expneurol.2014.06.019

39. Ronan T, Macdonald-Obermann JL, Huelsmann L, Bessman NJ, Naegle KM, Pike LJ. Different Epidermal Growth Factor Receptor (EGFR) agonists produce unique signatures for the recruitment of downstream signaling proteins. *J Biol Chem.* 2016; 291:5528–40. doi:10.1074/jbc.M115.710087
40. Kesler SR. Default mode network as a potential biomarker of chemotherapy-related brain injury. *Neurobiol Aging.* 2014 (Suppl 2); 35:S11–19. doi: 10.1016/j.neurobiolaging.2014.03.036
41. Wang X-M, Walitt B, Saligan L, Tiwari AF, Cheung CW, Zhang Z-J. Chemobrain: a critical review and causal hypothesis of link between cytokines and epigenetic reprogramming associated with chemotherapy. *Cytokine.* 2015; 72:86–96. doi: 10.1016/j.cyto.2014.12.006
42. Small BJ, Scott SB, Jim HS, Jacobsen PB. Is cancer a risk factor of cognitive decline in late life? *Gerontology.* 2015;61:561–66. doi: 10.1159/000381022
43. Zhang Q, Guo S, Zhang X, Tang S, Shao W, Han X, Wang L, Du Y. Inverse relationship between cancer and Alzheimer’s disease: a systemic review meta-analysis. *Neurol Sci.* 2015;36:1987–94. doi: 10.1007/s10072-015-2282-2
44. Adriaensen W, Matheï C, Vaes B, van Pottelbergh G, Wallemacq P, Degryse JM. Interleukin-6 predicts short-term global functional decline in the oldest old: results from the BELFRAIL study. *Age (Dordr).* 2014; 36:9723. doi:10.1007/s11357-014-9723-3
45. Wechsler D. Wechsler Memory Scale – Third Edition. San Antonio, TX: The Psychological Corporation, 1997.
46. Benton A, Hamsher K. Multilingual Aphasia Examination. AJA Associates, Iowa City, Iowa, 1989.
47. Lawton MP, Brody EM. Assessment of older people: self-maintaining and instrumental activities of daily living. *Gerontologist.* 1969; 9:179–86. doi: 10.1093/geront/9.3\_Part\_1.179
48. Hughes CP, Berg L, Danziger WL, Coben LA, Martin RL. A new clinical scale for the staging of dementia. *Br J Psychiatry.* 1982;140:566–72. doi: 10.1192/bjp.140.6.566
49. Waring S, O’Bryant SE, Reisch JS, Diaz-Arrastia R, Knebl J, Doody R; for the Texas Alzheimer’s Research Consortium. The Texas Alzheimer’s Research Consortium longitudinal research cohort: study design and baseline characteristics. *Texas Public Health Journal.* 2008;60:9–13.
50. Koch W, Ehrenhaft A, Griesser K, Pfeufer A, Müller J, Schömig A, Kastrati A. TaqMan systems for genotyping of disease-related polymorphisms present in the gene encoding apolipoprotein E. *Clin Chem Lab Med.* 2002;40:1123–31. doi: 10.1515/cclm.2002.197
51. Arbuckle JL. Analysis of Moment Structures-AMOS (Version 7.0) [Computer Program], SPSS, Chicago, 2006.
52. Grice JW. Computing and evaluating factor scores. *Psychol Methods.* 2001;6:430–50. doi: 10.1037/1082-989X.6.4.430
53. Spearman C, Wynn Jones LL. Human Ability, Macmillan & Co., London, 1951.
54. Kraemer HC, Stice E, Kazdin A, Offord D, Kupfer D. How do risk factors work together? Mediators, moderators, and independent, overlapping, and proxy risk factors. *Am J Psychiatry.* 2001; 158:848–56. doi:10.1176/appi.ajp.158.6.848
55. MacKinnon D. Analysis of mediating variables in prevention and intervention research. In: Czarees A, Beatty L (editors). Scientific methods for prevention intervention research. NIDA Research Monograph. 1994;139:137-153.
56. Metz CE. Basic principles of ROC analysis. *Semin Nucl Med.* 1978; 8:283–98. doi: 10.1016/S0001-2998(78)80014-2
57. Zweig MH, Campbell G. Receiver-operating characteristic (ROC) plots: a fundamental evaluation tool in clinical medicine. *Clin Chem.* 1993; 39:561–77.
58. Palmer RF, Royall DR. Missing data? Plan on it! *J Am Geriatr Soc.* 2010 (Suppl 2); 58:S343–48. doi: 10.1111/j.1532-5415.2010.03053.x
59. Schafer JL, Graham JW. Missing data: our view of the state of the art. *Psychol Methods.* 2002; 7:147–77. doi:10.1037/1082-989X.7.2.147
60. Graham JW. Missing data analysis: making it work in the real world. *Annu Rev Psychol.* 2009; 60:549–76. doi: 10.1146/annurev.psych.58.110405.085530
61. Statistics PA. 18, Release Version 18.0.0, SPSS, Inc., 2009, Chicago, IL.
62. Bollen KA, Long JS. Testing Structural Equation Models. Sage Publications, Thousand Oaks, CA, 1993.
63. Wheaton B, Muthén B, Alwin DF, Summer GF. Assessing reliability and stability in panel models. In D.R.Heise (Ed.) *Sociology Methodology* San Francisco, CA: Jossey-Bass, 1977.

64. Bentler PM. Comparative fit indexes in structural models. *Psychol Bull.* 1990; 107:238–46. doi: 10.1037/0033-2909.107.2.238
65. Browne M, Cudeck R. Alternative ways of assessing model fit. In *Testing structural equation models*, Bollen KA, Long JS, eds. Sage Publications, Thousand Oaks, CA, pp. 136–162, 1993.
66. Yesavage JA, Brink TL, Rose TL, Lum O, Huang V, Adey M, Leirer VO. Development and validation of a geriatric depression screening scale: A preliminary report. *J Am Geriatr Soc.* 1982; 29:164–71. doi: 10.1111/j.1532-5415.1981.tb01759.x
67. Folstein MF, Folstein SE, McHugh PR. “Mini-mental state”. A practical method for grading the cognitive state of patients for the clinician. *J Psychiatr Res.* 1975; 12:189–98. doi: 10.1016/0022-3956(75)90026-6

# Early and progressive deficit of neuronal activity patterns in a model of local amyloid pathology in mouse prefrontal cortex

Fani Koukoulis<sup>1</sup>, Marie Rooy<sup>2</sup>, Uwe Maskos<sup>1</sup>

<sup>1</sup>Institut Pasteur, Département de Neurosciences, Unité Neurobiologie intégrative des systèmes cholinergiques, 75724 Paris Cedex 15, France; CNRS, UMR 3571, Paris, France

<sup>2</sup>Group for Neural Theory, Laboratoire de Neurosciences Cognitives, INSERM Unité 969, Département d'Études Cognitives, École Normale Supérieure, Paris, France

**Correspondence to:** Uwe Maskos; email: [umaskos@pasteur.fr](mailto:umaskos@pasteur.fr)

**Keywords:** Alzheimer's Disease, AAV, human mutated APP, chronic two-photon imaging, neuronal synchronicity

**Received:** October 16, 2016 **Accepted:** November 29, 2016 **Published:** December 20, 2016 **doi:** [10.18632/aging.101136](https://doi.org/10.18632/aging.101136)

## ABSTRACT

Alzheimer's Disease (AD) is the most common form of dementia. The condition predominantly affects the cerebral cortex and hippocampus and is characterized by the spread of amyloid plaques and neurofibrillary tangles (NFTs). But soluble amyloid- $\beta$  (A $\beta$ ) oligomers have also been identified to accumulate in the brains of AD patients and correlate with cognitive dysfunction more than the extent of plaque deposition. Here, we developed an adeno-associated viral vector expressing the human mutated amyloid precursor protein (AAV-hAPP). Intracranial injection of the AAV into the prefrontal cortex (PFC) allowed the induction of AD-like deficits in adult mice, thereby modelling human pathology. AAV-hAPP expression caused accumulation of A $\beta$  oligomers, microglial activation, astrogliosis and the gradual formation of amyloid plaques and NFTs. *In vivo* two-photon imaging revealed an increase in neuronal activity, a dysfunction characteristic of the pathology, already during the accumulation of soluble oligomers. Importantly, we found that A $\beta$  disrupts the synchronous spontaneous activity of neurons in PFC that, as in humans, is characterized by ultraslow fluctuation patterns. Our work allowed us to track brain activity changes during disease progression and provides new insight into the early deficits of synchronous ongoing brain activity, the "default network", in the presence of A $\beta$  peptide.

## INTRODUCTION

Alzheimer's Disease (AD) is a devastating neurodegenerative condition that greatly impacts society, primarily affecting the elderly population, and will become an enormous burden as the population ages [1]. In the broad category of dementia, AD amounts to 70% of all cases and thereby is the most common form of dementia [2]. Although there are familial genetic mutations linked to AD, the sporadic form is the most prevalent. There is currently no cure available for AD, only symptomatic treatments are administered in order to slow down the progression of the clinical manifestations [3].

Several genes have been implicated in AD in humans, most notably, those encoding the mutated APP,

presenilin 1 and presenilin 2 [4]. Consequently, various transgenic mouse models of AD harboring mutations in these genes have been established to decipher the disease mechanism. Moreover, a significant advance in the field came from the development of transgenic rodent models that exhibit tau pathology [5,6]. Although the results from these models have unraveled specific components of the disease pathology and given indications for developing potential therapies, there is no transgenic model that replicates the broad spectrum of AD pathology. In some cases, the mutations are associated with other pathologies, like frontotemporal dementia that is not part of AD pathology [7]. Moreover, in transgenic mice that express human familial AD mutations, the gene is expressed throughout the brain, making it impossible to study disease induced changes in specific brain regions.

The two primary features associated with AD pathology are the senile plaques and the neurofibrillary lesions. Since deposited A $\beta$  in amyloid plaques had a lack of correlation with cognitive impairment and its location and quantity in the brain, the 'toxic A $\beta$  oligomer' hypothesis developed as a possible alternative mechanism [8]. A $\beta$  oligomers are associated with AD hallmarks, like inducing abnormal tau phosphorylation [9]. Soluble and highly toxic forms of A $\beta$  such as oligomers and protofibrils may be more directly linked to cellular pathology, however the balance between monomeric A $\beta$ , oligomers and insoluble A $\beta$  fibrils is poorly understood and the lack of an experimental description of the toxic A $\beta$  oligomer makes conclusions difficult [8]. In addition, the acute short-term injection of A $\beta$  oligomers, sometimes of defined composition, into the brain of rodents and non-human primates [10] does not allow studies on the progression of the disease over time. There still is a need for a model that replicates the regionality and timecourse of the disorder.

Here, we developed an adeno-associated virus (AAV) based model for replicating AD-like pathology. The AAV vector expresses the mutated form of human APP harboring three pathogenic mutations: Swedish, London and Austrian (hAPP-SLA) [11–13]. We chose these mutations because they are associated with early onset of the disease. We targeted the expression of hAPP-SLA to the PFC, due to this region's key role in cognitive processes and its crucial implication in AD pathology [14] and we recorded neuronal spontaneous activity patterns. Our findings reveal a distinct impact of A $\beta$  oligomers in the synchronous activity of the PFC neurons and provide a mechanistic basis for understanding the pathophysiology of the disorder.

## RESULTS

### Generation of an AAV vector to express human mutated hAPP

The mutant hAPP-SLA contained the Swedish, London and Austrian mutations. The Swedish mutation was chosen because it leads to familial AD, as seen in patients harboring just one allele of this dominant mutation [11]. It has been widely used to establish transgenic mouse models of AD, for example the Tg2576 line [15], and in combination with other fAD associated mutations, such as PS1 (M146V) and tau (P301L) in the 3x-Tg mouse model [16]. The Austrian (T714I) [12] and London (V717I) [13] mutations were added, that when present in hAPP are known to drive a higher production of A $\beta$ . In addition, we added a FLAG tag at the C-terminus of the hAPP sequence to be able to detect the protein with anti-FLAG tag antibodies. We

thus produced an AAV-hAPP-SLA-FLAG construct (Fig. 1A).

Protein expression was confirmed *in vitro* in the HEK cell line. HEK cells were transduced with the vector expressing hAPP-SLA. The anti-FLAG antibody confirmed the synthesis of the hAPP protein (Fig. 1B).

### *In vivo* detection of hAPP in the PFC

The main cellular pathology of AD consists of damage and loss of neurons in widespread areas of the cortex and hippocampus [17]. The cognitive impairments characteristic of dementia in humans, such as attentional deficits and short-term memory loss, indicate PFC pathology [18, 19]. For this reason, we targeted the prelimbic area (PrL) of the PFC. A series of stereotaxic injections were performed *in vivo* to verify the efficiency of the AAV-hAPP-SLA in the PrL cortex (PrLC) of 3 month old WT mice. The vector showed diffusion in the brain and sufficient expression of the transgene, as visualized one month post-injection using an anti-FLAG antibody (Fig. 2 panel 1) with the hAPP diffusing throughout the PFC. As shown in the mosaics, there is no labeling in other parts of the brain outside PFC (Fig. 2 panel 1).

### AAV-hAPP-SLA drives A $\beta$ oligomer synthesis and intracellular accumulation

Most AD transgenic models exhibit memory impairments, with the cognitive deficits occurring earlier than the appearance of extracellular plaques. Research shifted to identify the precursors to plaque formation and to determine whether, and how, aggregation of A $\beta$  was crucial to its toxicity. This led to the focus on soluble oligomeric A $\beta$  species. As in AD transgenic mouse models, cognitive decline in humans is not proportional to A $\beta$  plaque load [20], but does correlate with soluble A $\beta$  species [21]. Intraneuronal A $\beta$  has gained experimental support in recent years, as, similar to humans, many hAPP AD transgenic mice exhibit intraneuronal amyloid accumulation [22]. The accumulation of intracellular A $\beta$  has been shown to precede deposition. Interestingly, it was found that intraneuronal A $\beta$  strongly correlates with initial deficits on a hippocampal-based memory task [23] and that intraneuronal A $\beta$  is more neurotoxic than extracellular A $\beta$  [24].

We investigated whether the expression of the hAPP-SLA protein was able to drive A $\beta$  oligomer accumulation in our model. The presence of oligomeric A $\beta$  was confirmed with anti-VHH 31-1 antibody, specific for oligomeric forms of A $\beta$  [25]. Immunofluorescent images with this antibody in WT

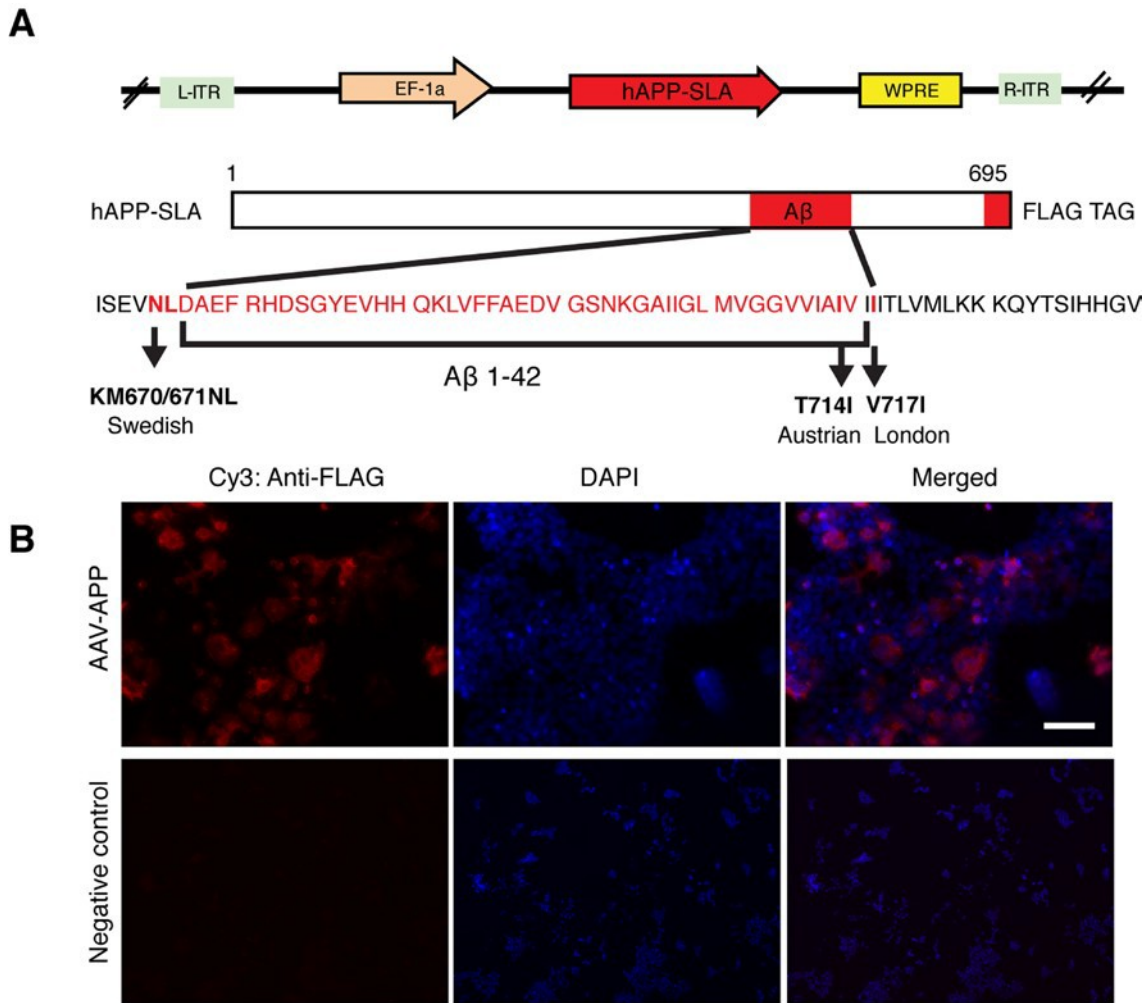


**Figure 1. Production of an AAV vector to express human mutated APP.** (A) Adeno-associated virus construct encoding for the 695 amino acid isoform of the human APP harbouring three pathogenic mutations (hAPP-SLA). The mutations in the APP sequence are highlighted. S: Swedish, L: London, A: Austrian mutations. (B) A HEK cell line was transfected with the viral vector expressing APP-SLA. Cells were positive for APP (red) and visualized with the anti-FLAG antibody. Negative control: HEK cells without being transduced with the viral vector and stained with the anti-FLAG antibody. Scale bar = 50  $\mu$ m.

mice injected with AAV-hAPP-SLA showed abundant intracellular A $\beta$  oligomer expression in the PFC at one month post-injection (1 mpi) of viral vector (Fig. 2, panels 2 to 3). A $\beta$  synthesis was strictly related to hAPP-SLA expression, since A $\beta$  oligomers were not observed in other brain areas, without viral transduction. There was no detection of A $\beta$  oligomers in sham mice injected with the control vector AAV-CAG-tdTomato (Fig. 2E, F). We followed the A $\beta$  oligomer accumulation over time and performed immunostaining analysis in mouse brains at various time points. Significant A $\beta$  production was also detected 4 and 6 mpi of AAV-hAPP-SLA. The diffusion of A $\beta$  was significantly higher 4 and 6 mpi in comparison to 1 mpi of the AAV-hAPP-SLA (Fig. 2G).

### Activation of microglia by AAV-hAPP-SLA

Neurological disorders trigger local inflammation and consequently activation of the immune response. Specifically, AD is characterized by an inflammatory response to A $\beta$ , including the activation of microglia and the recruitment of astrocytes around A $\beta$  deposits [26]. Cause or consequence of this activation in the disease progression is still not clear. Several studies in animal models suggest that microglia activation precedes amyloid plaques [27, 28] and the formation of NFTs [29, 30]. Once activated, microglia prominently change their morphology: the ramified processes swell and withdraw, while their cell bodies enlarge [31, 32]. Microglia activation occurs in the AD brain with micro-

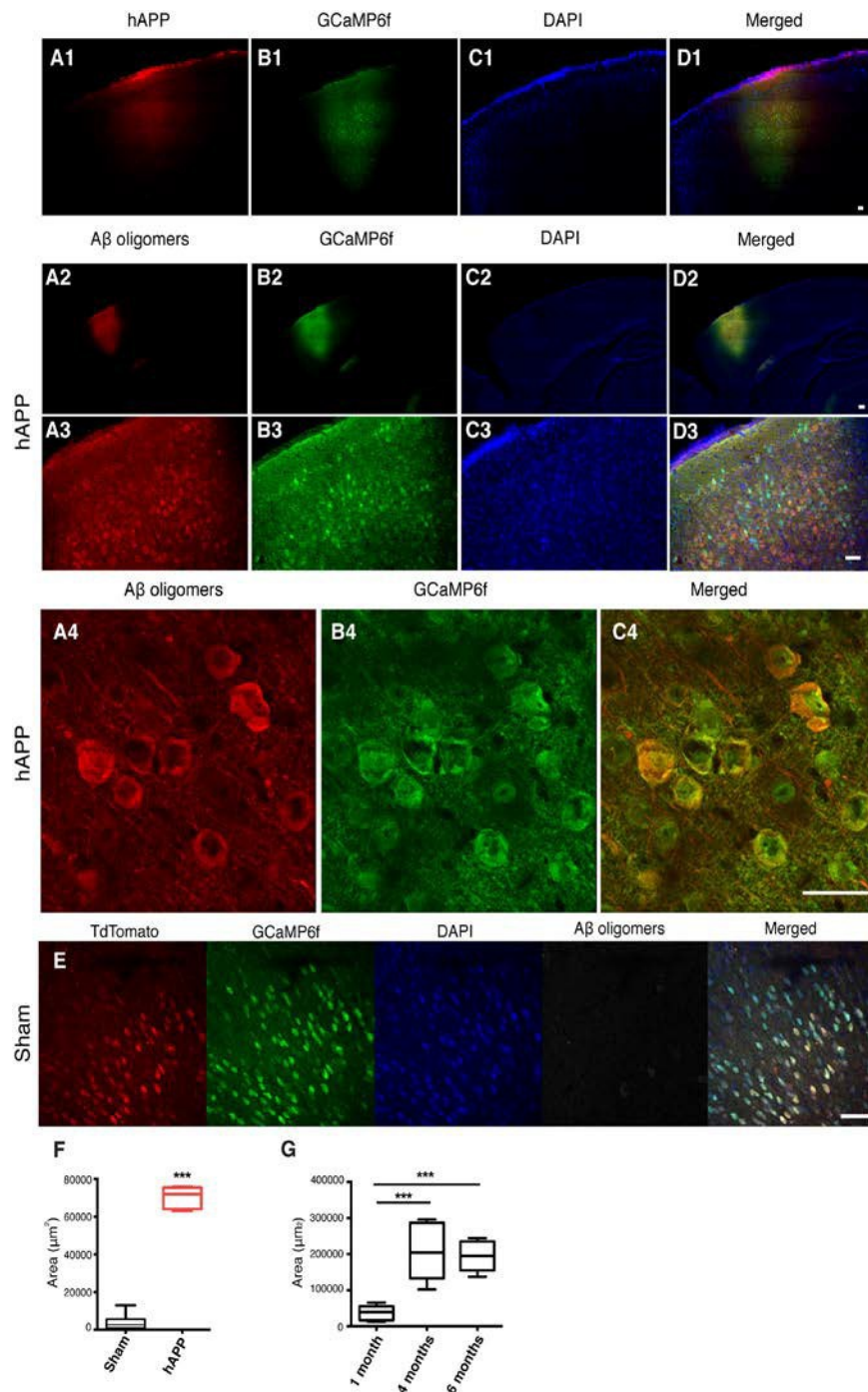


**Figure 2. Detection of hAPP and A $\beta$  oligomers in the PFC at 1 mpi of AAV-hAPP-SLA in WT mice.** *In vivo* detection of hAPP (A1), A $\beta$  oligomers (A2-A4), GCaMP6f (B), DAPI (C) and merged (D). Immunofluorescence images at low (1, 2), medium (3) and high (4) magnification. Scale bars = (1) 100  $\mu$ m, (2, 3) 200  $\mu$ m and (4) 50  $\mu$ m. (E) A $\beta$  oligomers were not detected in sham mice injected with the control vector AAV-tdTomato. Scale bar = 50  $\mu$ m. (F) Quantification of A $\beta$  oligomer diffusion in sham and hAPP mice. (G) Quantification of A $\beta$  oligomer diffusion in hAPP mice at three different timepoints. (Student's test,  $P < 0.0001$ , 3 mice for each group).

glia clusters forming around amyloid deposits as an early indicator of pathology and little is known about how this interaction is initiated. Here, we specifically focused on the early stages of the pathology and we validated our AD model by characterizing *in vivo* the process by which the microglia become activated in the presence of A $\beta$  peptide.

CX3CR1-GFP<sup>+/-</sup> mice [33] were used to visualize microglia in order to characterize the morphological

dynamics of microglia activation. The knockin of GFP at the Cx3cr1 locus in CX3CR1-GFP mice results in GFP-labeling of microglia. CX3CR1-GFP<sup>+/-</sup> mice were injected with a mixture of AAV-hAPP-SLA and the AAV1.CAG.tdTomato, whereas control mice were injected only with the AAV1.CAG.tdTomato vector specifically in the PrLC. A cranial window was implanted (see *Materials and Methods* for details) and four weeks after the injection, the microglia were imaged by two-photon microscopy with the mouse

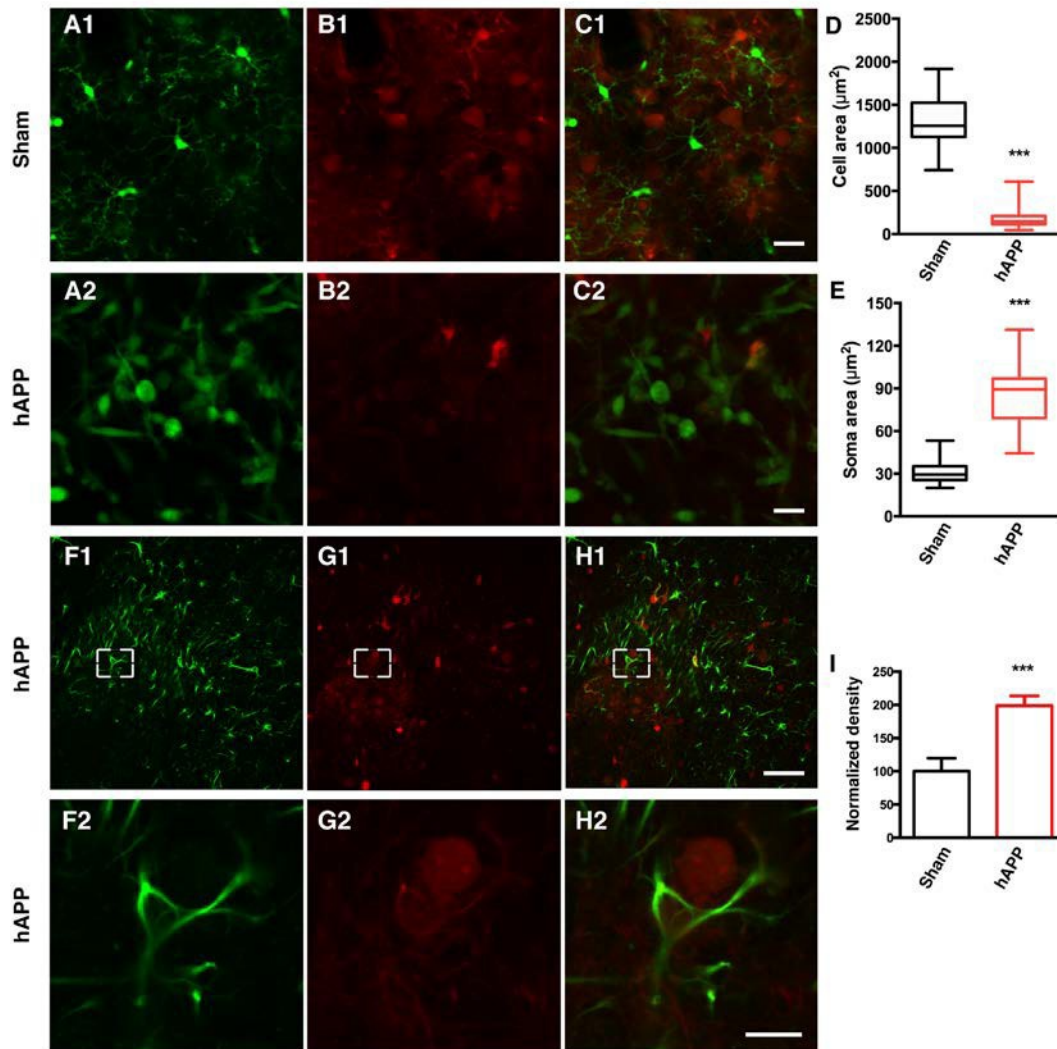


**Figure 3. AAV-hAPP-FLAG induces microglial activation and astroglyosis.** *In vivo* two-photon imaging of microglial activation in AAV-hAPP-SLA injected CX3CR1-GFP<sup>+/-</sup> mice. (A1-A2), GFP expressing microglial cells, (B1-B2), tdTomato and (C1-C2), merged. (1) Sham-operated mice indicating microglia cells in resting state, (2) AAV-hAPP-SLA injected mice indicating microglia cells in an activated state. Mean cell area (D) and mean soma area of microglia cells (E) in the sham and AAV-hAPP-SLA injected mice (Student's test,  $P < 0.0001$ ,  $n = 150$  cells, 3 mice). (F-H) Representative images showing GFAP immunostaining in the PFC. Immunofluorescence images at low (1) and high (2) magnification for GFAP (F), A $\beta$  oligomers (G) and merged (H). (I) Quantification of GFAP density. The density was normalized to control levels. The error bar is  $\pm$  SEM. (Student's test,  $P < 0.001$ , 6 slices were analyzed from 3 control mice and 6 slices from 3 AAV-hAPP-SLA injected mice). Scale bars = 50  $\mu\text{m}$ , for H2 scale bar = 10  $\mu\text{m}$ .

lightly anesthetized with isoflurane (0.8% isoflurane /O<sub>2</sub>). Ten-second interval imaging of control mice showed microglia that were characterized by a small cell body and highly elaborated thin processes, with multiple branches extending radially, a feature of the resting state (Fig. 3A1 and Supplementary Movies 1 and 2). Interestingly, in the mice injected with the AAV-hAPP-SLA vector, microglia were characterized by an amoeboid form, a feature of microglial activation (Fig. 3A2 and Supplementary Movie 3). Their processes were retracted and the soma enlarged. Most of the activated microglia had a large round morphology with one short or complete lack of processes. We estimated the level of microglial extension by measuring the cell area, including the soma and the processes and we found a significant difference between the two groups. The mean cell area of microglial cells in the sham mice

was  $1335 \pm 50.21 \mu\text{m}^2$ , and  $172.9 \pm 13.66 \mu\text{m}^2$  for the AAV-hAPP-SLA mice (Student's test,  $P < 0.0001$ ,  $n = 150$  cells, 3 mice) (Fig. 3D). The mean soma area of microglial cells in the sham mice was  $30.66 \pm 1.269 \mu\text{m}^2$ , and  $87.35 \pm 3.623 \mu\text{m}^2$  for the AAV-hAPP-SLA mice (Student's test,  $P < 0.0001$ ,  $n = 150$  cells, 3 mice) (Fig. 3E). Thus, the AAV-hAPP-SLA induces robust microglial activation.

### AAV-hAPP-SLA induces astrocyte activation

Reactive gliosis, including astrocyte activation, detected by increased glial fibrillary acidic protein (GFAP) expression, is another important characteristic of AD neuropathology [34]. Therefore, we aimed to investigate whether our model induces astrocyte activation.

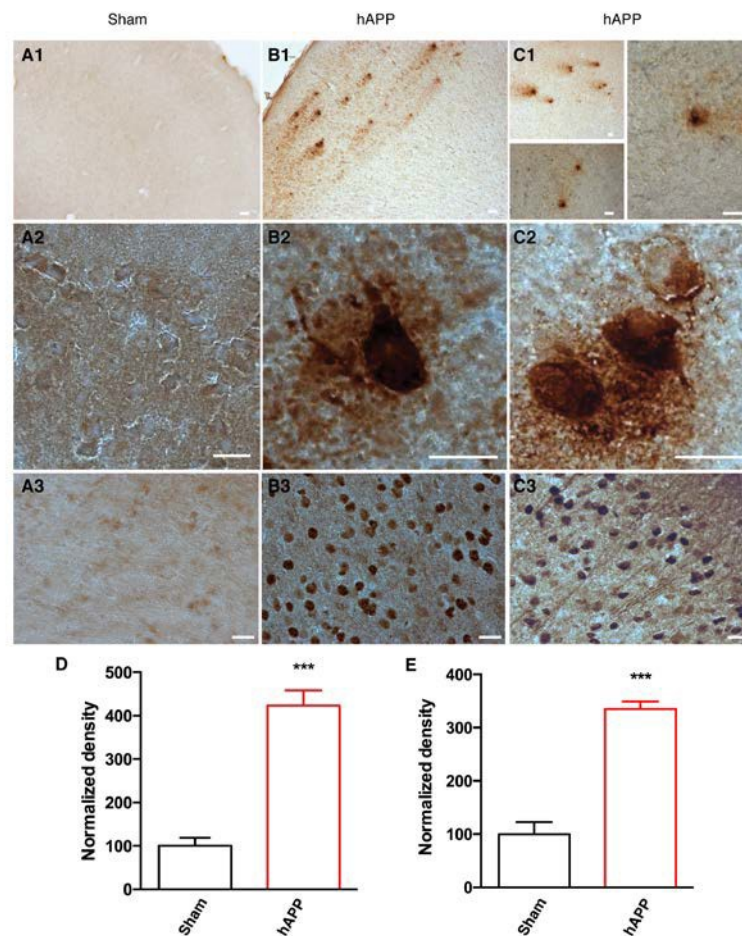


**Figure 4. Detection of amyloid plaques and NFTs in the PFC of AAV-hAPP-SLA injected mice at 12 mpi.** (A) Sham mouse brains injected with a control AAV and (B), (C) AAV-hAPP-SLA injected mice stained with the 4G8 antibody (1, 2) and AT100 antibody (phospho-tau at Ser212 and Thr214) (3). Scale bars = 20  $\mu\text{m}$ . Quantification of 4G8 optical density (D) and AT100 densities (E) and normalized to values obtained in sham operated mice. The error bar is  $\pm$  SEM. (Student's test,  $P < 0.001$ , for the quantification of amyloid plaques, 8 slices were analyzed from 4 control mice and 6 slices from 3 AAV-hAPP injected mice, whereas for the quantification of NFTs, 6 slices were analyzed from 3 control mice and 6 slices from 3 AAV-hAPP injected mice).

Sections from the PFC of control or AAV-hAPP-SLA injected mice were immunostained for the presence of astrocytes using an anti-GFAP antibody. The AAV-hAPP-SLA injected mice showed markedly increased immunoreactivity for GFAP, compared to the control (Fig. 3F to I). This suggests that the presence of astrocyte-mediated inflammatory processes is associated with the A $\beta$  oligomers.

### Amyloid plaque and neurofibrillary tangle formation in AAV-hAPP-SLA injected mice

As the disease advances, amyloid peptides accumulate and aggregate, eventually forming amyloid plaques. We were able to detect typical amyloid plaques in the PFC of AAV-hAPP-SLA mice at 12 mpi, but not in control mice (Fig. 4). Another hallmark pathology of human AD is the intra-neuronal aggregation of hyperphosphorylated tau forming NFTs. We aimed to evaluate abnormal tau phosphorylation in our model. We investigated the levels of paired helical filaments (PHFs) reactive to the anti-AT100 antibody, which recognizes tau phosphorylated at serine 212 and threonine 214 residues [10]. AT100-positive neurons represent early stage markers of tau pathology. Immunostaining with AT100 revealed tau pathology in the PFC of mice injected with the AAV-hAPP-SLA, but no immunoreactivity was observed to the PFC of control mice (Fig. 4). No amyloid plaques or tau pathology were detected before 12 mpi.

The amyloid cascade hypothesis predicts that tau hyperphosphorylation occurs as a downstream consequence of A $\beta$  accumulation [35]. APP-over-expressing transgenic mice have provided evidence both for and against this. Unlike humans with AD, many mouse models do not develop NFTs, yet many do show increased tau hyperphosphorylation.

### Higher rates of neuronal activity in layer II/III of PrLC in AAV-hAPP-SLA injected mice

There is accumulating experimental evidence that neuronal hyperactivity as a result of amyloid pathology is a major indicator of AD associated dysfunction [36].

Experimental analysis using various approaches, from single neurons to neuronal populations to large-scale networks, with a variety of electrophysiological and imaging techniques, have revealed two forms of AD-related hyperactivity and provided first insights into the synaptic mechanisms. A striking early observation from *in vivo* two-photon calcium imaging in mouse models of AD was the unexpected abundance of hyperactive neurons in networks of the cerebral cortex and the hippocampus. For instance, in the frontal cortex of amyloid plaque-bearing hAPP and PS1 double transgenic mice (the APP23 PS45 model), more than 20% of supragranular layer II/III neurons were found to be hyperactive [37]. These hyperactive neurons were located mostly in the direct vicinity of amyloid plaques, less than 60  $\mu$ m from the plaque border, whereas the fractions of the simultaneously present functionally silent neurons increased with plaque distance.

In order to assess neuron function in the PFC of our AD mouse model, we used dynamic two-photon microscopy to image the activity of neurons *in vivo* through a chronic imaging window (Fig. 5A). Neurons of PrLC were transduced with an AAV expressing the genetically encoded calcium indicator GCaMP6f driven by the synapsin promoter [38]. Four weeks after AAV injection, the majority of layer II/III neurons exhibited green fluorescence (Fig. 5B). The activity patterns of lightly anesthetized mice, 0.8% isoflurane/O<sub>2</sub>, were recorded. Three-month-old WT mice injected with the AAV-hAPP-SLA (hAPP) and sham mice, injected with the control vector (see *Materials and Methods*), were

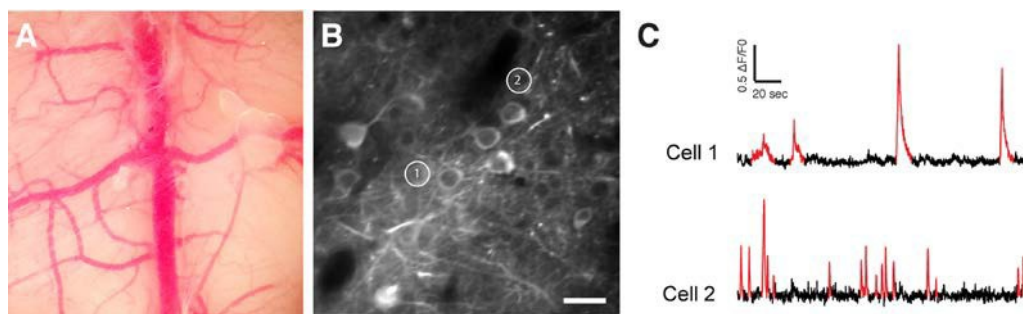


**Figure 5. *In vivo* two-photon calcium imaging.** (A) Chronic cranial window. (B) Two-photon image of GCaMP6f expressing neurons. (C) Spontaneous Ca<sup>2+</sup> transients (in red) of the two cells shown in (B). Scale bar = 50  $\mu$ m.

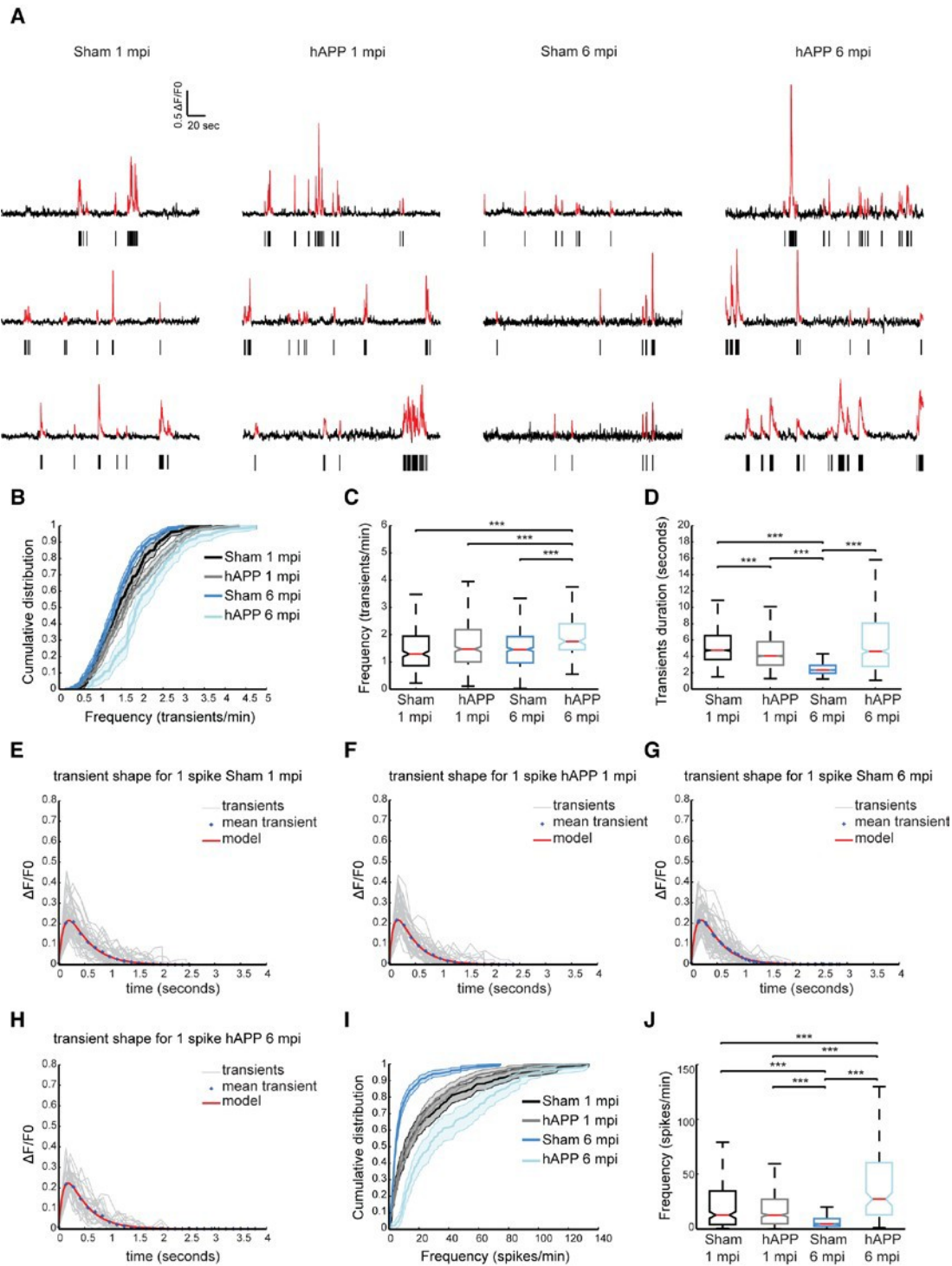


**Figure 6. Higher rates of neuronal activity in layer II/III of PrLC in AAV-hAPP-SLA injected mice.** (A) Representative spontaneous  $Ca^{2+}$  transients of sham-operated mice and hAPP mice and corresponding raster plots 1 and 6 mpi. (B) Population averaged cumulative plot of the distribution of spontaneous transients/min. (C) Median frequency of spontaneous calcium transients/min of the different mouse groups. (D) Median transient durations. (E-H) Kernel estimation for the different mouse groups. The kernel (model) is obtained from the fitting of an alpha function on the mean unitary calcium transient (crosses). In light gray, individual unitary calcium transients used to compute the mean for sham-operated and hAPP mice at 1 and 6 mpi of the vector. (I) Population averaged cumulative histograms of the distribution of spontaneous spikes/min. (J) Median frequency of spontaneous calcium spikes/min of the different mouse groups ( $n = 4$  animals for each group). Kruskal-Wallis test for all comparisons. (\* $P < 0.05$ , \*\* $P < 0.01$  and \*\*\* $P < 0.001$ )

**Table 1. Kernel estimation of amplitude, tau rise and tau decay of PFC layer II/III neurons in the different mouse groups.**

Mouse group	Amplitude ( $\Delta F/F$ ) (%)	tau rise (msec)	tau decay (msec)
Sham 1 mpi	21.5202 $\pm$ 0.576	200 $\pm$ 5	390 $\pm$ 10
hAPP 1 mpi	21.7686 $\pm$ 0.4782	160 $\pm$ 1	350 $\pm$ 1
Sham 6 mpi	21.5057 $\pm$ 0.35565	190 $\pm$ 1	370 $\pm$ 5
hAPP 6 mpi	22.2633 $\pm$ 0.99118	180 $\pm$ 1	370 $\pm$ 10

Data presented as mean  $\pm$  SEM.

used to monitor the spontaneously occurring somatic  $Ca^{2+}$  transients in individual cells (Fig. 5C). We analyzed the spontaneous neuronal activity at two time points: 1 and 6 mpi (Fig. 6A).

The distribution of spontaneous  $Ca^{2+}$  transients for the different time points is shown in Figure 6B. We found that the median frequency distribution of  $Ca^{2+}$  transients shifted towards higher values in hAPP mice at 6 mpi (1.75  $\pm$  0.08 transients/min, 160 cells, n = 4 mice), compared with the sham (1.458  $\pm$  0.04 transients/min, 829 cells, n = 4 mice, Kruskal Wallis test;  $P < 0.001$ ), although at 1 mpi no significant difference was found (sham, 1.29  $\pm$  0.05 transients/min in 451 cells; hAPP, 1.47  $\pm$  0.049 transients/min in 729 cells, n = 4 mice in each group) (Fig. 6C). We also analyzed the duration of  $Ca^{2+}$  transients between the different mouse groups. For the sham mice the median transient duration was 4.74  $\pm$  0.17 seconds (2542 transients) and 4.04  $\pm$  0.15 for the hAPP mice (3960 transients analyzed, Kruskal Wallis test;  $P < 0.001$ ), at 1 mpi. Interestingly, the sham mice at 6 mpi exhibited a much lower calcium transient duration when compared to the hAPP mice (sham, 2.32  $\pm$  0.04 seconds of 5524 transients analyzed; hAPP, 4.63  $\pm$  0.29 seconds of 887 transients analyzed n = 4 mice, Kruskal Wallis test;  $P < 0.001$ ) (Fig. 5D).

$Ca^{2+}$  transients were then selected according to their shape. Unitary calcium transients detected with GCaMP6f should have a rapid rise period, followed by a single peak value and a longer decay period [38]. We assumed that the smallest and fastest  $Ca^{2+}$  were a result of a single action potential. The mean shape and amplitude of this unitary event was used as a kernel for deconvolution to best estimate spike frequency. This procedure was performed on all recorded transients separately for each experimental condition, i.e., Sham and hAPP, 1 and 6 mpi (Fig. 6E to H and Table 1). We found layer II/III neuronal activity significantly

increased in PrLC of hAPP mice (27.14  $\pm$  3.33 spikes/min) compared to WT-control mice (4.46  $\pm$  0.71 spikes/min, Kruskal Wallis test;  $P < 0.001$ ), 6 mpi. There was no significant difference between the mice imaged at 1 mpi (WT control; 12.70  $\pm$  2.35 spikes/min, hAPP; 12.65  $\pm$  1.38 spikes/min,  $p = 0.397$  Kruskal Wallis test; Fig. 6I, J). Interestingly, sham mice showed a decrease in neuronal activity over time.

### Neuronal synchronicity is disrupted early in the disease

We have previously shown that the ongoing activity in the mouse PFC constantly fluctuates and exhibits synchronously firing neuronal activity, similar to humans [39]. These ultraslow fluctuations are considered to be related to elementary physiological processes associated with conscious processing in humans [39,40]. We aimed to identify ultraslow fluctuations in hAPP mice and compare their properties with the fluctuations observed in age-matched sham mice. Representative examples of simultaneously recorded neurons are shown in Fig. 7A. To identify patterns of activity characterized by high/low activity state transitions, we studied the distribution of their time varying mean activity, as before [39]. The high activity states correspond to population activities in red and low activity states correspond to population activities in blue (Fig. 7B and C). The activity patterns were then analyzed in order to detect synchronous activity in populations of simultaneously recorded neurons (Fig. 7D). We found that 66.25  $\pm$  6.88 % of simultaneously recorded populations exhibited high/low activity states in sham mice and 73.064  $\pm$  13.67 % in hAPP mice 1 mpi with no significant difference between groups ( $P = 0.65$ , ANOVA). In each population of simultaneously recorded neurons with high/low activity transitions, we determined the percentage of cells that exhibit an activity pattern in accordance with the population

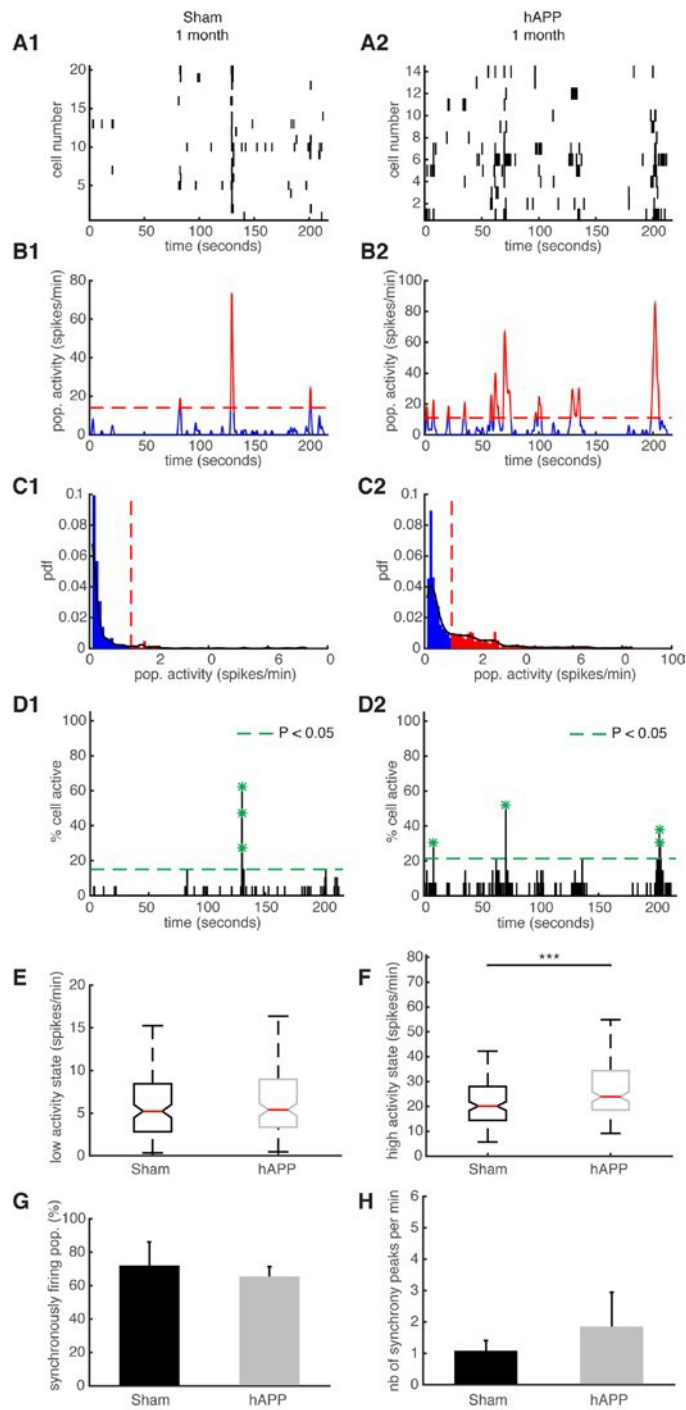


**Figure 7. Synchronous firing of simultaneously recorded neurons in sham and hAPP mice 1 mpi.** (A) Representative raster plots for one population of simultaneously recorded neurons. Each row corresponds to the spiking activity of one neuron. (B) Mean neural activity for the populations in A. The activity was smoothed through Gaussian filtering. The red periods correspond to the high activity states and the blue periods to the low activity states. The dotted red line represents the computed threshold between the two states. (C) Probability density function (pdf) of the population activity exhibited in (B). The black line represents the smoothed pdf, through Gaussian filtering. Red bars represent the high activity states and blue bars the low activity states. (D) Histogram representing the percentage of cells active in small time bins ( $\sim 0.144$  sec), for the population activity in (A). Asterisks mark significant peaks of synchrony. (E) Boxplots of low activity states for each mouse group (spikes/min). (F) Boxplots of high activity states for each mouse group (spikes/min). (G) Percentage of populations (simultaneously imaged neurons) exhibiting synchronous activity. (H) Mean number of synchrony peaks per minute for the different animal groups. (1) sham and (2) hAPP mice.

activity. In sham mice,  $73.91 \pm 8.67$  % of cells fire in accordance with their population activity and in hAPP,  $73.68 \pm 5.41$  % with no significant difference between the groups ( $P = 0.83$ , Kruskal-Wallis test). In addition, we found that  $45.96 \pm 10.63$  % of simultaneously recorded cells exhibited high/low activity states in sham mice and  $52.23 \pm 13.31$  % in hAPP mice 1 mpi with no significant difference ( $P = 0.73$ , ANOVA). Next, we computed the high/low activity properties in all populations. The low activity duration was  $5.2 \pm 2.26$  s for sham mice and  $6.5 \pm 2.9$  s for hAPP mice 1 mpi ( $P = 0.26$ , Kruskal-Wallis), whereas the high activity state duration was  $3.32 \pm 1.08$  s for sham mice and  $3.6 \pm 1.1$  s for hAPP mice 1 mpi, with no significant difference ( $P = 0.28$ ). The high activity state for hAPP mice was significantly higher ( $23.88 \pm 1.96$  spikes/min) than for sham mice 1 mpi ( $20.16 \pm 3.04$  spikes/min,  $P < 0.001$ ) whereas there was no significant difference for the low activity state (sham:  $5.22 \pm 2.09$  spikes/min, hAPP:  $5.4 \pm 0.55$  spikes/min;  $P = 0.74$ , Kruskal-Wallis) (Fig. 7E and F).

We then analyzed and compared the synchronicity in the two groups 1 mpi. In the sham mice, neurons displayed synchronous activity in  $72.12 \pm 14$ % of the recorded populations, whereas in hAPP mice neurons displayed synchronous activity in  $65.4 \pm 5.9$ % with no significant difference between groups ( $P = 0.37$ , ANOVA) (Fig. 7G). The number of synchrony peaks detected was similar between sham mice ( $1.27 \pm 0.34$  peaks/min) and hAPP ( $2.08 \pm 1.07$  peaks/min,  $P = 0.54$ , ANOVA) (Fig. 7H). Also, the percentage of coactive cells in the peaks of synchrony was similar between sham ( $50.66 \pm 2.21$  %) and hAPP mice ( $51.86 \pm 1.23$  %,  $P = 0.61$ ), 1 mpi.

We then performed the same type of analysis for the same mice at 6 mpi. Representative examples of simultaneously recorded neurons are shown in Fig. 8A. The high activity states correspond to population activities in red and low activity states correspond to population activities in blue (Fig. 8B and C). Synchronous activity in populations of simultaneously recorded neurons was detected for both mouse groups (Fig. 8D). We determined that  $79.33 \pm 11.57$  % of simultaneously recorded populations exhibited high/low activity states in sham mice and  $87.5 \pm 0.11$  % in hAPP mice 6 mpi with no significant difference between groups ( $P = 0.78$ , ANOVA). In sham mice,  $84.61 \pm 5.35$  % of cells fire in accordance with their population activity and in hAPP,  $85 \pm 5.2$  % with no significant difference between the groups ( $P = 0.95$ , Kruskal-Wallis). Moreover,  $54.61 \pm 12.02$  % of simultaneously recorded cells exhibited high/low activity states in sham mice and  $71.59 \pm 0.11$  % in hAPP mice 6 mpi with no significant difference ( $P = 0.59$ , ANOVA). The low

activity duration was  $16.96 \pm 2.74$  s for sham mice and  $9.96 \pm 2.98$  s for hAPP mice 6 mpi ( $P = 0.02$ , Kruskal-Wallis), whereas the high activity state duration was  $2.26 \pm 0.22$  s for sham mice and  $3.17 \pm 0.77$  s for hAPP mice 6 mpi, with a significant difference ( $P = 0.005$ ). The high activity state for hAPP mice was significantly higher ( $28.5 \pm 21.36$  spikes/min) than for sham mice 6 mpi ( $21.37 \pm 1.30$ ,  $P < 0.001$ ), but also the low activity state was significantly higher for hAPP mice than for sham mice 6 mpi (sham:  $1.69 \pm 0.69$  spikes/min, hAPP:  $5.3 \pm 2.17$  spikes/min;  $P < 0.001$ , Kruskal-Wallis) (Fig. 8E and F). In the sham mice, neurons displayed synchronous activity in  $69.29 \pm 14.79$ % of the recorded populations, whereas in hAPP mice neurons displayed synchronous activity in  $75 \pm 0.01$ % with no significant difference between groups ( $P = 0.88$ , ANOVA) (Fig. 8G). Importantly, the number of synchrony peaks detected was robustly decreased for the case of hAPP mice ( $0.72 \pm 0.23$  peaks/min) compared to sham mice 6 mpi ( $3.95 \pm 0.82$  peaks/min) ( $P = 0.049$ , ANOVA) (Fig. 8H). Also, the percentage of coactive cells in the peaks of synchrony was increased for hAPP mice ( $41.4 \pm 4.83$  %) compared to sham mice ( $31.18 \pm 0.52$  %,  $P < 0.001$  ANOVA), 6 mpi.

Overall, neuronal synchronicity is disrupted in the presence of A $\beta$  oligomers 6 mpi of the AAV-hAPP in the absence of amyloid plaques or NFTs.

## DISCUSSION

AD is a complex disease affecting discrete brain areas with defined specificity for certain regions and pathways [41]. To more effectively study AD pathology, it is necessary to dissect the pathological mechanisms using *in vivo* models and recording methods identifying the functional changes.

Here, we generated an AAV model that created AD-like pathology. The AAV was made to express mutant human APP harboring the Swedish, London and Austrian mutations that are associated with early onset of AD. Production of different AAVs for the expression of the tau protein or the mutant APP have previously been described without including any functional analysis on the role of soluble A $\beta$  [42]. With injection of our viral vector into the PFC of WT mice, we successfully induced A $\beta$  production as early as 1 mpi. This production of A $\beta$  oligomers in the initial phase of the pathology has the potential to greatly advance the understanding of the mechanisms centrally implicated in the early stages of AD pathogenesis, with applications for therapeutic development. It is thought that in AD the balance between A $\beta$  production and clearance is disrupted therefore causing an increase in cellular A $\beta$ . Over time, this disrupted balance leads to

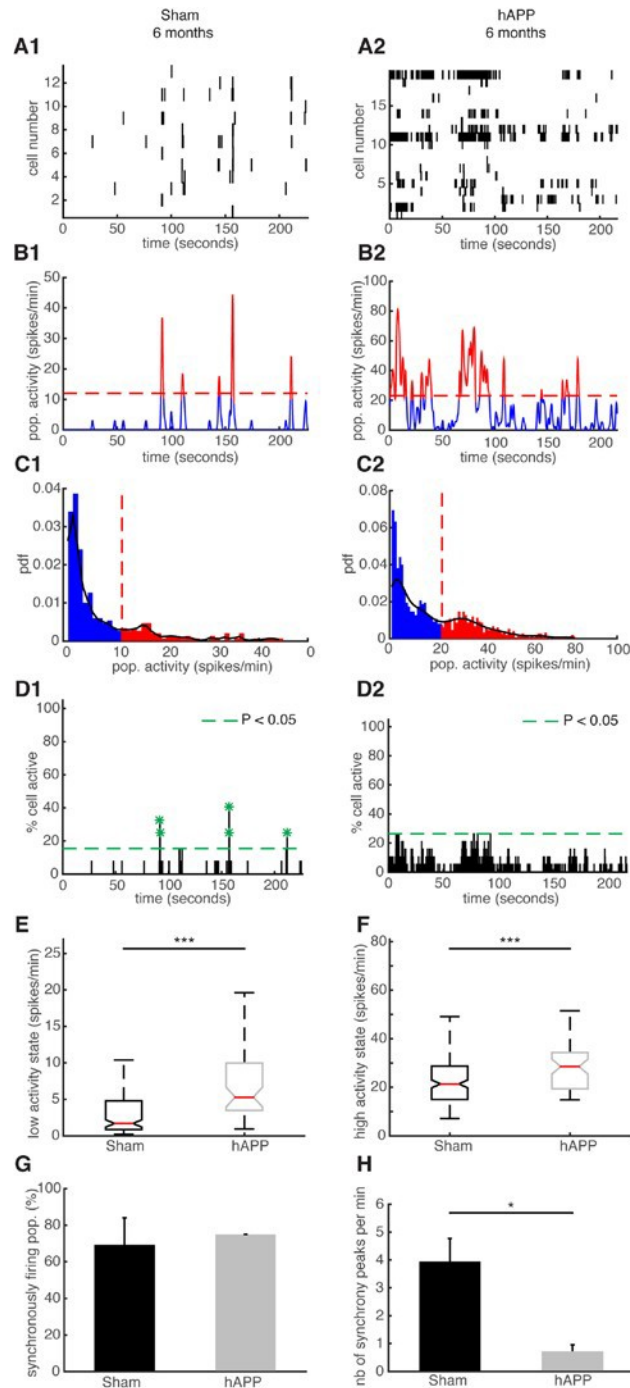


**Figure 8. Neuronal synchronicity is disrupted in the PFC of hAPP mice 6 mpi.** (A) Representative raster plots for one population of simultaneously recorded neurons. Each row corresponds to the spiking activity of one neuron. (B) Mean neural activity for the populations in (A). The activity was smoothed through Gaussian filtering. The red periods correspond to the high activity states and the blue periods to the low activity states. The dotted red line represents the computed threshold between the two states. (C) Probability density function (pdf) of the population activity exhibited in (B). The black line represents the smoothed pdf, through Gaussian filtering. Red bars represent the high activity states and blue bars the low activity states. (D) Histogram representing the percentage of cells active in small time bins ( $\sim 0.144$  sec), for the population activity in (A). Asterisks mark significant peaks of synchrony. (E) Boxplots of low activity states for each mouse group (spikes/min). (F) Boxplots of high activity states for each mouse group (spikes/min). (G) Percentage of populations (simultaneously imaged neurons) exhibiting synchronous activity. (H) Mean number of synchrony peaks per minute for the different animal groups. (1) sham and (2) hAPP mice.

large amyloid deposits. The deposition of A $\beta$  is a slowly progressive process that starts in the neocortex and then expands hierarchically into other brain regions, representing different phases of A $\beta$  deposition [43]. In accordance with the sequential involvement of brain regions in AD, we targeted the prefrontal area of the brain, a region associated with cognitive functions that could provide a basis for the understanding of the early phases of the disease. We were able to identify microglia activation, a feature of AD pathology, at 1 mpi of the vector. We followed the disease progression and identified hallmarks of AD pathology, such as the presence of amyloid plaques and tau hyperphosphorylation that appeared one year after vector injection.

Our method could be very useful to investigate region specific vulnerability in AD linked to A $\beta$  deposition and to follow the accumulation of amyloid deposition from one targeted brain structure to connected areas. In contrast, transgenic mouse models that express mutated hAPP globally in the brain throughout pre- and post-natal development into adulthood complicate the ability to measure the disease progression. Since all brain regions express the mutated APP, it is impossible to determine how the disease pathology spreads between an affected brain region to other initially unaffected areas. Our model allows targeted induction of AD-like pathology and therefore future studies exploring the spread to other brain regions will be possible.

Another advantage of this approach is that it is applicable to every animal model, strain or species. This includes knock-out animals for specific factors involved in the pathways that lead to AD pathology. Notably, the cholinergic pathway, and cholinergic neurons located in the basal forebrain in particular, are subject to degeneration in AD [44]. Nicotinic acetylcholine receptors are crucially implicated in cognitive processing and have been proposed to be involved in the cognitive decline observed in AD patients [45]. In human tissue, A $\beta$  oligomers have been identified in cholinergic neurons, suggesting a role in cholinergic deficiency [46]. The AAV vector we developed and characterized *in vivo* can be used to rapidly study the implications of different nicotinic receptor knock-out animals by using a single injection and therefore avoids the time and resource consuming crossbreeding between transgenic lines.

Furthermore, our new AD model is compatible with chronic long-term *in vivo* imaging and recording techniques. The importance of this is illustrated by previous slice and primary neuronal culture studies that concluded that high levels of A $\beta$  cause a reduction in excitatory neuronal transmission resulting in hypoactivity and synaptic failure [47]. However,

clinical observations suggested that patients with AD, and in particular early-onset familial AD, have a higher incidence of epileptic seizures, indicating an increase rather than decrease in neuronal excitability [48]. *In vivo* studies in the last few years have further confirmed these human results in mouse models. It was shown that hyperactive neurons were found in close proximity to amyloid plaques, suggesting a synaptotoxic microenvironment around the AD lesions [37]. Importantly, one study, in visual cortex, demonstrated that a progressive deterioration of neuronal tuning for the orientation of visual stimuli occurs in parallel with the age-dependent increase of the A $\beta$  load, and this deterioration was found only in neurons that are hyperactive during spontaneous activity [49]. The mechanisms underlying the changed neuronal activity in the diseased visual cortex are likely to involve a redistribution of synaptic inhibition and excitation, as it has been suggested for the impaired spontaneous activity in the frontal cortex [37]. In addition, local application of soluble A $\beta$  oligomers in the form of synthetic dimers provoked hyperactivity of CA1 neurons in WT mice [50].

Here, we examined the alterations in PFC neuronal activity at two different timepoints. By using *in vivo* two photon imaging, chronic cranial windows and monitoring neuronal activity with a genetically encoded calcium indicator, we were able to track neuronal activity in the same mice, at 1 and 6 mpi of the AAV-hAPP-SLA vector. Interestingly, we identified a robust increase in the median frequency of PFC neurons injected with the AAV-hAPP-SLA as compared to control mice. At 6 mpi, we did not detect amyloid plaques or the formation of NFTs, however, the expression of amyloid oligomers can explain the occurrence of the increased neuronal activity. Our results are in accordance with human studies where asymptomatic humans with high amyloid load were found to display abnormally increased activation in the default-mode network using blood-oxygen-level dependent (BOLD) fMRI. This increase was mainly found in the medial prefrontal cortex, the precuneus and the posterior cingulate cortex [51]. In addition, we observed reduced neuronal activity in the PFC of control mice at 6 mpi. This finding is in accordance with neuroimaging studies in humans where older adults have shown reduced activity in PFC and other brain regions critical for cognitive functions [52]. Our data show an evolution in the functional properties of the neurons and network since the brain activity of the same mouse was followed over time. A crucial role of soluble A $\beta$  on the spontaneous brain activity was identified, since increased neuronal activity was detected before the formation of amyloid plaques. Our findings indicate that A $\beta$  is able to increase spontaneous neuronal activity early in the disease progression in the

absence of amyloid plaques or NFTs and shed a different light on previous work that demonstrated a role of amyloid plaques in cortical hyperactivity [37].

In addition, we have previously shown that in the resting state, in the absence of any explicit task performance or external stimulus, the PFC exhibits a highly informative mode of spontaneous activity that is characterized by ultraslow fluctuations and synchronized activity patterns [39]. Here, we analyzed hAPP mice for the presence of ultraslow fluctuations and synchronously firing neurons and compared their properties with sham mice. Interestingly, high and low activity states were increased in the presence of A $\beta$  peptide 6 mpi, however, the number of synchronous peaks was robustly decreased. Computational and experimental studies had established that a neuronal group is the most fundamental unit in the cortex and it is not formed by a single neuron, but by a cluster of tightly coupled neural cells, which fire in synchrony [53]. We have previously shown that nicotinic acetylcholine receptors (nAChRs) are specifically required for synchronized activity patterns in the mouse PFC [39]. In addition, pharmacological intervention with nicotinic antagonists is enough for the disruption of neuronal synchronicity [39]. Here, we also found that A $\beta$  is able to disrupt neuronal synchronicity early in the disease progression in the absence of amyloid plaques or NFTs, implying a possible role of nAChRs in the A $\beta$ -mediated disruption of synchronicity.

In conclusion, our model induces A $\beta$  accumulation, astrocyte and microglia activation, amyloid plaque formation, and abnormal tau phosphorylation. Functional *in vivo* two-photon imaging of AAV-hAPP injected mice revealed an important role of soluble A $\beta$  on spontaneous brain activity, indicating that the spontaneous synchronous activity patterns are disrupted in an AD-like brain before the formation of amyloid plaques. These findings can further our understanding of AD mechanisms of pathogenesis since it replicates important features of AD and can therefore be applied to improve our efforts to develop future therapies, already targeting early AD stages. However, the exact mechanisms that lead to the disruption of neuronal activity in AD is indeed poorly understood and further studies must be performed in order to elucidate the complexity of AD mediated hyperactivity and disruption of synchronicity.

## MATERIALS AND METHODS

### Adeno-associated viral construction

The generation of the hAPP-SLA-FLAG plasmid in pGEM-T was described previously [54]. The hAPP-

SLA-FLAG cassette was recovered from the pGEM-T vector with XbaI and EcoRV restriction enzymes and inserted in an AAV-EF1a vector. The AAV-EF1a vector was derived from an AAV-EF1a-DIO-ChetA-EYFP plasmid ([http://www.everyvector.com/sequences/show\\_public/7300](http://www.everyvector.com/sequences/show_public/7300)) that was digested with the same restriction enzymes. Ligation of the two fragments with T4 DNA ligase (M0202, NEB) resulted in the adeno-associated viral vector AAV-EF1a-hAPP-SLA-FLAG. Virus production was performed by INSERM U649 Vector Core of Nantes University to a final titer of  $2.2 \times 10^{12}$  vg/ml.

### Animals

Experiments were performed with male wild-type mice (C57Bl/6J line) and were bred at Charles River Laboratories (L'Arbresle, France). All mice were transported to our facilities at eight weeks of age, housed under a 12h light-dark cycle with ad libitum access to food and water.

CX3CR1-GFP<sup>+/-</sup> mice [33] were kindly provided by the *Unité d'Histopathologie humaine et modèles animaux* of the Institut Pasteur in Paris, France.

The experiments described in the present work were conducted in accordance with the guidelines on the ethical use of animals from the European Community Council Directive of 24 November 1986 (86/609/EEC) and in accordance with institutional animal welfare guidelines and were approved by the CETEA Ethics committee, protocol number 2013-0056 Animalerie Centrale and Médecine du Travail, Institut Pasteur.

### Stereotaxic injections and chronic cranial window

Twelve week old mice were anesthetized with ketamine (Imalgen 1000, 10% in PBS; Rhone Mérieux) and xylazine (Rompun, 2% in PBS; Bayer AG), 10 ml/kg i.p. The stereotaxic injections and chronic cranial windows were performed as previously described [39, 55]. Briefly, the skull was carefully thinned using a dental drill over the region of interest and the thinned bone was removed using forceps, leaving the dura intact. 200 nl of GCaMP6f expressing Serotype 2.1 AAV virus under the synapsin-1 promoter (AAV.syn.GCaMP6f.WPRE.SV40,  $2.2 \times 10^{13}$  GC/ml, University of Pennsylvania Vector Core, catalog number; AV-1-PV2822, lot; CS0261WL) was injected bilaterally at the following coordinates into PrLC: AP, +2.8 mm from bregma; L,  $\pm 0.5$  mm; and DV, -0.3 to -0.1 mm from the skull using a Nanoject II<sup>TM</sup> (Drummond Scientific) at the slow infusion setting. For WT control mice, 2  $\mu$ l of AAV1.CAG.tdTomato.WPRE.SV40  $1.52 \times 10^{13}$  GC/ml (University of Pennsylvania Vector Core, catalog

number; AV-1-PV2126) diluted in PBS 1X, was injected bilaterally at the same coordinates as described above. For the WT-hAPP mice, 2  $\mu$ l of AAV-EF1a-hAPP-SLA-FLAG (2,2e12 GC/ml.) was also injected bilaterally at the same coordinates. The glass pipette was left in situ for an additional 5 min before being slowly withdrawn. The cranial window was covered with a circular coverglass (5mm diameter) and was sealed to the skull with dental cement (Coffret SUPERBOND complet, Phymep).

### Immunofluorescent staining

Mice were deeply anesthetized with a lethal dose of ketamine/xylazine before intracardiac perfusion with ice cold PBS, followed by 4% PFA (Sigma-Aldrich, Saint Louis, MO, USA). The brains were removed and post-fixed by immersion in 4% PFA for 2 days at 4° C. The brains were then immersed in 30% sucrose in PBS overnight at 4° C for cryoprotection. Serial 40  $\mu$ m coronal sections were cut using a sliding microtome (Leica Microsystems) and transferred to PBS. Slices were incubated in 10% normal goat serum (NGS) and 0.2% Triton X- 100 in PBS for one hour, then washed in PBS and incubated with various combinations of primary antibodies: rabbit anti-GFP (1:2000; Life Technologies, Invitrogen, Carlsbad, CA, USA), rabbit anti-GFAP (1:1000; Chemicon, AB5804, Temecula, CA), camel single-domain anti-VHH V31-1 (1:500; kindly provided by Pierre Lafaye [25]) and mouse anti-FLAG (1:1000; Sigma Life Science, F1804, France). A mouse anti-His antibody (1:1500; Sigma- Aldrich, Saint Louis, MO, USA) was used for amplifying the VHH signal. Fluorophore-conjugated secondary antibodies were used with cy3-anti-mouse and Alexa 488-anti-rabbit (Life technologies, Eugene, OR, USA) at a dilution of 1:500 for 3 hours at RT. After DAPI (Sigma-Aldrich, Saint Louis, MO, USA) incubation, the slices were mounted on slides ProLong Gold Antifade Reagent mounting medium (Life Technologies, Molecular Probes, Carlsbad, CA, USA). Images were acquired with a Zeiss epifluorescent microscope and a confocal microscope (Zeiss LSM 700, Heidelberg, Germany).

### Immunohistochemistry

40  $\mu$ m coronal sections were incubated for 30 min in NH<sub>4</sub>Cl 50 mM, Lysine 1 mM and Glycine 1 mM in PBS, then one hour in 3% H<sub>2</sub>O<sub>2</sub> in PBS for neutralisation of endogenous aldehydes and peroxidases, respectively. Slices were incubated in 10% NGS and 0.2% Triton X- 100 in PBS (Tx-PBS) for 1 hour and then with the primary biotinylated antibody, mouse anti-4G8 (1:500; Covance, Dedham, MA, lot: 09EC00860) or AT100 (1:100; Thermo Scientific, MN 1060, lot: QE202937), diluted in 2% NGS and 0.2% Triton X-100 in PBS and incubated overnight at 4°C.

Slices were rinsed with Tx-PBS and incubated in ABC mixture for 30 min with gentle shaking (Elite ABC, PK-6100, Vector Laboratories, Burlingame, CA). After 3 washes with Tx-PBS, the sections were developed in DAB solution (Vector Novared substrate kit, SK-4800, Vector Laboratories, Burlingame, CA) for 5-10 minutes. Finally, slices were washed with distilled H<sub>2</sub>O and mounted in aqueous mounting media. Amyloid plaques and NFTs were visualized with light microscopy.

### Quantitative analysis of immunofluorescent images

The analysis of the A $\beta$  diffusion, *in vivo* microglia images and the immunolabeling of astrocytes was performed using Fiji (ImageJ, NIH). For the microglia, 1024x1024 resolution images (163.225 x 163.225  $\mu$ m) were analyzed for both sham operated and AAV-hAPP injected mice. The same settings (laser power and gain) were used during the acquisition of the images. First, we set the scale in  $\mu$ m by adding the distance in pixels. For the quantification of cell area (somas and processes) the perimeter of the cells' process tips was manually marked using the polygon selection tool, whereas for the soma area, we manually traced the somas of the cells within the whole field. In the set measurements menu we selected "area and then measure". For the A $\beta$  diffusion 5 slices were analyzed from 3 control mice and 5 slices from 3 AAV-hAPP-SLA injected mice. For the microglia analysis, 10 *in vivo* two-photon images from 3 control mice and 8 *in vivo* two-photon images from 3 AAV-hAPP injected mice were analyzed, n = 150 cells. For the analysis of astrocytic density between sham and AAV-hAPP injected mice, the rectangle tool was used to select a region of interest (ROI) of 200 x 200  $\mu$ m. The same size of ROI was selected for both sham and hAPP brain slices in the injection area. A ROI was also drawn in an area without fluorescence to be used for background subtraction. The net average fluorescence intensity in the ROI was calculated for the different groups and the average intensity values of AAV- hAPP injected mice were normalized by values obtained in sham mice. 6 slices were analyzed from 3 control mice and 6 slices from 3 AAV-hAPP-SLA injected mice. For these experiments, all parameters during image acquisition were kept identical.

### Quantitative analysis of immunohistochemical labeling

The analysis of optical densities for the immunohistochemical labeling of amyloid plaques and neurofibrillary tangles was also performed in Fiji. The images first underwent color deconvolution. The H DAB setting was selected as the labeling method from the vectors and the analysis was performed and measurements were set to the mean grey value. ROIs were selected (the prelimbic cortex area was validated

by taking mosaics of each brain slice), always maintaining the same size of box for both sham and hAPP brain slices. Optical density numbers were acquired using the formula  $OD = \log(\text{max intensity/mean intensity})$ . The values were normalized by values obtained in sham mice. For the quantification of amyloid plaques, 8 slices were analyzed from 4 control mice and 6 slices from 3 AAV-hAPP injected mice, whereas for the quantification of NFTs, 6 slices were analyzed from 3 control mice and 6 slices from 3 AAV-hAPP injected mice.

### **In vivo two-photon imaging**

*In vivo* imaging was performed with an Ultima IV two-photon laser-scanning microscope system (Bruker), using a 16x 0.8 NA water immersion objective (Nikon) with a femtosecond laser (MaiTai DeepSee, Spectra Physics, Mountain View, CA, USA) tuned to 950 nm for imaging of GCaMP6f expressing cells. Time-series movies of neuronal populations expressing GCaMP6f were acquired at 7 Hz (182 x 182 microns). Each focal plane movie duration was 3.6 minutes (1500 frames) to track spontaneous neuronal activity. Care was taken to use less than 10 mW of laser power at the surface of the tissue. For *in vivo* two-photon imaging of microglia cells of the CX3CR1 mice (also injected with the AAV1.CAG.tdTomato vector), the femtosecond laser tuned to 960 nm and laser power was kept below 5 mW to avoid phototoxic effects. Time series were acquired (1024x1024 pixels) at a 10-second interval for a total of 10 min (60 iterations).

### **Two-photon data analysis**

Image analysis (also for immunostained images) was performed off-line with ImageJ software. The time series were registered using the “Image Stabilizer” plugin (K. Li, [http://www.cs.cmu.edu/~kangli/code/Image\\_Stabilizer.html](http://www.cs.cmu.edu/~kangli/code/Image_Stabilizer.html)). Regions of interest (ROIs) were manually selected in FIJI and processing of  $Ca^{2+}$  transients of individual neurons was performed automatically by using a custom-written toolbox in MATLAB (Mathworks) based on a previously published method [56]. A baseline correction algorithm was used in order to remove the slow time scale (< 0.05 Hz) changes in the fluorescence as previously described [56]. Based on the fact that action potential firing causes calcium influx into the cytoplasm via the opening of voltage-gated calcium channels and therefore one calcium transient is not necessarily translated to one action potential, we deconvolved spontaneous  $Ca^{2+}$  transients with a putative unitary (spike-evoked) event in order to estimate neuronal firing rates. The analysis of synchronously firing neuronal populations was performed as previously described [39].

### **Code availability**

The custom-written toolbox in MATLAB (Mathworks, 2014b) is available upon request.

### **Statistical analysis**

Data are presented as  $\pm$  SEM. The *P* values were obtained by a two-tail Students’s *t* test comparing control and APP injected groups’ images. Kruskal-Wallis one-way analysis of variance combined with multiple comparison testing was applied on the activities (transients/min and spikes/min) of the neurons in all mouse groups in order to study the statistical similarities. We used Welch’s Test ANOVA as a complementary test for heteroscedasticity. This test gave similar results as the Kruskal-Wallis test with the same level of significance.

### **ACKNOWLEDGEMENTS**

We acknowledge the imaging platform of the Department of Neuroscience at the Pasteur Institute funded by Ile-de-France Domaine d’Intérêt Majeur (NeRF/DIM), Dr Franck Verdonck and Dr Fabrice Chrétien for providing the CX3CR1 mice. We would like to thank Sylvia Lombardo and Stéphanie Pons for help with DNA constructs, and the GENIE Program and the Janelia Research Campus and specifically Vivek Jayaraman, Ph.D., Douglas S. Kim, Ph.D., Loren L. Looger, Ph.D., Karel Svoboda, Ph.D. from the GENIE Project, Janelia Research Campus, Howard Hughes Medical Institute for making the AAV.Syn.GCaMP6 and AAV.CAG.tdTom available.

### **CONFLICTS OF INTEREST**

The authors declare no competing financial interests

### **FUNDING**

F.K. is a scholar of the Pasteur Paris University Doctoral Program (PPU) and received a stipend from the Stavros Niarchos Foundation. This work was supported by the CNRS UMR 3571, the Fondation de la recherche médicale (FRM), the Agence nationale de la recherche (ANR), the Laboratoire d’Excellence BIO-PSY (salary support to F.K.) and the programme PasteurInnov 2012. The laboratory of U.M. is part of the École des Neurosciences de Paris Ile-de-France RTRA network. U.M. is member of the Laboratory of Excellence, LabEx BIO-PSY. As such this work was supported by French state funds managed by the ANR within the Investissements d’Avenir programme under reference ANR-11-IDEX-0004-02.

## REFERENCES

1. Castellani RJ, Rolston RK, Smith MA. Alzheimer disease. *Dis Mon.* 2010;56:484–546. doi: 10.1016/j.disamonth.2010.06.001
2. Fratiglioni L, De Ronchi D, Agüero-Torres H. Worldwide prevalence and incidence of dementia. *Drugs Aging.* 1999;15:365–75. doi: 10.2165/00002512-199915050-00004
3. Small GW, Greenfield S. Current and Future Treatments for Alzheimer Disease. *Am J Geriatr Psychiatry.* 2015;23:1101–05. doi: 10.1016/j.jagp.2015.08.006
4. McGowan E, Eriksen J, Hutton M. A decade of modeling Alzheimer's disease in transgenic mice. *Trends Genet.* 2006;22:281–89. doi: 10.1016/j.tig.2006.03.007
5. Oddo S, Caccamo A, Kitazawa M, Tseng BP, LaFerla FM. Amyloid deposition precedes tangle formation in a triple transgenic model of Alzheimer's disease. *Neurobiol Aging.* 2003;24:1063–70. doi: 10.1016/j.neurobiolaging.2003.08.012
6. Cohen RM, Rezai-Zadeh K, Weitz TM, Rentsendorj A, Gate D, Spivak I, Bholat Y, Vasilevko V, Glabe CG, Breunig JJ, Rakic P, Davtayan H, Agadjanyan MG, et al. A transgenic Alzheimer rat with plaques, tau pathology, behavioral impairment, oligomeric  $\alpha\beta$ , and frank neuronal loss. *J Neurosci.* 2013; 33:6245–56. doi:10.1523/JNEUROSCI.3672-12.2013
7. Götz J, Ittner LM. Animal models of Alzheimer's disease and frontotemporal dementia. *Nat Rev Neurosci.* 2008; 9:532–44. doi: 10.1038/nrn2420
8. Benilova I, Karran E, De Strooper B. The toxic  $A\beta$  oligomer and Alzheimer's disease: an emperor in need of clothes. *Nat Neurosci.* 2012; 15:349–57. doi: 10.1038/nn.3028
9. De Felice FG, Wu D, Lambert MP, Fernandez SJ, Velasco PT, Lacor PN, Bigio EH, Jerecic J, Acton PJ, Shughrue PJ, Chen-Dodson E, Kinney GG, Klein WL. Alzheimer's disease-type neuronal tau hyperphosphorylation induced by A beta oligomers. *Neurobiol Aging.* 2008;29:1334–47. doi: 10.1016/j.neurobiolaging.2007.02.029
10. Forny-Germano L, Lyra e Silva NM, Batista AF, Brito-Moreira J, Gralle M, Boehnke SE, Coe BC, Lablans A, Marques SA, Martinez AM, Klein WL, Houzel J-C, Ferreira ST, et al. Alzheimer's disease-like pathology induced by amyloid- $\beta$  oligomers in nonhuman primates. *J Neurosci.* 2014;34:13629–43. doi: 10.1523/JNEUROSCI.1353-14.2014
11. Mullan M, Crawford F, Axelman K, Houlden H, Lilius L, Winblad B, Lannfelt L. A pathogenic mutation for probable Alzheimer's disease in the APP gene at the N-terminus of  $\beta$ -amyloid. *Nat Genet.* 1992; 1:345–47. doi:10.1038/ng0892-345
12. Kumar-Singh S, De Jonghe C, Cruts M, Kleinert R, Wang R, Mercken M, De Strooper B, Vanderstichele H, Löfgren A, Vanderhoeven I, Backhovens H, Vanmechelen E, Kroisel PM, Van Broeckhoven C. Nonfibrillar diffuse amyloid deposition due to a gamma(42)-secretase site mutation points to an essential role for N-truncated A beta(42) in Alzheimer's disease. *Hum Mol Genet.* 2000; 9:2589–98. doi:10.1093/hmg/9.18.2589
13. Goate A, Chartier-Harlin MC, Mullan M, Brown J, Crawford F, Fidani L, Giuffra L, Haynes A, Irving N, James L, Mant R, Newton P, Rooke K, et al. Segregation of a missense mutation in the amyloid precursor protein gene with familial Alzheimer's disease. *Nature.* 1991;349:704–06. doi: 10.1038/349704a0
14. Grady CL, Furey ML, Pietrini P, Horwitz B, Rapoport SI. Altered brain functional connectivity and impaired short-term memory in Alzheimer's disease. *Brain.* 2001;124:739–56. doi: 10.1093/brain/124.4.739
15. Hsiao K, Chapman P, Nilsen S, Eckman C, Harigaya Y, Younkin S, Yang F, Cole G. Correlative memory deficits, Abeta elevation, and amyloid plaques in transgenic mice. *Science.* 1996;274:99–102. doi: 10.1126/science.274.5284.99
16. Oddo S, Caccamo A, Shepherd JD, Murphy MP, Golde TE, Kaye R, Metherate R, Mattson MP, Akbari Y, LaFerla FM. Triple-transgenic model of Alzheimer's disease with plaques and tangles: intracellular Abeta and synaptic dysfunction. *Neuron.* 2003; 39:409–21. doi: 10.1016/S0896-6273(03)00434-3
17. Serrano-Pozo A, Frosch MP, Masliah E, Hyman BT. Neuropathological alterations in Alzheimer disease. *Cold Spring Harb Perspect Med.* 2011; 1:a006189. doi:10.1101/cshperspect.a006189
18. Larson EB, Kukull WA, Katzman RL. Cognitive impairment: dementia and Alzheimer's disease. *Annu Rev Public Health.* 1992; 13:431–49. doi: 10.1146/annurev.pu.13.050192.002243
19. Storandt M, Grant EA, Miller JP, Morris JC. Rates of progression in mild cognitive impairment and early Alzheimer's disease. *Neurology.* 2002; 59:1034–41. doi:10.1212/WNL.59.7.1034
20. Terry RD, Masliah E, Salmon DP, Butters N, DeTeresa R, Hill R, Hansen LA, Katzman R. Physical basis of

- cognitive alterations in Alzheimer's disease: synapse loss is the major correlate of cognitive impairment. *Ann Neurol.* 1991; 30:572–80. doi: 10.1002/ana.410300410
21. Wang J, Dickson DW, Trojanowski JQ, Lee VM. The levels of soluble versus insoluble brain Abeta distinguish Alzheimer's disease from normal and pathologic aging. *Exp Neurol.* 1999; 158:328–37. doi: 10.1006/exnr.1999.7085
  22. LaFerla FM, Green KN, Oddo S. Intracellular amyloid-beta in Alzheimer's disease. *Nat Rev Neurosci.* 2007; 8:499–509. doi:10.1038/nrn2168
  23. Billings LM, Oddo S, Green KN, McGaugh JL, LaFerla FM. Intraneuronal Abeta causes the onset of early Alzheimer's disease-related cognitive deficits in transgenic mice. *Neuron.* 2005; 45:675–88. doi: 10.1016/j.neuron.2005.01.040
  24. Casas C, Sergeant N, Itier J-M, Blanchard V, Wirhth O, van der Kolk N, Vingtdoux V, van de Steeg E, Ret G, Canton T, Drobecq H, Clark A, Bonici B, et al. Massive CA1/2 neuronal loss with intraneuronal and N-terminal truncated Abeta42 accumulation in a novel Alzheimer transgenic model. *Am J Pathol.* 2004; 165:1289–300. doi:10.1016/S0002-9440(10)63388-3
  25. Lafaye P, Achour I, England P, Duyckaerts C, Rougeon F. Single-domain antibodies recognize selectively small oligomeric forms of amyloid beta, prevent Abeta-induced neurotoxicity and inhibit fibril formation. *Mol Immunol.* 2009; 46:695–704. doi: 10.1016/j.molimm.2008.09.008
  26. Sastre M, Klockgether T, Heneka MT. Contribution of inflammatory processes to Alzheimer's disease: molecular mechanisms. *Int J Dev Neurosci.* 2006; 24:167–76. doi:10.1016/j.ijdevneu.2005.11.014
  27. Itagaki S, McGeer PL, Akiyama H, Zhu S, Selkoe D. Relationship of microglia and astrocytes to amyloid deposits of Alzheimer disease. *J Neuroimmunol.* 1989; 24:173–82. doi: 10.1016/0165-5728(89)90115-X
  28. Jung CK, Keppler K, Steinbach S, Blazquez-Llorca L, Herms J. Fibrillar amyloid plaque formation precedes microglial activation. *PLoS One.* 2015; 10:e0119768. doi: 10.1371/journal.pone.0119768
  29. Yoshiyama Y, Higuchi M, Zhang B, Huang S-M, Iwata N, Saito TC, Maeda J, Suhara T, Trojanowski JQ, Lee VM. Synapse loss and microglial activation precede tangles in a P301S tauopathy mouse model. *Neuron.* 2007; 53:337–51. doi:10.1016/j.neuron.2007.01.010
  30. Bellucci A, Westwood AJ, Ingram E, Casamenti F, Goedert M, Spillantini MG. Induction of inflammatory mediators and microglial activation in mice transgenic for mutant human P301S tau protein. *Am J Pathol.* 2004; 165:1643–52. doi: 10.1016/S0002-9440(10)63421-9
  31. Stence N, Waite M, Dailey ME. Dynamics of microglial activation: a confocal time-lapse analysis in hippocampal slices. *Glia.* 2001; 33:256–66. doi: 10.1002/1098-1136(200103)33:3<256::AID-GLIA1024>3.0.CO;2-J
  32. Jonas RA, Yuan T-F, Liang Y-X, Jonas JB, Tay DK, Ellis-Behnke RG. The spider effect: morphological and orienting classification of microglia in response to stimuli in vivo. *PLoS One.* 2012; 7:e30763. doi: 10.1371/journal.pone.0030763
  33. Virgone-Carlotta A, Uhlrich J, Akram MN, Ressenkoff D, Chrétien F, Domenget C, Gherardi R, Despars G, Jurdic P, Honnorat J, Nataf S, Touret M. Mapping and kinetics of microglia/neuron cell-to-cell contacts in the 6-OHDA murine model of Parkinson's disease. *Glia.* 2013; 61:1645–58. doi:10.1002/glia.22546
  34. Serrano-Pozo A, Mielke ML, Gómez-Isla T, Betensky RA, Growdon JH, Frosch MP, Hyman BT. Reactive glia not only associates with plaques but also parallels tangles in Alzheimer's disease. *Am J Pathol.* 2011; 179:1373–84. doi:10.1016/j.ajpath.2011.05.047
  35. LaFerla FM, Green KN. Animal models of Alzheimer disease. *Cold Spring Harb Perspect Med.* 2012; 2:a006320. doi:10.1101/cshperspect.a006320
  36. Busche MA, Konnerth A. Neuronal hyperactivity--A key defect in Alzheimer's disease? *BioEssays.* 2015; 37:624–32. doi:10.1002/bies.201500004
  37. Busche MA, Eichhoff G, Adelsberger H, Abramowski D, Wiederhold K-H, Haass C, Staufenbiel M, Konnerth A, Garaschuk O. Clusters of hyperactive neurons near amyloid plaques in a mouse model of Alzheimer's disease. *Science.* 2008; 321:1686–89. doi:10.1126/science.1162844
  38. Chen T-W, Wardill TJ, Sun Y, Pulver SR, Renninger SL, Baohan A, Schreiter ER, Kerr RA, Orger MB, Jayaraman V, Looger LL, Svoboda K, Kim DS. Ultrasensitive fluorescent proteins for imaging neuronal activity. *Nature.* 2013; 499:295–300. doi: 10.1038/nature12354
  39. Koukoulis F, Rooy M, Changeux JP, Maskos U. Nicotinic receptors in mouse prefrontal cortex modulate ultraslow fluctuations related to conscious processing. *Proc Natl Acad Sci USA.* 2016; 201614417. doi:10.1073/pnas.1614417113
  40. Moutard C, Dehaene S, Malach R. Spontaneous fluctuations and non-linear ignitions: two dynamic faces of cortical recurrent loops. *Neuron.* 2015; 88:194–206. doi:10.1016/j.neuron.2015.09.018

41. Braak H, Braak E. Neuropathological staging of Alzheimer-related changes. *Acta Neuropathol.* 1991; 82:239–59. doi:10.1007/BF00308809
42. Jaworski T, Dewachter I, Lechat B, Croes S, Termont A, Demedts D, Borghgraef P, Devijver H, Filipkowski RK, Kaczmarek L, Kügler S, Van Leuven F. AAV-tau mediates pyramidal neurodegeneration by cell-cycle re-entry without neurofibrillary tangle formation in wild-type mice. *PLoS One.* 2009; 4:e7280. doi: 10.1371/journal.pone.0007280
43. Thal DR, Griffin WS, Braak H. Parenchymal and vascular Abeta-deposition and its effects on the degeneration of neurons and cognition in Alzheimer's disease. *J Cell Mol Med.* 2008; 12:1848–62. doi:10.1111/j.1582-4934.2008.00411.x
44. Auld DS, Kornecook TJ, Bastianetto S, Quirion R. Alzheimer's disease and the basal forebrain cholinergic system: relations to beta-amyloid peptides, cognition, and treatment strategies. *Prog Neurobiol.* 2002;68:209–45. doi: 10.1016/S0301-0082(02)00079-5
45. Dineley KT, Pandya AA, Yakel JL. Nicotinic ACh receptors as therapeutic targets in CNS disorders. *Trends Pharmacol Sci.* 2015;36:96–108. doi: 10.1016/j.tips.2014.12.002
46. Baker-Nigh A, Vahedi S, Davis EG, Weintraub S, Bigio EH, Klein WL, Geula C. Neuronal amyloid- $\beta$  accumulation within cholinergic basal forebrain in ageing and Alzheimer's disease. *Brain.* 2015; 138:1722–37. doi:10.1093/brain/awv024
47. Selkoe DJ. Alzheimer's disease is a synaptic failure. *Science.* 2002;298:789–91. doi: 10.1126/science.1074069
48. Palop JJ, Mucke L. Epilepsy and cognitive impairments in Alzheimer disease. *Arch Neurol.* 2009; 66:435–40. doi:10.1001/archneurol.2009.15
49. Grienberger C, Rochefort NL, Adelsberger H, Henning HA, Hill DN, Reichwald J, Staufenbiel M, Konnerth A. Staged decline of neuronal function in vivo in an animal model of Alzheimer's disease. *Nat Commun.* 2012; 3:774. doi:10.1038/ncomms1783
50. Busche MA, Chen X, Henning HA, Reichwald J, Staufenbiel M, Sakmann B, Konnerth A. Critical role of soluble amyloid- $\beta$  for early hippocampal hyperactivity in a mouse model of Alzheimer's disease. *Proc Natl Acad Sci USA.* 2012; 109:8740–45. doi:10.1073/pnas.1206171109
51. Sperling RA, Laviolette PS, O'Keefe K, O'Brien J, Rentz DM, Pihlajamaki M, Marshall G, Hyman BT, Selkoe DJ, Hedden T, Buckner RL, Becker JA, Johnson KA. Amyloid deposition is associated with impaired default network function in older persons without dementia. *Neuron.* 2009; 63:178–88. doi: 10.1016/j.neuron.2009.07.003
52. Morcom AM, Friston KJ. Decoding episodic memory in ageing: a Bayesian analysis of activity patterns predicting memory. *Neuroimage.* 2012; 59:1772–82. doi: 10.1016/j.neuroimage.2011.08.071
53. Soares GE, Borges HE, Gomes RM, Zeferino GM, Braga AP. Emergence of synchronicity in a self-organizing spiking neuron network: an approach via genetic algorithms. *Nat Comput. Springer Netherlands.* 2012;11:405–13. doi: 10.1007/s11047-011-9288-3
54. Lombardo S, Catteau J, Besson M, Maskos U. A role for  $\beta_2^*$  nicotinic receptors in a model of local amyloid pathology induced in dentate gyrus. *Neurobiol Aging.* 2016;46:221–34. doi: 10.1016/j.neurobiolaging.2016.06.005
55. Holtmaat A, Bonhoeffer T, Chow DK, Chuckowree J, De Paola V, Hofer SB, Hübener M, Keck T, Knott G, Lee W-C, Mostany R, Mrsic-Flogel TD, Nedivi E, et al. Long-term, high-resolution imaging in the mouse neocortex through a chronic cranial window. *Nat Protoc.* 2009;4:1128–44. doi: 10.1038/nprot.2009.89
56. Dombeck D, Tank D. Two-photon imaging of neural activity in awake mobile mice. *Cold Spring Harb Protoc.* 2014; 2014:726–36. doi: 10.1101/pdb.top081810

## SUPPLEMENTARY MATERIAL

Please browse the links in Full Text version of this manuscript to see Supplementary Movies.

### **Supplementary Movie 1.**

*In vivo* two-photon movie of a 3D projected z-stack of PFC in a CX3CR1-GFP<sup>+/-</sup> mouse. Microglia cells are shown in green. The red represents AAV1.CAG.tdTomato infected cells. The z-stack projected in 3D using Imaris software (Bitplane, Zurich, Switzerland).

### **Supplementary Movie 2.**

*In vivo* two-photon time-series of microglia cells in the PFC of a CX3CR1-GFP<sup>+/-</sup> mouse (sham not injected with the AAV-hAPP-SLA). Resting state microglia cells characterized by a small cell body and highly elaborated thin processes.

### **Supplementary Movie 3.**

*In vivo* two-photon time-series of microglial cells in the PFC of a CX3CR1-GFP<sup>+/-</sup> mouse injected with the AAV-hAPP-SLA. Microglia are characterized by an amoeboid form, a feature of microglial activation.

**Supplemental file.** Related paper in press.

# Long-term caloric restriction in *ApoE*-deficient mice results in neuroprotection via Fgf21-induced AMPK/mTOR pathway

Claire Rühlmann<sup>1,\*</sup>, Tjark Wölk<sup>1,\*</sup>, Tobias Blümel<sup>1</sup>, Laura Stahn<sup>1</sup>, Brigitte Vollmar<sup>1</sup>, Angela Kuhla<sup>1</sup>

<sup>1</sup>Institute for Experimental Surgery, Rostock University Medical Center, 18057 Rostock, Germany

\*Equal contribution

Correspondence to: Angela Kuhla; email: [angela.kuhla@uni-rostock.de](mailto:angela.kuhla@uni-rostock.de)

Keywords: *ApoE*-deficiency, caloric restriction, Fgf21, pAMPK, mTOR, Tau-phosphorylation, Alzheimer's disease

Received: July 1, 2016 Accepted: November 14, 2016 Published: November 29, 2016 doi: [10.18632/aging.101086](https://doi.org/10.18632/aging.101086)

## ABSTRACT

Caloric restriction (CR) decelerates the aging process, extends lifespan and exerts neuroprotective effects in diverse species by so far unknown mechanisms. Based on known neuroprotective effects of fibroblastic growth factor 21 (Fgf21) we speculate that CR upregulates Fgf21, which phosphorylates neuronal AMP-activated protein kinase (AMPK), leading to a decrease of mammalian target of rapamycin (mTOR) signaling activity and an inhibition of tau-hyperphosphorylation. This in turn reduces the formation of neurofibrillary tangles, a neuropathological hallmark of Alzheimer's disease. *ApoE*-deficient mice (*ApoE*<sup>-/-</sup>), serving as a model of neurodegeneration, showed upon CR vs. ad libitum feeding increased Fgf21 levels in both, plasma and brain as well as higher phosphorylation of fibroblastic growth factor receptor 1c (Fgfr1c), extracellular signal-regulated kinases 1/2 (ERK1/2) and AMPK in brain, lower activity of mTOR and decreased Tau-phosphorylation. Finally, CR in *ApoE*<sup>-/-</sup> mice caused neuroprotection as indicated by a higher synaptic plasticity shown by immunohistochemical analysis with increased numbers of PSD95-positive neurons and a better cognitive performance as analyzed with Morris water maze test. These data provide substantial evidence that neuroprotection upon CR seems to be Fgf21-dependent. Further experiments are necessary to evaluate Fgf21 as a therapeutic tool to treat tauopathy for improvement of cognitive performance.

## INTRODUCTION

In all species studied to date, restricted calorie intake by 20-50% while providing adequate micronutrient supply significantly extends mean and maximal lifespan [1, 2]. Moreover, age-related deficits in learning and motor coordination are ameliorated by caloric restriction (CR) in rodents [3, 4]. In line with this, CR attenuates amyloid deposition in monkeys and in transgenic mouse models of Alzheimer's disease (AD) [5, 6], leading to improvement of cognitive deficits [7] and to reduction of neuronal loss in neocortex, hippocampus, and striatum [8]. Further, it is described that CR promotes neurogenesis in adult rodents, probably by increasing brain-derived neurotrophic factor levels [9]. However, the underlying mechanisms in response to CR remain unclear.

Recently, the fibroblastic growth factor 21 (Fgf21) was described as starvation hormone [10]. Fgf21 is upregulated in response to CR in the liver and is secreted into plasma [11]. Fgf21 activity occurs when Fgf21 binds to fibroblast growth factors receptor (Fgfr) and  $\beta$ -klotho, a single transmembrane protein [12]. Fgfrs consist of seven major isoforms (1b, 1c, 2b, 2c, 3b, 3c and 4), whereby the isoform Fgfr1c is the primary receptor of Fgf21 in the mediation of its activity in *in vivo* studies [13]. When Fgf21 binds to its receptor, it leads to a rapid phosphorylation of downstream pathway components, including the MAPK cascade [14] and results via protein kinase A to activation of AMP-activated protein kinase (AMPK) [15]. In addition, *fgf21* is also a direct target gene of the peroxisome proliferator-activated receptor- $\alpha$  (*ppara*) [16, 17], a regulator for CR-induced lipolysis.

Therefore, Fgf21 plays an important role in adaptation to metabolic states, which require increased fatty acid oxidation and ketogenesis [18] as an alternative energy source [17]. Ketogenesis, which is basically triggered by Fgf21, leads to AMPK activation not only in the periphery [19] but also in the central nervous system [20], resulting in decreased mammalian target of

rapamycin (mTOR) signaling [21, 22]. It could additionally be shown that inhibition of the mTOR pathway with rapamycin protects the entorhinal cortex from Tau-mediated neurodegeneration [23].

Since plasma Fgf21 can cross the blood brain barrier by simple diffusion and can be detected in human

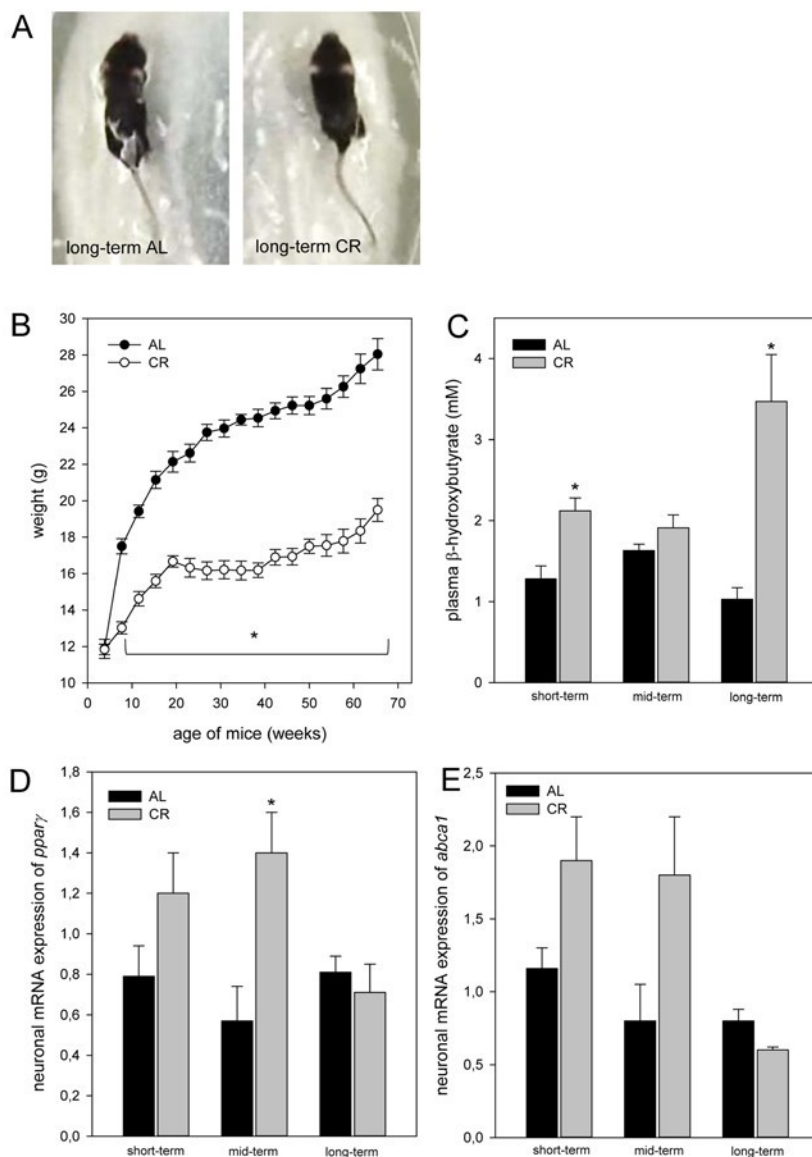


**Figure 1.** (A) Image of one long-term ad libitum (AL)- and of one caloric-restricted (CR)-fed *ApoE*<sup>-/-</sup> mouse. These mice were fed either AL or CR (60% of ad libitum). These images exemplarily show that in general CR-fed mice were smaller in body size than AL-fed mice. (B) Body weight (g) of AL- and CR-fed mice over a period of 68 weeks. In general, parameter of ketogenesis and lipolysis are increased in CR-fed mice when compared with the age-matched AL-fed mice indicated by a marked rise of (C) plasma  $\beta$ -hydroxybutyrate and of neuronal (D) *ppar $\gamma$*  and (E) *abca1* mRNA expressions. Values are given as mean $\pm$ SEM; ANOVA, post-hoc pairwise comparison tests: \*  $p < 0.05$  vs. AL.

cerebrospinal fluid and brain tissues in rodents [24, 25], it is conceivable to assume that Fgf21 contributes to regulation of brain metabolism. There is growing evidence that Fgf21 has neuroprotective effects and improves cognition [26]. It could be shown that incubation of human dopaminergic neurons with Fgf21 resulted in enhanced mitochondrial function and mitochondrial respiratory capacity [27]. Based on the neuronal functional activity of Fgf21 we speculate that Fgf21 phosphorylates neuronal AMPK. Activated AMPK leads to decrease of mTOR signaling activity [21] and in consequence to inhibition of Tau-hyperphosphorylation with reduction of neurofibrillary tangles (NFTs) [28] as a neuropathological hallmark of AD.

Apolipoprotein E (ApoE) binds to Tau-protein and prevents its hyperphosphorylation [29], leading to slow down of NFTs-formation. *ApoE*-deficient mice (*ApoE*<sup>-/-</sup>) represent a well-established mouse model of tauopathy [30] with memory deficits [31]. In addition, *ApoE*<sup>-/-</sup> compared to wild-type mice revealed throughout life a 2- to 7-fold lower expression of hepatic *fgf21* (own unpublished data). Since Fgf21 has neuroprotective properties, it may be assumed that low Fgf21 contributes to neurodegeneration. To pursue this issue, we fed *ApoE*<sup>-/-</sup> mice caloric-restricted for a long-term to raise hepatic as well as neuronal Fgf21 with the aim to prevent tauopathy via the AMPK/mTOR pathway and to improve cognitive performance.

## RESULTS

### Long-term CR slowed increase of body weight in *ApoE*<sup>-/-</sup> mice

In general, CR-fed mice were smaller in body size than the ad libitum (AL)-fed mice (Fig. 1A). The body weight of AL-fed *ApoE*<sup>-/-</sup> mice continuously increased 2-fold with aging up to  $28.10 \pm 0.85$  g. Long-term CR resulted in a very slow increase of body weight reaching values of  $19.6 \pm 0.63$  g. In general, at all time points CR-fed mice showed significantly lower levels of body weight when compared to AL-fed mice (Fig. 1B).

### CR increased ketogenesis and neuronal lipolytic gene expression in *ApoE*<sup>-/-</sup> mice

CR-fed mice revealed a continuous rise of ketone bodies, as given by an up to 2-fold increase of plasma  $\beta$ -hydroxybutyrate concentrations in long-term-fed mice when compared to short-term-fed mice. On the contrary, the concentrations of  $\beta$ -hydroxybutyrate remained almost unchanged in AL-fed mice averaging at low values of 1 mM up to 1.6 mM (Fig. 1C). Ketogenesis was significantly higher in CR- than in AL-

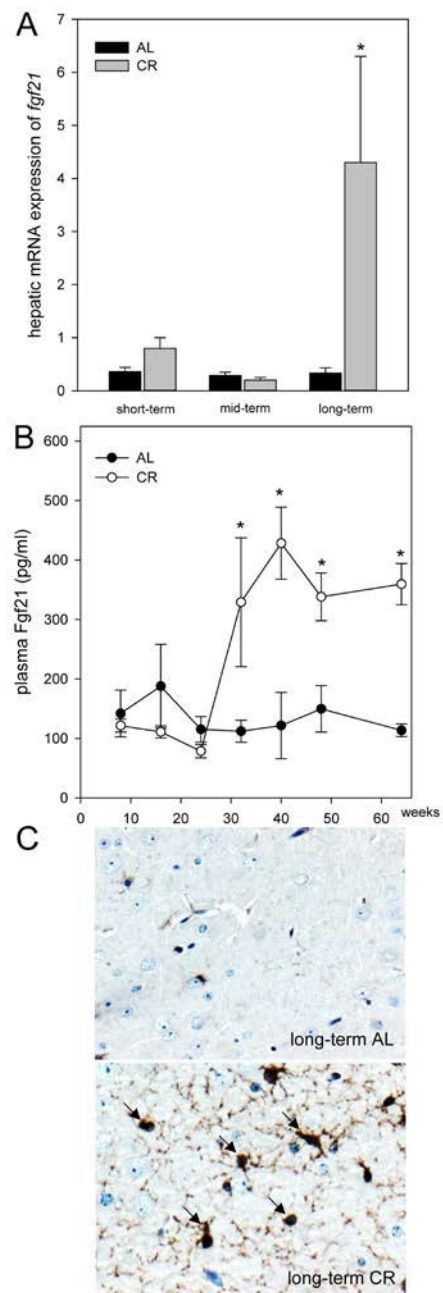


**Figure 2.** (A) Quantitative real-time PCR analysis of hepatic mRNA expression of *fgf21* and (B) quantitative analysis of plasma Fgf21 of *ApoE*<sup>-/-</sup> mice. Mice were fed either ad libitum (AL) or caloric-restricted (CR, 60% of ad libitum) for a short-term (4 weeks; n=14), mid-term (20 weeks; n=14) or long-term (64 weeks; n=14). At weeks 8, 16, 24, 32, 40, 48 and 64 plasma Fgf21 was measured. Signals were corrected to that of RPS18. Representative immunohistochemical images (C, original magnification x400) of Fgf21 accumulation in brain of long-term AL- (upper panel) and CR-fed *ApoE*<sup>-/-</sup> mice (lower panel) mice. Values are given as means  $\pm$  SEM; ANOVA, post-hoc pairwise comparison tests. \*  $p < 0.05$  vs. AL.

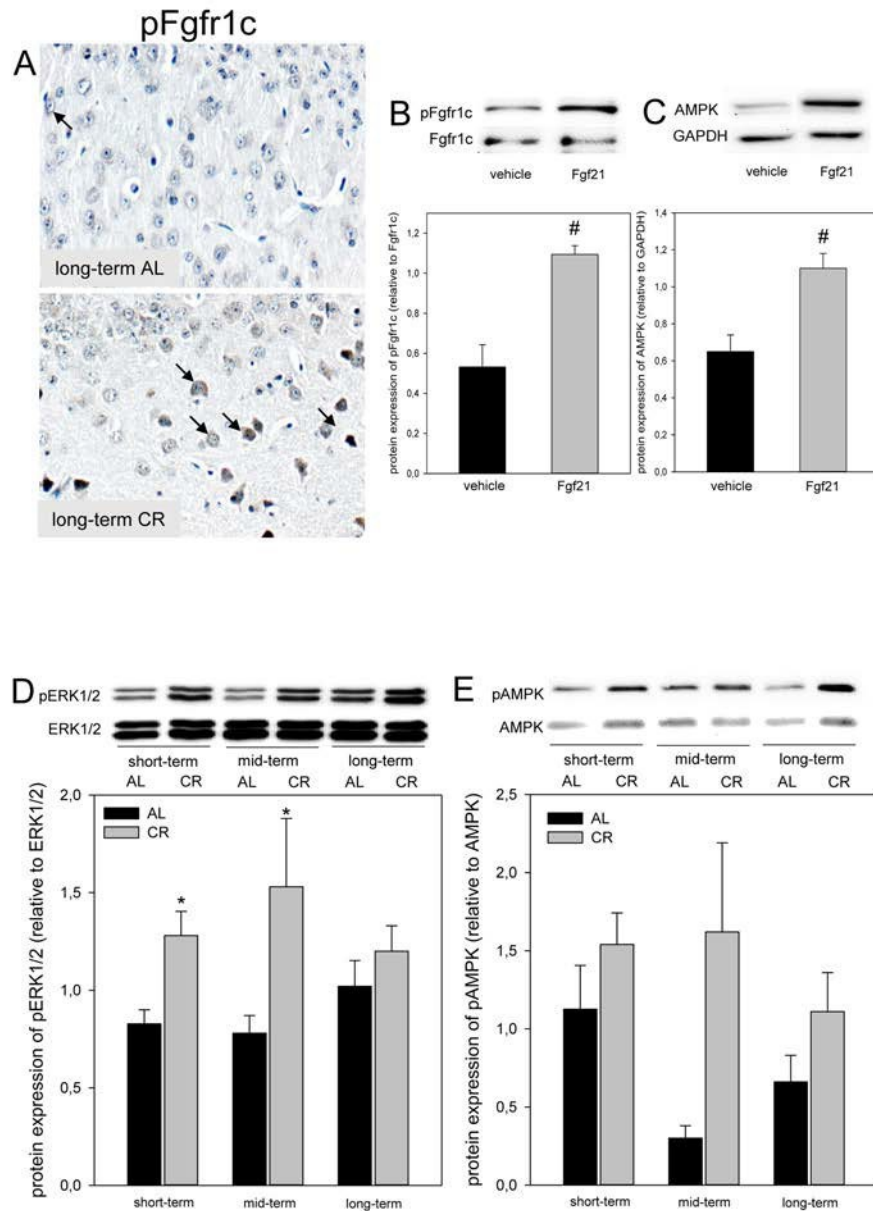


**Figure 3. (A)** Representative immunohistochemical images (original magnification x400) of pFgfr1c expression in brain of long-term ad libitum- (AL, upper panel, indicated by arrows) and of caloric-restricted-fed (CR, lower panel, indicated by arrows) *ApoE*<sup>-/-</sup> mice. Representative Western blots as well as densitometric analysis of **(B)** pFgfr1c and **(C)** AMPK expression in primary glial cells, which were treated with vehicle (DMEM/F12) and 5  $\mu$ g/ml Fgf21. Representative Western blot and densitometric analysis of **(D)** pERK1/2 and **(E)** pAMPK expression in brain of *ApoE*<sup>-/-</sup> mice. Mice were fed either AL or CR (60% of ad libitum) for a short-term (4 weeks; n=14), mid-term (20 weeks; n=14) or long-term (64 weeks; n=14). Signals were corrected to that of either ERK1/2 or AMPK. Values are given as means  $\pm$  SEM; ANOVA, post-hoc pairwise comparison tests: \*  $p < 0.05$  vs. AL, #  $p < 0.05$  vs. vehicle.

fed *ApoE*<sup>-/-</sup> mice after short- and long-term feeding. The neuronal mRNA expression of *ppary* and *abcal* remained unchanged with aging in AL-fed *ApoE*<sup>-/-</sup> mice (Fig.1 D and E) while short- and mid-term CR markedly increased the neuronal mRNA expression of *ppary* and *abcal* (Fig. 1 D and E).

### CR increased hepatic expression and systemic concentration of Fgf21 in *ApoE*<sup>-/-</sup> mice

Of note, the hepatic mRNA expression of *fgf21* in *ApoE*<sup>-/-</sup> mice was significantly increased upon long-term CR (Fig. 2A). Accordingly, the systemic Fgf21

concentration in *ApoE*<sup>-/-</sup> mice raised significantly and reached approx. 3-fold higher levels upon long-term CR when compared to AL feeding (Fig. 2B). Fgf21 was barely measurable in the brain of *ApoE*<sup>-/-</sup> mice (Fig. 2C; upper panel) but was detectable at a much higher level upon a long-term CR (Fig. 2C; arrows, lower panel) with a preferential location around glial cells in the cortex. Along with the higher neuronal Fgf21 levels upon long-term CR, the receptor for Fgf21, namely Fgfr1c, was activated, as indicated by an increased number of pFgfr1c-positive neuronal cells in the cortex (Fig. 3A; lower panel, arrows).

### CR increased Fgfr1c downstream signaling in *ApoE*<sup>-/-</sup> mice

Next we asked whether Fgf21 activates the neuronal downstream signaling pathway via Fgfr1c *in vitro* and could show that phosphorylation of Fgfr1c is significantly increased in Fgf21-treated primary glial cells compared to vehicle alone (Fig. 3B). Along with activation of Fgfr1c the AMPK protein expression was significantly increased in Fgf21-treated primary glial cells compared to vehicle alone (Fig. 3C). Further, a significant increase of ERK1/2-phosphorylation was found upon short- as well as mid-term CR vs. AL feeding in *ApoE*<sup>-/-</sup> mice (Fig. 3D). In addition, the

phosphorylation of AMPK was consistently increased upon CR (Fig. 3E).

### CR inhibited mTOR and Tau-phosphorylation in *ApoE*<sup>-/-</sup> mice

Since activation of AMPK inhibits mTOR, we analyzed the phosphorylation of mTOR by immunohistochemistry and could show that long-term CR reduced the activity of mTOR in the cortex of *ApoE*<sup>-/-</sup> mice, as indicated by a decreased number of pmTOR-positive neuronal cells (Fig. 4A; lower panel, arrows). It could further be demonstrated that an inhibition of mTOR upon CR feeding resulted in an almost 2-fold reduction of Tau-phosphorylation at all time points, which was significant upon long-term CR (Fig. 4B) while AL-fed mice revealed an age-dependent increase of Tau-phosphorylation (Fig. 4B).

### Long-term CR increased working memory and neuronal plasticity in *ApoE*<sup>-/-</sup> mice

Mice were tested in the spatial reference memory version of the Morris water maze. AL- and CR-fed *ApoE*<sup>-/-</sup> mice did not show significant differences in general swimming performance, which was determined by measurement of the swimming speed during the test

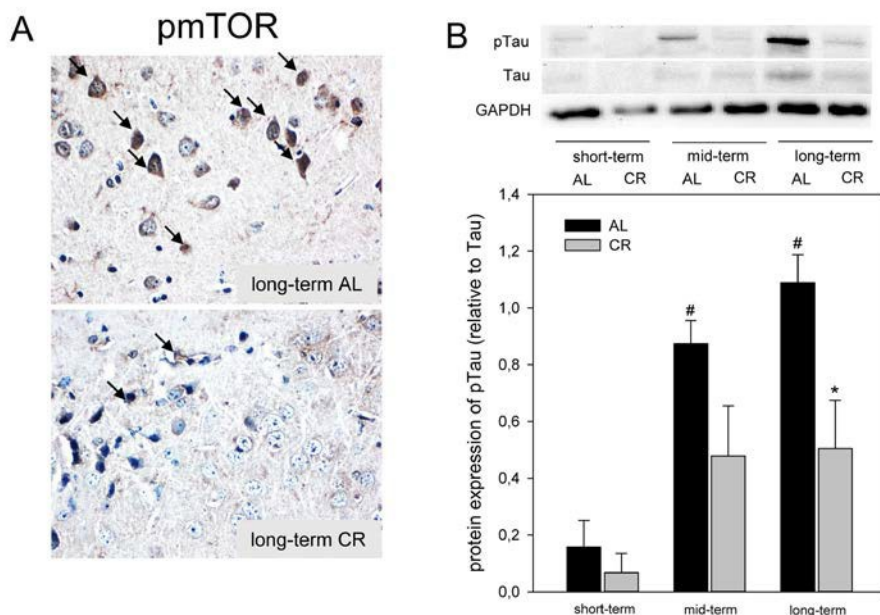


**Figure 4.** (A) Representative immunohistochemical images (original magnification x400) of pmTOR expression in brain of long-term ad libitum- (AL, upper panel) and of caloric-restricted-fed (CR, lower panel) *ApoE*<sup>-/-</sup> mice. (B) Representative Western blot and densitometric analysis of pTau in brain of *ApoE*<sup>-/-</sup> mice. Mice were fed either AL or CR (60% of ad libitum) for a short-term (4 weeks; n=14), mid-term (20 weeks; n=14) or long-term (64 weeks; n=14). Signals were corrected to Tau. GAPDH served as loading control. Values are given as means ± SEM; ANOVA, post-hoc pairwise comparison tests: \* p < 0.05 vs. AL.

trials (data not shown). Escape latencies were displayed in five blocks. Each block consisted of four consecutive trials. It is expected, escape latencies decreased throughout the training days. Thus, all mice were able to learn the task, whereas aged mice (long-term AL/CR) vs. younger mice (short- and mid-term AL/CR) started with a *per se* inferior performance (Fig. 5A, C, E). While short- and mid-term-fed mice of both groups

revealed almost comparable escape latency, long-term CR resulted in lower escape latency found for block 2 - 4 (Fig. 5E), suggesting that long-term CR caused a better training performance due to better cognitive activities.

All mice were exercised to the platform 4 (PF4) during training. Finally, the platform was removed and the

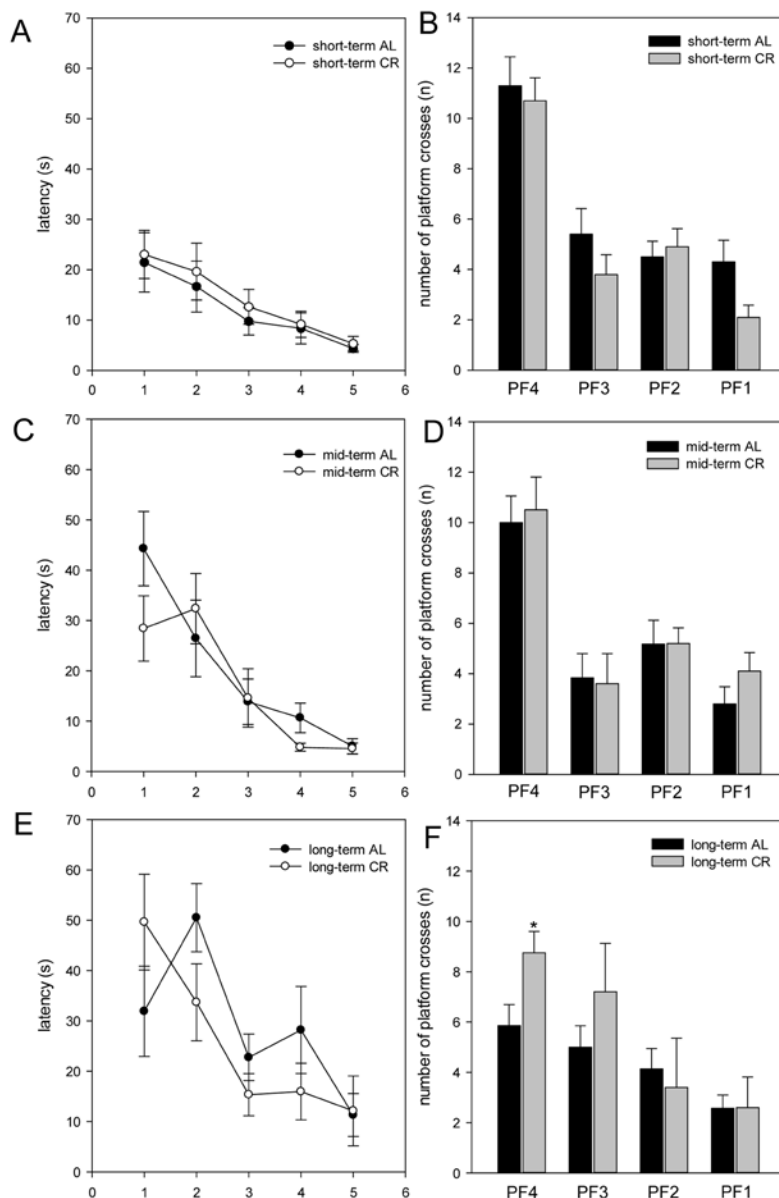


**Figure 5.** The escape latencies (in s) of the training were displayed in five blocks (A, C, E; x-axis 1-5). One block consisted of four consecutive trials. The escape latencies decreased throughout the training days. In the test trial, the number of platform crossings during 60 s was measured (B, D, F). *ApoE*<sup>-/-</sup> mice were fed either ad libitum (AL) or caloric-restricted (CR, 60% of ad libitum) for a short-term (A and B, 4 weeks; n=14), mid-term (C and D, 20 weeks; n=14) or long-term (E and F, 64 weeks; n=14) and were trained and tested 5 days before being sacrificed. Values are given as mean±SEM; ANOVA, post-hoc pairwise comparison tests: \*p < 0.05 vs. AL.

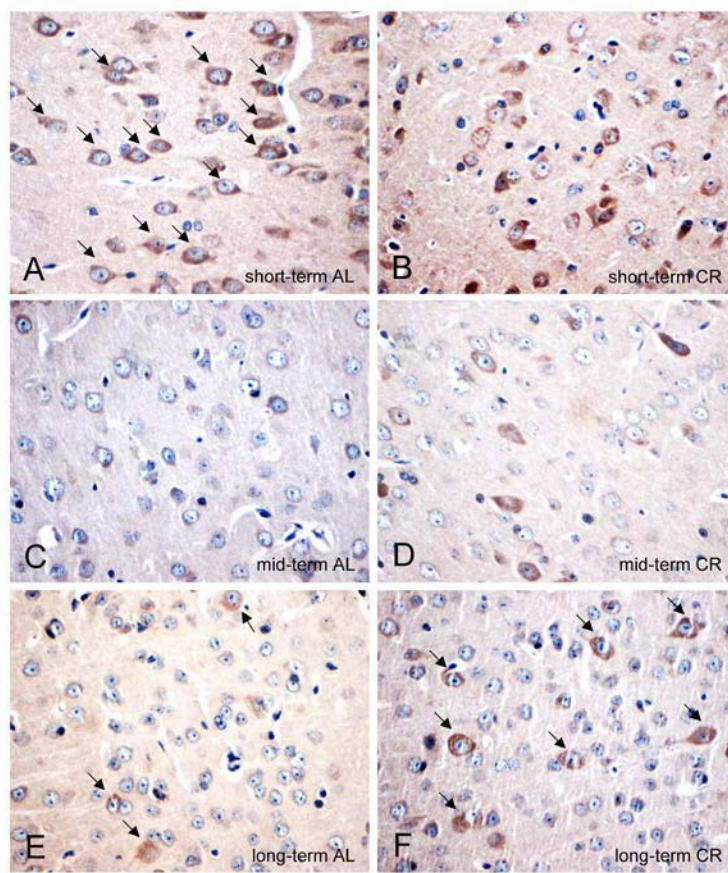


**Figure 6.** (A-F) Representative immunohistochemical images (original magnification x400) of PSD95 protein expression in brain of short-term (A and B), mid-term (C and D) and long-term (E and F) ad libitum- (AL, left panels) and caloric-restricted-fed (CR, right panels) *ApoE*<sup>-/-</sup> mice. Mice were fed either AL or CR (60 % of ad libitum) for a short-term (4 weeks; n=14), mid-term (20 weeks; n=14) or long-term (64 weeks; n=14). Note the decrease of PSD95-positive neurons in the AL-fed *ApoE*<sup>-/-</sup> mice while a long-term CR delayed the decline of PSD95-positive neurons in the *ApoE*<sup>-/-</sup> mice (indicated by arrows).

number of platform crossings during 60 s was measured. Thereby, it could be shown that short- as well as mid-term-fed mice of both groups crossed PF4 nearly with the same frequency (Fig. 5B, D, F). The most striking differences between the AL- and CR-fed mice were found in the number of platform crossings of long-term-fed mice. Long-term CR-fed mice crossed PF3 up to 30% and PF4 significantly more often than AL-fed mice (Fig. 5F). Thus, long-term CR resulted in a better working memory.

#### **CR delayed the decrease of neuronal PSD95 expression in *ApoE*<sup>-/-</sup> mice**

AL-fed *ApoE*<sup>-/-</sup> mice revealed an age-dependent decrease of the number of PSD95-positive neuronal cells (Fig. 6A, C, E; arrows) while this could not be observed in CR mice, as shown by an almost stable expression of PSD95 (Fig. 6B, D, F; arrows).

## **DISCUSSION**

The main finding of the present study is that long-term CR in *ApoE*<sup>-/-</sup> mice increased lipolysis and ketogenesis in the animals. This was reflected by higher systemic ketone body concentrations and increased neuronal mRNA expressions of *ppary* and *abca1*. CR further caused both, a systemic and neuronal increase of *Fgf21*, leading to higher activation of *Fgfr1c* in the brain and, in consequence, to activation of the AMPK/mTOR pathway. AMPK-induced inhibition of mTOR in CR-fed *ApoE*<sup>-/-</sup> mice reduced Tau-phosphorylation and improved their cognition performance.

Most recently, we could demonstrate that long-term CR i.e. starting at the age of weaning until pre-senescence reduced the normal age-related decline in cognitive performance [4]. This underlines the importance of lifestyle factors such as nutrition in the context of

metabolic syndrome-associated neurodegeneration [32]. However, the mechanism of CR-induced neuroprotection is not yet completely understood. To address this issue, we used *ApoE*<sup>-/-</sup> mice an accepted model of metabolics-driven neurodegeneration. The animals were maintained under CR for a long-term to evaluate neuroprotective molecular mechanisms. *ApoE*<sup>-/-</sup> mice are known for their significant loss of synapses with increasing age [33] and further are also described as model of tauopathy [30].

In response to fasting, lipolysis and  $\beta$ -oxidation are enhanced to provide alternative energy resources for the organism [17, 34]. In addition, marked elevations in Fgf21 expression were observed in mice upon fasting [18] and food restriction [11]. Elevated *fgf21* gene expression and serum Fgf21 concentrations in food-restricted animals were accompanied by an upregulation of *ppara* mRNA expression [11]. PPAR $\alpha$  regulates the hepatic lipid metabolism by induction of ketogenesis and lipolysis via increased  $\beta$ -oxidation [11, 35]. Accordingly, the present study shows an accumulation of ketone bodies upon CR. Ketone bodies may act neuroprotective [36] and thereby, enhance memory performance [37]. In addition, we found that lipolysis and  $\beta$ -oxidation are also enhanced in brain as shown by increased neuronal mRNA expression of *ppary* and of its target gene *abca1*. Since activation of PPAR $\gamma$  reduces AD-pathology and improves cognitive function in mouse models of AD [38] this current finding might also contribute to neuroprotection.

Fgf21 is present in the brain [39] including midbrain and *in vitro* is expressed by glial cells [27]. Mäkelä and coworkers found additionally that Fgf21 plays a regulatory role in brain energy metabolism as shown by enhanced mitochondrial capacity in Fgf21-treated dopaminergic neurons [27]. Further, it is known that Fgf21 can cross the blood brain barrier [24]. Thus, it is conceivable to state that CR-induced hepatic Fgf21 might be responsible for the positive immunostaining of glial cells *in vivo*, as observed in the present study (Fig. 2C). Fgfr1c, the receptor for Fgf21, is found to be expressed in hypothalamic region of the brain [40] and in cortical neurons (current study; Fig. 3A). Activation of Fgfr1c -most occasionally via Fgf21-positive glial cells- phosphorylates specific tyrosine residues that mediate interaction with cytosolic adaptor proteins and intracellular signaling pathways [14]. This view is supported by our *in vitro* data showing the activation of Fgfr1c and the increase of downstream AMPK protein upon Fgf21 exposure of glial cells and by our *in vivo* data showing increased Fgfr1c- as well as increased ERK1/2- and AMPK-phosphorylation in CR-fed mice. Since Fgf21 is capable to elevate phosphorylation of AMPK [19], we assume that CR-induced rise of Fgf21

triggers the AMPK pathway. However, it has to be mentioned that conditions of perceived energy deprivation, such as fasting, food restriction, and exercise, increase the AMP/ATP ratio, eventually causing an activation of AMPK [41 and current study].

AMPK is a suppressor of mTOR signaling [42]. Abrogation of TOR signaling causes rejuvenation in the *C. elegans* [43]. This new function for TOR signaling in ageing control may represent a link between nutrition, metabolism and longevity [43]. In support of this function, inhibition of mTOR is described to be protective in neurodegenerative diseases such as AD by enhancement of autophagy, a biological process that not only facilitates the clearance of mutant proteins but also significantly reduces the build-up and accumulation of toxic protein aggregates such as NTFs, being caused by Tau-hyperphosphorylation [44, 45]. Therefore, reduced mTOR and Tau-phosphorylation in the long-term CR-fed *ApoE*<sup>-/-</sup> mice can be most supposedly attributed to the activation of AMPK pathway by increased Fgf21. In parallel, Ma and coworkers showed that food restriction could lead to activation of SIRT1 and suppression of mTOR activation in mice and speculated that the SIRT1/mTOR signaling pathway may be involved in the neuroprotective effect of food restriction [46]. This view is supported by the study of Guo et al. [47], which demonstrated that food restriction-induced SIRT/mTOR activation contributed to brain integrity. In addition, positive properties of SIRT signaling in *ApoE*<sup>-/-</sup> mice was reported by the groups of Stein et al. [48] and Palacios et al. [49]. These studies showed that of SIRT-overexpression diminishes atherogenesis and that diet- and exercise-induced SIRT/AMPK pathway regulates muscle energy homeostasis.

Moreover limited Tau-phosphorylation by Fgf21-dependent AMPK/mTOR signaling, improved cognitive performance upon long-term CR restriction might also be due to maintenance of PSD95-positive cells and thus, neuronal plasticity.

In summary, these data provide substantial evidence that neuroprotection upon CR seems to be Fgf21/AMPK/mTOR-dependent. Further experiments are necessary to evaluate Fgf21 as a therapeutic tool to treat tauopathy for improvement of cognitive performance.

## MATERIALS AND METHODS

### Animals

Female Apolipoprotein (*Apo*) *E* deficient (*ApoE*<sup>-/-</sup>) mice at the age of 4 weeks were fed either ad libitum (AL) or caloric-restricted (CR, 60% of ad libitum) for 4

additional weeks (short-term, n=10 for each group), 20 weeks (mid-term, n=10 for each group) or 64 weeks (long-term, n=10 for each group). All mice were housed in standard cages in a temperature-controlled room (22°C±2°C) on a 12 h light/dark cycle with free access to food (4.2% fat) and water under specific pathogen free (SPF) conditions. The mice were weighed weekly and directly before they were sacrificed. The experimental protocol was approved by the local Animal Research Committee (Landesamt für Landwirtschaft, Lebensmittelsicherheit und Fischerei (LALLF) of the state Mecklenburg-Western Pomerania (LALLF M-V/TSD/7221.3-1.1-002/14)) and all animals received care according to the German legislation on protection of animals and the Guide for the Care and Use of Laboratory Animals (NIH publication 86-23 revised 1985).

### Sampling and assays

For the analysis of Fgf21-kinetics blood samples were taken from all mice at weeks 8, 16, 24, 32, 40, 48 and 64. At the end of the experiment, all mice were exsanguinated by puncture of the vena cava inferior for immediate separation of plasma, followed by harvest of brain and liver tissues. Measurements of Fgf21 and ketone bodies in plasma were performed using the Fgf21 immunoassay and  $\beta$ -hydroxybutyrate assay kit methods according to the manufacturer's instructions (Fgf21: R&D System;  $\beta$ -hydroxybutyrate: Cayman Chemical Company).

### Glial cell culture

Primary glial cells were cultured from postnatal day 0-3 C57BL/6J mice as described previously [50]. First, pups were decapitated, brains isolated in cold PBS (Gibco) with 1% penicillin/streptomycin (Invitrogen), and 0.1% glucose (Sigma), cerebellum, the meninges, and blood vessels were removed from the cortices. The latter were then minced and trypsinized with 0,05% trypsin-EDTA (Merck Millipore), 0.1% glucose (Sigma), 1%

penicillin/streptomycin (Invitrogen) and DNase (10  $\mu$ g/mL) for 10 min at 37°C. To stop trypsin digestion, DMEM/F12 (Merck Millipore) containing 10% heat-inactivated fetal bovine serum (HI-FBS, PAA) with supplement 1% penicillin/streptomycin was added. Cells were triturated, filtrated and centrifuged for 5 min at 200 xg. Supernatant was discarded and the pellet resuspended in DMEM/F12 containing 15% (HI-FBS) and 1% penicillin/streptomycin. Cortical cells were seeded in DMEM/F12 with 15% HI-FBS and 1% penicillin/streptomycin at a density of  $2 \times 10^6$ /well in a 6 well-plate (Cellstar, Greiner bio-one). Medium was changed the following day to fresh DMEM/F12 with 10% HI-FBS and 1% penicillin/streptomycin and incubated for 14-21 d at 37°C and 5% CO<sub>2</sub>. Medium was replaced every 4-5 d. Afterwards cells were exposed with 5  $\mu$ g/ml Fgf21 in medium or medium as vehicle and incubated for 24 h at 37°C, and 5% CO<sub>2</sub>. Subsequently, cells were harvested for protein analysis.

### RNA analysis of brain and liver tissue

Total RNA was isolated using the RNeasy<sup>®</sup> Mini Kit (Qiagen) in accordance with the manufacturer's instructions. 2  $\mu$ g of total RNA was reverse-transcribed with SuperScript<sup>™</sup> First Strand Synthese System (Invitrogen) as described by the manufacturer. Real-time quantitative PCR assays were performed by using Lightcycler 1.5 using the Lightcycler<sup>®</sup> FastStart DNA Master<sup>plus</sup> SYBR Green I kit (Roche Diagnostics). Each amplification mixture (20  $\mu$ l) contained 5  $\mu$ M primer, 19  $\mu$ l of universal PCR Mastermix, and 1  $\mu$ l 1:2 diluted cDNA solution. PCR thermocycling parameters were 95°C for 10 min and 40 cycles of 95°C for 10 s, 55°C for 5 s and 72°C for 10 s. All samples were analyzed for ribosomal protein S18 (RPS18) expression. For analysis of the relative change in gene expression we used the  $2^{-\Delta\Delta Ct}$  method. A cDNA pool of livers of untreated C57BL/6J mice served as the control and therefore as the first  $\Delta$ . The second  $\Delta$  is represented by Ct-values of RPS18 amplification. Specificity of the amplification was verified by melt-curve analysis and evaluation of

**Table 1.**

Transcript	forward primer	reverse primer
<i>ppary</i>	5'-TCATGACCAGGGAGTTCCTC-3'	5'-CAGGTTGTCTTGGATGCCTC-3'
<i>abca1</i>	5'-ACTGGAGACACCCTGTGAC-3'	5'-GGAGAGCTTTCGTTTGTTC-3'
<i>fgf21</i>	5'-GCTGTCTTCTGCTGGGG-3'	5'-CCTGGTTTGGGGAGTCCTC-3'
<i>rps18</i>	5'-AGGATGTGAAGGATGGGAAG-3'	5'-TTGGATACACCCACAGTTCG-3'

efficiency of PCR amplification. The primers are listed in Table 1.

### **Western Blot analysis of brain tissue and of glial cells**

Harvested brain tissues and glial cells were further processed for protein isolation. For this purpose, brain tissue and glial cells were homogenized in lysis buffer (10 mM Tris pH 7.5, 10 mM NaCl, 0.1 mM EDTA, 0.5% Triton-X 100, 0.02% NaN<sub>3</sub>, and 0.2 mM PMSF (a protease inhibitor cocktail), incubated for 30 min on ice and centrifuged for 10 min at 4°C and 10,000 xg. Protein contents were assayed by the bicinchoninic acid method (Pierce Biotechnology) with 2.5% BSA (Pierce Biotechnology) as standard. On 12% SDS gels, 20 µg (pTau, Tau, pERK1/2 and ERK1/2) and 40 µg (pAMPK and AMPK) protein from brain tissue was separated and transferred to a polyvinylidene difluoride membrane (Immobilon-P; Millipore). On 8% SDS gels, 20 µg (pFgfr1c, Fgfr1c and AMPK) protein from glial cells was separated and transferred to a polyvinylidene difluoride membrane (Immobilon-P; Millipore). After blockade with 2.5% BSA (Pierce Biotechnology), membranes were incubated overnight at 4°C with a mouse monoclonal anti-pAMPK (1:1,000), a rabbit polyclonal anti-AMPK (1:1,000), a mouse monoclonal anti-pTau (1:1,000), a mouse monoclonal anti-Tau (1:1,000), a rabbit polyclonal anti-pFgfr1c (1:1,000), a rabbit monoclonal anti-Fgfr1c (1:1,000), a rabbit monoclonal anti-ERK1/2 (1:1,000), or a rabbit polyclonal anti-pERK1/2 (1:1,000), respectively. Afterwards, a secondary peroxidase-linked horse anti-mouse (pAMPK, AMPK, pTau, Tau; 1:10,000) or a goat anti-rabbit (pFgfr1c, Fgfr1c; 1:10,000; pERK1/2, ERK1/2; 1:5,000) was applied. All antibodies were supplied by Cell Signaling. Protein expression was visualized by means of luminol-enhanced chemiluminescence (ECL plus; Amersham Pharmacia Biotech) and digitalized with ChemiDoc™ XRS System (Bio-Rad Laboratories). Signals were densitometrically assessed (Quantity One; Bio-Rad Laboratories) and densities normalized either to GAPDH (mouse monoclonal anti-GAPDH antibody; 1:20,000; Millipore) or to unphosphorylated proteins (AMPK, ERK1/2, Tau, Fgfr1c).

### **Immunohistology**

For immunohistochemical analysis, brain tissue was fixed in 4% phosphate-buffered formalin for 5-6 weeks and subsequently embedded in paraffin. From the paraffin-embedded tissue blocks, 4 µm thin sections were put on X-tra Adhesive Precleaned Micro Slides (Leica) and exposed to a rabbit monoclonal anti-Fgf21

antibody (1:500, Abcam), rabbit polyclonal anti-pFgfr1c antibody (1:100, Cell Signaling), rabbit monoclonal anti-pmTOR (IHC specific, 1:100, Cell Signaling) and rabbit polyclonal anti-PSD95 (1:1000, Abcam). For the development of the primary antibodies with DAB chromogen Universal LSAB® kits (System-HRP; DakoCytomation, Dako) were used according to the manufacturer's instructions. The sections were counterstained with hemalaun and analyzed with a light microscope (Olympus BX51). Images were acquired with a Color View II FW camera (Color View).

### **Morris water maze test**

The Morris water maze (MWM) was performed as a task to measure spatial reference memory. Mice under dim light conditions (indirect illumination, 3.0 Lux) at days -4 to -1 d were trained to locate a submerged hidden platform (11 cm diameter) in a fixed quadrant of a circular pool filled with opaque water (diameter of pool 107 cm, filled to a depth of 20 cm, water temperature 17° C, platform submerged 1 cm beneath the surface). For each trial (1 x at -4 d to familiarize the animals with test apparatus, 8 x at -3 d, 8 x at -2 d, 4 x -1 d = 5 training blocks each consisting of 4 consecutive trials) mice are gently placed in the water, hind legs first. On each trial, the starting position was randomized between four possible quadrant positions. The location of the platform remained constant throughout the whole training period. Each trial lasted until the animal located the platform. However, after max. 60 s the mouse was guided to the platform. The latter was given a latency score of 60 s. Mice were allowed to rest 10 s on the escape platform, were then removed, dried with a towel and warmed under a heating lamp. After further 30 s the next trial started. The time to reach the platform (latency to escape) was recorded for each trial. On day -1, mice finally were trained for four trials. All training trials were monitored online by a video camera [4]. After training, the platform was removed from the pool and the mouse performed a 60 s test trial. The start position of the test trial was located opposite to the quadrant that had contained the platform. The swimming route and the number of times the mouse crossed each of the four possible platform positions (the previous platform position and 3 imaginary platform position in the other quadrants and platform crossings) was monitored online by a video camera [4].

### **Statistical analysis**

All data are expressed as means ± SEM. Statistical differences were determined using one- or two-way ANOVA followed by post-hoc pairwise comparison

tests for analysis between either feeding groups or duration of feeding. Data were considered significant if  $p < 0.05$ . Statistical analysis was performed using the SigmaStat software package (Jandel Scientific).

## ACKNOWLEDGEMENTS

The authors cordially thank the technicians of the Institute for Experimental Surgery and of the Central Animal Care Facility, Rostock University Medical Center for their valuable assistance. We would like to thank Ottmar Herchenröder for editing the manuscript.

## CONFLICTS OF INTEREST

The other authors declare that they have no conflict of interest.

## FUNDING

This study was supported by a grant from the Deutsche Forschungsgemeinschaft, Bonn, Germany (KU 3280/1-1).

## REFERENCES

1. Weindruch R, Walford RL, Fligiel S, Guthrie D. The retardation of aging in mice by dietary restriction: longevity, cancer, immunity and lifetime energy intake. *J Nutr.* 1986;116:641–54.
2. Mulligan JD, Stewart AM, Saupe KW. Downregulation of plasma insulin levels and hepatic PPAR $\gamma$  expression during the first week of caloric restriction in mice. *Exp Gerontol.* 2008; 43:146–53. doi:10.1016/j.exger.2007.10.011
3. Duan W, Guo Z, Jiang H, Ware M, Mattson MP. Reversal of behavioral and metabolic abnormalities, and insulin resistance syndrome, by dietary restriction in mice deficient in brain-derived neurotrophic factor. *Endocrinology.* 2003; 144:2446–53. doi:10.1210/en.2002-0113
4. Kuhla A, Lange S, Holzmann C, Maass F, Petersen J, Vollmar B, Wree A. Lifelong caloric restriction increases working memory in mice. *PLoS One.* 2013; 8:e68778. doi:10.1371/journal.pone.0068778
5. Patel NV, Gordon MN, Connor KE, Good RA, Engelman RW, Mason J, Morgan DG, Morgan TE, Finch CE. Caloric restriction attenuates A $\beta$ -deposition in Alzheimer transgenic models. *Neurobiol Aging.* 2005;26:995–1000. doi: 10.1016/j.neurobiolaging.2004.09.014
6. Qin W, Chachich M, Lane M, Roth G, Bryant M, de Cabo R, Ottinger MA, Mattison J, Ingram D, Gandy S, Pasinetti GM. Calorie restriction attenuates Alzheimer's disease type brain amyloidosis in Squirrel monkeys (*Saimiri sciureus*). *J Alzheimers Dis.* 2006;10:417–22.
7. Halagappa VK, Guo Z, Pearson M, Matsuoka Y, Cutler RG, Laferla FM, Mattson MP. Intermittent fasting and caloric restriction ameliorate age-related behavioral deficits in the triple-transgenic mouse model of Alzheimer's disease. *Neurobiol Dis.* 2007; 26:212–20. doi:10.1016/j.nbd.2006.12.019
8. Roberge MC, Hotte-Bernard J, Messier C, Plamondon H. Food restriction attenuates ischemia-induced spatial learning and memory deficits despite extensive CA1 ischemic injury. *Behav Brain Res.* 2008; 187:123–32. doi:10.1016/j.bbr.2007.09.002
9. Vasconcelos AR, Yshii LM, Viel TA, Buck HS, Mattson MP, Scavone C, Kawamoto EM. Intermittent fasting attenuates lipopolysaccharide-induced neuroinflammation and memory impairment. *J Neuroinflammation.* 2014; 11:85. doi: 10.1186/1742-2094-11-85
10. Zhang Y, Xie Y, Berglund ED, Coate KC, He TT, Katafuchi T, Xiao G, Potthoff MJ, Wei W, Wan Y, Yu RT, Evans RM, Kliewer SA, Mangelsdorf DJ. The starvation hormone, fibroblast growth factor-21, extends lifespan in mice. *eLife.* 2012; 1:e00065. doi: 10.7554/eLife.00065
11. Kuhla A, Hahn S, Butschkau A, Lange S, Wree A, Vollmar B. Lifelong caloric restriction reprograms hepatic fat metabolism in mice. *J Gerontol A Biol Sci Med Sci.* 2014;69:915–22. doi: 10.1093/gerona/glt160
12. Kharitonov A. FGFs and metabolism. *Curr Opin Pharmacol.* 2009;9:805–10. doi: 10.1016/j.coph.2009.07.001
13. Yang C, Jin C, Li X, Wang F, McKeehan WL, Luo Y. Differential specificity of endocrine FGF19 and FGF21 to FGFR1 and FGFR4 in complex with KLB. *PLoS One.* 2012; 7:e33870. doi:10.1371/journal.pone.0033870
14. Ornitz DM, Marie PJ. Fibroblast growth factor signaling in skeletal development and disease. *Genes Dev.* 2015; 29:1463–86. doi: 10.1101/gad.266551.115
15. Cyphert HA, Alonge KM, Ippagunta SM, Hillgartner FB. Glucagon stimulates hepatic FGF21 secretion through a PKA- and EPAC-dependent posttranscriptional mechanism. *PLoS One.* 2014; 9:e94996. doi:10.1371/journal.pone.0094996

16. Lundåsen T, Hunt MC, Nilsson LM, Sanyal S, Angelin B, Alexson SE, Rudling M. PPAR $\alpha$  is a key regulator of hepatic FGF21. *Biochem Biophys Res Commun.* 2007;360:437–40. doi: 10.1016/j.bbrc.2007.06.068
17. Badman MK, Pissios P, Kennedy AR, Koukos G, Flier JS, Maratos-Flier E. Hepatic fibroblast growth factor 21 is regulated by PPAR $\alpha$  and is a key mediator of hepatic lipid metabolism in ketotic states. *Cell Metab.* 2007;5:426–37. doi: 10.1016/j.cmet.2007.05.002
18. Domouzoglou EM, Maratos-Flier E. Fibroblast growth factor 21 is a metabolic regulator that plays a role in the adaptation to ketosis. *Am J Clin Nutr.* 2011;93:901S–5. doi:10.3945/ajcn.110.001941
19. Chau MD, Gao J, Yang Q, Wu Z, Gromada J. Fibroblast growth factor 21 regulates energy metabolism by activating the AMPK-SIRT1-PGC-1 $\alpha$  pathway. *Proc Natl Acad Sci USA.* 2010;107:12553–58. doi:10.1073/pnas.1006962107
20. Genzer Y, Dadon M, Burg C, Chapnik N, Froy O. Ketogenic diet delays the phase of circadian rhythms and does not affect AMP-activated protein kinase (AMPK) in mouse liver. *Mol Cell Endocrinol.* 2015;417:124–30. doi:10.1016/j.mce.2015.09.012
21. Cai Z, Yan LJ, Li K, Quazi SH, Zhao B. Roles of AMP-activated protein kinase in Alzheimer's disease. *Neuromolecular Med.* 2012;14:1–14. doi: 10.1007/s12017-012-8173-2
22. Perluigi M, Di Domenico F, Butterfield DA. mTOR signaling in aging and neurodegeneration: at the crossroad between metabolism dysfunction and impairment of autophagy. *Neurobiol Dis.* 2015;84:39–49. doi:10.1016/j.nbd.2015.03.014
23. Siman R, Cocca R, Dong Y. The mTOR inhibitor rapamycin mitigates perforant pathway neurodegeneration and synapse loss in a mouse model of early-stage alzheimer-type tauopathy. *PLoS One.* 2015;10:e0142340. doi: 10.1371/journal.pone.0142340
24. Hsuchou H, Pan W, Kastin AJ. The fasting polypeptide FGF21 can enter brain from blood. *Peptides.* 2007;28:2382–86. doi: 10.1016/j.peptides.2007.10.007
25. Tan BK, Hallschmid M, Adya R, Kern W, Lehnert H, Randeve HS. Fibroblast growth factor 21 (FGF21) in human cerebrospinal fluid: relationship with plasma FGF21 and body adiposity. *Diabetes.* 2011;60:2758–62. doi:10.2337/db11-0672
26. Sa-Nguanmoo P, Chattipakorn N, Chattipakorn SC. Potential roles of fibroblast growth factor 21 in the brain. *Metab Brain Dis.* 2016; 31:239–48. doi: 10.1007/s11011-015-9789-3
27. Mäkelä J, Tselykh TV, Maiorana F, Eriksson O, Do HT, Mudò G, Korhonen LT, Belluardo N, Lindholm D. Fibroblast growth factor-21 enhances mitochondrial functions and increases the activity of PGC-1 $\alpha$  in human dopaminergic neurons via Sirtuin-1. *Springerplus.* 2014; 3:2. doi: 10.1186/2193-1801-3-2
28. Tang Z, Bereczki E, Zhang H, Wang S, Li C, Ji X, Branca RM, Lehtiö J, Guan Z, Filipcik P, Xu S, Winblad B, Pei JJ. Mammalian target of rapamycin (mTor) mediates tau protein dyshomeostasis: implication for Alzheimer disease. *J Biol Chem.* 2013; 288:15556–70. doi:10.1074/jbc.M112.435123
29. Roses AD. Apolipoprotein E affects the rate of Alzheimer disease expression: beta-amyloid burden is a secondary consequence dependent on APOE genotype and duration of disease. *J Neuropathol Exp Neurol.* 1994; 53:429–37. doi: 10.1097/00005072-199409000-00002
30. Genis I, Gordon I, Sehayek E, Michaelson DM. Phosphorylation of tau in apolipoprotein E-deficient mice. *Neurosci Lett.* 1995;199:5–8. doi: 10.1016/0304-3940(95)12007-Q
31. Gordon I, Grauer E, Genis I, Sehayek E, Michaelson DM. Memory deficits and cholinergic impairments in apolipoprotein E-deficient mice. *Neurosci Lett.* 1995; 199:1–4. doi:10.1016/0304-3940(95)12006-P
32. Cai H, Cong WN, Ji S, Rothman S, Maudsley S, Martin B. Metabolic dysfunction in Alzheimer's disease and related neurodegenerative disorders. *Curr Alzheimer Res.* 2012; 9:5–17. doi: 10.2174/156720512799015064
33. Masliah E, Mallory M, Ge N, Alford M, Veinbergs I, Roses AD. Neurodegeneration in the central nervous system of apoE-deficient mice. *Exp Neurol.* 1995; 136:107–22. doi:10.1006/exnr.1995.1088
34. Reitman ML. FGF21: a missing link in the biology of fasting. *Cell Metab.* 2007;5:405–07. doi: 10.1016/j.cmet.2007.05.010
35. Berger J, Moller DE. The mechanisms of action of PPARs. *Annu Rev Med.* 2002; 53:409–35. doi: 10.1146/annurev.med.53.082901.104018
36. Noh HS, Kim YS, Choi WS. Neuroprotective effects of the ketogenic diet. *Epilepsia.* 2008 (Suppl 8); 49:120–23. doi:10.1111/j.1528-1167.2008.01855.x
37. Krikorian R, Shidler MD, Dangelo K, Couch SC, Benoit SC, Clegg DJ. Dietary ketosis enhances memory in mild cognitive impairment. *Neurobiol Aging.* 2012; 33:425.e19–27.

doi: 10.1016/j.neurobiolaging.2010.10.006

38. Mandrekar-Colucci S, Landreth GE. Nuclear receptors as therapeutic targets for Alzheimer's disease. *Expert Opin Ther Targets*. 2011; 15:1085–97. doi:10.1517/14728222.2011.594043
39. Leng Y, Wang Z, Tsai LK, Leeds P, Fessler EB, Wang J, Chuang DM. FGF-21, a novel metabolic regulator, has a robust neuroprotective role and is markedly elevated in neurons by mood stabilizers. *Mol Psychiatry*. 2015;20:215–23. doi: 10.1038/mp.2013.192
40. Bookout AL, de Groot MH, Owen BM, Lee S, Gautron L, Lawrence HL, Ding X, Elmquist JK, Takahashi JS, Mangelsdorf DJ, Kliewer SA. FGF21 regulates metabolism and circadian behavior by acting on the nervous system. *Nat Med*. 2013; 19:1147–52. doi: 10.1038/nm.3249
41. Haigis MC, Sinclair DA. Mammalian sirtuins: biological insights and disease relevance. *Annu Rev Pathol*. 2010;5:253–95. doi: 10.1146/annurev.pathol.4.110807.092250
42. Kahn BB, Alquier T, Carling D, Hardie DG. AMP-activated protein kinase: ancient energy gauge provides clues to modern understanding of metabolism. *Cell Metab*. 2005; 1:15–25. doi: 10.1016/j.cmet.2004.12.003
43. Vellai T, Takacs-Vellai K, Zhang Y, Kovacs AL, Orosz L, Müller F. Genetics: influence of TOR kinase on lifespan in *C. elegans*. *Nature*. 2003; 426:620. doi: 10.1038/426620a
44. Caccamo A, Magrì A, Medina DX, Wisely EV, López-Aranda MF, Silva AJ, Oddo S. mTOR regulates tau phosphorylation and degradation: implications for Alzheimer's disease and other tauopathies. *Aging Cell*. 2013; 12:370–80. doi:10.1111/accel.12057
45. Cai Z, Yan LJ. Rapamycin, Autophagy, and Alzheimer's Disease. *J Biochem Pharmacol Res*. 2013;1:84–90.
46. Ma L, Dong W, Wang R, Li Y, Xu B, Zhang J, Zhao Z, Wang Y. Effect of caloric restriction on the SIRT1/mTOR signaling pathways in senile mice. *Brain Res Bull*. 2015;116:67–72. doi: 10.1016/j.brainresbull.2015.06.004
47. Guo W, Qian L, Zhang J, Zhang W, Morrison A, Hayes P, Wilson S, Chen T, Zhao J. Sirt1 overexpression in neurons promotes neurite outgrowth and cell survival through inhibition of the mTOR signaling. *J Neurosci Res*. 2011;89:1723–36. doi: 10.1002/jnr.22725
48. Stein S, Schäfer N, Breitenstein A, Besler C, Winnik S, Lohmann C, Heinrich K, Brokopp CE, Handschin C, Landmesser U, Tanner FC, Lüscher TF, Matter CM. SIRT1 reduces endothelial activation without affecting vascular function in ApoE<sup>-/-</sup> mice. *Aging (Albany NY)*. 2010;2:353–60. doi: 10.18632/aging.100162
49. Palacios OM, Carmona JJ, Michan S, Chen KY, Manabe Y, Ward JL 3rd, Goodyear LJ, Tong Q. Diet and exercise signals regulate SIRT3 and activate AMPK and PGC-1 $\alpha$  in skeletal muscle. *Aging (Albany NY)*. 2009;1:771–83. doi: 10.18632/aging.100075
50. Mandrekar-Colucci S, Karlo JC, Landreth GE. Mechanisms underlying the rapid peroxisome proliferator-activated receptor- $\gamma$ -mediated amyloid clearance and reversal of cognitive deficits in a murine model of Alzheimer's disease. *J Neurosci*. 2012; 32:10117–28. doi: 10.1523/JNEUROSCI.5268-11.2012

# An antioxidant specifically targeting mitochondria delays progression of Alzheimer's disease-like pathology

Natalia A. Stefanova<sup>1</sup>, Natalia A. Muraleva<sup>1</sup>, Kseniya Yi. Maksimova<sup>2</sup>, Ekaterina A. Rudnitskaya<sup>1</sup>, Elena Kiseleva<sup>1</sup>, Darya V. Telegina<sup>1</sup>, Nataliya G. Kolosova<sup>1,3</sup>

<sup>1</sup>Institute of Cytology and Genetics SB RAS, 630090, Novosibirsk, Russia

<sup>2</sup>Siberian State Medical University, 634055, Tomsk, Russia

<sup>3</sup>Novosibirsk State University, 630090, Novosibirsk, Russia

**Correspondence to:** Natalia A. Stefanova; Nataliya G. Kolosova; email: [stefanovan@mail.ru](mailto:stefanovan@mail.ru); [kolosova@bionet.nsc.ru](mailto:kolosova@bionet.nsc.ru)

**Keywords:** Alzheimer's disease, mitochondria, amyloid, synapse, neurodegeneration

**Abbreviations:** APP, amyloid precursor protein, SkQ1, plastoquinonyl-decyltriphenylphosphonium

**Received:** June 14, 2016 **Accepted:** September 18, 2016 **Published:** October 6, 2016 **doi:** [10.18632/aging.101054](https://doi.org/10.18632/aging.101054)

## ABSTRACT

Mitochondrial aberrations are observed in human Alzheimer's disease (AD) and in medical conditions that increase the risk of this disorder, suggesting that mitochondrial dysfunction may contribute to pathophysiology of AD. Here, using OXYS rats that simulate key characteristics of sporadic AD, we set out to determine the role of mitochondria in the pathophysiology of this disorder. OXYS rats were treated with a mitochondria-targeted antioxidant SkQ1 from age 12 to 18 months, that is, during active progression of AD-like pathology in these animals. Dietary supplementation with SkQ1 caused this compound to accumulate in various brain regions, and it was localized mostly to neuronal mitochondria. Via improvement of structural and functional state of mitochondria, treatment with SkQ1 alleviated the structural neurodegenerative alterations, prevented the neuronal loss and synaptic damage, increased the levels of synaptic proteins, enhanced neurotrophic supply, and decreased amyloid- $\beta$ 1-42 protein levels and tau hyperphosphorylation in the hippocampus of OXYS rats, resulting in improvement of the learning ability and memory. Collectively, these data support that mitochondrial dysfunction may play a key role in the pathophysiology of AD and that therapies with target mitochondria are potent to normalize a wide range of cellular signaling processes and therefore slow the progression of AD.

## INTRODUCTION

Alzheimer's disease (AD) is a progressive, age-dependent neurodegenerative disorder featuring progressive impairments in memory and cognition and ultimately leads to death [1]. According to the most widely accepted theory, the "amyloid cascade" hypothesis [2], AD arises when amyloid precursor protein (APP) is processed into amyloid- $\beta$ , which accumulates in plaques. The form of this protein that is most toxic to cells (amyloid- $\beta$ <sub>42</sub>) promotes tau hyperphosphorylation, which leads to formation of neurofibrillary tangles: the effect directly causing mitochondrial dysfunction, synaptic damage, and

neuronal cell death [3-4]. In many ways, the above hypothesis has been highly successful, in that it unites findings from many different investigative approaches to the disease and, most compellingly, helps to explain how mutations in genes *APP*, presenilin 1 (*PSEN1*), or *PSEN2* can cause the familial early-onset form of AD, which accounts for ~5% of all cases [4-5]. Nonetheless, the therapeutic strategies designed to eliminate amyloid- $\beta$  production as the key precipitating event in Alzheimer's pathogenesis have not been successful [1]. Consequently, the factors that initiate (or affect the risk and onset of) amyloid- $\beta$  accumulation in sporadic late-onset AD, which accounts for ~95% of all disease cases, remain poorly understood [6].

There is growing evidence that mitochondrial damage and oxidative stress lead to activation of the amyloid- $\beta$  cascade and, accordingly, the mitochondrial dysfunction is a significant contributing factor of the onset and progression of AD. According to the “mitochondrial cascade hypothesis” [7] amyloid- $\beta$  is a marker of brain aging, and not a singular cause of AD [8]. Many studies have confirmed that mitochondrial dysfunction is likely to be the leading cause of synaptic loss and neuronal death by apoptosis, representing the most likely mechanism underlying cortical shrinkage, especially in brain regions involved in learning and memory, such as the hippocampus [9]. The mitochondrial changes increase amyloid- $\beta$  production and cause its accumulation, which in turn can directly exert toxic action on mitochondria, thus aggravating the neurodegenerative processes. Triggering of the “vicious circle” of neurodegeneration leads to tau hyperphosphorylation, synaptic damage, and neuronal cell death and serves as a fatal hallmark event of Alzheimer’s pathophysiology. Naturally, the mitochondrial dysfunction is called the missing link separating brain aging and AD [10], and recent studies have provided substantial evidence that therapeutic strategies targeting mitochondria may shed some light on new strategies for treatment of AD [1, 11]. A promising approach to this problem may be the use of antioxidants specifically targeting mitochondria, for example, mitochondria-targeted antioxidants of the SkQ family [11]. These membrane-penetrating cations specifically accumulate in the inner mitochondrial membrane because the mitochondrial interior is the only negatively charged compartment in the cell; such compounds have been shown to have a beneficial effect in a number of age-related diseases [12-15]. In our studies involving senescence-accelerated OXYS rats, we demonstrated that dietary supplementation with plastoquinonyl-decyltriphenylphosphonium (SkQ1) in OXYS rats starting at a young age is clearly pleiotropic in nature, inhibits a large set of typical traits of aging, and suppress age-related diseases [16-23], including development of signs of AD [24-25]. Recently, we showed that OXYS rats simulate key characteristics of the sporadic form of AD [25-27]. More recently, we reported that an age-dependent increase in the levels of amyloid- $\beta_{1-42}$  and extracellular amyloid- $\beta$  deposits in the brain of OXYS rats occur later than do mitochondrial structural abnormalities, hyperphosphorylation of the tau protein, synaptic loss, and neuronal cell death [28]. On the basis of our results, we theorized that multiple age-associated degenerative processes may precede the toxic accumulation of amyloid- $\beta$ , which in turn triggers the final, currently irreversible stage of AD.

In the present study, we explored the role of mitochondria in the brain affected by AD using mitochondria-

targeted antioxidant SkQ1 as a possible therapeutic agent for alleviation of the deleterious consequences of this disease in a rat model. To obtain evidence of the hypothesized role of mitochondrial damage in AD, treatment with SkQ1 was started at the progressive stage of AD-like pathology in OXYS rats. Via improvement of the structural and functional state of mitochondria in the hippocampus of OXYS rats by SkQ1, we showed alleviation of structural neurodegenerative alterations, prevention of the neuronal loss and synaptic damage, improvement of the neurotrophic supply, a decrease in the toxic amyloid- $\beta$  protein levels and in tau hyperphosphorylation, and a recovery of reference memory. All these changes suggest that mitochondrial damage may play a key role in AD.

## RESULTS

### SkQ1 is predominantly localized to neuronal mitochondria in the brain

We first assessed the localization of SkQ1 in the brain, using a rhodamine derivative of SkQ1, 10(6'-plastoquinonyl) decylrhodamine 19 (SkQR1), which, as shown elsewhere [11, 14], also has neuroprotective properties. We found high-intensity fluorescent signals of SkQR1 in the brain neurons of OXYS rats treated with this antioxidant for 7 or 14 days ( $n=4$ ). Depending on duration of administration, the signal of SkQR1 increased (7 day < 14 days) and was most noticeable in neurons of the hippocampus (Fig. 1A–D), cortex (Fig. S1A), thalamus, myelencephalon, and cerebellum (Fig. S1B) of OXYS rats, suggesting that SkQ1 accumulates in cerebral neurons. Moreover, using the antibody to COX-IV (cytochrome *c* oxidase subunit 4, mitochondrial loading control), we found that SkQR1 is localized to neuronal mitochondria (Fig. 1C and D), suggesting that this antioxidant may play an important neuroprotective role by regulating and restoring the mitochondrial function.

### SkQ1 retards mitochondrial alterations

We next tested whether SkQ1 treatment from age 12 to 18 months (that is, during active progression of AD-like pathology in OXYS rats) affects mitochondrial alterations in the hippocampus. To this end, in OXYS rats, we evaluated the influence of SkQ1 administration on the ultrastructural state of the mitochondrial apparatus in pyramidal neurons of the hippocampal CA1 region, as the most vulnerable region of the hippocampus during the development of AD [29-30]. According to electron-microscopic analysis, in contrast to Wistar rats and SkQ1-treated OXYS rats, untreated OXYS rats showed significant changes in structural organization of the mitochondrial apparatus, such as

large intramitochondrial cristae-free areas of low electron density with an uneven contour of the external and internal membranes as well as localization of cristae near the periphery only; the latter picture corresponds to a de-energized state (Fig. 2A). In some locations, we could see contacts of the mitochondria with the nuclear envelope, the endoplasmic reticulum, and Golgi complex. SkQ1 treatment substantially improved the ultrastructure of the mitochondrial apparatus (Fig. 2A) and increased the specific area of mitochondria (Fig.

2B) in neurons in the hippocampal CA1 region of OXYS rats. In addition, in untreated OXYS rats, we seldom found mitochondria touching each other via membranes: this touching can be a sign of fusion or fission and was observed more frequently in Wistar rats and SkQ1-treated OXYS rats. To determine the state of mitochondrial dynamics, we immunostained rat brain tissue for Drp1 (dynamin-1-like protein; mitochondria in fission) and for Mfn2 (mitofusin 2; mitochondria in fusion).

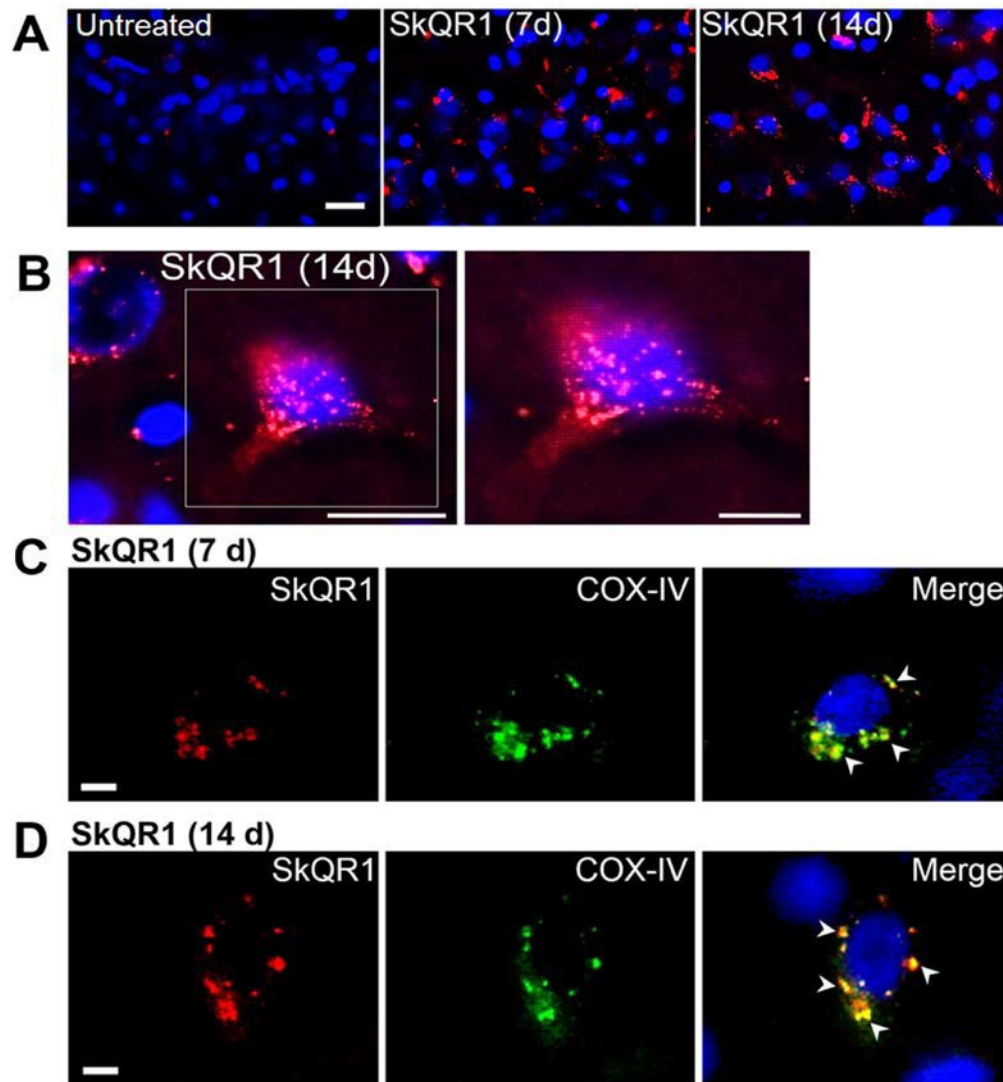


**Figure 1. SkQ1 is predominantly localized to (and accumulates in) neuronal mitochondria.** Four-month-old OXYS rats were treated with SkQR1 (250 nmol/kg) for 7 or 14 days ( $n = 4$ ) to assess localization and accumulation of SkQ1. **(A)** High intensity of fluorescence signals of fluorescence signals of rhodamine-labeled of SkQ1 (red fluorescence) in neurons of the hippocampus in SkQR1-treated OXYS rats and the absence of specific signals in untreated (control) OXYS rats. The SkQR1 signal increased depending on the duration of treatment with the antioxidant (7 days < 14 day). **(B)** An example of accumulation of SkQR1 (in red) in hippocampal neurons of an OXYS rat. **(C and D)** Immunolabeling with an anti-COX-IV antibody (mitochondrial loading control; in green) shows that SkQR1 (in red) is localized to neuronal mitochondria. The arrows show colocalization of SkQR1 and COX-IV. Cell nuclei are stained with DAPI (in blue). The scale bars are 20  $\mu\text{m}$  (**A** and **B**) and 5  $\mu\text{m}$  (**C** and **D**).

In the hippocampus, we found increased expression of Drp1 and Mfn2 in SkQ1-treated OXYS rats and Wistar rats compared to untreated OXYS rats (Fig. 2C); this result was suggestive of improvement of the mitochondria biogenesis processes in OXYS rats by SkQ1. Finally, using Microplate Assay Kits we found that enzymatic activity of complexes I and IV in the hippocampus of untreated OXYS rats was ~30% lower than that in Wistar rats. Less pronounced interstrain differences in these parameters compared to the scale of detected by electron microscopy mitochondrial destructions, we can assume methodological reasons.

The enzymatic activity of the respiratory chain complexes was determined in the isolated mitochondria, in which severely damaged mitochondria do not fall. Administration of SkQ1 slightly but not significantly increased enzymatic activity of complex I and significantly increased enzymatic activity of complex IV in OXYS rats to the level of Wistar rats (Fig. 2D). Taken together, these findings indicate that the mitochondrial alterations involved in progression of AD-like pathology in OXYS rats can be significantly attenuated by SkQ1-driven improvement of mitochondrial function.

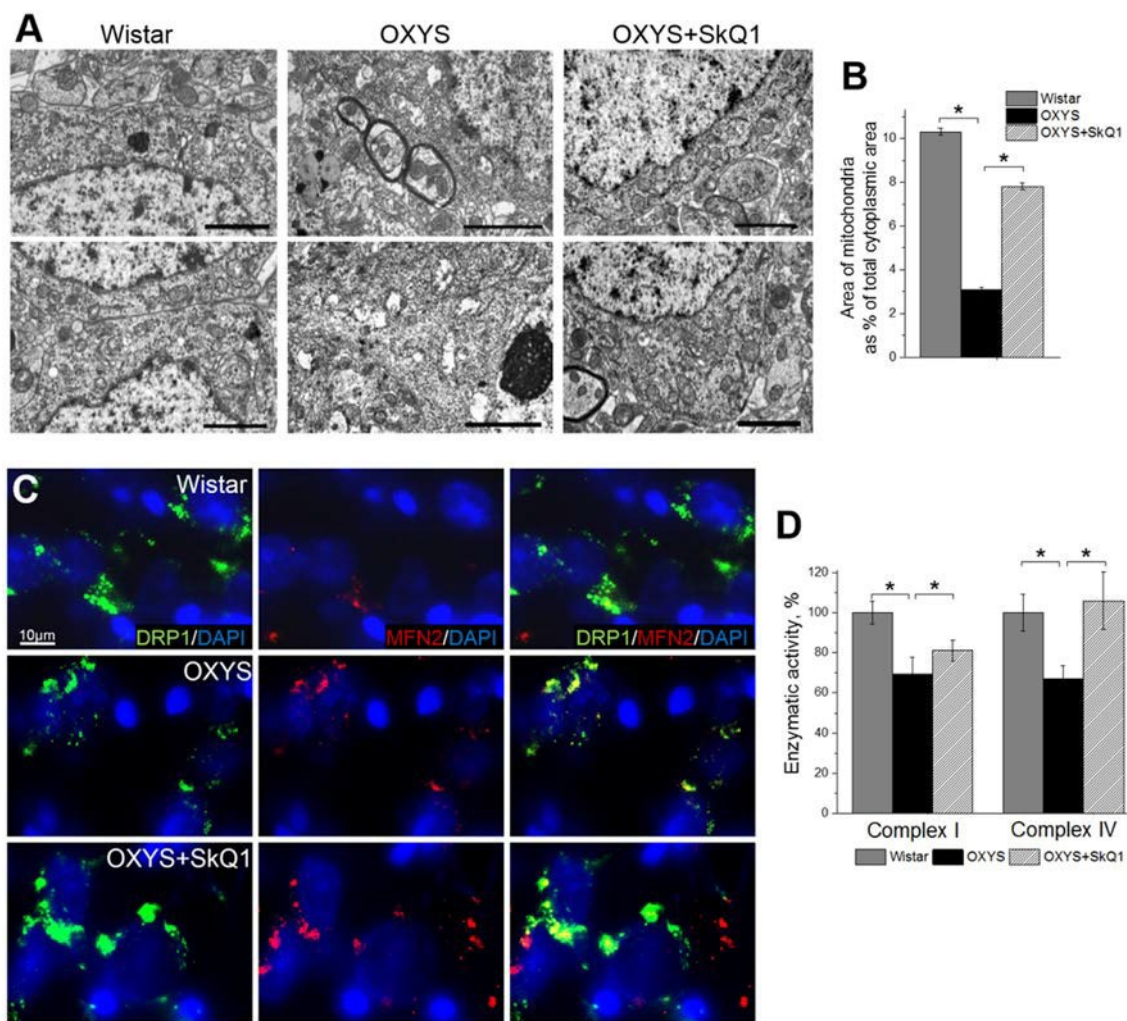


**Figure 2. SkQ1 retards mitochondrial alterations in the hippocampus.** (A) Alterations in the ultrastructure of the mitochondrial apparatus of CA1 pyramidal neurons in OXYS rats were attenuated by SkQ1 administration. (B) The area occupied by mitochondria within the hippocampal pyramidal neurons as a percentage of the total neuronal area in 18-month-old Wistar rats, untreated OXYS rats, and SkQ1-treated OXYS rats (n=4). Compared to Wistar rats, the untreated OXYS rats had a considerably smaller mitochondrial area. SkQ1 administration increased the mitochondria-occupied portion of the neuronal area. (C) Immunolabeling for mitochondrial fission mediator Drp1 (green) and mitochondrial fusion mediator Mfn2 (red) and cell nuclei (DAPI, blue) in the CA3 region of the hippocampus. (D) Enzymatic activities of complexes I and IV in the hippocampus of OXYS rats were ~30% lower than those in Wistar rats ( $p < 0.03$  and  $p < 0.02$ , respectively). Enzymatic activity did not change significantly in complex I but increased by ~30% in complex IV ( $p < 0.001$ ) in the hippocampus of SkQ1-treated OXYS rats (n=6). The data are shown as mean  $\pm$  SEM. Statistical significance ( $p < 0.05$ ) is denoted by the asterisk. The scale bar is 2  $\mu$ m (A).

### SkQ1 prevents neuronal loss and retards structural neurodegenerative alterations

An important and distinct feature of OXYS rats is that these rats show an overt neuronal loss in the hippocampus at the progressive stage of AD-like pathology [27]. When we evaluated the effects of SkQ1 in this crucial period, we stained brain tissue with

Cresyl violet to visualize cell nuclei and stereologically quantified the number of neurons in the hippocampus (Fig. 3A). Quantification of neuronal populations revealed a significant decrease in neuronal numbers in the CA1 and CA3 regions and in the dentate gyrus of OXYS rats, whereas SkQ1 treatment prevented this decrease (Fig. 3B). In addition, quantification using stereological counts revealed that the specific

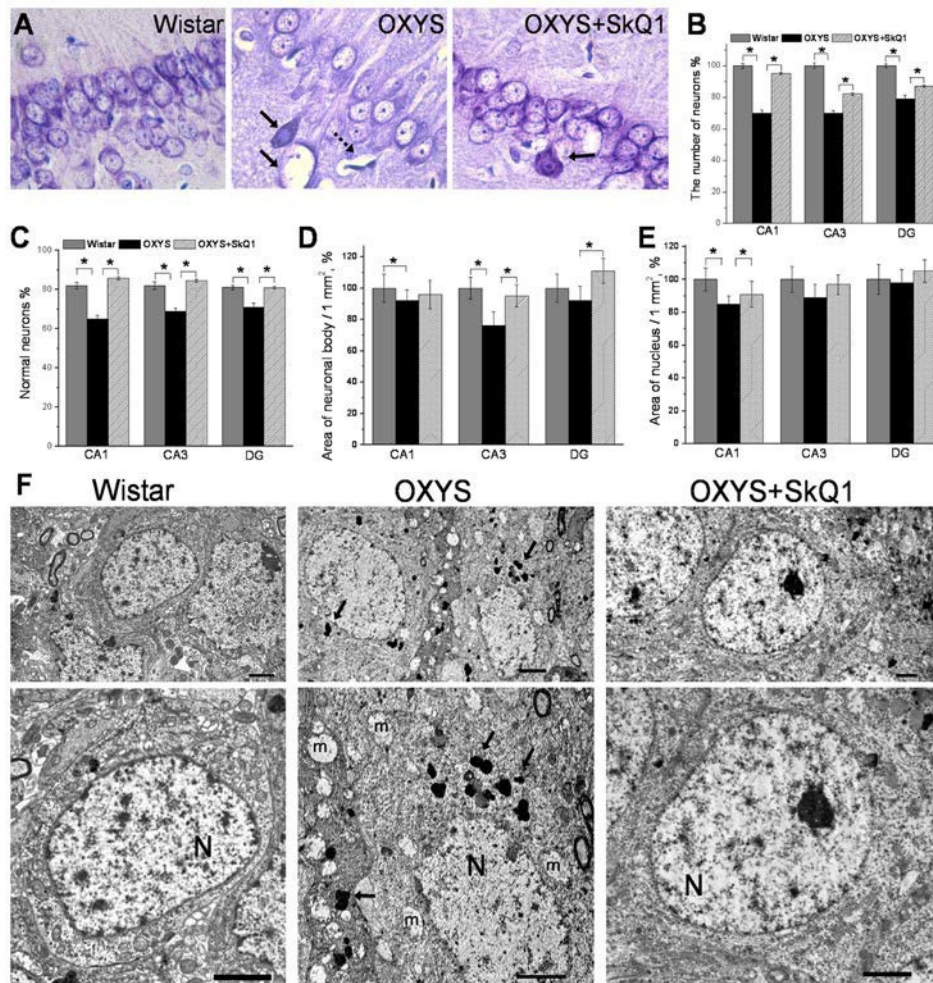


**Figure 3. SkQ1 prevents neuronal loss and retards structural neurodegenerative alterations.** (A) Representative 100 × histological Cresyl violet images of neurons of the hippocampal CA1 region in 18-month-old Wistar rats, untreated OXYS rats, and SkQ1-treated OXYS rats (n=4). The damaged neurons are indicated by solid arrows, and a dead neuron is indicated by a dashed arrow. (B) Quantification of neuronal populations revealed a significant decrease in neuronal number in the CA1 and CA3 regions and in the dentate gyrus of untreated OXYS rats compared to Wistar rats ( $p < 0.05$ ). Treatment with SkQ1 significantly increased neuronal populations in the hippocampus of OXYS rats ( $p < 0.05$ ). (C) The percentages of normal neurons were smaller in the examined hippocampal regions of OXYS rats compared to Wistar rats. Oral SkQ1 administration improved neuronal health in all the hippocampal regions examined in OXYS rats. (D) The small area of neuronal bodies in the CA3 region and dentate gyrus of the hippocampus in OXYS rats (n=5) is enlarged in response to SkQ1 treatment ( $p < 0.05$ ). (E) The small area of neuronal nuclei in the hippocampal CA1 region of OXYS rats (n=5) is enlarged in response to SkQ1 treatment ( $p < 0.05$ ). (F) SkQ1 improved the ultrastructure of pyramidal neurons in the hippocampal CA1 region in 18-month-old OXYS rats (n=4). The electron micrographs show examples of the normal ultrastructure of pyramidal neurons of Wistar rats and SkQ1-treated OXYS rats, and the substantial changes in the structural organization of cellular organelles in the CA1 region of untreated OXYS rats. The figure shows a pyramidal neuron containing a large cluster of lipofuscin granules (indicated by arrows), and massively swollen mitochondria (m). N: nucleus. The scale bars are 2  $\mu\text{m}$ . DG: dentate gyrus. The data are shown as mean  $\pm$  SEM. Statistical significance ( $p < 0.05$ ) is denoted by the asterisk.

proportion of unaffected neurons in the CA1 and CA3 areas in the dentate gyrus of the OXYS hippocampus was lower, whereas the proportion of dead or damaged neurons was higher than that in Wistar rats, in all hippocampal regions (Fig. 3C, Fig. S2). Administration of SkQ1 slowed the progression of degenerative alterations of hippocampal neurons in OXYS rats (Fig. S2): the number of damaged neurons in all the analyzed hippocampal regions in SkQ1-treated OXYS rats was substantially lower than that in untreated OXYS rats, and did not differ from these parameters in Wistar rats. Accordingly, the number of normal neurons in all hippocampal regions of SkQ1-treated OXYS rats was at the level of Wistar rats and higher than in untreated OXYS rats (Fig. 3C). Next, we analyzed the effects of SkQ1 treatment on the size of pyramidal neurons in the hippocampal CA1 and CA3 regions and dentate gyrus of OXYS rats. We found that in OXYS rats in the CA1 region, the average area of neuronal bodies and nuclei—and in the CA3 region, the average area of neuronal bodies—were less than those in the Wistar strain (Fig. 3D, E). SkQ1 treatment increased the area of neuronal bodies in the CA3 region and dentate gyrus of the OXYS hippocampus (Fig. 3D).

Besides, in SkQ1-treated OXYS rats, the area of the nuclei in the CA1 region was larger than that in untreated OXYS rats and was not different from this parameter in Wistar rats (Fig. 3E). Further analyses of the ultrastructural state of pyramidal neurons in the hippocampal CA1 region of the rats revealed significant changes (similar to those showed recently [31]) in the structural organization of the nucleus, nucleolus, Golgi complex, endoplasmic reticulum (Fig. 3F) and mitochondria (Fig. 2B) in OXYS rats compared to the Wistar strain. In addition, in many neurons of OXYS rats, there were numerous vacuoles and phagolysosomes of various sizes and shapes (Fig. 3F). Administration of SkQ1 substantially improved the ultrastructural state of neurons in OXYS rats (Fig. 3F) and according to morphometric analysis, significantly increased specific area of mitochondria (Fig. 2B) and the endoplasmic reticulum, decreased specific area of lysosomes and vacuoles, and slightly but not significantly decreased the specific area of the Golgi complex (Table S1). These data corroborate previous reports of neuronal loss and neurodegenerative changes in the hippocampus of OXYS rats at this age [31] and indicate that SkQ1 treatment prevented the neuronal loss and progression of neurodegeneration in these rats.

### SkQ1 improves the neurotrophic supply

We next assessed the effects of SkQ1 treatment on the levels of brain-derived neurotrophic factor (BDNF) and of neurotrophic receptors tyrosine kinase B (TrkB) and

p75 neurotrophin receptor (p75<sup>NTR</sup>), because we recently reported [32] that in OXYS rats, the cerebral level of BDNF compensatory increases in response to the development of neurodegenerative changes at early stages of AD-like pathology and dramatically decreases with age. Enzyme immunoassay analysis of BDNF (Fig. 4A) revealed no significant differences in protein levels of total BDNF between OXYS rats and Wistar rats. In addition, we found no effects of SkQ1 treatment on the BDNF protein level in OXYS rats. After that, we immunolabeled tissue samples with antibodies against the mature form of BDNF (mBDNF) and immature BDNF (proBDNF) to assess the contribution of each protein form to the total BDNF protein level in untreated or chronically SkQ1-treated OXYS rats and in Wistar rats (Fig. 4B). In the hippocampus, we found decreased mBDNF and increased proBDNF concentrations in OXYS rats and no differences in these proteins' levels between SkQ1-treated OXYS rats and Wistar rats. Therefore, the downregulation of mBDNF and upregulation of proBDNF in OXYS rats is indicative of a shift in the proBDNF/mBDNF balance in the direction of the immature form of the protein (proBDNF), which activates apoptosis.

Western blot analysis of the phospho-TrkB/TrkB ratio, which reflects activity of TrkB (a mBDNF receptor), revealed that in the OXYS hippocampus, this ratio was lower than that in Wistar rats (Fig. 4C). Immunolabeling of tissue samples with anti-TrkB and anti-phospho-TrkB antibodies confirmed this result (Fig. 4D). Moreover, immunolabeling for proBDNF and p75<sup>NTR</sup> revealed increased colocalization of proBDNF with p75<sup>NTR</sup>, apparently caused by upregulation of proBDNF in the OXYS hippocampus (Fig. 4E). This result is suggestive of initiation of neuronal apoptosis, and as a consequence, of progression of neurodegenerative changes. SkQ1 treatment of OXYS rats increased the protein level of mBDNF and decreased that of proBDNF (Fig. 4B). Thus, the increase in the phospho-TrkB/TrkB ratio (Fig. 4C, D), downregulation of proBDNF, upregulation of mBDNF (Fig. 4B), and reduced immunoreactivity of p75<sup>NTR</sup> as well as its colocalization with proBDNF (Fig. 4E) in the hippocampus of SkQ1-treated OXYS rats indicate activation of cellular processes promoting the growth of neurites, formation of new synapses, and neuronal survival.

### SkQ1 reverses synaptic deficits

In line with their hippocampus-dependent cognitive deficits, OXYS rats show a synaptic loss [31], prominent alterations of synaptic functions [33], and significant ultrastructural changes [28] in the hippocampus. Ultrastructural abnormalities in synaptic

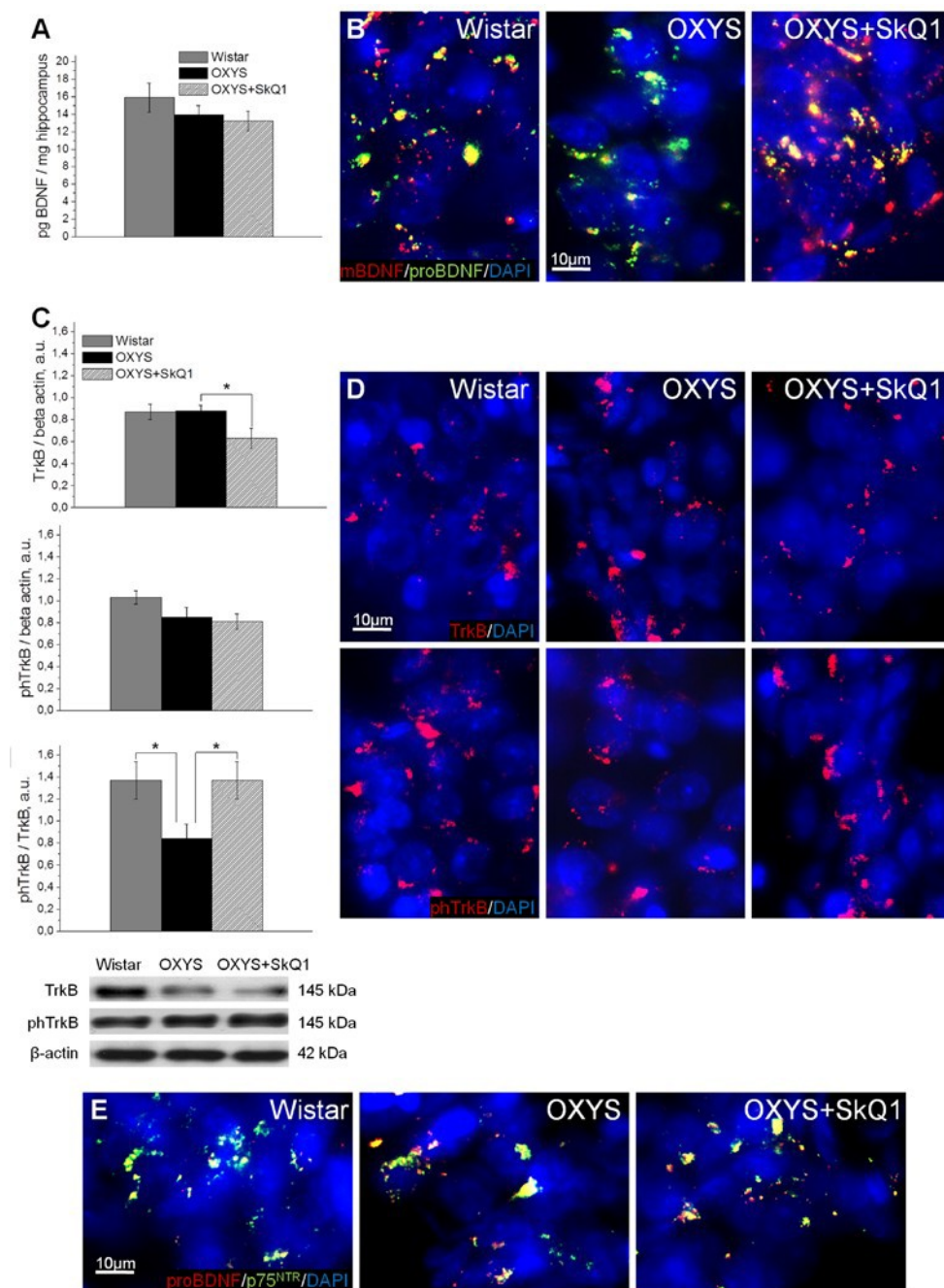


**Figure 4. SkQ1 improves neurotrophic supply in the hippocampus.** (A) Enzyme immunoassay analysis showed no differences in the levels of total hippocampal BDNF among 18-month-old Wistar rats, untreated OXYS rats, and SkQ1-treated OXYS rats (n=8). (B) Representative 40 × immunofluorescent images of staining for mBDNF (red), proBDNF (green), and cell nuclei (DAPI, blue) in the CA1 region of the hippocampus. (C) Hippocampus levels of TrkB and phTrkB were not different between Wistar rats and untreated OXYS rats (n=6). The level of TrkB decreased in the hippocampus of SkQ1-treated OXYS rats ( $p < 0.05$ ). Measurement of the phTrkB/TrkB ratio showed a significant decrease of this ratio in the hippocampus of OXYS rats ( $p < 0.04$ ). Treatment with SkQ1 increased the phTrkB/TrkB ratio in OXYS rats ( $p < 0.05$ ). (D) Representative 40× immunofluorescent images of staining for receptors TrkB (red; upper row) and phTrkB (red; lower row) and for cell nuclei (DAPI, blue) in the CA1 region of the hippocampus. (E) Representative 40× immunofluorescent images of colocalization of proBDNF (red), p75<sup>NTR</sup> receptor (green), and cell nuclei (DAPI, blue) in the CA1 region of hippocampus. A.u.: arbitrary units. The data are shown as mean ± SEM. Statistical significance ( $p < 0.05$ ) is denoted by the asterisk.

terminals of OXYS rats in the period of progression of AD-like pathology are characterized by decreased numbers of synaptic vesicles, by signs of their disorganization and destruction, by increased numbers of various vacuoles, and by swelling and disintegration of mitochondria [31]. To determine whether chronic SkQ1 treatment alleviates synaptic deficits in OXYS rats, we measured SkQ1's effects on synaptic density in the CA1 region of the hippocampus. Electron-microscopic analysis showed that the synaptic density was significantly lower in OXYS rats (Fig. 5A) than in Wistar rats. Furthermore, the number of asymmetric (excitatory) synapses (classified by morphometric criteria) was almost twofold lower in OXYS rats (Fig. 5C) than in Wistar rats. In SkQ1-treated OXYS rats, the synaptic density was 17% higher (Fig. 5A) than that in untreated OXYS rats (insignificantly). In contrast, the

number of excitatory synapses in SkQ1-treated OXYS rats was 42% greater (Fig. 5C) than that in untreated OXYS rats. The proportion of symmetric (inhibitory) synapses classified by morphometric criteria was twofold smaller in the SkQ1-treated OXYS rats than in untreated OXYS rats (Fig. 5B). In contrast to Wistar rats (Fig. 5D) and SkQ1-treated OXYS rats (Fig. 5F), in untreated OXYS rats, we observed degenerating synaptic terminals substantially more frequently (Fig. 5E); they showed characteristic clarification and swelling of the cytoplasm, disintegration of synaptic vesicles, an increase in the number of various vacuoles, and swelling and disintegration of mitochondria.

In addition, in SkQ1-treated OXYS rats, the share of excitatory synapses was 94% of total synaptic density, in untreated OXYS rats: 78%, and in Wistar rats: 86%.

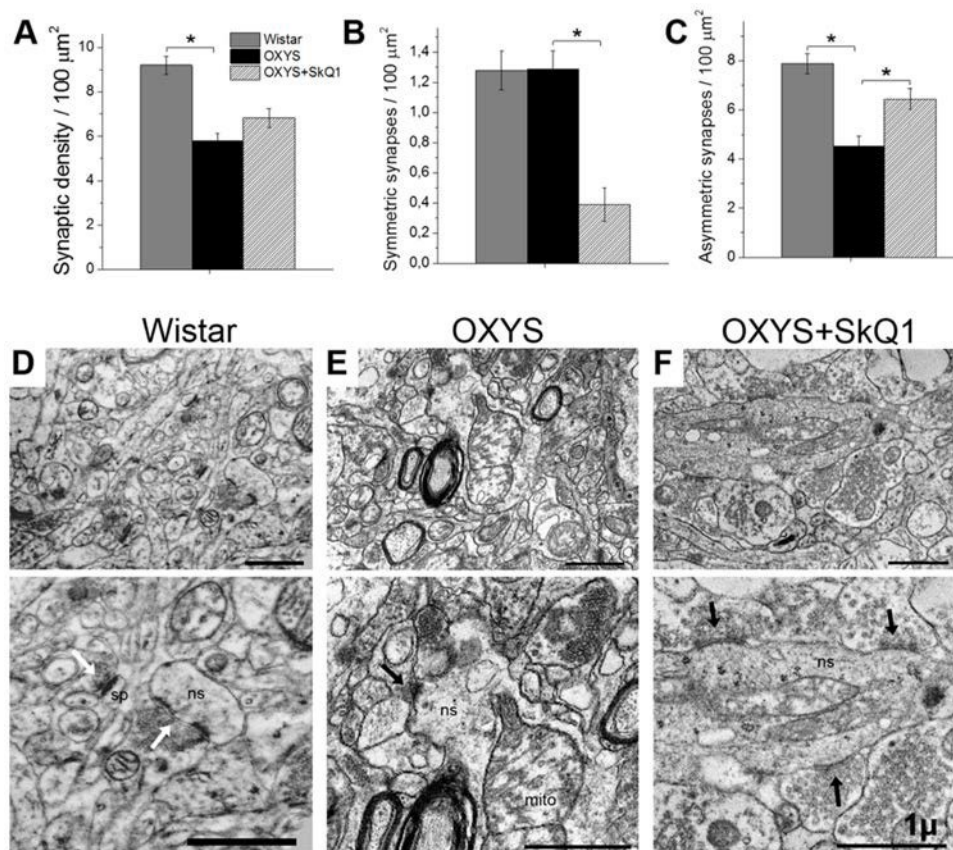


**Figure 5. SkQ1 increased the density of asymmetric synapses and improved synaptic structure in the CA1 region of the hippocampus.** (A) The low density of synapses in the hippocampus of OXYS rats ( $n=4$ ;  $p<0.05$ ) and an increase by 17% in response to SkQ1 treatment. (B) A decrease in the number of symmetric synapses in response to SkQ1 treatment ( $p<0.05$ ). (C) The low number of asymmetric synapses in the hippocampus of OXYS rats and an increase in response to SkQ1 treatment ( $p<0.05$ ). (D–F) Typical synaptic neuropil of the CA1 region in a Wistar rat, untreated OXYS rat, and SkQ1-treated OXYS rat. (D) Asymmetric synapses (white arrows) on a dendritic spine (sp) and on a nonspiny dendrite (ns) in a Wistar rat. (E) Symmetric synapse (black arrow) on a nonspiny dendrite (ns) containing a large mitochondrion (mito), and a degenerative myelinated axon in neuropil of an untreated OXYS rat. (F) Asymmetric synapses (black arrows) on a nonspiny dendrite (ns) in neuropil of an SkQ1-treated OXYS rat. The scale bar is 1  $\mu\text{m}$ . The data are shown as mean  $\pm$  SEM. Statistical significance ( $p<0.05$ ) is denoted by an asterisk.

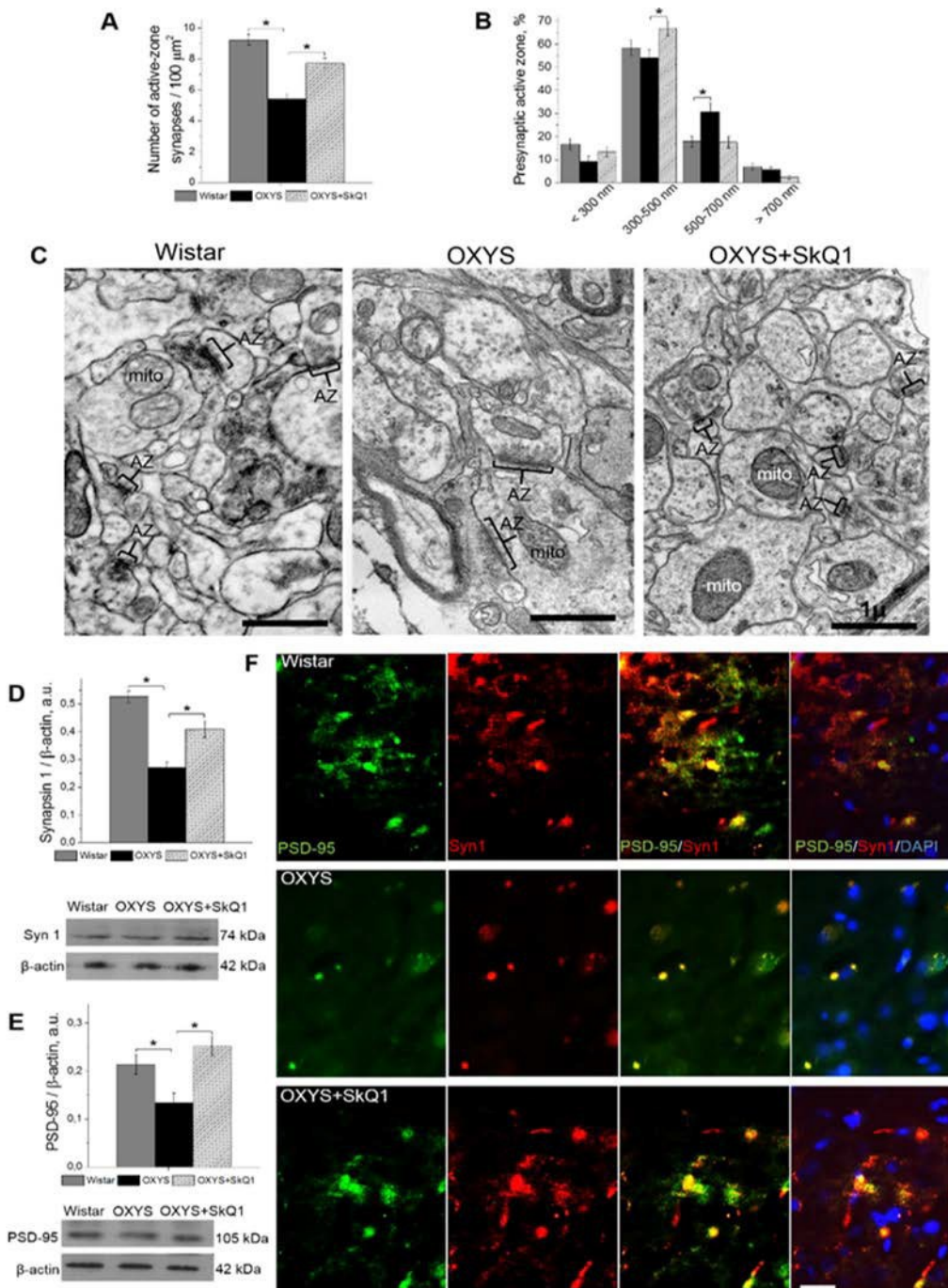


**Figure 6. SkQ1 increased the number of presynaptic active zones in the hippocampal CA1 region and increased the levels of pre- and postsynaptic proteins in the hippocampus.** (A) The low number of presynaptic active zones in the hippocampus of OXYS rats ( $n=4$ ;  $p<0.05$ ) and an increase in response to SkQ1 treatment ( $p<0.05$ ). (B) The elevated number of large presynaptic active zones (judging by the length of an active zone in the micrographs) in the hippocampus of OXYS rats ( $p<0.05$ ) and an increase in the number of medium presynaptic active zones in response to SkQ1 treatment ( $p<0.05$ ). (C) The electron micrographs show an active zone (AZ) in the CA1 region of the hippocampus in a Wistar rat and untreated and SkQ1-treated OXYS rats. (D, E) Synapsin I and PSD-95 levels were low in the hippocampus of untreated OXYS rats ( $p<0.05$ ) and increased in response to SkQ1 treatment ( $p<0.05$ ) according to western blot analyses ( $n=6-8$ ). (F) Immunohistochemical staining ( $n=4$ ) of synapsin I (red) and PSD-95 (green). The DAPI (blue) staining shows cell nuclei. The scale bar is 1  $\mu\text{m}$  in (C) and 5  $\mu\text{m}$  in (F). Mito: mitochondria, Syn I: synapsin I, a.u.: arbitrary units. The data are shown as mean  $\pm$  SEM. Statistical significance ( $p<0.05$ ) is denoted by an asterisk.

Accordingly, the proportion of active zones – a specialized portion of the presynaptic membrane to which synaptic vesicles dock and where they get primed for the release [34] – was greater in SkQ1-treated OXYS rats than in untreated OXYS rats (Fig. 6A). In this context, the increase in the proportion of large active zones in untreated OXYS rats (Fig. 6B) may reflect the processes of plastic reorganization directed at compensation for the regressive alterations of synaptic connections. Although in SkQ1-treated OXYS rats, the number of presynaptic active zones significantly increased (Fig. 6A, B), mostly due to medium active zones (300–500 nm), this change probably represents the mechanism of plastic reorganization of synapses and formation of new contacts among neurons. The result of the rearrangement of synaptic organization of the hippocampus in SkQ1-treated OXYS rats was an increased number of synaptic vesicles docked with the presynaptic membrane (Fig. 6C).

The conclusions of the morphometric assessment of the synaptic status were confirmed by the results of evaluation of SkQ1's influence on the hippocampal amounts of protein markers of pre- and postsynaptic density: synapsin I, participating in the regulation of the process of neurotransmitter release in synapses, and postsynaptic density protein 95 (PSD-95): the main protein of postsynaptic density. According to western blot analysis, the hippocampal level of both proteins in untreated OXYS rats was significantly lower (Fig. 6D, E) than that in Wistar rats. Prolonged administration of SkQ1 significantly increased the levels of synapsin I and PSD-95 in the hippocampus of OXYS rats (Fig. 6D, E), to the level of the Wistar strain. Finally, we immunolabeled tissue samples with anti-synapsin I and anti-PSD-95 antibodies to assess the effects of SkQ1 treatment on expression of the proteins (Fig. 6F). In the hippocampus, we observed decreased levels of synapsin I and PSD-95 in OXYS rats and no differences in these proteins' levels between SkQ1-treated OXYS rats and Wistar rats. Thus, these results indicate that chronic SkQ1 treatment probably not only ensured integrity of the existing neuronal connections but also promoted formation of new functionally active neuronal relations.

### **SkQ1 decreases amyloid- $\beta$ levels, tau hyperphosphorylation, and attenuates memory deficits**

Because progressive accumulation of toxic amyloid- $\beta$  species in the brain of OXYS rats starts at age 12 months [27-28], we tested whether treatment with SkQ1 since 12 months of age affects amyloid- $\beta_{1-40}$  and amyloid- $\beta_{1-42}$  levels in the hippocampus of 18-month-old OXYS rats. Enzyme immunoassay analysis of amyloid- $\beta_{1-40}$  and amyloid- $\beta_{1-42}$  (Fig. 7A) revealed

significantly increased levels of these polypeptides in OXYS rats compared to Wistar rats. SkQ1 significantly lowered the protein levels of amyloid- $\beta_{1-40}$  and amyloid- $\beta_{1-42}$  in OXYS rats, to the level of Wistar rats. Finally, we immunolabeled tissue samples with an anti-amyloid- $\beta_{1-42}$  antibody, to assess the influence of SkQ1 treatment on protein expression (Fig. 7B). In the hippocampus, we found increased amyloid- $\beta_{1-42}$  levels in OXYS rats and no differences in amyloid- $\beta_{1-42}$  content between SkQ1-treated OXYS rats and Wistar rats.

Because the levels of tau protein and of its phosphorylated form are increased in the brain of OXYS rats already at age 3 months [28], we then evaluated the ability of SkQ1 to slow down the hyperphosphorylation of tau protein in the hippocampus during progression of AD-like pathology. Western blot analysis of Tau and of its phosphorylated forms pT181, pS262, and pS396 (Fig. 7C, D) revealed significantly increased protein levels of all of the above in 18-month-old OXYS rats compared to Wistar rats. SkQ1 significantly lowered the protein expression of Tau, pT181, and pS262 in OXYS rats, to the level of Wistar rats (Fig. 7C, D).

Finally, we assessed hippocampus-dependent learning and memory of untreated or chronically SkQ1-treated OXYS rats in the Morris water maze as compared with Wistar rats. In the spatial (hidden-platform) component of the test, Wistar rats and SkQ1-treated OXYS rats learned better and faster than OXYS rats did (Fig. 7E). Moreover, untreated OXYS rats did not show any decrease in escape latency during the training. In addition, compared to Wistar rats, OXYS rats spent 2.5-fold less time in the target quadrant (Fig. 7F) on the sixth day (when the platform was removed); this is an indication of worsened reference memory. SkQ1-treated OXYS rats showed a significant decrease in escape latency already on the second trial day (Fig. 7E) and spent almost 2.5-fold as much time in the target quadrant on the sixth day (Fig. 7F) as compared to the untreated OXYS rats. Taken together, these data confirm our previous findings of increased amyloid- $\beta$  levels, tau hyperphosphorylation, and cognitive deficits in OXYS rats at the progressive stage of AD-like pathology [28] and indicate that chronic SkQ1 treatment attenuates these processes, by decreasing amyloid- $\beta$  levels and tau hyperphosphorylation and by restoring reference memory.

## **DISCUSSION**

The main purpose of this study was to assess the impact of mitochondrial dysfunction on the development of the sporadic form of AD using a nontransgenic rat model of this disease (the OXYS strain) and to test whether

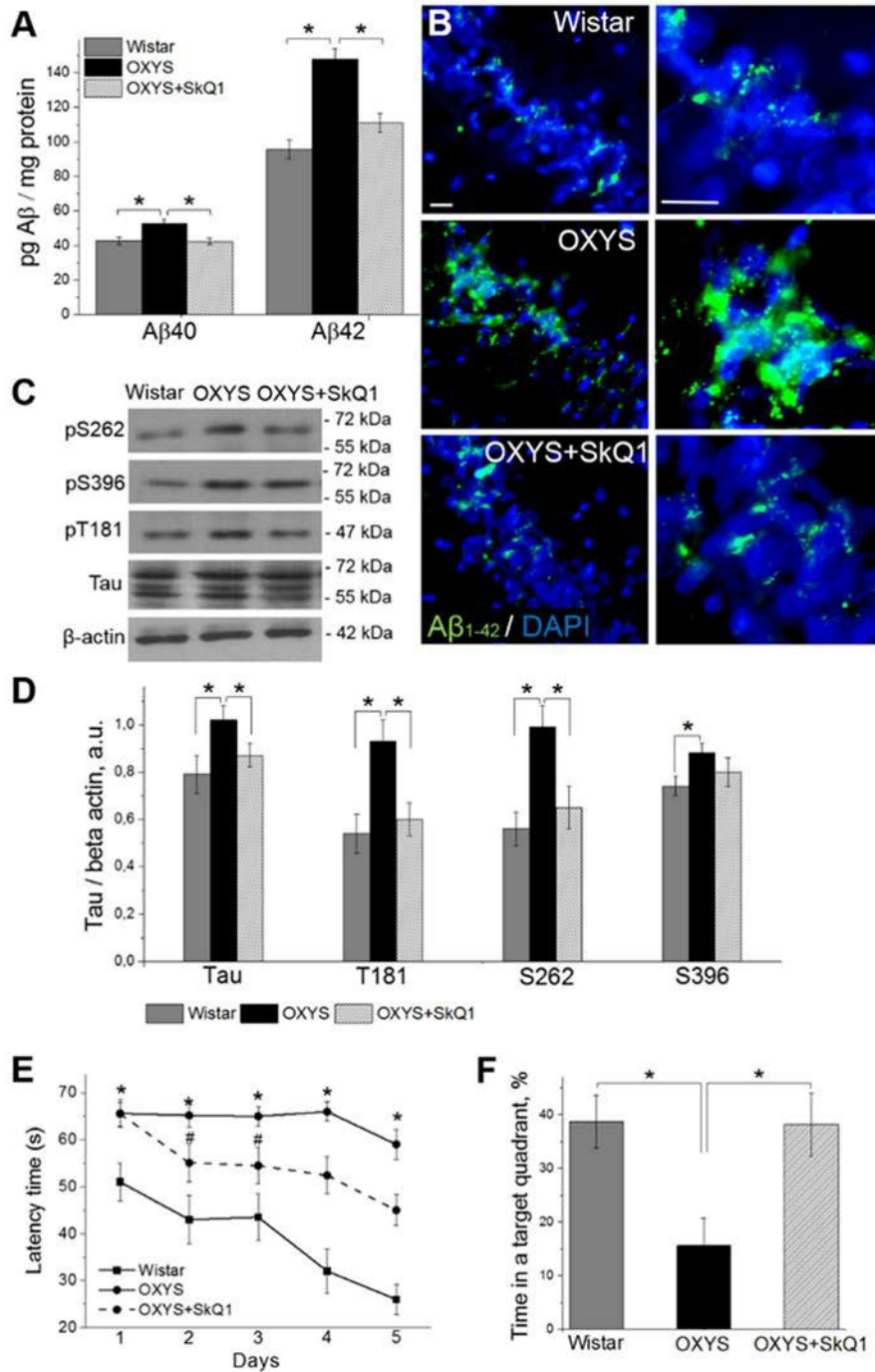


**Figure 7. SkQ1 decreases amyloid- $\beta$  levels and tau hyperphosphorylation and attenuates memory deficits. (A)** The increased levels of amyloid- $\beta_{1-40}$  and amyloid- $\beta_{1-42}$  in the hippocampus of untreated OXYS rats ( $n=8$ ;  $p<0.05$ ) were attenuated in response to SkQ1 treatment ( $p<0.05$ ). **(B)** Immunostaining for amyloid- $\beta_{1-42}$  ( $A\beta_{1-42}$  in green) in the hippocampus of Wistar rats, untreated OXYS rats, and SkQ1-treated OXYS rats. The DAPI (blue) staining shows cell nuclei. **(C and D)** The increased levels of Tau, pT181, pS262, and pS396 in the hippocampus of untreated OXYS rats ( $n=6$ ;  $p<0.05$ ) were significantly attenuated (except for pS396) in response to SkQ1 treatment ( $p<0.05$ ). **(E)** Compared to Wistar rats, OXYS rats ( $n=8$ ) showed increased escape latencies on all trial days ( $p<0.01$ ) and **(F)** spent less time in the target quadrant on the sixth day ( $p<0.05$ ). SkQ1 decreased escape latency of OXYS rats on the second trial day ( $p<0.02$ ) and increased the time spent by OXYS rats in the target northwest quadrant on the sixth day ( $p<0.02$ ). The scale bar is 5  $\mu$ m.  $A\beta$ : amyloid- $\beta$ , a.u.: arbitrary units. The data are shown as mean  $\pm$  SEM. \* $p<0.05$ ; # $p<0.05$  for effects of SkQ1.

correction of mitochondrial dysfunction by means of the mitochondria-targeted antioxidant SkQ1 is an effective way to slow AD. According to our past and present data, we believe that the development and progression of AD-like pathology in OXYS rats may be caused by mitochondrial dysfunction. Five lines of evidence support this conclusion.

First, the development of early disturbances in mitochondrial function in OXYS rats is indicated by the significant increase in the prevalence of a common deletion (4834 bp) in mitochondrial DNA (mtDNA), especially at the stage of completion of brain development in the postnatal period [35]; this event is much earlier than accumulation of toxic forms of amyloid- $\beta$  in the brain [28]. Meanwhile, the prevalence of mtDNA with the deletion in the hippocampus of OXYS rats stays elevated both at the stages preceding the development of signs of AD and during their progression. Accumulation of mtDNA deletions is considered one of the causes of the age-related decrease in the efficiency of oxidative phosphorylation. It also affects age-associated development of neurodegenerative diseases, including AD [36]. In particular, the lowered efficiency of the respiratory chain leads to enhanced accumulation of mtDNA deletions and oxidative damage to mtDNA; these processes may promote the buildup of toxic forms of amyloid- $\beta$ , including because of the disruption in the production/clearance balance of this protein [37].

Second, the expression profile of mitochondrial genes in the brain of OXYS rats is significantly different from that of normal control rats [38], including the possible mitochondrial energy deficiency.

Third, enzymatic activity of complexes of the respiratory chain is decreased, and biosynthetic processes are aberrant in the hippocampus of old OXYS rats. Downregulation of oxidative phosphorylation and functional insufficiency of the fusion/fission system of mitochondria (associated with the development of AD) trigger mitochondrial disorders and activation of apoptotic processes. Both high activity of mitophagy in neurons and weakened elimination of mitochondria with structural or functional disturbances tend to shift the balance between functionally normal and defective mitochondria in favor of the latter [39-42].

Fourth, OXYS rats have (increasing with age) structural and functional mitochondrial alterations, detectable in various tissues and cells [20-22, 28, 31, 43-44], pointing to systemic disturbances in mitochondrial function; these problems can result in accelerated aging.

And fifth, treatment with the mitochondria-targeted

antioxidant SkQ1 slows the development and progression of age-dependent diseases in OXYS rats [16-23], including AD-like pathology [24-25]. Recently, we showed that treatment of OXYS rats with SkQ1—starting at a young age—protected the rats from accumulation of mtDNA deletions in the hippocampus [35] and from neurodegeneration [25].

The main finding in the present study is that restoration of mitochondrial function by means of SkQ1 prevents and/or significantly slows the development of all signs of AD-like pathology in OXYS rats in the period of its active progression. We found that the proportion of damaged neurons in the hippocampus of SkQ1-treated OXYS rats was significantly smaller than that in untreated OXYS rats and was not different from this proportion in the Wistar strain. At the same time, according to analysis of the ultrastructural state of pyramidal neurons in the hippocampal CA1 region, in SkQ1-treated OXYS rats, there was a significant improvement of structural organization of organelles as well as increased specific area of mitochondria and endoplasmic reticulum, with decreased specific area of lysosomes and vacuoles. Our results revealed that SkQ1 did not affect the level of total BDNF in the OXYS hippocampus but upregulated mBDNF and downregulated proBDNF; these changes are suggestive of a shift in the proBDNF/mBDNF balance in favor of the mature form of the protein. Indeed, the increased phospho-TrkB/TrkB ratio and normalization of the balance of mature/immature forms of BDNF in the hippocampus of SkQ1-treated OXYS rats reflects activation of cellular processes promoting the growth of neurites, formation of new synapses, and neuronal survival.

The progression of AD-like pathology in OXYS rats is linked with substantial structural and functional alterations of synapses and with decreased synaptic density [31, 45]. Administration of SkQ1 not only ensured preservation of numerical density of synapses in the hippocampus of OXYS rats but, possibly, also facilitated activation of the remaining undamaged neurons and synapses and improved intraneuronal processes and axonal transport. This notion is supported by the increased proportion of asymmetric (excitatory) synapses and a greater number of active zones of synaptic contact as well as upregulation of pre- and postsynaptic proteins synapsin I and PSD-95, whose downregulation is considered an indicator event in AD [46-47].

We found that supplementation with SkQ1 in OXYS rats during active progression of AD-like pathology substantially improved their cognitive abilities, possibly as a result of the unique ability of SkQ1 to restore the

processes of synaptic plasticity (as demonstrated in this study), not so much as a result of amyloid- $\beta$  downregulation. Our hypothesis is that the pathogenesis of the familial form of AD differs from that of the sporadic form of this disease. We obtained additional evidence that the consequence of toxic accumulation of amyloid- $\beta$  (in the brain of patients with the familial form of AD) is a disruption of A $\beta$ PP processing, whereas in patients with the sporadic form of AD, the accumulation of amyloid- $\beta$  can be mediated by synaptic processes [48]. Lately, the decisive role in progression of AD is attributed to trans-synaptic migration of toxic amyloid- $\beta$  under the conditions of reorganization of interneuronal connections [49].

It should be emphasized that accumulation of amyloid- $\beta$  in the brain of OXYS rats is a secondary event during the development of AD signs [28]. Manifestation of behavioral aberrations and deterioration of cognitive abilities in OXYS rats take place during mitochondrial dysfunction and hyperphosphorylation of tau protein [25, 27-28, 31]. Oxidative stress, chronic inflammation, and cellular stress are conducive to hyperphosphorylation of tau protein [50-53], whose consequence is disturbances of axonal transport [54]. These alterations can lead to destructive changes in axons, accumulation of damaged mitochondria there (mitochondrial abnormalities) and of other defective organelles [55-56], as we frequently saw in the hippocampus of 18-month-old untreated OXYS rats and in rare cases, in Wistar rats and in SkQ1-treated OXYS rats. Recently, in OXYS rats, we uncovered signs structural disturbances of myelin fibers of axons, structural changes in microtubules, and their disarray [31], which, to a substantial extent, can be a consequence of hyperphosphorylation of tau protein, as we demonstrated previously [25, 27-28] and in the present work. The neurotoxic action of tau protein can be mediated by amyloid- $\beta$ , which promotes enhanced phosphorylation of tau protein and therefore, formation of neurofibrillary tangles via activation of kinases Cdk5 and GSK3b and by activating caspase 3, caspase 9, and calpain [57-58]. As shown in our previous studies, progression of the signs of AD in OXYS rats is accompanied by downregulation of the *Gsk3b* gene's mRNA in the cortex and increased mRNA expression of genes *Cdk5*, *Casp9*, and *Capn1*; these changes may also be triggered by the toxic forms of amyloid- $\beta$  from neurodegenerative processes [38]. On the basis of the present results, we can hypothesize that the observed substantial improvement in the structure of myelin fibers and in the structure and organization of microtubules in SkQ1-treated OXYS rats are related to the ability of this antioxidant to attenuate the age-associated enhancement of tau protein phosphorylation; the latter improvement

apparently led to normalization of transport pathways in cerebral neurons.

Studies involving primary neuronal cultures and hippocampal slices from A $\beta$ PP transgenic mice showed that mitochondria-targeted antioxidants can prevent and/or slow down the amyloid- $\beta$ -driven increase in ROS production, mitochondrial aberrations, disturbances of long-term post-tetanic potentiation, and neuronal death [59-61]. The ability of SkQ1 to slow down toxic effects of exogenous amyloid- $\beta$  on formation of long-term post-tetanic potentiation in the hippocampus has also been demonstrated *in vitro* as well as *in vivo* [62]. Previously, we have shown that prophylactic dietary supplementation with SkQ1, starting before the manifestation of AD-like pathology (at the age of 1.5 months), significantly suppresses the accumulation of toxic forms of amyloid- $\beta$  in the OXYS rats' brain and inhibits the development of all other signs of the disease [25]. Here, for the first time, we showed the ability of SkQ1 to suppress their development in elderly OXYS rats during active progression of AD-like pathology.

We cannot name the specific mechanisms of action of SkQ1 today, but the focus of this study is on the novel finding (by means of SkQR1) that dietary supplementation with SkQ1 allows this compound to penetrate and accumulate in the mitochondria of cerebral neurons. Earlier, effective penetration of SkQR1 into brain structures was shown only for its intranasal administration [63]. We can assume that the effects of SkQ1 are due to a direct antioxidant effect [64] as well as the ability to suppress mitochondrial production of ROS, and thereby to enhance the fatty-acid-driven mild decoupling of oxidation and phosphorylation [65]. We can also speculate that the effects of SkQ1, like those of another powerful neuroprotector, melatonin [31; 66], which are considered in recent years as a mitochondria-targeted antioxidant, are mediated by improved coordination of cellular signaling pathways responsible for tissue homeostasis [67]. In any case, this hypothesis is supported by the improved structural and functional state of mitochondria (and neurons on the whole) in SkQ1-treated OXYS rats as well as downregulation of amyloid- $\beta$  and of tau protein hyperphosphorylation, recovery of synaptic processes and as a consequence, restoration of cognitive functions.

Thus, although the specific mechanisms of action of SkQ1 remain unclear, the fact that it specifically restores mitochondrial function and inhibits the development and progression of AD in a rat model is a compelling argument for its testing in clinical strategies

targeting mitochondria for prevention and possibly treatment of this disease.

## MATERIALS AND METHODS

### Compounds

SkQ1 and SkQR1 (a rhodamine derivative of the former: SkQ1 decylrhodamine 19) were synthesized and provided by the Institute of Mitoengineering of Moscow State University (Moscow, Russia).

### Animal treatments

All experimental procedures were in compliance with the European Communities Council Directive of 24 November 1986 (86/609/EEC). The protocol of the animal study was approved by the Commission on Bioethics of the Institute of Cytology and Genetics, Novosibirsk, Russia. Male senescence-accelerated OXYS rats and Wistar rats were obtained from the Center for Genetic Resources of Laboratory Animals at the Institute of Cytology and Genetics, the Siberian Branch of the Russian Academy of Sciences (RFMEFI61914X0005 and RFMEFI61914X0010). The OXYS strain was derived from the Wistar strain of rats at the Institute of Cytology and Genetics as described earlier [24] and was registered in the Rat Genome Database (<http://rgd.mcw.edu/>). At this point, we have the 109<sup>th</sup> generation of OXYS rats, with spontaneously developing cataract and accelerated senescence syndrome inherited in a linked manner.

At the age of 4 weeks, the pups were weaned, housed in groups of five animals per cage (57 × 36 × 20 cm), and kept under standard laboratory conditions (22°C ± 2°C, 60% relative humidity, and 12-hour light/12-hour dark cycle; lights on at 9 a.m.). The animals were provided with standard rodent feed (PK-120-1; LaboratorSnab, Ltd., Moscow, Russia) and water *ad libitum*.

To assess the influence of oral SkQ1 administration (from age 12 to 18 months) on progression of AD-like pathology, 12-month-old male OXYS rats were randomly assigned to one of two groups (n=15). One group consumed a control diet with addition of dried bread slices, and the other the same diet supplemented with SkQ1 (250 nmol/[kg body weight]) on the dried bread slices. Each rat in the treatment group received SkQ1 daily. As controls, we used a group of Wistar rats (n=15).

To assess the localization and accumulation of SkQ1 in the brain by means of SkQR1, 4-month-old OXYS rats were randomly assigned to one of four groups (n=4). Two groups consumed a control diet supplemented with

dried bread slices for 7 days or 14 days. The other two groups consumed the same diet supplemented with SkQR1 (250 nmol/kg) for 7 days or 14 days, respectively.

After treatment with SkQR1 in the 4.2- to 4.5-month-old cohorts, and after behavioral testing in the 18-month-old cohort, the rats were euthanized via CO<sub>2</sub> asphyxiation. In both series of experiments, brains were carefully excised, and hemispheres were separated along the midline. For histological and immunohistochemical assays, the hemispheres were immediately fixed in 4% paraformaldehyde in phosphate-buffered saline. Fixed hemispheres were sliced at 5 or 20 μm (n=4-5; 4–6 serial tissue sections per animal) using a Microm HM-505 N cryostat. For western blot analysis and an enzyme-linked immunosorbent assay (ELISA), the hippocampus of 18-month-old rats (n=6-8) was separated from the brain, placed in a microcentrifuge tube for protein isolation, and frozen in liquid nitrogen. For assays of activities of mitochondrial complexes I and IV, the mitochondrial fraction was isolated from the rat hippocampus. For electron microscopic examination, the hippocampus samples (n=4) were fixed with 2.5% glutaraldehyde in sodium cacodylate buffer.

### Western blotting

Immunoblotting was performed as previously described [28]. Antibodies and dilutions used in this study include: anti-TrkB (1:1000; # ab18987, Abcam), anti-phospho-TrkB (phTrkB Y817; 1:1000; # ab81288, Abcam), anti-synapsin I (1:1000; # ab64581, Abcam), anti-PSD-95 (1:1000; # ab12093, Abcam), anti-tau (1:1000; # ab75714, Abcam), anti-phospho-tau (phospho T181; 1:1000; # ab75679, Abcam), anti-phospho-tau (phospho S262; 1:1000; # ab131354, Abcam), anti-phospho-tau (phospho S396; 1:1000; # ab109390, Abcam), and anti-β-actin (1:1000; # ab1801, Abcam). Quantitative densitometric analyses were performed on digitized images of immunoblots in the ImageJ software (NIH, USA).

### ELISAs

ELISAs for BDNF (BDNF [Rat] ELISA Kit; #KA0330, Abnova), for amyloid-β<sub>1-40</sub> (Human/Rat ELISA Kit; # 294-62501, Wako), and for amyloid-β<sub>1-42</sub> (Human/Rat ELISA Kit; # 290-62601, Wako) were performed on the isolated protein samples. Quantitation was carried out by measuring optical density on a microtiter plate reader, and the concentration was calculated in picograms of BDNF per milligram of hippocampal tissue or in picograms of amyloid-β<sub>1-40</sub> or amyloid-β<sub>1-42</sub> protein per milligram of total protein of hippocampal tissue.

## Assays of activity of mitochondrial complexes I and IV

Mitochondrial complex I activity was determined with the Complex I Rodent Enzyme Activity Microplate Assay Kit (# ab109721, Abcam) by quantifying oxidation of NADH to NAD<sup>+</sup> and the simultaneous reduction of a dye, which causes an absorbance increase at 450 nm within 30 min using a CLARIO Star spectrophotometer (BMGLabtech). The Mitochondrial Complex IV Rodent Enzyme Activity Microplate Assay Kit (# ab109911, Abcam) was used to determine the activity of cytochrome c oxidase by quantifying oxidation of reduced cytochrome c using the absorbance change at 550 nm within 2 hours by means of CLARIO Star. The linear rate was examined, and enzymatic activity was expressed as an optic density (OD) alteration rate (OD/min) per  $\mu\text{g}$  of the isolated protein samples added per well.

## Histological examination

This analysis was performed as described elsewhere [31]. For the estimates of neuron numbers and to evaluate morphological features of the neurons in the middle molecular layer of the dentate gyrus, and CA1 and CA3 pyramidal layer, a set of 4–6 serial sections from each animal was used. A 100 $\times$  objective lens (Axioplan 2, Zeiss) was used to count >200 neurons per visual field. The dead and damaged neurons were identified by their morphological features. The data were presented as a percentage of normal (no change), damaged, and dead neurons among all neurons in each visual field of a hippocampus sample. We measured the average area of the body and nucleus of the neurons per  $\text{mm}^2$ . Images of the same region of the hippocampus were analyzed using the ImageJ software.

## Immunofluorescent staining

This procedure was performed by a standard indirect method as described previously [28]. Primary antibodies and dilutions were as follows: anti-COX IV (1:250; # ab16056, Abcam), anti-DRP1 (1:250; # ab56788, Abcam), anti-Mfn2 (1:250; # ab50838, Abcam), anti-proBDNF (1:250; # ab72440, Abcam), anti-mBDNF (1:250; # GF35L, Millipore), anti-TrkB (1:250; # ab18987, Abcam), anti-phospho-TrkB (phospho TrkB Y817; 1:250; # ab81288, Abcam), anti-p75<sup>NTR</sup> (1:250; # ab93934, Abcam), anti-synapsin I (1:250; # ab64581, Abcam), anti-PSD-95 (1:250; # ab12093, Abcam), and anti-amyloid beta peptide (MOAB-2; 1:250; # MABN254, Millipore). After incubation with the respective secondary antibodies DyLight-650 or Alexa Fluor 488 (## ab96886,

ab150073, Abcam) diluted 1:250, the slices were coverslipped with the Fluoro-shield mounting medium containing 4',6-diamidino-2-phenylindole (DAPI; # ab104139, Abcam) and examined under an Axioplan 2 microscope (Zeiss).

## Electron-microscopic examination

The hippocampal samples of rats were prepared as described elsewhere [31]. For quantitative analysis, electron-transparent regions were identified on the electron micrographs of synapses and pyramidal neurons of the CA1 region (30 photos per animal). Then, all organelles that are located in these regions were painted using software. The photos were processed in Adobe Photoshop; for each photo, the following parameter was determined: the total area of each type of organelle located in the electron-transparent areas of the neurons. Then, the organelle-occupied proportion of the neuron area was calculated. We determined the number of interneuronal contacts (per visual field of  $50 \mu\text{m}^2$ ) and calculated the numerical density of synapses per  $100 \mu\text{m}^2$ . Asymmetrical and symmetrical synapses were also counted. The synapses were classified (by the length of the active contact zone) into small (<300 nm), medium (300–500 nm), large (500–700 nm), and very large (>700 nm).

## Cognitive testing

The Morris water maze test [68] was used to analyze spatial memory: the rats ( $n=7$ ) had to find a submerged platform in a pool of water, using external visual cues. Behavioral testing was carried out from 17.5 to 18 months of age as described previously [25].

## Statistical analysis

The data were subjected to ANOVA (Statistica 8.0 software). The Newman–Keuls test was applied to significant main effects and interactions in order to assess the differences between some sets of means. The data were presented as mean  $\pm$  SEM. The differences were considered statistically significant at  $p<0.05$ .

## ACKNOWLEDGEMENTS

The experiments on cognitive abilities and neurochemistry in OXYS and Wistar rats were supported by grants from the Russian Foundation for Basic Research (15-04-01938 and 15-04-06066), whereas the histological examination and electron-microscopic analysis were supported by a Russian Scientific Foundation grant (16-15-10005).

## CONFLICTS OF INTEREST

The authors declare no conflicts of interest.

## REFERENCES

1. Feng Y, Wang X. Antioxidant therapies for Alzheimer's disease. *Oxid Med Cell Longev*. 2012; 2012:472932. doi:10.1155/2012/472932
2. Hardy JA, Higgins GA. Alzheimer's disease: the amyloid cascade hypothesis. *Science*. 1992; 256:184–85. doi:10.1126/science.1566067
3. Morley JE, Armbrecht HJ, Farr SA, Kumar VB. The senescence accelerated mouse (SAMP8) as a model for oxidative stress and Alzheimer's disease. *Biochim Biophys Acta*. 2012; 1822:650–56.
4. Schon EA, Area-Gomez E. Mitochondria-associated ER membranes in Alzheimer disease. *Mol Cell Neurosci*. 2013; 55:26–36. doi: 10.1016/j.mcn.2012.07.011
5. Krstic D, Knuesel I. Deciphering the mechanism underlying late-onset Alzheimer disease. *Nat Rev Neurol*. 2013; 9:25–34. doi:10.1038/nrneurol.2012.236
6. Castellano JM, Deane R, Gottesdiener AJ, Verghese PB, Stewart FR, West T, Paoletti AC, Kasper TR, DeMattos RB, Zlokovic BV, Holtzman DM. Low-density lipoprotein receptor overexpression enhances the rate of brain-to-blood A $\beta$  clearance in a mouse model of  $\beta$ -amyloidosis. *Proc Natl Acad Sci USA*. 2012; 109:15502–07. doi: 10.1073/pnas.1206446109
7. Swerdlow RH, Khan SM. A “mitochondrial cascade hypothesis” for sporadic Alzheimer's disease. *Med Hypotheses*. 2004; 63:8–20. doi: 10.1016/j.mehy.2003.12.045
8. Swerdlow RH, Burns JM, Khan SM. The Alzheimer's disease mitochondrial cascade hypothesis: progress and perspectives. *Biochim Biophys Acta*. 2014; 1842:1219–31. doi:10.1016/j.bbadis.2013.09.010
9. Mattson MP. Pathways towards and away from Alzheimer's disease. *Nature*. 2004; 430:631–39. doi: 10.1038/nature02621
10. Grimm A, Friedland K, Eckert A. Mitochondrial dysfunction: the missing link between aging and sporadic Alzheimer's disease. *Biogerontology*. 2016; 17:281–96. doi:10.1007/s10522-015-9618-4
11. Skulachev VP. Mitochondria-targeted antioxidants as promising drugs for treatment of age-related brain diseases. *J Alzheimers Dis*. 2012; 28:283–89.
12. Neroev VV, Archipova MM, Bakeeva LE, Fursova AZ, Grigorian EN, Grishanova AY, Iomdina EN, Ivashchenko ZN, Katargina LA, Khoroshilova-Maslova IP, Kilina OV, Kolosova NG, Kopenkin EP, et al. Mitochondria-targeted plastoquinone derivatives as tools to interrupt execution of the aging program. 4. Age-related eye disease. SkQ1 returns vision to blind animals. *Biochemistry (Mosc)*. 2008; 73:1317–28. doi: 10.1134/S0006297908120043
13. Skulachev VP, Anisimov VN, Antonenko YN, Bakeeva LE, Chernyak BV, Elichev VP, Filenko OF, Kalinina NI, Kapelko VI, Kolosova NG, Kopnin BP, Korshunova GA, Lichinitser MR. An attempt to prevent senescence: a mitochondrial approach. *Biochim Biophys Acta*. 2009; 1787:437–61.
14. Plotnikov EY, Morosanova MA, Pevzner IB, Zorova LD, Manskikh VN, Pulkova NV, Galkina SI, Skulachev VP, Zorov DB. Protective effect of mitochondria-targeted antioxidants in an acute bacterial infection. *Proc Natl Acad Sci USA*. 2013; 110:E3100–08. doi: 10.1073/pnas.1307096110
15. Weidinger A, Müllebnner A, Paier-Pourani J, Banerjee A, Miller I, Lauterböck L, Duvigneau JC, Skulachev VP, Redl H, Kozlov AV. Vicious inducible nitric oxide synthase-mitochondrial reactive oxygen species cycle accelerates inflammatory response and causes liver injury in rats. *Antioxid Redox Signal*. 2015; 22:572–86. doi:10.1089/ars.2014.5996
16. Obukhova LA, Skulachev VP, Kolosova NG. Mitochondria-targeted antioxidant SkQ1 inhibits age-dependent involution of the thymus in normal and senescence-prone rats. *Aging (Albany NY)*. 2009; 1:389–401. doi:10.18632/aging.100043
17. Amstislavskaya TG, Maslova LN, Gladkikh DV, Belousova II, Stefanova NA, Kolosova NG. Effects of the mitochondria-targeted antioxidant SkQ1 on sexually motivated behavior in male rats. *Pharmacol Biochem Behav*. 2010; 96:211–16. doi: 10.1016/j.pbb.2010.05.007
18. Markovets AM, Fursova AZ, Kolosova NG. Therapeutic action of the mitochondria-targeted antioxidant SkQ1 on retinopathy in OXYS rats linked with improvement of VEGF and PEDF gene expression. *PLoS One*. 2011; 6:e21682. doi: 10.1371/journal.pone.0021682
19. Kolosova NG, Stefanova NA, Muraleva NA, Skulachev VP. The mitochondria-targeted antioxidant SkQ1 but not N-acetylcysteine reverses aging-related biomarkers in rats. *Aging (Albany NY)*. 2012; 4:686–94. doi:10.18632/aging.100493

20. Kolosova NG, Stefanova NA, Korbolina EE, Fursova AZ, Kozhevnikova OS. Senescence-accelerated OXYS rats: A genetic model of premature aging and age-related diseases. *Adv Gerontol.* 2014;4:294–98. doi: 10.1134/S2079057014040146
21. Saprunova VB, Lelekova MA, Kolosova NG, Bakeeva LE. SkQ1 slows development of age-dependent destructive processes in retina and vascular layer of eyes of wistar and OXYS rats. *Biochemistry (Mosc).* 2012; 77:648–58. doi:10.1134/S0006297912060120
22. Vays VB, Eldarov CM, Vangely IM, Kolosova NG, Bakeeva LE, Skulachev VP. Antioxidant SkQ1 delays sarcopenia-associated damage of mitochondrial ultrastructure. *Aging (Albany NY).* 2014; 6:140–48. doi: 10.18632/aging.100636
23. Rumyantseva YV, Ryabchikova EI, Fursova AZ, Kolosova NG. Ameliorative effects of SkQ1 eye drops on cataractogenesis in senescence-accelerated OXYS rats. *Graefes Arch Clin Exp Ophthalmol.* 2015; 253:237–48. doi:10.1007/s00417-014-2806-0
24. Stefanova NA, Fursova AZ, Kolosova NG. Behavioral effects induced by mitochondria-targeted antioxidant SkQ1 in Wistar and senescence-accelerated OXYS rats. *J Alzheimers Dis.* 2010; 21: 479–91.
25. Stefanova NA, Muraleva NA, Skulachev VP, Kolosova NG. Alzheimer’s disease-like pathology in senescence-accelerated OXYS rats can be partially retarded with mitochondria-targeted antioxidant SkQ1. *J Alzheimers Dis.* 2014;38:681–94.
26. Kozhevnikova OS, Korbolina EE, Stefanova NA, Muraleva NA, Orlov YL, Kolosova NG. Association of AMD-like retinopathy development with an Alzheimer’s disease metabolic pathway in OXYS rats. *Biogerontology.* 2013;14:753–62. doi: 10.1007/s10522-013-9439-2
27. Stefanova NA, Kozhevnikova OS, Vitovtov AO, Maksimova KY, Logvinov SV, Rudnitskaya EA, Korbolina EE, Muraleva NA, Kolosova NG. Senescence-accelerated OXYS rats: a model of age-related cognitive decline with relevance to abnormalities in Alzheimer disease. *Cell Cycle.* 2014; 13:898–909. doi: 10.4161/cc.28255
28. Stefanova NA, Muraleva NA, Korbolina EE, Kiseleva E, Maksimova KY, Kolosova NG. Amyloid accumulation is a late event in sporadic Alzheimer’s disease-like pathology in nontransgenic rats. *Oncotarget.* 2015;6:1396–413. doi: 10.18632/oncotarget.2751
29. Brun A, Englund E. Regional pattern of degeneration in Alzheimer’s disease: neuronal loss and histopathological grading. *Histopathology.* 1981; 5:549–64. doi: 10.1111/j.1365-2559.1981.tb01818.x
30. Wright AL, Zinn R, Hohensinn B, Konen LM, Beynon SB, Tan RP, Clark IA, Abdipranoto A, Vissel B. Neuroinflammation and neuronal loss precede Ab plaque deposition in the hAPP-J20 mouse model of Alzheimer’s disease. *PLoS One.* 2013;8:1–14. doi: 10.1371/journal.pone.0059586
31. Stefanova NA, Maksimova KY, Kiseleva E, Rudnitskaya EA, Muraleva NA, Kolosova NG. Melatonin attenuates impairments of structural hippocampal neuro-plasticity in OXYS rats during active progression of Alzheimer’s disease-like pathology. *J Pineal Res.* 2015;59:163–77. doi: 10.1111/jpi.12248
32. Rudnitskaya EA, Maksimova KY, Muraleva NA, Logvinov SV, Yanshole LV, Kolosova NG, Stefanova NA. Beneficial effects of melatonin in a rat model of sporadic Alzheimer’s disease. *Biogerontology.* 2015; 16:303–16. doi:10.1007/s10522-014-9547-7
33. Beregovoy NA, Sorokina NS, Starostina MV, Kolosova NG. Age-specific peculiarities of formation of long-term posttetanic potentiation in OXYS rats. *Bull Exp Biol Med.* 2011; 151:71–73. doi: 10.1007/s10517-011-1262-7
34. Harris KM, Weinberg RJ. Ultrastructure of synapses in the mammalian brain. *Cold Spring Harb Perspect Biol.* 2012;4:a005587. doi: 10.1101/cshperspect.a005587
35. Loshchenova PS, Sinityna OI, Fedoseeva LA, Stefanova NA, Kolosova NG. Influence of antioxidant SkQ1 on accumulation of mitochondrial DNA deletions in the hippocampus of senescence-accelerated OXYS rats. *Biochemistry (Mosc).* 2015;80:596–603. doi: 10.1134/S0006297915050120
36. Krishnan KJ, Ratnaike TE, De Gruyter HL, Jaros E, Turnbull DM. Mitochondrial DNA deletions cause the biochemical defect observed in Alzheimer’s disease. *Neurobiol Aging.* 2012;33:2210–14. doi: 10.1016/j.neurobiolaging.2011.08.009
37. Mawuenyega KG, Sigurdson W, Ovod V, Munsell L, Kasten T, Morris JC, Yarasheski KE, Bateman RJ. Decreased clearance of CNS beta-amyloid in Alzheimer’s disease. *Science.* 2010; 330:1774. doi: 10.1126/science.1197623
38. Stefanova NA, Korbolina EE, Ershov NI, Rogaev EI, Kolosova NG. Changes in the transcriptome of the prefrontal cortex of OXYS rats as the signs of Alzheimer’s disease development. *Vavilov Journal of Genetics and Breeding.* 2015; 19:74–82. doi: 10.18699/VJ15.059

39. Sullivan PG, Dragicevic NB, Deng JH, Bai Y, Dimayuga E, Ding Q, Chen Q, Bruce-Keller AJ, Keller JN. Proteasome inhibition alters neural mitochondrial homeostasis and mitochondria turnover. *J Biol Chem.* 2004;279:20699–707. doi: 10.1074/jbc.M313579200
40. Lee CS, Han ES, Han YS, Bang H. Differential effect of calmodulin antagonists on MG132-induced mitochondrial dysfunction and cell death in PC12 cells. *Brain Res Bull.* 2005;67:225–34. doi: 10.1016/j.brainresbull.2005.07.003
41. Sierra A, Gottfried-Blackmore AC, McEwen BS, Bulloch K. Microglia derived from aging mice exhibit an altered inflammatory profile. *Glia.* 2007; 55:412–24. doi:10.1002/glia.20468
42. Navarro A, Boveris A. Brain mitochondrial dysfunction and oxidative damage in Parkinson's disease. *J Bioenerg Biomembr.* 2009;41:517–21. doi: 10.1007/s10863-009-9250-6
43. Shabalina IG, Kolosova NG, Grishanova AI, Solov'ev VN, Salganik RI, Solov'eva NA. [Oxidative phosphorylation activity, F0F1-ATPase and level of liver mitochondrial cytochromes in rats with congenitally increased ability for free radical formation]. *Biokhimiia.* 1995;60:2045–52.
44. Kolosova NG, Aidagulova SV, Nepomnyashchikh GI, Shabalina IG, Shalbueva NI. Dynamics of structural and functional changes in hepatocyte mitochondria of senescence-accelerated OXYS rats. *Bull Exp Biol Med.* 2001;132:814–19. doi: 10.1023/A:1013014919721
45. Maksimova KY, Logvinov SV, Stefanova NA. Ultrastructure of synapses in the hippocampus of rats in aging. *Bull Siberian Medicine.* 2014;13:49–54.
46. Gylys KH, Fein JA, Yang F, Wiley DJ, Miller CA, Cole GM. Synaptic changes in Alzheimer's disease: increased amyloid-beta and gliosis in surviving terminals is accompanied by decreased PSD-95 fluorescence. *Am J Pathol.* 2004;165:1809–17. doi: 10.1016/S0002-9440(10)63436-0
47. Scheff SW, Neltner JH, Nelson PT. Is synaptic loss a unique hallmark of Alzheimer's disease? *Biochem Pharmacol.* 2014;88:517–28. doi: 10.1016/j.bcp.2013.12.028
48. Shinohara M, Fujioka S, Murray ME, Wojtas A, Baker M, Rovelet-Lecrux A, Rademakers R, Das P, Parisi JE, Graff-Radford NR, Petersen RC, Dickson DW, Bu G. Regional distribution of synaptic markers and APP correlate with distinct clinicopathological features in sporadic and familial Alzheimer's disease. *Brain.* 2014; 137: 1533–49. doi:10.1093/brain/awu046
49. Spires-Jones TL, Hyman BT. The intersection of amyloid beta and tau at synapses in Alzheimer's disease. *Neuron.* 2014;82:756–71. doi: 10.1016/j.neuron.2014.05.004
50. Zhu X, Raina AK, Perry G, Smith MA. Alzheimer's disease: the two-hit hypothesis. *Lancet Neurol.* 2004; 3:219–26. doi:10.1016/S1474-4422(04)00707-0
51. Gómez-Ramos A, Díaz-Nido J, Smith MA, Perry G, Avila J. Effect of the lipid peroxidation product acrolein on tau phosphorylation in neural cells. *J Neurosci Res.* 2003;71:863–70. doi: 10.1002/jnr.10525
52. Lovell MA, Xiong S, Xie C, Davies P, Markesbery WR. Induction of hyperphosphorylated tau in primary rat cortical neuron cultures mediated by oxidative stress and glycogen synthase kinase-3. *J Alzheimers Dis.* 2004;6:659–71.
53. Krstic D, Madhusudan A, Doehner J, Vogel P, Notter T, Imhof C, Manalastas A, Hilfiker M, Pfister S, Schwerdel C, Riether C, Meyer U, Knuesel I. Systemic immune challenges trigger and drive Alzheimer-like neuropathology in mice. *J Neuroinflammation.* 2012; 9:151. doi:10.1186/1742-2094-9-151
54. Kanaan NM, Morfini GA, LaPointe NE, Pigino GF, Patterson KR, Song Y, Andreadis A, Fu Y, Brady ST, Binder LI. Pathogenic forms of tau inhibit kinesin-dependent axonal transport through a mechanism involving activation of axonal phosphotransferases. *J Neurosci.* 2011;31:9858–68. doi: 10.1523/JNEUROSCI.0560-11.2011
55. Shemesh OA, Erez H, Ginzburg I, Spira ME. Tau-induced traffic jams reflect organelles accumulation at points of microtubule polar mismatching. *Traffic.* 2008;9:458–71. doi: 10.1111/j.1600-0854.2007.00695.x
56. Shahpasand K, Uemura I, Saito T, Asano T, Hata K, Shibata K, Toyoshima Y, Hasegawa M, Hisanaga S. Regulation of mitochondrial transport and inter-microtubule spacing by tau phosphorylation at the sites hyperphosphorylated in Alzheimer's disease. *J Neurosci.* 2012;32:2430–41. doi: 10.1523/JNEUROSCI.5927-11.2012
57. Chung CW, Song YH, Kim IK, Yoon WJ, Ryu BR, Jo DG, Woo HN, Kwon YK, Kim HH, Gwag BJ, Mook-Jung IH, Jung YK. Proapoptotic effects of tau cleavage product generated by caspase-3. *Neurobiol Dis.* 2001; 8:162–72. doi:10.1006/nbdi.2000.0335
58. Cho JH, Johnson GV. Glycogen synthase kinase 3 beta induces caspase-cleaved tau aggregation in situ. *J Biol Chem.* 2004;279:54716–23. doi: 10.1074/jbc.M403364200

59. Manczak M, Mao P, Calkins MJ, Cornea A, Reddy AP, Murphy MP, Szeto HH, Park B, Reddy PH. Mitochondria-targeted antioxidants protect against amyloid-beta toxicity in Alzheimer's disease neurons. *J Alzheimers Dis.* 2010 (Suppl 2);20:S609–31.
60. Ma T, Hoeffler CA, Wong H, Massaad CA, Zhou P, Iadecola C, Murphy MP, Pautler RG, Klann E. Amyloid  $\beta$ -induced impairments in hippocampal synaptic plasticity are rescued by decreasing mitochondrial superoxide. *J Neurosci.* 2011; 31:5589–95. doi: 10.1523/JNEUROSCI.6566-10.2011
61. Calkins MJ, Manczak M, Reddy PH. Mitochondria-targeted antioxidant SS31 prevents amyloid beta-induced mitochondrial abnormalities and synaptic degeneration in Alzheimer's disease. *Pharmaceuticals (Basel).* 2012;5:1103–19. doi: 10.3390/ph5101103
62. Kapay NA, Popova OV, Isaev NK, Stelmashook EV, Kondratenko RV, Zorov DB, Skrebitsky VG, Skulachev VP. Mitochondria-targeted plastoquinone antioxidant SkQ1 prevents amyloid- $\beta$ -induced impairment of long-term potentiation in rat hippocampal slices. *J Alzheimers Dis.* 2013;36:377–83.
63. Silachev DN, Plotnikov EY, Zorova LD, Pevzner IB, Sumbatyan NV, Korshunova GA, Gulyaev MV, Pirogov YA, Skulachev VP, Zorov DB. Neuroprotective effects of mitochondria-targeted plastoquinone and thymoquinone in a rat model of brain ischemia/reperfusion injury. *Molecules.* 2015; 20:14487–503. doi:10.3390/molecules200814487
64. Skulachev VP, Antonenko YN, Cherepanov DA, Chernyak BV, Izyumov DS, Khailova LS, Korshunova GA, Lyamzaev KG, Pletjushkina OY, Roginsky VA, Rokitskaya TI, Severin FF, Severina II. Prevention of cardiolipin oxidation and fatty acid cycling as two antioxidant mechanisms of cationic derivatives of plastoquinone (SkQs). *Biochim Biophys Acta.* 2010; 1797:878-89.
65. Plotnikov EY, Silachev DN, Jankauskas SS, Rokitskaya TI, Chupyrkina AA, Pevzner IB, Zorova LD, Isaev NK, Antonenko YN, Skulachev VP, Zorov DB. Mild uncoupling of respiration and phosphorylation as a mechanism providing nephro- and neuroprotective effects of penetrating cations of the SkQ family. *Biochemistry (Mosc).* 2012;77:1029–37. doi: 10.1134/S0006297912090106
66. Rudnitskaya EA, Muraleva NA, Maksimova KY, Kiseleva E, Kolosova NG, Stefanova NA. Melatonin attenuates memory impairment, amyloid- $\beta$  accumulation, and neurodegeneration in a rat model of sporadic Alzheimer's disease. *J Alzheimers Dis.* 2015; 47:103–16. doi:10.3233/JAD-150161
67. Lambeth JD. Nox enzymes, ROS, and chronic disease: an example of antagonistic pleiotropy. *Free Radic Biol Med.* 2007;43:332–47. doi: 10.1016/j.freeradbiomed.2007.03.027
68. Morris R. Developments of a water-maze procedure for studying spatial learning in the rat. *J Neurosci Methods.* 1984;11:47–60. doi: 10.1016/0165-0270(84)90007-4

SUPPLEMENTARY MATERIAL

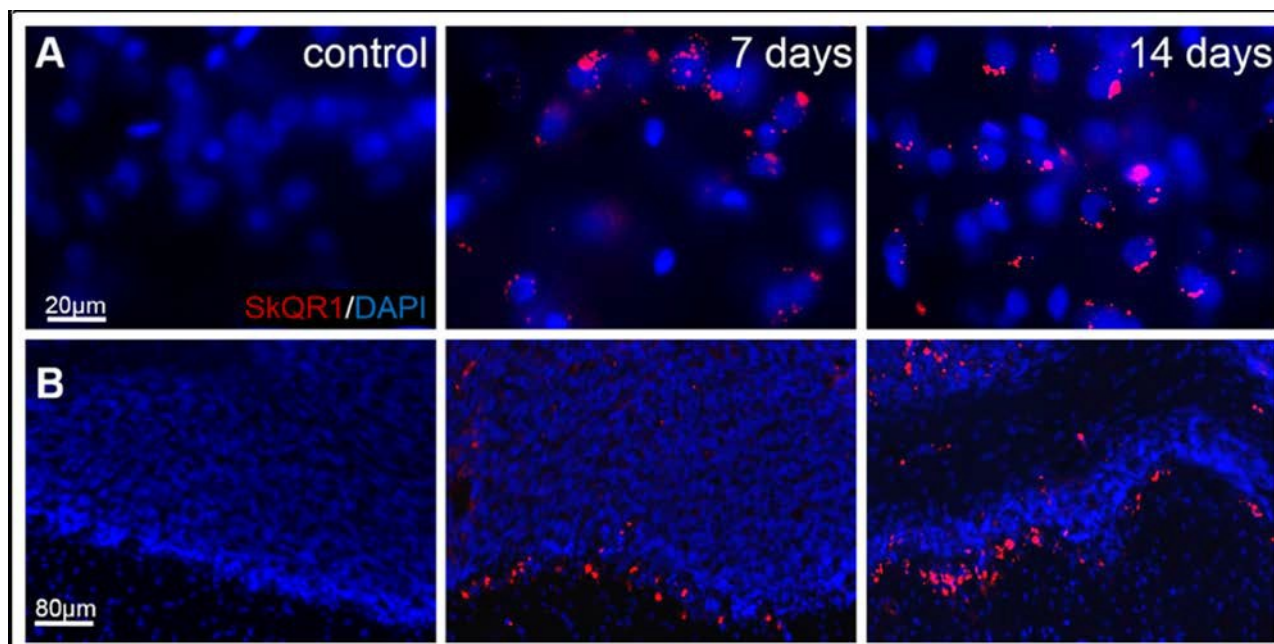


**Figure S1. Accumulation of SkQ1 in the brain of OXYS rats.** (A and B) Representative images showing accumulation of SkQR1 (a rhodamine derivative of SkQ1: SkQ1 decylrhodamine 19, red) in the frontal cortex (40×) and cerebellum (10×) of 4-month-old OXYS rats (n=4) depending on the duration of treatment. Cell nuclei are stained with DAPI (blue).

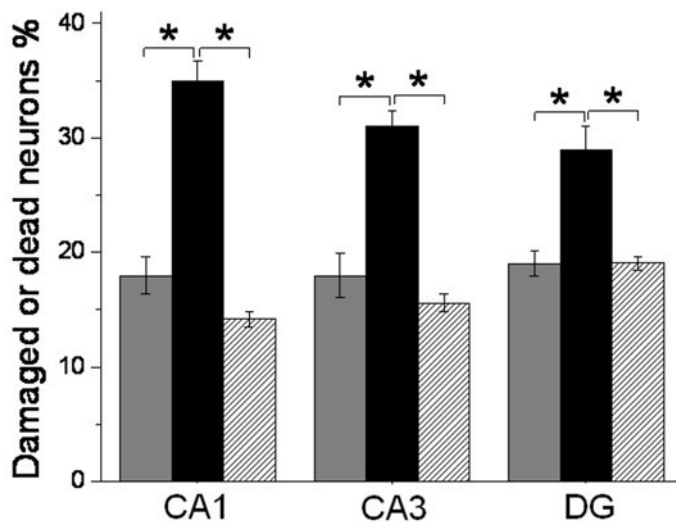


**Figure S2. SkQ1 retards structural neurodegenerative alterations.** The percentages of dead or damaged neurons in the examined hippocampal regions were greater in OXYS rats compared to Wistar rats. Oral SkQ1 administration improved neuronal health in all the hippocampal regions examined in OXYS rats. DG: dentate gyrus. The data are shown as mean ± SEM; \*p< 0.05.

**Table S1. The specific area of organelles in the cytoplasm of neurons (according to electron micrographs)**

	Mitochondria, %	Lysosomes, %	Golgi apparatus, %	Rough ER, %	Vacuoles, %
Wistar	10.3±0.12	8.5±0.24	1.04±0.04	25.8±0.32	4.11±0.29
OXYS	3.1±0.1 <sup>#</sup>	12.1±0.28 <sup>#</sup>	1.19±0.03 <sup>#</sup>	10.4±0.34 <sup>#</sup>	8.58±0.32 <sup>#</sup>
OXYS+SkQ1	7.8±0.16*	9.4±0.25*	1.08±0.05	18.1±0.42*	6.81±0.38

The data are presented as mean ± SEM (n=4). ER: endoplasmic reticulum. <sup>#</sup>p< 0.05 compared to Wistar rats; \*p<0.05 compared to OXYS rats.

## Targeting therapy for homocysteic acid in the blood represents a potential recovery treatment for cognition in Alzheimer's disease patients

Tohru Hasegawa<sup>1</sup> and Wataru Ukai<sup>2</sup>

<sup>1</sup>Saga Woman Junior College, Saga 840-8550, Japan

<sup>2</sup>Department of Neuropsychiatry, Sapporo Medical University, School of Medicine, S-1, W-16, Chuo-ku, Sapporo, 0608543, Japan

**Correspondence to:** Tohru Hasegawa; email: [hasegawa-t@leo.bbiq.jp](mailto:hasegawa-t@leo.bbiq.jp)

**Key words:** Alzheimer's cognitive decline, homocysteic acid in peripheral blood, homocysteic acid in urine, decreasing homocysteic acid in blood

**Received:** June 13, 2016    **Accepted:** September 2, 2016    **Published:** September 14, 2016    **doi:** [10.18632/aging.101046](https://doi.org/10.18632/aging.101046)

### ABSTRACT

At present, we have no reliable means of recovering cognitive impairment in Alzheimer's disease (AD) patients. We hypothesized that homocysteic acid (HA) in the blood might represent one such pathogen that could be excreted into the urine. Since DHA is known to reduce circulating levels of homocysteine, and since exercise attenuates this effect, it follows that supplementation of the diet with DHA, along with increased levels of physical activity, may help to reduce cognitive impairment in AD patients. Our hypothesis was proven to be correct because memory problems in 3xTg- AD mice (a model for AD in which animals develop amyloid pathology), and in a mouse model of familial AD, were recovered following treatment with an anti-HA antibody and not by amyloid treatment. Interestingly, 3xTg-AD mice with amyloid pathology showed increased levels of HA level. This could perhaps be explained by the fact that amyloid precursor protein and/or presenilin increases calcium influx, which could then increase levels of superoxide and consequently increase levels of HA from homocysteine or methionine. Our hypothesis is also partially supported by an open clinical trial of certain dietary supplements that has shown impressive results. Also there are other treatments hypothesis which would be possible for the effective therapies, such as ribonucleoprotein therapy, a  $\beta$ -secretase inhibitor treatment and the metabolic enhancement treatment.

Amyloid cascade hypothesis is strong and main stream hypothesis in Alzheimer's field [1]. The enormous articles of amyloid toxicities were published and the antibody which reduces a quantity of amyloid has been developed and finally this therapy was conducted for human Alzheimer.

Recent big two clinical trials of amyloid beta treatment for Alzheimer's disease were all failed to recover the cognitive impairment [2,3], it has forced us to reconsider this central hypothesis of amyloid pathogen for Alzheimer's disease. Yes, it is very obvious that AD patients have a large amount of amyloid beta in their

brains [4]. However it is also obvious that normal brain also accumulates amyloid beta, and this normal brain can show the normal cognitive ability [5]. This is a key point. The amyloid cannot disturb the normal brain work. But why did many papers report its toxicity? And why did the clinical trial of amyloid treatment not succeed to recover the cognition? First we should consider that many amyloid toxicities were observed in animal experiment, especially the amyloid gene activated model mice were used. It is a famous scientific fact that human cannot synthesize vitamin C, but mice can synthesize vitamin C [6]. And human case of Alzheimer's disease, amyloid pathology is usually

observed with aging, but mice do not accumulate amyloid with aging. Yes, it is obvious that mice has more powerful anti-oxidant efficacy than human and we should keep a mind that mice model for AD are carefully considered to adapt for human case.

Second if the amyloid beta cannot induce a toxic cascade flow by an unknown physiological effect, amyloid pathology will not show any degenerative effect to the neuron and consequently amyloid accumulation will occur in the normal brain. That is a next point. It is known that the amyloid pathology stimulates the calcium influx [7], which stimulate oxygen radical formation [8] to produce homocysteic acid from homocysteine or methionine. And if some physiological antioxidant effect will be large enough, this oxygen radical formation will not be produced and consequently will not produce such a toxic HA. Now we hypothesize why normal brain can accumulate the amyloid beta [5] and that the cognitive reserve ability will be shown in such a typical AD brain.

The familial AD [9] will be observed by a such amyloid mechanism, because it is well known that some genes such as APP and/or Presenilina induces a familial AD and these genes stimulate calcium influx [7,10]. The stimulated calcium induces the superoxide formation [8,45] to produce HA from homocysteine or methionine. However if the familial AD patient's brain can show the effective antioxidant power to the amyloid pathology, the amyloid toxicity does not appear until their physiological antioxidant power will decrease. The produced HA can destruct the cognitive reserve ability and consequently induces AD pathology. The familial AD (FAD) pathology will be occurred in an earlier age. Because FAD genes will be activated in an earlier age. The amyloid pathology will not be occurred in some physiological conditions.

Also some papers reported the physiological effect of amyloid on neurons [11–34]. For example, low concentration (picomole) of amyloid could act as trophic factor [11–15] and APP (amyloid precursor protein) could act as neuronal controller [13,17]. Also low concentration of amyloid beta could act as neurological modulator [18–24]. And anti-oxidant effect of amyloid is very interesting [23–25], because it is well-known that aging process induced oxidative stress and the aging brain contained more amount of amyloid that younger one.

Recently some papers have reported that our peripheral blood may have some pathogens for the AD cognitive impairment, not in the brain itself.

In earlier studies published in Nature [35, 36], scientists at the Stanford University School of Medicine identified substances in the blood of old mice that made the brains of younger mice act older. These substances, whose levels rise with increasing age, appeared to inhibit the brain's ability to produce new nerve cells critical for memory and learning. These findings raise the question of whether it is possible to shield the brain from aging by eliminating or mitigating the effects of these apparently detrimental blood-borne substances.

APOE4 is a gene involved in the mechanisms underlying the development of AD. It increases permeability of the blood–brain barrier (BBB) [37], which thus allows pathogens present in the peripheral blood to readily traverse the BBB and ultimately disturb brain function. This report indicates the possibility that APOE4 represents an early-onset gene.

Another report [38] described an early AD patient showing destruction of the hippocampal BBB. However, this report did not describe which blood-borne pathogen was involved or the causative factor underlying increased permeability of the BBB in aged hippocampus. It is possible that these same blood-borne pathogens can be excreted in the urine as a result of increased blood circulation during exercise, which would thus stop the cognitive decline of AD patients. It also follows that the pathogens involved cannot be large molecules such as proteins, as these cannot be excreted into the urine. As yet, the precise identity of the small molecule pathogens involved remains elusive.

It has been reported that HA is a probable blood-borne pathogen for AD [39–42] and increases BBB permeability via the activation of HA by NMDA receptors [43]. HA is a known glutamate receptor agonist [44] with a molecular weight of 183 KDa. JAD [39] study reported a significant negative relationship between MMSE scores and HA levels in the blood. Consequently, it follows that HA might represent one of the blood-borne pathogens responsible for AD.

We already observed the positive statistical significant relationship between an urinary HA level and the MMSE score, which indicated that the cognitive function was high if there were many urinary HA discharges [39]. However, a key point to consider is how HA might be related to the amyloid pathology of AD. First, it is important to consider the potential neurodegenerative effects of HA. An earlier study [41] described such degenerative effects of HA. The mouse model for AD, the 3xTg-AD mouse, was originally developed by Professor Laferal and was created specifically to develop amyloid pathology that

destroyed normal memory function. It has been shown that memory problems in this mouse model can be rescued by treatment with an anti-HA antibody. It should be pointed out that this was a polyclonal anti-HA antibody, which could have reacted with other HA-related compounds, although our own observations confirmed that HA levels in the brain were indeed reduced following treatment with this antibody. It is also worth noting that HA is completely independent of amyloid toxicity. Since 3xTg-AD mice are a good model for familial AD and that an anti-HA antibody can rescue memory problems in this mouse model, it follows that an anti-HA antibody could potentially recover amyloid-induced cognitive impairment in familial and other types of AD in humans.

However, the question remains as to why 3xTg-AD mice exhibited increased HA levels that were not related to amyloid pathology. Recent studies have shown that APP and Presenilin stimulate calcium influx [8,10], which then stimulates the production of superoxide radicals [8], and these superoxide radicals stimulate the production of HA from methionine and homocysteine [45]. Collectively, these reports suggest that HA levels increase via amyloid pathology. However, this does not explain why amyloid treatment is unable to rescue cognitive impairment. This suggests significant differences between the relevant physiology of mice and humans. In humans, there is increased production of HA in the brain from amyloid, and increased levels of HA in the blood, with the progression of age [39]. However, HA levels are not known to increase with aging in mice (unpublished observation). Consequently, amyloid treatment can recover cognitive impairment in mice. This aging effect in humans can still destroy cognitive function following amyloid treatment. A recently published article reported that the amino acid, methionine, can induce the formation of amyloid plaques, characteristic pathological changes associated with AD, via phosphorylated-tau protein [46]. This is particularly interesting because HA can be produced from heavily-oxidized methionine [8,45]. Therefore, we can hypothesize that amyloid treatment, in combination with other treatments such as anti-HA treatment, are likely to show positive curative effects.

Presently, a range of treatments are under evaluation such as those that prevent inflammation or the phosphorylation of tau or involve mitochondrial treatment [47]. And the metabolic enhancement treatment [48],  $\beta$ -secretase inhibitor treatment [49] and ribonucleoprotein therapy [50] are also interesting hypotheses. Such treatments appear to be effective and are very promising. However, it is important to consider

that these treatments may involve drugs that may have deleterious side effects.

The development of an effective anti-HA therapy requires consideration of several factors. Firstly we need to take into account the fact that HA in the blood will be discharged into the urine by stimulating the circulation of blood. Aerobic exercise stimulates the blood circulation to stimulate the discharge of HA discharge. A recent paper showed that aerobic exercise was very effective in preventing AD pathology[51].

We conducted the open clinical trial of HBF supplement for the cognitive recovery of 91 AD patients of all stage. This HBF supplement decreased the HA levels in blood, which induced the remarkable cognitive recovery processes of all stages of AD patients (unpublished data). From our open clinical trial, our hypothesis is proved. Targeting treatment of HA in blood will be useful and effective therapy for the cognitive recovery of AD patients. Our clinical trial presented the one powerful answer to the question. That is, when the amyloid treatment failed to recover the cognition, it is thought that the treatment time was too late to recover the patients's cognition, because the patients' neurons were already lost. However our trial presents that patient's cognition could be recovered as such. Of course, the final stage of patient could not recover his cognition as normal stage, because such as hippocampus organ already degenerated. The regenerative medicine becomes important at this stage. However we should keep a mind that the regenerative therapy should be conducted after the pathogen such as HA will be treated.

Our hypothesis, the destruction of HA will induce the cognitive reserve ability and its realization is urgent hypothesis to be solved.

## CONFLICTS OF INTEREST

There are no conflicts of interest for all the contributors.

## REFERENCES

1. Karran E, Mercken M, De Strooper B. The amyloid cascade hypothesis for Alzheimer's disease: an appraisal for the development of therapeutics. *Nat Rev Drug Discov.* 2011; 10:698–712. doi.org/10.1038/nrd3505
2. Bapineuzumab Phase 3: Target Engagement. But No Benefit. *Alzheimer Research Forum.* September 12, 2012. Available at <http://www.Alzforum.org/new/detail.asp?id=3268>

3. The Solanezumab Benefit. Oh. So, Small, But Probably Real. Alzheimer Research Forum. October 9, 2012. Available at <http://www.Alzforum.org/new/detail.asp?id=3288>
4. Sadigh-Eteghad S, Sabermarouf B, Majdi A, Talebi M, Farhoudi M, Mahmoudi J. Amyloid-beta: a crucial factor in Alzheimer's disease. *Med Princ Pract*. 2015; 24:1–10. doi.org/10.1159/000369101
5. Aizenstein HJ, Nebes RD, Saxton JA, Price JC, Mathis CA, Tsopelas ND, Ziolkowski SK, James JA, Snitz BE, Houck PR, Bi W, Cohen AD, Lopresti BJ, et al. Frequent amyloid deposition without significant cognitive impairment among the elderly. *Arch Neurol*. 2008; 65:1509–17. doi.org/10.1001/archneur.65.11.1509
6. Ha MN, Graham FL, D'Souza CK, Muller WJ, Igdoura SA, Schellhorn HE. Functional rescue of vitamin C synthesis deficiency in human cells using adenoviral-based expression of murine l-gulonolactone oxidase. *Genomics*. 2004; 83:482–92. doi.org/10.1016/j.ygeno.2003.08.018
7. Leissring MA, Murphy MP, Mead TR, Akbari Y, Sugarman MC, Jannatipour M, Anliker B, Müller U, Saftig P, De Strooper B, Wolfe MS, Golde TE, LaFerla FM. A physiologic signaling role for the gamma-secretase-derived intracellular fragment of APP. *Proc Natl Acad Sci USA*. 2002; 99:4697–702. doi.org/10.1073/pnas.072033799
8. Scully SP, Segel GB, Lichtman MA. Relationship of superoxide production to cytoplasmic free calcium in human monocytes. *J Clin Invest*. 1986; 77:1349–56. doi.org/10.1172/JCI112440
9. Ertekin-Taner N. Genetics of Alzheimer's disease: a centennial review. *Neurol Clin*. 2007; 25:611–67, v. doi.org/10.1016/j.ncl.2007.03.009
10. Honarnejad K, Herms J. Presenilins: role in calcium homeostasis. *Int J Biochem Cell Biol*. 2012; 44:1983–86. doi.org/10.1016/j.biocel.2012.07.019
11. Luo Y, Sunderland T, Roth GS, Wolozin B. Physiological levels of beta-amyloid peptide promote PC12 cell proliferation. *Neurosci Lett*. 1996; 217:125–28. doi.org/10.1016/0304-3940(96)13087-1
12. Moya KL, Benowitz LI, Schneider GE, Allinquant B. The amyloid precursor protein is developmentally regulated and correlated with synaptogenesis. *Dev Biol*. 1994; 161:597–603. doi.org/10.1006/dbio.1994.1055
13. Mileusnic R, Lancashire CL, Johnston AN, Rose SP. APP is required during an early phase of memory formation. *Eur J Neurosci*. 2000; 12:4487–95.
14. Plant LD, Boyle JP, Smith IF, Peers C, Pearson HA. The production of amyloid beta peptide is a critical requirement for the viability of central neurons. *J Neurosci*. 2003; 23:5531–35.
15. Atwood CS, Obrenovich ME, Liu T, Chan H, Perry G, Smith MA, Martins RN. Amyloid-beta: a chameleon walking in two worlds: a review of the trophic and toxic properties of amyloid-beta. *Brain Res Brain Res Rev*. 2003; 43:1–16. doi.org/10.1016/S0165-0173(03)00174-7
16. Pearson HA, Peers C. Physiological roles for amyloid beta peptides. *J Physiol*. 2006; 575:5–10. doi.org/10.1113/jphysiol.2006.111203
17. Kamenetz F, Tomita T, Hsieh H, Seabrook G, Borchelt D, Iwatsubo T, Sisodia S, Malinow R. APP processing and synaptic function. *Neuron*. 2003; 37:925–37. doi.org/10.1016/S0896-6273(03)00124-7
18. Garcia-Osta A, Alberini CM. Amyloid beta mediates memory formation. *Learn Mem*. 2009; 16:267–72. doi.org/10.1101/lm.1310209
19. Puzzo D, Privitera L, Leznik E, Fà M, Staniszewski A, Palmeri A, Arancio O. Picomolar amyloid-beta positively modulates synaptic plasticity and memory in hippocampus. *J Neurosci*. 2008; 28:14537–45. doi.org/10.1523/JNEUROSCI.2692-08.2008
20. Puzzo D, Privitera L, Fa' M, Staniszewski A, Hashimoto G, Aziz F, Sakurai M, Ribe EM, Troy CM, Mercken M, Jung SS, Palmeri A, Arancio O. Endogenous amyloid- $\beta$  is necessary for hippocampal synaptic plasticity and memory. *Ann Neurol*. 2011; 69:819–30. doi.org/10.1002/ana.22313
21. Morley JE, Farr SA, Banks WA, Johnson SN, Yamada KA, Xu L. A physiological role for amyloid-beta protein: enhancement of learning and memory. *J Alzheimers Dis*. 2010; 19:441–49.
22. Smith DG, Cappai R, Barnham KJ. The redox chemistry of the Alzheimer's disease amyloid beta peptide. *Biochim Biophys Acta*. 2007; 1768:1976–90. doi.org/10.1016/j.bbamem.2007.02.002
23. Baruch-Suchodolsky R, Fischer B. Abeta 40, either soluble or aggregated, is a remarkably potent antioxidant in cell-free oxidative systems. doi.org/10.1021/bi802361k
24. Kontush A, Atwood CS. Amyloid-beta: phylogenesis of a chameleon. *Brain Res Brain Res Rev*. 2004; 46:118–20. doi.org/10.1016/j.brainresrev.2004.05.001
25. Smith DG, Cappai R, Barnham KJ. The redox chemistry of the Alzheimer's disease amyloid beta peptide. *Biochim Biophys Acta*. 2007; 1768:1976–90. doi.org/10.1016/j.bbamem.2007.02.002

26. Baruch-Suchodolsky R, Fischer B. Abeta40, either soluble or aggregated, is a remarkably potent antioxidant in cell-free Oxidative systems. *Biochemistry*. 2009; 48:4354–70. doi.org/10.1021/bi802361k
27. Kontush A, Atwood CS. Amyloid-beta: phylogenesis of a chameleon. *Brain Res Brain Res Rev*. 2004; 46:118–20. doi.org/10.1016/j.brainresrev.2004.05.001
28. López-Toledano MA, Shelanski ML. Neurogenic effect of beta-amyloid peptide in the development of neural stem cells. *J Neurosci*. 2004; 24:5439–44. doi.org/10.1523/JNEUROSCI.0974-04.2004
29. Heo C, Chang KA, Choi HS, Kim HS, Kim S, Liew H, Kim JA, Yu E, Ma J, Suh YH. Effects of the monomeric, oligomeric, and fibrillar Abeta42 peptides on the proliferation and differentiation of adult neural stem cells from subventricular zone. *J Neurochem*. 2007; 102:493–500. doi.org/10.1111/j.1471-4159.2007.04499.x
30. Chen Y, Dong C. Abeta40 promotes neuronal cell fate in neural progenitor cells. *Cell Death Differ*. 2009; 16:386–94. doi.org/10.1038/cdd.2008.94
31. Giuffrida ML, Caraci F, Pignataro B, Cataldo S, De Bona P, Bruno V, Molinaro G, Pappalardo G, Messina A, Palmigiano A, Garozzo D, Nicoletti F, Rizzarelli E, Copani A. Beta-amyloid monomers are neuroprotective. *J Neurosci*. 2009; 29:10582–87. doi.org/10.1523/JNEUROSCI.1736-09.2009
32. Yankner BA, Duffy LK, Kirschner DA. Neurotrophic and neurotoxic effects of amyloid beta protein: reversal by tachykinin neuropeptides. *Science*. 1990; 250:279–82. doi.org/10.1126/science.2218531
33. Díaz-Moreno M, Hortigüela R, Gonçalves A, García-Carpio I, Manich G, García-Bermúdez E, Moreno-Estellés M, Eguiluz C, Vilaplana J, Pelegrí C, Vilar M, Mira H. Aβ increases neural stem cell activity in senescence-accelerated SAMP8 mice. *Neurobiol Aging*. 2013; 34:2623–38. doi.org/10.1016/j.neurobiolaging.2013.05.011
34. Sotthibundhu A, Li QX, Thangnipon W, Coulson EJ. Abeta(1-42) stimulates adult SVZ neurogenesis through the p75 neurotrophin receptor. *Neurobiol Aging*. 2009; 30:1975–85. doi.org/10.1016/j.neurobiolaging.2008.02.004
35. Scudellari M. Ageing research: blood to blood. *Nature*. 2015; 517:426–29. doi.org/10.1038/517426a
36. Villeda SA, Luo J, Mosher KI, Zou B, Britschgi M, Bieri G, Stan TM, Fainberg N, Ding Z, Eggel A, Lucin KM, 6 negatively regulates neurogenesis and cognitive function. *Nature*. 2011; 477:90–94. doi.org/10.1038/nature10357
37. Bell RD, Winkler EA, Singh I, Sagare AP, Deane R, Wu Z, Holtzman DM, Betsholtz C, Armulik A, Sallstrom J, Berk BC, Zlokovic BV. Apolipoprotein E controls cerebrovascular integrity via cyclophilin A. *Nature*. 2012; 485:512–16.
38. Blood-Brain Barrier Breakdown in the Aging Human Hippocampus. *Neuron*. 2015; 85:296–302. doi.org/10.1016/j.neuron.2014.12.032
39. Hasegawa T, Ichiba M, Matsumoto SE, Kasanuki K, Hatano T, Fujishiro H, Iseki E, Hattori N, Yamada T, Tabira T. Urinary homocysteic acid levels correlate with mini-mental state examination scores in Alzheimer's disease patients. *J Alzheimers Dis*. 2012; 31:59–64. 10.3233/JAD-2012-120022
40. Hasegawa T, Mikoda N, Kitazawa M, LaFerla FM. B6 deficient feeding or homocysteic acid induces the earlier Alzheimer's pathological change in normal C57BL male mice. *Nature Precedings*. 2009. http://hdl.handle.net/10101/npre.2009.2764.1
41. Hasegawa T, Mikoda N, Kitazawa M, LaFerla FM. Treatment of Alzheimer's disease with anti-homocysteic acid antibody in 3xTg-AD male mice. *PLoS One*. 2010; 5:e8593. doi.org/10.1371/journal.pone.0008593
42. Hasegawa T, Ukai W, Jo DG, Xu X, Mattson MP, Nakagawa M, Araki W, Saito T, Yamada T. Homocysteic acid induces intraneuronal accumulation of neurotoxic Abeta42: implications for the pathogenesis of Alzheimer's disease. *J Neurosci Res*. 2005; 80:869–76. doi.org/10.1002/jnr.20514
43. Miller RD, Monsul NT, Vender JR, Lehmann JC. NMDA- and endothelin-1-induced increases in blood-brain barrier permeability quantitated with Lucifer yellow. *J Neurol Sci*. 1996; 136:37–40. doi.org/10.1016/0022-510X(95)00309-P
44. Do KQ, Herrling PL, Streit P, Cuénod M. Release of neuroactive substances: homocysteic acid as an endogenous agonist of the NMDA receptor. *J Neural Transm*. 1988; 72:185–90. doi.org/10.1007/BF01243418
45. Bern M, Saladino J, Sharp JS. Conversion of methionine into homocysteic acid in heavily oxidized proteomics samples. *Rapid Commun Mass Spectrom*. 2010; 24:768–72. doi.org/10.1002/rcm.4447
46. Tapia-Rojas C, Lindsay CB, Montecinos-Oliva C, Arrazola MS, Retamales RM, Bunout D, Hirsch S, Inestrosa NC. Is L-methionine a trigger factor for Alzheimer's-like neurodegeneration?: changes in Aβ oligomers, tau phosphorylation, synaptic proteins,

Wnt signaling and behavioral impairment in wild-type mice. *Mol Neurodegener.* 2015; 10:62.  
[doi.org/10.1186/s13024-015-0057-0](https://doi.org/10.1186/s13024-015-0057-0)

47. [http://www.alz.org/research/science/alzheimers\\_treatment\\_horizon.asp#hope](http://www.alz.org/research/science/alzheimers_treatment_horizon.asp#hope)
48. Bredesen DE. Reversal of cognitive decline: a novel therapeutic program. *Aging (Albany NY).* 2014; 6:707–17. [doi.org/10.18632/aging.100690](https://doi.org/10.18632/aging.100690)
49. Tang J, Ghosh A. Treating transgenic Alzheimer mice with a  $\beta$ -secretase inhibitor, what have we learned? *Aging (Albany NY).* 2011; 3:14–16.  
[doi.org/10.18632/aging.100267](https://doi.org/10.18632/aging.100267)
50. Yoon JH, Gorospe M. Ribonucleoprotein therapy in Alzheimer's disease? *Aging (Albany NY).* 2014; 6:428–29. [doi.org/10.18632/aging.100672](https://doi.org/10.18632/aging.100672)
51. [https://www.alz.org/aaic/\\_downloads/thurs-1130am-exercise.pdf](https://www.alz.org/aaic/_downloads/thurs-1130am-exercise.pdf)

## Biological and biophysics aspects of metformin-induced effects: cortex mitochondrial dysfunction and promotion of toxic amyloid pre-fibrillar aggregates

Pasquale Picone<sup>1</sup>, Silvia Vilasi<sup>2</sup>, Fabio Librizzi<sup>2</sup>, Marco Contardi<sup>2,4</sup>, Domenico Nuzzo<sup>1</sup>, Luca Caruana<sup>1</sup>, Sara Baldassano<sup>3</sup>, Antonella Amato<sup>3</sup>, Flavia Mulè<sup>3</sup>, Pier Luigi San Biagio<sup>2</sup>, Daniela Giacomazza<sup>2</sup>, and Marta Di Carlo<sup>1</sup>

<sup>1</sup>Istituto di Biomedicina e Immunologia Molecolare, CNR, Palermo, Italy

<sup>2</sup>Istituto di Biofisica, CNR, Palermo, Italy

<sup>3</sup>Dipartimento di Scienze e Tecnologie Biologiche, Chimiche e Farmaceutiche, University of Palermo, Palermo, Italy

<sup>4</sup>Current address: Italian Institute of Technology, Genova, Italy

**Correspondence to:** Daniela Giacomazza; Marta Di Carlo; email: [daniela.giacomazza@cnr.it](mailto:daniela.giacomazza@cnr.it); [marta.dicarlo@ibim.cnr.it](mailto:marta.dicarlo@ibim.cnr.it)

**Key words:** Alzheimer's disease, metformin, mitochondrial dysfunction, cell degeneration, mitochondrial pores,  $\beta$ -amyloid aggregation

**Received:** June 28, 2016 **Accepted:** July 15, 2016 **Published:** July 28, 2016 **doi:** [10.18632/aging.101004](https://doi.org/10.18632/aging.101004)

### ABSTRACT

The onset of Alzheimer disease (AD) is influenced by several risk factors comprising diabetes. Within this context, antidiabetic drugs, including metformin, are investigated for their effect on AD. We report that in the C57B6/J mice, metformin is delivered to the brain where activates AMP-activated kinase (AMPK), its molecular target. This drug affects the levels of  $\beta$ -secretase (BACE1) and  $\beta$ -amyloid precursor protein (APP), promoting processing and aggregation of  $\beta$ -amyloid ( $A\beta$ ), mainly in the cortex region. Moreover, metformin induces mitochondrial dysfunction and cell death by affecting the level and conformation of Translocase of the Outer Membrane 40 (TOM40), voltage-dependent anion-selective channels 1 (VDAC1) and hexokinase I (HKI), proteins involved in mitochondrial transport of molecules, including  $A\beta$ . By using biophysical techniques we found that metformin is able to directly interact with  $A\beta$  influencing its aggregation kinetics and features. These findings indicate that metformin induces different adverse effects, leading to an overall increase of the risk of AD onset.

### INTRODUCTION

According to Rotterdam Study, individuals with metabolic pathologies such as Type2 diabetes (T2DM) or Obesity have almost a two-fold greatest risk of developing Alzheimer's disease (AD) [1]. AD is the most common cause of dementia in the elderly and it is associated with a progressive impairment of cognitive function, orientation, and difficulties with problem-solving or language. Thus, in patients with AD, gradually, over the time, more parts of the brain are damaged developing progressive symptoms, leading to death. Thirty-five millions of persons in the world are now considered to be affected by AD and this number is expected to double in the next few decades [2]. Even if

the etiological defects in AD are not well known, prevalent ideas implicate build-up of soluble  $\beta$ -amyloid ( $A\beta$ ) oligomers or insoluble plaques or neurofibrillary tangles [3,4].  $A\beta$  is a 39–43 amino acid peptide formed from the cleavage of amyloid precursor protein (APP), a transmembrane glycoprotein. Neurofibrillary tangles are, instead, produced by hyperphosphorylation of Tau, a protein associated with microtubules in neurons [5]. Aging is the primary risk factor for the development of AD and many other pathological conditions occurring in older people, including T2DM. Change in cognitive function and increase of neurodegeneration markers were found both in patients with T2DM and/or obesity [6] and in insulin-resistant obese mice [7], suggesting the existence of a common molecular mechanism. Some

studies have identified in insulin resistance condition the link among the pathophysiology of metabolic disorders and the brain alteration [8–10]. Insulin has a significant role in modulation of synaptic plasticity and learning memory and a high number of Insulin Receptor (IR) are present in brain [9,11]. Modification in the insulin concentration and IR number have been reported in AD cell model [12] and AD brain, leading to the result that AD can be considered as a brain diabetes or “Type 3 Diabetes” [13]. On the basis of this association between metabolic disorders and impaired cognition it should be relevant to investigate whether a potential risk or benefit could occur by using antidiabetic treatments on brain health [14,15].

Evidences on the association between antidiabetic medication and the risk of AD are conflicting and not well documented [16]. One of the few classes of therapeutics, efficient in lowering glucose production are the biguanides, which include molecules as phenformin (2-N-phenethylcarbamimidoyl guanidine) and metformin (1,2-dimethylbiguanide hydrochloride). In particular, the last is the most frequently prescribed drug for T2DM or other metabolic diseases. On the basis of its physicochemical structure and properties, metformin is a small amphoteric molecule (129 Da) with pKa values of 2.8 and 11.5. These characteristics are associated to high water solubility and low lipid solubility. Studies both *in vitro* and *in vivo*, indicate that metformin increases the production of A $\beta$  [17], suggesting that its long-term administration may promote AD onset. On the contrary, a neuropathological study has reported that people treated both with insulin and oral antidiabetic drugs had developed a significantly lower amyloid plaque density [18]. A recent population-based case-control study examined the relationship between T2DM and administration of different antidiabetic drugs and risk of AD development. The authors conclude that long-term users of metformin may have a somewhat higher risk of AD onset and development [19]. However, poor information is available about the molecular mechanism activated by metformin. Some reports indicate that it is able to stimulate AMP activated protein kinase (AMPK), an enzyme activated when cellular energy levels are altered [20]. Recently, *in vitro* and *ex vivo* studies have demonstrated that metformin favors APP and presenilin increase and induces A $\beta$  production and aggregation [21]. Furthermore, metformin acts as a pro-oxidant molecule inducing oxidative stress and mitochondrial dysfunction that, in turn, activates Nf- $\kappa$ B, a transcription factor involved in regulation of APP and presenilin gene expression. Lastly, these molecular mechanisms are counteracted by insulin co-administration [21].

Functional and structural mitochondrial defects contribute to the pathogenesis of aged-related diseases. Metformin affects mitochondria by inducing depolarization of the mitochondrial phospholipidic membrane [21,22] and inhibiting the mitochondrial complex I of the respiratory chain [23,24]. Moreover, the use of metformin changes the expression of several proteins involved in metabolic processes, the regulation of apoptosis and the structural preservation of brain mitochondria [25]. Impairing of exchange of molecule between cytoplasm and mitochondria is one of the cause of mitochondrial dysfunction. The Translocase of the Outer Membrane (TOM) complex, of which TOM40 is the key subunit, is the main gateway for the import of most mitochondrial proteins synthesized in the cytoplasm. The complex is relevant also for mitochondrial biogenesis and its damage triggers mitochondrial dysfunction [26]. Furthermore, opening and closure of the mitochondrial permeability transition (MPT) pore, in which voltage-dependent anion-selective channels 1 (VDAC1), also known as mitochondrial porin, is one of the main proteins, is impaired in patients with neurodegenerative diseases [27]. Moreover, VDAC1 interacts with hexokinase I (HKI) and this binding protects against cell death [28]. Thus, the correct mitochondrial transport of ions, metabolites and molecules affects cell survival and death mechanisms.

From a molecular point of view, the overproduction and aberrant self-assembly of the amyloid  $\beta$  peptide (A $\beta$ ) into fibrillar aggregates constitute the first step of the so-called amyloid cascade hypothesis, thought to trigger AD [29]. These extremely toxic oligomers [30,31] have high hydrophobicity, are small [32] and constitute a heterogeneous group characterized by several highly dynamic different assemblies with multiple conformational states. Although the mechanism of cytotoxicity is not yet fully understood, it has been ascertained that amyloid oligomers are the most toxic species [30,31]; in fact, they directly interact with and affect cell plasma membranes by forming pores and consequently disrupting several cellular processes. Amyloid fibrils have also been recently demonstrated to modify the membrane integrity. In fact, they interacting with lipid bilayers are destabilized and disassembled in the pre-fibrillar toxic forms, inducing cell dysfunction, although to a lesser extent [31,33–35].

From a molecular point of view, the self-assembly of A $\beta$  peptides in well-ordered fibrils constituting the senile plaques found in AD brains, is a complex process composed by several steps. It is characterized by multiple transitional aggregation species as initial seeds, soluble small oligomers, protofibrils and insoluble

amyloid fibrils, with a  $\beta$ -sheet conformation. The kinetics of amyloid formation is best described by a sigmoid curve and can be schematically described in three stages [36,37]:

- 1) the slow lag nucleation phase, in which monomers gradually undergo a secondary structure conformational change from random coil to  $\beta$ -sheet and associate to form oligomeric nuclei/protofibrils;
- 2) the fast exponential elongation phase, in which the soluble species are progressively arranged at the ends of preformed  $\beta$ -sheet rich structures in a thermodynamically favorable process. The initial oligomeric nuclei rapidly grow by further addition of monomers forming larger fibrils;
- 3) the saturation phase, in which the fibrils are completely formed and associate each other giving rise to stable mature fibers.

In this study we assessed the molecular effects of metformin in specific brain area of mice. Difference in A $\beta$  deposits, expression of AD markers and proteins involved in mitochondrial dysfunction were found between cortex and hippocampus regions of quite young mice. Furthermore, the direct interaction between metformin and A $\beta$  aggregate formation was determined by in vitro biophysical study.

## RESULTS

### Metformin is a fluorescent molecule able to reach the brain

Absorption or fluorescence phenomena of ultraviolet or visible lights by a molecule depend on electron transitions between molecular orbital energy levels. Due to the presence of two double conjugated bonds the possibility of fluorescence phenomenon in metformin has been investigated. The emission spectrum obtained by fluorescence measurements indicates that metformin, once excited at 395 or 488 nm, has the emission peaks at 475 and 520 nm, respectively (data not shown). This property allows analyzing the presence of metformin into the brain of mice after its dispersion in drinking water. Metformin was administered to C57B6/J mice and after seven days the mice were sacrificed and the brains analyzed by using an imaging instrument. A strong signal was detected in the treated mice whereas no signal was found in the control, thus indicating that metformin has reached the brain (Fig. 1a,b). The delivery of metformin to the brain was confirmed by the increased levels of phosphorylated AMP-activated kinase (AMPK), one of the main molecular target of metformin (Fig. 1c,d). Thus, metformin crosses the blood brain barrier (BBB) and has an impact on the brain biochemical pathways.

### Chronic metformin treatment stimulates APP processing mainly in brain cortex region

To ascertain the possibility that metformin is a risk factor for AD onset, especially in long term administration, C57B6/J mice were treated with metformin for seven days or three months. After these treatments proteins extracted from cortex and hippocampus, two-brain area mainly damaged in AD, were submitted to Western blot. Changes in the levels of BACE1, an enzyme required for APP processing to produce A $\beta$ , its pathogenic cleavage product, and the same APP were measured. Activation of AMPK was evaluated for confirming the biochemical activity of metformin in the brain (Fig. 2). An increase of the levels of BACE1 and APP expression was detected in the cortex after seven days of treatment (Fig. 2a). In contrast, an increase of BACE1, and a decrease of APP were found after chronic treatment in the cortex, suggesting that an enhanced processing may be occurred (Fig. 2c). Furthermore, after both treatments, no significant differences in BACE1 and APP expression in the hippocampus were detected (Fig. 2b, d). To validate the hypothesis that the decreased presence of APP in the cortex was a consequence of the  $\beta$ -secretase increased activity, a quantitative real-time PCR (qRT-PCR) experiment was performed. No significant change was observed in APP transcript, strongly signifying that the produced protein was quickly processed (Fig. 2e).

### Metformin induces accumulation of A $\beta$ aggregates mainly in brain cortex region

Since the obtained results after three months of treatment suggested an augmented processing of APP mainly in the cortex, we explored the possibility that an increase of A $\beta$  production could have enhanced its aggregation and deposition in the extracellular area. By immunofluorescence analysis, using coronary brain sections, in which cerebral cortex and hippocampus were visible, and anti-APP antibody we observed a diffuse staining around the nuclei of the control and a punctate staining around the cells of treated cortex, suggesting presence of aggregates due to increased processing (Fig. 3a). However, this result was confirmed by staining with Thioflavin T (Fig. 3b), a dye used to reveal the presence of  $\beta$ -sheet protein aggregates because of the increase of its fluorescence emission intensity upon binding to the linear array of  $\beta$ -strand aggregates [38,39]. In particular, we observed aggregates with a dimension ranging below 1  $\mu$ m mainly in the cortex (Fig. 3b). In contrast, no significant immunoreactivity, or presence of A $\beta$  aggregates, was detectable in hippocampus (Fig. 3a,b).

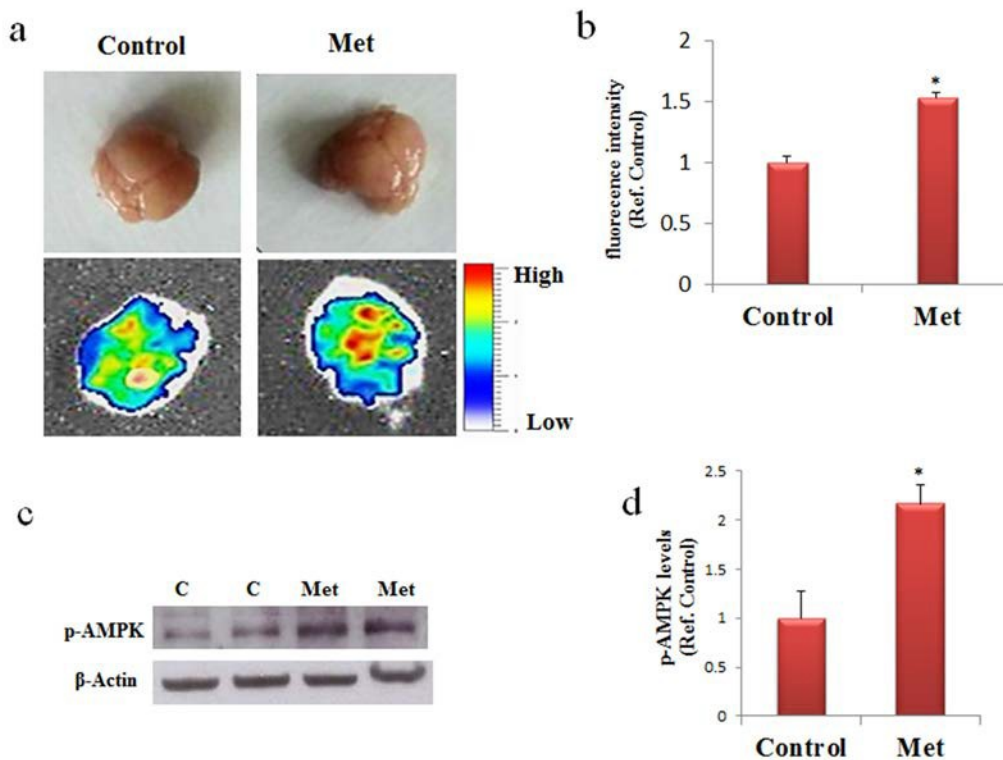


**Figure 1. Metformin reaches the brain and activate AMPK.** (a) and (b) Mice were untreated or treated with metformin for seven days and the fluorescence in the brain was quantified by bioimaging. Fluorescence values are referred to the control. (c) Western blot of proteins extracted from brains of metformin untreated (C) or treated mice (Met) and incubated with phospho-AMPK (p-AMPK) and  $\beta$ -Actin (loading control) antibodies. (d) Quantification of immunoreactivity using densitometric analysis. Representative images from 2 animals for condition are shown. n=5 per group.

### Metformin induces mitochondrial dysfunction by impairing MPT pores and membrane channels

Specific mitochondrial proteins involved in distinctive structures regulate cross talk and transport of proteins and metabolites between cytoplasm and mitochondria. We addressed the question if metformin treatment might contribute to the alteration of the components of mitochondrial machinery. After three months of treatment changes in levels of expression were analyzed for some proteins involved in mitochondrial transport of different molecules and markers of mitochondrial dysfunction such as TOM40, VDAC1 and HKI. Western blot of proteins extracted from both cortex and hippocampus of mice treated with metformin and controls were incubated with antibodies against TOM40, VDAC1 and HKI. In agreement with previous data, Western blot analysis showed changes in the levels of expression of the analyzed proteins only in the cortex region. An increase of TOM40 was detected indicating an impairing of MPT pores (Fig. 4a). Further,

an increase of total VDAC1 levels were observed in cortex where, in particular, we found together with VDAC1 monomers some dimers and trimers, suggesting that a fraction of the VDAC1 in the membrane is organized in oligomers (Fig. 4c). Moreover, the lower band, indicated by the red arrow in Figure 4C, represents a monomeric species whose electrophoretic mobility is modified by the intramolecular crosslinking of the VDAC1 N-terminal domain. A decrease of HKI amount was also detected suggesting that probably a detachment from VDAC1 was occurred (Fig. 4e). TOM40, VDAC1 and HKI levels were not significantly affected in the hippocampus brain area (Fig. 4b, d, f).

### Metformin induces neuronal apoptosis

To assess whether, after chronic metformin treatment, apoptotic cell death occurred *in vivo*, presence of fragmented DNA was examined in cortex and hippocampus brain sections by the terminal deoxynucleotidyl

transferase-mediated, dUTP, nick end labeling (TUNEL) method. TUNEL-positive cells in brain sections of

metformin treated mice were markedly higher in cortical region than in hippocampal region or control (Fig. 5a, b).

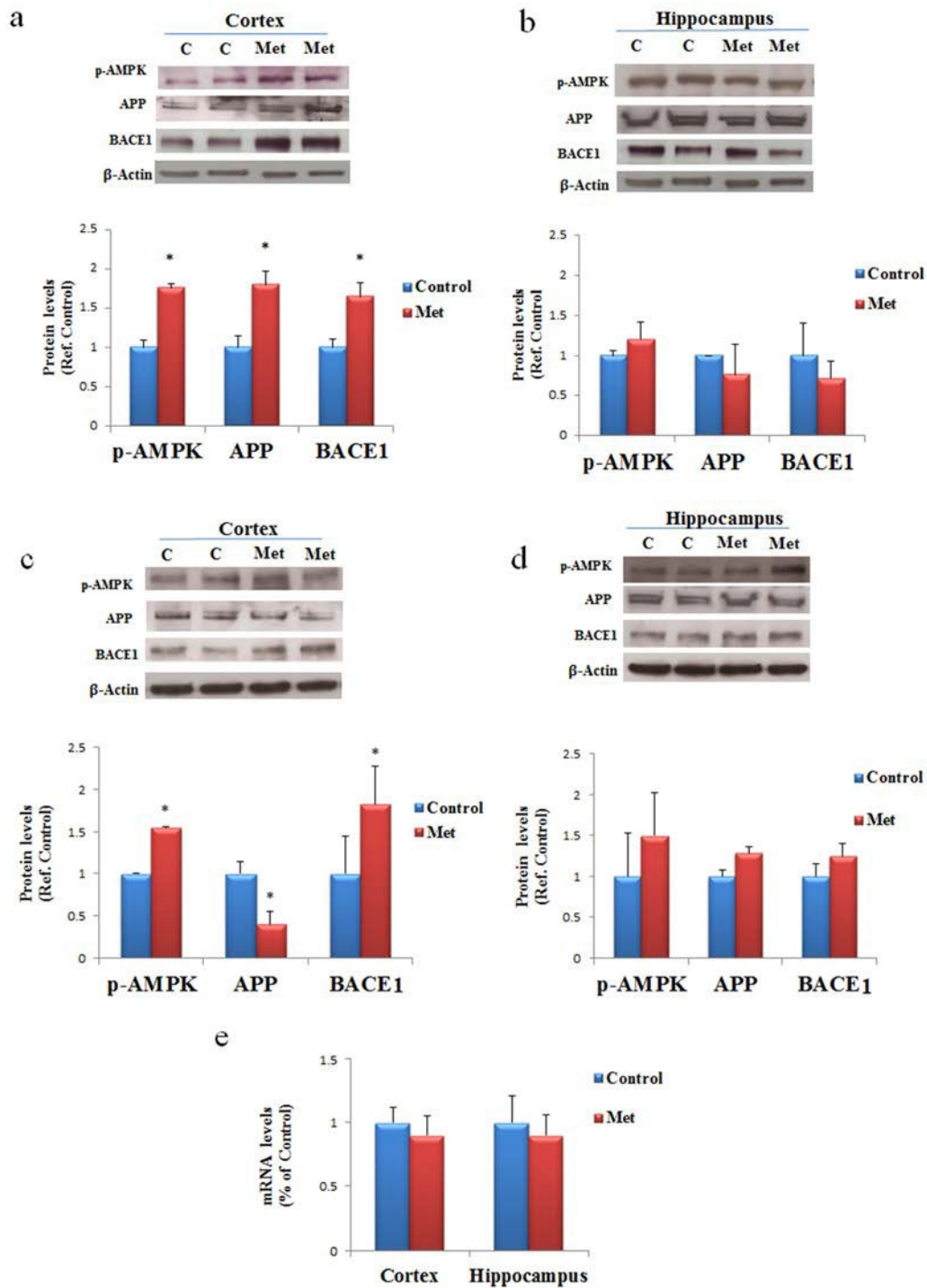


**Figure 2. AD biomarkers are differently activated by metformin treatment in brain regions.** Western blot of protein extracted from brain lysates of mice cortex (a) and hippocampus (b) after seven days of metformin treatment and incubated with anti-phospho-AMPK (p-AMPK), APP, BACE and  $\beta$ -Actin (loading control) antibodies. Western blot of protein extracted from brain lysates of mice cortex (c) and hippocampus (d) after chronic metformin treatment and incubated with anti-phospho-AMPK (p-AMPK), APP, BACE1 and  $\beta$ -Actin (loading control) antibodies. Quantification of immunoreactivity was performed using densitometric analysis. (e) Effect of chronic metformin treatment on APP transcript levels determined by quantitative real-time PCR in cortex and hippocampus regions. n=5 per group.

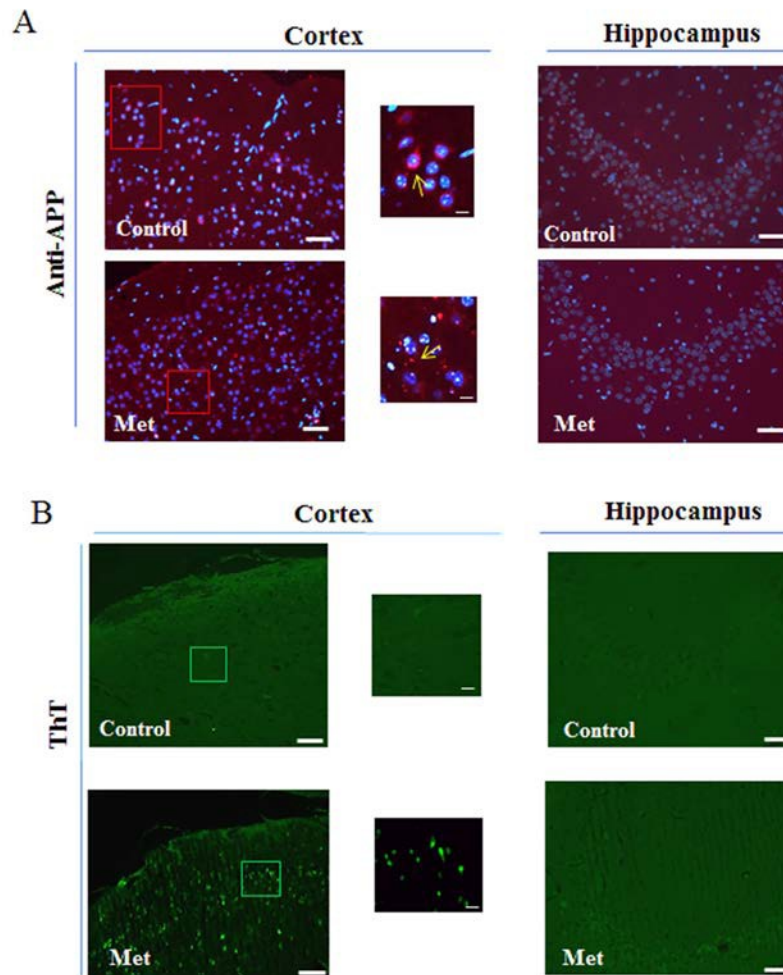


**Figure 3. Metformin induces accumulation of Aβ aggregates.** (a) Immunofluorescence of cerebral cortex and hippocampus sections of metformin treated mice stained using anti-APP. Nuclei were stained with Hoechst 33258 and merged images with anti-APP staining are shown. (b) ThT staining of Aβ aggregates on coronary sections. High magnification of the squared areas is shown. Yellow arrows in the zoomed images indicate diffuse or punctate anti-APP staining. 20X original magnification. Scale bars = 50 μm and 5 μm in the zoomed images. n=5 per group.

### Metformin directly interacts with Aβ peptide influencing its aggregation kinetics in vitro

In order to assess whether metformin is also able to directly interact with Aβ peptide influencing its aggregation process we performed the fibrillogenesis kinetics by ThT assay. Figure 6 shows the time course of the ThT signal during the fibrillation kinetics of 50 μM Aβ incubated at 37°C in the absence and in the presence of 2mM metformin. The kinetics followed the typical nucleation-polymerization process, described by the sigmoidal profile [36]. In the presence of metformin, the lag phase increased and the amount of final fibrils is

reduced in comparison with control. Metformin addition seemed to reduce the effective Aβ concentration leading to initial nuclei, thus interfering with lag-phase.

This result was confirmed by circular dichroism (CD) experiments. CD spectra are sensitive to the secondary structure variation accompanying amyloid cross-β-structure formation during fibrillogenesis. In the initial phase of the aggregation process, the Aβ CD spectrum presents a single minimum that, typical of a random coil structure, is around 200 nm. The minimum shifts towards higher wavelength during amyloid formation. Our results have shown that the presence of 2mM of

metformin delayed the  $\beta$ -sheet structure formation of a 50  $\mu$ M A $\beta$ 1-40 solution. In fact, while the control sample reached the end point of the aggregation reaction (Fig. 7a) after 0.5 h, no significant changes were observed in the presence of the drug in the same time interval indicating that the peptide retained its disordered structure (Fig. 7b), in fully agreement with the fluorescence data. Always in accordance with ThT assay, after 2 h both the samples completed their conversion.

The reduced amount of A $\beta$ 1-40 fibrils detected by ThT assay in the presence of metformin was confirmed by AFM measurements. In Figure 8a-d the morphology of the aggregates formed at the end of the kinetics in the absence and in the presence of metformin are reported. Amyloid fibrils result reduced in number and length when metformin is added in solution. Moreover, prefibrillar oligomeric aggregates are observed at the end of the kinetics of the peptide incubated with the drug.

The characterization of the action of metformin on the aggregation process of A $\beta$ 1-40 peptide was followed by Dynamic Light Scattering (DLS) experiments. Although not specifically focused on chemo-physical features characterizing amyloid formation, like conversion to cross- $\beta$ -structure, the addition of DLS to other biophysical techniques provides important quantitative information on the hydrodynamic size variation occurring during an aggregation process. In this sense, it represents a suitable technique to monitor the influence of an exogenous molecule on the protein assembly, and, therefore, it is often used for testing drugs for therapeutic purposes. Moreover, light scattering technique does not need the use of extrinsic probes, whose evaluation of their potential influence on the process under study requires high carefulness [40]. Figures 8e and f show the hydrodynamic diameter DH distribution functions of a sample of A $\beta$ 1-40 peptide undergone to the amyloid formation protocol (37°C and 200 rpm under stirring) with and without metformin,

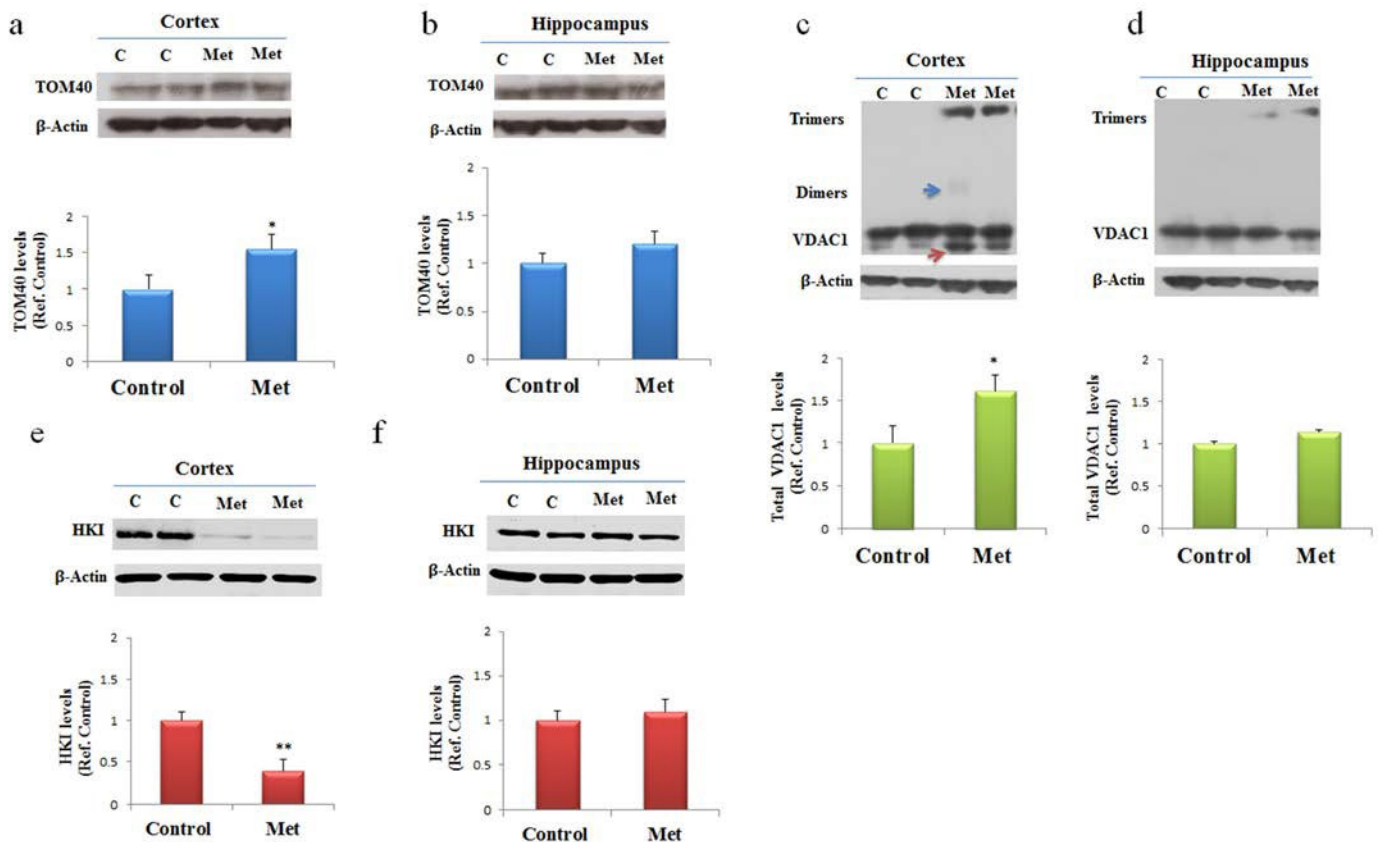


**Figure 4. Metformin after chronic administration, changes TOM40 expression levels and induces VDAC1 oligomerization, and affects Hexokinase I (HKI) in the cortex region.** We stern blot of protein extracted from brain lysates of mice cortex (a, c, e) and hippocampus (b, d, f) after chronic metformin treatment and incubated with anti- TOM40, VDAC1, Hexokinase I (HKI), and  $\beta$ -Actin (loading control) antibodies. Quantitative analysis of total VDAC1, HKI and TOM40 levels relative to  $\beta$ -actin was performed using densitometric analysis. The blue arrow indicates a VDAC1 dimers and the red arrow indicates VDAC1 monomers with modified electrophoretic mobility. n=5 per group.

respectively after 0.5 h from the beginning of the process and at the end of the experiment observation (2 h). The increase in ThT assay (Fig. 6) and variation in CD spectra (Fig. 7) reveal that, at that time, in the absence of metformin a significant amyloid cross- $\beta$ -structure has already formed. Correspondently, two size

distributions are revealed by DLS analysis: one centered at around 300 nm and the other one corresponding to larger species of the order of microns. At the same time, in the presence of metformin this higher size species is not formed and only the appearance of species at around 300 nm occurs.

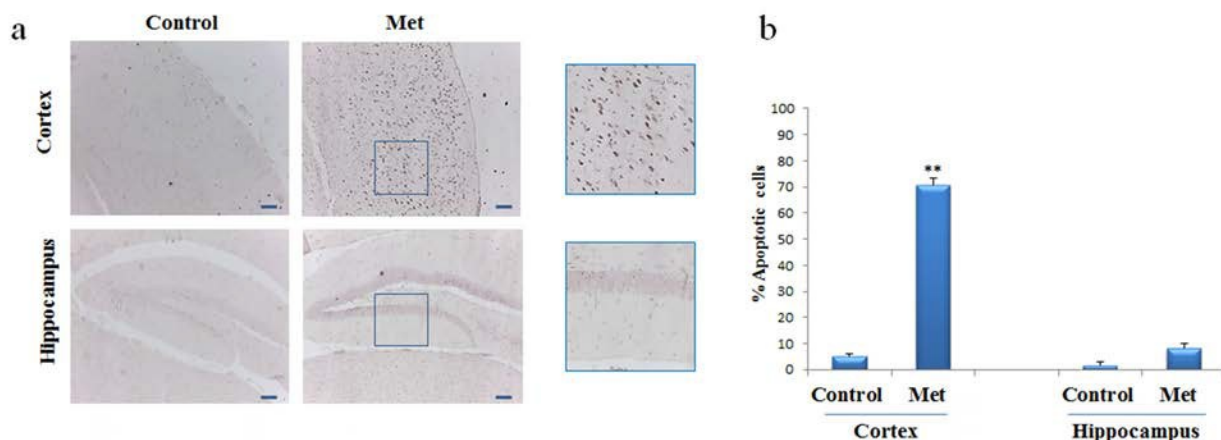


**Figure 5. Metformin induces apoptosis mainly in neurons of cortex region.** TUNEL assay was performed on the paraffin sections of cortex and hippocampus obtained from mice untreated or treated with metformin to detect apoptotic nuclei (brown). (a) Representative cortex and hippocampus brain sections stained with TUNEL in control and metformin treated mice. High magnification of the squared areas is shown. (b) The histogram indicates the percentage of positive cells both in cortex and hippocampus regions normalized to the control. 10X original magnification. Scale bars = 100  $\mu$ m. n=5 per group.

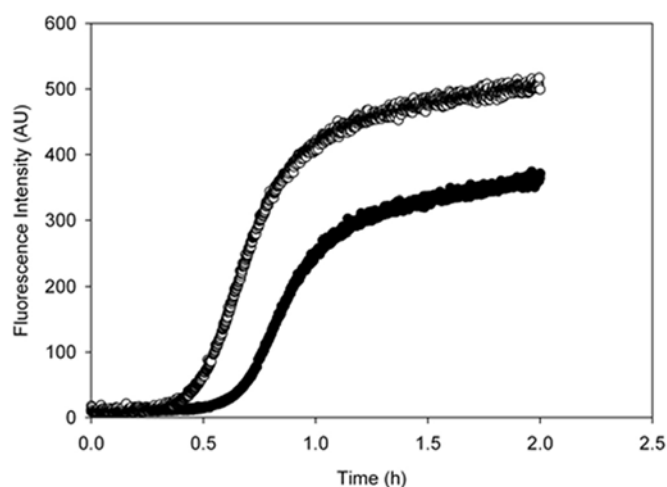


**Figure 6. Metformin increases the lag-phase duration and reduces the final amount of amyloid fibrils.** Aggregation kinetics of 50  $\mu$ M  $A\beta_{1-40}$  was followed in the absence (empty circles) and in the presence (black circles) of 2mM metformin by ThT assay. The dye concentration was 12 $\mu$ M.

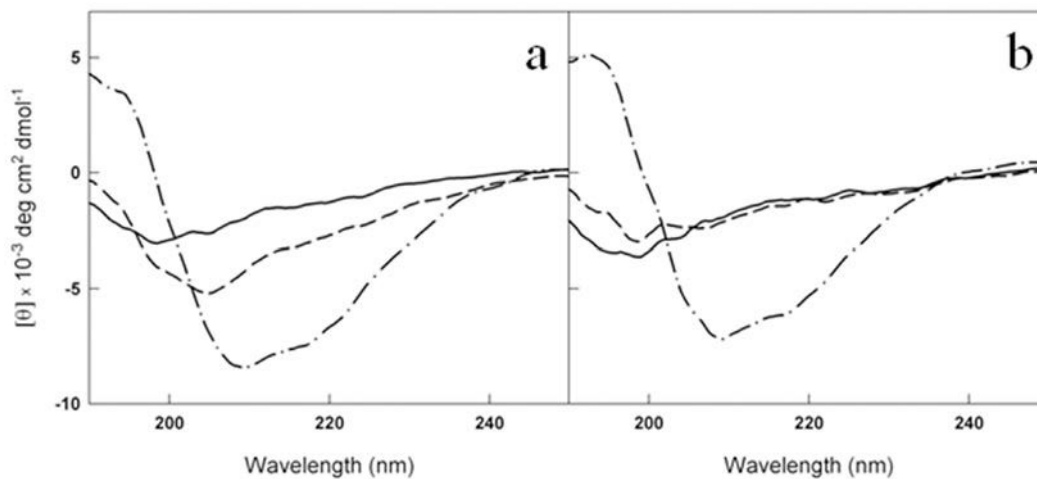


**Figure 7. Metformin delays the conversion of A $\beta$ <sub>1-40</sub> from disordered coil to  $\beta$ -sheet structure.** Far-UV CD spectra of 50  $\mu$ M A $\beta$ <sub>1-40</sub> at t<sub>0</sub> (solid lines), t=0.5 h (dashed lines) and t=2h (dot dashed lines) at 37 °C in the absence (a) and in the presence (b) of 2mM metformin. The signals from the buffer and metformin in buffer have been subtracted from the spectra in (a) and (b), respectively.

The size distribution for samples collected at the end of aggregation kinetics reveals for the A $\beta$ <sub>1-40</sub> sample grown in the absence of metformin, a marked shift towards higher values in comparison to the initial time, probably corresponding to mature fibril formation. In contrast, only a little increase in the average hydrodynamic diameter (from 300 to 600 nm) in the correspondent sample incubated with the drug is detectable. The overall results from biophysical techniques converge in indicating that the metformin delays amyloid aggregation of A $\beta$ <sub>1-40</sub> peptide, reduces the amount of mature fibrils formed and, more important, stabilizes prefibrillar oligomeric species.

## DISCUSSION

We analyzed both biological and biophysical aspects to understand the molecular mechanisms induced by metformin and leading to neurodegeneration in mouse brain. Fluorescence measurements of ex vivo mouse brain performed by using the intrinsic fluorescence signal of the metformin gave us the direct confirmation that the drug had reached the central organ by crossing the BBB. For mouse treatment, an experimental dose, deduced by those utilized in other works, which uses the same C57B6/J strain, was employed [17,21]. In particular, Chen et al. administering 2mg/ml, and using liquid chromatography-mass spectrometry, measured that metformin reaches a concentration of about 2  $\mu$ M and 1  $\mu$ M in the plasma and in the brain, respectively, well below the 10–40  $\mu$ M achieved in human plasma

[20]. Moreover, since the drug is eliminated via renal secretion in few hours, the mice were treated for three months to determine the incidence of long-term administration on the risk of AD developing. Activation of AMPK was considered as a marker of metformin-induced biochemical answer in brain, even if we cannot exclude that the response to metformin could not be limited only to its activation, but mediated by additional mechanisms depending directly or not by AMPK. Furthermore, these data are supported by the finding that metformin uptake in the brain can be mediated by the organic cation transporter 3 (OCT3), a member of the SLC22A family, which in turn modulates the pharmacologic action of metformin on AMPK [41]. After metformin chronic treatment BACE1 and APP, the enzyme-substrate required for A $\beta$  production, are differently modulated, mainly in the cortex where an enhanced APP processing was assumed. This result coincides with the discovery that metformin increases A $\beta$  generation in cultured neurons due to induction of BACE expression [17]. Modulation of BACE transcription has been reported to depend on the pathway involving activated AMPK, being antagonized by the AMPK inhibitor compound C [17]. It has been postulated that metformin modulates BACE1 and APP transcription activating a signal including AMPK and leading to increase A $\beta$  production [17]. More recently it has been demonstrated that metformin induces up-regulation of APP and PSN1 through a mechanism involving oxidative stress, mitochondrial dysfunction and Nf- $\kappa$ B activation [21]. Further support to these

findings was given by immunofluorescence analysis in the mouse brain regions that are vulnerable in AD pathogenesis. The inspection showed a large number of A $\beta$  aggregates in the cerebral cortex, whereas no significant A $\beta$  deposits were detected in the hippocampus. In particular, in the cortex we found a quite different distribution of APP in control and metformin treated mice, confirming that an increased processing leading to A $\beta$  oligomerization or aggregate formation were occurred.

However, this result was in agreement with the evolution of the temporal-spatial accumulation of A $\beta$  described in AD [42]. In line with these results, increase of typical AD biomarkers and A $\beta$  aggregates in the cortex area and no in the hippocampus, denotes that we have focalized a molecular moment comparable to an early neurodegenerative stage. However, we can hypothesize that the different effects of metformin in cortex and hippocampus areas could be due to a diverse metformin distribution or accumulation. In fact, analysis

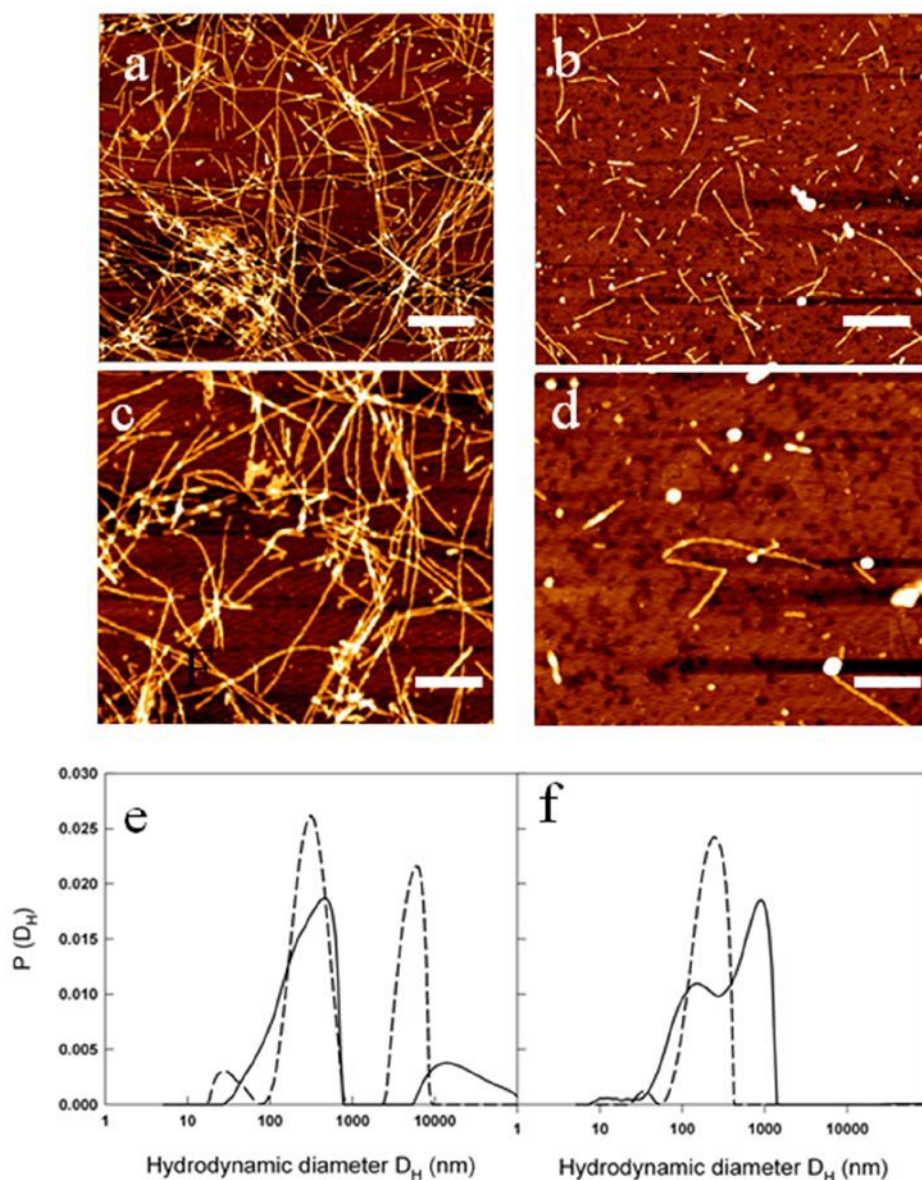


**Figure 8. Metformin effects on fibril size and growth.** (a-d) AFM images acquired for: 50 μM A $\beta$ <sub>1-40</sub> at the end of the kinetics at 37 °C and 200 rpm at two different magnifications: scale bar = 1 μm and Z-range = 8.9 nm (a); scale bar = 500 nm; Z-range = 8.3 nm (b). The samples were compared with 50 μM A $\beta$ <sub>1-40</sub> + 2 mM metformin at the end of the kinetics at 37 °C and 200 rpm at two different magnifications: scale bar = 1 μm and Z-range = 7.0 nm (c); scale bar = 500 nm; Z-range = 8.3 nm (d). Particle size distribution from DLS of 50 μM A $\beta$ <sub>1-40</sub> incubated at 37 °C and 200 rpm in the absence (e) and in the presence (f) of 2 mM metformin after 0.5 h (dashed lines) and 2 hrs (solid lines) from the beginning of amyloid aggregation process.

of seven rat brain regions, by HPLC method, has demonstrated that metformin concentrations varied in the different brain regions and, both after acute and chronic administration, it was higher in the cortex than in the hippocampus [43].

Our findings suggest that increased APP and A $\beta$  production, due to metformin exposition, could impair mitochondrial function in brain neurons acting in multiple ways on different targets. Metformin treatment changes the levels of expression of TOM40, VDAC1 and HKI, proteins involved in mitochondrial import and export of molecules and metabolites, in cortex region where A $\beta$  aggregates are mainly present. Studies on human brain biopsies have demonstrated that TOM40 pore mediates the internalization of A $\beta$  and APP [44]. Depending on the size of the molecules, the whole APP can block TOM40 channel and the small A $\beta$  can be imported in the inner membrane where affects the respiratory chain. Moreover, influx of A $\beta$  via the TOM40 pore increases Reactive Oxygen Species (ROS) within the organelle, leading to mitochondrial dysfunction and structural and functional damage of neurons [45]. In addition, ROS triggers events that include the increase of A $\beta$  production thus nourishing a vicious circle by which A $\beta$  self-feed its own production [21]. Thus, increased TOM40 could favor transport of A $\beta$  into the mitochondria and their impairing. In their physiological state, the dimensions of the VDAC1 pores are sufficient to selectively allow the passage of small molecules. During cell death processes, in which the release of folded proteins like cytochrome C is required, the formation of larger channels is necessary [46]. In line with this study we found VDAC1 in monomeric, with different electrophoretic mobility, dimeric and oligomeric configurations. VDAC1 is a  $\beta$ -barrel protein with a flexible N-Terminal domain that can be located within the pore by intramolecular crosslinking (Cys-Lys) or exposed to the cytosolic face that could associate with the N-Terminal region of another VDAC1 molecule leading to oligomerization [47]. Moreover, using different stimuli it has been demonstrated that the lower monomeric band appears only when apoptosis is induced [48], indicating that a neurodegenerative process has been locally produced. Furthermore, VDAC1 N-terminus has been found mediate the interaction of VDAC1 with anti-apoptotic proteins such as HKI [47], and VDAC1 oligomerization is considered relevant for interactions with proteins involved in apoptosis [46]. In the cortex region, where metformin-induced A $\beta$  aggregates are accumulated, and apoptotic neurons were observed, a decrease in the amount of monomers and an increase of intramolecular crosslinked products with a concomitant increase in oligomers formation were found. Furthermore, decrease

of HKI suggests that its binding to VDAC1 was displaced and the increased concentration of free VDAC1 molecules has promoted VDAC1 oligomerization. This is in line with the observation that A $\beta$  mediated neurodegeneration involves detachment of HKI from VDAC1 that oligomerizes and promotes cytochrome C release, events leading to apoptosis [28]. Thus, the increased presence of A $\beta$ , due to metformin treatment, could compete with the binding of HKI and/or other anti-apoptotic proteins with VDAC1 and be the apoptotic stimulus for enhancing VDAC1 oligomerization to produce enlarged pores capable to change permeability and mediate cytochrome C release, in critical brain region. In support of this observation direct interaction of A $\beta$  and phosphorylated tau with VDAC1 has been demonstrated [27,28]. A $\beta$  interaction is able to block mitochondrial pores and interfere with the transport of ATP, ADP and other metabolites between mitochondria and cytoplasm, leading to mitochondrial dysfunction and neurodegeneration [27]. Thus, the observed related increase of VDAC1, A $\beta$  and apoptotic cells, due to metformin administration, mainly in the cortex, could be an initial neurodegenerative event that could be spread to other brain regions as the disease progresses. However, this concept need of additional experimental supports. Lastly, being mitochondrial dysfunction considered an early pathophysiological event in AD, TOM40 and VDAC1 may be proposed as potential timeline biomarkers for this pathology [49]. Consistent with data is the change in expression levels of TOM40 and VDAC1 mainly in cerebral cortex, in a very local specific manner. However, our observations suggest a strong association between metformin-induced A $\beta$  accumulation and mitochondrial dysfunction via impaired TOM40 and VDAC1 expression that is cause of mitochondrial stress and, in turn, source of increased A $\beta$  production. Because many of these factors can be either a cause or a consequence of the others, it is difficult to establish a clear sequence of events. Finally, we cannot exclude that the effect of metformin seen in brain of mice after three months of exposition could be exacerbated by the damage induced by the physiological aging. However, the potentiality of this drug to produce side effects could be counteracted, as suggested in other studies, by its use in combination with insulin [17,18,21].

Very interestingly, by biophysical methods, our study also demonstrates that metformin is able to directly interact with A $\beta$  amyloid species involved in AD influencing their aggregation kinetics and features. Indeed, in the presence of metformin the typical sigmoidal profile of the fibrillogenesis shows an increased lag-phase and final reduction of amyloid fibrils, stabilizing the prefibrillar oligomeric species.

The direct influence on lag-phase reveals that metformin is able to influence the nucleation step of the process by the formation of a drug-A $\beta$  complex [50]. The molecule could exert a stabilizing effect on the on-pathway seeding species involved in  $\beta$ -sheet formation and monomer amyloid assembly.

From DLS and AFM, the presence of metformin sizably reduces the formation of large amyloid fibers, favoring the formation of smaller aggregates. Furthermore, these aggregates have dimensions comparable to that observed in mouse brains even if we cannot exclude that in vivo the size of the aggregates could be influenced by other entrapped extracellular components [3].

These results could provide the hypothesis on a different route by which, together with the others above described, metformin could be negatively correlated to AD pathogenesis. Indeed, in the wide structural polymorphism of A $\beta$  oligomers, the accredited assumption is that, rather than mature fibrils, the species more involved in pathogenesis of AD are prefibrillar oligomeric species that form at the beginning of the process [51,52]. These species expose larger hydrophobic

surfaces to the solvent and, therefore, could directly interact with cell membranes influencing calcium homeostasis and ROS production. It cannot be excluded, therefore, that the smaller species stabilized by metformin in vitro are those with higher cytotoxic potentiality, whereas mature fibrils, considered harmless, are much reduced in length and number. In this respect, also by a direct action on the product of APP cleavage, i.e. A $\beta$  peptide, the use of metformin could contribute to toxicity associated to AD.

The high prevalence of AD and T2DM in the elderly population suggests that concomitant pharmacotherapy could be desirable. Our findings indicate that metformin, the drug usually administered for T2DM, is able to reach the brain in C57B6/J mice, where it activates neurodegenerative pathways, including mitochondrial dysfunction and apoptosis, mainly in the brain cortex. Furthermore, metformin is able to directly interacts in vitro with A $\beta$ , modifying its aggregation profile, reducing the amount of mature fibrils and stabilizing toxic prefibrillar oligomeric species. A summary of the proposed mechanism is shown in figure 9. Thus, metformin induces different adverse effects, possibly leading to an overall increase of the risk of AD onset.

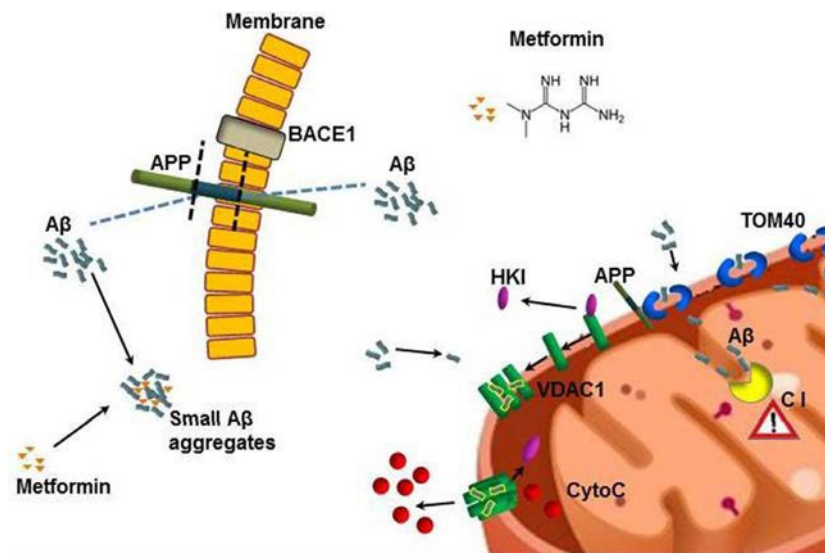


**Figure 9. Model describing how metformin induces A $\beta$  aggregates formation and mitochondrial dysfunction.** Metformin increases BACE1 production that stimulates APP processing and A $\beta$  production at cell membrane level. Metformin stabilizes small A $\beta$  aggregates that could be internalized. TOM40 pore mediates the mitochondrial internalization of A $\beta$  and APP. The whole APP can block TOM40 channel and the small A $\beta$  can be imported in the inner membrane where affects the Complex I (C I) of the respiratory chain. Small A $\beta$  aggregates displace the binding of HKI with mitochondrial VDAC1 leading to its oligomerization and the formation of large pores that are capable to change permeability and mediate the cytochrome C release. All these coexistent events lead to mitochondrial dysfunction and neuronal apoptosis.

## MATERIALS AND METHODS

### Mice

The experimental procedures employed in the present study were in accordance with the Italian D.L. no. 116 of 27 January 1992 and subsequent variations and the recommendations of the European Economic Community (86/609/ECC). The studies were approved by Ministero della Sanità (Rome, Italy). Male C57BL/6J (B6) mice, purchased from Harlan Laboratories (San Pietro al Natisone Udine, Italy) at 4 weeks of age, were housed under standard conditions of light (12h light: 12h darkness cycle) and temperature (22–24°C), with free access to water and food. After acclimatization (1 week), the animals were divided in two groups (n=10 per group), control and metformin treated. Mice were provided food and received metformin in drinking water (2 mg/mL) for 7 days or three months. After this treatment, animals were sacrificed by cervical dislocation and the brain of age-matched animals were immediately exported and processed for subsequent analysis, as previously described [7]. When necessary, hippocampus and cortex were separated. Biodistribution of metformin in ex vivo brain was detected by using Biospace Lab Imaging Instrument.

### Total protein extraction and western blotting

Brain of mice were homogenized in RIPA buffer (20 mM Tris, pH 7.4, 150 mM NaCl, 1 mM Na<sub>3</sub>VO<sub>4</sub>, 10 mM NaF, 1mM EDTA, 1 mM EGTA, 0.2 mM phenyl-methylsulfonyl fluoride, 1% Triton, 0.1%SDS, and 0.5% deoxycholate) with protease inhibitors (Amersham) and phosphatase inhibitor cocktail II and III (SIGMA). To remove insoluble material, tissue lysates were sonicated and centrifuged (14,000 rpm, at 4°C, for 30 min). Proteins (50 µg) were resolved by 10% SDS-PAGE gel and transferred onto nitrocellulose filters for Western blotting using anti-APP (1:1000), anti-BACE1 (1:1000) anti-phospho-AMPK (1:1000), anti-TOM40 (1:1000), anti-VDAC1 (1:1000), and anti-HKI (1:1000) purchased from Santa Cruz, anti-β-actin (1:5000) purchased from Sigma. Secondary antibodies conjugated to horseradish peroxidase (1:2000) purchased from Cell Signaling were detected using the NOVEX® ECL HRP chemiluminescence kit (Cat. n° WP20005, Invitrogen) according to the manufacturer's instructions. In some instances, antibodies were stripped from blots with Restore Western Blot Stripping Buffer (Thermo Scientific) for 10 minutes at room temperature, for antibody reprobing. Band intensities were analyzed with a gel documentation system (BioRad), expression was normalized with β-actin expression. The protein

levels were expressed as densitometry and percentage of controls.

### Immunofluorescence

For immunofluorescence the brains (n=5 per group) were embedded in paraffin as previously described [7] and coronally sectioned (5µm) using a microtome. Brain sections including the cerebral cortex and the hippocampus were mounted on slides and deparaffinized in xylene solution. Then, the slides were hydrated in a series of graded ethanol (96%, 85%, 70%, 50%) for 5 minutes each. After washing in water and PBS the slides were incubated with 3% BSA/PBS for 1 h. Next, the sections were incubated with anti-APP (1:50) (Santa Cruz) at 4 °C overnight. After washing in PBS, the samples were incubated with anti-rabbit Cy3-conjugate secondary antibody (1:500; SIGMA). For nuclear staining, the sections were incubated with Hoechst 33258 (5µg/ml) for 20 minutes. After washing in PBS the slides were mounted with cover slips and images were visualized by using a Leica DM5000 upright microscope (Leica Microsystems, Heidelberg, Germany) at 20X magnification.

### Thioflavin T staining

For Thioflavin-T (ThT) staining the brain sections including the cerebral cortex and the hippocampus were mounted on slides. The slides were deparaffinized in xylene solution and hydrated in a series of graded ethanol (96%, 85%, 70%, 50%) for 5 minutes each. After washing in water, the sections were incubated in filtered 1% aqueous ThT solution for 8 minutes at room temperature. The slides were then dehydrated in ethanol 80% and 95%, for 5 minutes each. After washing in water the slides were mounted with cover slips and the images were visualized by using a Leica DM5000 upright microscope (Leica Microsystems, Heidelberg, Germany) at 20x magnification.

### TUNEL assay

Terminal deoxynucleotidyl Transferase Biotin-dUTP Nick End Labeling (TUNEL)-positive apoptotic nuclei were detected in brain paraffin sections using an in situ cell death detection kit (Promega) according to manufacturer's instructions. The number of apoptotic cells was counted in randomly selected fields to calculate the ratio of apoptotic cell per brain area.

### Quantitative real-time PCR

Total RNA was extracted using RNEasy Mini Kit (Qiagen). Two ng of RNA was used to synthesize the

first strand cDNA using RT First-Strand kit (Qiagen). Synthesized cDNAs were amplified using RT2 SYBR Green/ROX qPCR Mastermix (Qiagen) and StepOne Real-Time instrument (Applied Biosystem). Gene expression validation was performed using RT2 qPCR Primer Assay for human APP, Presenilin1,  $\beta$ -actin (SABiosciences). Gene expression was normalized to  $\beta$ -actin.

### Statistical analysis

All experiments were repeated at least three times and each experiment was performed in triplicate. The results are presented as mean + SD. A one-way ANOVA was performed, followed by Dunnet's post hoc test for analysis of significance. Results with a p-value <0.05 were considered statistically significant, \*P < 0.05, \*\*P<0.02.

### Sample preparation for biophysics experiments

The synthetic peptide A $\beta$ <sub>1-40</sub> (Anaspec) was pretreated according to the procedure of Fezoui et al. [53] for improving the reliability of experiments at neutral pH. Stock aliquots (200  $\mu$ g each) were stored at -80 °C. Metformin was purchased from Sigma Aldrich. A $\beta$ <sub>1-40</sub> samples were prepared by dissolving the lyophilized peptide in 50 mM phosphate buffer, pH 7.4, at a concentration of about 70  $\mu$ M. The solution was filtered through 0.22  $\mu$ m and 20 nm filters into a fluorescence quartz cuvette containing a small magnetic stirring bar. A $\beta$ <sub>1-40</sub> concentration was determined by tyrosine absorption at 276 nm using an extinction coefficient of 1390 cm<sup>-1</sup>M<sup>-1</sup>. The sample was then diluted to the working concentration of 50  $\mu$  M by adding the appropriate amount of buffer, concentrated solution of ThT (1mM), and concentrated solution of metformin (20 mM) when required.

Final samples containing A $\beta$  and metformin were obtained by appropriate aseptically mixing of the protein solutions and placed in closed cuvettes in a cold room at 4 °C, before incubation at higher temperatures. The aggregation kinetics were followed at controlled temperature (37 °C) and under controlled stirring (200 rpm) for 24 hours.

### ThT spectrofluorometric measurements

ThT fluo-rescence emission was monitored by using a JASCO FP-6500 spectrometer. The excitation and emission wavelengths were 450 and 485 nm, respectively, with 3 nm slit width. ThT concentration was 12  $\mu$ M. The sample was placed at 37 °C in the thermostated cell compartment (10 mm). When

required, a magnetic stirrer at 200 rpm (mod. 300, Rank Brothers Ltd., Cambridge) was used.

Control fluorimetric experiments between Thioflavin T and metformin with the purpose of excluding undesired pitfalls due to potential interaction between the dye and the molecule [54] have been performed under the same conditions of aggregation kinetics (37 °C, under stirring).

### Circular dichroism spectroscopy

CD measurements were acquired by using a JASCO J-815 CD Spectrometer. Particularly, during the aggregation kinetics, withdrawals of samples at appropriate time were observed. Spectra were recorded at 20 °C using a quartz cell with 0.2 mm path length. Each spectrum measurement was obtained by averaging over eight scans and subtracting the blank solvent contribution.

The aggregation of A $\beta$  peptide in the presence or absence of metformin was investigated by Dynamic Light Scattering. The samples were placed into a dust-free quartz cell without further filtering and kept at 37°C in the thermostatic cell compartment of a Brookhaven Instruments BI200-SM goniometer. The temperature was controlled within 0.1 °C using a thermostatic recirculating bath. The light scattered intensity and its autocorrelation function were measured at  $\theta = 90^\circ$  by using a Brookhaven BI-9000 correlator and a 50 mW He-Ne laser tuned at a wavelength  $\lambda = 632.8$  nm. Due to their Brownian motion, particles moving in solution give rise to fluctuations in the intensity of the scattered light [55, 56]. The autocorrelator measures the homodyne intensity-intensity correlation function that, for a Gaussian distribution of the intensity profile of the scattered light, is related to the electric field correlation function:

$$g^{(2)}(q, t) = [A + Bg^{(1)}(q, t)]^2 \quad (1)$$

where  $A$  and  $B$  are the experimental baseline and the optical constant, respectively. For polydisperse particles,  $g^{(1)}(q, t)$  is given by:

$$g^{(1)}(q, t) = \int_0^\infty G(\Gamma) \exp(-\Gamma t) d\Gamma \quad (2)$$

Here,  $G(\Gamma)$  is the normalized number distribution function for the decay constant  $\Gamma = q^2 D_T$ , where  $q = (4\pi n/\lambda) \sin(\theta/2)$  is the scattering vector defining the spatial resolution with  $n$  and  $D_T$  being the solvent refractive index and the translational diffusion coefficient, respectively. The hydrodynamic diameter

$D_H$  is calculated from  $D_T$  through the Stokes–Einstein relationship:

$$D_T = \frac{k_B T}{3\eta r_{H,DH}} \quad (3)$$

where  $k_B$  is the Boltzmann constant,  $T$  is the absolute temperature, and  $\eta$  is the solvent viscosity. Intensity-weighted distribution functions  $P_i$  of the z-average hydrodynamic diameter  $D_H$  were obtained by the analysis of the intensity autocorrelation functions were analyzed by means of a CONTIN-like smoothing-constrained regularization method [57].

### Atomic Force Microscopy (AFM)

AFM measurements were performed by using a Nanowizard III (JPK Instruments, Germany) mounted on an Axio Observer D1 (Carl Zeiss, Germany) or on an Eclips Ti (Nikon, Japan) inverted optical microscope. Aliquots of protein solutions were deposited onto freshly cleaved mica surfaces (Agar Scientific, Assing, Italy) and incubated for up to 20 min before rinsing with deionized water and drying under a low pressure nitrogen flow. Imaging of the protein was carried out in intermittent contact mode in air by using NCHR silicon cantilever (Nanoworld, Switzerland) with nominal spring constant ranging from 21 to 78 N/m and typical resonance frequency ranging from 250 to 390 kHz.

### ACKNOWLEDGEMENTS

The authors wish to thank Alessia Provenzano and Fulvio Ferrante for their useful technical support.

### FUNDING

This research was partially supported by the grant from the Department of Productive Activities of the Sicilian Region (PO FESR 2007/2013) “Piattaforma Regionale di Ricerca Traslationale per la Salute” (B65E12000570008) and by the Italian grant FIRB “Future in Research” RBF12SIPT MIND: “Multidisciplinary Investigations for the Development of Neuroprotective Drugs”.

### CONFLICTS OF INTEREST

The authors declare no conflicts of interest.

### REFERENCES

1. Ott A, Stolk RP, van Harskamp F, Pols HA, Hofman A, Breteler MM. Diabetes mellitus and the risk of dementia: the Rotterdam Study. *Neurology*. 1999;53:1937–42.
2. Alzheimer’s Association. Alzheimer’s disease facts and figures Alzheimer’s & Dementia. 2015; 11:1-83.
3. Selkoe DJ. The cell biology of  $\beta$ -amyloid precursor protein and presenilin in Alzheimer’s disease. *Trends Cell Biol*. 1998; 8:447–53.
4. Walsh DM, Klyubin I, Fadeeva JV, Cullen WK, Anwyl R, Wolfe MS, Rowan MJ, Selkoe DJ. Naturally secreted oligomers of amyloid beta protein potently inhibit hippocampal long-term potentiation in vivo. *Nature*. 2002; 416:535–39.
5. Weingarten MD, Lockwood AH, Hwo SY, Kirschner MW. A protein factor essential for microtubule assembly. *Proc Natl Acad Sci USA*. 1975; 72:1858–62.
6. Hildreth KL, Van Pelt RE, Schwartz RS. Obesity, insulin resistance, and Alzheimer’s disease. *Obesity (Silver Spring)*. 2012; 20:1549–57.
7. Nuzzo D, Picone P, Baldassano S, Caruana L, Messina E, Marino Gammazza A, Cappello F, Mulè F, Di Carlo M. Insulin resistance as common molecular denominator linking obesity to Alzheimer’s disease. *Curr Alzheimer Res*. 2015; 12:723–35.
8. Watson GS, Craft S. The role of insulin resistance in the pathogenesis of Alzheimer’s disease: implications for treatment. *CNS Drugs*. 2003; 17:27–45.
9. Watson GS, Craft S. Modulation of memory by insulin and glucose: neuropsychological observations in Alzheimer’s disease. *Eur J Pharmacol*. 2004; 490:97–113.
10. De Felice FG. Alzheimer’s disease and insulin resistance: translating basic science into clinical applications. *J Clin Invest*. 2013; 123:531–39.
11. Ghasemi R, Haeri A, Dargahi L, Mohamed Z, Ahmadiani A. Insulin in the brain: sources, localization and functions. *Mol Neurobiol*. 2013; 47:145–71.
12. Picone P, Giacomazza D, Vetri V, Carrotta R, Militello V, San Biagio PL, Di Carlo M. Insulin-activated Akt rescues  $A\beta$  oxidative stress-induced cell death by orchestrating molecular trafficking. *Aging Cell*. 2011; 10:832–43.
13. Steen E, Terry BM, Rivera EJ, Cannon JL, Neely TR, Tavares R, Xu XJ, Wands JR, de la Monte SM. Impaired insulin and insulin-like growth factor expression and signaling mechanisms in Alzheimer’s disease—is this type 3 diabetes? *J Alzheimers Dis*. 2005; 7:63–80.
14. Di Carlo M, Picone P, Carrotta R, Giacomazza D, San Biagio PL. Insulin promotes survival of amyloid-beta oligomers neuroblastoma damaged cells via caspase 9 inhibition and Hsp70 upregulation. *J Biomed Biotechnol*. 2010; 2010:147835.
15. Picone P, Ditta LA, Sabatino MA, Militello V, San Biagio PL, Di Giacinto ML, Cristaldi L, Nuzzo D, Dispenza C, Giacomazza D, Di Carlo M. Ionizing radiation-engineered nanogels as insulin nanocarriers for the development of a new strategy for the treatment of Alzheimer’s disease. *Biomaterials*. 2016; 80:179–94.

16. Wang J, Gallagher D, DeVito LM, Cancino GI, Tsui D, He L, Keller GM, Frankland PW, Kaplan DR, Miller FD. Metformin activates an atypical PKC-CBP pathway to promote neurogenesis and enhance spatial memory formation. *Cell Stem Cell*. 2012; 11:23–35.
17. Chen Y, Zhou K, Wang R, Liu Y, Kwak YD, Ma T, Thompson RC, Zhao Y, Smith L, Gasparini L, Luo Z, Xu H, Liao FF. Antidiabetic drug metformin (GlucophageR) increases biogenesis of Alzheimer's amyloid peptides via up-regulating BACE1 transcription. *Proc Natl Acad Sci USA*. 2009; 106:3907–12.
18. Beeri MS, Schmeidler J, Silverman JM, Gandy S, Wysocki M, Hannigan CM, Purohit DP, Lesser G, Grossman HT, Haroutunian V. Insulin in combination with other diabetes medication is associated with less Alzheimer neuropathology. *Neurology*. 2008;71:750–57.
19. Imfeld P, Bodmer M, Jick SS, Meier CR. Metformin, other antidiabetic drugs, and risk of Alzheimer's disease: a population-based case-control study. *J Am Geriatr Soc*. 2012; 60:916–21.
20. Zhou G, Myers R, Li Y, Chen Y, Shen X, Fenyk-Melody J, Wu M, Ventre J, Doebber T, Fujii N, Musi N, Hirshman MF, Goodyear LJ, Moller DE. Role of AMP-activated protein kinase in mechanism of metformin action. *J Clin Invest*. 2001; 108:1167–74.
21. Picone P, Nuzzo D, Caruana L, Messina E, Barera A, Vasto S, Di Carlo M. Metformin increases APP expression and processing via oxidative stress, mitochondrial dysfunction and NF- $\kappa$ B activation: use of insulin to attenuate metformin's effect. *Biochim Biophys Acta*. 2015; 1853:1046-1059.
22. Schäfer G, Rieger E. Interaction of biguanides with mitochondrial and synthetic membranes. Effects on ion conductance of mitochondrial membranes and electrical properties of phospholipid bilayers. *Eur J Biochem*. 1974; 46:613–23.
23. Detaille D, Guigas B, Leverve X, Wiernsperger N, Devos P. Obligatory role of membrane events in the regulatory effect of metformin on the respiratory chain function. *Biochem Pharmacol*. 2002;63:1259–72.
24. Carvalho C, Correia S, Santos MS, Seica R, Oliveira CR, Moreira PI. Metformin promotes isolated rat liver mitochondria impairment. *Mol Cell Biochem*. 2008; 308:75–83.
25. Suski M, Olszanecki R, Chmura Ł, Stachowicz A, Madej J, Okoń K, Adamek D, Korbut R. Influence of metformin on mitochondrial subproteome in the brain of apoE knockout mice. *Eur J Pharmacol*. 2016;772:99–107.
26. Gottschalk WK, Lutz MW, He YT, Saunders AM, Burns DK, Roses AD, Chiba-Falek O. The broad impact of TOM40 on neurodegenerative diseases in aging. *J Parkinsons Dis Alzheimers Dis*. 2014; 1:1–25.
27. Manczak M, Reddy PH. Abnormal interaction of VDAC1 with amyloid beta and phosphorylated tau causes mitochondrial dysfunction in Alzheimer's disease. *Hum Mol Genet*. 2012; 21:5131–46.
28. Smilansky A, Dangoor L, Nakdimon I, Ben-Hail D, Mizrahi D, Shoshan-Barmatz V. The voltage-dependent anion channel 1 mediates amyloid  $\beta$  toxicity and represents a potential target for Alzheimer disease therapy. *J Biol Chem*. 2015; 290:30670–83.
29. Karran E, Mercken M, De Strooper B. The amyloid cascade hypothesis for Alzheimer's disease: an appraisal for the development of therapeutics. *Nat Rev Drug Discov*. 2011; 10:698–712.
30. Carrotta R, Di Carlo M, Manno M, Montana G, Picone P, Romancino D, San Biagio PL. Toxicity of recombinant beta-amyloid prefibrillar oligomers on the morphogenesis of the sea urchin *Paracentrotus lividus*. *FASEB J*. 2006; 20:1916–17.
31. Picone P, Carrotta R, Montana G, Nobile MR, San Biagio PL, Di Carlo M. A $\beta$  oligomers and fibrillar aggregates induce different apoptotic pathways in LAN5 neuroblastoma cell cultures. *Biophys J*. 2009;96:4200–11.
32. Mannini B, Mulvihill E, Sgromo C, Cascella R, Khodarahmi R, Ramazzotti M, Dobson CM, Cecchi C, Chiti F. Toxicity of protein oligomers is rationalized by a function combining size and surface hydrophobicity. *ACS Chem Biol*. 2014; 9:2309–17.
33. Novitskaya V, Bocharova OV, Bronstein I, Baskakov IV. Amyloid fibrils of mammalian prion protein are highly toxic to cultured cells and primary neurons. *J Biol Chem*. 2006; 281:13828–36.
34. Bucciantini M, Nosi D, Forzan M, Russo E, Calamai M, Pieri L, Formigli L, Quercioli F, Soria S, Pavone F, Savistchenko J, Melki R, Stefani M. Toxic effects of amyloid fibrils on cell membranes: the importance of ganglioside GM1. *FASEB J*. 2012; 26:818–31.
35. Bucciantini M, Rigacci S, Stefani M. Amyloid aggregation: role of biological membranes and the aggregate–membrane system. *J Phys Chem Lett*. 2014; 5:517–27.
36. Lomakin A, Teplow DB, Kirschner DA, Benedek GB. Kinetic theory of fibrillogenesis of amyloid beta-protein. *Proc Natl Acad Sci USA*. 1997; 94:7942–47.
37. Lee CC, Nayak A, Sethuraman A, Belfort G, McRae GJ. A three-stage kinetic model of amyloid fibrillation. *Biophys J*. 2007; 92:3448–58.
38. LeVine H 3rd. Thioflavine T interaction with synthetic Alzheimer's disease beta-amyloid peptides: detection of amyloid aggregation in solution. *Protein Sci*. 1993; 2:404–10.
39. Naiki H, Higuchi K, Hosokawa M, Takeda T. Fluorometric determination of amyloid fibrils in vitro using the fluorescent dye, thioflavin T1. *Anal Biochem*. 1989; 177:244–49.
40. Coelho-Cerqueira E, Pinheiro AS, Follmer C. Pitfalls associated with the use of Thioflavin-T to monitor anti-fibrillogenic activity. *Bioorg Med Chem Lett*. 2014; 24:3194–98.

41. Chen L, Pawlikowski B, Schlessinger A, More SS, Stryke D, Johns SJ, Portman MA, Chen E, Ferrin TE, Sali A, Giacomini KM. Role of organic cation transporter 3 (SLC22A3) and its missense variants in the pharmacologic action of metformin. *Pharmacogenet Genomics*. 2010;20:687–99.
42. Khan UA, Liu L, Provenzano FA, Berman DE, Profaci CP, Sloan R, Mayeux R, Duff KE, Small SA. Molecular drivers and cortical spread of lateral entorhinal cortex dysfunction in preclinical Alzheimer's disease. *Nat Neurosci*. 2014; 17:304–11.
43. Łabuzek K, Suchy D, Gabryel B, Bielecka A, Liber S, Okopień B. Quantification of metformin by the HPLC method in brain regions, cerebrospinal fluid and plasma of rats treated with lipopolysaccharide. *Pharmacol Rep*. 2010; 62:956–65.
44. Hansson Petersen CA, Alikhani N, Behbahani H, Wiehager B, Pavlov PF, Alafuzoff I, Leinonen V, Ito A, Winblad B, Glaser E, Ankarcrona M. The amyloid  $\beta$ -peptide is imported into mitochondria via the TOM import machinery and localized to mitochondrial cristae. *Proc Natl Acad Sci USA*. 2008; 105:13145–50.
45. Reddy PH. Amyloid beta, mitochondrial structural and functional dynamics in Alzheimer's disease. *Exp Neurol*. 2009; 218:286–92.
46. Zalk R, Israelson A, Garty ES, Azoulay-Zohar H, Shoshan-Barmatz V. Oligomeric states of the voltage-dependent anion channel and cytochrome c release from mitochondria. *Biochem J*. 2005;386:73–83.
47. Geula S, Ben-Hail D, Shoshan-Barmatz V. Structure-based analysis of VDAC1: n-terminus location, translocation, channel gating and association with anti-apoptotic proteins. *Biochem J*. 2012; 444:475–85.
48. Keinan N, Tyomkin D, Shoshan-Barmatz V. Oligomerization of the mitochondrial protein voltage-dependent anion channel is coupled to the induction of apoptosis. *Mol Cell Biol*. 2010; 30:5698–709.
49. Reddy PH. Is the mitochondrial outer membrane protein VDAC1 therapeutic target for Alzheimer's disease?. *Biochim Biophys Acta*. 2013; 1832:67–75.
50. Bartolini M, Bertucci C, Bolognesi ML, Cavalli A, Melchiorre C, Andrisano V. Insight into the kinetic of amyloid beta (1-42) peptide self-aggregation: elucidation of inhibitors' mechanism of action. *ChemBioChem*. 2007; 8:2152–61.
51. Hata S, Saito Y, Suzuki T. Alzheimer's Disease as a Membrane-Associated Enzymopathy of  $\beta$ -Amyloid Precursor Protein (APP) Secretases In: *Lipids and cellular membranes in amyloid diseases*, R Jelinek editor. 2011. New York: John Wiley.
52. Canale C, Seghezza S, Vilasi S, Carrotta R, Bulone D, Diaspro A, San Biagio PL, Dante S. Different effects of Alzheimer's peptide A $\beta$ (1-40) oligomers and fibrils on supported lipid membranes. *Biophys Chem*. 2013; 182:23–29.
53. Fezoui Y, Hartley DM, Harper JD, Khurana R, Walsh DM, Condron MM, Selkoe DJ, Lansbury PT Jr, Fink AL, Teplow DB. An improved method of preparing the amyloid beta-protein for fibrillogenesis and neurotoxicity experiments. *Amyloid*. 2000; 7:166–78.
54. Hudson SA, Ecroyd H, Kee TW, Carver JA. The thioflavin T fluorescence assay for amyloid fibril detection can be biased by the presence of exogenous compounds. *FEBS J*. 2009; 276:5960–72.
55. Pusey PN. Introduction to scattering experiments In: *Neutrons, X-ray and light: scattering method applied to soft condensed matter*, Th Zemb, P Lindner, editors. Amsterdam: Elsevier; 2002; 3-22.
56. Berne BJ, Pecora R. *Dynamic Light Scattering*. New York: John Wiley; 1976.
57. Stepanek P. The method and some applications In: *Dynamic light scattering*, W Brown editor. Oxford, UK: Clarendon Press; 1993.

## Reversal of cognitive decline in Alzheimer's disease

Dale E. Bredesen<sup>1,2</sup>, Edwin C. Amos<sup>3</sup>, Jonathan Canick<sup>4</sup>, Mary Ackerley<sup>5</sup>, Cyrus Raji<sup>6</sup>, Milan Fiala<sup>7</sup>, and Jamila Ahdidan<sup>8</sup>

<sup>1</sup>Easton Laboratories for Neurodegenerative Disease Research, Department of Neurology, University of California, Los Angeles, CA 90095, USA

<sup>2</sup>Buck Institute for Research on Aging, Novato, CA 94945, USA

<sup>3</sup>Department of Neurology, University of California, Los Angeles, CA 90095, USA

<sup>4</sup>Memory Clinic, California Pacific Medical Center, San Francisco, CA 94115, USA

<sup>5</sup>Private Practice of Psychiatry, Tucson, AZ 85718, USA

<sup>6</sup>Department of Radiology, University of California, Los Angeles, CA 90095, USA

<sup>7</sup>Department of Surgery, University of California, Los Angeles, CA 90095, USA

<sup>8</sup>Brainreader, Horsens, Denmark

**Key words:** neurodegeneration, cognition, biomarkers, dementia, neuropsychology, imaging, Alzheimer's disease, Apolipoprotein E

**Received:** 04/12/16; **Accepted:** 05/30/16; **Published:** 06/12/16

**doi:** [10.18632/aging.100981](https://doi.org/10.18632/aging.100981)

**Correspondence to:** Dale E. Bredesen, MD; **E-mail:** [dbredesen@buckinstitute.org](mailto:dbredesen@buckinstitute.org)

**Abstract:** Alzheimer's disease is one of the most significant healthcare problems nationally and globally. Recently, the first description of the reversal of cognitive decline in patients with early Alzheimer's disease or its precursors, MCI (mild cognitive impairment) and SCI (subjective cognitive impairment), was published [1]. The therapeutic approach used was programmatic and personalized rather than monotherapeutic and invariant, and was dubbed metabolic enhancement for neurodegeneration (MEND). Patients who had had to discontinue work were able to return to work, and those struggling at work were able to improve their performance. The patients, their spouses, and their co-workers all reported clear improvements. Here we report the results from quantitative MRI and neuropsychological testing in ten patients with cognitive decline, nine ApoE4+ (five homozygous and four heterozygous) and one ApoE4-, who were treated with the MEND protocol for 5-24 months. The magnitude of the improvement is unprecedented, providing additional objective evidence that this programmatic approach to cognitive decline is highly effective. These results have far-reaching implications for the treatment of Alzheimer's disease, MCI, and SCI; for personalized programs that may enhance pharmaceutical efficacy; and for personal identification of ApoE genotype.

### INTRODUCTION

Alzheimer's disease is now the third leading cause of death in the United States, following only cardiovascular disease and cancer [1]. There are approximately 5.2 million Americans with AD, but this estimate ignores the many young Americans destined to develop AD during their lifetimes: given the lifetime risk of approximately 15% when including all ApoE genotypes, as many as 45 million of the 318 million Americans now living may develop AD during their lifetimes if no prevention is instituted[2].

Effective treatment of Alzheimer's disease has been lacking, but recently a novel programmatic approach involving metabolic enhancement was described, with promising anecdotal results [3]. This treatment is based on connectomic studies [4] and previous transgenic findings [5] as well as epidemiological studies of various monotherapeutic components of the overall program [6]. The approach is personalized, responsive to suboptimal metabolic parameters that reflect a network imbalance in synaptic establishment and maintenance vs. reorganization, and progressive in

that continued optimization is sought through iterative treatment and metabolic characterization.

Here we report the initial follow-up of ten patients who were treated with this metabolic programmatics approach. One patient had well documented mild cognitive impairment (MCI), with a strongly positive amyloid-PET (positron emission tomography) scan, positive FDG-PET scan (fluorodeoxyglucose PET scan), abnormal neuropsychological testing, and hippocampal volume reduced to 17<sup>th</sup> percentile; after 10 months on the MEND protocol, his hippocampal volume had increased to 75<sup>th</sup> percentile, in association with a reversal of cognitive decline. Another patient had well documented early Alzheimer's disease, with a positive FDG-PET scan and markedly abnormal neuropsychological testing. After 22 months on the MEND protocol, he showed marked improvement in his neuropsychological testing, with some improvements reaching three standard deviations from his earlier testing.

The initial results for these patients show greater improvements than have been reported for other patients treated for Alzheimer's disease. The results provide further support for the suggestion that such a comprehensive approach [3] to treat early Alzheimer's disease and its precursors, MCI and SCI, is effective. The results also support the need for a large-scale, personalized clinical trial using this protocol.

## RESULTS

### Case studies

**Patient 1.** A 66-year-old professional man presented with what he described as "senior moments" (for example, forgetting where his keys were or forgetting appointments) of two-years duration, and difficulty performing his work. There was a positive family history of dementia in both parents. He was an ApoE4 heterozygote (3/4), his amyloid PET scan was markedly positive, and his fluorodeoxyglucose (FDG) PET scan showed temporoparietal reduced glucose utilization indicative of Alzheimer's disease. An MRI showed hippocampal volume at only 17<sup>th</sup> percentile for his age. His neuropsychological testing was compatible with a diagnosis of MCI. His hs-CRP was 9.9mg/l, albumin: globulin ratio was 1.6, homocysteine 15.1 $\mu$ mol/l, fasting glucose 96mg/dl, hemoglobin A1c 5.5%, fasting insulin 32mIU/l, 25-hydroxychole-calciferol 21ng/ml, TSH 2.21mIU/l, and testosterone 264ng/dl.

He began the MEND protocol [3], lost 18 pounds, and after three months his wife reported that his memory

had improved. He noted that his work came more easily to him. However, after five months, he discontinued the majority of the program for approximately three weeks. His wife came home to find his car in the driveway, idling with the keys in the ignition, while he was inside the house, working and unaware that he had left the car idling in the driveway. He re-initiated the program, and had no further such episodes.

After 10 months on the program, he returned for a follow-up MRI, which was subjected to volumetric analyses by both Neuroquant [7] and Neuroreader [8] programs. The former indicated an increase in hippocampal volume from 17<sup>th</sup> percentile to 75<sup>th</sup> percentile, with an associated absolute increase in hippocampal volume of 11.7%. The Neuroreader program showed an absolute increase from 7.65cc to 8.3cc, which represents an 8.5% absolute increase in size. The associated Z-scores were -4.6 and +1.6, respectively, disclosing an increase from <5<sup>th</sup> percentile to the 90<sup>th</sup> percentile. Thus although the Neuroquant and Neuroreader analyses differed somewhat in the amplitude of the effect detected, they were in agreement that a relatively large magnitude increase in hippocampal volume had occurred.

Follow-up metabolic analysis also disclosed improvement, with hs-CRP having decreased from 9.9mg/l to 3mg/l, fasting insulin having decreased from 32mIU/l to 8mIU/l, homocysteine having decreased from 15.1 $\mu$ mol/l to 8 $\mu$ mol/l, and 25-hydroxychole-calciferol having increased from 21ng/ml to 40ng/ml. See Table 1 for a summary of the responses of all patients to the treatment program.

Comment: This patient had well documented Alzheimer's disease, with a strongly positive amyloid PET scan, characteristic FDG PET scan, abnormal neuropsychological studies, positive family history, ApoE4-positive (3/4) genotype, and hippocampal volume of 17<sup>th</sup> percentile. During his 10 months on the MEND protocol, he interrupted his otherwise good compliance once, and this was associated with an episode of memory loss, in which he failed to remember that he had left his car in the driveway while he was working in his house. He returned to the protocol at that time, and after 10 months in total, he demonstrated not only a marked symptomatic improvement (which had begun after approximately three months on the protocol), but also a dramatic increase in hippocampal volume. More modest hippocampal volumetric increases have been described with exercise [9] and with a brain-training program [10], but to our knowledge the magnitude of hippocampal volume

increase that occurred with this patient has not been reported previously.

**Patient 2.** This is a follow-up on patient 2 from a previous publication [3]. A 69-year-old entrepreneur and professional man presented with 11 years of slowly progressive memory loss, which had accelerated over the past one to two years. In 2002, at the age of 58, he had been unable to recall the combination of the lock on his locker, and he felt that this was out of the ordinary for him. In 2003, he had an FDG PET scan, which was read as showing a pattern typical for early Alzheimer’s disease, with reduced glucose utilization in the parietotemporal cortices bilaterally and left > right temporal lobes, but preserved utilization in the frontal lobes, occipital cortices, and basal ganglia. In 2003, 2007, and 2013, he had quantitative neuropsychological testing, which showed a reduction in CVLT (California

Verbal Learning Test), a Stroop color test at 16<sup>th</sup> percentile, and auditory delayed memory at 13<sup>th</sup> percentile. In 2013, he was found to be heterozygous for ApoE4 (3/4). He noted that he had progressive difficulty recognizing the faces at work (prosopagnosia), and had to have his assistants prompt him with the daily schedule. He also recalled an event during which he was several chapters into a book before he finally realized that it was a book he had read previously. In addition, he lost an ability he had had for most of his life: the ability to add columns of numbers rapidly in his head.

He was advised that, given his status as an Alzheimer’s disease patient and his clear progression, as well as his poor performance on the 2013 test, he should begin to “get his affairs in order.” His business was in the process of being shut down due to his inability to continue work.

**Table 1. Patient responses to the MEND treatment protocol [3].**

<b>Patient</b>	<b>Diagnosis</b>	<b>ApoE Genotype</b>	<b>Treatment Outcome<sup>1</sup></b>
66yoM	MCI, type 1 (inflammatory)	3/4	Marked subjective improvement, hippocampal volume increase 17 <sup>th</sup> ->75 <sup>th</sup> %ile
69yoM	AD, type 2 (atrophic)	3/4	Marked subjective improvement, quantitative neuropsychological testing improvement
49yoF	MCI, type 2 (and possibly type 3 (toxic))	4/4	Marked subjective improvement, neuropsychological testing improvement
49yoF	MCI, type 2	2/4	Marked subjective improvement, neuropsychological testing improvement
55yoF	MCI, type 2	4/4	Marked subjective improvement, neuropsychological testing improvement
74yoM	AD, type 1	4/4	Subjective improvement, MMSE 23->30
62yoM	AD, type 1.5 (glycotoxic)	4/4	Subjective improvement, MMSE 22->29
68yoM	MCI, type 1.5	3/4	Subjective improvement, neuropsychological testing improvement
54yoF	AD, type 3	3/3	Clear subjective improvement, MoCA 19->21
54yoF	MCI, type 2	4/4	Subjective improvement, neuropsychological testing improvement

<sup>1</sup>See text for details of treatment outcome.

His laboratory values included a homocysteine of 18  $\mu\text{mol/l}$ , CRP  $<0.5\text{mg/l}$ , 25-hydroxycholecalciferol 28ng/ml, hemoglobin A1c 5.4%, serum zinc 78mcg/dl, serum copper 120mcg/dl, copper:zinc ratio of 1.54, ceruloplasmin 25mg/dl, pregnenolone 6ng/dl, testosterone 610ng/dl, albumin:globulin ratio of 1.3, cholesterol 165mg/dl (on atorvastatin), HDL 92mg/dl, LDL 64mg/dl, triglycerides 47mg/dl, AM cortisol 14mcg/dl, free T3 3.02pg/ml, free T4 1.27ng/l, TSH 0.58mIU/l, and BMI 24.9.

He began on the MEND therapeutic program, and after six months, his wife, co-workers, and he all noted improvement. He lost 10 pounds. He was able to recognize faces at work unlike before, was able to remember his daily schedule, and was able to function at work without difficulty. He was also noted to be quicker with his responses. His life-long ability to add columns of numbers rapidly in his head, which he had lost during his progressive cognitive decline, returned. His wife pointed out that, although he had clearly shown improvement, the more striking effect was that he had been accelerating in his decline over the prior year or two, and this had been completely halted.

After 22 months on the program, he returned for follow-up quantitative neuropsychological testing, which revealed marked improvement: his CVLT-IIB had increased from 3<sup>rd</sup> percentile to 84<sup>th</sup> percentile (3 standard deviations), total recognized hits from  $<1^{\text{st}}$  percentile to 50<sup>th</sup> percentile, CVLT-II from 54<sup>th</sup> percentile to 96<sup>th</sup> percentile, auditory delayed memory from 13<sup>th</sup> percentile to 79<sup>th</sup> percentile, reverse digit span from 24<sup>th</sup> percentile to 74<sup>th</sup> percentile, and processing speed from 93<sup>rd</sup> percentile to 98<sup>th</sup> percentile. His business, which had been in the process of termination, was reinvigorated, and a new site was added to the previous sites of operation.

Comment: This patient had well-documented Alzheimer's disease, with an ApoE4-positive genotype, characteristic FDG-PET scan, characteristic abnormalities on neuropsychological testing, well documented decline on longitudinal quantitative neuropsychological testing, and progression of symptoms. After two years on the protocol, his symptoms and neuropsychological testing improved markedly. The neuropsychologist who performed and evaluated his testing pointed out that his improvement was beyond that which had been observed in the neuropsychologist's 30 years of practice.

**Patient 3.** A woman late in her fifth decade began to note episodes of forgetfulness, such as returning home from shopping without the items she had purchased.

She also placed household items in the wrong locations repeatedly, and frequently failed to recognize previously familiar faces. She had difficulty remembering which side of the road on which to drive. A male cousin had developed Alzheimer's disease in his fifth decade. She was found to be an ApoE4 homozygote. On-line cognitive evaluation showed her to be at the 35<sup>th</sup> percentile for her age, despite her having been an excellent student earlier in her life.

She began various parts of the MEND protocol, and slowly added protocol features over several months. She began to note improvement, and her on-line cognitive evaluation improved to the 98<sup>th</sup> percentile, where it has remained to the current time, with her having been on the protocol for 3.5 years.

Comment: This patient showed early but definite cognitive decline, documented by on-line quantitative cognitive testing. Her marked improvement has now been sustained for 3.5 years. As described for patient 3 in a previous report [3], her improvement was iterative, with continued optimization over several months.

**Patient 4.** A 49-year-old woman noted progressive difficulty with word finding, and noted that her vocabulary had become more limited. She also began to feel unsure about her navigation during driving. She also complained of difficulty with facial recognition (prosopagnosia). Her recall was affected, and she described the requirement of "more energy" for recall of events. She had difficulty with remembering scheduled events. She also noted that her clarity and sharpness were reduced, leading to difficulties assisting her children with schoolwork. She had difficulty with complex conversations, and with reading comprehension. She also lost the ability she had had to speak two foreign languages.

Her family history was positive for Alzheimer's disease in her father, and her ApoE genotype was 2/4. Her MRI was read as normal, but volumetrics were not included. She underwent quantitative neuropsychological testing at a major university center, and was told that she was in the early stages of cognitive decline and therefore ineligible for the Alzheimer's prevention program, since she was already too late in the disease course for prevention. Her homocysteine was 10 $\mu\text{M}$ , hs-CRP 0.6mg/l, hemoglobin A1c 5.2%, fasting insulin 7mIU/l, TSH 1.6mIU/l, and 25-hydroxycholecalciferol 35ng/ml.

She began on the MEND protocol, and over the next several months she noted a clear improvement in recall, reading, navigating, vocabulary, mental clarity, and facial recognition. Her foreign language abilities

returned. Nine months after her initial neuropsychological testing, the testing was repeated at the same university site, and she was told that she no longer showed evidence of cognitive decline. Immediate and delayed recall, as well as semantic knowledge, executive function, and processing speed, had all shown improvement.

Comment: This patient had typical early amnesic MCI, which reverted over several months, resulting in a normal neuropsychological examination after nine months. She remains asymptomatic after one year on the program.

**Patient 5.** A 55-year-old woman presented with memory concerns of two-years duration. She had a positive family history of dementia in an aunt and a grandmother. She was an ApoE4 homozygote and a TOMM40 homozygote (G/G).

She experienced difficulties with word recall several times a day, either being unable to recall the word at all or substituting the wrong word in its place. For example, she would say a word like "tweezers" when she meant to say "tongs" (semantic paraphasic errors). She also experienced an increase in spelling errors as she typed on her computer. As a professional writer and editor with a master's degree in English, she found these issues very troubling. She often lost her train of thought while speaking, requiring her to ask others what she had just said. In addition, she would misplace items and forget why she had walked into a room. She would also forget some things her husband had told her or asked her to do.

She began the MEND protocol, and after four months her husband reported that her memory had improved. She noted that her word recall was as good as it had ever been, and she was no longer experiencing an increase in spelling errors. She also reported that she rarely lost her train of thought, but if she went off on a tangent or if someone interrupted her, that issue might return. However, if she paused and gave herself a few seconds, she could find her way back to her original train of thought without asking for help. In addition, she no longer forgot why she had entered a room, and only rarely misplaced items.

Her primary care provider noted that, in her professional opinion, her cognition had returned to normal after four months on the protocol, and an on-line cognitive test (CNS Vital Signs), performed prior to the start of the protocol and then again after five months on the protocol, confirmed this opinion: her overall cognitive assessment (neurocognitive index) had

increased from 16<sup>th</sup> percentile to 73<sup>rd</sup> percentile; composite memory from 1<sup>st</sup> percentile to 61<sup>st</sup> percentile; verbal memory from 3<sup>rd</sup> percentile to 93<sup>rd</sup> percentile; visual memory from 5<sup>th</sup> percentile to 14<sup>th</sup> percentile; executive function from 14<sup>th</sup> percentile to 58<sup>th</sup> percentile; and processing speed from 37<sup>th</sup> percentile to 81<sup>st</sup> percentile. Improvement had occurred in all sub-tests.

Comment: This patient is homozygous for ApoE4, and presented with amnesic MCI. She showed a clear response, both subjectively and objectively, to the metabolic protocol, and has sustained improvement over seven months.

**Patient 6.** A 74-year-old attorney presented with a five-year history of memory loss and word-finding difficulty. His family history was positive for dementia in his mother, beginning at the age of 75 years. He had been evaluated at an Alzheimer's disease center at the onset of his memory loss, and was found to be ApoE4/4, with MRI showing ventricular enlargement and temporal lobe atrophy, right > left, and FDG-PET showing reduced glucose utilization in the temporal lobes and the precuneus, compatible with Alzheimer's disease. Neuropsychological testing was compatible with a diagnosis of amnesic MCI. He was treated with donepezil, memantine, and intravenous immunoglobulin, and his MMSE fell from 27 to 23 over three years. He noted no improvement with the treatment.

He began the MEND protocol, and after six months, his MFI (phagocytosis index) was measured at 1260, with normal being >500 and most Alzheimer's patients scoring <500 [11, 12]. His MMSE was 29. He returned three months later, his MMSE was 30, and his MFI was 1210. He then returned three months after that, complaining that he had taken a trip, gone off much of the protocol, come under stress, and he felt that his memory had declined. His MFI at that visit had dropped to 230, a typical score for a patient with Alzheimer's disease, and his MMSE was 28. He was placed back on the protocol, and returned two months later, with MFI of 1100 and MMSE of 30. Over the ensuing 12 months, his MFI remained >1000 and his MMSE remained at 30.

Comment: This patient, homozygous for ApoE4/4, had a typical amnesic presentation and well documented Alzheimer's disease, unresponsive to donepezil, memantine, and intravenous immunoglobulin. His MMSE improved to a perfect 30 on the metabolic protocol, where it has remained for over one year. His longitudinal MFI supports the notion that MFI may

provide a “real time” method for following inflammatory/metabolic status, given the marked reduction when off the protocol with return to normal when he re-initiated the protocol.

**Patient 7.** A 57-year-old man began to have difficulty with memory and in work performance as a computer programmer, leading to dismissal from his job. Over the next five years his cognition continued to decline, he developed navigational difficulties, had difficulty with attention and multi-tasking, and became quieter and less self-assured. He had been a superb guitarist, and he lost both the chord progression memory and the nuance in his playing. Family history was positive for dementia in his mother, in her ninth decade. Evaluation by a neurologist included an unremarkable brain MRI without volumetrics, and he was placed on Aricept, which he discontinued after two months.

Seven years after his symptom onset, he was again evaluated, and found to be homozygous for ApoE4. An FDG PET scan was strongly suggestive of Alzheimer’s disease, with reductions in glucose utilization in the temporal, parietal, posterior cingulate, and frontal regions, with some asymmetry. He scored 22/30 on the mini-mental state examination, having lost points for failing to know the date or day, location, and failing tasks of attention and short-term recall. His BMI was 23.

A diagnosis of Alzheimer’s disease was made. His laboratory evaluation included an hs-CRP of 0.2mg/l, homocysteine 9.5µmol/l, albumin:globulin ratio of 1.6, hemoglobin A1c 5.7%, fasting insulin 4.9mIU/l, free T3 2.8pg/ml, free T4 1.3ng/l, TSH 2.1mIU/l, testosterone 281ng/dl, pregnenolone 44ng/dl, 25-hydroxycholecalciferol 38ng/ml, total cholesterol 145mg/dl (on atorvastatin), RBC magnesium 4.7mg/dl, serum copper 93mcg/dl, serum zinc 76mcg/dl, copper:zinc ratio 1.22, and AM cortisol 6.8mcg/dl. His Cyrex Array 2 was positive for gastrointestinal hyperpermeability, Cyrex Array 3 (for gluten sensitivity) was negative, and Cyrex Array 20 (for blood-brain barrier disruption) was negative.

He was placed on the MEND protocol, and his MMSE increased to 26 after four months, and to 29 after 10 months. His wife noticed clear improvement in his memory and navigation. His guitar skills improved, both his chord progressions and the nuances of his playing, such that he was able to play several pieces for the neurologist.

Comment: This patient had well documented Alzheimer’s disease, with a characteristic presentation,

characteristic FDG-PET scan, and an ApoE4 homozygous genotype. For the seven years prior to beginning the MEND protocol, his cognition declined, again in keeping with the diagnosis of Alzheimer’s disease. Therefore, the chance that his MMSE improved from 22 to 26 and then to 29 over the 10 months on the protocol, as a random event unrelated to the MEND protocol, is slim. Although a score of 29 on the MMSE is within the normal range, both the patient and his wife recognize that subjectively he has not returned completely to normal, and continued optimization of his metabolic status is ongoing.

**Patient 8.** A 68-year-old business executive presented with a five-year history of progressive memory loss, forcing him to retire from his company. He had difficulty navigating while driving, as well. Family history was positive in his mother. He underwent amyloid PET imaging, which was positive. His ApoE genotype was 3/4.

After six months on the MEND protocol, his BMI improved from 27.7 to 24.6, and his hemoglobin A1c improved from 5.9% to 5.7%. Both he and his family noted improvement in memory and navigation. His improvement was documented by on-line neuropsychological testing (Brain HQ), which showed increase from 0 (baseline) to 2221, which represented 52<sup>nd</sup> percentile for his age.

Comment: This patient had typical Alzheimer’s disease with mnemonic and visuospatial deficits, progressive course, positive family history, ApoE4 heterozygosity, and a positive amyloid PET scan. He responded to treatment with an improvement in BMI, reduction in hemoglobin A1c, symptomatic improvements in both memory and navigation, and objective improvement in on-line neuropsychological testing.

**Patient 9.** This is a follow-up description of a patient presented in a previous publication [13]. A 50-year-old woman developed depression following a hysterectomy. She received hormone replacement therapy, but the depression continued. At the age of 54, she began to have word-finding difficulty, disorientation, difficulty driving, difficulty following recipes and other instructions, and memory complaints, and these problems progressed. She became quieter and slower to respond. Her depression deepened when her son left home.

She underwent neuropsychological testing, which disclosed frontal, temporal, and parietal abnormalities. A PET scan was typical for Alzheimer’s disease, with temporoparietal decreases in glucose utilization as well

as a modest frontal decrease. She was placed on duloxetine, which reduced her depression, and donepezil, which improved her cognition. However, she continued to decline.

At the age of 57, she was again evaluated. Her ApoE genotype was 3/3, MoCA was 19/30, BMI was 18, hs-CRP 0.2mg/l, homocysteine 8μM, fasting insulin 4.2uIU/ml, hemoglobin A1c 5.1%, free T3 2.1pg/ml, free T4 1.33ng/dl, reverse T3 23ng/dl, fT3:rT3 9, TSH 1.16uIU/ml, progesterone 0.3ng/ml, AM cortisol 7.2mcg/dl, pregnenolone 19ng/dl, 25-hydroxycholecalciferol 37ng/ml, vitamin B12 799pg/ml, alpha-tocopherol 12.5mg/l, zinc 82mcg/l, copper 99mcg/l, copper:zinc ratio 1.2, ceruloplasmin 20mg/dl, total cholesterol 221mg/dl, HDL cholesterol 67mg/dl, non- HDL cholesterol 167mg/dl, triglycerides 82mg/dl, urinary mercury:creatinine < 2.8, Lyme antibodies negative, C4a 5547ng/ml, TGF-β1 7037pg/ml, and VEGF (vascular endothelial growth factor) 56pg/ml (normal range 31-86pg/ml). VIP (vasoactive intestinal peptide) was not evaluated. HLA-DR/DQ was 13-6-52A (mycotoxin sensitive) and 15-6-51 (Borrelia sensitive). MARCoNS (multiple-antibiotic-resistant coagulase-negative Staph) culture was negative. Anti-thyroglobulin antibodies were strongly positive at 2076IU/ml (normal range 0-0.9IU/ml) and anti-thyroid peroxidase antibodies positive at 58IU/ml (normal range 0-34IU/ml).

She was placed on the MEND protocol, and intranasal VIP (vasoactive intestinal peptide) was administered. After three months, she showed improvement. She was able to babysit her grandchildren. She was able to follow written and verbal instructions without any problems, which had not been possible prior to treatment. She was able to read and remember overnight, and discuss her reading with her husband, which she had not been able to do prior to treatment. She also routinely remembered events of the previous day, which had not occurred in the few years prior to treatment. She had a follow-up MoCA test, and scored 21/30.

Comment: This patient had progressed beyond MCI to Alzheimer's disease, well documented by characteristic PET scan abnormalities, neuropsychological testing deficits, and progression. Despite an initial subjective response to donepezil, she continued to decline and displayed significant impairment. She was diagnosed with type 3 Alzheimer's disease [13, 14], and laboratory data supported this diagnosis with characteristic HLA-DR/DQ and abnormal C4a and TGF-β1, as well as anti-thyroglobulin antibodies and anti-thyroid peroxidase antibodies, although MARCoNS culture was negative.

After three months of therapy, she showed clear subjective improvement and modest objective improvement. Her previous three years of relentless decline argued against the possibility that the improvement was random and unrelated to her treatment.

**Patient 10.** A 54-year-old woman presented with a two-year history of memory loss. She noted that she did not retain new information the way she formerly had, she had to re-read information a number of times to remember it, especially technical or scientific information, and noted that her reading speed had decreased. She also noted a reduction in vocabulary, word-finding problems, and repeated use of the same word instead of using synonyms. She also noted increased difficulty with grammar and spelling, as well as loss of names of friends and of famous people. Her writing declined, her typographical errors increased, and she had difficulty remembering passwords. She had increasing difficulty driving, organizing, and with her motivation. Activities of daily living were preserved.

Her ApoE genotype was 4/4, homocysteine 7.5μmol/l, hs-CRP 0.26mg/l, albumin:globulin ratio 2.0, hemoglobin A1c 5.3%, fasting insulin 2.7mIU/l, fasting glucose 81mg/dl, alpha-tocopherol 18.3mg/l, and 25-hydroxycholecalciferol 188ng/ml.

On-line quantitative neuropsychological testing disclosed a composite memory score at the 32<sup>nd</sup> percentile, visual memory at 10<sup>th</sup> percentile, and verbal memory at 73<sup>rd</sup> percentile. This testing was repeated after four months on the protocol, at which time the composite memory score was at the 61<sup>st</sup> percentile, visual memory score at the 25<sup>th</sup> percentile, and verbal memory score at the 84<sup>th</sup> percentile.

Comment: This person, who is homozygous for the ApoE ε4 allele, demonstrated both subjective and objective evidence of cognitive decline, with preserved activities of daily living, and thus would fit best with a diagnosis of mild cognitive impairment. After four months on the protocol, repeat on-line quantitative neuropsychological testing revealed improvements in visual and verbal memory. Although these improvements were relatively modest, they are in contrast to the natural history of progressive decline in cognition for MCI associated with ApoE4 homozygosity.

## DISCUSSION

These observations provide further support for the previously reported finding that the personalized

protocol for metabolic enhancement (note that the metabolic evaluation included parameters shown to affect Alzheimer's disease pathophysiology, such as homocysteine [15], glucose [16], and inflammation [17], as well as numerous others as previously described [3]) in Alzheimer's disease leads to the reversal of cognitive decline in at least some patients with early Alzheimer's disease or its precursors, MCI (mild cognitive impairment) and SCI (subjective cognitive impairment). To our knowledge, the magnitude of the improvements documented in patients 1 and 2 is unequalled in previous reports: in patient 1, the increase in hippocampal volume from 17<sup>th</sup> percentile to 75<sup>th</sup> percentile supports the marked symptomatic improvement that he (and others) achieved on the protocol. In patient 2, quantitative neuropsychological testing demonstrated improvements of up to three standard deviations (CVLT-IIb, from 3<sup>rd</sup> percentile to 84<sup>th</sup> percentile), with multiple tests all showing marked improvements. These findings complement and support the marked subjective improvement already published for this patient [3].

It is noteworthy that these patients met criteria for Alzheimer's disease or MCI prior to treatment, but failed to meet criteria for either Alzheimer's disease or MCI following treatment—i.e., following treatment, most had returned to the normal range for their cognitive testing. Furthermore, as noted in the initial description of the protocol used here [3], discontinuation of the protocol was associated with cognitive decline (here, in patient 1). It is not yet known for how many months or years the marked improvements will be sustained, but loss of improvement in patients maintaining the protocol has not yet been observed, and follow-ups of up to four years have now occurred.

The hippocampal volumetric increase observed for patient 1 does not discriminate between the possibility that synaptic number increased, or glial cell number or volume increased, or endogenous stem cell survival increased, or neuronal cell number or volume increased, or the vascular compartment increased, or some combination of these possibilities. This volumetric increase, and the marked symptomatic improvement that accompanied it, raises the question of whether it is possible that the patient's diagnosis of mild cognitive impairment associated with Alzheimer's disease was incorrect. However, the diagnostic evaluation makes this possibility extremely unlikely: given the strong family history of dementia, the ApoE4 heterozygosity, markedly positive amyloid PET scan, the FDG-PET scan characteristic of Alzheimer's disease with reduced glucose utilization in a temporoparietal distribution, the

abnormal neuropsychological testing, and the MRI showing hippocampal volume at 17<sup>th</sup> percentile for age, the possibility that the underlying pathological process was something other than Alzheimer's disease is remote. Thus it would be expected that hippocampal volume would decrease over time, and that cognitive decline would occur. Therefore, the likelihood that his improvement was random and unrelated to the intervention is extremely low.

Similarly, for patient 2, it is highly unlikely that the diagnosis of Alzheimer's disease was incorrect: the ApoE4-positive genotype, the FDG-PET scan typical of Alzheimer's disease with temporoparietal reduction in glucose utilization, the pattern and severity of quantitative neuropsychological abnormalities, and the well documented progressive nature of the deficits all provide strong support for the diagnosis of Alzheimer's disease. Furthermore, the severity of the abnormalities documented by the quantitative neuropsychological assessment was also compatible with the diagnosis of Alzheimer's disease. The variations that may occur when different examiners perform the same set of quantitative neuropsychological tests is an obvious concern when there is a significant change in the results of the tests in one subject. However, in this case, the same examiner performed the same set of tests in each instance, arguing against the possibility that the major improvement observed was simply the result of examiner-related variability. The magnitude of the improvement also argued against this possibility.

In each of these cases, obvious subjective improvement, noted by the patient, his/her significant other, and his/her co-workers, was accompanied by clear, quantitated, objective improvement. In the cases of patients 1 and 2, the improvement was of a magnitude not reported previously for patients with Alzheimer's disease. None of the 10 patients exhibited the cognitive decline that is characteristic of Alzheimer's disease, and the improvement experienced by all 10 has been sustained, with the longest time on the program being four years.

It has been claimed that there is nothing that will prevent, delay, or reverse Alzheimer's disease ([www.nih.gov/news-events/news-releases/independent-panel-finds-insufficient-evidence-support-preventive-measures-alzheimers-disease](http://www.nih.gov/news-events/news-releases/independent-panel-finds-insufficient-evidence-support-preventive-measures-alzheimers-disease)). Therefore, it is typically recommended that the ApoE genotype, which represents the most important genetic risk factor for Alzheimer's disease, not be evaluated in asymptomatic individuals, and many physicians do not evaluate ApoE genotype even in symptomatic patients. However, the examples described here complement and extend

previously published data that argue that these claims are no longer valid. Thus, given the success of the therapeutic regimen used with these patients, it may be appropriate to evaluate the ApoE genotype as part of prevention and early reversal of symptoms. Given the approximately 75 million Americans who are heterozygous for the ApoE  $\epsilon$ 4 allele, and the approximately seven million Americans who are homozygous, early identification and treatment (presymptomatic or symptomatic) could potentially have a major impact on the prevalence of Alzheimer's disease-mediated cognitive decline.

## ACKNOWLEDGEMENTS

I thank Dr. Rammohan Rao, Dr. Aida Lasheen Bredesen, and Dr. Alexei Kurakin for discussions, and Ms. Rowena Abulencia for preparing the manuscript.

## Funding

I am grateful for support from James and Phyllis Easton, the NIH (AG16570, AG034427 and AG036975), the Mary S. Easton Center for Alzheimer's Disease Research at UCLA, the Douglas and Ellen Rosenberg Foundation, the Stephen D. Bechtel, Jr. Foundation, the Joseph Drown Foundation, the Alzheimer's Association, the Accelerate Fund, the Buck Institute and Marin Community Foundation, the Michael and Catherine Podell Fund, Mr. Craig Johnson, Mr. Allan Bortel, Mr. Wright Robinson, Mr. Jeffrey Lipton, Mr. Lawrence Dingus, and Ms. Michaela Hoag.

## Conflict of interest statement

The author of this manuscript declares no conflict of interest.

## REFERENCES

1. James BD, Leurgans SE, Hebert LE, Scherr PA, Yaffe K and Bennett DA. Contribution of Alzheimer disease to mortality in the United States. *Neurology*. 2014;82:1045-50.
2. Seshadri S, Drachman DA and Lippa CF. Apolipoprotein E epsilon 4 allele and the lifetime risk of Alzheimer's disease. What physicians know, and what they should know. *Arch Neurol*. 1995;52:1074-79.
3. Bredesen DE. Reversal of cognitive decline: A novel therapeutic program. *Aging (Albany NY)*. 2014; 6:707-17. doi: 10.18632/aging.100690.
4. Kurakin A and Bredesen DE. Dynamic self-guiding analysis of Alzheimer's disease. *Oncotarget*. 2015; 6:14092-14122. doi: 10.18632/oncotarget.4221.
5. Galvan V, Gorostiza OF, Banwait S, Ataie M, Logvinova AV, Sitaraman S, Carlson E, Sagi SA, Chevallier N, Jin K, Greenberg DA

and Bredesen DE. Reversal of Alzheimer's-like pathology and behavior in human APP transgenic mice by mutation of Asp664. *Proc Natl Acad Sci U S A*. 2006; 103:7130-35.

6. Bredesen DE, John, V. Next generation therapeutics for Alzheimer's disease. *EMBO Mol Med*. 2013;5:795-98.
7. Ross DE, Ochs, A.L., Seabaugh, J., Henshaw, T. NeuroQuant® revealed hippocampal atrophy in a patient with traumatic brain injury. *J Neuropsychiatry Clin Neuroscience*. 2012; 24:1:33.
8. Ahdidan J, Raji CA, DeYoe EA, Mathis J, Noe KO, Rimestad J, Kjeldsen TK, Mosegaard J, Becker JT and Lopez O. Quantitative Neuroimaging Software for Clinical Assessment of Hippocampal Volumes on MR Imaging. *J Alzheimers Dis*. 2015;49:723-32.
9. Erickson KI, Voss MW, Prakash RS, Basak C, Szabo A, Chaddock L, Kim JS, Heo S, Alves H, White SM, Wojcicki TR, Mailey E, Vieira VJ, et al. Exercise training increases size of hippocampus and improves memory. *Proc Natl Acad Sci U S A*. 2011;108:3017-22.
10. Fotuhi M, Lubinski B, Trullinger M, Hausterman N, Riloff T, Hadadi M, Raji CA. A personalized 12-week "Brain Fitness Program" for improving cognitive function and increasing the volume of hippocampus in elderly with mild cognitive impairment. *The Journal of Prevention of Alzheimer's Disease*. 2016.
11. Fiala M, Lin J, Ringman J, Kermani-Arab V, Tsao G, Patel A, Lossinsky AS, Graves MC, Gustavson A, Sayre J, Sofroni E, Suarez T, Chiappelli F, et al. Ineffective phagocytosis of amyloid-beta by macrophages of Alzheimer's disease patients. *J Alzheimers Dis*. 2005; 7:221-232; 255-62.
12. Masoumi A, Goldenson B, Ghirmai S, Avagyan H, Zaghi J, Abel K, Zheng X, Espinosa-Jeffrey A, Mahanian M, Liu PT, Hewison M, Mizwickie M, Cashman J, et al. 1alpha,25-dihydroxyvitamin D3 interacts with curcuminoids to stimulate amyloid-beta clearance by macrophages of Alzheimer's disease patients. *J Alzheimers Dis*. 2009;17:703-17.
13. Bredesen DE. Metabolic profiling distinguishes three subtypes of Alzheimer's disease. *Aging (Albany NY)*. 2015; 7:595-600. doi: 10.18632/aging.100801.
14. Bredesen DE. Inhalational Alzheimer's disease: an unrecognized - and treatable - epidemic. *Aging (Albany NY)*. 2016; 8:304-13. doi: 10.18632/aging.100896.
15. Hooshmand B, Solomon A, Kareholt I, Leiviska J, Rusanen M, Ahtiluoto S, Winblad B, Laatikainen T, Soininen H and Kivipelto M. Homocysteine and holotranscobalamin and the risk of Alzheimer disease: a longitudinal study. *Neurology*. 2010; 75:1408-14.
16. Yang Y, Wu Y, Zhang S and Song W. High glucose promotes Abeta production by inhibiting APP degradation. *PLoS One*. 2013;8:69824.
17. Calsolaro V and Edison P. Neuroinflammation in Alzheimer's disease: Current evidence and future directions. *Alzheimers Dement*. 2016; 12:719-32.

## Epigenetic mechanisms underlying cognitive impairment and Alzheimer disease hallmarks in 5XFAD mice

Christian Griñán-Ferré<sup>1</sup>, Sara Sarroca<sup>3</sup>, Aleksandra Ivanova<sup>1</sup>, Dolors Puigoriol-Illamola<sup>1</sup>, Fernando Aguado<sup>2</sup>, Antoni Camins<sup>1</sup>, Coral Sanfeliu<sup>3</sup>, and Mercè Pallàs<sup>1</sup>

<sup>1</sup>Department of Pharmacology and Therapeutic Chemistry (Pharmacology Section) and Institute of Neuroscience, University of Barcelona, 08028 Barcelona, Spain

<sup>2</sup>Department of Cellular Biology, University of Barcelona, 08028 Barcelona, Spain

<sup>3</sup>Institut d'Investigacions Biomèdiques de Barcelona (IIBB), CSIC, and IDIBAPS, 08036 Barcelona, Spain

**Key words:** Alzheimer disease, neurodegeneration, behavior, cognition, deacetylase, methyltransferase

**Received:** 12/16/15; **Accepted:** 01/23/16; **Published:** 03/21/16

**doi:** [10.18632/aging.100906](https://doi.org/10.18632/aging.100906)

**Correspondence to:** Mercè Pallàs, PhD; **E-mail:** [pallas@ub.edu](mailto:pallas@ub.edu)

**Copyright:** Griñán-Ferré et al. This is an open-access article distributed under the terms of the Creative Commons Attribution License, which permits unrestricted use, distribution, and reproduction in any medium, provided the original author and source are credited

**Abstract:** 5XFAD is an early-onset mouse transgenic model of Alzheimer disease (AD). Up to now there are no studies that focus on the epigenetic changes produced as a result of A $\beta$ -42 accumulation and the possible involvement in the different expression of related AD-genes. Under several behavioral and cognition test, we found impairment in memory and psychoemotional changes in female 5XFAD mice in reference to wild type that worsens with age.

Cognitive changes correlated with alterations on protein level analysis and gene expression of markers related with tau aberrant phosphorylation, amyloidogenic pathway (*APP*, *BACE1*), Oxidative Stress (*iNOS*, *Aldh2*) and inflammation (astrogliosis, *TNF- $\alpha$*  and *IL-6*); no changes were found in non-amyloidogenic pathway indicators such as ADAM10.

Epigenetics changes as higher CpG methylation and transcriptional changes in DNA methyltransferases (DNMTs) family were found. *Dnmt1* increases in younger 5XFAD and *Dnmt3a* and *b* high levels in the oldest transgenic mice. Similar pattern was found with histone methyltransferases such as *Jarid1a* and *G9a*. Histone deacetylase 2 (*Hdac2*) or *Sirt6*., both related with cognition and memory, presented a similar pattern. Taken together, these hallmarks presented by the 5XFAD model prompted its use in assessing different potential therapeutic interventions based on epigenetic targets after earlier amyloid deposition.

### INTRODUCTION

Alzheimer's disease (AD) is a progressive and irreversible neurodegenerative disorder [1] and the most common cause of dementia, affecting about 35 million people worldwide [2]. A three-fold increase there is estimated for the number of cases of AD (114 million) by 2050 [1]. According to statistical analyses approved by the World Health Organization, (WHO), AD and the others forms of dementia rank as the fourth cause of death in economically developed countries with a rate of 4,1% of total deaths [3,4]. The disease involves degeneration of certain regions of the brain, which results in memory loss and declining cognitive functions

and leads to a decrease in physiological functions and death. The neuropathological hallmarks comprise the production of senile plaques, the formation of neurofibrillary tangles, and the accumulation of neuronal lesions in the brain [5]. Despite that Late-Onset AD (LOAD) has a relatively high heritability of around 70% [6], the sole long-established, unequivocal genetic risk factor has been the  $\epsilon$ 4-allele of the Apolipoprotein E gene (*APOE*) [7-10]. The precise mechanism by which *APOE* exerts this influence remains largely undefined, with indications including a key role in mediating A $\beta$  metabolism and clearance [11]. Numerous candidate gene, genetic linkage, and association studies have been carried out over the past

two decades to elucidate the remaining genetic risk for AD [12]. However, none of these candidates has proven to consistently influence disease risk or onset age in more than a handful of samples [13]. Reasons for lack of reproducibility may include the following: insufficient study power to detect variants with minor contributions; biologic, genetic, and allelic heterogeneity; difference in study design, and the presence of population substructure [14]. The occurrence of phenotypical differences in monozygotic twins over time is thought to arise from epigenetic changes induced by different environments or by stochastic events [15]; thus, it appears plausible that epigenetic changes resulting in altered gene expression may also be involved in the pathogenesis of LOAD.

In addition to genetic factors, growing evidences demonstrated that the effects of environmental factors and epigenetic mechanisms also play an important role in the pathogenesis of AD [16-20]. Epigenetic information is principally encoded in two types of synergistically acting covalent modifications: DNA methylation and chromatin modifications; these changes afford the epigenetic complexity that directly affects regulation of the gene expression and other genomic functions [21]. For example, hypomethylation of the Amyloid Precursor Protein (APP) gene in the brain of a patient with AD was found [22]. Subsequently, several studies have linked DNA methylation changes in hippocampus and cortex of patients with AD, showing that DNA hypomethylation is associated with a huge number of Amyloid  $\beta$  (A $\beta$ ) plaques [22]. DNA methylation is also involved in APP processing and A $\beta$  production through the regulation of Presenilin1 (PS1) and  $\beta$ -secretase (BACE) expression [23]. Monitoring the frontal cortex of patients with AD, indicated that DNA hypomethylation leads to expanded regulation of proinflammatory genes, Nuclear Factor- $\kappa$ B (NF- $\kappa$ B) and the encoding of cyclooxygenase-2 that catalyzes the production of prostaglandins and some prostanoids [24,25]. This assumes that abnormal DNA methylation may cause nerve inflammation. Hypermethylation of Brain Derived Neurotrophic Factor (BDNF) and cAMP Response Element Binding (CREB) promoters would harm the plasticity of the synapses [25]. Although these studies report AD brain global DNA methylation changes in opposite directions, differences are likely due to the fact that the authors studied different brain regions and employed different methylation detection techniques.

In addition, A $\beta$  changes in DNA methylation are associated with induction of several genes, causing apoptotic and cell loss. It remains unclear how these changes in DNA methylation began, but it is suggested

that various cellular mechanisms, such as OS and A $\beta$ -42, are involved [26]. OS and A $\beta$ -42 may modify DNA methylation, and evidences for the dynamic modulation of learning and memory suggest the functional importance of abnormal methylation of DNA in the cases of AD [27].

The detection and identification of mutations in APP, PS1 and PS2 genes associated with Familial AD (FAD) have allowed the generation of various transgenic murine models. These transgenic models have the potential to enable us to understand the pathogenesis of the disease, and to develop and evaluate new and effective therapeutic targets. The 5XFAD mouse was formally established and declared in 2006 by Oakley and the specific characteristic of this model being that it is generated to promote rapid, aggressive and complete development of AD pathological interactions. This novel model of A $\beta$  pathology consists of two APP mutations (APP K670N/ M671L (Swedish), I716V (Florida), and V717 (London) and two PS1 mutations (PS1 M146 and L286V) on B6/SJL and each transgene is regulated by Thy1 promoter [28,29].

The present work focuses on the study of the possible involvement of A $\beta$ -42 accumulation in the production of OS and in subsequent modifications in the epigenetic machinery in the murine model of AD, 5XFAD. We aimed to discuss the role of global DNA methylation and the histone epigenetic enzymes involved in epigenetic modification acting in the control of gene expression and memory in this AD mouse model.

## RESULTS

### 5XFAD showed cognitive impairment but no changes in emotional parameters with age

NORT analysis demonstrated significant differences between the 5XFAD and Wt strains at 8, but not at 2 months of age (age,  $F(1,28) = 4.5631$ ,  $p = 0.0416$ ; genotype,  $F(1,28) = 4.563$ ,  $p = 0.001$ , and interaction age  $\times$  genotype  $F(1,28) = 6,211$ ,  $p = 0.0189$ ). The DI was significantly decreased in 5XFAD mice at 8 months of age compared with young 5XFAD mice and with age-matched Wt, indicating impairment in hippocampal memory processes (Fig. 1A). Although, all mouse groups were able to learn through trial days in the MWM paradigm, statistical differences were found comparing young 5XFAD compared with old Wt. (Fig. 1B). On the test day, it was observed that 5XFAD mice aged 2 and 8 months showed impairment in spatial memory, with a significant decrease in time spent in the platform quadrant and with erratic preference for the platform area (age,  $F(1,28) = 0.8253$ ,  $p = 0.3720$ ;

genotype,  $F(1,28) = 19.67$ ,  $p = 0.0001$ , and interaction age  $\times$  genotype  $F(1,28) = 0.3977$ ,  $p = 0.5334$ ) (Figs. 1C and 1D).

Behavioral and emotional tests showed differences in anxiety-like behavior, through EPM test (Figs. 2A and 2B). Old 5XFAD mice demonstrated less anxious behavior, spending a longer time in open than in closed arms (age,  $F(1,32) = 0.7973$ , n.s.; genotype,  $F(1,32) = 3.842$ ,  $p = 0.0587$ , and interaction age  $\times$  genotype

$F(1,32) = 5.761$ ,  $p = 0.0024$ ). Locomotor activity was reduced significantly in 5XFAD (age,  $F(1,32) = 8.123$ ,  $p = 0.0076$ ; genotype,  $F(1,32) = 0.2784$ , n.s., and interaction age  $\times$  genotype  $F(1,32) = 6.921$ ,  $p = 0.0338$ ) (Fig. 2C and E) whereas vertical activity in EPM was significantly reduced in old 5XFAD (age,  $F(1,32) = 6.167$ ,  $p < 0.0184$ ; genotype,  $F(1,32) = 1.827$ , n.s., and interaction age  $\times$  genotype  $F(1,28) = 6.211$ ,  $p = 0.0189$ ) (Fig. 2D). A summary of the parameters measured are presented in Table 2. O The OFT demonstrated that

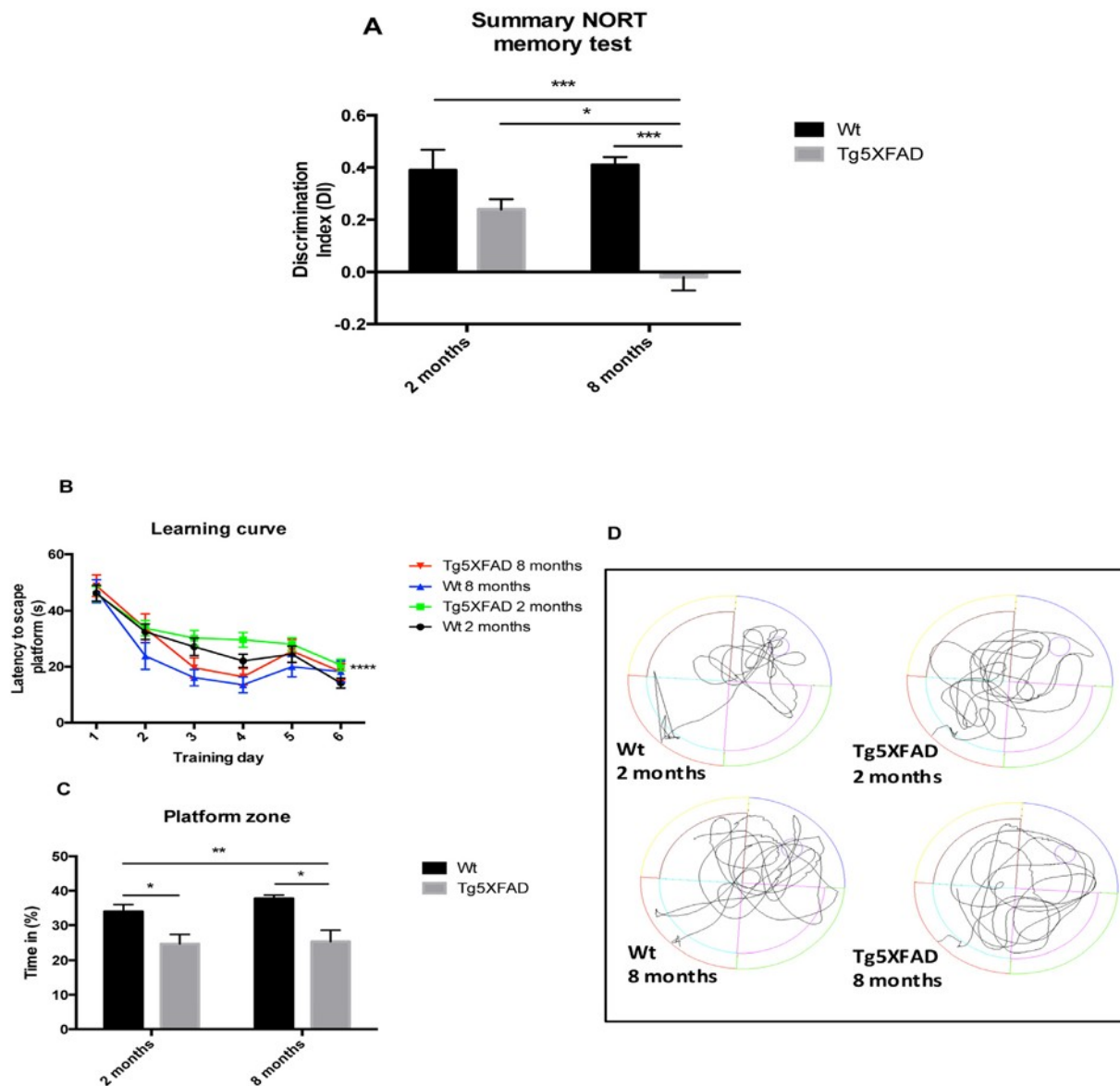


**Figure 1.** Results of Discrimination index of NORT in female mice aged 2 and 8 months (Wt and 5XFAD) (A). Learning curves during MWM trials (B), Percentage of time spent in platform zone during 60 sec probe trial of the MWM test (C), Representative swim paths from the memory day test on day 7 (D). Data represented as observed mean  $\pm$  Standard Error of the Mean (SEM) ( $n = 10$  for each group). \* $p < 0.05$ ; \*\* $p < 0.01$ ; \*\*\* $p < 0.001$ .

both female Wt and 5XFAD exhibited increased fear with age, reducing time in center zone (age,  $F(1,28) = 43.25$ ,  $p < 0.0001$ ; genotype,  $F(1,28) = 13.57$ ,  $p = 0.001$ , and interaction age  $\times$  genotype  $F(1,28) = 2.887$ , n.s.) (Fig. 3A), increasing time in border zone (age,  $F(1,28) = 34.69$ ,  $p < 0.001$ ; genotype,  $F(1,28) = 8.494$ ,  $p = 0.0069$ , and interaction age  $\times$  genotype  $F(1,28) = 0.9871$ , n.s.) (Fig. 3B). According to the results obtained in EPM paradigm, locomotor activity was reduced in 5XFAD aged 8 months (age,  $F(1,28) = 11.73$ ,  $p = 0.0019$ ; genotype,  $F(1,28) = 1.021$ , n.s., and interaction age  $\times$  genotype  $F(1,28) = 6.625$ ,  $p = 0.0156$ ) and vertical activity or rears (age,  $F(1,28) = 23.33$ ,  $p < 0.0001$ ; genotype,  $F(1,28) = 1.029$ , n.s., and interaction age  $\times$  genotype  $F(1,28) =$

4.190,  $p = 0.0502$ ) (Figs. 3C-E). A summary of results obtained in the OFT is depicted in Table 3.

#### Alzheimer's disease hallmarks and oxidative stress in female 5XFAD: changes with age

Molecular analysis demonstrated that there a significant increase in BACE1 and APP gene expression (Figs. 4A and 4B) in 8 month-old 5XFAD compared with Wt (BACE1: age,  $F(1,8) = 0.8420$ , n.s.; genotype,  $F(1,8) = 19.13$ ,  $p = 0.0009$ , and interaction age  $\times$  genotype  $F(1,8) = 0.0004$ , n.s., and APP: age,  $F(1,8) = 8.292$ ,  $p = 0.0138$ ; genotype,  $F(1,8) = 3.969$ , n.s., and interaction age  $\times$  genotype  $F(1,8) = 3.475$ ; n.s.).

**Table 1.** Antibodies used in Western blot and Immunohistochemical studies

Antibody	Host	Source/Catalog	WB dilution	ICH dilution
BACE1	Rabbit	Abcam/ab5832	1:500	
4-HNE	Rabbit	Abcam/ab46545	1:1000	
SOD1	Sheep	Calbiochem/574597	1:1000	
sAPP beta	Rabbit	Covance/SIG-39138-050	1:1000	
Sinaptophysin	Mouse	Dako/Clone SY38	1:2000	
GAPDH	Mouse	Millipore/MAB374	1:2000	
NeuN	Mouse	Millipore/MAB377	1:1000	
GFAP	Mouse	Abcam/ab48050-100		1:1000
TAU s396	Rabbit	Invitrogen/44752G	1:1000	
TAU total	Goat	Santa cruz/sc-1995	1:1000	
Alexa Fluor 546 donkey anti-rabbit IgG A		Molecular probes/AF488:A21202		1:400
Alexa Fluor 488 donkey anti-mouse IgG A Alexa		Molecular probes/AF555:A31572		1:400
Donkey-anti-goat HRP conjugated		Santa Cruz Biotech/ sc-2020	1:3000	
Goat-anti-mouse HRP conjugated		Biorad/# 170-5047	1:2000	
Goat-anti-rabbit HRP conjugated		Cell Signaling/# 7074	1:2000	

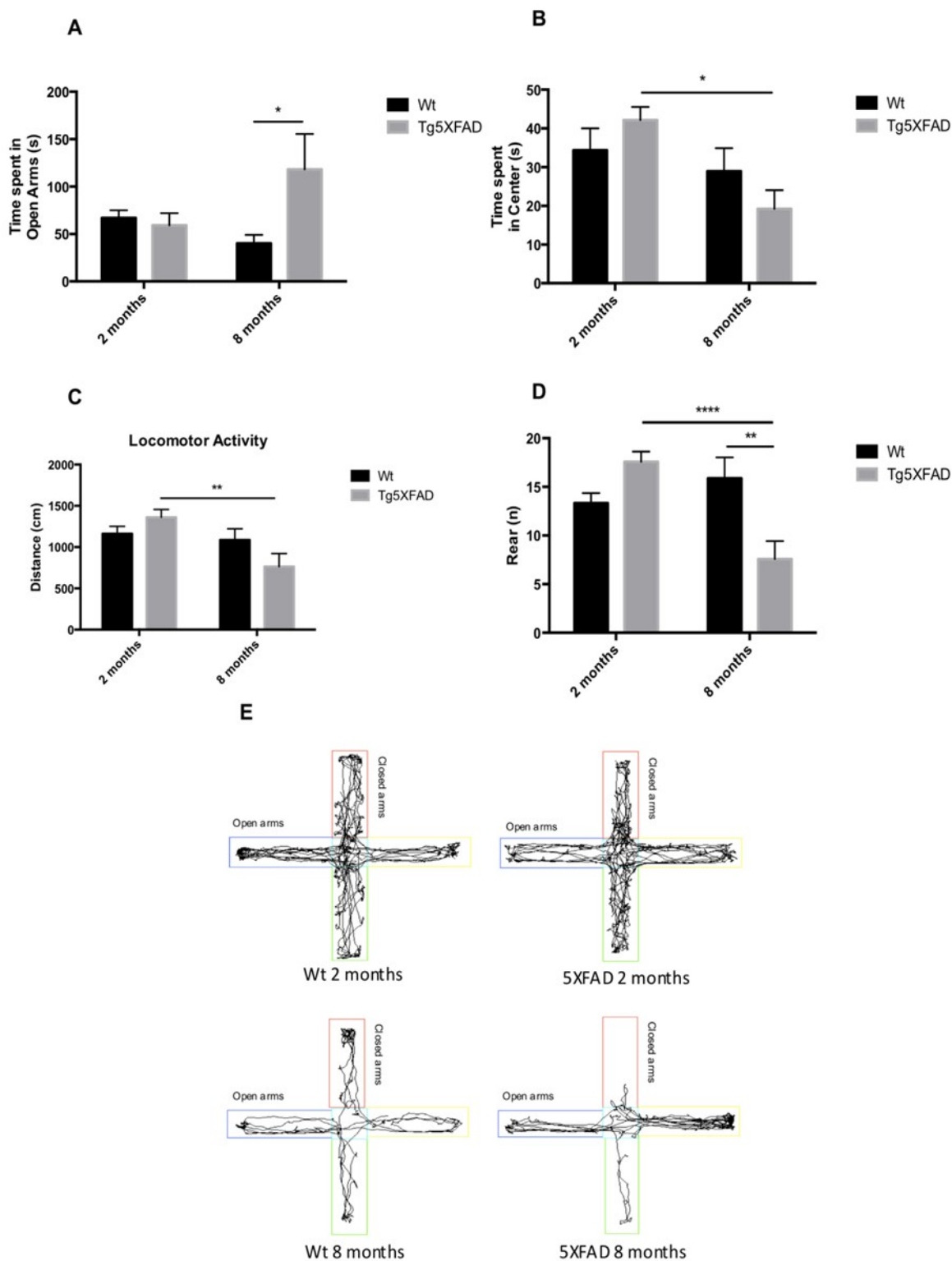


**Figure 2.** Results of Elevated Plus Maze (EPM) in female mice aged 2 and 8 months (Wt and 5XFAD). Time spent in open arms (A), Time spent in center maze (B), Locomotor activity (C), Rears/vertical activity (D), Representative track sheets showing duration dependent changes in time spent in and number of entries on the open arm and closed arm in EPM (E). Data represented as observed mean  $\pm$  Standard Error of the Mean (SEM); ( $n = 10$  for each group). \* $p < 0.05$ ; \*\* $p < 0.01$ ; \*\*\*\* $p < 0.0001$ .

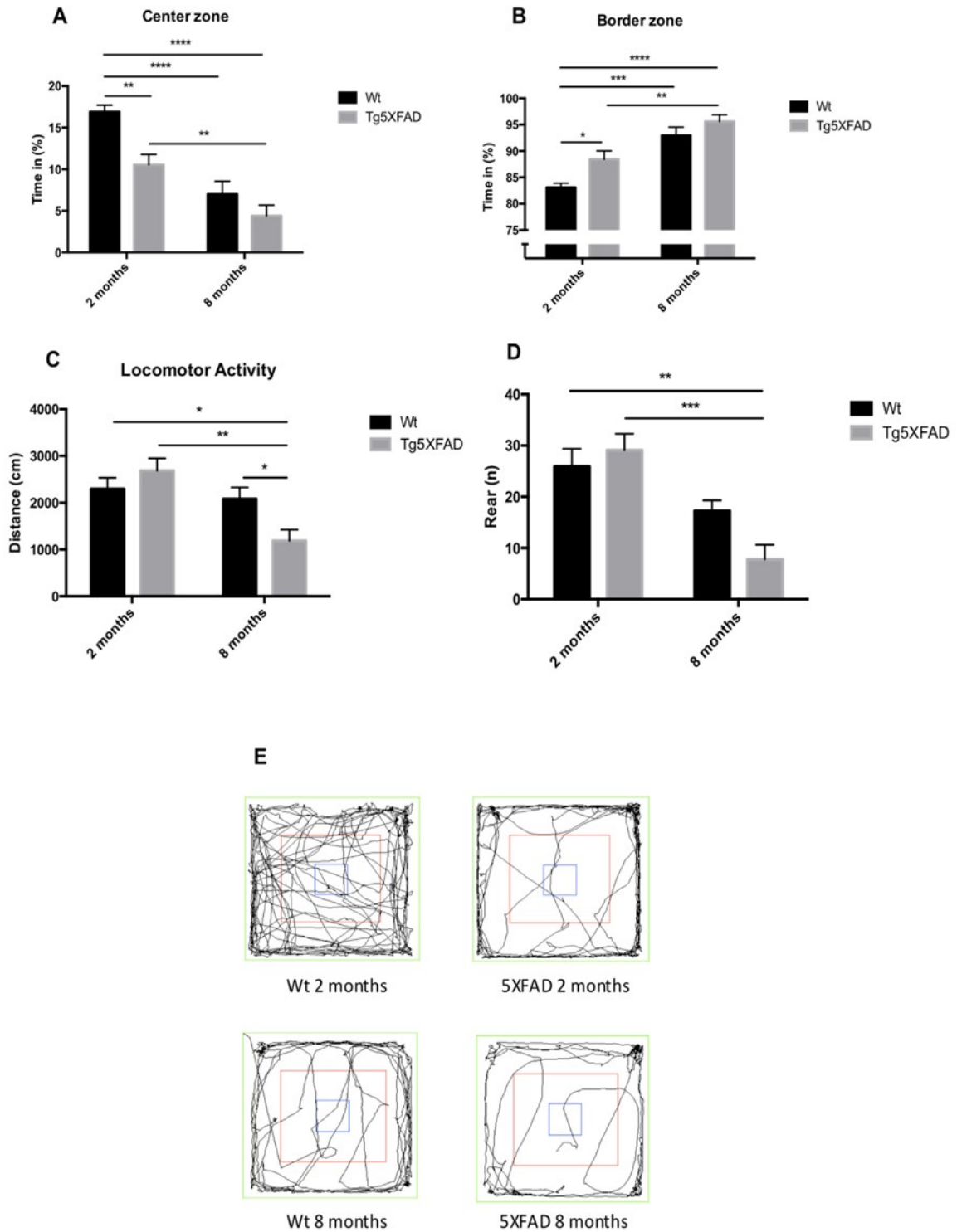


**Figure 3.** Results of Open field test in female mice aged 2 and 8 months (Wt and 5XFAD). Time spent in center zone., (A), Time spent in border maze (B), Locomotor activity (C) and Rears (D). Representative tracks for the OFT (E). Data represented as observed mean  $\pm$  Standard Error of the Mean (SEM) ( $n = 10$  for each group). \* $p < 0.05$ ; \*\* $p < 0.01$ ; \*\*\* $p < 0.001$ ; \*\*\*\* $p < 0.0001$ .

According to gene expression results, when protein levels for BACE1 were studied significant increases of BACE1 in 5XFAD in comparison with Wt were demonstrated (age,  $F(1,8) = 0.5599$ , n.s.; genotype,  $F(1,8) = 15.05$ ,  $p = 0.0047$ , and interaction age  $\times$  genotype  $F(1,8) = 11.17$ ,  $p = 0.0102$ ) (Fig. 4C). sAPP $\beta$  protein levels were studied as a indicative of APP processing and A $\beta$  production; the results showed that sAPP $\beta$  levels increased in 8 month-

old 5XFAD compared with age-mated Wt (age,  $F(1,8) = 1.647$ , n.s.; genotype,  $F(1,8) = 1.449$ , n.s., and interaction age  $\times$  genotype  $F(1,8) = 18.45$ ,  $p = 0.0026$ ) (Fig. 4D). This is in agreement with increases in thioflavine-S staining in 5XFAD in front over Wt, as described elsewhere (age,  $F(1,8) = 149.6$ ,  $p < 0.0001$ ; genotype,  $F(1,8) = 278.2$ ,  $p < 0.0001$ , and interaction age  $\times$  genotype  $F(1,8) = 149.6$ ,  $p < 0.0001$ ) (Figs. 7A and 7B).

**Table 2.** Parameters measured in the Elevated Plus Maze Test (EPM). (n): number of events.

	Wt 2 months	5XFAD 2 months	Wt 8 months	5XFAD 8 months
Locomotor activity (cm)	1,161.79 $\pm$ 89.91	1,360.81 $\pm$ 94.74	1,087.42 $\pm$ 135.49	764.18 $\pm$ 157.50 <sup>##</sup>
Time in zone-Center (sec)	34.35 $\pm$ 5.67	42.13 $\pm$ 3.45	28.93 $\pm$ 6.42	19.22 $\pm$ 4.86 <sup>#</sup>
Time in zone-Open Arms (sec)	67.16 $\pm$ 7.93	59.28 $\pm$ 12.85	40.17 $\pm$ 8.96	118.25 $\pm$ 37.15 <sup>\$</sup>
Time in zone-Closed Arms (sec)	198.11 $\pm$ 10.03	198.06 $\pm$ 14.87	230.15 $\pm$ 13.43	162.23 $\pm$ 35.18
Rearings (n)	13.33 $\pm$ 1.02	17.58 $\pm$ 1.05	15.88 $\pm$ 2.15	7.57 $\pm$ 1.86 <sup>####, \$\$</sup>
Defecations (n)	0.67 $\pm$ 0.27	0.83 $\pm$ 0.33	0.75 $\pm$ 0.49	0.29 $\pm$ 0.29
Urinations (n)	0.22 $\pm$ 0.17	0.17 $\pm$ 0.14	0.25 $\pm$ 0.16	0.14 $\pm$ 0.14

Results are expressed as a mean  $\pm$  Standard error of the mean (SEM). \* $p < 0.05$ ; \*\* $p < 0.05$ ; \*\*\* $p < 0.001$  vs Wt, 2 months. # $p < 0.05$ ; ## $p < 0.001$  vs 5XFAD, 2 months. \$ $p < 0.05$  vs Wt, 8 months.

**Table 3.** Parameters measured in the Open Field Test (OFT).

	Wt 2 months	5XFAD 2 months	Wt 8 months	5XFAD 8 months
Total Distance (cm)	2,296.28 $\pm$ 235.08	2,686.37 $\pm$ 260.57	2,083 $\pm$ 246.02	1,383.31 $\pm$ 291.40 <sup>*, ##, \$</sup>
Distance in Zone Center (cm)	46.64 $\pm$ 10.01	40.62 $\pm$ 8.06 <sup>**</sup>	266.05 $\pm$ 48.34 <sup>****</sup>	166.72 $\pm$ 44.46 <sup>****, ##</sup>
Distance in Zone Periphery	2,249.65 $\pm$ 228.66	2,645.76 $\pm$ 258.96 <sup>*</sup>	1,817.83 $\pm$ 221.38 <sup>***</sup>	1,218.98 $\pm$ 255.46 <sup>****, ##</sup>
Center (%)	16.91 $\pm$ 1.82	11.60 $\pm$ 1.63	7.00 $\pm$ 1.55 <sup>**</sup>	4.81 $\pm$ 1.26 <sup>***, #</sup>
Periphery (%)	83.09 $\pm$ 0.80	88.40 $\pm$ 1.63 <sup>*</sup>	93.00 $\pm$ 1.55 <sup>****</sup>	95.19 $\pm$ 1.26 <sup>****, ##</sup>
Rearings (n)	25.89 $\pm$ 3.45	29.08 $\pm$ 3.20	17.29 $\pm$ 2.04	7.29 $\pm$ 2.68 <sup>**, ###</sup>
Defecations (n)	0.44 $\pm$ 0.19	0.33 $\pm$ 0.25	1.14 $\pm$ 0.51	0.57 $\pm$ 0.20
Urinations (n)	0.33 $\pm$ 0.18	0.08 $\pm$ 0.11	0.00 $\pm$ 0.00	0.00 $\pm$ 0.00

(n): number of events. Results are expressed as a mean  $\pm$  Standard error of the mean (SEM). \* $p < 0.05$ ; \*\* $p < 0.05$ ; \*\*\* $p < 0.001$  vs Wt, 2 months. # $p < 0.05$ ; ## $p < 0.001$  vs 5XFAD, 2 months. \$ $p < 0.05$  vs Wt, 8 months.

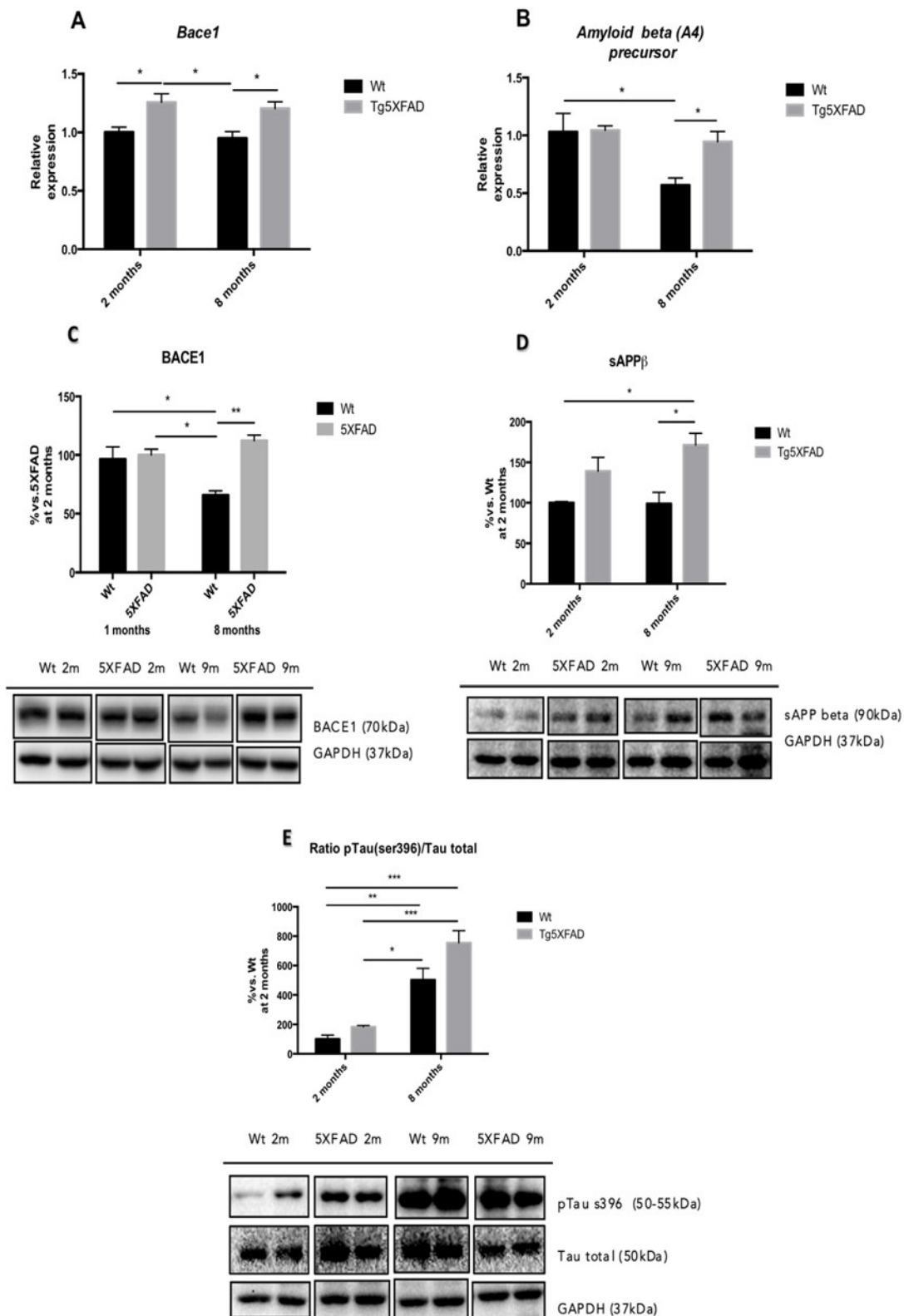


**Figure 4.**  $\beta$ -amyloid pathway gene expression in in female mice aged 2 and 8 months (Wt and 5XFAD) for *Bace1* (A), *Amyloid Beta (A4) precursor* (B) and representative Western blot for BACE1 (C), sAPP (D) and p-Tau (Ser 396) /Tau ratio quantifications (E). Bars represent mean  $\pm$  Standard Error of the Mean (SEM), and values are adjusted to 100% for levels Wt at 2 months. \*\* $p < 0.05$ ; \*\*\* $p < 0.001$ .

Tau hyperphosphorylation was also studied with a focus on pTau (Ser396), whose levels exhibited an age dependent increase in pTau both in Wt and in 5XFAD mice (age,  $F(1,8) = 69.06$ ,  $p < 0.0001$ ; genotype,  $F(1,8) = 8.256$ ,  $p = 0.0207$ , and interaction age  $\times$  genotype  $F(1,8) = 2.108$ , n.s.) (Fig. 4E).

OS is an earlier event in AD mouse models, including 5XFAD. Increased levels in SOD1 (age  $F(1,8) = 17.9969$ ,  $p < 0.0028$ ; genotype,  $F(1,8) = 6.875$ ,  $p = 0.0306$ , and interaction age  $\times$  genotype  $F(1,8) = 5.446$ ,  $p = 0.049$ ), jointly with 4-HNE (age,  $F(1,8) = 76.55$ ,  $p < 0.0001$ ; genotype,  $F(1,8) = 36.13$ ,  $p = 0.0003$ , and interaction age  $\times$  genotype  $F(1,8) = 3.451$ , n.s.) (Figs. 5A and 5B) were found in 5XFAD older mice and in reference to Wt. According to an increase in 4-HNE diminutions in *Aldh2* enzyme transcription levels were

demonstrated in older 5XFAD (age,  $F(1,8) = 9.098$ ,  $p = 0.0107$ ; genotype,  $F(1,8) = 1.789$ ,  $p = \text{n.s.}$ , and interaction age  $\times$  genotype  $F(1,8) = 16.06$ ,  $p = 0.0017$ ) (Fig. 5C) although not differences were found for *iNOS* gene expression among the studied groups (Fig. 5D). With reference to inflammation development, significant gene upregulation of *TNF- $\alpha$*  (age,  $F(1,12) = 97.05$ ,  $p < 0.001$ ; genotype,  $F(1,12) = 136.4$ ,  $p < 0.0001$ , and interaction age  $\times$  genotype  $F(1,12) = 135.0$ ,  $p < 0.0001$ ) and *IL-6* (age,  $F(1,12) = 17.74$ ,  $p < 0.0119$ ; genotype,  $F(1,12) = 51.40$ ,  $p < 0.04871$ , and interaction age  $\times$  genotype  $F(1,12) = 17.74$ ,  $p < 0.0012$ ) were found among animal groups. Both cytokines were significant higher in 8 months-old 5XFAD mice compared with young animals and age mated Wt indicating an age dependent inflammatory process (Figs. 5C and 5D).

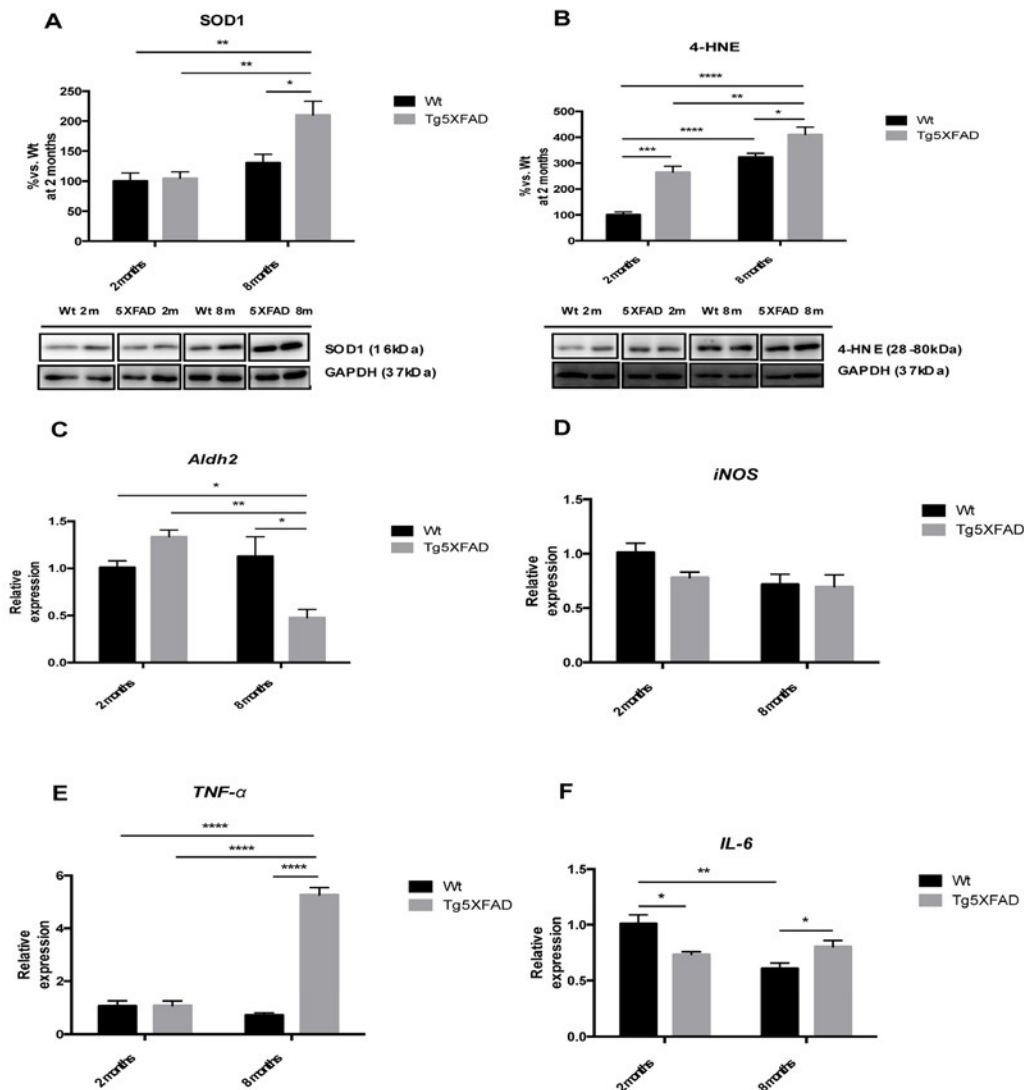


**Figure 5.** Oxidative stress and pro-inflammatory markers in female mice aged 2 and 8 months (Wt and 5XFAD), representative Western blot for SOD1 (A), 4-HNE (B), representative gene expression for *Aldh2* (C), *iNOS* (D), *TNF- $\alpha$*  (E), and *IL-6* (F). Mean  $\pm$  Standard Error of the Mean (SEM) from five independent experiments performed in triplicate are represented. \* $p < 0.05$ ; \*\* $p < 0.01$ ; \*\*\* $p < 0.001$ ; \*\*\*\* $p < 0.0001$ .

OS leads to gliosis and neuronal loss. In our hands increases in Glial Fibrillary Acidic Protein (GFAP) staining was found in 5XFAD animals compared with Wt, indicating harmful environment (Fig. 6A).

Quantification of fluorescence intensity demonstrated higher astrogliosis in hippocampus of 5XFAD with regard to Wt and significant worsening with age (See Figs. 6B-D for statistical notations). Moreover, signifi-

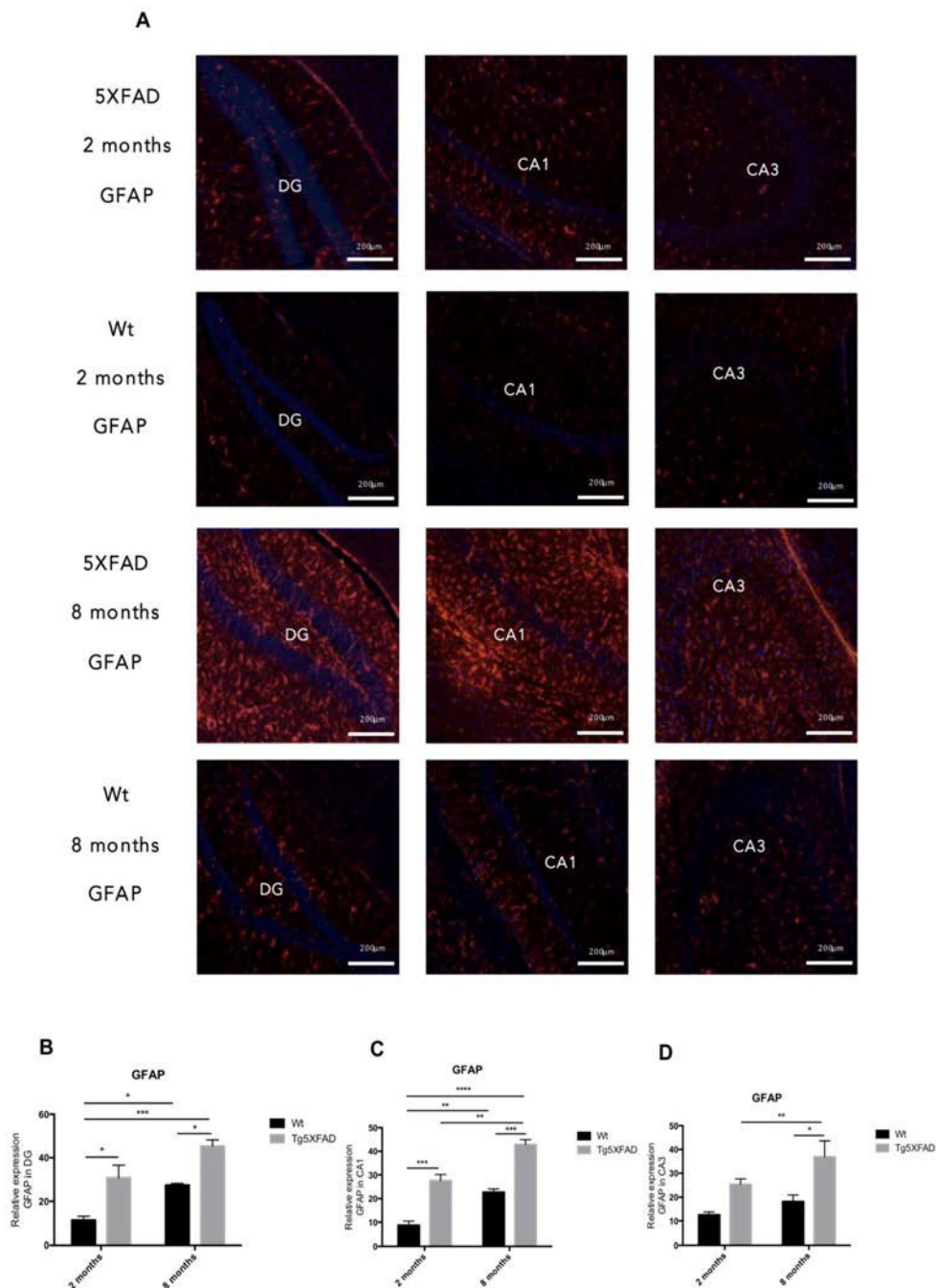


**Figure 6.** Representative images for GFAP immunostaining (A) and quantification on the bar chart (B-D) in female mice aged 2 and 8 months (Wt and 5XFAD). Bars represent mean  $\pm$  Standard Error of the Mean (SEM); ( $n = 4$  for each group). \*\*\* $p < 0.001$ ; \*\*\*\* $p < 0.0001$ . DG: Dentate Gyrus. Scale bar for immunohistochemical images is 200  $\mu\text{m}$ .

cant neuronal loss measured as NeuN levels accompanied gliosis with strain and age (Figs. 7C and 7D) (age,  $F(1,8) = 4.029$ ,  $p = 0.0796$ ; genotype,  $F(1,8) = 18.53$ ,  $p = 0.0026$ , and interaction age  $\times$  genotype  $F(1,8) = 4.029$ , n.s.). On the other hand, reduction in synaptic

structures, measured by Synaptophysin protein levels was also determined in 5XFAD in reference to Wt mice (Figs. 7C-E) (age,  $F(1,8) = 6.047$ , n.s.; genotype,  $F(1,8) = 14.14$ ,  $p = 0.0055$ , and interaction age  $\times$  genotype  $F(1,8) = 0.211$ , n.s.).

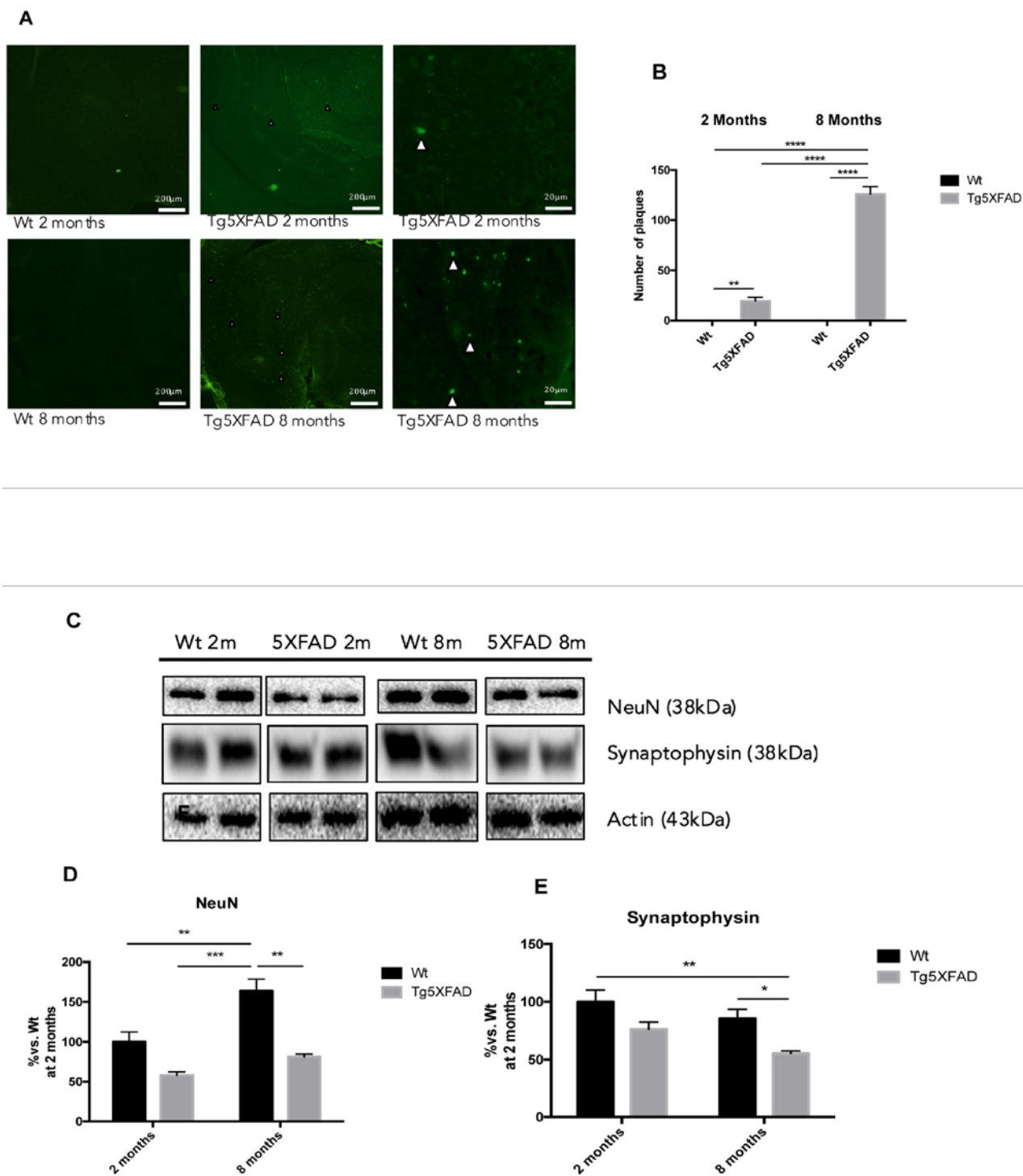


**Figure 7.** Histological images of amyloid plaques stained with thioflavin-S in female mice aged 2 and 8 months (Wt and 5XFAD). There is a heavy load of plaques in the majority of the brain areas illustrated in 5XFAD the brain section (A). Representative Western blot for NeuN (B, C) and Synaptophysin (D, E). Bars represent mean  $\pm$  Standard Error of the Mean (SEM),  $n = 4$  for each group; DG: Dentate Gyrus. Scale bar for histochemical images is indicated in the Picture; \* $p < 0.05$ ; \*\* $p < 0.01$ ; \*\*\* $p < 0.001$ .

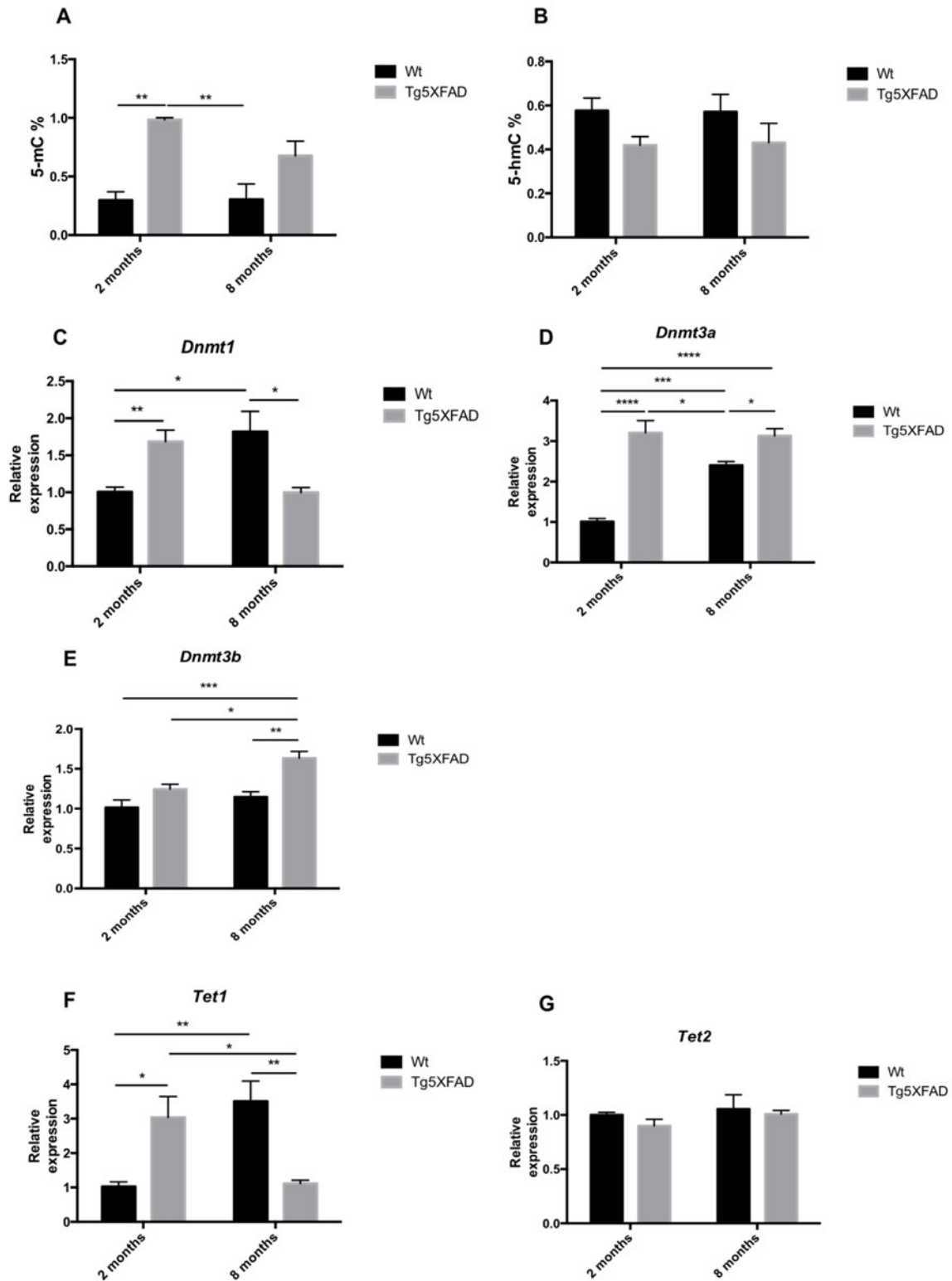


**Figure 8.** Global 5-methylated cytosine (A) and 5-hydroxymethylated cytosine levels (B) in female mice aged 2 and 8 months (Wt and 5XFAD). Gene expression for *Dnmt1* (C), *Dnmt3a* (D), *Dnmt3b* (E), *Tet1* (F), and *Tet 2* (G). Gene expression levels were determined by real-time PCR. Mean  $\pm$  Standard Error of the Mean (SEM) from five independent experiments performed in triplicate are represented. \* $p < 0.05$ ; \*\* $p < 0.01$ ; \*\*\* $p < 0.001$ ; \*\*\*\* $p < 0.0001$ .

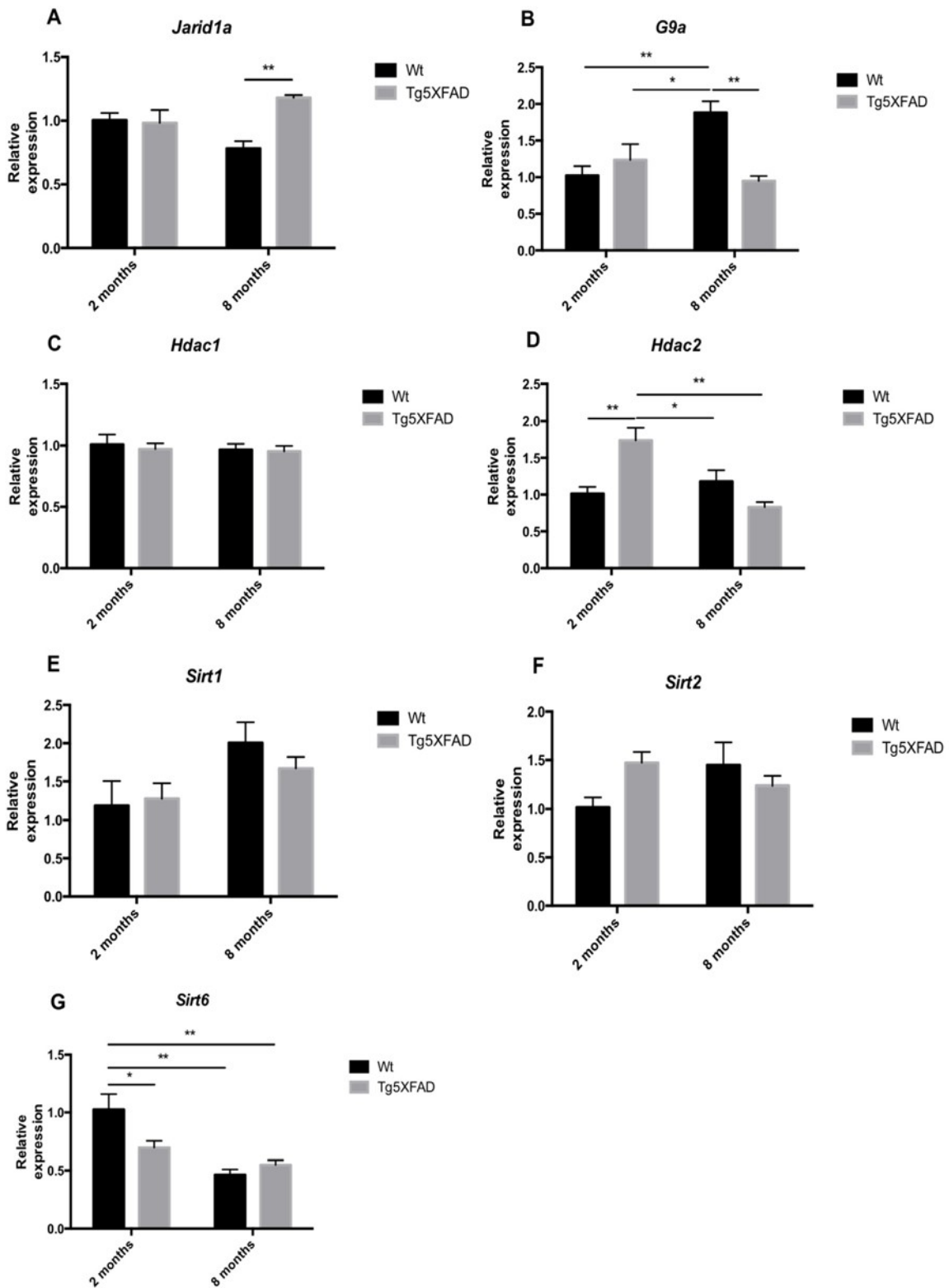


**Figure 9.** Gene expression for *Jarid1a* (A), *G9a* (B), *Hdac1* (C), *Hdac2* (D), *Sirt1* (E), *Sirt2* (F), and *Sirt6* (G) in female mice aged 2 and 8 months (Wt and 5XFAD). Gene expression levels were determined by real-time PCR. Mean  $\pm$  Standard Error of the Mean (SEM) from five independent experiments performed in triplicate are represented. \* $p < 0.05$ ; \*\* $p < 0.01$ ; \*\*\* $p < 0.001$ ; \*\*\*\* $p < 0.0001$ .

## Epigenetic enzymes gene expression differences in female 5XFAD

Global methylation and hydroxymethylation was measured by ELISA. Results demonstrated a superior levels in DNA methylation (5-mC) in 5XFAD mice with respect to Wt which reached significance at the age of 2 (age,  $F(1,8) = 2.383$ , n.s.; genotype,  $F(1,8) = 29.32$ ,  $p = 0.0006$ , and interaction age  $\times$  genotype  $F(1,8) = 2.583$ , n.s.) (Fig. 8A), whereas 5-hmC presented a diminution trend, which was not statistically significant (Fig. 8B). DNMTs, HDMs and HDACs gene expression was determined by RT-PCR, and non-transgenic and 5XFAD mice at ages 2 and 8 months were compared. The results demonstrated a significant increase in the levels of *Dnmt1* in young transgenic mice, this rise is inverted at the older age being higher in Wt groups (age  $F(1,12) = 0.1417$ , n.s.; genotype,  $F(1,12) = 0.1785$ , n.s., and interaction age  $\times$  genotype  $F(1,12) = 20.68$ ,  $p = 0.007$ ) (Fig 8C). *Dnmt3a* and *Dnmt3b* levels increased in the mice at 8 months of age, being significant higher in 5XFAD groups (*Dnmt3a*: age,  $F(1,12) = 12.90$ ,  $p = 0.0037$ ; genotype,  $F(1,12) = 63.51$ ,  $p < 0.0001$ , and interaction age  $\times$  genotype  $F(1,12) = 16.18$ ,  $p = 0.0017$ ; *Dnmt3b*: age,  $F(1,12) = 11.06$ ,  $p = 0.0060$ ; genotype,  $F(1,12) = 20.76$ ,  $p < 0.0007$ , and interaction age  $\times$  genotype  $F(1,12) = 2.668$ , n.s.) (Figs. 8D-E). TET oxidized 5-mC and create 5-hmC, which may represent epigenetic markers of their own with a role for priming the epigenome. *Tet1* was found significantly reduced in old 5XFAD in comparison with Wt (age,  $F(1,12) = 0.4151$ , n.s.; genotype,  $F(1,12) = 0.1934$ , n.s. and interaction age  $\times$  genotype  $F(1,12) = 25.93$ ,  $p = 0.003$ ), without changes in *Tet2* (Fig. 8F).

Another epigenetic modification is histone demethylation and deacetylation. *Jarid1a*, a specific H3K4 histone demethylase, increased in older 5XFAD (age,  $F(1,12) = 12.90$ ,  $p = 0.0037$ ; genotype,  $F(1,12) = 0.0367$ , n.s., and interaction age  $\times$  genotype  $F(1,12) = 8.272$ ,  $p = 0.0139$ ) (Fig. 9A). In addition, the results demonstrated significant differences in the expression of *G9a* (a specific H3K9 histone methyltransferase) between non-transgenic and 5XFAD mice. In Wt mice, there was a significant *G9a* increase with age, that was absent in 5XFAD animals (age,  $F(1,12) = 3.604$ , n.s.; genotype,  $F(1,12) = 5.779$ ,  $p = 0.0333$ , and interaction age  $\times$  genotype  $F(1,12) = 14.61$ ,  $p = 0.0024$ ) (Fig. 9B). In terms of deacetylases, we observed a significant increase of *Hdac2* in 2-months-old 5XFAD in terms of Wt, but non-significant changes in older mice (age,  $F(1,12) = 8.394$ ,  $p = 0.0134$ ; genotype,  $F(1,12) = 2.184$ , n.s., and interaction age  $\times$  genotype  $F(1,12) = 17.60$ ,  $p = 0.0012$ ) (Fig. 9D). No differences in *Hdac1* gene expression of were found in 5XFAD mice compared

with non-transgenic mice at any age (Fig. 9C). Sirtuin family deacetylases as with memory were also explored. No significant changes were found in the gene expression of *Sirt1* and *Sirt2* (Figs. 9E-F), but an earlier decrease in *Sirt6* expression was found in young transgenic mice, and in both strains in older mice (age,  $F(1,12) = 19.88$ ,  $p = 0.0008$ ; genotype,  $F(1,12) = 2.378$ , n.s., and interaction age  $\times$  genotype  $F(1,12) = 6.581$ ,  $p = 0.0225$ ) (Fig. 9G).

## DISCUSSION

Epigenetic modifications such as global DNA methylation/hydroxymethylation, histone demethylation levels and histone acetylation levels play a crucial role in gene regulation [30]. Epigenetic changes could be the basis for the presentation of senescence and for neurodegenerative diseases, such as AD [31]. In fact, impaired global DNA methylation has been found in aged and AD brain, but in addition other changes can be related with AD. For example, AD brain showed hyper- and hypomethylated CpG islands in promoter regions for CREB and NF- $\kappa$ B genes, respectively. Moreover, AD brain demonstrated increased global histone H3 acetylation and hypermethylation of the promotor region for the drebrin-like protein gene and many other epigenetic changes observed were inversely related with respective changes in messenger RNA and protein levels [25]. Because OS may be induced by A $\beta$ , it can be an important contributor to DNA epigenetic modifications. It has been shown that ROS can command epigenetic modification by histone acetylation and deacetylation by HATs and HDACs, respectively, linking OS to chromatin remodeling [32]. However, the exact relationship among A $\beta$ , ROS and epigenetics remains largely unknown, in terms of whether A $\beta$  does, in fact, cause DNA methylation/demethylation or whether it is responsible for other epigenetic changes that exert an influence on the progression of AD.

5XFAD mice are characterized by higher levels in amyloidogenic pathology [33]. These mice accumulate high levels of intraneuronal A $\beta$ -42 at around 1.5 months of age with amyloid deposition rapidly following at around two months of age, first in the subiculum and layer 5 of the cortex and increasing rapidly with age [34]. Plaques spread throughout the hippocampus and cortex by 6 months of age. Gliosis also begins at around 2 months of age, developing in parallel with plaque deposition. Synapse degeneration is also observed (at approximately 4 months of age) as well as neuronal loss and deficits in spatial learning (at approximately 4 to 5 months of age) [35]. Tangles are not typical in this model but tau hyperphosphorylation has been described

[36,37]. We demonstrated, as expected, that in our hands female 5XFAD exhibited an increase in AD markers with age, including, an increase in *APP* and *Bace1* expression, higher protein levels of BACE1 and sAPP $\beta$ , and higher number of amyloid plaques indicating the development of AD pathology as described elsewhere in aged 5XFAD [38]. Another hallmark demonstrated in these transgenic animals comprised the increase in oxidative environment that parallels with the degree of disease development [39]. In our hands, oxidative stress initiated with 4-HNE increases at 2 months of age, but a complete development of oxidative markers was found at older ages, accordingly to the higher levels of amyloid pathology and also of tau hyperphosphorylation. AD brain undergoes a general OS process, as documented by significant protein oxidation, lipid peroxidation, and DNA oxidation [40]. Interestingly, 4-HNE, a reactive end-product of lipid peroxidation that is found increased in AD brains, has been observed to bind to histone lysine residues.

These molecular and biochemical findings are phenotypically demonstrated by loss in memory abilities and also by impairment in behavioral and emotional parameters in aged 5XFAD. Therefore, in our hands female 5XFAD initiate the AD characteristics as earlier as 2 months but the disease is completely developed at 8 months of age in a similar way described by Oakley and coworkers (2006).

Here we confront the implication of epigenetic changes with AD hallmarks in female 5XFAD (including A $\beta$  deposition and OS processes), which we addressed from a holistic point of view, in order to demonstrate a possible relationship between the processes gated to earlier A $\beta$  deposition that account for, in the 5XFAD brain, the epigenetic response, both to delay or to contribute the evolution of the disease.

By means of this approach, we demonstrate that a significant increase in global DNA methylation, measured by 5-methylCytosine (5-mC) levels in young animals when A $\beta$  initiate deposition and with concomitant increase of *Dnmt1* and *Dnmt3a*. *Dnmt3b* is maintained as increased in older mice. Although no changes in hydroxymethylCytosine (5-hmC) levels were found, *Tet1* but not *Tet2* (which catalyze the conversion of 5-mC into 5-hmC) increases in 2 month-old transgenic mice, followed by a reduction in older animals. In reference to histone modification by acetylation or deacetylation, again we found differences in transgenic mice, with increases in *Hdac2*, *Jarid1a* or *G9a*.

It was described elsewhere that DNMT3a and DNMT3b are essential for memory formation and that they participated in neuronal and synaptic plasticity changes. Recently, it is has been reported that DNMT3b moderates cognitive decline in subjects with mild cognitive impairment [41,42]. The significant changes found in *Dnmt1* and *Dnmt3b* in young 5XFAD lead to

**Table 4.** Partial correlation controlling for group coefficients between selected variables included in the study.

Control Variables	NORT DI	EPM Time open arms	OFT Locomotor activity	Amyloid plaques	SOD1	4-HNE	DNMT1	HDAC2
NORT (DI)	1.000	-0.251	0.238	<b>-0.485***</b>	-0.155	0.241	0.344	<b>0.469*</b>
EPM Time open arms		1.000	-0.208	<b>0.480***</b>	0.327	0.330	-0.388	-0.392
OFT Locomotor activity			1.000	<b>-0.424*</b>	-0.308	<b>-0.427*</b>	0.096	0.368
Amyloid plaques				1.000	<b>0.721***</b>	0.005	<b>0.633**</b>	<b>-0.750***</b>
SOD1					1.000	<b>0.442*</b>	-0.361	<b>-0.714***</b>
4-HNE						1.000	0.402	-0.198
DNMT1							1.000	<b>0.456*</b>
HDAC2								1.000

The values used to calculate Partial correlation controlling for group coefficients were Amyloid pathology obtained with S-Thioflavin staining (showed in Figure 7B); behavioral parameters from NORT, EPM and OFT (showed in Figures 1A, 2A and 3C); protein expression for SOD1 and 4-HNE (showed in Figure 5A and 5B); and gene expression for *Dnmt1* and *Hdac2* (showed in Figures 8C and 9D) Correlation(2-tailed) is significant \* p<0.05; \*\*p<0.01 and \*\*\*p<0.001; (-) Negative covariation of two variables.

higher cytosine methylation, prior to the development of AD hallmark in this mouse, underlying the earlier participation for methylation processed at the onset of the pathology. Some authors reported that in aged mice there occurs a diminution in hippocampal expression of *Dnmt3a*, and that increasing this expression reverses memory deficits whereas knockdown in young mice impairs memory formation [43]. The increases in *Dnmt3a* and *Dnmt3b* in transgenic animals could be an attempt to surpass the harmful effect of the A $\beta$  increment as well as the high oxidant environment that occurs in 5XFAD when the disease is completely developed, as depicted in negative correlations found among the results obtained in the present work (Table 4).

JumonjiC (JmjC) and ARID domain, containing histone lysine demethylase 1a (JARID1a) increased histone acetylation by inhibiting histone deacetylase 1 function and modifying gene transcription in a demethylase-independent manner. *Jarid1a* and *Jarid1b* catalyzed H3K4 demethylation contributing to the silencing of retinoblastoma target genes in senescent cells. Therefore *Jarid1a* and *Jarid1b* are tumor-suppressors that control cellular senescence [44]. Moreover, depletion of JARID1a in mammalian cells reduced per histone acetylation promoter, dampened gene expression and, for example, shortened the period of circadian rhythms [45].

Different histone methylations are also associated with behavioral disorders. G9a methylates H3K9 and this hypermethylation leads to the downregulation of BDNF [46]. It well established that BDNF plays an important role in neuron formation, maintenance and memory formation, and memory formation affects acetylation of H3 and H4 N-terminal tails. The lowest level of *G9a* gene expression in 5XFAD compared with non-transgenic mice is coincident with the loss of memory in this AD mouse model.

Finally, histone modification also plays an important role in epigenetic control. Histone deacetylases have been implicated in memory and cognition, and concretely, HDAC2 plays a central role in coupling lysine acetylation with synaptic plasticity and its modulation is implicated in cognition and disease [47]. Sirtuins are a family of nicotinamide adenine dinucleotide-dependent deacetylases that are implicated in a number of physiological and pathological processes, such as control of glucose and lipid metabolism, cancer, genomic stability and DNA repair [48]. SIRT6 plays a role in synaptic function and neuronal maturation and may be implicated in the regulation of neuronal survival [49] and the overexpression of the SIRT6 extended life span [50]. It

is noteworthy that, in the 5XFAD model, *Hdac2* increased significantly in 2-month old transgenic mice whereas diminution of *Sirt6* was found. No significant changes were found for these and other histone acetylases or deacetylases tested at older age (*Hdac1*, *Sirt1* and *Sirt2*). A very significant negative correlation between amyloid plaques and HDAC2 was found (Table 4), supporting the previously reported role of HDAC2 in synaptic plasticity [51] and working memory results obtained in 5XFAD.

Our results support that the A $\beta$  pathology that is characteristic for 5XFAD mouse correlates with behavior, OS markers and specific epigenetic enzymes in 5XFAD (Table 4). Depending on disease stage development, DNA transcription modification processes, such as methylation or acetylation, may form part of a vicious cycle involving OS because the increase in A $\beta$  accumulation, and that of, in turn, A $\beta$  may induce global DNA changes in methylation and acetylation that correlated with the progression of the pathology from earlier onset to final stages of the disease in 5XFAD, including neuronal loss, gliosis and the disturbances in cognition and behavior present in this animal model of AD.

## METHODS

**Animals.** Female Wild type (Wt, n = 10) and 5XFAD (Tg5XFAD, n = 10) mice at both 2 and 8 months of age, were used. These animals had *ad libitum* access to a standard chow diet (2018 Teklad Global 18% Protein Rodent Diet; Harlan Teklad, Madison, WI, USA) and tap water and were maintained under standard temperature conditions ( $22 \pm 2^\circ\text{C}$ ) and 12h:12h light-dark cycles (300 lux/0 lux).

Studies were performed in accordance with the Institutional Guidelines for the Care and Use of Laboratory Animals established by the Ethical Committee for Animal Experimentation at the University of Barcelona.

### Behavioral and cognitive experiments

**Elevated Plus Maze test.** This test is employed to assess anxiety [52]. The basic measurement is the animal's preference for dark, enclosed over bright, exposed places. The animal is placed in the center of the apparatus and observed for a set time. Measurements include total time spent in open and closed arms (and central platform), as well as entries into open and closed arms. Each mouse was individually placed at the center of the maze facing one of the enclosed arms and allowed to explore the maze freely during a 5-min

observation period. Maze performance was video-recorded for later analysis. Time spent in open arms and numbers of arm entries were analyzed as indices of emotional behavior utilizing SMART<sup>®</sup> ver. 3.0 software (PanLab, SLU, Spain).

**Open Field Test.** Open Field Test (OFT) apparatus was constructed of white plywood (50 × 50 × 25 cm) [53]. Red lines were drawn on dividing the floor into 25-cm squares. Behavior was scored with SMART<sup>®</sup> ver. 3.0 software, and each trial were recorded for later analysis, utilizing a camera fixed to the ceiling at a height of 2.1 m situated above the apparatus. Mice were placed at the center, or at one of the four corners, of the Open Field and allowed to explore the apparatus for 5 min. After the 5-min test, the mice were returned to their home cages and the Open Field was cleaned with 70% ethyl alcohol and allowed to dry between tests. To assess the animal's habituation process to the novelty of the arena, the mice were exposed to the apparatus for 5 min on 2 consecutive days. The behaviors scored included Line Crossing, Center Entries, Center Stay Duration, Rearing, Defecation, and Urination. Each animal was then given a score for total locomotor activity, which was calculated as the sum of total distance, line crosses and number of rears.

**Novel Object Recognition Test (NORT).** This test was conducted in a 90-degree, two-arm, 25-cm-long, 20-cm-high maze [54]. Light intensity in the middle of the field was 30 lux. The objects to be discriminated were plastic figures (object A, 5.25-cm high, and object B, 4.75-cm high). First, mice were individually habituated to the apparatus for 10 min for 3 days. On day 4, they were submitted to a 10-min acquisition trial (first trial), during which they were placed in the maze in the presence of two identical novel objects (A+A or B+B) placed at the end of each arm. A 10-min retention trial (second trial) occurred 2 h later. During this second trial, objects A and B were placed in the maze, and the times that the animal took to explore the new object (tn) and the old object (to) were recorded. A Discrimination Index (DI) was defined as  $(tn-to)/(tn+to)$ . In order to avoid object preference biases, objects A and B were counterbalanced so that one half of the animals in each experimental group were first exposed to object A and then to object B, whereas the other one half first saw object B and then object A was presented. The maze, the surface, and the objects were cleaned with 96° ethanol between the animals' trials to eliminate olfactory cues.

**Morris Water Maze test.** An open circular pool (100 cm in diameter, 50 cm in height) was filled halfway with water [55] and water temperature was maintained at

22°C ± 1. Two principal perpendicular axes were defined; thus, the water surface was divided into four quadrants (NE, SE, SW, and NW), and five starting points were set (NE, E, SE, S, and SW). Four visual clues were placed on the walls of the tank (N, E, S, and W). Non-toxic white latex paint was added to make the water opaque, and a white escape platform was submerged 1 cm below the water level (approximately in the middle of one of the quadrants).

The animal's swimming paths were recorded by a video camera mounted above the center of the pool, and the data were analyzed with SMART<sup>®</sup> ver. 3.0 statistical software. The learning phase consisted of 6 days of trials for each mouse. The animals were submitted to five trials each day starting from the positions set (in random order) and without a resting phase between each trial and the subsequent one. At each trial, the mouse was placed gently into the water, facing the wall of the pool, and allowed to swim for 60 sec. If not able to locate the platform in this period of time, the mouse was guided to the platform by the investigator. Animals were left on the platform each time for 30 sec in order to allow spatial orientation.

The parameters measured were latency time in finding the platform, time spent in each quadrant, and distance swum for each trial; the mean was calculated for each trial day. A memory test was performed at the end of the learning days, in which the platform was removed and the time spent by each mouse in each quadrant was measured.

**Brain isolation and immunoanalysis assays.** Mice were euthanized 3 days after the last trial was conducted, and the brain was quickly removed from the skull. Hippocampus were dissected and frozen in powdered dry ice and maintained at -80°C for further use. Tissue samples were homogenized in lysis buffer containing phosphatase and protease inhibitors (Protease Inhibitor Cocktail 2, Sigma), and cytosol and nuclear fractions was obtained as described elsewhere. Protein concentration was determined by the Bradford method. Fifteen µg of protein was separated by Sodium Dodecyl Sulfate-PolyAcrylamide Gel Electrophoresis (SDS-PAGE) (8–15%) and transferred onto PolyVinylidene DiFlouride (PVDF) membranes (Millipore). The membranes were blocked in 5% non-fat milk in Tris-Buffered Saline containing 0.1% Tween 20 (TBS-T) for 1 h at room temperature, followed by overnight incubation at 4°C with primary antibodies diluted in TBS-T and 5% Bovine Serum Albumin (BSA) (See details in Table 1). Membranes were then washed and incubated with secondary antibodies for 1 h at room temperature. Immunoreactive proteins were visualized

utilizing an Enhanced ChemiLuminescence-based detection kit (ECL Kit; Millipore) and digital images were acquired employing a ChemiDoc XRS+System (BioRad). Band intensities were quantified by densitometric analysis utilizing Image Lab software (BioRad) and values were normalized to GAPDH.

For immunohistochemical studies, the frozen brains were embedded into OCT Cryostat Embedding Compound (Tissue-Tek, Torrance, CA, USA), cut into 20- $\mu$ m-thick sections on a cryostat (Leyca Microsystems, Germany) at  $-20^{\circ}\text{C}$ , and placed on slides. After 3 h of drying time at room temperature, the slices were fixed with acetone at  $4^{\circ}\text{C}$  for 10 min, allowed to dry overnight, and finally stored at  $-20^{\circ}\text{C}$  until their further staining. For the staining procedure, the brain sections were first rehydrated by 5-min incubation in Phosphate-Buffered Solution (PBS). Afterward, the blocking/permeabilization step was performed (20 min in PBS 1% BSA + 1% Triton). Following two, 5-min washings in PBS, the slices were incubated overnight at  $4^{\circ}\text{C}$  with the primary antibodies (see Table 1 for dilutions). Two further washings were carried out prior to incubation with the fluorescent secondary antibody (1 h at room temperature, see Table for dilutions). Finally, before mounting with Fluoromount-G<sup>TM</sup> (EMS, Hatfield, NJ, USA), nuclear staining was performed with Hoechst 2  $\mu\text{g}/\text{mL}$  for 5 min at room temperature. Slides were allowed to dry overnight after mounting and image acquisition was performed with a fluorescence laser microscope (Olympus BX41; Germany). At least four images from four different individuals by group were analyzed with ImageJ/Fiji software available online from the National Institutes of Health, NIH).

Thioflavin S staining. Slides were allowed to defreeze at room temperature and then were rehydrated with PBS solution for 5 min. Later, the brain sections were incubated with 0.3% thioflavin S (Sigma-Aldrich) for 20 min at room temperature in the dark. Subsequently, these were submitted to washes in 3-min series, specifically with 80% ethanol (two washes), 90% ethanol (one wash), and three washes with PBS. Finally, the slides were mounted using Fluoromount (EMS), allowed to dry overnight at room temperature in the dark, and stored at  $4^{\circ}\text{C}$ . Image acquisition was performed with an epifluorescence microscope (BX41; Olympus, Germany). For plaque quantification, similar and comparable histological areas were selected, focusing on adjacent positioning of the hippocampus and the whole cortical area.

RNA extraction and gene expression determination. Total RNA isolation was carried out by means of Trizol reagent following the manufacturer's instructions. RNA

content in the samples was measured at 260 nm, and sample purity was determined by the A260/280 ratio in a NanoDrop<sup>TM</sup> ND-1000 (Thermo Scientific). Samples were also tested in an Agilent 2100B Bioanalyzer (Agilent Technologies) to determine the RNA integrity number. Reverse Transcription-Polymerase Chain Reaction (RT-PCR) was performed as follows: 2  $\mu\text{g}$  of messenger RNA (mRNA) was reverse-transcribed using the High Capacity (complementary DNA) cDNA Reverse Transcription kit (Applied Biosystems). Real-time quantitative PCR (qPCR) was employed to quantify the mRNA expression of Aldehyde dehydrogenase 2 (*Aldh2*), amyloid beta A4 Precursor (*PreAPP*),  $\beta$ -secretase 1 (*Bace1*) and Disintegrin and Metalloproteinase 10 (*Adam10*), inflammatory genes Interleukin 6 (*IL-6*) and Tumor necrosis factor alpha (*TNF- $\alpha$* ), inducible Nitric Oxide Synthase (*iNOS*), epigenetic enzymes genes DNA (cytosine-5)-methyltransferase 1 (*Dnmt1*), DNA (cytosine-5)-methyltransferase 3 alpha (*Dnmt3a*), DNA (cytosine-5)-methyltransferase 3 beta (*Dnmt3b*), Tet methylcytosine dioxygenase 1 (*Tet1*), Tet methylcytosine dioxygenase 2 (*Tet2*), lysine (K)-specific demethylase 5A (*Jarid1a*), histone-lysine N-methyltransferase 2 (*G9a*), histone deacetylase 1 (*Hdac1*), histone deacetylase 2 (*Hdac2*), sirtuin 1 (*Sirt1*), sirtuin 2 (*Sirt2*), sirtuin 6 (*Sirt6*). Normalization of expression levels was performed with *Actin* for SYBER Green and TATA-binding protein (*Tbp*) for TaqMan. The primers were as follows: for *Aldh2*, forward 5'-GCAGGCGTACACAGAAGTGA-3' and reverse 5'-TGAGCTTCATCCCCTACCCA-3', for *PreAPP*, forward 5'-AGGACTGACCCTCGACCAG-3' and reverse 5'-CTTCCGAGATCTCTTCCGTCT-3', for *Bace1*, forward 5'-AAGCTGCCGTCAAGTCCATC-3' and reverse 5'-GCGGAAGGACTGATTGGTGA-3', for *Adam10*, forward 5'-GGGAAGAAATGCAAGCTGAA-3' and reverse 5'-CTGTACAGCAGGGTCTTCTGAC-3', for *IL-6*, forward 5'-ATCCAGTTGCCTTCTTGGGACTGA-3' and reverse 5'-TAAGCCTCCGACTTGTGAAGTGGT-3', for *TNF- $\alpha$* , forward 5'-TCGGGGTGATCGGTCCCCAA-3' and reverse 5'-TGGTTTGCTACGACGTGGGCT-3', for *iNOS*, forward 5'-GGCAGCCTGTGAGACCTTTG-3' and reverse 5'-GAAGCGTTTCGGGATCTGAA-3', for *Dnmt1*, (Mm01151063\_m1), for *Dnmt3a*, forward 5'-GGGCCACACGGCAGAG-3' and reverse 5'-CACGGTTCTCCTCCTGTTC-3', for *Dnmt3b*, forward 5'-TGCCAGACCTTGAAACCTC-3' and reverse 5'-GCTGGCACCTCTTCTTCAT-3', for *Tet1*, forward 5'-CTGCCAACTACCCCAAACCTCA-3' and reverse 5'-TCGGGGTTTTGTCTTCCGTT-3', for *Tet2*, forward 5'-CCATCATGTTGTGGGACGGA-3' and reverse 5'-ATTCTGAGAACAGCGACGGT-3', for *Jarid1a*, forward 5'-TCCGTGTGTCATCAGCCAAA-3' and reverse 5'-CAAGCCTACGCCAGAGTCAA-3',

for *G9a*, forward 5'-TTCCTTGTCTCCCCTCCCAG-3' and reverse 5'-GACGGTGACAGTGACAGAGG-3', for *Hdac1*, forward 5'- TCACCGAATCCGCATGACTC-3' and reverse 5'-TCTGGGCGAATAGAACGCAG-3', for *Hdac2*, forward 5'- CTATCCCGCTCTGTGCCCT-3' and reverse 5'- GAGGCTTCATGGGATGACCC-3', for *Sirt1*, forward 5'-AACACACACACAAAATCCA GCA-3' and reverse 5'-TGCAACCTGCTCCAAGGT AT-3', for *Sirt2*, forward 5'-TGCAGGAGGCTCAGG ATTC-3' and reverse 5'-GTCACCTCTCGAGGGT CAG-3', for *Sirt6*, forward 5'-GTCTCACTGTGTCC CTTGTCC-3' and reverse 5'-GCGGGTGTGATTGG TAGAGA-3', for *Actin*, forward 5'-CAACGAGCGGT TCCGAT-3' and reverse 5'-GCCACAGGTTCCATAC CCA-3', *Tbp*, (Mm00446971\_m1).

Real-time PCR was performed on the Step One Plus Detection System (Applied Biosystems) employing SYBR Green PCR Master Mix (Applied Biosystems). Each reaction mixture contained 7.5  $\mu$ L of cDNA, whose concentration was 2  $\mu$ g, 0.75  $\mu$ L of each primer (whose concentration was 100 nM), and 7.5  $\mu$ L of SYBR Green PCR Master Mix (2X) and for TaqMan gene expression assays (Applied Biosystems), each 20  $\mu$ L of TaqMan reaction, 9  $\mu$ L cDNA (18ng) was mixed with the 1  $\mu$ L 20x probe of TaqMan Gene Expression Assays and 10  $\mu$ L of 2X TaqMan Universal PCR Master Mix.

Data were analyzed utilizing the comparative Cycle threshold (Ct) method ( $\Delta\Delta$ Ct), where the actin transcript level was utilized to normalize differences in sample loading and preparation. Each sample (n=4–5) was analyzed in triplicate, and the results represented the n-fold difference of transcript levels among different samples.

**Statistical analysis.** Data are expressed as the mean  $\pm$  Standard Error of the Mean (SEM) from at least 4–5 samples. Data analysis was conducted using GraphPad Prism ver. 6 statistical software. Means were compared with two-way Analysis of Variance (ANOVA) and post hoc analysis. Comparisons between groups were performed by the unpaired Student *t* test for independent samples. Statistical significance was considered when *p* values were  $<0.05$ . Statistical outliers were performed out with the Grubs test and were removed from analysis.

In addition, partial correlation controlling for group were calculated using SPSS 19.00, between the following variables: DI, Time in open arms, Locomotor activity, Amyloid plaques, SOD1, 4-HNE, DNMT1 and HDAC2. Partial correlation coefficients were calculated using the data from number of Amyloid plaques

obtained with S-Thioflavin staining; behavioral parameters from NORT, EPM and OFT; protein expression for SOD1 and 4-HNE; and gene expression for *Dnmt1* and *Hdac2*.

## ACKNOWLEDGEMENTS

We thank Maggie Brunner, M.A., for reviewing the language and style of the manuscript.

## Funding

This study was supported by Spanish MINECO, and the European Regional Development Funds (SAF-2012-39852, BFU2013-48822-R and CSD2010-00045). CG-F, AC, and MP belong to 2014 SGR 525; and SS and CS to 2014 SGR 625.

## Conflict of interest statement

The authors have no conflict of interests to declare.

## REFERENCES

1. Ferri CP, Prince M, Brayne C, Brodaty H, Fratiglioni L, Ganguli M, Hall K, Hasegawa K, Hendrie H, Huang Y, Jorm A, Mathers C, Menezes PR, Rimmer Scazufca M. Global prevalence of dementia: a Delphi consensus study. *Lancet*. 2005; 366:2112-2117.
2. Prince M, Bryce R, Albanese E, Wimo A, Ribeiro W, Ferri CP, Rao AT, Degan. The global prevalence of dementia: a systematic review and metaanalysis. *Alzheimers Dement*. 2013; 9:63-75.e2.
3. Zanetti O, Solerte SB, Cantoni. Life expectancy in Alzheimer's disease (AD). *Arch Gerontol Geriatr*. 2009; 49 Suppl1:237-243.
4. World Health Organization report. 2011.
5. Roberson ED, Mucke L. 100 years and counting: prospects for defeating Alzheimer's disease. *Science*. 2006;314:781–784.
6. Avramopoulos D. Genetics of Alzheimer's disease: recent advances. *Genome Medicine*. 2009;1:34.
7. Grupe A, Abraham R, Li Y, Rowland C, Hollingworth P, Morgan A, Jehu L, Segurado R, Stone D, Schadt E, Karnoub M, Nowotny P, Tacey K, Catanese J, Sninsky J, Brayne C, Rubinsztein D, Gill M, Lawlor B, Lovestone S, Holmans P, O'Donovan M, Morris JC, Thal L, Goate A, Owen MJ. and Williams, J. Evidence for novel susceptibility genes for late-onset Alzheimer's disease from a genome-wide association study of putative functional variants. *Human Molecular Genetics*. 2007;16:865-873.
8. Harold D, Abrahams R, Hollingworth P, Sims R, Gerrish A, et al. Genome-wide association study identifies variants at *CLU* and *PICALM* associated with Alzheimer's disease. *Nat Genet*. 2009; 41:1088-1093.
9. Naj AC, Jun G, Beecham GW, Wang L-S, Vardarajan BB, et al. Common variants at *MS4A6E*, *CD2AP*, *CD33* and *EPHA1* are associated with late-onset Alzheimer's disease. *Nature Genetics*. 2011; 43:436-441.
10. Genin E, Hannequin D, Wallon D, Sleegers K, Hiltunen M, et al. *APOE* and Alzheimer Disease: A Major Gene with Semi-Dominant Inheritance. *Molecular psychiatry*. 2011; 16:903-907.

11. Mohandas E, Rajmohan V, and Raghunath B. Neurobiology of Alzheimer's disease. *Indian Journal of Alzheimer's Disease*. 2009; 21:1077-1087.
12. Bertram L, McQueen MB, Mullin K, Blacker D, Tanzi RE. Systematic meta-analyses of Alzheimer disease genetic association studies: the AlzGene database. *Nat Genet*. 2007; 39:17-23.
13. Bertram L. Alzheimer's disease genetics: Current status and future perspectives. *Alzheimer's and Dementia*. 2009; 5:147.
14. Bettens K, Slegers K, and Van Broeckhoven C. Current status on Alzheimer disease molecular genetics: from past, to present, to future. *Hum. Mol. Genet*. 2010; ddq142.
15. Fraga MF, Ballestar E, Paz MF, Ropero S, Setien F, Ballestar ML, Heine-Suñer D, Cigudosa JC, Urioste M, Benitez J, Boix-Chornet M, Sanchez-Aguilera A, Ling C, Carlsson E, Poulsen P, Vaag A, Stephan Z, Spector TD, Wu Y-Z, Plass C, and Esteller M. Epigenetic differences arise during the lifetime of monozygotic twins. *Proceedings of the National Academy of Sciences of the United States of America*. 2005; 102:10604-10609.
16. Mastroeni D, McKee A, Grover A, Rogers J, and Coleman PD. Epigenetic Differences in Cortical Neurons from a Pair of Monozygotic Twins Discordant for Alzheimer's Disease. *PLoS ONE*. 2009; 4:e6617.
17. Millan MJ. The epigenetic dimension of Alzheimer's disease: causal, consequence, or curiosity? *Dialogues Clin Neurosci*. 2014; 16:373-393.
18. Bradley-Whitman MA and Lovell MA. *Mech Aging Dev*. 2013; 134:486-495. Doi: 10.1016/j.mad.2013.08.005.
19. Zhenyun Yuan, Mingwei Wang, Baoyong Yan, Ping Gu, Xiangming Jiang, Xiufen Yang, and Dongsheng Cui. An enriched environment improves cognitive performance in mice from the senescence-accelerated prone mouse 8 strain. *Neural Regen Res*. 2012; 7:1797-1804.
20. Griñan-Ferré C, Pérez-Cáceres D, Martínez Gutiérrez-Zetina S, Camins A, Palomera-Ávalos V, Ortuño-Sahagún D, Teresa-Rodrigo MT, Pallàs M. Environmental Enrichment Improves Behavior, Cognition, and Brain Functional Markers in Young Senescence-accelerated Prone Mice (SAMP8). *Molecular Neurobiology*. 2015; DOI:10.1007/s12035-015-9210-6.
21. Kaminski Z, Wang SC, Petronisa. Complex disease, gender and epigenetics. *Annals of Medicine*. 2006; 38:530-544
22. West et al. Hypomethylation of the amyloid precursor protein gene in the brain of an Alzheimer's disease patient. *J Mol Neurosci*. 1995; 6:141-146.
23. Fuso A, Seminara L, Cavallaro RA, D'Anselmi F, Scarpa S. S-adenosylmethionine/homocysteine cycle alterations modify DNA methylation status with consequent deregulation of PS1 and BACE and beta-amyloid production. *Mol Cell Neurosci*. 2005; 28:195-204.
24. Chaudhry U, Zhuang H, Doré S. Microsomal prostaglandin E synthase-2: cellular distribution and expression in Alzheimer's disease. *Exp Neurol*. 2010; 223:359-365.
25. Rao, JS, Keleshian VL, Klein S, and Rapoport SI. Epigenetic modifications in frontal cortex from Alzheimer's disease and bipolar disorder patients. *Translational Psychiatry*. 2012; 2: e132.
26. Fleming JL, Phiel CJ, Toland AE. The role for oxidative stress in aberrant DNA methylation in Alzheimer's disease. *Curr Alzheimer Res*. 2012; 9:1077-96.
27. Coppieters N, Dragunow M. Epigenetics in Alzheimer's disease: a focus on DNA modifications. *Curr Pharm Des*. 2011; 17:3398-3412.
28. Zhang C, McNeil E, Dressler L, Siman R. Long-lasting impairment in hippocampal neurogenesis associated with amyloid deposition in a knock-in mouse model of familial Alzheimer's disease. *Exp Neurol*. 2007; 204:77-87.
29. Chang EH, Savage MJ, Flood DG, Thomas JM, Levy RB, Mahadomrongkul V, Shirao T, Aoki C, Huerta PT. AMPA receptor downscaling at the onset of Alzheimer's disease pathology in double knockin mice. *Proc Natl Acad Sci U S A*. 2006; 103:3410-3415.
30. Andrew J Bannister and Tony Kouzarides. Regulation of chromatin by histone modifications. *Cell Res*. 2011; 21:381-395.
31. Mastroeni D, Grover A, Delvaux E, Whiteside C, Coleman PD, Rogers J. Epigenetic mechanisms in Alzheimer's disease. 2011; *Neurobiol Aging*. 32:1161-80. Doi.1016/j.neurobiolaging.2010.08.017.
32. Afanas'ev I. Mechanisms of superoxide signaling in epigenetic processes: relation to aging and cancer. *Aging Dis*. 2015; 6:216-227.
33. Jaszberenyi M, Rick FG, Szalontay L, Block NL, Zarandi M, Cai RZ, Schally AV. Beneficial effects of novel antagonists of GHRH in different models of Alzheimer's disease. *Aging (Albany NY)*. 2012; 4:755-767.
34. Jawhar S, Trawicka A, Jenneckens C, Bayer TA, Wirths O. Motor deficits, neuron loss, and reduced anxiety coinciding with axonal degeneration and intraneuronal A $\beta$  aggregation in the 5XFAD mouse model of Alzheimer's disease. *Neurobiol Aging*. 2012; 33:196.e29-24.
35. Oakley H, Cole SL, Logan S, Maus E, Shao P, Craft J, Guillozet-Bongaarts A, Ohno M, Disterhoft J, Van Eldik L, Berry R, Vassar R. Intraneuronal beta-amyloid aggregates, neurodegeneration, and neuron loss in transgenic mice with five familial Alzheimer's disease mutations: potential factors in amyloid plaque formation. *Journal of Neuroscience*. 2006; 26:10129-10140.
36. Saul A, Sprenger F, Bayer TA, Wirths O. Accelerated tau pathology with synaptic and neuronal loss in a novel triple transgenic mouse model of Alzheimer's disease. *Neurobiol Aging*. 2013; 34:2564-2573.
37. Kanno T, Tsuchiya A, Nishizaki T. Hyperphosphorylation of Tau at Ser396 occurs in the much earlier stage than appearance of learning and memory disorders in 5XFAD mice. *Behav Brain Res*. 2014; 274:302-306.
38. Rojas S, Herance JR, Gispert JD, Abad S, Torrent E, Jiménez X, Pareto D, Perpiña U, Sarroca S, Rodríguez E, Ortega-Aznar A, Sanfeliu C. In vivo evaluation of amyloid deposition and brain glucose metabolism of 5XFAD mice using positron emission tomography. *Neurobiol Aging*. 2013; 34:1790-1798.
39. Yang E-J, Ahn S, Ryu J, Choi M-S, Choi S, Chong YH, et al. Phloroglucinol Attenuates the Cognitive Deficits of the 5XFAD mouse Model of Alzheimer's Disease. 2015; *PLoS ONE* 10: e0135686. Doi.10.1371/journal.pone.0135686.
40. Butterfield DA, Lauderback CM. Lipid peroxidation and protein oxidation in Alzheimer's disease brain: potential causes and consequences involving amyloid  $\beta$ -peptide-associated free radical oxidative stress. *Free Radic Biol Med*. 2002; 32:1050-1060.
41. Chouliaras L, Kenis G, Visser PJ, Scheltens P, Tsolaki M, Jones RW, Kehoe PG, Graff C, Girtler NG, Wallin ÅK, Rikkert MO, Spiru L, Elias-Sonnenschein LS, Ramakers IH, Pishva E, van Os J, Steinbusch HW, Verhey FR, van den Hove DL, Rutten BP. DNMT3A moderates cognitive decline in subjects with mild

cognitive impairment: replicated evidence from two mild cognitive impairment cohorts. *Epigenomics*. 2015; 7:533-537.

42. Córdova-Palomera A, Fatjó-Vilas M, Kebir O, Gastó C, Krebs MO, Fañanás L. Polymorphic variation in the epigenetic gene DNMT3B modulates the environmental impact on cognitive ability: a twin study. *Eur Psychiatry*. 2015;30:303-308.

43. Su, SC, Tsai, LH. DNA methylation in cognition comes of age. *Nature Neuroscience*. 2012; 15:1061–1062.

44. Chicas A, Kapoor A, Wang X, Aksoy O, Everitts AG, Zhang MQ, Garcia BA, Bernstein E, Lowe SW. H3K4 demethylation by Jarid1a and Jarid1b contributes to retinoblastoma-mediated gene silencing during cellular senescence. *Proc Natl Acad Sci USA*. 2012; 109: 897-896.

45. DiTacchio, L, Le HD, r Vollmers C, Hatori M, Witcher M, Secombe J, Panda S. Histone Lysine Demethylase JARID1a Activates CLOCK-BMAL1 and Influences the Circadian Clock Science. 2011;333:1881-1885.

46. Schweizer S, Harms C, Lerch H, Flynn J, Hecht J, Yildirim F, Meisel A, Märzsch S. *J Cereb Blood Flow Metab*. 2015; 350:1640-1647.

47. Penney J, Tsai LH. Histone deacetylases in memory and cognition. *Sci Signal*. 2014;7:re12.

48. Duan W. Sirtuins: from metabolic regulation to brain aging. *Front Aging Neurosci*. 2013;5:36.

49. Cardinale A, de Stefano MC, Mollinari C, Racaniello M, Garaci E, Merlo D. Biochemical characterization of sirtuin 6 in the brain and its involvement in oxidative stress response. *Neurochem Res*. 2015; 40:59-56.

50. Kanfi Y., Naiman S., Amir G., Peshti V., Zinman G., Nahum L., Bar-Joseph Z, Cohen HY. The sirtuin SIRT6 regulates lifespan in male mice. *Nature*. 2012;483:218–221.

51. Guan JS, Haggarty SJ, Giacometti E, Dannenberg JH, Joseph N, Gao J, Nieland TJ, Zhou Y, Wang X, Mazitschek R, Bradner JE, DePinho RA, Jaenisch R, Tsai LH. HDAC2 negatively regulates memory formation and synaptic plasticity. *Nature*. 2009; 459:55–60.

52. Pellow S, Chopin P, File SE and Briley M. Validation of open: closed arm entries in an elevated plus-maze as a measure of anxiety in the rat. *J. Neurosci. Methods*. 1985;14:149–167.

53. Hall, C. S. Emotional behavior in the rat. I. Defecation and urination as measures of individual differences in emotionality. *Journal of Comparative Psychology*. 1934;18:385-403.

54. Ennaceur A, Delacour J. A new one-trial test for neurobiological studies of memory in rats. *Behavioral data. Behav Brain Res*. 1988; 31:47-59.

55. Morris water maze: procedures for assessing spatial and related forms of learning and memory. Charles V Vorhees and Michael T Williams. *Nat Protoc*. 2006; 1:848-858.doi:10.1038/nprot.2006.116.

# Inhalational Alzheimer's disease: an unrecognized—and treatable—epidemic

Dale E. Bredesen<sup>1,2</sup>

<sup>1</sup>Easton Laboratories for Neurodegenerative Disease Research, Department of Neurology, University of California, Los Angeles, CA 90095, USA;

<sup>2</sup>Buck Institute for Research on Aging, Novato, CA 94945, USA

**Key words:** mycotoxins, neurodegeneration, cognition, chronic inflammatory response syndrome, biomarkers, dementia, biotoxins

**Received:** 10/30/15; **Accepted:** 02/03/16; **Published:** 02/10/16      **doi:** [10.18632/aging.100896](https://doi.org/10.18632/aging.100896)

**Correspondence to:** Dale E. Bredesen, MD; **E-mail:** [dbredesen@buckinstitute.org](mailto:dbredesen@buckinstitute.org)

**Copyright:** Bredesen. This is an open-access article distributed under the terms of the Creative Commons Attribution License, which permits unrestricted use, distribution, and reproduction in any medium, provided the original author and source are credited

**Abstract:** Alzheimer's disease is one of the most significant healthcare problems today, with a dire need for effective treatment. Identifying subtypes of Alzheimer's disease may aid in the development of therapeutics, and recently three different subtypes have been described: type 1 (inflammatory), type 2 (non-inflammatory or atrophic), and type 3 (cortical). Here I report that type 3 Alzheimer's disease is the result of exposure to specific toxins, and is most commonly inhalational (IAD), a phenotypic manifestation of chronic inflammatory response syndrome (CIRS), due to biotoxins such as mycotoxins. The appropriate recognition of IAD as a potentially important pathogenetic condition in patients with cognitive decline offers the opportunity for successful treatment of a large number of patients whose current prognoses, in the absence of accurate diagnosis, are grave.

## INTRODUCTION

Alzheimer's disease is now the third leading cause of death in the United States, following only cardiovascular disease and cancer [1]. There are approximately 5.2 million Americans with AD, but this estimate ignores the many young Americans destined to develop AD during their lifetimes: given the lifetime risk of approximately 15% when including all ApoE genotypes, as many as 45 million of the 318 million Americans now living may develop AD during their lifetimes if no prevention is instituted [2].

Effective treatment of Alzheimer's disease has been lacking, but recently a novel programmatic approach involving metabolic enhancement (MEND) was described, with promising anecdotal results [3]. One of the strategies to optimize treatment development is to identify specific subtypes of Alzheimer's disease that may respond to different optimal programs. Metabolic

profiling has revealed three readily distinguishable types of Alzheimer's disease [4]: type 1 is characterized by systemic inflammation, reflected in such laboratory results as a high hs-CRP (high-sensitivity C-reactive protein), low albumin:globulin ratio, and high cytokine levels such as interleukin-1 and interleukin-6. Type 2 is characterized by an atrophic profile, with reduced support from molecules such as estradiol, progesterone, testosterone, insulin, and vitamin D, often accompanied by increased homocysteine and insulin resistance. Type 3 is very dissimilar to the other two types, and may be mediated by a fundamentally different pathophysiological process (although, by definition, still  $\beta$ -amyloid positive and phospho-tau positive): the onset is typically younger (late 40s to early 60s); ApoE genotype is usually 3/3 instead of 4/4 or 3/4; the family history is typically negative (or positive only at much greater age); symptom onset usually follows a period of great stress, sleep loss, anesthesia, or menopause/andropause; presentation is not predominantly amnesic but is instead

cortical, with dyscalculia, aphasia, executive dysfunction, or other cortical deficits; and the neurological presentation is often preceded by, or accompanied by, depression. Consonant with these deficits, the imaging studies often indicate extra-hippocampal disease, with more general cerebral atrophy and frontal-temporal-parietal abnormalities on FDG-PET (as opposed to the more restricted, typical temporoparietal reductions in glucose utilization seen in type 1 and type 2). Neuropsychological studies also indicate non-amnestic abnormalities such as executive dysfunction. Laboratory studies often, but not always, feature hypozincemia and/or a high copper:zinc ratio, and may also suggest adrenal fatigue with reduced pregnenolone, DHEA-S (dehydroepiandrosterone sulfate), and/or AM cortisol.

Over the past two decades, elegant work from Dr. R. Shoemaker and his colleagues has demonstrated unequivocally that biotoxins such as mycotoxins are associated with a broad range of symptoms, including cognitive decline (summarized in [5]). These researchers and clinicians identified a constellation of symptoms, signs, genetic predisposition (HLA-DR/DQ haplotypes), and laboratory abnormalities characteristic of patients exposed to, and sensitive to, these biotoxins. The resulting syndrome has been designated chronic inflammatory response syndrome (CIRS). The most common cause of CIRS is exposure to mycotoxins, typically associated with molds such as *Stachybotrys*, *Penicillium*, or *Aspergillus*, present in water-damaged buildings. However, other biotoxins, from the *Borrelia burgdorferi* of Lyme disease or from other tick-borne pathogens, or aquatoxins such as those from dinoflagellates, may also cause CIRS. Laboratory evaluation of CIRS reveals increases in C4a (complement component 4a), TGF- $\beta$ 1 (transforming growth factor beta-1), MMP9 (matrix metalloproteinase 9), specific cytokines, and decreases in MSH (melanocyte-stimulating hormone), VEGF (vascular endothelial growth factor), and ADH (anti-diuretic hormone), as well as frequent hypercortisolemia, hypozincemia, and other abnormalities. These laboratory abnormalities are frequently accompanied by nasal colonization by MARCoNS (multiple-antibiotic-resistant coagulase-negative *Staphylococcus*) and compromised visual contrast sensitivity. Specific HLA-DR/DQ haplotypes are associated with sensitivity to mycotoxins, and thus account for the vast majority of CIRS cases.

Most importantly, Dr. Shoemaker and his colleagues developed an effective therapeutic regimen for CIRS. This is a complicated, multi-step regimen that includes toxin binding by cholestyramine, treatment of

MARCoNS by BEG (Bactroban, EDTA, and gentamicin) nasal spray, intranasal VIP (vasoactive intestinal peptide), removal of toxin source, addressing all of the hormonal, gastrointestinal, and other biochemical abnormalities (e.g., anti-diuretic hormone administration if indicated), and follow-up laboratory tests to ensure return to normal.

Here I report that type 3 Alzheimer's disease is a phenotypic manifestation of CIRS. Both may present with cognitive decline that goes beyond a restricted amnestic presentation to include executive dysfunction and other deficits; as well as depression, hypozincemia, hypersensitivity to stress, and dysfunction of the hypothalamic-pituitary-adrenal (HPA) axis. In the description of the three types of Alzheimer's disease [4], it was pointed out that all of the initial six patients described with type 3 Alzheimer's disease had a significant history of toxic exposures, including in some cases mycotoxins. Follow-up evaluation of these and other patients with type 3 Alzheimer's disease revealed that a majority of these patients meet criteria for CIRS.

## RESULTS

### Case studies

**Patient 1.** This is a follow-up description of the first patient described in a previous report [4]. A 52-year-old woman presented with a two-year history of cognitive decline, beginning with dyscalculia. Her cognitive decline had been preceded by severe stress with employment changes, menopause at 51 years of age, and four episodes of general anesthesia for relatively minor procedures. She declined over several months and developed a simple, childlike affect. Despite these symptoms, she learned and remembered the names of all 28 children on the playground at her son's school. Family history was negative for dementia. Her MoCA score was 19/30. Her MRI showed global cerebral and cerebellar atrophy. There were several areas of FLAIR (fluid-attenuated inversion recovery) hyperintensity in the subcortical and periventricular white matter. An amyloid PET (positron emission tomography) scan was positive. Her CSF (cerebrospinal fluid) included reduced A $\beta$ 2 of 294pg/ml and increased p-tau of 133pg/ml, strongly supporting the diagnosis of Alzheimer's disease.

BMI was 24.9. ApoE was 3/3, klotho variant negative (SNP Rs9536314), hs-CRP 1.4mg/l, albumin:globulin ratio 1.57, IL-6 1.4pg/dl, hemoglobin A1c 5.3%, fasting insulin 4.5mIU/l, TSH 2.14mIU/l, free T3 4.2pg/ml, reverse T3 11ng/dl, free T4 1.0pg/ml, progesterone < 0.21ng/ml, estradiol 3pg/ml, 17-hydroxypregnenolone

14ng/dl, AM cortisol 9mcg/dl, 25-hydroxycholecalciferol 22ng/ml, total cholesterol 264mg/dl, HDL-cholesterol 67mg/dl, LDL-cholesterol 167mg/dl, triglycerides 61mg/dl, cholesterol:HDL ratio 3.7, serum copper 101mcg/dl, serum zinc 56mcg/dl, and Cu:Zn ratio 1.8. Heavy metal evaluation from blood was negative.

She was started on the MEND protocol [3], and because of the presentation consistent with type 3 AD, further history was obtained and additional laboratory evaluation undertaken. She had moved into a new home two years before the onset of symptoms. Her symptoms tended to worsen when she returned home from travel. Evaluation of the home by a mold expert isolated *Stachybotrys*, *Penicillium*, and *Aspergillus*, all mold genera associated with neurotoxin production. Her C4a was 22,799ng/ml (normal <2800ng/ml), TGF- $\beta$ 1 (transforming growth factor beta-1) was 6660pg/ml (normal <2382pg/ml), and MMP9 (matrix metalloproteinase 9) was 620ng/ml (normal <332ng/ml). Serum test for Lyme disease was negative. Her nasal cavity was positive for MARCoNS (multiple-antibiotic-resistant coagulase-negative *Staphylococcus*), a common finding associated with CIRS. She underwent visual contrast sensitivity testing, which she failed. Since these findings, taken together, are strongly suggestive of a diagnosis of CIRS, she was started on the Shoemaker Protocol [5]. After five weeks on this protocol, she began to show modest subjective improvement, and her C4a had decreased to 2750ng/ml.

Comment: This patient fulfilled diagnostic criteria for both Alzheimer's disease and CIRS. She presented in a manner typical for type 3 Alzheimer's disease, with a non-amnesic onset (although her memory was affected later in the course), multiple stresses, onset at a young age (50 years of age), in association with hormonal reduction, ApoE  $\epsilon$ 4-negative genotype, hypozincemia, hypothalamic-pituitary-adrenal axis (HPA) abnormality, and negative family history. Her laboratory values were strongly supportive of CIRS, with a very high C4a, as well as high TGF- $\beta$ 1 and MMP9, and the presence of MARCoNS, as well as reduced visual contrast sensitivity (VCS). Typical for the patients in this report (and those with CIRS in general), the chronic inflammation was not accompanied by a marked elevation of hs-CRP, although the value of 1.4mg/l represents a slight elevation above normal. The inciting agents for the CIRS in her case are likely to have been mycotoxins, based on the presence of *Stachybotrys*, *Penicillium*, and *Aspergillus* in the patient's home and the negative test for Lyme disease. These mycotoxins may include trichothecenes (from *Stachybotrys*), aflatoxin (from *Aspergillus*), and ochratoxin A (from

*Aspergillus* and *Penicillium*), among others, all of which exhibit well-described neurotoxic effects. In addition, inflammagens, microbes, microbial fragments, endotoxins, lipopolysaccharides, and biologically-produced VOCs (volatile organic compounds) may have contributed to the CIRS [6]. It is noteworthy that, as has been described repeatedly with CIRS, the mold exposure had not been suspected by patient, family, or healthcare providers prior to the recognition of the syndrome. At the current time, it is too early to tell how much improvement the patient will experience with the Shoemaker Protocol, but she has begun to show modest improvement, which is in stark contrast to her severe decline over the previous two years.

**Patient 2.** This is a follow-up description of the second patient described in a previous report [4]. A 59-year-old man began to note word-finding difficulties, followed by difficulties with arithmetic. These symptoms had been preceded by depression for seven years. He had been a type A personality with a high-powered position, whose neurological symptoms had begun after two years of the most stressful time of his career. His personality changed, and he became passive and timid. Neuropsychological testing showed profound impairment in semantic fluency, executive functioning, attention, overall mental status, processing, and visual memory. Fluorodeoxyglucose PET scan showed reduced metabolism in temporal and parietal lobes, left > right precuneus, and left frontal lobe. A diagnosis of Alzheimer's disease was made at a nationally recognized dementia clinic.

His BMI was 24.9, ApoE genotype 2/3, hs-CRP 0.5mg/l, albumin 4.5g/dl, globulin 2.4g/dl, albumin:globulin ratio 1.9, AM cortisol 15.8mcg/dl, total cholesterol 235mg/dl, HDL-cholesterol 70mg/dl, LDL-cholesterol 150mg/dl, triglycerides 75mg/dl, cholesterol:HDL ratio 3.4, DHEA-S 130mcg/dl, progesterone 0.4ng/ml, fasting insulin 6mIU/l, 25-hydroxycholecalciferol 44.5ng/ml, alpha-tocopherol 22.5mg/l, beta-gamma-tocopherol 0.5mg/l, TSH 2.98mIU/l, free T3 2.7ng/ml, free T4 1.2ng/dl, reverse T3 21ng/dl, pregnenolone <5ng/dl, homocysteine 7.3 $\mu$ mol/l, folate 16.6ng/ml, RBC Mg 5.5mg/dl, serum iron 135mcg/dl, serum copper 97mcg/dl, serum zinc 59mcg/dl, Cu:Zn ratio 1.6, blood arsenic/lead/mercury all <2mcg/l, TNF 1.2pg/ml, and IL-61.7pg/ml.

A sleep study showed mild obstructive sleep apnea, with an apnea/hypopnea index of 7 events per hour. No REM behavioral disturbance was noted.

Because of the presentation consistent with type 3 Alzheimer's disease, further history was obtained and

additional laboratory evaluation was undertaken. He had spent time in foreclosed homes that had suffered water damage. His HLA-DR/DQ (Table 1) was 12-3-52B, which is uncommon (less than 5% of the population) and strongly associated with hypersensitivity to biotoxins [5]. His TGF-β1 was elevated at 9040pg/ml, and C4a was elevated, as well. His nasal cavity was colonized by MARCoNS, an association of CIRS. Because his history and laboratory evaluation were suggestive of a diagnosis of CIRS, he was treated with the Shoemaker Protocol [5], and began to show subjective improvement in cognition after several weeks.

Comment: This patient was typical both in his presentation of type 3 Alzheimer’s disease and in his presentation of CIRS. His relatively rapid initial response to treatment with the Shoemaker Protocol supports the diagnosis of CIRS and the relationship between type 3 Alzheimer’s disease and CIRS.

**Patient 3.** A 72-year-old man who had been a high school mathematics state champion with an IQ of 164 began to have word-finding difficulty, as well as dyscalculia. There was no family history of dementia except in his mother, who in her 90s had undergone cognitive decline. Genetic analysis disclosed his ApoE genotype as 3/3. His neuropsychological testing was suggestive of subcortical dementia, and thus Alzheimer’s disease was initially felt to be unlikely.

However, his CSF showed reduced Aβ42 and increased p-tau, strongly suggestive of Alzheimer’s disease.

His homocysteine was 10.4μM, hs-CRP 0.2mg/l, albumin 4.6g/dl, albumin:globulin ratio 2.0, 25-hydroxycholecalciferol 32.5ng/ml, alpha-tocopherol 13.4mg/l, hemoglobin A1c 5.4%, fasting insulin 5.6mIU/l, total cholesterol 167mg/dl, HDL cholesterol 94mg/dl, LDL cholesterol 62mg/dl, triglycerides 56mg/dl, TSH 1.0mIU/l, free T4 1.29ng/dl, reverse T3 23.2ng/dl, AM cortisol 21.7ug/dl, pregnenolone 48ng/dl, and RBC magnesium 4.9mg/dl.

Because of his presentation suggestive of type 3 AD (his advanced age compared to other patients notwithstanding), he underwent HLA-DR/DQ testing, which revealed that he carried the uncommon, multiple biotoxin sensitivity haplotype 4-3-53. Urine testing was positive for mycotoxins.

Comment: This patient was atypical for type 3 Alzheimer’s disease in his late age of onset, but was in all other respects typical, including a cortical presentation with aphasia and dyscalculia, ApoE ε4-negative genotype, lack of family history (except in the tenth decade), neuropsychological testing suggesting an atypical presentation for Alzheimer’s, with CSF indicative of Alzheimer’s disease. His high reverse T3 and high AM cortisol are both suggestive of ongoing stress, and his HLA-DR/DQ is supportive of CIRS given the uncommon, multiple biotoxin-sensitive haplotype and the positive urine test formycotoxins.

**Table 1. HLA-DR/DQ haplotypes in patients with type 3 Alzheimer’s disease.**

Age at symptom onset (years)	Major symptoms	HLA-DR/DQ	Comment
50	Dyscalculia, executive	10-3-52B 10-5 (low MSH)	ApoE3/3
54	Executive, visual	11-3-52B ** 7-2-53 *	ApoE3/3
72	Executive, dyscalculia	4-3-53 ** 15-6-51 * (Lyme)	ApoE3/3
65	Spatial > verbal memory, attention, irritability, depression	11-3-52B ** 13-6-52B *	ApoE3/3
54	Executive, visuospatial, memory, depression	17-2-52A * 1-5 (low MSH)	ApoE4/4
59	Aphasia, executive, dyscalculia, depression	12-3-52B ** 15-6-51 * (Lyme)	ApoE2/3
59	Headache, executive	4-3-53 ** 15-6-51 * (Lyme)	ApoE ND
66	Headache, executive, memory	11-3-52B ** 13-6-52C *	ApoE ND

\*Pathogen-specific HLA-DR/DQ-related sensitivity (mold or Lyme).

\*\*Multiple-biotoxin-sensitive HLA-DR/DQ association.

**Patient 4.** A 54-year-old man developed depression after 70% of his company's employees were laid off. He was treated with an antidepressant, and three years later began to have difficulty understanding the difference between left-turn lanes, failing to appreciate the difference between the more acute left turn (far left lane) and the more gentle left turn (second lane from the left), leading to lane crosses and near accidents. He then developed executive, visuospatial, and memory deficits. He was unable to organize, unable to understand how to set the table, had difficulty with drawing and writing, and was unable to work. He was unable to pay bills, and had difficulty speaking multi-syllabic words.

He was evaluated at a university dementia center, where he was found to carry the ApoE4/4 genotype, his MMSE (mini-mental status exam) was 24, and a diagnosis of early onset Alzheimer's disease was made. He was treated with donepezil, to which he responded with improvement, and memantine was later added. He was also involved in a clinical trial in which he was given an antibody to amyloid-beta peptide, and his wife noted that each time he received the antibody, he declined markedly, with several days of severe confusion and non-communication, followed by a slow return to baseline. Over the ensuing two years he declined rapidly, and his MoCA (Montreal Cognitive Assessment) score at that time was 6/30.

His wife and he had lived in the same home for 19 years. She had suffered from asthma during part of that time. *Stachybotrys*, *Penicillium*, and *Aspergillus* were identified in the home by ERMI (environmental relative moldiness index) testing. His TGF- $\beta$ 1 was elevated at 3260pg/ml, and his HLA-DR/DQ was 17-2-52A, a mold-sensitive haplotype. His *Borrelia burgdorferi* Western blot was negative. His methylmercury was markedly elevated, twice the 95th percentile, and inorganic mercury was at the 90th percentile. His BMI was 22, fasting glucose 90mg/dl, hemoglobin A1c 5.5%, fasting insulin 2.2 mIU/l, homocysteine 15.1 < M, vitamin B12 333pg/ml, folate 9.8ng/ml, 25-hydroxycholecalciferol 45.9ng/ml, zinc 78mcg/dl, copper 73mcg/dl, free T3 2.1pg/ml, free T4 1.23ng/dl, reverse T3 19.7ng/dl, TSH 4.0uIU/ml, AM cortisol 17.7mcg/dl, total cholesterol 231mg/dl, LDL cholesterol 110mg/dl, HDL cholesterol 112mg/dl, and triglycerides 43mg/dl. Cyrex Arrays 2 (for gastrointestinal permeability), 3 (for gluten sensitivity), and 20 (for blood-brain barrier permeability) were negative.

Comment: This patient presented with typical type 3 Alzheimer's disease, with the single exception that his

ApoE genotype was not  $\epsilon$ 4-negative. In searching for potential toxic etiologies, both mycotoxins and mercury were identified as candidates. His mold-sensitive haplotype, 17-2-52A, along with elevated TGF- $\beta$ 1 and cognitive decline, coupled with definitive evidence of molds within the home, all support a diagnosis of CIRS.

**Patient 5.** A 50-year-old woman experienced depression following a hysterectomy, despite hormone-replacement therapy (although resulting hormone levels were not determined, so it is unknown whether optimal levels were achieved). Four years later she began to have word-finding difficulty, disorientation, difficulty driving, difficulty following recipes and other instructions, and increased depression following her son's leaving home. Her husband noted that she improved markedly following several days of rest, and declined markedly with sleep deprivation, viral illness, or stress. On neuropsychological evaluation, it was noted that she could not remember her own family history (which based on the recall of knowledgeable others was negative for dementia), that she exhibited paucity of speech, poor semantic fluency, confabulation on memory tests, and that she was anosmic. The diagnostic impression was of frontal, temporal, and parietal deficits. Her MRI was read as normal, but quantitative volumetrics were not performed. Her FDG-PET was abnormal, with reduced glucose utilization in the parietotemporal regions, and to a much lesser extent in the frontal region.

Her BMI was 18, ApoE genotype was 3/3, hs-CRP 0.2mg/l, homocysteine 8 $\mu$ M, fasting insulin 4.2uIU/ml, hemoglobin A1c 5.1%, free T3 2.1pg/ml, free T4 1.33ng/dl, reverse T3 23ng/dl, fT3:rT3 9, TSH 1.16uIU/ml, progesterone 0.3ng/ml, AM cortisol 7.2mcg/dl, pregnenolone 19ng/dl, 25-hydroxycholecalciferol 37ng/ml, vitamin B12 799pg/ml, alpha-tocopherol 12.5mg/l, zinc 82mcg/l, copper 99mcg/l, copper:zinc ratio 1.2, ceruloplasmin 20mg/dl, total cholesterol 221mg/dl, HDL cholesterol 67mg/dl, non-HDL cholesterol 167mg/dl, triglycerides 82mg/dl, urinary mercury:creatinine < 2.8, Lyme antibodies negative, C4a 5547ng/ml, and TGF- $\beta$ 1 7037pg/ml.

She was treated with donepezil, to which she responded well, and duloxetine, which reduced her depression. However, her cognitive function continued to decline.

Comment: This patient's presentation was typical for type 3 Alzheimer's disease in age of onset, preceding depression, ApoE non- $\epsilon$ 4 genotype, executive dysfunction, predominantly non-amnesic onset, negative family history, and strong response to stress

and sleep. Her failure to recall her own family history, demonstrating the loss of long-term storage or recall, rather than a restriction to recent memory, is also typical. Patients with type 3 Alzheimer's disease often have relatively low triglyceride levels (in the 40-70 range), and this patient's higher triglyceride level of 82 may have been associated with her hypothyroidism. Although the copper:zinc ratio is not as high as for most patients with type 3 Alzheimer's disease, the free copper (estimated by serum copper minus three times ceruloplasmin) is high. The high reverse T3 and low FT3:rT3 ratio of 9 (normal > 20) both suggest ongoing stress, and the low AM cortisol and low pregnenolone are compatible with HPA axis dysfunction. The low progesterone shows that her hormone-replacement therapy is suboptimal, a potential contributor to both type 3 Alzheimer's disease and CIRS. CIRS is suspected based on the high C4a; the negative Lyme antibody titer, along with lack of exposure to dinoflagellates and other water-borne CIRS-related agents, suggests that the most likely cause of CIRS in this patient is mycotoxins.

**Patient 6.** A 54-year-old woman began to have difficulty driving at night, followed by difficulty writing numbers, along with exhaustion. This was initially ascribed to menopause. She was unable to complete her work in a timely fashion, and had to check her work many times over because of a propensity to make mistakes, all of which was highly unusual for her. She had difficulty with organization and with visual recognition, including difficulty reading. She had to resign from work, and this led to severe stress.

There was no family history of dementia, and her ApoE genotype was 3/3. Her MoCA was 23, with 4/5 on memory (5/5 on a subsequent test) but missing all serial 7s except the first (which she missed on a subsequent test), and missing the clock numbers and hands, cube copying, as well as part of one of the repeated sentences. Her primary care provider made the diagnosis of MCI. A brain MRI showed mild atrophy, without hippocampal predilection, and a second MRI, two and one-half years later, showed slightly more severe generalized atrophy. A neurologist noted mild EEG abnormalities and therefore prescribed anticonvulsants, which had no noticeable effect on her condition.

Because of the presentation typical for type 3 Alzheimer's disease, further evaluation was undertaken, revealing that her HLA-DR/DQ haplotypes were 11-3-52B (uncommon, multiple-biotoxin sensitive) and 7-2-53 (mold sensitive). Her TGF- $\beta$ 1 was elevated at 5780pg/ml (normal 344-2382pg/ml). She failed a visual contrast sensitivity (VCS) test.

Comment: This patient's presentation was typical for type 3 Alzheimer's disease, and the combination of elevated TGF- $\beta$ 1 and HLA-DR/DQ multiple-biotoxin sensitive and mold-sensitive haplotypes, along with a failed VCS test, supports the diagnosis of CIRS.

**Patient 7.** A 64-year-old man began to complain of headache, leg cramps, irritability, distractibility, and difficulty with memory. Evaluation noted in addition a peripheral neuropathy and hyposmia. Neuropsychological assessment revealed a high-functioning individual with mild reductions in spatial > verbal memory. CT angiogram did not disclose a source for the headaches, and an MRI revealed generalized cerebral atrophy and areas of FLAIR (fluid-attenuated inversion recovery) hyperintensity. A diagnosis of amnesic mild cognitive impairment was made, and over the next seven years his headaches abated but cognitive decline progressed slowly, and he became frustrated, irritable, and occasionally depressed.

His fasting glucose was 101mg/dl, hemoglobin A1c 5.4%, fasting insulin 3mIU/l, homocysteine 10.6 $\mu$ M, vitamin B12 543pg/ml, hs-CRP 1.1mg/l, albumin:globulin ratio 1.8, free T3 2.8pg/ml, free T4 1.2pg/ml, TSH 1.19mIU/l, vitamin D 37ng/ml, total cholesterol 191mg/dl, HDL 92mg/dl, LDL 91mg/dl, triglycerides 45mg/dl, serum copper 97mcg/dl, serum zinc 57mcg/dl, copper:zinc ratio 1.7. His HLA-DR/DQ haplotypes were 11-3-52B, a multiple-biotoxin-sensitive haplotype, and 13-6-52B, a mold-sensitive haplotype. His TGF- $\beta$ 1 was markedly elevated at 20,657, and MMP9 was 684. Nasopharyngeal culture was positive for MARCoNS. Evaluation of his home revealed *Penicillium* and *Aspergillus*. His Cyrex Arrays 2, 3, 5, and 20 were all abnormal: Cyrex Array 2 revealed IgM anti-occludin/zonulin of 2.5 (0.1-2.1), indicative of gastrointestinal hyperpermeability; Cyrex Array 3 revealed a high level of IgA anti-omega gliadin; Cyrex Array 5 disclosed a high level of auto-antibodies to myelin basic protein and glutamic acid decarboxylase 65; and Cyrex Array 20 was compatible with hyperpermeability of the blood-brain barrier.

Comment: This patient was atypical for type 3 AD in that he presented with single domain, amnesic MCI. However, his other symptoms and laboratory values supported both a diagnosis of CIRS and a diagnosis of type 3 AD: his headache, depression, irritability, markedly elevated TGF- $\beta$ 1, HLA haplotypes characteristic of biotoxin sensitivity (11-3-52B) and mold sensitivity (13-6-52B), positive nasopharyngeal culture for MARCoNS, autoantibodies, and the presence of *Aspergillus* and *Penicillium* in his home, are all compatible with a diagnosis of CIRS. His

depression, difficulty focusing and keeping his train of thought, hypozincemia, hypotriglyceridemia, and general atrophy on MRI with areas of FLAIR hyperintensity, are all compatible with type 3 AD.

## DISCUSSION

These findings suggest that patients with presentations compatible with type 3 Alzheimer's disease should be evaluated for CIRS (as well as other toxic exposures, such as mercury and copper). These are treatable etiologic agents, and thus treatable causes of Alzheimer's disease. Furthermore, it may be particularly important to identify or exclude these toxins in patients with type 3 Alzheimer's disease since amyloid may be protective against toxins, especially metals, so reducing the amyloid burden without reducing the toxic exposure may potentially exacerbate the pathophysiology (and, indeed, may have done so in patient 4). Conversely, the exclusion of patients with type 3 Alzheimer's disease may potentially enhance the group efficacy of anti-amyloid therapies. While the patients described here are still too early in their courses to know the final therapeutic outcome, it is important to note that improvement in cognitive decline has been observed routinely in the treatment of CIRS with the Shoemaker Protocol.

It is noteworthy that a recent report described the direct detection of fungi in the brains of patients who had died with Alzheimer's disease, contrasting with a lack of detection of fungi in control brains [7]. This finding raises the possibility that the mycotoxic effects that occur in CIRS associated with type 3 Alzheimer's disease may be accompanied by active infection. However, unlike in the case of CIRS, there is as yet no indication that treating the putative fungal infection has any ameliorative effect on the cognitive decline (unless a specific diagnosis such as Cryptococcal meningitis is made).

The increasing number of reports of various pathogens identified in the brains of patients with Alzheimer's disease—from viruses such as *Herpes simplex* [8] to oral bacteria such as *P. gingivalis* [9] to fungi such as *C. glabratus* [7]—raises the possibility that what is referred to as Alzheimer's disease may actually be the result of a protective response to various brain perturbations. Indeed, the three different types of Alzheimer's disease that are distinguishable based on metabolic profiling fit well with the three known effects of amyloids such as A $\beta$ : A $\beta$  is produced in response to infection, and exhibits antimicrobial effects [10]; furthermore, A $\beta$  is a component of the inflammatory response, with NF $\kappa$ B inducing proteases involved in its formation. These inflammatory/antimicrobial effects

are prominent in type 1 AD, in which systemic inflammation is reflected in high hs-CRP levels, reduced albumin:globulin ratios, and increased cytokine levels. In contrast, A $\beta$  is also produced in response to the withdrawal of trophic support [11], and indeed APP processing to A $\beta$  peptides is influenced by factors involved in trophic support, such as estradiol and SirT1. This atrophic response is compatible with the metabolic profile in type 2 Alzheimer's disease, in which hormonal support is typically reduced and the biochemical mediators of systemic inflammation are not increased.

Thus amyloid may function as part of an inflammatory/antimicrobial response or as part of an atrophic response; however, the third major cause of amyloid production is as part of an anti-toxin response, especially as part of the response to the toxic accumulation of divalent metals such as mercury, copper, or iron [12]. The liberation of amyloid as part of a response to toxins forms the underpinning of type 3 Alzheimer's disease. Although some of these patients did indeed demonstrate laboratory values compatible with metal toxicity, the majority, including the seven described above, had instead, histories, exposures, genetics, laboratory values, visual contrast sensitivities, and at least initial, subjective therapeutic responses that were all compatible with a diagnosis of CIRS.

Interestingly, the pathophysiology of CIRS includes effects that are relevant to all three types of Alzheimer's disease: chronic inflammation is produced by the ongoing activation of the innate immune system, infection is at least theoretically possible due to the exposure to mold species and other aerosol-derived microbes, trophic support may be reduced due to pathogen-derived proteases, and, as noted above, multiple different mycotoxins may be included in the aerosols of water-damaged buildings. Therefore, it is perhaps not surprising that CIRS may be causally associated with Alzheimer's disease.

Since the majority of patients with CIRS have a combination of genetic sensitivity plus exposure to a complex aerosolic mixture of mycotoxins, spores, bacteria, microbial fragments, inflammagens, volatile organic compounds, and other molecular species, the majority of patients with type 3 Alzheimer's disease and CIRS are likely to have an inhalational cause of Alzheimer's disease (IAD). This recognition may be critical to optimizing therapeutic approaches to patients with this form of Alzheimer's disease.

It is noteworthy that patients with IAD did not in most cases exhibit extraneural symptoms of CIRS, such as

asthma, pruritus, rhinorrhea, chronic fatigue, epistaxis, dyspnea on exertion, hemoptysis, diarrhea, vomiting, loss of appetite, alopecia, chronic sinus infections, chronic bronchitis, arthralgias, or otitis. This raises the obvious question of how patients who exhibit the laboratory abnormalities, genetics, and exposures characteristic of CIRS might develop neural abnormalities yet, in large measure, escape the characteristic extraneural manifestations. There are several possible explanations: one possibility is that the autoimmune component of the response may be more significant in the typical CIRS patients than in the IAD patients, or that the overall innate system immune stimulation (ISIS) characteristic of CIRS may be more active in the typical CIRS patients. Another possibility is that the genetics may favor a chronic neurodegenerative syndrome over a more typical immune-mediated systemic illness. Evaluation of the HLA-DR/DQ haplotypes in eight patients with IAD may provide some support for this possibility: whereas about 95% of CIRS patients display one of the four multiple-biotxin-sensitive haplotypes (4-3-53, 11-3-52B, 12-3-52B, 14-5-52B) or one of the seven mold-sensitive haplotypes (7-2-53, 7-3-53, 13-6-52A, 13-6-52B, 13-6-52C, 17-2-52A, 18-4-52A), six of the eight IAD patients displayed both a multiple-biotxin-sensitive haplotype and a pathogen-sensitive (mold or Lyme) haplotype (of the other two, one was an ApoE4 homozygote and the other was an ApoE4 heterozygote with a mold-sensitive haplotype). Based on the frequencies of these haplotypes, the chance of picking eight people at random and having six of them display both one of the uncommon multiple-biotxin-sensitive haplotypes and one of the pathogen-sensitive haplotypes is less than one in one million. Finally, a third possibility is that the neurodegenerative phenotype may represent a late-stage effect, analogous to the tertiary lues syndromes, whereas the typical CIRS symptoms may be analogous to the primary and secondary syndromes. These three possibilities are not mutually exclusive.

As noted previously, type 3 Alzheimer's disease is readily distinguished from types 1 and 2 biochemically, genetically, and symptomatically [4]. Given previous descriptions of cortical presentations in Alzheimer's disease, as well as the current studies, it is possible that type 3 represents on the order of 10% of patients with Alzheimer's disease, thus potentially affecting hundreds of thousands of Americans. This percentage would be much higher for the subgroup of patients who are ApoE4-negative and whose symptoms begin prior to the age of 65. This potential epidemic may have gone unrecognized to date for several reasons: (1) because it has been hidden beneath the large umbrella of

Alzheimer's disease diagnoses grouped without respect to metabolic profiling-based type; (2) because CIRS is neither widely recognized nor typically considered in evaluations at neurological centers specializing in dementia; and (3) because standard evaluations for patients presenting with dementia or mild cognitive impairment do not include laboratory testing for the innate system immune stimulation (ISIS) that is characteristic of CIRS.

There are many cases of CIRS without dementia, and conversely, there are examples of type 3 Alzheimer's disease without CIRS. Nonetheless, the concordance of symptoms and laboratory values suggests an important and potentially extensive overlap. Given the relatively common presentation of AD with cortical symptoms, it is possible that CIRS may contribute to a significant minority of patients with AD. It is unlikely that the coexistence of type 3 Alzheimer's disease and CIRS described here is simply a coincidence: although both Alzheimer's disease and CIRS are relatively common illnesses, the finding that most patients with type 3 Alzheimer's disease also have laboratory abnormalities typical of CIRS, the repeated finding of biotoxin-sensitive HLA-DR/DQ haplotypes in type 3 Alzheimer's disease patients, the discovery of well-described neurotoxin-producing mold genera in the homes of these individuals, the initial response to treatment, and the similarity of the symptoms all argue that type 3 Alzheimer's disease is most commonly IAD, a phenotypic manifestation of CIRS.

It is not yet clear why IAD occurs in a subset of CIRS patients but not in all. It is possible that genotype plays a role, or that specific mycotoxins or inflammagens or other inciting agents may predispose to this phenotypic manifestation of CIRS, or that other contributing factors, such as metal toxicity or stress or HPA axis dysfunction, may increase risk for IAD with CIRS. It is also possible that a combination of these factors may be critical in the development of this syndrome.

Since the toxins associated with IAD are addressable therapeutically, it will be important to recognize and evaluate candidates appropriately. IAD should be suspected if more than two of the characteristics listed in Table 2 are present in a patient with Alzheimer's disease, mild cognitive impairment, or subjective cognitive impairment.

The appropriate recognition of IAD as a potentially important pathogenetic condition in patients with cognitive decline offers the opportunity for successful treatment of a large number of patients whose current prognoses, in the absence of accurate diagnosis, are

grave. Furthermore, the possibility that inhalational factors may contribute not only to the clinically distinct syndrome of IAD but also, partially, to typical type 1 or 2

Alzheimer's disease, or to other neurodegenerative diseases, should be considered in the evaluation of these patients.

**Table 2. Symptoms, signs, and laboratory values suggestive of type 3 Alzheimer's disease.**

Characteristic	Comment
Age at symptom onset less than 65 years.	Symptoms often begin in the 50s or late 40s.
ApoE ε4-negative genotype.	Typically ApoE3/3 unless there are other risk factors.
Negative family history or family history positive with symptom onset only in much older individuals than the patient.	
Symptom onset in association with menopause or andropause.	
Depression as a preceding or significant accompaniment of the cognitive decline.	
Headache as an early or preceding symptom.	
Atypical presentation, in which memory consolidation is not the initial and dominant characteristic.	Typical deficits include executive deficits, dyscalculia, paraphasias, or aphasia.
Precipitation or exacerbation by a period of great stress (e.g., loss of employment or marriage dissolution or family change) and sleep loss.	The degree of dysfunction is also markedly affected by stress and sleep loss.
Exposure to mycotoxins or metals (e.g., inorganic mercury via amalgams, or organic mercury via the consumption of large fish such as tuna) or both.	
Diagnosis of CIRS with cognitive decline.	Cognitive decline is common with CIRS.
Imaging suggestive of more than typical Alzheimer's involvement.	FDG-PET may show frontal as well as temporoparietal reductions in glucose utilization, even early in the course of the illness; MRI may show generalized cerebral and cerebellar atrophy, especially with mild FLAIR (fluid-attenuated inversion recovery) hyperintensity.
Low serum triglycerides or triglyceride:total cholesterol ratio.	Triglycerides are often in the 50s.
Low serum zinc (<75mcg/dl) or RBC zinc, or high copper:zinc ratio (>1.3).	
HPA axis dysfunction, with low pregnenolone, DHEA-S, and/or AM cortisol.	
High serum C4a, TGF-β1, or MMP9; or low serum MSH (melanocyte-stimulating hormone). Positive deep naso-pharyngeal culture for MARCoNS.	See reference 5.
HLA-DR/DQ associated with multiple biotoxin sensitivities or pathogen-specific sensitivity.	See reference 5.

## ACKNOWLEDGEMENTS

I am grateful to Dr. Mary Ackerley, Dr. Raj Patel, and Dr. Richard Podell, for their expertise, discussion, and evaluation and treatment of some of the patients described. I thank Dr. Rammohan Rao, Dr. Aida Lasheen Bredesen, and Dr. Alexei Kurakin for discussions, and Ms. Rowena Abulencia for preparing the manuscript.

## Funding

I am grateful for support from the NIH (AG16570, AG034427 and AG036975), the Mary S. Easton Center for Alzheimer's Disease Research at UCLA, the Douglas and Ellen Rosenberg Foundation, the Stephen D. Bechtel, Jr. Foundation, the Joseph Drown Foundation, the Alzheimer's Association, the Accelerate Fund, the Buck Institute and Marin Community Foundation, the Michael and Catherine Podell Fund, Mr. Craig Johnson, Mr. Allan Bortell, and Ms. Michaela Hoag.

## Conflict of interest statement

The author of this manuscript declares no conflict of interest.

## REFERENCES

1. James BD, Leurgans SE, Hebert LE, Scherr PA, Yaffe K and Bennett DA. Contribution of Alzheimer disease to mortality in the United States. *Neurology*. 2014;82:1045-1050.
2. Seshadri S, Drachman DA and Lippa CF. Apolipoprotein E epsilon 4 allele and the lifetime risk of Alzheimer's disease. What physicians know, and what they should know. *Arch Neurol*. 1995;52:1074-1079.
3. Bredesen DE. Reversal of cognitive decline: A novel therapeutic program. *Aging (Albany NY)*. 2014;6:1-11.
4. Bredesen DE. Metabolic profiling distinguishes three subtypes of Alzheimer's disease. *Aging (Albany NY)*. 2015;7:595-600.
5. Shoemaker RT, MD. 2010. *Surviving mold: life in the era of dangerous buildings*. (Baltimore, MD: Otter Bay Books).
6. Shoemaker RC and House DE. Sick building syndrome (SBS) and exposure to water-damaged buildings: time series study, clinical trial and mechanisms. *Neurotoxicol Teratol*. 2006;28:573-588.
7. Pisa D, Alonso R, Rabano A, Rodal I and Carrasco L. Different Brain Regions are Infected with Fungi in Alzheimer's Disease. *Scientific reports*. 2015;5:15015.
8. Harris SA and Harris EA. Herpes Simplex Virus Type 1 and Other Pathogens are Key Causative Factors in Sporadic Alzheimer's Disease. *J Alzheimers Dis*. 2015;48:319-353.
9. Poole S, Singhrao SK, Kesavalu L, Curtis MA and Crean S. Determining the presence of periodontopathic virulence factors in short-term postmortem Alzheimer's disease brain tissue. *J Alzheimers Dis*. 2013;36:665-677.
10. Soscia SJ, Kirby JE, Washicosky KJ, Tucker SM, Ingelsson M, Hyman B, Burton MA, Goldstein LE, Duong S, Tanzi RE and Moir RD. The Alzheimer's disease-associated amyloid beta-protein is an antimicrobial peptide. *PLoS One*. 2010;5:e9505.
11. Matrone C, Ciotti MT, Mercanti D, Marolda R and Calissano P. NGF and BDNF signaling control amyloidogenic route and Abeta production in hippocampal neurons. *Proc Natl Acad Sci U S A*. 2008;105:13139-13144.
12. Singh I, Sagare AP, Coma M, Perlmutter D, Gelein R, Bell RD, Deane RJ, Zhong E, Parisi M, Ciszewski J, Kasper RT and Deane R. Low levels of copper disrupt brain amyloid-beta homeostasis by altering its production and clearance. *Proc Natl Acad Sci U S A*. 2013;110:14771-14776.

# Epigenetic age of the pre-frontal cortex is associated with neuritic plaques, amyloid load, and Alzheimer's disease related cognitive functioning

Morgan E. Levine<sup>1,2</sup>, Ake T. Lu<sup>1</sup>, David A. Bennett<sup>3,4</sup>, and Steve Horvath<sup>1,5</sup>

<sup>1</sup>Human Genetics, David Geffen School of Medicine, University of California Los Angeles, Los Angeles, CA 90095, USA;

<sup>2</sup>Center for Neurobehavioral Genetics, University of California Los Angeles, Los Angeles, CA 90095, USA;

<sup>3</sup>Rush Alzheimer's Disease Center, Rush University Medical Center, Chicago, IL 60612, USA;

<sup>4</sup>Department of Neurological Sciences, Rush University Medical Center, Chicago, IL 60612, USA;

<sup>5</sup>Biostatistics, School of Public Health, University of California Los Angeles, Los Angeles, CA 90095, USA.

**Key words:** epigenetics; neuritic plaques; amyloids; cognitive functioning; memory; Alzheimer's disease, epigenetic clock; DNA methylation

**Received:** 11/08/15; **Accepted:** 11/30/15; **Published:** 12/18/15 **doi:** [10.18632/aging.100864](https://doi.org/10.18632/aging.100864)

**Correspondence to:** Steve Horvath, PhD; **E-mail:** [shorvath@mednet.ucla.edu](mailto:shorvath@mednet.ucla.edu)

**Copyright:** Levine et al. This is an open-access article distributed under the terms of the Creative Commons Attribution License, which permits unrestricted use, distribution, and reproduction in any medium, provided the original author and source are credited

**Abstract:** There is an urgent need to develop molecular biomarkers of brain age in order to advance our understanding of age related neurodegeneration. Recently, we developed a highly accurate epigenetic biomarker of tissue age (known as epigenetic clock) which is based on DNA methylation levels. Here we use n=700 dorsolateral prefrontal cortex (DLPFC) samples from Caucasian subjects of the Religious Order Study and the Rush Memory and Aging Project to examine the association between epigenetic age and Alzheimer's disease (AD) related cognitive decline, and AD related neuropathological markers.

Epigenetic age acceleration of DLPFC is correlated with several neuropathological measurements including diffuse plaques ( $r=0.12$ ,  $p=0.0015$ ), neuritic plaques ( $r=0.11$ ,  $p=0.0036$ ), and amyloid load ( $r=0.091$ ,  $p=0.016$ ). Further, it is associated with a decline in global cognitive functioning ( $\beta=-0.500$ ,  $p=0.009$ ), episodic memory ( $\beta=-0.411$ ,  $p=0.009$ ) and working memory ( $\beta=-0.405$ ,  $p=0.011$ ) among individuals with AD. The neuropathological markers may mediate the association between epigenetic age and cognitive decline. Genetic complex trait analysis (GCTA) revealed that epigenetic age acceleration is heritable ( $h^2=0.41$ ) and has significant genetic correlations with diffuse plaques ( $r=0.24$ ,  $p=0.010$ ) and possibly working memory ( $r=-0.35$ ,  $p=0.065$ ). Overall, these results suggest that the epigenetic clock may lend itself as a molecular biomarker of brain age.

## INTRODUCTION

Cognitive aging is on a continuum from normality, to mild cognitive impairment (MCI), to dementia [1-3]. Aging is also tied to an increasing susceptibility for a number of neurodegenerative diseases. After the age of 65 the risk of developing a neurodegenerative form of dementia, such as Alzheimer's Disease (AD), has been

shown to double every five years, and by age 85, the prevalence of dementia is estimated to be as high as 31% [4].

AD dementia is an irreversible progressive neurodegenerative disease affecting the central nervous system. It is typically characterized by the presence of amyloid-beta plaques and hyperphosphorylated paired

helical filament tau protein-rich neurofibrillary tangles (NFT) [5]. Both types of lesions have been linked to AD dementia, MCI, and cognitive decline. There is also evidence that NFT mediates the association between amyloid plaques and clinical manifestations of AD [6]. While the exact physiology through which NFT and amyloid-beta plaques influence AD pathogenesis remains somewhat unclear, the presence of such deposits among those afflicted with AD is typically associated with much steeper trajectories of cognitive deficit accumulation with age [7, 8]. Cognition is not a unitary process but is composed of several dissociable cognitive systems, such as episodic memory the clinical hallmark of AD dementia.

Epigenetic alterations, such as DNA methylation (DNAm), have been linked to the both AD pathology [9] and cognitive aging in the absence of AD dementia [10]. DNAm refers to the addition of a methyl group to a cytosine nucleotide at cytosine-phosphate-guanine (CpG) sites. Hyper- or hypo methylation of sites can change over time, as a function of genes and environment, and have implications for gene expression via alterations in chromatin structure. We recently developed a highly accurate molecular biomarker of aging based on DNA methylation (DNAm) levels [11], known as “epigenetic clock”, which can be used to measure the age of human cells, tissues, and organs. Given that aging is associated with a normal loss in cognitive ability as well as the rapidly increasing susceptibility to AD, an aging biomarker based on DNAm could account for between-person differences in either the rate of cognitive aging among non-demented individuals or the rate of disease progression among those with AD. As a result, the goals of our study were to 1) examine the association between DNAm age and AD neuropathology, 2) test whether DNAm age relates to AD dementia status and measures of cognitive functioning, 3) determine if differences in DNAm age reflect cognitive decline in persons with or without AD-dementia, 4) examine whether neuropathology underlies the association between higher DNAm age and worse cognitive functioning. We hypothesize that participants who have higher levels of neuropathology, lower cognitive functioning, and/or who are diagnosed with AD will have higher DNAm age in PFC samples at death—signifying that their brains are biologically older. We also hypothesize that neuropathology will mediate the association between DNAm age and cognition.

## RESULTS

### Study Sample

Our analytic sample included Caucasian subjects from the Religious Order Study (ROS) and the Rush Memory

and Aging Project (MAP) [12, 13]. Both are longitudinal community based cohort studies of aging and dementia. The majority of participants in both studies are 75-80 years old at baseline with no known dementia. All participants agree to organ donation at death. Participants sign and informed consent, repository consent, and Anatomical Gift Act. The studies were approved by the Institutional Review Board of Rush University Medical Center. Inclusion in the studies requires participants to consent to undergoing annual clinical evaluations as well as postmortem organ donation. The ROS sample includes Catholic priests, nuns, and brothers from across the United States, whereas the MAP sample includes a more general community based population from northeastern Illinois. For our analysis, we excluded subjects with missing DNAm age, or who were diagnosed with dementias other than AD leaving us with 700 Caucasian subjects. Participants were administered annual structured interviews and a battery of cognitive tests such as episodic memory (EM), working memory (WM), and semantic memory (SM), perceptual orientation (PO), and perceptual speed (PS). Tests were averaged to yield a measure of global cognitive functioning (GCF). Neuropathological assessments were carried out postmortem as described in Methods.

### Sample characteristics

As shown in Table 1, upon enrollment into the two studies, subjects were 63-102 years of age (mean=81.36, standard deviation=6.59). Cognitive follow-up time after baseline ranged from 0 to 16 years, with a mean of 4.07 years (s.d.=3.42). Of 700 participants, 615 had at least three measures of cognitive functioning (baseline plus two follow-up), while half of our participants had seven or more cognitive measures. Average lifespan was approximately 89 years (s.d.=6.44). Overall, subjects from ROS (n=375) were 5 years younger at baseline and lived 1.5 years longer compared to those from MAP (n=325). Nearly two-thirds of participants (63.6%) were female.

Just over 300 of our 700 participants were diagnosed with AD dementia. Mean GCF, EM, WM, SM, PO, and PS were -0.33 (s.d.=0.90), -0.28 (s.d.=1.08), -0.23 (s.d.=0.90), -0.31 (s.d.=0.99), -0.34 (s.d.=0.92), and -0.53 (s.d.=1.06), respectively. Additionally, between- and within-person standard deviations were 0.82 and 0.47 for GCF, respectively; 1.00 and 0.55 for EM, respectively; 0.77 and 0.53 for WM, respectively; 0.91 and 0.53 for SM, respectively; 0.83 and 0.52 for PO, respectively; and 0.95 and 0.59 for PS, respectively. Finally, mean overall amyloid level was 3.47

(s.d.=3.68), mean neuritic plaque average 0.80 (s.d.=0.84), mean diffuse plaque average 0.71 (s.d.=0.80), mean NFT (silverstain) average 0.60 (s.d.=0.77), and mean overall paired helical filament (PHF) tangle score 6.52 (s.d.=8.16).

### Epigenetic age relates to neuropathological variables

We estimated the epigenetic age (also known as DNAm age) of each brain samples by averaging the DNAm levels of 353 CpGs as described in Methods and [11].

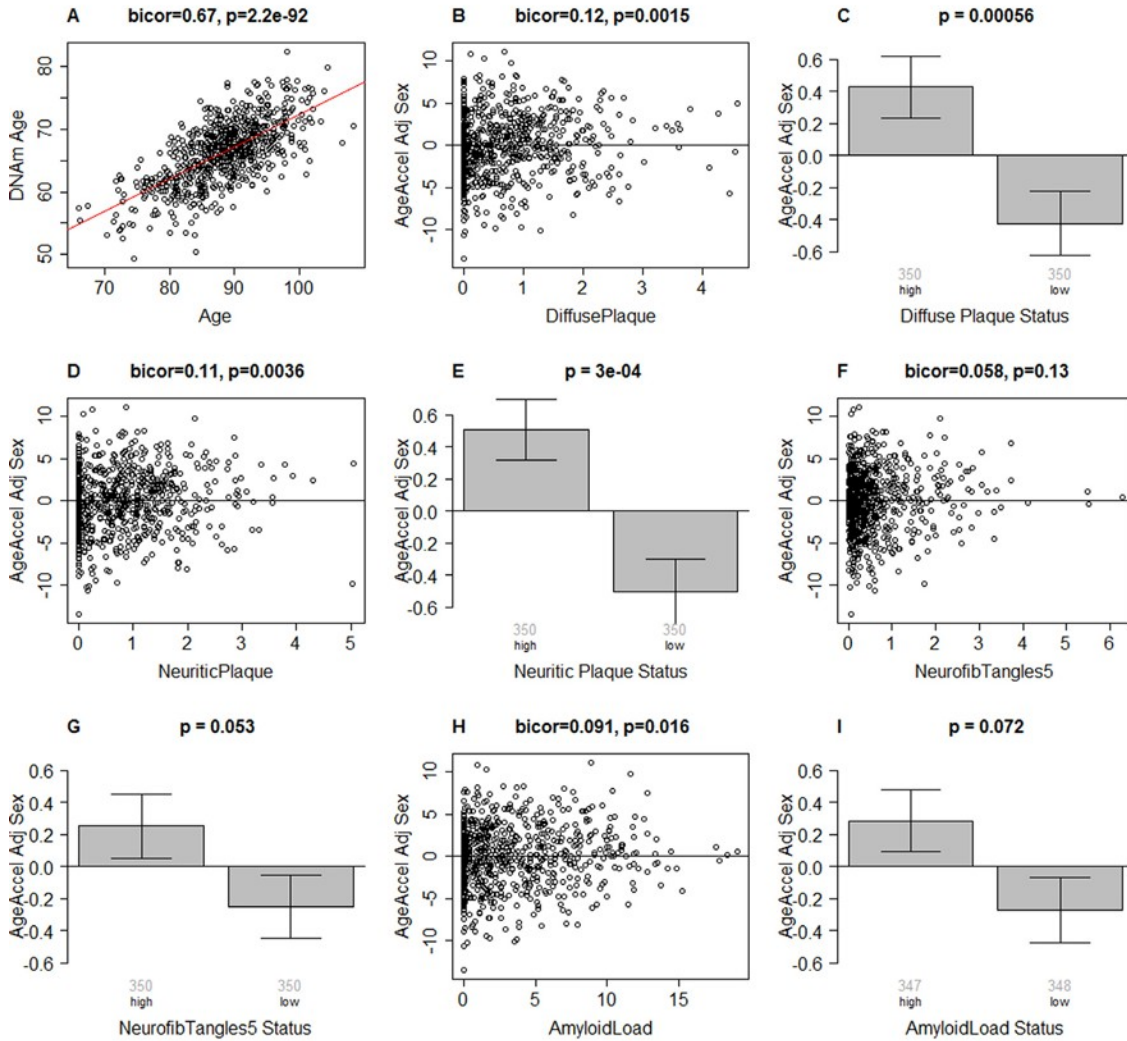


**Figure 1. Epigenetic age of DLPFC samples versus neuropathological measures.** (A) Scatter plot relating the DNAm age of each PFC sample (y-axis) versus chronological age at time of death (x-axis). The red line depicts a linear regression line. The y-axis of the remaining panels (B-I) involves the measure of epigenetic age acceleration which has been adjusted for sex. The scatter plots relate epigenetic age acceleration (y-axis) to (B) diffuse plaques, (D) neuritic plaques, (F) NFTs, and (H) amyloid load. The title of each scatter plot reports a robust correlation coefficient (biweight midcorrelation) and a corresponding p-value. (C,E,G,I) The x-axis of the bar plots involve a binary grouping variable that results from using the median value for dichotomizing (C) diffuse plaques, (E) neuritic plaques, (G) NFT, and (I) beta-amyloid load, respectively. Each bar plot depicts the mean value, one standard error, and reports the p-value results from a non-parametric group comparison test (Kruskal Wallis test). The title of each scatter plot reports a robust correlation coefficient (biweight midcorrelation) and a corresponding p-value.

**Table 1. Sample characteristics**

Variable	Statistic
Age at Enrollment, Mean (Std. Dev.)	81.4 (6.95)
Age at Death, Mean (Std. Dev.)	88.1 (6.60)
DNAm Age, Mean (Std. Dev.)	66.2 (5.04)
GCF, Mean (Std. Dev.)	-0.33 (0.90)
EM, Mean (Std. Dev.)	-0.28 (1.08)
WM, Mean (Std. Dev.)	-0.23 (0.90)
SM, Mean (Std. Dev.)	-0.31 (0.99)
PO, Mean (Std. Dev.)	-0.34 (0.92)
PS, Mean (Std. Dev.)	-0.53 (1.06)
Amyloid Load, Mean (Std. Dev.)	3.47 (3.68)
NP, Mean (Std. Dev.)	0.80 (0.84)
DP, Mean (Std. Dev.)	0.71 (0.80)
NFT, Mean (Std. Dev.)	0.60 (0.77)
Tangle Score, Mean (Std. Dev.)	6.52 (8.16)
Sex (Female=1), Frequency	0.636
Study (ROS=1), Frequency	0.536
AD Status, Frequency	0.433

DNAm age (in units of years) estimates the number of years that passed since birth. DNAm age was highly correlated with chronological age at time of death across all samples (correlation  $r=0.67$ , Figure 1A). We defined a measure of epigenetic age acceleration as residual resulting from regressing DNAm age on chronological age and sex. Thus, a positive value of age acceleration indicates that the epigenetic age is higher than expected based on chronological age and sex. Our study addresses the hypothesis that epigenetic age acceleration (that measures deviations between DNAm age and chronological age) captures aspects of the biological age of brain tissue. We test this hypothesis by relating epigenetic age acceleration to various measures of neuropathology and cognitive functioning.

Results from biweight midcorrelation showed that epigenetic age acceleration is associated with several postmortem neuropathological indices. Epigenetic age acceleration had a correlation of 0.12 with diffuse plaques ( $p=0.0015$ , Figure 1B,C), 0.11 with neuritic plaques ( $p=0.0036$ , Figure 1D,E), and 0.019 with amyloid load ( $p=0.016$ , Figure 1H,I). Further, it showed a marginally significant association with neurofibrillary tangle status ( $p=0.053$  in Figure 1G) when the latter was defined by dichotomizing the NFT variable by its median value. These associations were also examined using multivariate models (Table 2), adjusting for age at death, sex, and study (ROS vs MAP), and again, we found positive associations between DNAm age and neuritic plaques ( $\beta=0.45$ ,  $p=0.004$ ), diffuse plaques

( $\beta=0.47$ ,  $p=0.004$ ), amyloid load ( $\beta=0.10$ ,  $p=0.006$ ), NFT ( $\beta=0.38$ ,  $p=0.021$ ), and Tangle Score ( $\beta=0.03$ ,  $p=0.041$ ).

### DNAm age, cognitive functioning and AD status

As shown in Table 3, we used linear models, adjusting standard errors to account for multiple observations, to examine whether postmortem estimates of DNAm age were associated with GCF, EM, WM, SM, PO, PS, and/or AD status. We found associations between DNAm age and both GCF and EM, the clinical hallmark

of AD. For instance, results showed that a one unit decrease in GCF was associated with about a one third of a year increase in DNAm age ( $\beta = -0.34$ ,  $P = 0.019$ ), while a one unit decrease in EM was also associated with about a one third of a year increase in DNAm age ( $\beta = -0.30$ ,  $P = 0.009$ ). By contrast, we did not find a relationship between DNAm age and WM ( $\beta = -0.16$ ,  $P = 0.172$ ), SM ( $\beta = -0.21$ ,  $P = 0.072$ ), PO ( $\beta = -0.10$ ,  $P = 0.270$ ), or PS ( $\beta = -0.13$ ,  $P = 0.191$ ). We also examined whether AD dementia status was associated with higher DNAm age. Results showed a moderate, but non-significant association ( $\beta = 0.38$ ,  $P = 0.103$ ).

**Table 2. Multivariate associations between DNAm age and neuropathological measures**

Beta Coefficient (One-Tailed P-Value)	
Amyloid Load	0.100 (0.006)
NP	0.451 (0.004)
DP	0.468 (0.004)
NFT	0.377 (0.021)
Tangle Score	0.030 (0.041)
Results are from independent multivariate models that adjust for age at death, study, and sex	

**Table 3. Associations between DNAm age and cognitive functioning, and mediation by AD status**

	$\beta$ (SE)	P-value
GCF	-0.340 (0.163)	0.019
EM	-0.297 (0.126)	0.009
WM	-0.160 (0.170)	0.172
SM	-0.205 (0.140)	0.072
PO	-0.102 (0.166)	0.270
PS	-0.134 (0.153)	0.191
AD Status	0.377 (0.298)	0.103

DNAm age was used as the dependent variable for all models. All models were run adjusting for study (ROS or MAP), age at death, age a clinical evaluation (accept for the model for AD), and sex. GCF=Global Cognitive Functioning, EM=Episodic Memory, WM=Working Memory, SM=Semantic Memory, PO=Perceptual Orientation, PS=Processing Speed. P-values represent significance assuming a one-tailed hypothesis test. Standard errors were adjusted via clustering by Sample ID, in order to account for multiple observations (except for the model for AD).

**Table 4. Associations between DNAm age and cognitive functioning, by AD status**

	Non-Demented Participants (n=397)		AD Participants (n=303)	
	$\beta$ (SE)	P-value	$\beta$ (SE)	P-value
GCF	-0.059 (0.503)	0.454	-0.500 (0.210)	0.009
EM	-0.209 (0.322)	0.258	-0.411 (0.173)	0.009
WM	0.340 (0.328)	0.836	-0.405 (0.177)	0.011
SM	-0.047 (0.429)	0.456	-0.262 (0.160)	0.051
PO	-0.049 (0.312)	0.437	-0.102 (0.210)	0.313
PS	-0.058 (0.304)	0.425	-0.178 (0.205)	0.193

DNAm age was used as the dependent variable for all models. All models were run adjusting for study (ROS or MAP), age at death, age at clinical evaluation, and sex. GCF=Global Cognitive Functioning, EM=Episodic Memory, WM=Working Memory. P-values represent significance assuming a one-tailed hypothesis test. Standard errors were adjusted via clustering by Sample ID, in order to account for multiple observations.

Using linear models, we then examined the association between DNAm age and cognitive functioning by AD dementia status (Table 4). Overall, we found no association between DNAm age and any of the cognitive functioning measures among participants without AD dementia which might reflect the relatively low variance of cognitive measures among controls. However, among participants with AD dementia, GCF, EM, and WM were all associated with DNAm age. Results showed that for persons who developed AD dementia, every one unit decrease in GCF was associated with a half a year increase in DNAm ( $\beta = -0.50$ ,  $P = 0.009$ ). Similarly, for persons who developed AD dementia, every one unit decrease in EM or WM was associated with about a 0.4 year increase in DNAm (EM:  $\beta = -0.41$ ,  $P = 0.009$ ; WM:  $\beta = -0.40$ ,  $P = 0.011$ ).

**Mediation analysis involving neuropathological variables and cognitive scores**

Using multivariate linear models, with DNAm age as the dependent variable and adjusting for study (ROS vs MAP), age at clinical assessment, age at death, and sex, we examined whether neuropathological measures accounted for the association between worse cognitive functioning (GCF, EM) and higher DNAm age (Table 5 and Table 6). All models were run on n=695 participants

who had complete neuropathology data. Standard errors were adjusted to account for repeat cognitive measures. For each cognitive measure, seven models were run. The first model shows the association between the cognitive measure and DNAm age, after adjusting for covariates. We find that (as reported previously), GCF and EM were inversely associated with DNAm age (GCF:  $\beta=-0.336$ ,  $P=0.020$ ; EM:  $\beta=-0.286$ ,  $P=0.012$ ). Model 2, is similar to model 1, but includes the addition of amyloid load, to examine whether it alters the association between cognitive functioning and DNAm age. We find that amyloid load is significantly associated with DNAm age. Furthermore, it accounts for 31.8% and 30.8% of the association between DNAm age and GCF and EM, respectively. Model 3, is similar to model 1, but with the addition of neuritic plaques. We find that NP is significantly associated with DNAm age and accounts for 66.1% of the association between DNAm age and GCF, as well as 65.0% of the association between DNAm age and EM. Model 4, includes the addition of diffuse plaques, which is significantly associated with DNAm age. However, diffuse plaques only account for 15.5% of the association between DNAm age and GCF, and 17.8% of the association between DNAm age and EM. Model 5, includes the addition of neurofibrillary tangles, which is not significantly associated with DNAm age, yet NFT

accounts for 25.9% of the association between DNAm age and GCF, and 23.4% of the association between DNAm age and EM. Model 6, includes the addition of overall tangle score, which, like NFT, is not significantly associated with DNAm age, yet it account for a significant proportion of the association between DNAm age and GCF (24.4%), as well as DNAm age and EM (19.9%). Finally, Model 7 is similar to model 1, but with the addition of all five neuropathology variables. We find that the inclusion of all these measures accounts for 52.4% of the association between DNAm age and GCF, and 51.4% of the association between DNAm age and EM.

### Heritability and genetic correlation analysis

We estimated the heritability of epigenetic age accelera-

tion using the GCTA software [14, 15] from SNP markers measured on the same subjects. We find that epigenetic age acceleration in DLPFC is highly heritable ( $h^2=0.41$ , Table 7), which is similar to heritability estimate reported for blood [11, 16].

We find that diffuse plaques are highly heritable ( $h^2=0.38$ , Table 7) and have a significant genetic correlation with epigenetic age acceleration ( $r=0.24$ ,  $p=0.010$ , Table 7). Neuritic plaques also exhibit a significant genetic correlation with epigenetic age acceleration ( $r=0.78$ ,  $p=0.014$ ) but the result needs to be interpreted with caution since neuritic plaques are at best weakly heritable ( $h^2=0.05$ ). We also find a suggestive genetic correlation with working memory at the last assessment ( $r=-0.35$ ,  $p=0.065$ ) but working memory is only weakly heritable ( $h^2=0.07$ ).

**Table 5. Neuropathological mediation of the association between GCF and DNAm age**

	Beta Coefficient (One-Tailed P-Value)						
	Model1	Model2	Model3	Model4	Model5	Model6	Model7
GCF	-0.336 (0.020)	-0.229 (0.087)	-0.114 (0.256)	-0.284 (0.044)	-0.249 (0.088)	-0.254 (0.084)	-0.160 (0.193)
Amyloid		0.094 (0.015)					0.026 (0.305)
Neuritic Plaques			0.553 (0.004)				0.514 (0.025)
Diffuse Plaques				0.360 (0.044)			0.144 (0.268)
NFT					0.231 (0.139)		-0.028 (0.537)
Tangles						0.019 (0.165)	-0.016 (0.720)

**Table 6. Neuropathological mediation of the association between EM and DNAm age**

	Beta Coefficient (One-Tailed P-Value)						
	Model 1	Model 2	Model 3	Model 4	Model 5	Model 6	Model 7
EM	-0.286 (0.012)	-0.198 (0.064)	-0.100 (0.229)	-0.235 (0.032)	-0.219 (0.057)	-0.229 (0.048)	-0.139 (0.161)
Amyloid		0.094 (0.015)					0.028 (0.287)
Neuritic Plaques			0.538 (0.005)				0.487 (0.033)
Diffuse Plaques				0.368 (0.044)			0.165 (0.243)
NFT					0.210 (0.164)		-0.032 (0.540)
Tangles						0.016 (0.202)	-0.017 (0.725)

## DISCUSSION

Overall, we found that postmortem DNAm age in DLPFC was associated with neuropathological variables (Figure 1 and Table 2) and with pre-mortem measures of cognitive decline, after adjusting for chronological age, sex, and other possible confounders (Tables 3 and 4). Our mediation analysis (Tables 5-6) suggests that a proportion (up to 66%) of the association between DNAm age and measures of cognitive function is mediated by neuropathological measures. Our genetic analysis (Table 7) indicates that pleiotropic genetic loci affect epigenetic age acceleration, neuropathological variables, and cognitive traits.

The association between cognitive function and DNAm age is consistent with previous work showing that general cognitive ability—defined as a composite score for six cognitive function tests comprising working memory, non-verbal reasoning, constructional ability,

and processing speed—was associated with DNAm age in pre-mortem blood samples [17]. However, previous work has not examined the role of neuropathology or AD dementia in the association between DNAm age and cognitive decline. Our study showed that about half of the association between DNAm age and cognition was accounted for by variations in neuropathological variables. For instance, we found that worse GCF and EM was associated with higher DNAm age; however, this association was significantly reduced or eliminated after adjusting for amyloid load or neuritic plaques.

Previous studies have shown that there is little or no age effect on many cognitive domains after accounting for common neuropathologies [18]. The extended preclinical phase of dementia is typically characterized by an accumulation of neuropathology underlying cognitive decline, and as such, pathologies have been shown to relate to decline across the entire continuum, from normal, to MCI, to dementia [19, 20].

**Table 7. Heritability analysis and genetic correlations**

<b>Trait (residuals)</b>	<b>Heritability</b>		<b>Genetic correlation with epigenetic age acceleration</b>	
	<b>Estimate</b>	<b>P</b>	<b>Estimate</b>	<b>P</b>
DNAm age	0.41	0.19	--	--
Mean GCF	<0.01	0.50	--	--
Mean WM	0.17	0.32	-0.19	0.12
Mean EM	< 0.01	0.50	--	--
Last GCF	< 0.01	0.50	--	--
Last WM	0.07	0.43	-0.35	0.065
Last EM	< 0.01	0.50	--	--
Amyloid	0.03	0.46	--	--
Neuritic plaque	0.05	0.43	0.78	0.014
Diffuse plaque	0.38	0.080	0.24	0.010
NFT	< 0.01	0.50	--	--
Tangles	< 0.01	0.50	--	--

The GCTA software was used to estimate the heritability (first two columns) and the genetic correlations with epigenetic age acceleration (last two columns).

Nevertheless, declines in cognitive functioning have been shown to be significantly steeper among those with AD [21-24]. In contrast to those with non-pathological cognitive aging, the more drastic cognitive decline associated with AD is thought to reflect AD-mediated neuronal injury, larger decreases in brain volume, functional disconnection between PFC and the hippocampus, and dramatic increases in ventricle size [3, 25].

While our results showed that DNAm age was associated with cognitive decline among persons with a clinical diagnosis of AD, we did not find an association between AD dementia status and DNAm age. One poten-

tial explanation for the lack of association between AD dementia status and DNAm age is that the clinical diagnosis AD is only an incomplete measure of the underlying neuropathology such as the accumulation of amyloid-beta plaques and NFT. For this reason, AD reflects a heterogeneous group, which is why the severity of AD (as estimated by cognitive decline or neuropathology) may be more strongly associated with DNAm age than AD dementia status alone. Among our participants, we found that both the between-person and within-person variance in GCF and EM change was much higher for those with AD versus those without AD dementia (Table 8), suggesting that 1) the AD group may be far more heterogeneous in regards to

neurocognitive decline, and 2) experience far more cognitive aging changes. Additionally, this interpretation is supported by our analysis of neuropathological variables, for which we found strong associations between DNAm age and all five measures (amyloid load, neuritic plaques, diffuse plaques, NFT, and overall tangle score). Additionally, results from step-wise models showed that neuropathological variables, especially amyloid load and neuritic plaques, may explain the association between DNAm age and cognitive functioning. This suggests that increased DNAm age may influence changes in the regulation of amyloid proteins, contributing to AD neuropathology, and thus manifesting as steeper cognitive declines [26].

Finally, our genetic analysis showed that DNAm age, neuropathology, and cognitive decline may be pleiotropic, which could reflect mediation among these factors. For instance, alleles could be associated with faster cognitive decline via acceleration of the biological aging process, which in turn leads to a faster accumulation of neuropathology (Figure 2A). Another alternative is that physiological consequences associated with neuropathological accumulation could influence both biological brain aging and cognitive decline, simultaneously (Figure 2B). Finally, loci could pleiotropically influence both neuropathology and biological aging, independently, with no causal pathway between them (Figure 2C). In moving forward, examina-

**Table 8. Between- and within-person statistics for cognitive function, by AD**

		No AD			AD		
		Mean	Std. Dev.	N	Mean	Std. Dev.	N
GCF	Overall	0.126	0.496	2554	-0.894	0.954	2105
	Between		0.448	397		0.786	300
	Within		0.235			0.649	
EM	Overall	0.252	0.649	2482	-0.928	1.139	2029
	Between		0.607	397		0.951	300
	Within		0.323			0.731	

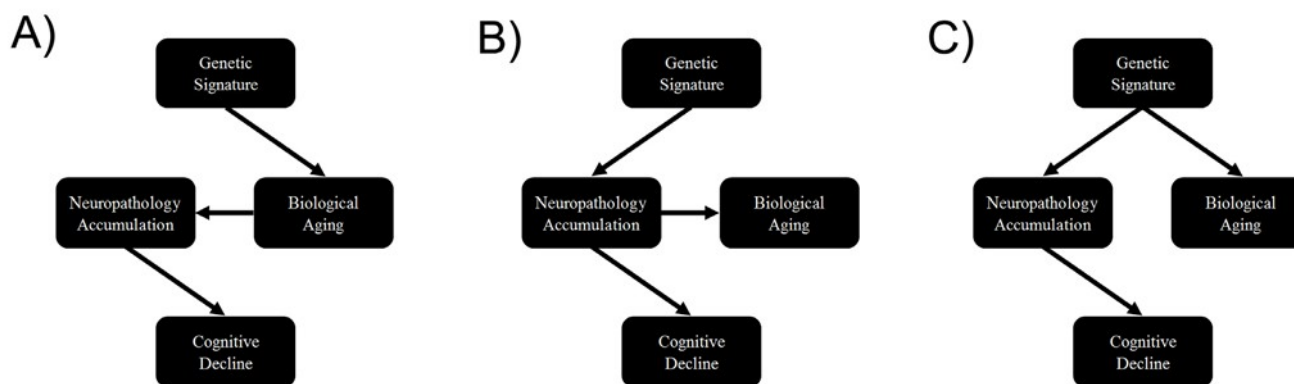


**Figure 2. Causal scenarios that might explain the significant genetic correlations between epigenetic age, neuropathology and cognitive decline.** Genetic variants form a causal anchor that affect biological age (and associated measures such as epigenetic age) and various measures of neuropathology and cognitive decline.

tion of these pathways will be important for facilitating our understanding of brain aging and neurodegenerative disease.

There are limitations to this study. First, DNAm age was only measured postmortem, which prevented us from determining if it was predictive of AD status or cognitive decline. Furthermore, DNAm age changes with time, yet in our sample it was only measured at a single time-point. For that reason we were unable to examine if larger changes in DLPFC DNAm age were associated with steeper cognitive decline or AD. Nevertheless, our study was strengthened by the inclusion of neuropathological variables, longitudinal measurements of multiple cognitive functioning domains, measurement of DNAm age in DLPFC rather than whole blood, and availability of postmortem data for neuropathologic indices.

Overall, our study shows that epigenetic aging in DLPFC is associated with the severity of cognitive decline as well as neuropathological hallmarks of AD. These results strongly suggests that the epigenetic clock lend itself as a molecular biomarker of brain age.

## METHODS

Study sample. Our analytic sample included 700 non-Latino white subjects from the Religious Order Study (ROS) and the Rush Memory and Aging Project (MAP) [12, 13]. Both are longitudinal community based cohort studies of aging and dementia. The majority of participants in both studies are 75-80 years old at baseline with no known dementia. Inclusion in the studies requires participants to consent to undergoing annual clinical evaluations as well as postmortem organ donation. The ROS sample includes Catholic priests, nuns, and brothers from across the United States, whereas the MAP sample includes a more general community based population from northeastern Illinois. For our analysis, excluded subjects included those with missing DNAm age, or who were diagnosed with dementias other than AD.

Clinical evaluations. Participants were administered annual structured interviews to assess cognitive functioning. These included tests for EM (immediate recall (word list), delayed recall (word list), word recognition (word list), immediate recall (East Boston story), delayed recall (East Boston story), logical memory immediate recall, logical memory delayed recall), WM (digits forward, digits backward, digit ordering), SM (Boston naming, category fluency, reading test), PO (line orientation, progressive matrices), and PS (symbol digits modality-oral, number

comparison, stroop color naming, stroop color reading). For each domain, composite measures were calculated as the average across tests. Before taking the average, each cognitive test was converted to a z-score (with mean of zero and standard deviation of 1). Finally, GCF is meant to represent overall cognitive functioning. At each wave it was estimated as the average across z-scores from the 19 cognitive tests for EM, WM, SM, PO, and PS.

Neuropathological examination. Upon participants' death, brains were extracted, weighed, sectioned into 1 cm-thick coronal slabs, and stored. Neuropathological indices were examined in order to diagnose cognitive pathologies such as AD, Lewy Body diseases, and cerebrovascular disease [27]. Modified Bielschowsky silver stain was used to identify AD pathology based on NIA-Reagan and modified CERAD criteria. Global AD pathologic burden was estimated by averaging standardized numbers of neuritic plaques, diffuse plaques, and NFT across five brain regions as described in [28]. Moreover, amyloid load was quantified as abundance of amyloid- $\beta$ , labeled with a N-terminal directed monoclonal antibody, while PHFtau tangles, was quantified as the density of paired helical filament tau tangles.

We focused on the following aggregated neuropathological variables (Figure 1 and elsewhere):

- a) "neuritic plaques" and "diffuse plaques" were defined as average of 5 scaled scores (namely scaled mid-frontal, temporal cortex, inferior parietal cortex, entorhinal cortex, and hippocampus plaques) [29,30].
- b) "NFT" measures the tangle average across 5 regions (mid-frontal cortex, mid-temporal cortex, inferior parietal cortex, entorhinal cortex, and hippocampus CA1) [29].
- c) "Amyloid load" measures the overall amyloid load, which was defined as the mean amyloid scores across 8 regions (namely hippocampus entorhinal cortex, mid-frontal, inferior parietal cortex, anterior gyrus, calcarine cortex, cingulate regions, superior frontal gyrus) [29, 31, 32].
- d) Overall tangle score which reports the PHFtau tangle score across 8 regions (hippocampus, entorhinal cortex, midfrontal gyrus, inferior temporal, anterior gyrus, calcarine cortex, cingulate region, superior frontal gyrus).

DNA methylation data. DNAm was measured using the Illumina Infinium HumanMethylation450 BeadChip. The Illumina BeadChips measures bisulfite-conversion-based, single-CpG resolution DNA methylation levels at 485577 different CpG sites in the human genome. These data were generated by following the standard

protocol of Illumina methylation assays, which quantifies methylation levels by the  $\beta$  value using the ratio of intensities between methylated and unmethylated alleles. Specifically, the  $\beta$  value is calculated from the intensity of the methylated (M corresponding to signal A) and unmethylated (U corresponding to signal B) alleles, as the ratio of fluorescent signals  $\beta = \text{Max}(M,0) / [\text{Max}(M,0) + \text{Max}(U,0) + 100]$ . Thus,  $\beta$  values range from 0 (completely unmethylated) to 1 (completely methylated) (Dunning, 2008). The DNA methylation data are available at the following webpage <https://www.synapse.org/#!Synapse:syn3168763>. We focused on brain samples of Caucasian subjects from ROS and MAP that include brain donation at the time of death (n=700) [12, 13]. Additional details on the DNA methylation data can be found in [9].

Epigenetic clock analysis and DNAm age. Several recent studies have proposed to measure the age of tissue samples by combining the DNA methylation levels of multiple dinucleotide markers, known as Cytosine phosphate Guanines or CpGs [11, 33, 34]. In particular, the epigenetic clock based on 353 Cytosine phosphate Guanine (CpG) markers was developed to measure the age (known as "DNA methylation age" or "epigenetic age") of human tissues, organs and cell types—including brain, breast, kidney, liver, lung, blood [11], and even applies to prenatal brain samples [35]. The epigenetic clock method - applied to two commercially standardized methylation platforms: the Illumina 450K array and the 27K arrays - is an attractive biomarker of aging because (1) it applies to most human tissues; (2) its accurate measurement of chronological age is unprecedented [11]; (3) it is predictive of all-cause mortality even after adjusting for a variety of known risk factors [16]; (4) it correlates with measures of cognitive and physical fitness in the elderly [17]; (5) it has already been useful in detecting accelerated aging due to obesity [36], Down syndrome [37], Parkinson's disease [38], and HIV infection [39]; and . Further, the epigenetic clock was used to show that age acceleration of blood may predict the future onset of lung cancer [40], that the cerebellum ages slowly [41], that the blood of subjects with a severe developmental disorder ages normally [42], and that semi-supercentenarians and their offspring age more slowly [47].

Weighted DNAm measures across the 353 CpGs from the epigenetic clock were used to measure the DNAm age of DLPFC samples. These CpGs and their weights (coefficient values) were chosen in independent data sets by regressing chronological age on CpGs. DNAm age is then defined as predicted age, in years [43].

Statistical analysis. Biweight midcorrelations and ordinary least squares regression models were used to examine whether postmortem neuropathology was associated with postmortem DNAm age in DLPFC, after controlling for age at death, study (ROS vs. MAP), and sex. For the bar plots in Figure 1, we defined a grouping variable (high versus low) by dichotomizing the respective neuropathological variable according to the median value. The median was chosen in order to arrive at equal group sizes (high versus low) and to avoid overfitting due to the selection of an optimal threshold. Multivariate linear regression models were fit in the whole sample and in strata defined by AD dementia status (according to the clinical diagnosis). Here we did not use a linear mixed effects model since our dependent variable (DNAm age) is a time-invariant variable based on postmortem brain tissue. The linear models were used to determine whether GCF, WM, EM, SM, PO, and PS over all waves leading up to death were related to postmortem DNAm age in DLPFC. Standard errors for cognitive decline models were adjusted to account for multiple observations. These models also included potential confounders, such as age of clinical evaluation, age at death, study (ROS vs. MAP), and sex. Finally, step-wise linear models were run with DNAm age as the dependent variable and cognitive measures as the independent models. For these models we examined how the association between DNAm age and cognition was altered with the inclusion of either one or all of the neuropathology measure.

We report one-sided (one-tailed) p-values for the cognitive scores and neuropathology variables in our multivariate model analyses because our hypotheses involving cognitive scores are one-sided (e.g. that *higher* DNAm age is associated with *worse* cognitive functioning and *higher* levels of neuropathology).

Genetic analysis. Of the study samples, a total of 1102 individuals (632 normal/ 470 AD) were available with both genotypes and cognitive functioning or neuropathological measure. The GCTA software was used to estimate the heritability and genetic correlations based on both genotyped and imputed SNP markers. We used IMPUTE2 [44, 45] with haplotypes phased using SHAPEIT[46] to impute SNP and INDEL markers, with a reference panel based on the 1000 Genome haplotypes from 2,504 individuals (released in October 2014). As study individuals were genotyped on either Affymetrix SNP Array 6.0 or Illumina HumanOmniExpress, we performed imputation on each subset of individuals stratified by platform. We merged the imputation outputs across platforms and pruned in the markers with info measure > 0.4 in both sets. The other quality control was based on minor allele

frequency (MAF)  $\geq 0.02$ . We converted the IMPUTE2 output format to MaCH dosage format in order to use it as input for the GCTA software.

## Funding

This research was supported by NIH/NIA 5R01AG042511-02 (Horvath, Levine) and NIH/NINDS T32NS048004 (Levine), and NIH/NIA 1U34AG051425-01 (Horvath). The Religious Order study and Rush Memory and Aging Project were funded by P30AG10161, R01AG17917, RF1AG15819, R01AG34374, R01AG36042, U01AG46152 (Bennett). The funding bodies played no role in the design, the collection, analysis, or interpretation of the data.

## Conflict of interest statement

The authors declare no conflict of interest.

## REFERENCES

1. Deary IJ, Corley J, Gow AJ, Harris SE, Houlihan LM, Marioni RE, Penke L, Rafnsson SB and Starr JM. Age-associated cognitive decline. *Br Med Bull.* 2009;92:135-152.
2. Singh-Manoux A, Kivimaki M, Glymour MM, Elbaz A, Berr C, Ebmeier KP, Ferrie JE and Dugravot A. Timing of onset of cognitive decline: results from Whitehall II prospective cohort study. *BMJ.* 2012; 344:d7622.
3. Sperling RA, Aisen PS, Beckett LA, Bennett DA, Craft S, Fagan AM, Iwatsubo T, Jack CR, Jr., Kaye J, Montine TJ, Park DC, Reiman EM, Rowe CC, et al. Toward defining the preclinical stages of Alzheimer's disease: recommendations from the National Institute on Aging-Alzheimer's Association workgroups on diagnostic guidelines for Alzheimer's disease. *Alzheimers Dement.* 2011; 7:280-292.
4. von Strauss E, Viitanen M, De Ronchi D, Winblad B and Fratiglioni L. Aging and the occurrence of dementia: findings from a population-based cohort with a large sample of nonagenarians. *Archives of neurology.* 1999;56:587-592.
5. Rosenberg RN. The molecular and genetic basis of AD: the end of the beginning: the 2000 Wartenberg lecture. *Neurology.* 2000; 54:2045-2054.
6. Bennett DA, Schneider JA, Wilson RS, Bienias JL and Arnold SE. Neurofibrillary tangles mediate the association of amyloid load with clinical Alzheimer disease and level of cognitive function. *Archives of neurology.* 2004;61:378-384.
7. Petersen RC. Mild Cognitive Impairment. *The New England Journal of Medicine.* 2011:2227-2234.
8. Bennett DA, Wilson RS, Arvanitakis Z, Boyle PA, de Toledo-Morrell L and Schneider JA. Selected Findings from the Religious Orders Study and Rush Memory and Aging Project. *Journal of Alzheimer's disease : JAD.* 2013; 33:S397-S403.
9. De Jager PL, Srivastava G, Lunnon K, Burgess J, Schalkwyk LC, Yu L, Eaton ML, Keenan BT, Ernst J, McCabe C, Tang A, Raj T, Replogle J, et al. Alzheimer's disease: early alterations in brain DNA methylation at ANK1, BIN1, RHBDF2 and other loci. *Nat Neurosci.* 2014; 17:1156-1163.
10. Marioni RE, Shah S, McRae AF, Ritchie SJ, Muniz-Terrera G, Harris SE, Gibson J, Redmond P, Cox SR and Pattie A. The epigenetic clock is correlated with physical and cognitive fitness in the Lothian Birth Cohort 1936. *International journal of epidemiology.* 2015:dyu277.
11. Horvath S. DNA methylation age of human tissues and cell types. *Genome Biol.* 2013;14(R115).
12. Bennett DA, Schneider JA, Arvanitakis Z and Wilson RS. Overview and findings from the religious orders study. *Curr Alzheimer Res.* 2012; 9:628-645.
13. Bennett DA, Schneider JA, Buchman AS, Barnes LL, Boyle PA and Wilson RS. Overview and findings from the rush Memory and Aging Project. *Curr Alzheimer Res.* 2012; 9:646-663.
14. Lee SH, Wray NR, Goddard ME and Visscher PM. Estimating missing heritability for disease from genome-wide association studies. *Am J Hum Genet.* 2011;88:294-305.
15. Visscher PM, Hemani G, Vinkhuyzen AA, Chen GB, Lee SH, Wray NR, Goddard ME and Yang J. Statistical power to detect genetic (co)variance of complex traits using SNP data in unrelated samples. *PLoS Genet.* 2014;10:e1004269.
16. Marioni R, Shah S, McRae A, Chen B, Colicino E, Harris S, Gibson J, Henders A, Redmond P, Cox S, Pattie A, Corley J, Murphy L, et al. DNA methylation age of blood predicts all-cause mortality in later life. *Genome Biol.* 2015;16:25.
17. Marioni RE, Shah S, McRae AF, Ritchie SJ, Muniz-Terrera G, Harris SE, Gibson J, Redmond P, Cox SR, Pattie A, Corley J, Taylor A, Murphy L, et al. The epigenetic clock is correlated with physical and cognitive fitness in the Lothian Birth Cohort 1936. *Int J Epidemiol.* 2015;44:1388-1396.
18. Yu L, Boyle PA, Leurgans S, Schneider JA and Bennett DA. Disentangling the effects of age and APOE on neuropathology and late life cognitive decline. *Neurobiol Aging.* 2014; 35:819-826.
19. Boyle PA, Wilson RS, Yu L, Barr AM, Honer WG, Schneider JA and Bennett DA. Much of late life cognitive decline is not due to common neurodegenerative pathologies. *Ann Neurol.* 2013; 74:478-489.
20. Boyle PA, Yu L, Wilson RS, Schneider JA and Bennett DA. Relation of neuropathology with cognitive decline among older persons without dementia. *Frontiers in Aging Neuroscience.* 2013; 5:50.
21. Hatanpaa K, Isaacs KR, Shirao T, Brady DR and Rapoport SI. Loss of proteins regulating synaptic plasticity in normal aging of the human brain and in Alzheimer disease. *J Neuropathol Exp Neurol.* 1999; 58:637-643.
22. Ohnishi T, Matsuda H, Tabira T, Asada T and Uno M. Changes in brain morphology in Alzheimer disease and normal aging: is Alzheimer disease an exaggerated aging process? *AJNR American journal of neuroradiology.* 2001; 22(9):1680-1685.
23. Grundman M, Petersen RC, Ferris SH, Thomas RG, Aisen PS, Bennett DA, Foster NL, Jack Jr CR, Galasko DR and Doody R. Mild cognitive impairment can be distinguished from Alzheimer disease and normal aging for clinical trials. *Archives of neurology.* 2004; 61:59-66.
24. Kensinger EA, Brierley B, Medford N, Growdon JH and Corkin S. Effects of normal aging and Alzheimer's disease on emotional memory. *Emotion (Washington, DC).* 2002; 2:118-134.
25. Grady CL, Furey ML, Pietrini P, Horwitz B and Rapoport SI. Altered brain functional connectivity and impaired short-term memory in Alzheimer's disease. *Brain.* 2001;124:739-756.

26. Levine ZA, Larini L, LaPointe NE, Feinstein SC and Shea J-E. Regulation and aggregation of intrinsically disordered peptides. *Proceedings of the National Academy of Sciences of the United States of America*. 2015;112:2758-2763.
27. Schneider JA, Arvanitakis Z, Leurgans SE and Bennett DA. The neuropathology of probable Alzheimer disease and mild cognitive impairment. *Ann Neurol*. 2009;66:200-208.
28. Bennett DA, Wilson RS, Schneider JA, Evans DA, Aggarwal NT, Arnold SE, Cochran EJ, Berry-Kravis E and Bienias JL. Apolipoprotein E epsilon4 allele, AD pathology, and the clinical expression of Alzheimer's disease. *Neurology*. 2003;60:246-252.
29. Barnes LL, Schneider JA, Boyle PA, Bienias JL and Bennett DA. Memory complaints are related to Alzheimer disease pathology in older persons. *Neurology*. 2006;67:1581-1585.
30. Hensley K, Barnes LL, Christov A, Tangney C, Honer WG, Schneider JA, Bennett DA and Morris MC. Analysis of postmortem ventricular cerebrospinal fluid from patients with and without dementia indicates association of vitamin E with neuritic plaques and specific measures of cognitive performance. *J Alzheimers Dis*. 2011;24:767-774.
31. Bell KF, Ducatzenzeiler A, Ribeiro-da-Silva A, Duff K, Bennett DA and Cuello AC. The amyloid pathology progresses in a neurotransmitter-specific manner. *Neurobiol Aging*. 2006;27:1644-1657.
32. Bennett DA, Schneider JA, Wilson RS, Bienias JL and Arnold SE. Education modifies the association of amyloid but not tangles with cognitive function. *Neurology*. 2005;65:953-955.
33. Hannum G, Guinney J, Zhao L, Zhang L, Hughes G, Sada S, Klotzle B, Bibikova M, Fan J-B, Gao Y, Deconde R, Chen M, Rajapakse I, et al. Genome-wide Methylation Profiles Reveal Quantitative Views of Human Aging Rates. *Mol Cell*. 2013;49:359-367.
34. Weidner CI, Lin Q, Koch CM, Eisele L, Beier F, Ziegler P, Bauerschlag DO, Jockel KH, Erbel R, Muhleisen TW, Zenke M, Brummendorf TH and Wagner W. Aging of blood can be tracked by DNA methylation changes at just three CpG sites. *Genome Biol*. 2014;15:R24.
35. Spiers H, Hannon E, Schalkwyk LC, Smith R, Wong CC, O'Donovan MC, Bray NJ and Mill J. Methylomic trajectories across human fetal brain development. *Genome research*. 2015;25:338-352.
36. Horvath S, Erhart W, Brosch M, Ammerpohl O, von Schönfels W, Ahrens M, Heits N, Bell JT, Tsai P-C, Spector TD, Deloukas P, Siebert R, Sipos B, et al. Obesity accelerates epigenetic aging of human liver. *Proc Natl Acad Sci U S A* 2014;111:15538-15543.
37. Horvath S, Garagnani P, Bacalini M, Pirazzini C, Salvioli S, Gentilini D, DiBlasio A, Giuliani C, Tung S, Vinters H and Franceschi C. Accelerated Epigenetic Aging in Down Syndrome. *Aging Cell*. 2015;14:491-495.
38. Horvath S and Ritz BR. Increased epigenetic age and granulocyte counts in the blood of Parkinson's disease patients. *Aging (Albany NY)*. 2015; this issue.
39. Horvath S and Levine AJ. HIV-1 infection accelerates age according to the epigenetic clock. *J Infect Dis*. 2015; 212:1563-1573.
40. Levine ME, Hosgood HD, Chen B, Absher D, Assimes T and Horvath S. DNA methylation age of blood predicts future onset of lung cancer in the women's health initiative. *Aging (Albany NY)*. 2015; 7:690-700.
41. Horvath S, Mah V, Lu AT, Woo JS, Choi OW, Jasinska AJ, Riancho JA, Tung S, Coles NS, Braun J, Vinters HV and Coles LS. The cerebellum ages slowly according to the epigenetic clock. *Aging (Albany NY)*. 2015; 7:294-306.
42. Walker RF, Liu JS, Peters BA, Ritz BR, Wu T, Ophoff RA and Horvath S. Epigenetic age analysis of children who seem to evade aging. *Aging (Albany NY)*. 2015;7:334-339.
43. Horvath S, Zhang Y, Langfelder P, Kahn R, Boks M, van Eijk K, van den Berg L and Ophoff RA. Aging effects on DNA methylation modules in human brain and blood tissue. *Genome Biol*. 2012;13:R97.
44. Howie B, Fuchsberger C, Stephens M, Marchini J and Abecasis GR. Fast and accurate genotype imputation in genome-wide association studies through pre-phasing. *Nat Genet*. 2012;44:955-959.
45. Howie BN, Donnelly P and Marchini J. A Flexible and Accurate Genotype Imputation Method for the Next Generation of Genome-Wide Association Studies. *PLoS Genet*. 2009;5:e1000529.
46. O'Connell J, Gurdasani D, Delaneau O, Pirastu N, Ulivi S, Cocca M, Traglia M, Huang J, Huffman JE, Rudan I, McQuillan R, Fraser RM, Campbell H, et al. A General Approach for Haplotype Phasing across the Full Spectrum of Relatedness. *PLoS Genet*. 2014;10:e1004234.
47. Horvath S, Pirazzini C, Bacalini MG, Gentilini D, DiBlasio AM, Delledonne M, Mari D, Arosio B, Passarino DMG, DeRango F, D'Aquila P, Giuliani C, Marasco E, Collino S, Descombes P, Garagnani P, Franceschi C. Decreased epigenetic age of PBMCs from Italian semi-supercentenarians and their offspring. *Aging (Albany, NY)*; 2015; this issue

## A comprehensive multiomics approach toward understanding the relationship between aging and dementia

Antonio Currais<sup>1</sup>, Joshua Goldberg<sup>1</sup>, Catherine Farrokhi<sup>1</sup>, Max Chang<sup>1</sup>, Marguerite Prior<sup>1</sup>, Richard Dargusch<sup>1</sup>, Daniel Daugherty<sup>1</sup>, Aaron Armando<sup>2</sup>, Oswald Quehenberger<sup>2</sup>, Pamela Maher<sup>1</sup>, and David Schubert<sup>1</sup>

<sup>1</sup> The Salk Institute for Biological Studies, La Jolla, CA 92037, USA;

<sup>2</sup> Department of Medicine, University of California San Diego, CA 92093-0601, USA.

**Key words:** aging, Alzheimer's disease, multiomics, SAMP8 mice, inflammation, J147

**Received:** 09/15/15; **Accepted:** 10/30/15; **Published:** 11/11/15      **doi:** [10.18632/aging.100838](https://doi.org/10.18632/aging.100838)

**Correspondence to:** David Schubert, PhD; **E-mail:** [schubert@salk.edu](mailto:schubert@salk.edu)

**Copyright:** Currais et al. This is an open-access article distributed under the terms of the Creative Commons Attribution License, which permits unrestricted use, distribution, and reproduction in any medium, provided the original author and source are credited

**Abstract:** Because age is the greatest risk factor for sporadic Alzheimer's disease (AD), phenotypic screens based upon old age-associated brain toxicities were used to develop the potent neurotrophic drug J147. Since certain aspects of aging may be primary cause of AD, we hypothesized that J147 would be effective against AD-associated pathology in rapidly aging SAMP8 mice and could be used to identify some of the molecular contributions of aging to AD. An inclusive and integrative multiomics approach was used to investigate protein and gene expression, metabolite levels, and cognition in old and young SAMP8 mice. J147 reduced cognitive deficits in old SAMP8 mice, while restoring multiple molecular markers associated with human AD, vascular pathology, impaired synaptic function, and inflammation to those approaching the young phenotype. The extensive assays used in this study identified a subset of molecular changes associated with aging that may be necessary for the development of AD.

### INTRODUCTION

There is currently no drug to prevent or slow down the progression of AD pathology. Our laboratory uses a drug discovery paradigm based upon a set of cell-based screening assays that mimic numerous aspects of old age-associated neurodegeneration and AD pathology [1]. This approach has led to the identification of J147, a very potent neuroprotective small molecule that is orally active in transgenic human familial AD (hFAD) animal models [2, 3].

Age is by far the greatest risk factor for dementia [4]. One model of aging is the senescence-accelerated prone 8 (SAMP8) mouse, that has a progressive, age-associated decline in brain function similar to human AD patients [5, 6]. As they age, SAMP8 mice develop an early deterioration in learning and memory as well as a number of pathophysiological alterations in the brain

including increased oxidative stress, inflammation, vascular impairment, gliosis, A $\beta$  accumulation and tau hyperphosphorylation. Therefore, the SAMP8 mice together with their response to J147 may help to delineate an understanding of the molecular mechanisms that are shared by aging and disease. These insights could lead to novel interventions for old age-associated sporadic AD.

To investigate the interaction between aging and the AD drug candidate J147 on brain function as well as brain and systemic metabolism, an integrative multi-omics approach was carried out in SAMP8 mice. Changes in behavior, protein expression, levels of metabolites and the whole transcriptome in old SAMP8 mice fed with control or J147 diets were compared with young SAMP8 control mice. These data identify a subset of metabolic changes associated with aging that may be relevant to sporadic AD and other forms of dementia.

Importantly, the data demonstrate the ability of J147 to suppress many of these changes.

## RESULTS

To address the effect of J147 on the SAMP8 phenotype, two groups of three-month old mice were fed with control or J147 diet for an additional seven months, while another group of three-month old mice was used as a young control group. The SAMP8 mice are an inbred strain and, as such, young SAMP8 mice were chosen as controls for young age. Given the seven-month duration of the feeding paradigm, the effect of the J147 diet could only be assessed in old SAMP8 mice, and age-related changes were defined by comparison to the young SAMP8 animals. At 10 months of age, SAMP8 mice present strong age- and AD-associated brain deterioration [5-8]. The overall goal of this work was to use an in depth multiomics approach to identify molecules that mediate the physiological effects of J147 on the aging and AD-associated phenotypes of these mice.

## Behavioral assessment

By monitoring the spontaneous behavior of mice in the open field assay, we found a decline in activity parameters between the young and the old SAMP8 (Fig. 1 A-D). J147 had a positive effect on locomotor activity as it improved the average velocity and the number of vertical counts in the old SAMP8 mice. J147 had no effect on the body weights (Fig. S1).

To investigate whether J147 could prevent age-associated cognitive decline, mice were tested using the elevated plus maze (Fig. 1 E), the object recognition test (Fig. 1 F) and the Barnes maze (Fig. 1 G). The elevated plus maze examines disinhibition behavior based on the aversion of normal mice to open spaces. Dementia is clinically associated with disinhibition and AD mouse models tend to exhibit increased disinhibition [3]. Accordingly, old SAMP8 mice spent significantly more time in the open arms compared to the young SAMP8 mice (Fig. 1 E). However, this was not altered by J147 treatment.

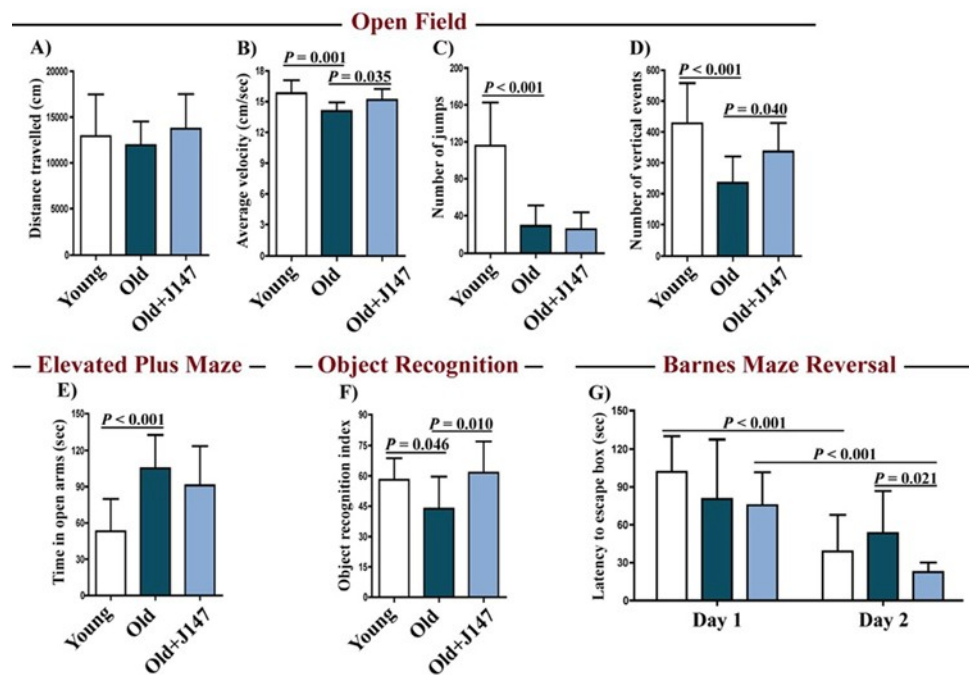


**Figure 1. J147 improves locomotor and cognitive function in old SAMP8 mice.** Distance travelled (A), average velocity (B), number of jumps (C) and number of vertical events (D) were assessed in young mice and old SAMP8 mice fed with control or J147 diets with the open field test. The elevated plus maze (E) was used to measure anxiety levels. Recognition memory and spatial learning/memory were evaluated by the object recognition (F) and the Barnes maze (G) assays, respectively. One-way ANOVA followed by Tukey-Kramer post-hoc test and two-way repeated measures ANOVA and post hoc Bonferroni corrected t-test ( $n = 12-16/\text{group}$ ). All data are mean  $\pm$  SD.

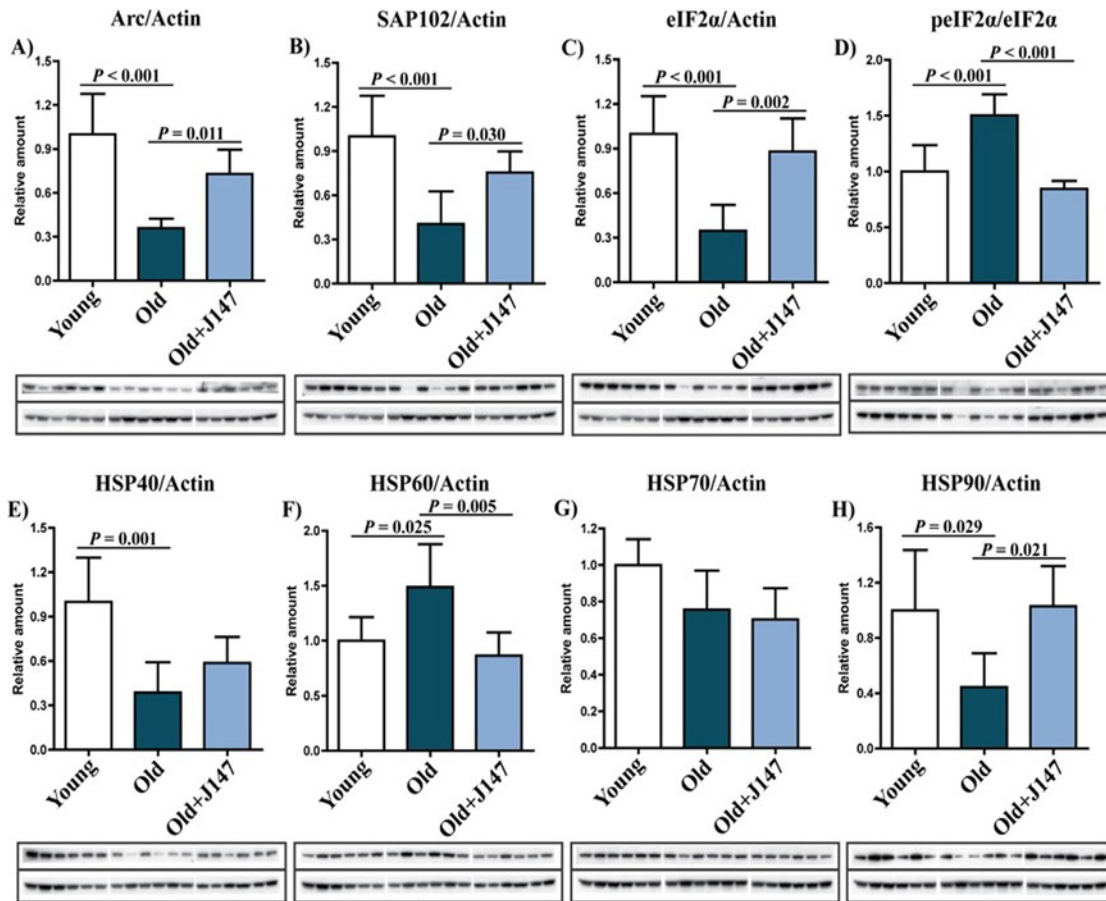


**Figure 2. Dysregulation of neuronal homeostasis and stress responses in the hippocampus of old SAMP8 mice is partially restored by J147.** RIPA-soluble fractions from hippocampal tissue were analyzed by Western blotting for relevant markers of neuronal homeostasis and stress and are presented relative to actin or the unphosphorylated molecule: Arc (A), SAP102 (B), eIF2 $\alpha$  (C), pEIF2 $\alpha$  (D), HSP40 (E), HSP60 (F), HSP70 (G), HSP90 (H). One-way ANOVA followed by Tukey-Kramer post-hoc test (n = 6/group). All data are mean  $\pm$  SD.

The object recognition test evaluates recognition memory and is based on the spontaneous tendency of mice to spend more time exploring a novel object than a familiar one. The choice to explore the novel object reflects the use of learning and recognition memory. There was a significant decrease in the recognition index with age in SAMP8 mice, which was reversed by J147 (Fig. 1 F).

The Barnes maze is used to analyze spatial learning and hippocampal-dependent memory. In this assay, mice use visual cues to locate a hidden box. With repeated trials, animals with an intact memory show a significant reduction in the time (latency) to locate the box. If the box is moved to another location in the maze (reversal test), normal animals rapidly disengage from the previously learned information and re-learn the new

location. No changes between the three groups were found in the escape latencies during the learning and the retention phases (data not shown). However, when tested during the reversal phase, which is more sensitive to smaller deficits in memory and learning, differences were found in the capacity of mice to relearn the new location of the escape box (Fig. 1 G). Importantly, J147 significantly improved learning of the new location. Altogether, these data show that J147 prevents the deterioration of several aspects of behavior and memory that are altered in old SAMP8 mice.

### Brain hippocampal protein expression

Western blotting was used to investigate both protein alterations underlying the decline in cognitive performance of old SAMP8 mice and the therapeutic

effects of J147. The expression of activity-regulated cytoskeleton-associated protein (Arc) and synapse-associated protein 102 (SAP102) decreased in old mice compared to young mice (Fig. 2 A and B), and treatment with J147 prevented these decreases. It was then asked if these changes were accompanied by alterations in the levels of proteins involved in the cellular responses to stress relevant to aging and AD (Fig. 2 C-H). Phosphorylation of eukaryotic initiation factor 2a (eIF2 $\alpha$ ) occurs under a variety of stress conditions to control protein synthesis. Although total levels of eIF2 $\alpha$  were decreased in old SAMP8 mice compared to young controls, its phosphorylation was increased (Fig. 2 C and D), as has been reported in AD patients [9]. Importantly, J147 reverted the changes in both the total levels and the phosphorylation of eIF2 $\alpha$ . Additionally, while the levels of heat shock protein 70 (HSP70) were not significantly altered between groups, changes in HSP40, HSP60 and HSP90 were detected in the old SAMP8 mice (Fig. 2 E-H). J147 restored HSP60 and HSP90 to levels similar to those found in the young control mice.

One hallmark of the AD brain is extracellular A $\beta$

plaques. Although SAMP8 mice do not develop classical plaque pathology, they have a high content of A $\beta$  and amyloid deposition around blood vessels [5, 7]. A $\beta$  is the product of sequential cleavages of the amyloid precursor protein (APP). Processing of APP involves the formation of the C83 and C99 C-terminal fragments by  $\alpha$  and  $\beta$ -secretases, respectively. Amyloidogenic processing of C99 by  $\gamma$ -secretase then generates A $\beta$  [10]. Although no significant changes in the total levels of APP and the C99 and C83 fragments across the three groups were identified, there was a trend towards lower levels of APP and both the C99 and C83 fragments after treatment with J147 (Fig. 3 A and B). More importantly, an increase in the level of A $\beta$ <sub>1-40</sub> was detected in the hippocampus of old SAMP8 mice, which was significantly prevented by J147 (Fig. 3 C). A $\beta$ <sub>1-42</sub> was below the limit of detection (data notshown).

Tau pathology is another important feature of AD. Old SAMP8 mice showed increases in both tau protein and its phosphorylation at Ser396 (Fig. 3 D and E), an epitope affected in the human AD brain [11]. J147 prevented both of these alterations.

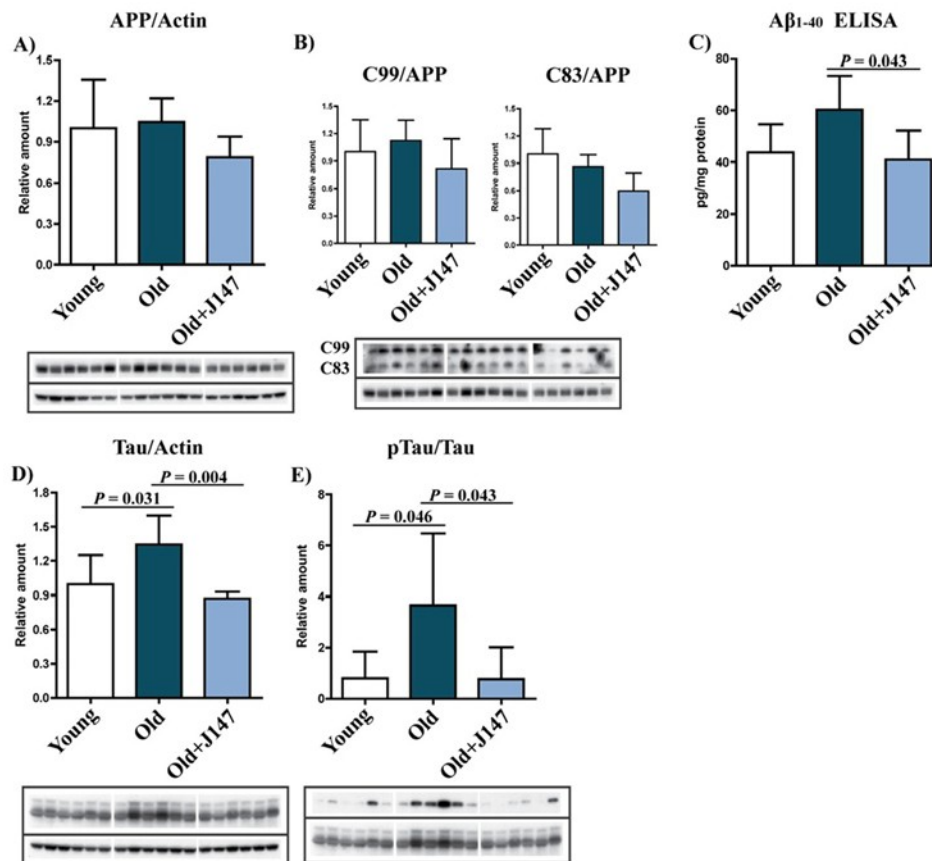


**Figure 3. J147 prevents alterations in A $\beta$  and tau homeostasis in the hippocampus of old SAMP8 mice.** (A and B) Western blot analysis of APP processing in hippocampal tissue using an antibody against the C-terminus of APP. Full-length APP and the APP cleavage products C99 and C83 were detected. (C) ELISA for A $\beta$ . Western blot analysis of total Tau (D) and pTau Ser396 (E). One-way ANOVA followed by Tukey-Kramer post-hoc test (n = 6/group). All data are mean  $\pm$  SD.

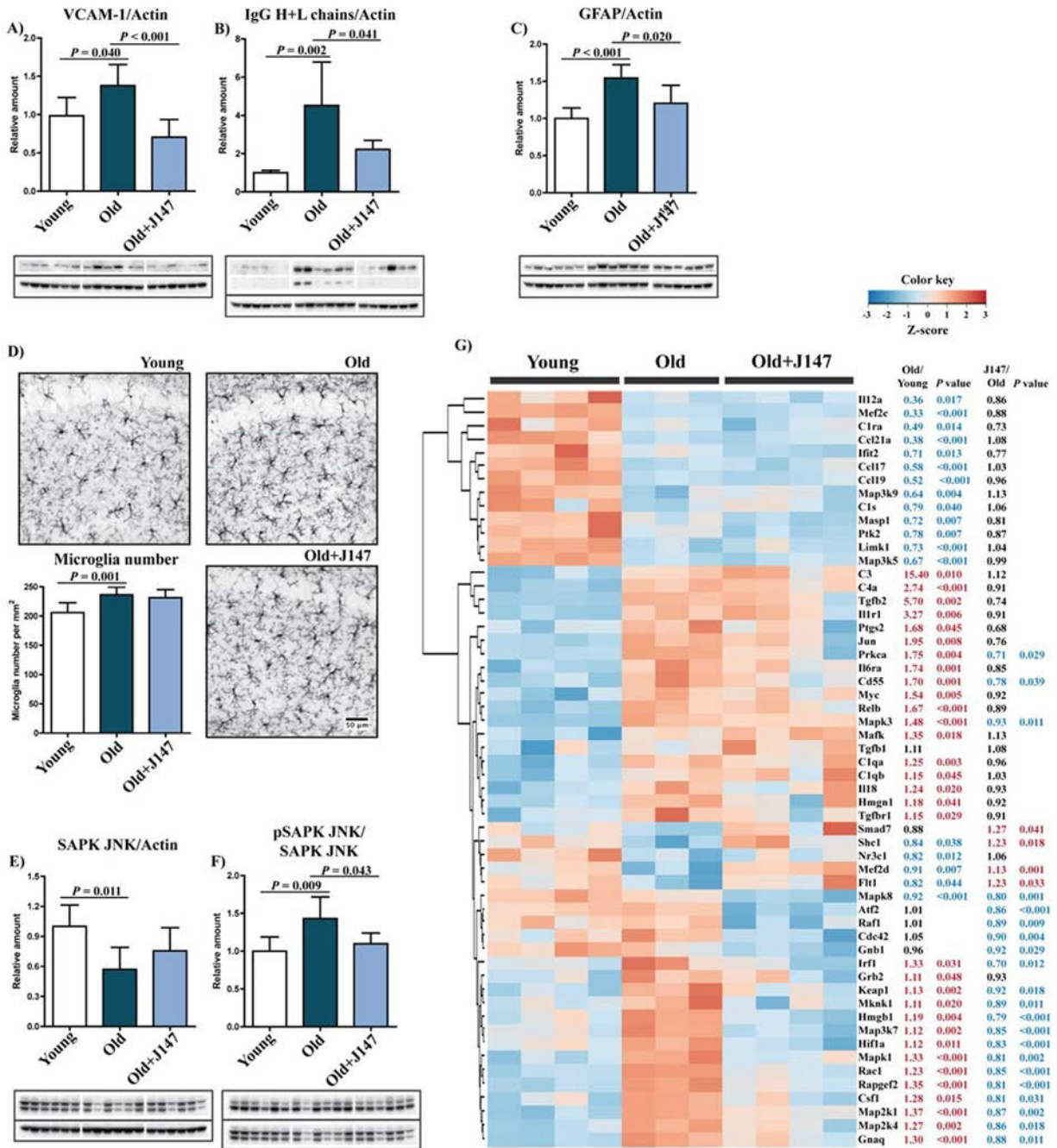


**Figure 4. Increased inflammation and gliosis in the hippocampus of old SAMP8 mice are prevented by J147.** Western blot analysis of the marker for vascular endothelial inflammation VCAM-1 (A) and of the IgG (Heavy + Light chains) content (B). (C) Astrocytosis, measured by Western blot of GFAP levels. One-way ANOVA followed by Tukey-Kramer post-hoc test ( $n = 6$ /group). (D) Microgliosis was assessed by immunohistochemical (IHC) staining and number of Iba-1-positive cells per mm<sup>2</sup> of total hippocampus calculated. Original magnification: x100. One-way ANOVA followed by Tukey-Kramer post-hoc test ( $n = 8$ /group). (E and F) Activation of the stress/inflammation-associated SAPK/JNK was measured by Western blot analysis of its phosphorylation at Thr183/Tyr185. One-way ANOVA followed by Tukey-Kramer post-hoc test ( $n = 6$ /group). All data are mean  $\pm$  SD. (G) Quantitative RNA analysis of altered genes related to inflammation. Heatmap and hierarchical clustering of scaled gene expression with respective fold changes and  $P$  values for the comparisons Old/Young and Old+J147/Old. Scaled expression value (Z-score) is plotted in red–blue color scale with red indicating high expression and blue indicating low expression. One-way ANOVA followed by Tukey-Kramer post-hoc test ( $n = 3$ -4/group).

## Vascular dysfunction and inflammation

Given the relevance of inflammation in aging and AD, a detailed characterization of the inflammatory status of the aged SAMP8 brain and of the effects of J147 was carried out. AD is often accompanied by inflammation of the brain blood barrier (BBB), and the disruption of its permeability severely compromises neuronal homeostasis [12, 13]. A significant increase in the levels of vascular cell adhesion molecule 1 (VCAM-1), a protein associated with vascular endothelium inflammation, was detected in the hippocampus of old SAMP8 mice compared to the young SAMP8 controls (Fig. 4 A). This increase was completely prevented by J147 treatment. In addition, old mice showed significantly higher levels of endogenous immunoglobulin G (IgG) (Fig. 4 B), a consequence of disrupted BBB permeability [14], which was also prevented by J147. Together these results suggest that J147 helps to preserve BBB homeostasis and vascular function in aged SAMP8 mice.

Astrocytes are key constituents of the BBB, and astrocytic reactivity is increased in AD [15]. We previously reported an increased expression of glial fibrillary acidic protein (GFAP), a marker for astrocytes, due to an increased number of astrocytes in the hippocampus of old SAMP8 mice [7]. The current study confirmed an increase in GFAP levels from young to old SAMP8 mice and showed that J147 reduced GFAP expression (Fig. 4 C). The number of microglia increased in the hippocampus of old mice compared to young (Fig. 4 D), but J147 did not significantly alter their number.

Western blot analysis revealed an activation of the stress-activated protein kinase/Jun-amino-terminal kinase (SAPK/JNK), determined by its phosphorylation, in the hippocampus of old SAMP8 mice (Fig. 4 E and F). SAPK/JNK is activated in AD brains and may be the cause of abnormal tau phosphorylation [16]. Importantly, J147 prevented the activation of SAPK/JNK in the old mice.

To expand upon these findings, the expression of a comprehensive panel of inflammatory genes was analyzed. The expression of a large number of genes was altered between young and old SAMP8 mice (50/248); most were upregulated (Fig. 4 G). The vast majority of changes associated with J147 reverted alterations found in old SAMP8 mice toward expression levels in young mice. These include mitogen-activated protein kinase (MAPK) kinases, such as Map3k7 and Map2k4, that are direct activators of SAPK/JNK, in accordance with the Western blotting data (Fig. 4 E and F).

J147 treatment was largely associated with an overall decrease in the expression of inflammatory markers in old mice, indicative of a reduction in stress-associated inflammation. However, the expression of some genes that are elevated in old mice, such as the components of the complement system C1qa, C1qb, C3 and C4a, were not altered by J147. Interestingly, there was a group of inflammation-associated genes whose expression was lowered in the old mice. Although most of these were not changed by J147, one that was restored by J147 is *Flt1* that encodes the vascular endothelial growth factor receptor 1 and may be related to the effect of J147 on the brain vasculature. These data show that J147 prevents a portion of the pro-inflammatory changes associated with aging in the SAMP8 mice.

## Eicosanoid metabolism

To further elucidate the effects of J147 on inflammation, a detailed analysis of eicosanoid production in the brain cortex was conducted. Eicosanoids are a class of bioactive lipid mediators derived from the metabolism of polyunsaturated fatty acids (PUFAs) by cyclooxygenases (COXs), lipoxygenases (LOXs) and cytochrome P450s as well as nonenzymatic pathways [17]. They are potent regulators of the inflammatory response in the periphery, but are much less studied in the brain. Several fatty acids, including arachidonic acid (AA), docosahexaenoic acid (DHA), linoleic acid (LA) and adrenic acid, as well as their respective metabolites were analyzed (Fig. 5). J147 significantly increased the levels of DHA and restored those of adrenic acid. J147 also had a strong anti-oxidant effect, since most of the metabolites derived from the non-enzymatic oxidation of the different fatty acids were decreased in mice treated with J147 as compared to either young or old SAMP8 mice. These include the AA-metabolites 9-HETE and 8-iso-15-keto PGF2 $\beta$ ; the DHA-metabolites 11- and 13-HDoHEs; and the LA-metabolites 9-HODE and 13-HODE. Therefore, J147 may reduce the pro-oxidant status in the brain of old animals.

The levels of the cytochrome P450 metabolites 19-HETE and 20-HETE (AA derivatives), 19(20)-EpDPE (DHA derivative) and 9,10-DiHOME (LA derivative), which are known regulators of vascular dynamics [18, 19], were altered with J147 treatment. 20-HETE and 9,10-DiHOME were also altered by aging and this was prevented by J147. In addition, several COX metabolites were changed. TXB2, a product of TXA2, was increased in old SAMP8 mice and lowered by J147. The thromboxane pathway is implicated in platelet aggregation, adhesion and vascular contraction during inflammation [20]. Thus, these data further support the idea that J147 reduces the decline in brain vascular health that occurs during aging.

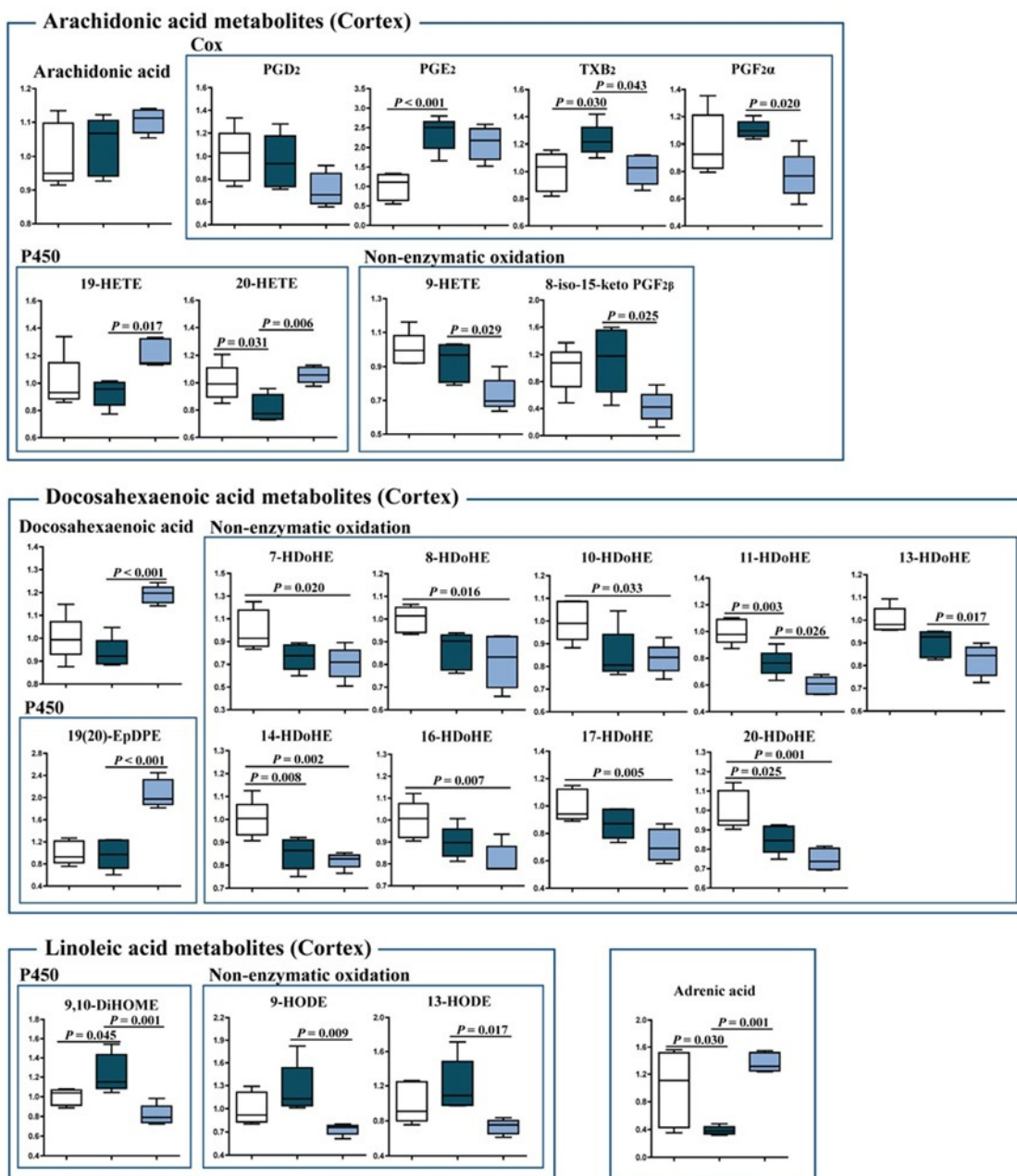


**Figure 5. Changes in eicosanoid metabolism of fatty acids in the cortex of young SAMP8, old SAMP8 and old SAMP8 mice fed with J147.** Significant changes in the metabolites of arachidonic acid, docosahexaenoic acid, linoleic acid and adrenic acid derived from the actions of COX and cytochrome P450 and non-enzymatic oxidation. One-way ANOVA followed by Tukey-Kramer post-hoc test ( $n = 5/\text{group}$ ). Values are expressed as box-and-whisker plots.

### Small molecule metabolism

To address the possible therapeutic effects of J147 on brain and whole body health, a global metabolic profiling study was carried out with blood plasma and brain cortical tissue. 195 of 593 (32.9%) and 105 of 493 (21.3%) assayed biochemicals differed significantly in the plasma and cortex, respectively, between the three

groups. The heatmaps in Figures 6 A and B depict the major altered biological pathways. Global pathway changes regarding the metabolism of amino acids, peptides and lipids were detected in the plasma (Fig. 6 A). In the brain, significant changes were associated with amino acid and lipid metabolism and, importantly, neurotransmission and energy production (Fig. 6 B).

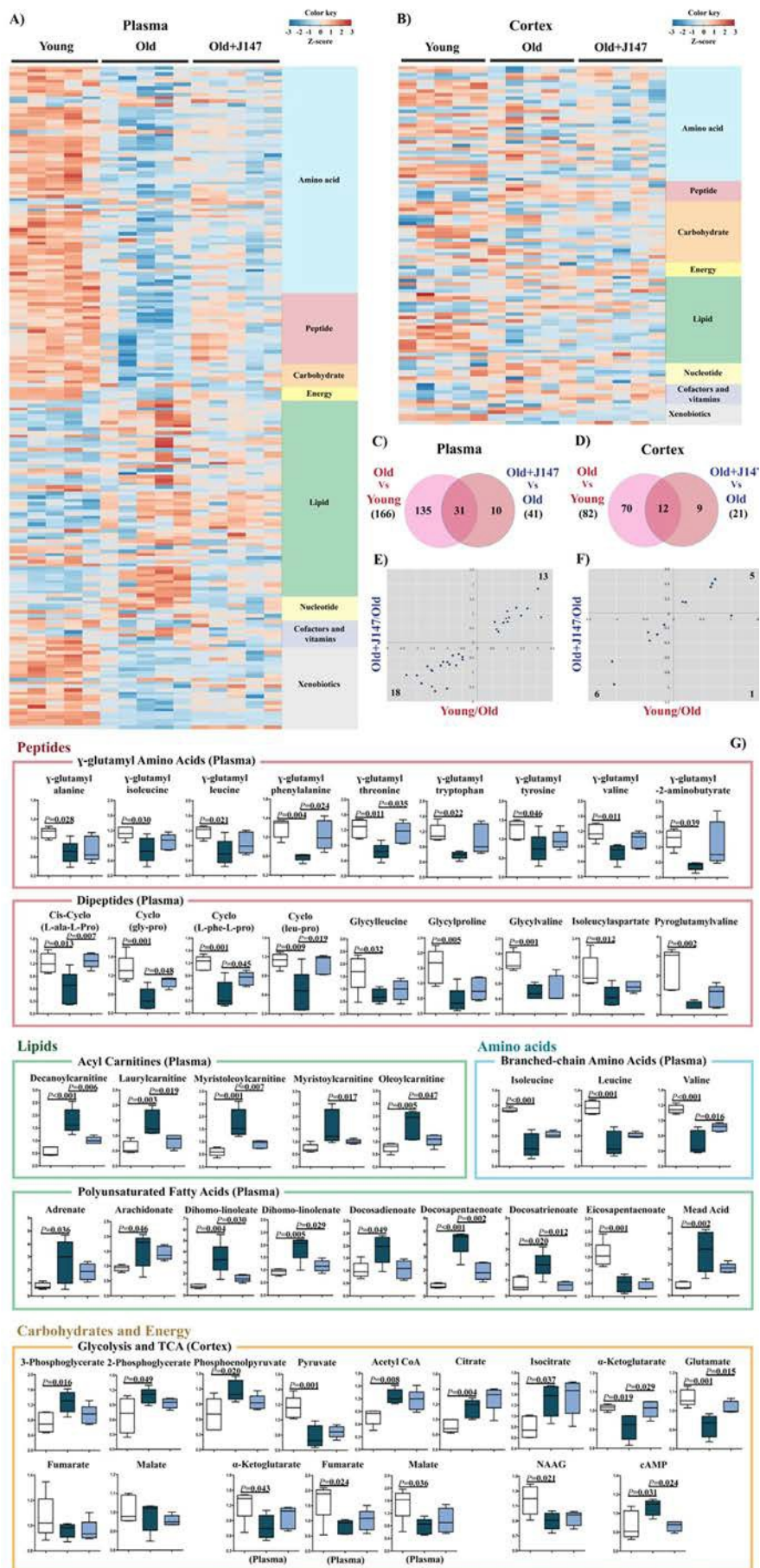


**Figure 6. Metabolomic analysis of plasma and cortex demonstrate that alterations in biological pathways between young SAMP8 and old SAMP8 mice are partially rescued by J147.** Plasma (A) and cortex (B) heatmaps of the biochemicals found significantly modified, organized by major biological groups. Scaled expression value (Z-score) is plotted in red–blue color scale with red indicating high expression and blue indicating low expression. Venn diagrams illustrating shared and uniquely affected metabolites in plasma (C) and cortex (D). Correlation of metabolite levels altered in Young/Old and Old+J147/Old in plasma (E) and cortex (F) (units are  $-\log(\text{fold change})$ ). (G) Selection of relevant biochemicals changed between young and old SAMP8 mice affected by J147, including  $\gamma$ -glutamyl amino acids, dipeptides, BCAAs, acyl carnitines and PUFAs in the plasma, and metabolites related to neurotransmission and energetic pathways in the cortex. One-way ANOVA followed by Tukey-Kramer post-hoc test ( $n = 5/\text{group}$ ). Values are expressed as box-and-whisker plots.

Venn diagrams highlighting the significant changes in plasma and cortex that differentiate the comparisons between the young, old and old+J147 groups are shown in Figures 6 C and D. Fold changes of the overlapping metabolites were correlated between the two comparisons (Fig. 6 E and F). Treatment with J147 rescued changes in all of the 31 plasma metabolites also found altered in old SAMP8 mice. This accounts for 76% of all differences between old SAMP8 treated with J147 and old SAMP8 fed with control diet. In the cortex, J147 rescued changes in 11 biochemicals (out of 12), representing 55% of all differences between J147 treated and untreated old SAMP8 mice. Figure 6 G shows the specific biological groups of metabolites found affected in the plasma (for all biochemicals see Table S1). Numerous  $\gamma$ -glutamyl amino acids, branched-chain amino acids (BCAAs) and dipeptides were downregulated with age, while several acylcarnitines and PUFAs were highly elevated in the old SAMP8 mice. In both cases, J147 reversed most of these changes towards the younger phenotype.

To investigate which biological pathways and diseases/functions could be associated with these alterations, Ingenuity Pathways Analysis (IPA) was carried out with biochemicals present in the Human Metabolome Database (HMDB). It is important to note that many of the metabolites identified in Figure 6 do not have an established biological pathway in HMDB; therefore, this analysis has limitations. The top canonical pathways altered in the plasma are shown in Figure S2 A and B, and confirm changes in amino acid, protein metabolism, urea cycle and mitochondrial energetics (tricarboxylic acid cycle (TCA) and oxidative phosphorylation) found between the young and old SAMP8 mice. Some of the diseases and functions predicted to be associated with these changes relevant to aging include cancer, gastrointestinal and hepatic dysfunction, endocrine system, energy metabolism and inflammatory responses (Fig. S2 C). Most of these were also found associated with the metabolites changed by J147, indicative that J147 might be rescuing certain aspects of these diseases and functions that are changed with age.

Although the total number of metabolites altered in the brain of old SAMP8 mice was lower than in the plasma, the associations determined by IPA were strong (Fig. S2 E and F). Some of the metabolites of interest participate in energy production processes, amino acid metabolism, G protein-coupled receptor (GPCR) and cAMP signaling, neuronal homeostasis and lipid metabolism (Fig. S2 E) (for all biochemicals see Table S2). Specifically, alterations in glycolytic and TCA intermediates in old SAMP8 mice (Fig. 6 G) are

indicative of mitochondrial dysfunction, which is characteristic of aging and AD [21]. J147 also preserved the levels of glutamate, the principal neurotransmitter in the brain and a product of the TCA intermediate  $\alpha$ -ketoglutarate, which was also rescued by J147 (Fig. 6 G). The levels of cAMP were elevated in old SAMP8 mice and were lowered by J147. cAMP is an intracellular signal transduction molecule crucial for many biological processes and its upregulation has been associated with AD [22]. The predicted diseases and functions are consistent with these alterations and include cancer, stress pathways, cellular survival/growth and maintenance, neurological disease and energy metabolism (Fig. S2 F).

### Whole transcriptome

To elucidate how changes in behavior, proteomics and metabolomics are related to alterations in gene expression, whole transcriptome analysis was carried out with hippocampal tissue. 5279 genes were altered between the old and young SAMP8 mice and 150 genes were changed with J147 treatment (Fig. 7 A). The heatmap in Figure 7 B shows a rescuing effect by J147 of changes verified between the young and old SAMP8 mice. Correlation of the expression of the overlapping 121 genes between the two comparisons confirms that most of these (116 genes; 77% of total genes changed with J147) are indeed associated with a rescue of age-related changes in gene expression (Fig. 7 C).

The IPA of canonical pathways revealed a number of important signaling pathways related to brain function, including axonal guidance, G-protein coupled receptor (GPCR), protein kinase A (PKA), cAMP and neuronal cAMP response element-binding protein (CREB) signaling (Fig. 7 D). Importantly, treatment with J147 altered the expression of genes associated with some of these pathways, namely cAMP, GPCR and CREB signaling. Also of interest are the changes in the renin-angiotensin and endothelin-1 signaling in old SAMP8 mice, which are important regulators of vascular function, supporting the Western blotting data regarding alterations in the brain vasculature (Fig. 4 A and B).

The large dataset obtained with the whole transcriptome allowed for a more informative prediction on the diseases and functions associated with aging. These included cancer as well as neurological disorders and nervous system homeostasis. The mosaics (Fig. 7 E) depict the activation state of specific components in each disease/function group. It is worth noting that the changes associated with J147 are related to decreases in neurological disease and increases in neuronal function and cancer signaling. The whole transcriptome data

also correlated well with the data obtained using the Nano-string technology for inflammatory genes (not shown).

In summary, the RNA analysis strongly complements

the rest of the data presented here and further supports the potential protective effects of J147 on the central nervous system (CNS) by virtue of its ability to rescue specific aspects of aging that are associated with CNS dysfunction with particular relevance to AD.

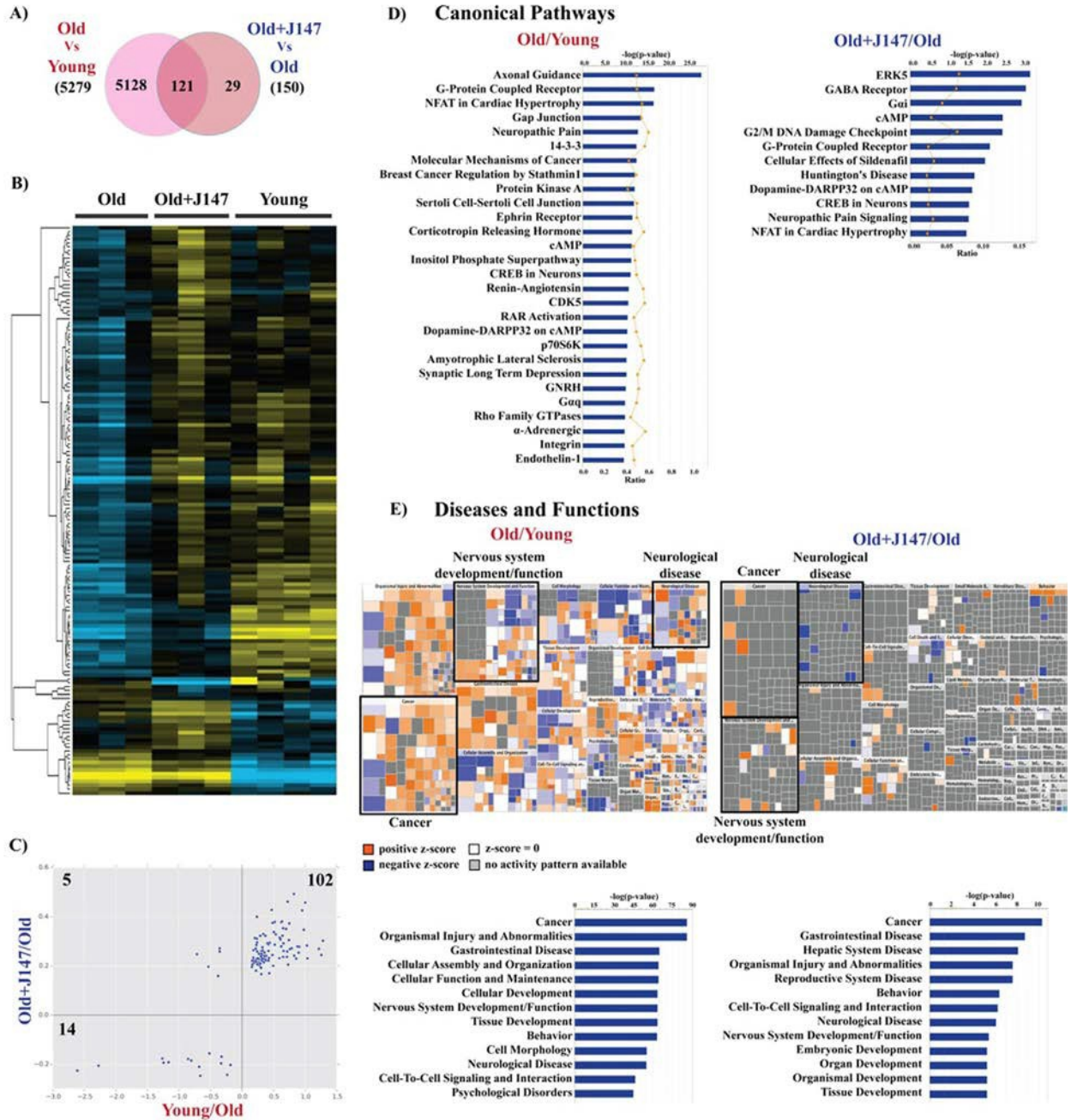


**Figure 7. Whole transcriptome analysis of hippocampus shows a rescue of some age-related changes in RNA expression by J147.** (A) Venn diagram illustrating shared and uniquely affected genes. (B) Heatmap of the 150 genes found significantly modified between Old, Old+J147 and Young SAMP8 mice. Scaled expression value (Z-score) is plotted in yellow–blue color scale with yellow indicating high expression and blue indicating low expression. (n = 3-4/group). (C) Correlation of gene expression altered in Young/Old and Old+J147/Old (units are  $-\log(\text{fold change})$ ). Predicted canonical biological pathways (D) and diseases/functions (E) associated with the alterations in gene expression. Only the top significant pathways are indicated.

## DISCUSSION

We used an integrated multiomics approach to investigate the interaction at the molecular level between an AD drug candidate and aging in the SAMP8 model of aging and early sporadic AD. Our data show that the detrimental changes in behavior that occur with age are accompanied by alterations in protein and RNA expression, as well as in the levels of many key metabolites. Most importantly, our study identifies a large set of parameters in old SAMP8 mice that are associated with stress, vascular pathology, and inflammation that are also observed in human aging and AD. J147 prevented the alteration of many of the metabolic parameters of aging as well as features directly related to the clinical hallmarks of AD, including memory impairment, A $\beta$  content and tau hyperphosphorylation.

SAMP8 mice develop a progressive, age-associated decline in brain function as well as pathophysiological features similar to those found in the brains of sporadic AD patients. Therefore, they may represent an excellent model for studying the relationship between aging and sporadic AD [5, 6]. Our data greatly expand the existing knowledge of the age and AD-associated SAMP8 phenotype at both the brain and system levels. Since the positive effects of J147 in old SAMP8 mice included an improvement in physical and cognitive parameters, reflecting a preservation of their health in general, our results suggest that J147 might be acting by preventing specific metabolic changes that result as a consequence of old age-associated stress.

HSPs represent a major cellular defense against the proteotoxic stress that is characteristic of age-related neurodegenerative disorders. HSP expression depends upon the type of HSP, the disease, cell type and brain region [23]. The changes in HSP40, 60 and 90 observed in the hippocampus of old SAMP8 mice are indicative of stress, and J147 returned the levels of HSP60 and 90 to those of young mice. eIF2 $\alpha$  is also involved in protein homeostasis and potentially AD [9]. J147 returned both its level and phosphorylation state to those of young animals.

One of the most prominent manifestations of stress during aging is the production of inflammatory mediators accompanied by metabolic alterations. Although clinical trials with a few anti-inflammatory drugs failed to prevent AD disease progression, epidemiological studies suggest that long-term use of anti-inflammatory drugs may reduce the risk [12]. The data presented here show an increase in inflammatory parameters in old SAMP8 mice. In the CNS,

inflammation is often characterized by the activation of glial cells, mainly astrocytes and microglia. This age-associated phenotype is characteristic of the AD brain [24]. SAMP8 mice also develop astrogliosis [7], and we demonstrate here that J147 reduces astrocytic reactivity. Microglia are the resident macrophages of the brain and play a central role during inflammation in the aging and AD brains [25]. Although J147 did not reduce the increased number of microglia cells found in the hippocampus of old SAMP8 mice, it reduced activation of the stress-induced SAPK/JNK as well as the RNA expression of a number of markers of inflammation in the brain. Activation of SAPK/JNK is associated with the inflammatory response in activated microglia [26] and it is possible that J147 preserved microglial function without affecting their number.

Interestingly, the altered expression of several components of the complement system in old SAMP8 mice was not changed by J147. This is important given that the complement system is also activated in human AD patients but that it is thought to be part of a neuroprotective response that helps clear apoptotic cells and A $\beta$  peptide [27]. Therefore, there are parts of the innate immune system that may be beneficial in the context of aging and AD. The fact that J147 did not alter the levels of these components yet reduced A $\beta$  levels, inflammation and vascular pathology supports this idea.

A potentially harmful aspect of inflammation in the aging brain is that it may lead to the impairment of vascular integrity and alterations in neuronal homeostasis [13]. Accordingly, aged SAMP8 mice display disrupted BBB permeability [14]. Our data strongly support the idea that neurovascular dysregulation is an important pathophysiological feature of brains from old SAMP8 mice, and that J147 may protect brain function in these old mice at least in part by preserving BBB homeostasis. The evidence includes the reduction in the levels of VCAM-1, the prevention of IgG infiltration into the hippocampus and the modulation of eicosanoids that regulate vascular dynamics.

Also important is the observation that J147 significantly increased the levels of DHA in the brain. DHA is the primary structural fatty acid in the human brain and has been linked to cognitive performance. While low plasma levels of DHA are associated with cognitive decline in elderly and AD patients, higher DHA intake and plasma levels inversely correlate with AD risk [28]. DHA supplementation in aged animals enhances learning and memory, and protects against A $\beta$  and tau pathology in AD mouse models [28-30]. The increase in

DHA with J147 could be a consequence of its reduced oxidation, as suggested by lower levels of its oxidized metabolites HDoHes. Furthermore, a dramatic reduction of other oxidized eicosanoids was also observed with J147 treatment.

Aging is accompanied by strong metabolic alterations at the organismal level that are often associated with mitochondrial dysfunction [21, 31]. Our analysis of the metabolomic profile of the plasma of old SAMP8 mice revealed profound changes in several biological pathways in comparison to the young SAMP mice. The levels of several amino acids and peptides were found lowered in the old SAMP8 mice. These included  $\gamma$ -glutamyl amino acids, dipeptides and the BCAAs.  $\gamma$ -glutamyl amino acids are generated during the  $\gamma$ -glutamyl cycle, which is involved in the transport of glutathione (GSH) between different organs [32]. GSH is the major intracellular antioxidant. Extracellular GSH is usually broken down to its constituent amino acids by the enzyme  $\gamma$ -glutamyl transpeptidase (GGT) and then those are transported across the plasma membrane to regenerate GSH intracellularly [32]. This enzymatic reaction transfers the  $\gamma$ -glutamyl moiety from GSH to acceptor amino acids. The fact that several  $\gamma$ -glutamyl amino acids were lower in the plasma of old SAMP8 could be related to impaired GSH homeostasis in themice.

Amino acid metabolism is of particular relevance to aging because studies with animals and humans strongly suggest that dietary supplementation with essential and branched chain amino acids positively affects physical health and promotes survival [33]. It was proposed that the positive effects of BCAAs are directly associated with improvement of mitochondrial function [33]. J147 restored to young levels many of the alterations in  $\gamma$ -glutamyl amino acids and BCAAs found in the old SAMP8 mice, as well as the levels of several dipeptides.

In a study that compared the plasma metabolome of young with older mice, there was an increase in fatty acids (C18:0 and C20:4 $\omega$ 6) with age [34]. Similarly, old SAMP8 mice have significantly increased levels of both C18:0 and C20:4 $\omega$ 6 (Table S1) as well as many other fatty acids, in particular a large group of PUFAs. However, in contrast with the earlier report, we found striking increases in the levels of several acylcarnitines. This is a very important observation because fatty acids must be transported into the mitochondria using the carnitine shuttle in order to produce energy via  $\beta$ -oxidation. When mitochondrial  $\beta$ -oxidation is defective, plasma levels of acylcarnitines rise, as we found in old SAMP8 mice. That J147 restored the levels of

acylcarnitines suggests a positive effect on mitochondrial dynamics. In addition, it has been shown that acylcarnitines can directly activate pro-inflammatory pathways [35], supporting the idea that J147 also reduces stress-associated inflammation in old age at the systemic level. These data are strengthened by the IPA, which identified diseases related to hepatic dysfunction and inflammatory responses associated with these metabolic alterations.

The analysis of brain metabolites revealed an alteration in glycolysis and the TCA cycle in old SAMP8 mice, further supporting the idea that mitochondrial function is affected with old age. Our data are in accordance with a recent study comparing the metabolome of plasma and CSF of AD patients and cognitively normal age-matched controls, where disturbances in multiple pathways related to energy metabolism and mitochondrial function were identified[36].

J147 had an impact on some of the metabolites within the brain, but this was not as pronounced as those found in the plasma. However, it did restore the reduced levels of glutamate detected in old mice to that of young animals. Glutamate can be synthesized from the TCA intermediate  $\alpha$ -ketoglutarate, which was also restored by J147. Glutamate is the major neurotransmitter in the brain and is involved in learning and memory processes. Studies have shown a decrease in brain glutamate levels with aging [37], as well as in the AD brain [38, 39].

Another metabolite altered in the hippocampus of old SAMP8 mice whose levels were restored by J147 was cAMP. Upregulation of cAMP signaling has been implicated in AD pathophysiology and increased cAMP-PKA signaling in the aging brain is associated with impaired cognition and increased vulnerability to neurodegeneration [22]. PKA is a tau kinase and its dysregulation might be partially responsible for AD-related abnormal tau phosphorylation [40], which could explain in part its increased phosphorylation in the hippocampus of old SAMP8 mice and the protection by J147. PKA signaling was also one of the canonical pathways predicted by the RNA IPA to be affected in old mice.

The relevance of cAMP in the old SAMP8 mice and the therapeutic effect of J147 were validated by the transcriptomic analysis, which identified the cAMP and CREB signaling pathways as being significantly altered. This is a good example of how omic approaches that target different cell physiological components can complement each other in order to provide solid readouts about relevant pathways. Importantly, changes given by J147 were associated with both the cAMP and

CREB signaling pathways, suggesting that J147 might be exerting its protective effects in the brain by preserving the proper function of these pathways. The latter result is in agreement with our previous data showing that CREB, a transcription factor with a crucial role in neuronal plasticity and memory, is activated by J147 [3].

Cancer was one of the top diseases associated with aging predicted by the IPA from both the RNA and metabolite data. Although we have seen no indication of tumorigenesis in our SAMP8 model, it is known that the incidence of cancer increases with age [41]. The changes reported here may thus reflect metabolic alterations associated with cellular senescence, a known contributor to cancer development [41].

An important observation derived from our multiomics approach is that both the metabolomic and transcriptomic analyses revealed that the vast majority of the changes associated with J147 treatment rescued physiological alterations that were observed with aging. These findings strongly suggest that J147 might be lowering the AD-related pathology in old SAMP8 mice by preventing some of the deterioration associated with aging.

The purpose of this study was to combine data derived from different technological approaches to assess the relationship between aging and the therapeutic effects of J147 in the SAMP8 mouse model of aging and sporadic AD. In this regard, the RNA data showed alterations associated with behavior, dysfunction of the nervous system and neurological disease. These predictions given by the IPA not only are in agreement with those found in the metabolite analysis, but also are consistent with the cognitive impairment assessed by the behavioral testing and the changes in proteins required for synaptic function and relevant to AD assessed by Western blotting. The IPA also identified altered pathways in the old SAMP8 mice linked to vascular homeostasis, which are consistent with the increased vascular inflammation and BBB disruption found with aging, as well as with the changes in eicosanoids involved in vascular function.

Overall, the integration of the data acquired with the multiple scientific techniques applied here not only allowed us to identify with a high level of confidence specific pathologies and molecular pathways characteristic of old age and critical in AD, but also to define a subset that are reverted to youthful levels by J147, suggesting that J147 may be effective at treating the primary causes of the disease. Finally, our study strongly supports the use of this and other rodent models of aging that develop AD-related pathology

[42], to address fundamental questions and test new therapeutic interventions.

## METHODS

**Study design.** The aim of this project was to investigate whether the AD drug candidate J147 protects SAMP8 mice from aging and AD-associated pathology and to assay the associated metabolic changes. Seventeen three-month old male SAMP8 mice were fed with control diet (LabDiet 5015, TestDiet, Richmond, IN) and eighteen three-month old male SAMP8 mice were fed with J147 diet (LabDiet 5015 + 200ppm J147, TestDiet) until they reached ten months old. At this age, SAMP8 mice present a strong phenotype [7]. The dose of J147 used was 200 ppm (~10mg/kg/day), which previously proved effective in AD transgenic mice [2, 3]. Fourteen three-month old male SAMP8 mice were used as the young control group. The SAMP8 mice are an inbred strain and, as such, young SAMP8 mice were chosen as controls for young age. Given the seven month duration of the feeding paradigm, the effect of J147 diet could only be assessed in old SAMP8 mice, and any age-related changes defined by the comparison to the young SAMP8 animals. All mice were randomly assigned to experimental groups. The number of mice per group was determined based on previous experiments [7] and was sufficient to attain statistical power. Six old SAMP8 mice fed with control diet and two old SAMP8 mice fed with J147 diet died throughout the course of this study. Behavioral testing was carried out one month prior to sacrifice and collection of biological material. Data were analysed by blinded researchers when appropriate.

**SAMP8 mice.** The SAMP8 line was acquired from Harlan Laboratories (U.K.). Mouse body weights were measured regularly and no significant differences were found between the groups (Fig. S1). All experiments were performed in accordance with the US Public Health Service Guide for Care and Use of Laboratory Animals and protocols approved by the IACUC at the Salk Institute.

**Behavioral assays.** For detailed descriptions of the materials and methods regarding the open field, the elevated plus maze, the object recognition test and the Barnes maze assays, please see supplemental information.

**Tissue preparation.** Mice were anesthetized and their blood collected by cardiac puncture. After perfusing with PBS, their brains were removed. Half of the brain was fixed and processed for histology and the other half was dissected (to collect cortex and hippocampus) and

prepared for Western blot (WB), RNA extraction, eicosanoid and metabolomic analysis.

Western blotting. Western blots were carried out as described previously [43]. A list of the antibodies used can be found in the supplemental information. IgG heavy and light chains were detected by blotting the membrane directly with the mouse secondary antibody.

Immunohistochemistry. Immunohistochemistry was carried out as described previously [43]. Anti-Iba-1 (#019-19741, 1/4000, from Wako) and biotinylated rabbit secondary antibody (#BA1000, 1/400 from Vector Laboratories) were used. Number of microglia per mm<sup>2</sup> of hippocampus was quantified using the Image J software (NIH). Total counts in 2-4 sections per eight mouse brains of each group were determined in an unbiased fashion.

A $\beta$  ELISA. A $\beta$  1-40 and 1-42 levels in hippocampal lysates were analyzed using the A $\beta$ 1-40 and A $\beta$ 1-42 ELISA kits from Invitrogen (# KMB3481 and # KMB3442, respectively).

Eicosanoid analysis. Eicosanoids were prepared and analyzed as described previously [43].

Metabolomic analysis. Metabolomic analyses were conducted at Metabolon as described previously [44]. For statistical analyses and data display, any missing values were assumed to be below the limits of detection and imputed with the compound minimum (minimum value imputation). An estimate of the false discovery rate (Q-value) was calculated to take into account the multiple comparisons that normally occur in metabolomic-based studies, with  $Q < 0.05$  used as an indication of high confidence in a result.

RNA analysis. RNA was isolated from hippocampus using the RNeasy Plus Universal mini kit (Qiagen) and RNA analysis performed by Nanostring.

Nanostring. The nCounter GX Mouse Inflammation Kit (Nanostring, Seattle, USA) was used to measure a comprehensive set of 248 inflammation related mouse genes and six internal reference genes.

Whole transcriptome analysis. RNA-Seq libraries were prepared using the Illumina TruSeq Stranded mRNA Sample Prep Kit according to the manufacturer's instructions. Briefly, poly-A RNA was selected using poly dT-beads. mRNA was then fragmented and reverse transcribed. cDNA was end-repaired, adenylated and ligated with Illumina adapters with indexes. Adapter-ligated cDNA was then amplified. Libraries were

pooled and sequenced single-end 50 base-pair (bp) on the Illumina HiSeq 2500 platform. Sequencing reads were mapped to the mm9 mouse genome using the spliced aligner STAR (2.3.0e) with default parameters [45]. Indices for the alignment were built using the Illumina iGenomes gene annotation for mm9 as a splice junction database and the sjdbOverhang parameter set to 100. Raw gene-level read counts were calculated using this same gene annotation with feature Counts (1.4.6) from the Subread package [46]. Expression normalization and differential analysis were carried out with DESeq2, using a false discovery rate cut-off of 0.1 [47]. The data discussed in this publication have been deposited in NCBI's Gene Expression Omnibus [48] and are accessible through GEO Series accession number GSE69244 (<http://www.ncbi.nlm.nih.gov/geo/query/acc.cgi?acc=GSE69244>).

Bioinformatics and statistics. Data in figures is presented as group mean  $\pm$  SD or as box-and-whisker plots indicating the group minimum, lower quartile, median, upper quartile, and group maximum. Data from the Western blotting and eicosanoids analyses were normalized to the average of the young SAMP8 control group. For metabolites, the measured values across the three groups were median-normalized to 1.

Data were analysed and the functional/network analyses were generated through the use of QIAGEN's Ingenuity Pathway Analysis (IPA<sup>®</sup>, QIAGEN Redwood City, [www.qiagen.com/ingenuity](http://www.qiagen.com/ingenuity)).

Metaboanalyst [49] was used to generate the heatmaps. Values were mean-centered and divided by the SD of each variable (scaled Z-score). Hierarchical clustering of RNA expression was performed using Euclidean distances and the Ward algorithm.

Statistical analysis of the three groups was carried out by one-way ANOVA followed by Tukey-Kramer multiple comparison *post hoc* test was used. For data regarding multiple time points, two-way repeated-measures ANOVA and post hoc Bonferroni corrected *t* tests were applied. GraphPad Prism 6 was used and exact *P* values are indicated (for  $P < 0.050$ ). All data are mean  $\pm$  SD.

## ACKNOWLEDGEMENT

We thank Joseph Chambers, Maria Encizo and Karen Suter for most valuable help with breeding and husbandry of mice; the Waitt Advanced Biophotonics Center; Dr. Amandine Chaix for support on the metabolomic analysis.

## Funding

This study was supported by the Salk Institute Pioneer Fund Postdoctoral Scholar Award and the Salk Nomis Fellowship Award (AC), fellowships from the Hewitt Foundation (JG) and Bundy Foundation (MP), and grants from the Alzheimer's Association, Burns Foundation and NIH (RO1 AG046153 and RO1 AG035055) to PM and DS.

## Conflict of interest statement

Salk has an issued patent on J147 licensed to Abrexa Pharmaceuticals. MP and DS are scientific advisors for Abrexa.

## REFERENCES

1. Prior M, Chiruta C, Currais A, Goldberg J, Ramsey J, Dargusch R, Maher PA and Schubert D. Back to the future with phenotypic screening. *ACS Chem Neurosci*. 2014;5:503-513.
2. Chen Q, Prior M, Dargusch R, Roberts A, Riek R, Eichmann C, Chiruta C, Akaishi T, Abe K, Maher P and Schubert D. A novel neurotrophic drug for cognitive enhancement and Alzheimer's disease. *PLoS One*. 2011;6:e27865.
3. Prior M, Dargusch R, Ehren JL, Chiruta C and Schubert D. The neurotrophic compound J147 reverses cognitive impairment in aged Alzheimer's disease mice. *Alzheimers Res Ther*. 2013;5:25.
4. Swerdlow RH. Is aging part of Alzheimer's disease, or is Alzheimer's disease part of aging? *Neurobiol Aging*. 2007;28:1465-1480.
5. Cheng XR, Zhou WX and Zhang YX. The behavioral, pathological and therapeutic features of the senescence-accelerated mouse prone 8 strain as an Alzheimer's disease animal model. *Ageing Res Rev*. 2014;13:13-37.
6. Morley JE, Armbrecht HJ, Farr SA and Kumar VB. The senescence accelerated mouse (SAMP8) as a model for oxidative stress and Alzheimer's disease. *Biochim Biophys Acta*. 2012;1822:650-656.
7. Currais A, Prior M, Lo D, Jolival C, Schubert D and Maher P. Diabetes exacerbates amyloid and neurovascular pathology in aging-accelerated mice. *Ageing Cell*. 2012;11:1017-1026.
8. Morley JE, Farr SA, Kumar VB and Armbrecht HJ. The SAMP8 mouse: a model to develop therapeutic interventions for Alzheimer's disease. *Curr Pharm Des*. 2012;18:1123-1130.
9. Chang RC, Wong AK, Ng HK and Hugon J. Phosphorylation of eukaryotic initiation factor-2alpha (eIF2alpha) is associated with neuronal degeneration in Alzheimer's disease. *Neuroreport*. 2002;13:2429-2432.
10. Thinakaran G and Koo EH. Amyloid precursor protein trafficking, processing, and function. *J Biol Chem*. 2008;283:29615-29619.
11. Ikura Y, Kudo T, Tanaka T, Tanii H, Grundke-Iqbal I, Iqbal K and Takeda M. Levels of tau phosphorylation at different sites in Alzheimer disease brain. *Neuroreport*. 1998;9:2375-2379.
12. Wyss-Coray T and Rogers J. Inflammation in Alzheimer disease—a brief review of the basic science and clinical literature. *Cold Spring Harb Perspect Med*. 2012;2:a006346.
13. Grammas P. Neurovascular dysfunction, inflammation and endothelial activation: implications for the pathogenesis of Alzheimer's disease. *J Neuroinflammation*. 2011;8:26.
14. Pelegri C, Canudas AM, del Valle J, Casadesus G, Smith MA, Camins A, Pallas M and Vilaplana J. Increased permeability of blood-brain barrier on the hippocampus of a murine model of senescence. *Mech Ageing Dev*. 2007;128:522-528.
15. Rodriguez JJ, Olabarria M, Chvatal A and Verkhratsky A. Astroglia in dementia and Alzheimer's disease. *Cell Death Differ*. 2009;16:378-385.
16. Ploia C, Antoniou X, Sclip A, Grande V, Cardinetti D, Colombo A, Canu N, Benussi L, Ghidoni R, Forloni G and Borsello T. JNK plays a key role in tau hyperphosphorylation in Alzheimer's disease models. *J Alzheimers Dis*. 2011;26:315-329.
17. Buczynski MW, Dumlao DS and Dennis EA. Thematic Review Series: Proteomics. An integrated omics analysis of eicosanoid biology. *J Lipid Res*. 2009;50:1015-1038.
18. Morin C, Fortin S and Rousseau E. 19,20-EpDPE, a bioactive CYP450 metabolite of DHA monoacylglyceride, decreases Ca(2)(+) sensitivity in human pulmonary arteries. *Am J Physiol Heart Circ Physiol*. 2011;301:H1311-1318.
19. Viswanathan S, Hammock BD, Newman JW, Meerarani P, Toborek M and Hennig B. Involvement of CYP 2C9 in mediating the proinflammatory effects of linoleic acid in vascular endothelial cells. *J Am Coll Nutr*. 2003;22:502-510.
20. Hardwick JP, Eckman K, Lee YK, Abdelmegeed MA, Esterle A, Chilian WM, Chiang JY and Song BJ. Eicosanoids in metabolic syndrome. *Adv Pharmacol*. 2013;66:157-266.
21. Lin MT and Beal MF. Mitochondrial dysfunction and oxidative stress in neurodegenerative diseases. *Nature*. 2006;443:787-795.
22. Carlyle BC, Nairn AC, Wang M, Yang Y, Jin LE, Simen AA, Ramos BP, Bordner KA, Craft GE, Davies P, Pletikos M, Sestan N, Arnsten AF, et al. cAMP-PKA phosphorylation of tau confers risk for degeneration in aging association cortex. *Proc Natl Acad Sci U S A*. 2014;111:5036-5041.
23. Leak RK. Heat shock proteins in neurodegenerative disorders and aging. *J Cell Commun Signal*. 2014.
24. Li C, Zhao R, Gao K, Wei Z, Yin MY, Lau LT, Chui D and Hoi Yu AC. Astrocytes: implications for neuroinflammatory pathogenesis of Alzheimer's disease. *Curr Alzheimer Res*. 2011;8:67-80.
25. Mosher KI and Wyss-Coray T. Microglial dysfunction in brain aging and Alzheimer's disease. *Biochem Pharmacol*. 2014;88:594-604.
26. Waetzig V, Czeloth K, Hidding U, Mielke K, Kanzow M, Brecht S, Goetz M, Lucius R, Herdegen T and Hanisch UK. c-Jun N-terminal kinases (JNKs) mediate pro-inflammatory actions of microglia. *Glia*. 2005;50:235-246.
27. Rubio-Perez JM and Morillas-Ruiz JM. A review: inflammatory process in Alzheimer's disease, role of cytokines. *ScientificWorldJournal*. 2012;2012:756357.
28. Yurko-Mauro K. Cognitive and cardiovascular benefits of docosahexaenoic acid in aging and cognitive decline. *Curr Alzheimer Res*. 2010;7:190-196.
29. Green KN, Martinez-Coria H, Khashwji H, Hall EB, Yurko-Mauro KA, Ellis L and LaFerla FM. Dietary docosahexaenoic acid and docosapentaenoic acid ameliorate amyloid-beta and tau pathology via a mechanism involving presenilin 1 levels. *J Neurosci*. 2007;27:4385-4395.

30. Lim GP, Calon F, Morihara T, Yang F, Teter B, Ubeda O, Salem N, Jr., Frautschy SA and Cole GM. A diet enriched with the omega-3 fatty acid docosahexaenoic acid reduces amyloid burden in an aged Alzheimer mouse model. *J Neurosci.* 2005; 25:3032-3040.
31. Navarro A and Boveris A. Brain mitochondrial dysfunction in aging, neurodegeneration, and Parkinson's disease. *Front Aging Neurosci.* 2010; 2:1-11.
32. Zhang H, Forman HJ and Choi J. Gamma-glutamyl transpeptidase in glutathione biosynthesis. *Methods Enzymol.* 2005; 401:468-483.
33. Valerio A, D'Antona G and Nisoli E. Branched-chain amino acids, mitochondrial biogenesis, and healthspan: an evolutionary perspective. *Aging (Albany NY).* 2011; 3:464-478.
34. Houtkooper RH, Argmann C, Houten SM, Canto C, Jenjira EH, Andreux PA, Thomas C, Doenlen R, Schoonjans K and Auwerx J. The metabolic footprint of aging in mice. *Sci Rep.* 2011; 1:134.
35. Rutkowski JM, Knotts TA, Ono-Moore KD, McCoin CS, Huang S, Schneider D, Singh S, Adams SH and Hwang DH. Acylcarnitines activate proinflammatory signaling pathways. *Am J Physiol Endocrinol Metab.* 2014; 306:E1378-1387.
36. Trushina E, Dutta T, Persson XM, Mielke MM and Petersen RC. Identification of altered metabolic pathways in plasma and CSF in mild cognitive impairment and Alzheimer's disease using metabolomics. *PLoS One.* 2013; 8:e63644.
37. Zahr NM, Mayer D, Pfefferbaum A and Sullivan EV. Low striatal glutamate levels underlie cognitive decline in the elderly: evidence from in vivo molecular spectroscopy. *Cereb Cortex.* 2008; 18:2241-2250.
38. Fayed N, Modrego PJ, Rojas-Salinas G and Aguilar K. Brain glutamate levels are decreased in Alzheimer's disease: a magnetic resonance spectroscopy study. *Am J Alzheimers Dis Other Dement.* 2011; 26(6):450-456.
39. Rupsingh R, Borrie M, Smith M, Wells JL and Bartha R. Reduced hippocampal glutamate in Alzheimer disease. *Neurobiol Aging.* 2011; 32:802-810.
40. Liu F, Liang Z, Shi J, Yin D, El-Akkad E, Grundke-Iqbal I, Iqbal K and Gong CX. PKA modulates GSK-3 $\beta$ - and cdk5-catalyzed phosphorylation of tau in site- and kinase-specific manners. *FEBS Lett.* 2006; 580:6269-6274.
41. de Magalhaes JP. How ageing processes influence cancer. *Nat Rev Cancer.* 2013; 13:357-365.
42. Stefanova NA, Muraleva NA, Korbolina EE, Kiseleva E, Maksimova KY and Kolosova NG. Amyloid accumulation is a late event in sporadic Alzheimer's disease-like pathology in nontransgenic rats. *Oncotarget.* 2015; 6:1396-1413.
43. Currais A, Prior M, Dargusch R, Armando A, Ehren J, Schubert D, Quehenberger O and Maher P. Modulation of p25 and inflammatory pathways by fisetin maintains cognitive function in Alzheimer's disease transgenic mice. *Aging Cell.* 2014; 13:379-390.
44. Shin SY, Fauman EB, Petersen AK, Krumsiek J, Santos R, Huang J, Arnold M, Erte I, Forgetta V, Yang TP, Walter K, Menni C, Chen L, et al. An atlas of genetic influences on human blood metabolites. *Nat Genet.* 2014; 46:543-550.
45. Dobin A, Davis CA, Schlesinger F, Drenkow J, Zaleski C, Jha S, Batut P, Chaisson M and Gingeras TR. STAR: ultrafast universal RNA-seq aligner. *Bioinformatics.* 2013; 29:15-21.
46. Liao Y, Smyth GK and Shi W. featureCounts: an efficient general purpose program for assigning sequence reads to genomic features. *Bioinformatics.* 2014; 30:923-930.
47. Love MI, Huber W and Anders S. Moderated estimation of fold change and dispersion for RNA-seq data with DESeq2. *Genome Biol.* 2014; 15:550.
48. Edgar R, Domrachev M and Lash AE. Gene Expression Omnibus: NCBI gene expression and hybridization array data repository. *Nucleic Acids Res.* 2002; 30(1):207-210.
49. Xia J, Mandal R, Sinelnikov IV, Broadhurst D and Wishart DS. MetaboAnalyst 2.0--a comprehensive server for metabolomic data analysis. *Nucleic Acids Res.* 2012; 40:W127-133.

## Defective mitochondrial respiration, altered dNTP pools and reduced AP endonuclease 1 activity in peripheral blood mononuclear cells of Alzheimer's disease patients

Scott Maynard<sup>1,\*</sup>, Anne-Mette Hejl<sup>2</sup>, Thuan-Son T. Dinh<sup>1</sup>, Guido Keijzers<sup>1</sup>, Åse M. Hansen<sup>3,4</sup>, Claus Desler<sup>1</sup>, Maria Moreno-Villanueva<sup>5</sup>, Alexander Bürkle<sup>5</sup>, Lene J. Rasmussen<sup>1</sup>, Gunhild Waldemar<sup>2</sup>, and Vilhelm A. Bohr<sup>1,6</sup>

<sup>1</sup>Department of Cellular and Molecular Medicine, Center for Healthy Aging, University of Copenhagen, 2200 Copenhagen, Denmark

<sup>2</sup>Department of Neurology, Danish Dementia Research Centre, Rigshospitalet, University of Copenhagen, 2100 Copenhagen, Denmark

<sup>3</sup>Department of Public Health, University of Copenhagen, 1014 Copenhagen, Denmark

<sup>4</sup>The National Research Centre for the Working Environment, 2100 Copenhagen, Denmark

<sup>5</sup>Molecular Toxicology Group, University of Konstanz, D-78457 Konstanz, Germany

<sup>6</sup>Laboratory of Molecular Gerontology, National Institute on Aging, National Institutes of Health, Baltimore, MD 21224-6825, USA

\*Present address: Danish Cancer Society Research Center, 2100 Copenhagen, Denmark

**Key words:** Alzheimer's disease; APE1; bioenergetics; dNTP pools; DNA repair; mitochondria; peripheral blood mononuclear cells; reactive oxygen species

**Abbreviations:** AD, Alzheimer's disease; APE1, AP-endonuclease 1; BER, base excision repair; dNTPs, deoxyribonucleoside triphosphates; ECAR, extracellular acidification rate; MMSE, mini-mental state examination; OCR, oxygen consumption rate; OGG1, 8-oxoG DNA glycosylase 1; PBMC, peripheral blood mononuclear cells; ROS, reactive oxygen species

**Received:** 08/25/15; **Accepted:** 09/15/15; **Published:** 10/21/15 **doi:** [10.18632/aging.100810](https://doi.org/10.18632/aging.100810)

**Correspondence to:** Scott Maynard, PhD; **E-mail:** [scottm@cancer.dk](mailto:scottm@cancer.dk)

**Copyright:** Maynard et al. This is an open-access article distributed under the terms of the Creative Commons Attribution License, which permits unrestricted use, distribution, and reproduction in any medium, provided the original author and source are credited

**Abstract:** **AIMS:** Accurate biomarkers for early diagnosis of Alzheimer's disease (AD) are badly needed. Recent reports suggest that dysfunctional mitochondria and DNA damage are associated with AD development. In this report, we measured various cellular parameters, related to mitochondrial bioenergetics and DNA damage, in peripheral blood mononuclear cells (PBMCs) of AD and control participants, for biomarker discovery.

**METHODS:** PBMCs were isolated from 53 patients with AD of mild to moderate degree and 30 age-matched healthy controls. Tests were performed on the PBMCs from as many of these participants as possible. We measured glycolysis and mitochondrial respiration fluxes using the Seahorse Bioscience flux analyzer, mitochondrial ROS production using flow cytometry, dNTP levels by way of a DNA polymerization assay, DNA strand breaks using the Fluorometric detection of Alkaline DNA Unwinding (FADU) assay, and APE1 incision activity (in cell lysates) on a DNA substrate containing an AP site (to estimate DNA repair efficiency).

**RESULTS:** In the PBMCs of AD patients, we found reduced basal mitochondrial oxygen consumption, reduced proton leak, higher dATP level, and lower AP endonuclease 1 activity, depending on adjustments for gender and/or age.

**CONCLUSIONS:** This study reveals impaired mitochondrial respiration, altered dNTP pools and reduced DNA repair activity in PBMCs of AD patients, thus suggesting that these biochemical activities may be useful as biomarkers for AD.

## INTRODUCTION

Current diagnosis of Alzheimer's disease (AD) is based on clinical examination, neuropsychological testing and brain imaging; however, a definite diagnosis can only be made by postmortem examination. Although brain imaging and cerebrospinal fluid biomarkers are applied in patients with mild or questionable symptoms to increase the level of diagnostic certainty, no definitive diagnostic tests based on peripheral biofluids are available yet. Biomarkers that reliably predict AD would greatly assist preventative and management treatments. Several reports describe alterations in peripheral blood cell DNA repair, reactive oxygen species (ROS) production and mitochondrial activities in AD patients [1-4], suggesting that these biochemical activities could potentially serve as peripheral biomarkers for early detection of AD. In fact, mitochondrial electron transport chain dysfunction and oxidative DNA damage are associated with amyloid beta (A $\beta$ ) and tau pathologies and neuronal damage in AD [5]. Because neurons have a high rate of oxygen consumption and low levels of antioxidants, they are particularly susceptible to ROS-induced oxidative DNA damage [6]. Mitochondrial dysfunction has been demonstrated in the neurons of AD patients [7] and further shown to be linked to alterations in ROS production [8]; many of these biochemical defects in the brain appear to be reflected in peripheral blood cells [9]. Reports suggest that mitochondria are central players in maintaining genomic stability by controlling a balanced supply of deoxyribonucleoside triphosphates (dNTPs) [10, 11], the substrates for DNA polymerizing enzymes. Thus, mitochondrial dysfunction in AD cells may be reflected by altered dNTP ratios (i.e. imbalance in dNTP pools). There are no published reports on dNTP pools in AD cohorts. However, recent published data from our group points to the potential utility of dNTP levels as peripheral indicators of probable disease, by revealing that low subjective vitality is linked to both a lower dCTP and higher dTTP level [12].

Deficiencies in DNA repair of nuclear and mitochondrial DNA damage have been linked to several neurodegenerative disorders [13]. Base excision repair (BER) is the main DNA repair pathway for removing oxidative DNA lesions, such as the prolific 8-oxoguanine (8-oxoG) lesion. During BER, a glycosylase enzyme (such as 8-oxoG DNA glycosylase 1; OGG1) excises the damaged base to yield an apurinic/apyrimidinic (AP) site. This AP-site is then incised by AP-endonuclease 1 (APE1). Polymerase and ligase proteins complete the repair in processes overlapping with those used in single strand break repair [14]. We recently reported that a new

mouse model of AD, generated from a cross of a common AD mouse model (3xTgAD) with a mouse heterozygous for the BER enzyme DNA polymerase  $\beta$  (Pol $\beta$ ), had aggravated features of AD relative to the 3xTgAD mouse [15]: the reduction in Pol $\beta$  in these 3xTg/Pol $\beta$  mice induced neuronal dysfunction, cell death, and impaired memory and synaptic plasticity. This is consistent with a previous study showing that cortical neurons isolated from OGG1-deficient mice showed enhanced oxidative DNA base lesions and cell death under ischemic conditions [16].

Defective expression or function of proteins required for BER or proteins that regulate BER have been consistently associated with neurological dysfunction and disease in humans [17]. Studies report defects in BER in AD brain [18, 19] and AD lymphocytes [20, 21], and reduced capacity to remove oxidative lesions in cultured neural stem/progenitor cells as they undergo differentiation [22, 23]. Previously, we measured BER activities in brain specimens from patients with AD and from normal controls, and found that several BER enzyme activities were deficient in AD brain regions, specifically uracil incision activity (i.e. enzyme activity of uracil DNA glycosylase, UDG), single nucleotide gap filling (i.e. DNA polymerase  $\beta$  activity), and 8-oxoG incision activity (i.e. enzyme activity of OGG1) [19]; these results were consistent with previous reports of lower UDG activity [24] and lower OGG1 activity [25] in AD brain. However, in our study, the AP-site incision activity (APE1 activity) was not altered in AD brains relative to control brains; this differs from previous reports of increased APE1 expression in AD brain [26, 27]. Notably, only expression levels, and not APE1 activity, were reported in the previous studies. However, a study by Huang et al. [28] demonstrated that Cdk5-mediated attenuation of APE1 incision activity resulting in the accumulation of DNA damage and enhanced neuronal death in cultured cortical neurons; this suggests that the neuronal death seen in AD may in part be caused by defective APE1 activity.

In light of the above, we investigated cellular bioenergetics respiratory fluxes (to estimate glycolysis and mitochondrial respiration), mitochondrial ROS production, dNTP levels (to look for imbalance in the dNTP pools), DNA strand breaks (estimate of DNA damage) and APE1 incision activity on a DNA substrate containing an AP site (estimate of BER), as potential peripheral biomarkers of AD. We adjusted for gender and/or age, both of which are known risk factors in AD (higher risk in women is likely mostly due to their longer lifespan [29]).

## RESULTS

### Comparison of PBMC biochemical parameters in AD and control participants

Demographic and clinical characteristics of the cohort are outlined in Table 1. There was no significant difference in age between the two groups. The higher number of AD compared to controls (53 and 30, respectively) was due to practical issues. The average MMSE score of 22.9 (+/- 4.2) is indicative of the patient selection of mild to moderate AD; a score of 23 or lower, out of a maximum of 30, suggests cognitive impairment. Mean values obtained for the various parameters in control and AD groups are presented in Table 2. We measured mitochondrial oxygen consumption rates (OCRs; respiratory parameters that estimate the efficiency of mitochondrial respiration [38]; specifically basal OCR, ATP turnover, reserve capacity, maximum capacity, and proton leak), extracellular acidification rates (ECARs; parameters that estimate of the level of glycolysis [38]; specifically basal ECAR and glycolytic reserve), levels of the four dTNPs (dTTP, dATP, dGTP, dCTP), DNA strand breaks, and APE1 DNA incision activity (indicator of DNA base excision repair capability) in the seeded PMBCs. Outcomes ( $R^2$  and  $P$  values) were either unadjusted (model 1), or adjusted for gender (model 2), age (model 3) or for both gender and age (model 4). The mean values and confidence intervals for models 2, 3 and 4 were slightly altered as expected and are shown in Supplemental Tables S1, S2 and S3, respectively; the relevant outcomes ( $R^2$  and  $P$  values) based on the average values obtained for all models are shown in Table 2. Basal OCR was significantly lower in AD, after adjustment for age (model 3;  $P = .037$ ) and after adjustment for both gender and age (model 4;  $P = .023$ ).

**Table 1.** Participant characteristics

Characteristic	Controls	Alzheimer
Population number, N	30	53
Age (mean/SD)	66.0 (8.7)	69.2 (9.6)
Sex (M/F in percent)	40/60	43/57
MMSE (mean/SD)	-	22.9 (4.2)

Abbreviation: MMSE, Mini Mental State Examination; SD, standard deviation. As many as possible of the cohort participants were used for the various tests performed in this study (see Table 2).

Proton leak was significantly lower in AD, with or without the adjustments ( $P = .039, .033, .030, .024$  for models 1, 2, 3, 4, respectively). The dATP level was significantly higher in AD, without adjustment (model 1;  $P = .039$ ) and after adjustment for gender (model 2;  $P = .035$ ). The APE1 activity was significantly lower in AD, with no adjustment (model 1;  $P = .035$ ), adjustment for gender (model 2;  $P = .003$ ) and adjustment for both gender and age (model 4;  $P = .006$ ). Gel images of the APE1 activity assays are shown in Figure 1A. The graphical form of the APE1 data for each model is shown in Figure 1B; since model 1 has no statistical adjustments, we were able to display the results as a dot plot to illustrate the raw values for each participant.

### Effects of gender, age and MMSE on the parameters

We also stratified the data of the cohort into two groups, men and women, and found that women had a significantly higher mitochondrial maximum capacity, lower ROS production and lower APE1 activity (Figure 2A). In addition to the significant effect on maximum capacity, there was an apparent trend for higher levels of the other four OCR parameters in women. We also stratified for both gender and control/AD (Figure 2B); crossover of the trend lines, or large differences in the slopes of the lines, would suggest that the differences in the parameter levels between men and women that we saw in Figure 2A may be group (control, AD) specific, or that the differences in the parameter levels between control and AD that we saw in Table 2 may in fact be gender specific. This approach reduces the statistical power due to lower population numbers, and in fact we found significant differences by this approach only in the case of the APE1 incision parameter, as follows. The significantly lower APE1 activity observed in women for the entire cohort (control plus AD) (Figure 2A) was recapitulated in the control group ( $P = .007$ ) and the AD group ( $P = .046$ ) (see Figure 2B) and thus is not strongly group specific. We also found a significant difference in the APE1 level between controls and AD in the case of men ( $P = .021$ ), but the difference was not significant in the case of women ( $P = .082$ ), suggesting that the lower APE1 activity in AD as tabulated in Table 2 may have some degree of gender specificity. This is consistent with the improved  $P$  value obtained when we corrected for gender in Table 2 ( $P = .003$  compared to unadjusted  $P$  value of  $.035$ ). The trendlines for the other parameters, although showing no statistical significance, may be informative. Notably, in the case of each of the OCR parameters, the slopes of the men and women lines are similar, indicating that the trends for higher OCRs in women that we see in the “control plus AD” cohort of Figure 2A are not specific for

control or AD groups. In the case of glycolytic reserve, dTTP, and dGTP, the trend lines have obvious crossover, indicating group (control, AD) specificity; such crossovers indicate that the gender-specific differences in the “control plus AD” cohort (Figure 2A) for these parameters are blunted by the use of both controls and AD in the Figure 2A analysis. In the case of ROS produc-

tion there was no obvious difference between men and women in the AD group, however, there was an apparently higher level in men in the control group (Figure 2B). These ROS production trend lines, albeit not significant, suggest that the lower ROS production in women seen in Figure 2A may be mediated by the control participants.

**Table 2.** Levels of various biochemical parameters in PBMCs of AD and control participants, before and after adjustments for gender, age, and for both gender and age

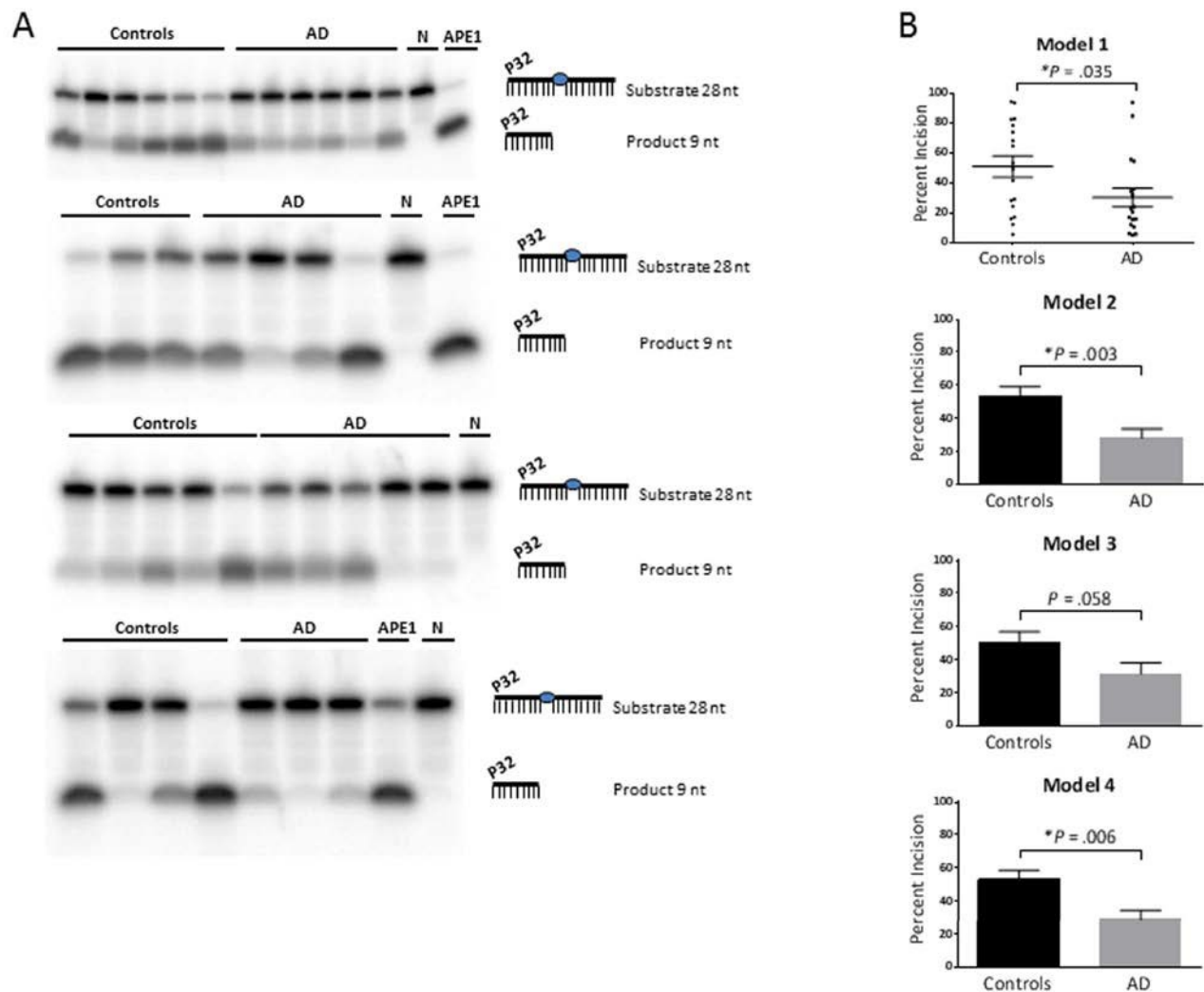
Variable	N	Model 1				Model 2†		Model 3†		Model 4†	
		Mean (± SEM)	95% CI	R <sup>2</sup>	P						
Basal OCR	C 25	45.39 (16.36)	38.77-52.02	0.041	.096	0.1	.071	0.092	.037*	0.157	.023*
	AD 43	38.34 (16.72)	33.30-43.40								
ATP turnover	C 25	36.85 (13.59)	31.42-42.28	0.013	.357	0.06	.303	0.059	.183	0.111	.140
	AD 43	33.67 (13.61)	29.53-37.81								
Reserve capacity	C 25	21.80 (19.06)	12.98-30.62	0.032	.146	0.053	.163	0.038	.213	0.061	.242
	AD 43	29.98 (23.65)	23.25-36.70								
Maximum capacity	C 25	67.20 (30.21)	55.22-79.18	0.000	.882	0.061	.965	0.036	.820	0.102	.710
	AD 43	68.32 (29.88)	59.19-77.46								
Proton leak	C 25	8.56 (5.93)	6.47-10.65	0.063	.039*	0.086	.033*	0.07	.03*	0.095	.024*
	AD 43	5.78 (4.79)	4.19-7.37								
Basal ECAR	C 25	5.73 (1.84)	4.73-6.73	0.016	.297	0.039	.287	0.05	.508	0.071	.492
	AD 43	6.39 (2.82)	5.63-7.16								
Glycolytic reserve	C 25	5.08 (2.42)	4.10-6.07	0.002	.729	0.004	.735	0.01	.873	0.012	.880
	AD 43	5.30 (2.49)	4.55-6.05								
ROS production	C 16	8.76 (5.01)	6.77-10.76	0.082	.077	0.176	.087	0.089	.069	0.181	.080
	AD 23	6.43 (2.99)	4.77-8.10								
dTTP	C 27	0.92 (0.85)	0.58-1.26	0.03	.205	0.032	.204	0.05	.264	0.05	.272
	AD 28	1.22 (0.91)	0.89-1.56								
dATP	C 27	8.73 (3.64)	7.42-10.04	0.078	.039*	0.094	.035*	0.109	.060	0.116	.055
	AD 28	10.66 (3.14)	9.38-11.95								
dGTP	C 27	4.87 (1.70)	4.04-5.71	0.004	.663	0.004	.666	0.024	.772	0.025	.797
	AD 28	5.13 (2.52)	4.31-5.94								
dCTP	C 27	1.50 (0.91)	1.17-1.83	0.001	.791	0.044	.721	0.003	.830	0.044	.711
	AD 28	1.44 (0.82)	1.11-1.76								
DNA Strand breaks	C 26	37.60 (8.98)	34.21-40.99	0.001	.808	0.012	.749	0.001	.832	0.013	.780
	AD 44	38.12 (8.49)	35.52-40.73								
APE1 activity	C 18	50.93 (29.81)	37.52-64.35	0.124	.035*	0.389	.003*	0.15	.059	0.399	.006*
	AD 18	30.47 (26.08)	17.05-43.88								

Model 1, no adjustment; Model 2, adjusted for gender; Model 3, adjusted for age; Model 4, adjusted for both gender and age. Abbreviations: OCR, oxygen consumption rate; ECAR, extracellular acidification rate; C, normal control participants; AD, Alzheimer's disease participants; N, population number; SEM, standard error of the mean.

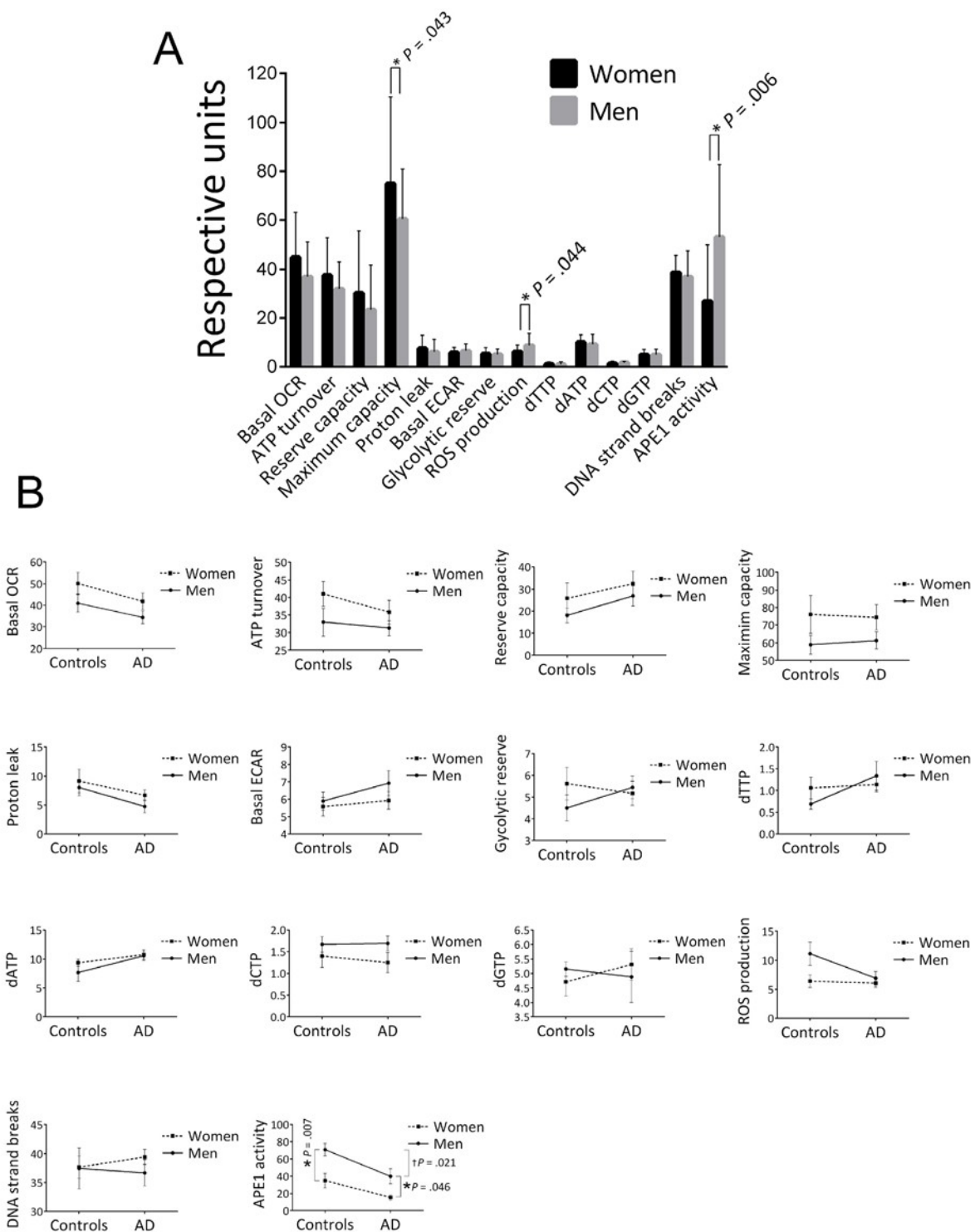
Units: OCRs (Basal OCR, ATP turnover, Reserve capacity, Maximum capacity, Proton leak), pmol oxygen/min; ECARs (Basal ECAR, Glycolytic reserve), mpH/min; ROS production, fluorescence; dNTPs, pmol/million cells; DNA strand breaks, percent fluorescence; APE1 activity, percent incision.

\*Significant difference ( $P < .05$ ).

†Mean/SEM and 95% CI for model 2, 3 and 4 are shown in Supplemental Tables S1, S2 and S3, respectively.



**Figure 1. APE1 activity levels.** The average APE1 activity is significantly lower in the AD group relative to the control group, without statistical adjustment (model 1) and after adjustment for gender (model 2) and both gender and age (model 4); and trended lower after adjustment for age (model 3). **(A)** Gel images of radiolabeled DNA substrate and incision product, indicating the APE1 incision activities in PBMCs from AD patients and controls. The combined data from the four gels is equivalent to N of 18 for each (controls and AD). Samples were run on triplicate gels so that each value is the average of three lanes, run on separate gels; one gel from each triplicate is shown. APE1 = purified enzyme as positive control; N = negative control (no enzyme). **(B)** Comparison of APE1 incision activities in PBMCs from AD patients and controls, as generated from band intensities of 1A, and adjusted for gender and/or age. Percent incision was calculated as the amount of radioactivity in the product relative to total radioactivity per assay. Background correction was performed using no-enzyme control. *P* values were determined using the unpaired t test; the *P* values for models 2, 3, 4 above were generated in GraphPad Prism 6 using the average and SEM from Table 2. All graphs were generated in GraphPad Prism 6. Error bars represent  $\pm$  SEM. As shown here and in Table 2, APE1 activity is significantly lower in AD in models 1, 2 and 4. Since model 1 has no statistical adjustments, it can be displayed as a dot plot to illustrate the raw values for each participant. \*Significant difference ( $P < .05$ ) in the average level of APE1 activity between the controls and AD.

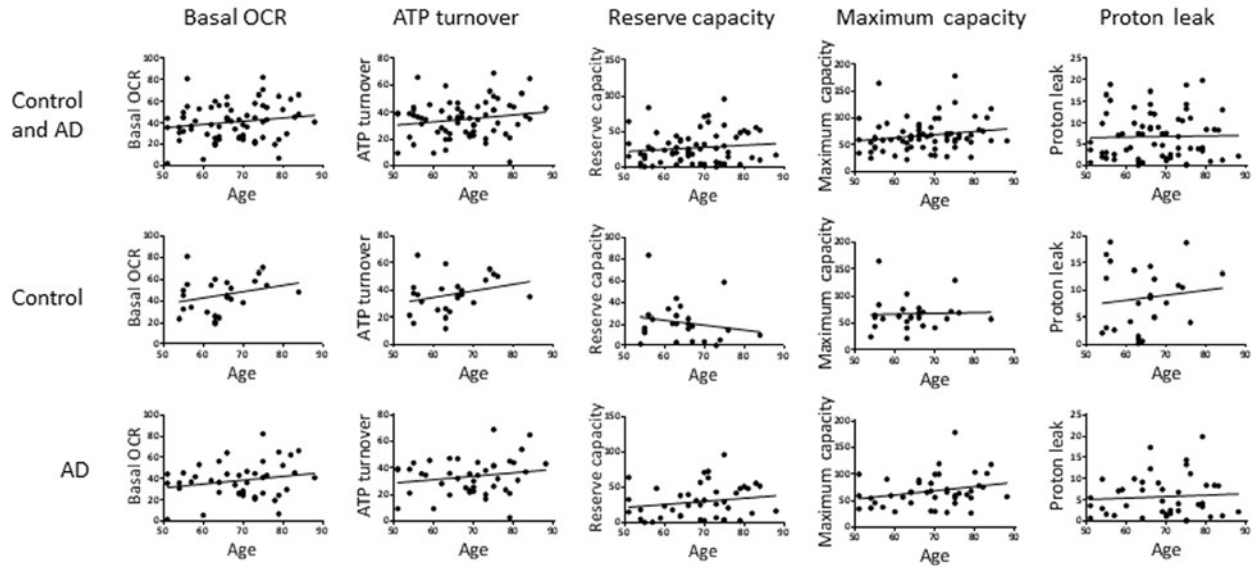
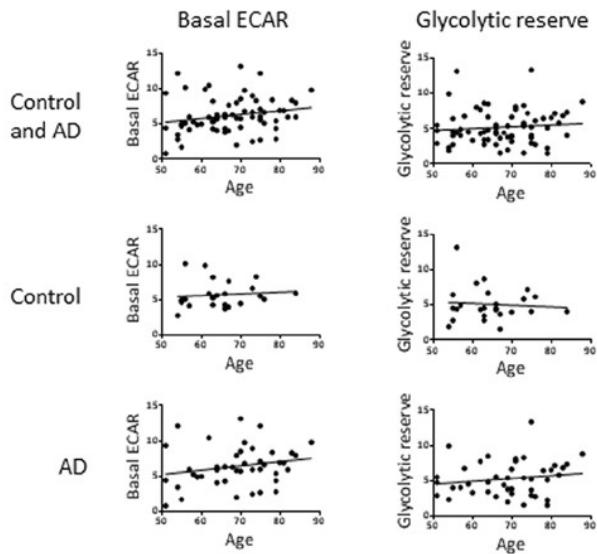
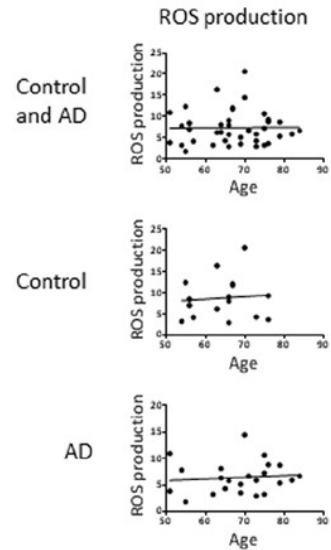


**Figure 2. Effects of gender on the average values of the biochemical parameters. (A)** Stratified for gender. Population numbers are as follows: OCRs (Basal OCR, ATP turnover, Reserve capacity, Maximum capacity, Proton leak) and ECARs (Basal ECAR, Glycolytic reserve), men = 33, women = 35; ROS production, men = 18, women = 21; all dNTPs, men = 22, women = 33; DNA strand breaks, men = 31, women = 39; APE1 activity, men = 19, women = 17. Error bars represent  $\pm$  standard deviation.

\* Significant difference ( $P < .05$ ) in the average level of the parameter between men and women.

**(B)** Stratified for both gender and control/AD. Population numbers in the order of control/men, control /women, AD/men, AD/women for each parameter were as follows: all OCR and ECARs, 13, 12, 20, 23; all dNTPs, 10, 17, 12, 16; ROS production, 8, 8, 10, 13; DNA strand breaks, 10, 16, 21, 23; APE1 activity, 8, 10, 11, 7. Error bars represent  $\pm$  standard deviation.

\*Significant difference ( $P < .05$ ) in the average level of the parameter between men and women.

**A****B****C**

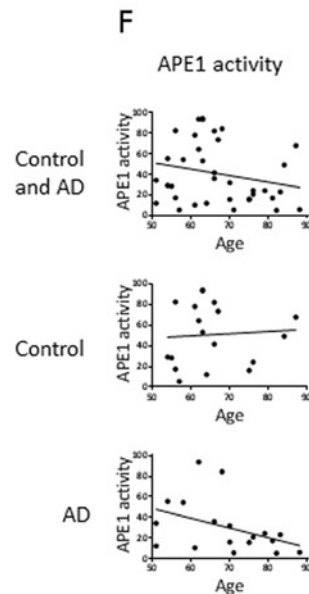
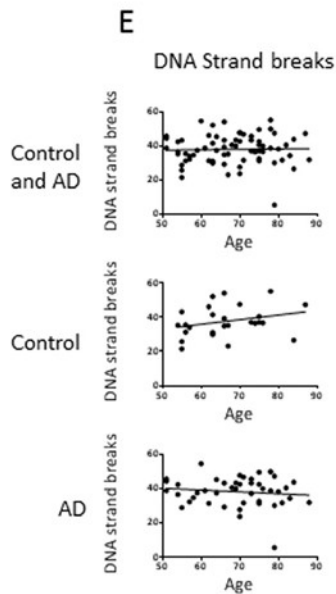
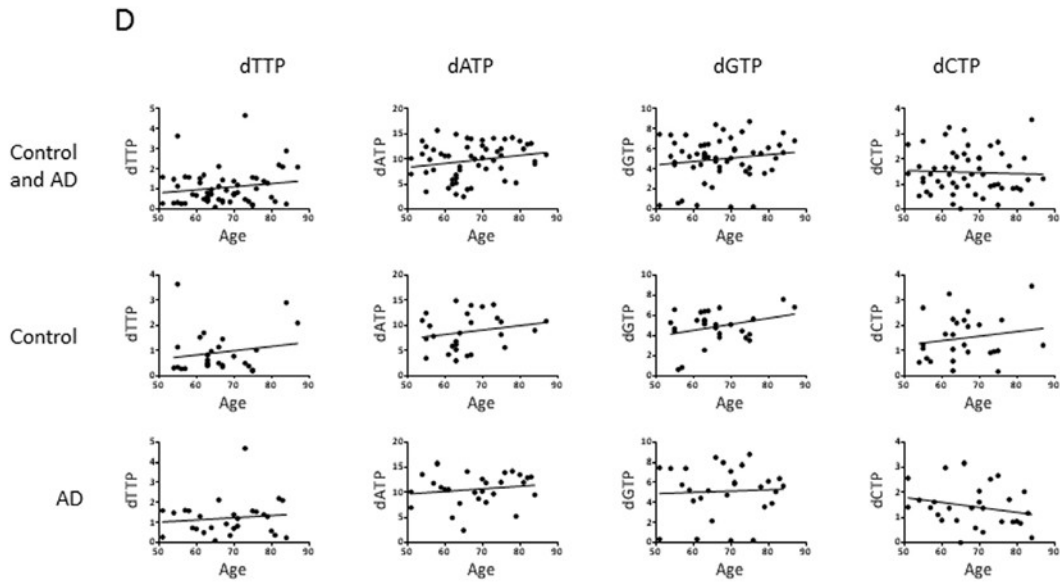


**Figure 3. Effects of age on the values of the biochemical parameters in controls and AD participants.** Pearson correlation analysis of age with (A) OCR parameters, (B) ECAR parameters, (C) ROS production, (D) dNTPs, (E) DNA strand breaks, (F) APE1 activity. Units: OCRs (Basal OCR, ATP turnover, Reserve capacity, Maximum capacity, Proton leak), pmol oxygen/min; ECARs (Basal ECAR, Glycolytic reserve), mpH/min; ROS production, fluorescence; dNTPs, pmol/million cells; DNA strand breaks, percent fluorescence; APE1 activity, percent incision.

We also performed correlation analysis to investigate potential associations of the parameters with age (Figure 3) and with disease progression (MMSE score) (Figure 4). In Figure 3, the aim of the analyses within the control group was to give insight into potential biochemical links to age, independent of AD pathology;

the analyses within the AD group will then indicate if age trends interact with AD pathology. There was no significant association of any of the measured parameters with age of the participants (within the entire group or within the controls or AD separately), or with MMSE score in the AD patients. However, the

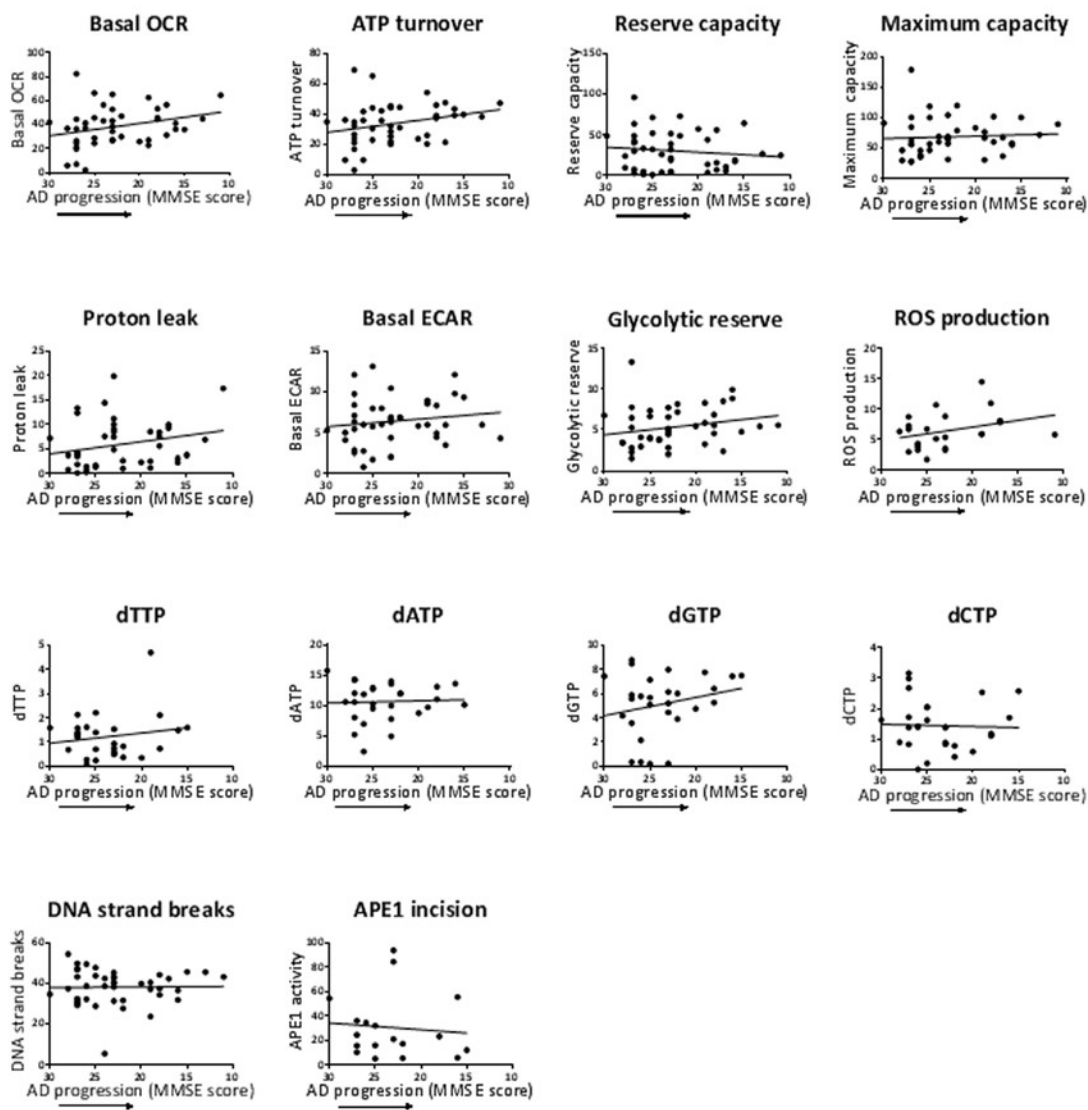


**Figure 4. Effects of MMSE of the AD patients on the values of the biochemical parameters.** Pearson correlation analysis of MMSE with the biochemical parameters, as indicated. MMSE scores are listed high to low on the x-axis to correspond to AD progression (reduction in cognitive function as measured by MMSE). Units: OCRs (Basal OCR, ATP turnover, Reserve capacity, Maximum capacity, Proton leak), pmol oxygen/min; ECARs (Basal ECAR, Glycolytic reserve), mpH/min; ROS production, fluorescence; dNTPs, pmol/million cells; DNA strand breaks, percent fluorescence; APE1 activity, percent incision.

trends may be informative. Notably, there is a trend for higher levels of basal OCR and ATP turnover with increased age (in the control and the AD groups with a similar slope of the trend lines, indicating no interaction of AD pathology with the age trends) and disease progression (lower MMSE score). This suggests that the PBMCs may be compensating for both age and AD development by increasing the mitochondrial production of ATP. There was also a trend for higher proton leak with increased age (in the control group; the age effect on proton leak was blunted in the AD group) and with lower MMSE, suggesting that PBMCs may be compensating for age and AD development by fine-tuning respiration efficiency (see discussion). In the case of glycolysis parameters (basal ECAR and glycolytic reserve) there was no obvious trend with age in the control groups, but both parameters trended to higher levels with lower MMSE, suggesting that glycolysis is compensating higher with disease progression (but not with age). ROS production was strikingly unaltered with age, but did show a trend for higher levels with lower MMSE. All four dNTPs, as well as DNA strand breaks and, to a very small degree, APE1 activity, had higher levels with advanced age in the control group; these trends were blunted within the AD group. The dGTP and dTTP parameters showed an increase with disease progression, but dATP, dCTP, DNA strand breaks and APE1 activity parameters did not; especially notable is the lack of dATP association with MMSE score since we did see a significantly higher dATP level in the AD group in Table 2. The DNA damage and repair (APE1 activity) trends indicate that DNA strand breaks increase with age (but not with disease progression) and the cells attempt to compensate with increased BER.

### **Correlation analyses among the biochemical parameters**

To examine links between the biochemical activities, we performed correlation analysis between all the parameters measured in this study (Supplemental Table S4). Consistent with our previous correlation analysis in PBMCs of normal (healthy) participants [12], where we compared many of the same biochemical parameters that we examine in this current report, we found that there were significant associations among the bioenergetics parameters and among the dNTP levels. These associations are to be expected [10, 39, 40] (also see Supplemental Figure S1), assuming that the parameters are measured accurately. This helps verify the specificity of our data for the biochemical activities being investigated (for example, a participant with high basal OCR, should also have a high maximum capacity OCR if the mitochondrial flux modifiers were added

correctly). Focusing on the parameters that gave a significant outcome in Table 2: basal OCR was significantly associated with ATP turnover, maximum capacity, proton leak and glycolytic reserve (all with  $P < .0001$ ); proton leak was additionally associated with ATP turnover ( $P = .007$ ) and maximum capacity ( $P = .0068$ ), but not with glycolytic reserve ( $P = .9499$ ); dATP was not associated with any of the other three dNTPs, yet the other three were associated with each other (all with  $P < .005$ ). APE1 activity was not associated with any of the other parameters.

## **DISCUSSION**

### **APE1 activity in AD**

The gender adjusted outcome for APE1 activity (significantly lower activity in the AD group) stood out as particularly compelling since it showed the strongest statistical result relative to any other parameter ( $R^2 = 0.389$ ,  $P = .003$ ). Correction of APE1 outcome for both gender and age did not improve the strength of this outcome ( $R^2 = 0.399$ ,  $P = .006$ ). This relatively strong outcome, does not appear to be linked to the other parameters, since the level of APE1 activity was not associated with any of the parameters (Supplemental Table S4). Studies report an increased level of the APE1 protein in AD brain [26, 27]; it has been suggested that this supports the view that AD brain compensates or adapts to higher oxidative stress by increasing the level of APE1 in an attempt to better repair damaged DNA. However, here we find lower level of APE1 activity, suggesting that BER efficiency is reduced in AD PBMCs, which in turn would contribute to accumulation of oxidative lesions. Published data from our group has reported a lower activity of the BER enzymes OGG1 and DNA polymerase  $\beta$ , but no change in APE1 activity, in AD post mortem brain tissue, relative to controls [19]. However, our finding in this current report is consistent with several studies reporting evidence of reduced BER capacity in peripheral cells (blood cells or dermal fibroblasts) or postmortem brains of AD patients [18, 20, 25, 41-44]. Moreover, a recent study reported reduced AP-site incision activity of APE1 in addition to reduced APE1 protein level upon differentiation of neuronal cells; OGG1 and UDG activities were also reduced, however the levels of these BER enzymes were not significantly altered [23]. Inconsistencies among studies, regarding activity and levels of BER components, may be a reflection of tissue-specific differences in the individual steps in BER, for example in peripheral blood compared to the central nervous system. If our data is reproduced in follow-up studies, APE1 activity could potentially be incorporated into a DNA repair panel of risk factors for

AD risk assessment or early detection, as suggested in the case of lung cancer [45]; in that study, the suggested risk factor panel consists of enzymatic DNA repair activities (in PBMCs) of APE1, OGG1, and methylpurine DNA glycosylase.

### **Mitochondrial respiration in AD**

The outcome for proton leak (significantly lower proton leak in AD PBMCs in all models) is intriguing since optimal proton leak is important in thermogenesis, protection against reactive oxygen species, endowment of metabolic sensitivity and maintenance of carbon fluxes [46]. Our data on proton leak suggests that AD patients are not well equipped at using proton leak to adjust respiration in response to mitochondrial stress or changes in ATP demand. The age adjusted (model 3) and the gender and age adjusted (model 4) outcomes for basal OCR suggest that AD PBMCs are deficient in basal mitochondrial respiration. This data is consistent with a recent study by Leuner et al [3], who reported a reduced basal rate of respiration in AD lymphocytes using the Oroboros Oxygraph-2 k system. In contrast, two previous reports found no changes in the enzyme activity of the respiratory chain complexes in AD lymphocytes [47, 48]. This suggests that perhaps measurement of bioenergetic fluxes is a more sensitive biomarker for AD compared to enzyme activity of respiratory chain complexes. It has also been suggested by Leuner et al. [3] that AD severity (MMSE level) may in part explain differences found between studies.

According to mitochondrial flux circuitry, a lower basal OCR could be due to a decrease in ATP turnover (reduced ATP demand), or a decrease on proton leak (with corresponding increase in membrane potential) [40]. This agrees with our data in which AD PBMCs displayed a significantly lower proton leak and a trend for lower ATP turnover (Table 2). The lower proton leak could be due to lower uncoupling protein activity and in fact this has been demonstrated in plasma of AD patients [49]. However, lower basal OCR and accompanying lower proton leak (more coupled, higher membrane potential) would be predicted to be accompanied by an increase in ROS [1] due to a more reduced electron transport chain [50]. In fact, Leutner et al [4] reported enhanced ROS production in AD lymphocytes (measured by the intracellular fluorescence dye dihydrorhodamine123). However, in our study we did not observe a higher ROS production in AD PBMCs (measured by MitoSox red), and in fact the trend was for lower ROS production in the AD PMBCs. It is possible that the mixture of white blood cells that make up PBMCs (lymphocytes, monocytes, macrophages) dilute any trend in lymphocytes alone. Also, it

has become apparent that mitochondrial ROS production can be regulated independently of oxygen consumption in many tissues and in different physiological situations, such as aerobic exercise bouts, chronic exercise training, hyperthyroidism and dietary restriction [51]. Interestingly, within the AD group there was a trend for increased ROS production with disease progression (Figure 4). We speculate that the participants within the AD group have more consistent physiological situations and thus ROS production would be more closely associated with oxygen consumption, however, more work needs to be done to assess the impact of tissue and physiological conditions on mitochondrial ROS production.

Our data indicating reduced basal OCR in AD is consistent with the underlying theme of the “mitochondrial cascade hypothesis” for sporadic AD in which it is proposed that inherited electron transport chain gene combinations determine basal mitochondrial respiration rate and persons with low rates may be at higher risk for AD [52]. The theory has come about to a large part based on the findings that amyloid  $\beta$  is transported to the mitochondria and binds respiratory complex IV where it is thought to then inhibit mitochondrial oxygen consumption [53]. However, the theory also proposes that the mechanism involves increased mitochondrial ROS and compensatory glycolysis stemming from mitochondrial dysfunction. Our data in Table 2 does not support this aspect of the model, since we do not see a significant increase in ROS production or basal ECAR in AD; however, both of these parameters show a trend for higher levels with disease progression (Figure 4).

### **dNTPs in AD**

The altered dATP level in AD, without significant alteration in the other three dNTPs, implies an imbalance in dNTP pools that may reflect mitochondrial dysfunction [39]. This finding is consistent with our correlation analysis indicating that dATP was not associated with any of the other three dNTPs, which were all associated with each other (Supplemental Table S4). There are no previous reports on dNTP imbalance in AD. However, studies suggest a model in which dTNP imbalance leads to mitochondrial DNA mutations, which are known to contribute to a range of human diseases, including neurodegenerative disorders, heart conditions, and cancer [11, 54]. Also, dATP is critical in feedback inhibition of ribonucleotide reductase (RNR), a key enzyme in de novo dNTP synthesis [55, 56]; this is important for optimal coupling of dNTP production to utilization. Since the enhanced dATP level is not accompanied by reduced levels of the

other dNTPs, it appears that dATP feedback inhibition process is impaired in AD patients. However, we cannot declare in this study the reason for the enhanced levels of dATP in AD PBMCs.

### Gender effects

Within the entire “control plus AD” cohort, there was an obvious trend for higher OCRs in women relative to men (Figure 2A) and there was in fact a significantly higher level of the maximum capacity OCR parameter in women. These trends were also apparent within both controls and AD as separate groups (Figure 2B). There are limited publications comparing mitochondrial bioenergetics in men and women, but a recent study using the oxygraph respirometer found no significant association between mitochondrial respiratory parameters and gender in intact and permeabilized platelets [57]. However, there are many differences in their approach compared to ours that may explain the differences in outcome, such as the specific type of blood cells, apparatus for measuring mitochondrial bioenergetics, and participant characteristics (ours includes AD patients, and all are over 50 years of age).

There was also a significantly lower APE1 activity in the women relative to men in the entire cohort (Figure 2A), and in both the control and AD groups (Figure 2B). This is consistent with the results from a recent study by Slysokova et al. [58], in which DNA repair (both BER and nucleotide excision repair) was lower in women relative to men, in PBMCs. We also found that the average ROS production value was significantly lower in women (Figure 2A). Based on these data, we speculate that in men we see a compensation for higher ROS-induced DNA damage via enhancement of DNA repair.

### Effects of age and MMSE

The trend-lines described in the Results (parameter values in participant PBMCs versus age or MMSE; Figures 3 and 4) suggest the following biochemical events in the PBMCs: 1. Accumulation of DNA damage (DNA strand breaks) with age in healthy individuals, 2. Increased ROS production with disease progression, 3. Compensation by the mitochondrial flux parameters basal OCR, ATP turnover, and proton leak with age in healthy individuals, and with disease progression, 4. Compensation with disease progression by the glycolysis parameters, 4. Compensation by APE1 activity (DNA repair) with age in healthy individuals, 5. The trend for higher dNTPs with age in healthy individuals (all four dNTPs) or disease progression (dGTP and dTTP) may represent a response to

genotoxic stress [56], and/or defective dATP feedback inhibition of ribonucleotide reductase, with age or disease progression (see above, Section 4.3). However, none of these trends reached statistical significance; note that the analysis *among* controls or *among* AD involved relative smaller population numbers, compared to the analysis *between* controls and AD of Table 2, resulting in diminished statistical power.

The aim of the MMSE correlation analysis was to see if the parameters that showed a statistically altered mean value in AD PBMCs (Table 2) (basal OCR, proton leak, dATP, APE1 activity) also showed an association (or trend) with disease progression (lower MMSE score). Basal OCR and proton leak levels in AD trended towards higher levels with disease progression; however the mean values of these mitochondrial flux parameters were significantly lower in the AD group compared to the control group (depending on gender/age adjustment) (Table 2). We speculate that basal OCR and proton leak are considerably reduced early before significant AD neuropathology, and then the cells attempt to compensate higher (to generate more ATP) as the disease progresses to more advanced stages as measured by reduced cognitive function (reduced MMSE scores). Future analyses to test and expand on this hypothesis, could entail measuring these cellular mitochondrial flux parameters in groups of high (or normal) MMSE and significantly declined MMSE score (without significant AD neuropathology), in addition to groups of control (or early AD) and severe AD (severe neuropathology). The dATP level did not show an obvious trend with disease progression; yet the mean value of dATP was significantly higher in the AD group compared to the control group (depending on gender/age adjustment) (Table 2). This suggests that dATP alteration may also be an early event, and in this case not further altered with disease severity. APE1 activity weakly trended lower with disease progression, in accord with the lower mean values in AD compared to controls (depending on gender/age adjustment) (Table 2). Notably, a recent study by Simpson et al. [59] demonstrated an increased expression of DNA damage response (DDR)-associated (double strand break repair) proteins  $\gamma$ H2AX and DNA-PKcs associated with lower MMSE score, in the frontal neocortex of participants at the earliest stages of AD pathology, before appreciable AD pathology. In contrast, we observed a reduced activity of the DDR protein of our study, i.e. APE1, in AD PBMCs. However, our study differed in several ways from that study: assays were performed on peripheral blood cells; APE1 is associated with a different aspect of the DDR than the DDR factors of the above study, namely BER; the AD patients were of a later stage of disease (diagnosed as mild to moderate AD) where AD

pathology may impede with the ability of cells to produce a vigorous DDR (such as impairing the APE1 enzyme activity).

Several studies dealing with markers of oxidative DNA and RNA damage in early stage AD neurons and association of these markers with progression of A $\beta$  plaques and neurofibrillary tangles, suggest that oxidative damage to DNA and RNA is greatest early in the disease, and reduces as the extent of AD pathology progresses [60-63]. In our cohort, the extent of DNA damage (DNA strand breaks) was not altered in AD PBMCs relative to controls, and showed no trend with MMSE score. However, our measure of DNA damage is not specific to oxidative DNA damage. A more appropriate comparison from our study with the above studies would be the APE1 activity, since it is an indicator of DNA repair of oxidative lesions. The lower APE1 activity in the AD group of our study (Table 2) is consistent with high oxidative DNA damage; however, the slight inverse trend of APE1 activity with AD progression in our AD group is not consistent with reduced oxidative DNA damage as AD pathology progresses. However, there are many differences between our study and those studies, including our use of only mild to moderate AD, and our tissue source (PBMCs).

### Limitations of the study

A limitation in this study is that the population size was restricted due to practical issue associated with the large number of tests performed (five different assays, and a total of 14 parameters measured). Also, due to the multifaceted aspect of this study, the number of participants varied depending on which test was performed (see Table 2). However, our population size for each test is in accord with many peripheral blood cell biomarker studies which typically have a population number for each of the control and AD participants of less than 50; moreover, such studies typically involve only one parameter being measured [64, 65]. In addition, the bioenergetics and ROS analyses required live cells, which for practical reasons limits the population size. It is also possible that some tests have low sensitivity due to multiple biochemical sources that determine their levels (thus, the sum effect may be blunted). For example, our measure of DNA strand breaks indicates total DNA breaks that could arise from a number of endogenous or exogenous sources. It may be necessary to measure more specific damage, to detect differences in AD tissue, such as extent of oxidative lesions. Indeed, studies have reported elevated levels of oxidized bases in AD, by making use of lesion-specific endonucleases in the

comet assay [2, 41]. Also, with regards to the gender comparisons of Figure 2A, the cohort is not ideal since it includes control and AD. We attempted to discern gender effects within the control and within the AD by stratifying for both gender and AD/control in Figure 2B, however the statistical power becomes reduced with the lower group population numbers; in fact, only APE1 activity retained statistical significance for gender effect (on both control and AD) and for significant alteration in AD (only retained in men).

We included patients with mild to moderate AD. We did not find any statistically significant associations between MMSE (global cognitive performance) and our molecular parameters. MMSE is a screening tool and, particularly in countries with a high level of education, many patients will score well during the early phases of AD, where it may not be sensitive to change. In further studies the performance of our molecular parameters in reflecting progression should be addressed in a longitudinal design, using other cognitive measures as well as global staging scales, such as the Clinical Dementia Rating Scale (CDR).

### Strengths of the study

The strengths of our study were that the diagnosis of AD was rigorous, our adjustments for age and gender were shown to be informative in that it suggests potential otherwise hidden alterations in AD PMBCs, and the techniques are potentially high throughput (especially determination of dNTP levels, since many frozen samples can be assayed simultaneously) which could make them useful as biomarkers for probable AD. Although our technique for measuring APE1 activity involved radioactivity (not ideal for high throughput biomarker testing) similar non-radioactive and equally sensitive BER assays for APE1 and other BER enzymes are being developed that have reduced costs, require very small amounts of protein extract, and that are easily automated [66, 67]. Our data is consistent with numerous reports of mitochondrial dysfunction in many neurological diseases, including AD, Parkinson's disease, Huntington's disease, and amyotrophic lateral sclerosis [68]. However, due to the cross-sectional design of this study, we cannot imply causality.

### METHODS

Patient selection. Patients with mild to moderate AD were recruited from the Memory Clinic at Rigshospitalet, University of Copenhagen. The NINDS-ARDRA criteria were used for the diagnosis of probable AD. The diagnosis was established by clinical interview, neurological examination, cognitive tests, CT

or MRI of the brain, and in selected cases, supplemental investigations. Patients who were unable to give informed consent were excluded. Healthy controls were age-matched volunteers, recruited from advertising, who had no major neurological or psychiatric disease and no significant cognitive deficits. In total, we recruited 53 patients with Alzheimer's disease with a mean age of 69.2 years and 30 age-matched healthy controls with a mean age of 66 years (Table 1). The sample size was calculated using power analysis. This analysis was performed with the assumption that the percentage of random missing data would be 5% as well as the other assumptions on expected means, standard deviations,  $\alpha$  value (0.05) and tails (two-tailed test). The estimated means and standard deviations for the power analysis were derived from our previous study, in which these same parameters were measured in PBMCs of healthy participants [12]. Disease severity (i.e. AD progression) was determined by the mini-mental state examination (MMSE) to assess cognitive function including orientation, attention, recall, language and visuospatial functions. The MMSE consists of 11 items in a questionnaire, with a maximum score of 30 points. A score of 23 or lower indicates cognitive impairment, but is dependent on age and level of education [30].

Isolation and storage of PBMCs. The isolation and freezing of the PBMCs for storage was performed as described previously [10, 12]. Briefly, PBMCs were isolated using BD Vacutainer Cell Preparation Tubes (CPT) containing sodium citrate (BD bioscience), according to the manufacturers protocol. PBMC isolation was performed on 8 ml of blood sample per participant, within 4 hours after blood withdrawal. Cells were counted by a cell counter (CASY<sup>®</sup> cell counter, Roch Innovatis AG) and aliquoted for the various tests. Fresh cells were used for bioenergetics (Seahorse XP analyzer) and ROS measurements (flow cytometry). Cells were frozen in liquid nitrogen for later testing of dNTPs, DNA strand breaks and APE1 activity. For the dNTP assay, two million PBMCs were centrifuged in freezer tubes and the cell pellet was resuspended in 60% methanol and directly frozen and stored in liquid nitrogen. For the DNA strand breaks assay, one million PBMCs were centrifuged and the cell pellet snap frozen and stored in liquid nitrogen. For the APE1 activity assay, one million PBMCs were resuspended in freezing medium (50% fetal bovine serum, 40% DMEM, 10% DMSO) in freezing tubes, and then frozen first in -80°C in a pre-cooled (4°C) freezing container overnight (-1°C/min cooling rate) and then moved for long term storage to liquid nitrogen.

Bioenergetics. The mitochondrial bioenergetic parameters were measured using the Seahorse Bioscience extracellular flux analyzer. This system is based on a

pharmacological profiling approach that makes use of four added pharmaceutical modulators of mitochondrial electron transport chain fluxes, as described previously [12] and in Supplemental Figure S1 with representative OCR and ECAR profiles. Briefly, cells were seeded at 300,000 cells per well onto XF24 V7 cell culture microplates (Seahorse Bioscience, Billerica, MA) after coating the plates with Cell-Tak adhesive (BD Bioscience). We measured mitochondrial oxygen consumption rates (OCRs; indicators of mitochondrial respiration; specifically basal OCR, ATP turnover, reserve capacity, maximum capacity, and proton leak) and extracellular acidification rates (ECARs; indicators of glycolysis; specifically basal ECAR and glycolytic reserve), in the seeded PMBCs. This was accomplished by automated injection of pharmaceutical modulators of mitochondrial oxidative phosphorylation fluxes to the medium; the specific compounds added, sequentially, were 1  $\mu$ M oligomycin, 0.3  $\mu$ M FCCP and 2  $\mu$ M antimycin A (Supplemental Figure S1). The chemical concentrations and PBMC seeding density were determined by titration. The reported level of each parameter from PBMCs of each participant was determined from the average of 10 wells.

ROS production. The mitochondrial superoxide production was measured quantitatively by flow cytometry combined with MitoSOX red (Molecular Probes, Invitrogen). Two million PMBCs were pelleted and resuspended in 5  $\mu$ M MitoSOX. After 10 minutes of incubation, cells were washed three times with PBS. All samples were prepared in triplicate. Determination of mitochondrial ROS was carried out using a FACScalibur (BD Bioscience). MitoSOX Red was excited at 488 nm and data collected at FSC, SSC and 585/42 nm (FL2) channels. The geometric mean fluorescence intensity values of the samples were obtained by subtracting the fluorescence of the control cells (not stained with MitoSOX) from the fluorescence of the MitoSOX stained cells.

dNTPs. Whole cell levels of deoxyadenosine triphosphate (dATP), deoxycytidine triphosphate (dCTP), deoxyguanosine triphosphate (dGTP) and deoxythymidine triphosphate (dTTP) were determined using the DNA polymerase assay previously described [12]. Cellular dNTPs were extracted from two million PBMCs with 60% methanol. Radioactivity was measured in a Tri-Carb 2900TR liquid scintillation counter (Packard) and normalized to pmol/ $1 \times 10^6$  cells using a standard curve of known dNTP concentrations. All samples were prepared in triplicate.

Fluorometric detection of alkaline DNA unwinding. The levels of endogenous DNA strand breaks were

measured using the Fluorometric detection of Alkaline DNA Unwinding (FADU) assay, as previously described [31, 32]. This assay measures both single and double strand DNA breaks but cannot distinguish between them. Decreased fluorescence signal as percentage of total fluorescence (= 100%) was used as the level of endogenous DNA damage; thus a higher value is indicative of a higher amount of DNA damage, in the form of DNA strand breaks. All samples were prepared in triplicate, at one million cells per well.

**APE1 incision assay.** Cell extracts of one million cells were made and assayed as described previously [6]. The oligonucleotide DNA substrate used in this assay contains a tetrahydrofuran (THF) residue (= AP site), and has been used extensively by our group and others; the oligonucleotides are as follows: AP site strand, 5'-GAA CGA CTG T (AP site) A CTT GAC TGC TAC TGA T; complementary strand, 3'- CTT GCT GAC A CT GAA CTG ACG ATG ACT A. Reaction products were analyzed by electrophoresis under denaturing conditions; 20% acrylamide, 7 M urea, 1x TBE. Gel images were visualized by phosphorimaging (Typhoon 9410, Amersham Bioscience) and analyzed by ImageQuant 5.2 (Molecular Dynamics). Incision activity was determined, from the average of triplicate lanes (on separate gels), as the intensity of product bands relative to the combined intensities of substrate and product bands.

**Statistical analysis.** To test for differences in the average values of each parameter between AD and control groups (Table 2) we used ANOVA, using GLM Univariate Analysis from IBM SPSS20 statistics software, New York, USA. In model 1, there were no adjustments for gender or age. In model 2 we adjusted for gender (men/women; categorical variable). In model 3 we adjusted for age (years; continuous variable), and in model 4 we adjusted for both gender and age. Gender effects on the parameters (Figure 2) were determined by two-tailed t-tests in GraphPad Prism 6 (La Jolla, CA, USA). For the association analysis of the parameter values with age (Figure 3) and with MMSE score (Figure 4), and association analysis among the biochemical parameters (Table S4), we used Pearson's correlation analysis with GraphPad Prism 6 software.  $P < .05$  was considered significant. Several studies suggest that health behaviors such as physical activity, smoking and alcohol consumption are determinants of AD development [33]; in the case of smoking, the epidemiological studies suggest inconsistent results, suggesting either detrimental or even beneficial effects in AD [34]. However, health behaviors may be in the potential causal pathways between the biochemical

parameters and AD development [35-37], and so they were not adjusted for. We did not adjust for hypertension since several participants (all controls) did not have blood pressure recorded.

**Ethical and safety aspects.** This study was conducted according to the ethical principles of the Helsinki II declaration. The project was approved by the Ethical Review Committee of the Capital Region of Copenhagen (H-3-2011-137).

## Conclusion

We observed several biochemical defects in AD PBMCs, in the form of reduced basal respiration rate and proton leak, higher dATP level and lower APE1 activity. This data suggests that peripheral blood cells in AD patients display measurable defects in mitochondrial respiration, dNTP pool balance, and BER activity. Specifically, after statistical adjustment for gender, age, or both gender and age, our data suggest the following three concepts. 1. Proton leak and dATP level may be relevant as biomarkers without correction for gender or age: there was a significant difference in the average level of these parameters between control and AD without adjustment and moreover the adjustments had no striking effect on the strength of the outcome as indicated by the  $R^2$  and  $P$  values (see Table 2), 2. The utility of APE1 activity as a biomarker may be best if correction for gender is included: although the difference in average APE1 activity between control and AD was significant without correction ( $R^2 = .124$ ,  $P = .035$ ), the outcome was much improved after correction for gender ( $R^2 = .389$ ,  $P = .003$ ), 3. The utility of basal OCR as a biomarker appears to have the requirement for age correction: there was no significant difference in average basal OCR level between control and AD unless correction for age was performed ( $R^2 = .092$ ,  $P = .037$ ). To validate the clinical utility of these results, an independent study is required of an equal or greater size to re-examine and further characterize the effects of AD or cognitive decline on mitochondrial bioenergetics, dNTP pools and DNA repair activity in AD.

## Author contributions

S.M, A-M.H, G.W, G.K, A.B, L.J.R and V.A.B designed the study; S.M, T-S.T.D, G.K, C.D, and M.M-V performed the laboratory research; S.M, G.K, and Å.M.H analyzed and interpreted the data; A-M.H collected the patient samples and clinical data. S.M drafted the manuscript; V.A.B helped develop the manuscript, and all authors critically reviewed the manuscript and gave their final approval.

## Funding

This work was supported by grants from Nordeafonden.

## Conflict of interest statement

The authors declare no conflict of interest.

## REFERENCES

1. Kramer PA, Ravi S, Chacko B, Johnson MS, Darley-Usmar VM. A review of the mitochondrial and glycolytic metabolism in human platelets and leukocytes: Implications for their use as bioenergetic biomarkers. *Redox Biol.* 2014; 2:206-210.
2. Leandro GS, Lobo RR, Oliveira DV, Moriguti JC, Sakamoto-Hojo ET. Lymphocytes of patients with Alzheimer's disease display different DNA damage repair kinetics and expression profiles of DNA repair and stress response genes. *Int J Mol Sci.* 2013; 14: 12380-12400.
3. Leuner K, Schulz K, Schutt T, Pantel J, Prvulovic D, Rhein V, Savaskan E, Czech C, Eckert A, Muller WE. Peripheral mitochondrial dysfunction in Alzheimer's disease: focus on lymphocytes. *Mol Neurobiol.* 2012; 46:194-204.
4. Leutner S, Schindowski K, Frolich L, Maurer K, Kratzsch T, Eckert A, Muller WE. Enhanced ROS-generation in lymphocytes from Alzheimer's patients. *Pharmacopsychiatry.* 2005; 38: 312-315.
5. Mao P, Reddy PH. Aging and amyloid beta-induced oxidative DNA damage and mitochondrial dysfunction in Alzheimer's disease: implications for early intervention and therapeutics. *Biochim Biophys Acta.* 2011; 1812:1359-1370.
6. Yang JL, Tadokoro T, Keijzers G, Mattson MP, Bohr VA. Neurons efficiently repair glutamate-induced oxidative DNA damage by a process involving CREB-mediated up-regulation of apurinic endonuclease 1. *J Biol Chem.* 2010; 285:28191-28199.
7. Mancuso M, Orsucci D, LoGerfo A, Calsolaro V, Siciliano G. Clinical features and pathogenesis of Alzheimer's disease: involvement of mitochondria and mitochondrial DNA. *Adv Exp Med Biol.* 2010; 685:34-44.
8. Hroudova J, Singh N, Fisar Z. Mitochondrial dysfunctions in neurodegenerative diseases: relevance to Alzheimer's disease. *Biomed Res Int.* 2014; 2014: 175062.
9. Rezai-Zadeh K, Gate D, Szekely CA, Town T. Can peripheral leukocytes be used as Alzheimer's disease biomarkers? *Expert Rev Neurother.* 2009; 9:1623-1633.
10. Desler C, Munch-Petersen B, Stevnsner T, Matsui S, Kulawiec M, Singh KK, Rasmussen LJ. Mitochondria as determinant of nucleotide pools and chromosomal stability. *Mutat Res.* 2007; 625: 112-124.
11. Kunz BA, Kohalmi SE, Kunkel TA, Mathews CK, McIntosh EM, Reidy JA. International Commission for Protection Against Environmental Mutagens and Carcinogens. Deoxyribonucleoside triphosphate levels: a critical factor in the maintenance of genetic stability. *Mutat Res.* 1994; 318:1-64.
12. Maynard S, Keijzers G, Gram M, Desler C, Bendix L, Budtz-Jorgensen E, Molbo D, Croteau DL, Osler M, Stevnsner T, Rasmussen LJ, Dela F, Avlund K, Bohr VA. Relationships between human vitality and mitochondrial respiratory parameters, reactive oxygen species production and dNTP levels in peripheral blood mononuclear cells. *Aging (Albany NY).* 2013; 5: 850-864.
13. Jeppesen DK, Bohr VA, Stevnsner T. DNA repair deficiency in neurodegeneration. *Prog Neurobiol.* 2011; 94:166-200.
14. Maynard S, Schurman SH, Harboe C, de Souza-Pinto NC, Bohr VA. Base excision repair of oxidative DNA damage and association with cancer and aging. *Carcinogenesis.* 2009; 30:2-10.
15. Sykora P, Misiak M, Wang Y, Ghosh S, Leandro GS, Liu D, Tian J, Baptiste BA, Cong WN, Brennerman BM, Fang E, Becker KG, Hamilton RJ, Chigurupati S, Zhang Y, Egan JM, Croteau DL, Wilson DM, III, Mattson MP, Bohr VA. DNA polymerase beta deficiency leads to neurodegeneration and exacerbates Alzheimer disease phenotypes. *Nucleic Acids Res.* 2015; 43: 943-959.
16. Liu D, Croteau DL, Souza-Pinto N, Pitta M, Tian J, Wu C, Jiang H, Mustafa K, Keijzers G, Bohr VA, Mattson MP. Evidence that OGG1 glycosylase protects neurons against oxidative DNA damage and cell death under ischemic conditions. *J Cereb Blood Flow Metab.* 2011; 31: 680-692.
17. Akbari M, Morevati M, Croteau D, Bohr VA. The role of DNA base excision repair in brain homeostasis and disease. *DNA Repair (Amst).* 2015.
18. Subba RK. Mechanisms of disease: DNA repair defects and neurological disease. *Nat Clin Pract Neurol.* 2007; 3:162-172.
19. Weissman L, Jo DG, Sorensen MM, de Souza-Pinto NC, Markesbery WR, Mattson MP, Bohr VA. Defective DNA base excision repair in brain from individuals with Alzheimer's disease and amnesic mild cognitive impairment. *Nucleic Acids Res.* 2007; 35: 5545-5555.
20. Bradley WG, Polinsky RJ, Pendlebury WW, Jones SK, Nee LE, Bartlett JD, Hartshorn JN, Tandan R, Sweet L, Magin GK, . DNA repair deficiency for alkylation damage in cells from Alzheimer's disease patients. *Prog Clin Biol Res.* 1989; 317:715-732.
21. Dorszewska J, Kempisty B, Jaroszewska-Kolecka J, Rozycka A, Florczak J, Lianeri M, Jagodzinski PP, Kozubski W. Expression and polymorphisms of gene 8-oxoguanine glycosylase 1 and the level of oxidative DNA damage in peripheral blood lymphocytes of patients with Alzheimer's disease. *DNA Cell Biol.* 2009; 28: 579-588.
22. Hildrestrand GA, Diep DB, Kunke D, Bolstad N, Bjaras M, Krauss S, Luna L. The capacity to remove 8-oxoG is enhanced in newborn neural stem/progenitor cells and decreases in juvenile mice and upon cell differentiation. *DNA Repair (Amst).* 2007; 6: 723-732.
23. Sykora P, Yang JL, Ferrarelli LK, Tian J, Tadokoro T, Kulkarni A, Weissman L, Keijzers G, Wilson DM, III, Mattson MP, Bohr VA. Modulation of DNA base excision repair during neuronal differentiation. *Neurobiol Aging.* 2013; 34:1717-1727.
24. Focher F, Mazzarello P, Verri A, Hubscher U, Spadari S. Activity profiles of enzymes that control the uracil incorporation into DNA during neuronal development. *Mutat Res.* 1990; 237: 65-73.
25. Lovell MA, Xie C, Markesbery WR. Decreased base excision repair and increased helicase activity in Alzheimer's disease brain. *Brain Res.* 2000; 855:116-123.
26. Davydov V, Hansen LA, Shackelford DA. Is DNA repair compromised in Alzheimer's disease? *Neurobiol Aging.* 2003; 24: 953-968.
27. Tan Z, Sun N, Schreiber SS. Immunohistochemical localization of redox factor-1 (Ref-1) in Alzheimer's hippocampus. *Neuroreport.* 1998; 9: 2749-2752.

28. Huang E, Qu D, Zhang Y, Venderova K, Haque ME, Rousseau MW, Slack RS, Woulfe JM, Park DS. The role of Cdk5-mediated apurinic/aprimidinic endonuclease 1 phosphorylation in neuronal death. *Nat Cell Biol.* 2010; 12:563-571.
29. Seshadri S, Wolf PA. Lifetime risk of stroke and dementia: current concepts, and estimates from the Framingham Study. *Lancet Neurol.* 2007; 6: 1106-1114.
30. Velayudhan L, Ryu SH, Raczek M, Philpot M, Lindesay J, Critchfield M, Livingston G. Review of brief cognitive tests for patients with suspected dementia. *Int Psychogeriatr.* 2014; 26: 1247-1262.
31. Moreno-Villanueva M, Pfeiffer R, Sindlinger T, Leake A, Muller M, Kirkwood TB, Burkle A. A modified and automated version of the 'Fluorimetric Detection of Alkaline DNA Unwinding' method to quantify formation and repair of DNA strand breaks. *BMC Biotechnol.* 2009; 9:39.
32. Maynard S, Keijzers G, Hansen AM, Osler M, Molbo D, Bendix L, Moller P, Loft S, Moreno-Villanueva M, Burkle A, Hvitby CP, Schurman SH, Stevnsner T, Rasmussen LJ, Avlund K, Bohr VA. Associations of subjective vitality with DNA damage, cardiovascular risk factors and physical performance. *Acta Physiol (Oxf).* 2014.
33. Lee Y, Back JH, Kim J, Kim SH, Na DL, Cheong HK, Hong CH, Kim YG. Systematic review of health behavioral risks and cognitive health in older adults. *Int Psychogeriatr.* 2010; 22: 174-187.
34. Mehta M, Adem A, Kahlon MS, Sabbagh MN. The nicotinic acetylcholine receptor: smoking and Alzheimer's disease revisited. *Front Biosci (Elite Ed).* 2012; 4: 169-180.
35. Eggers AE. Why do Alzheimer's disease and Parkinson's disease target the same neurons? *Med Hypotheses.* 2009; 72: 698-700.
36. Linert W, Bridge MH, Huber M, Bjugstad KB, Grossman S, Arendash GW. In vitro and in vivo studies investigating possible antioxidant actions of nicotine: relevance to Parkinson's and Alzheimer's diseases. *Biochim Biophys Acta.* 1999; 1454: 143-152.
37. Radak Z, Chung HY, Goto S. Systemic adaptation to oxidative challenge induced by regular exercise. *Free Radic Biol Med.* 2008; 44: 153-159.
38. Wu M, Neilson A, Swift AL, Moran R, Tamagnine J, Parslow D, Armistead S, Lemire K, Orrell J, Teich J, Chomicz S, Ferrick DA. Multiparameter metabolic analysis reveals a close link between attenuated mitochondrial bioenergetic function and enhanced glycolysis dependency in human tumor cells. *Am J Physiol Cell Physiol.* 2007; 292:C125-C136.
39. Desler C, Lykke A, Rasmussen LJ. The effect of mitochondrial dysfunction on cytosolic nucleotide metabolism. *J Nucleic Acids.* 2010; 10.4061/2010/701518 [doi].
40. Hill BG, Benavides GA, Lancaster JR, Jr., Ballinger S, Dell'Italia L, Jianhua Z, Darley-Usmar VM. Integration of cellular bioenergetics with mitochondrial quality control and autophagy. *Biol Chem.* 2012; 393: 1485-1512.
41. Kadioglu E, Sardas S, Aslan S, Isik E, Esat KA. Detection of oxidative DNA damage in lymphocytes of patients with Alzheimer's disease. *Biomarkers.* 2004; 9:203-209.
42. Ramamoorthy M, Sykora P, Scheibye-Knudsen M, Dunn C, Kasmer C, Zhang Y, Becker KG, Croteau DL, Bohr VA. Sporadic Alzheimer disease fibroblasts display an oxidative stress phenotype. *Free Radic Biol Med.* 2012; 53:1371-1380.
43. Gabbita SP, Lovell MA, Markesbery WR. Increased nuclear DNA oxidation in the brain in Alzheimer's disease. *J Neurochem.* 1998; 71: 2034-2040.
44. Lyras L, Cairns NJ, Jenner A, Jenner P, Halliwell B. An assessment of oxidative damage to proteins, lipids, and DNA in brain from patients with Alzheimer's disease. *J Neurochem.* 1997; 68: 2061-2069.
45. Sevilya Z, Leitner-Dagan Y, Pinchev M, Kremer R, Elinger D, Rennert HS, Schechtman E, Freedman LS, Rennert G, Paz-Elizur T, Livneh Z. Low integrated DNA repair score and lung cancer risk. *Cancer Prev Res (Phila).* 2014; 7:398-406.
46. Rolfe DF, Brand MD. The physiological significance of mitochondrial proton leak in animal cells and tissues. *Biosci Rep.* 1997; 17: 9-16.
47. Casademont J, Miro O, Rodriguez-Santiago B, Viedma P, Blesa R, Cardellach F. Cholinesterase inhibitor rivastigmine enhance the mitochondrial electron transport chain in lymphocytes of patients with Alzheimer's disease. *J Neurol Sci.* 2003; 206: 23-26.
48. Molina JA, de BF, Jimenez-Jimenez FJ, Benito-Leon J, Gasalla T, Orti-Pareja M, Vela L, Bermejo F, Martin MA, Campos Y, Arenas J. Respiratory chain enzyme activities in isolated mitochondria of lymphocytes from patients with Alzheimer's disease. *Neurology.* 1997; 48: 636-638.
49. Cornelius C, Trovato SA, Scuto M, Fronte V, Cambria MT, Pennisi M, Bella R, Milone P, Graziano A, Crupi R, Cuzzocrea S, Pennisi G, Calabrese V. Cellular stress response, sirtuins and UCP proteins in Alzheimer disease: role of vitagenes. *Immun Ageing.* 2013; 10: 41.
50. Skulachev VP. Role of uncoupled and non-coupled oxidations in maintenance of safely low levels of oxygen and its one-electron reductants. *Q Rev Biophys.* 1996; 29:169-202.
51. Barja G. Mitochondrial oxygen consumption and reactive oxygen species production are independently modulated: implications for aging studies. *Rejuvenation Res.* 2007; 10: 215-224.
52. Swerdlow RH, Khan SM. A "mitochondrial cascade hypothesis" for sporadic Alzheimer's disease. *Med Hypotheses.* 2004; 63: 8-20.
53. Pesini A, Iglesias E, Garrido N, Bayona-Bafaluy MP, Montoya J, Ruiz-Pesini E. OXPHOS, pyrimidine nucleotides, and Alzheimer's disease: a pharmacogenomics approach. *J Alzheimers Dis.* 2014; 42: 87-96.
54. Song S, Pursell ZF, Copeland WC, Longley MJ, Kunkel TA, Mathews CK. DNA precursor asymmetries in mammalian tissue mitochondria and possible contribution to mutagenesis through reduced replication fidelity. *Proc Natl Acad Sci U S A.* 2005; 102: 4990-4995.
55. Thelander L, Reichard P. Reduction of ribonucleotides. *Annu Rev Biochem.* 1979; 48: 133-158.
56. Chabes A, Georgieva B, Domkin V, Zhao X, Rothstein R, Thelander L. Survival of DNA damage in yeast directly depends on increased dNTP levels allowed by relaxed feedback inhibition of ribonucleotide reductase. *Cell.* 2003; 112:391-401.
57. Sjovalf F, Ehinger JK, Marelsson SE, Morota S, Frostner EA, Uchino H, Lundgren J, Arnbjornsson E, Hansson MJ, Fellman V, Elmer E. Mitochondrial respiration in human viable platelets--methodology and influence of gender, age and storage. *Mitochondrion.* 2013; 13:7-14.
58. Slyskova J, Lorenzo Y, Karlsen A, Carlsen MH, Novosadova V, Blomhoff R, Vodicka P, Collins AR. Both genetic and dietary

factors underlie individual differences in DNA damage levels and DNA repair capacity. *DNA Repair (Amst)*. 2014; 16: 66-73.

59. Simpson JE, Ince PG, Matthews FE, Shaw PJ, Heath PR, Brayne C, Garwood C, Higginbottom A, Wharton SB. A neuronal DNA damage response is detected at the earliest stages of Alzheimer's neuropathology and correlates with cognitive impairment in the Medical Research Council's Cognitive Function and Ageing Study ageing brain cohort. *Neuropathol Appl Neurobiol*. 2015; 41:483-496.

60. Nunomura A, Perry G, Pappolla MA, Wade R, Hirai K, Chiba S, Smith MA. RNA oxidation is a prominent feature of vulnerable neurons in Alzheimer's disease. *J Neurosci*. 1999; 19: 1959-1964.

61. Nunomura A, Perry G, Aliev G, Hirai K, Takeda A, Balraj EK, Jones PK, Ghanbari H, Wataya T, Shimohama S, Chiba S, Atwood CS, Petersen RB, Smith MA. Oxidative damage is the earliest event in Alzheimer disease. *J Neuropathol Exp Neurol*. 2001; 60: 759-767.

62. Simpson JE, Ince PG, Haynes LJ, Theaker R, Gelsthorpe C, Baxter L, Forster G, Lace GL, Shaw PJ, Matthews FE, Savva GM, Brayne C, Wharton SB. Population variation in oxidative stress and astrocyte DNA damage in relation to Alzheimer-type pathology in the ageing brain. *Neuropathol Appl Neurobiol*. 2010; 36: 25-40.

63. Wang J, Markesbery WR, Lovell MA. Increased oxidative damage in nuclear and mitochondrial DNA in mild cognitive impairment. *J Neurochem*. 2006; 96:825-832.

64. Guzman-Martinez L, Farias GA, Maccioni RB. Emerging noninvasive biomarkers for early detection of Alzheimer's disease. *Arch Med Res*. 2012; 43:663-666.

65. Veitinger M, Varga B, Guterres SB, Zellner M. Platelets, a reliable source for peripheral Alzheimer's disease biomarkers? *Acta Neuropathol Commun*. 2014; 2:65.

66. Georgiadis P, Polychronaki N, Kyrtopoulos SA. Progress in high-throughput assays of MGMT and APE1 activities in cell extracts. *Mutat Res*. 2012; 736:25-32.

67. Hamann I, Hartwig A. Quantification of DNA repair capacity towards oxidatively damaged DNA in subcellular and cellular systems by a nonradioactive cleavage assay. *Methods Mol Biol*. 2015; 1208: 73-84.

68. Karbowski M, Neutzner A. Neurodegeneration as a consequence of failed mitochondrial maintenance. *Acta Neuropathol*. 2012; 123: 157-171.

## Metabolic profiling distinguishes three subtypes of Alzheimer's disease

Dale E. Bredesen<sup>1, 2</sup>

<sup>1</sup> Mary S. Easton Center for Alzheimer's Disease Research, Department of Neurology, University of California, Los Angeles, CA 90095, USA;

<sup>2</sup> Buck Institute for Research on Aging, Novato, CA 94945, USA

**Key words:** inflammation, neurodegeneration, cognition, insulin resistance, biomarkers, dementia, dyscalculia

**Received:** 07/13/15; **Accepted:** 08/28/15; **Published:** 08/31/15 **doi:** [10.18632/aging.100801](https://doi.org/10.18632/aging.100801)

**Correspondence to:** Dale E. Bredesen, MD; **E-mail:** [dbredesen@mednet.ucla.edu](mailto:dbredesen@mednet.ucla.edu) or [dbredesen@buckinstitute.org](mailto:dbredesen@buckinstitute.org)

**Copyright:** Bredesen. This is an open-access article distributed under the terms of the Creative Commons Attribution License, which permits unrestricted use, distribution, and reproduction in any medium, provided the original author and source are credited

**Abstract:** The cause of Alzheimer's disease is incompletely defined, and no truly effective therapy exists. However, multiple studies have implicated metabolic abnormalities such as insulin resistance, hormonal deficiencies, and hyperhomocysteinemia. Optimizing metabolic parameters in a comprehensive way has yielded cognitive improvement, both in symptomatic and asymptomatic individuals. Therefore, expanding the standard laboratory evaluation in patients with dementia may be revealing. Here I report that metabolic profiling reveals three Alzheimer's disease subtypes. The first is inflammatory, in which markers such as hs-CRP and globulin:albumin ratio are increased. The second type is non-inflammatory, in which these markers are not increased, but other metabolic abnormalities are present. The third type is a very distinctive clinical entity that affects relatively young individuals, extends beyond the typical Alzheimer's disease initial distribution to affect the cortex widely, is characterized by early non-amnesic features such as dyscalculia and aphasia, is often misdiagnosed or labeled atypical Alzheimer's disease, typically affects ApoE4-negative individuals, and is associated with striking zinc deficiency. Given the involvement of zinc in multiple Alzheimer's-related metabolic processes, such as insulin resistance, chronic inflammation, ADAM10 proteolytic activity, and hormonal signaling, this syndrome of Alzheimer's-plus with low zinc (APLZ) warrants further metabolic, genetic, and epigenetic characterization.

### INTRODUCTION

Alzheimer's disease represents a major healthcare problem, with over five million Americans estimated to suffer from this disease, and a recent study showing that AD has now become the third leading cause of death, trailing only cardiovascular disease and neoplasia [1]. The cause(s) of AD remain incompletely determined, and there is currently no truly effective treatment. However, accumulating data suggest important contributions from metabolic abnormalities such as insulin resistance, metabolic syndrome, chronic inflammation, hypovitaminosis D, hormonal deficiencies, and hyperhomocysteinemia, among others [2]. Despite this, most clinical evaluations of patients with cognitive decline do not include extensive metabolic or genomic evaluations. Furthermore, given

the perceived poor prognosis for AD, in patients with evidence of amyloid- $\beta$  accumulation by amyloid PET imaging or, indirectly, by cerebrospinal fluid profile, there has been little incentive to perform extensive evaluations of hormonal status, nutritional status, toxicity status, metal status, gastrointestinal permeability, or other laboratory evaluations perceived by healthcare systems as "non-standard." However, studies such as the recent FINGER study [3] suggest that metabolic factors may play important roles in the neurodegenerative process, at least early in the pathogenetic process. Recent results from the evaluation of neural exosomes and nanosomes support the notion that metabolic abnormalities are present in patients with cognitive decline, often years prior to diagnosis of AD [4]. Therefore, it may be productive, both from the standpoint of identifying novel

biomarkers and from the standpoint of identifying treatable metabolic abnormalities, to perform metabolic profiling of patients with cognitive decline and those at risk for such decline.

I recently described a protocol for metabolic enhancement in neurodegeneration [5]. Evaluating these same metabolic parameters in patients with cognitive decline revealed three subtypes of Alzheimer's disease, which are described in greater detail below. Such metabolic subtyping may provide novel insights into the pathogenesis in specific patients, as well as suggesting therapeutic approaches that may be effective only in specific subgroups of patients.

## RESULTS

### Case studies

#### **Subtype 1: Inflammatory**

It has been well documented via numerous methods and observations that inflammation plays an important role in AD pathogenesis. Among the many findings implicating inflammation in AD mechanisms: the presence of pro-inflammatory cytokines, chemokines, acute-phase reactants, and other mediators of inflammation in AD brains [6, 7]; the mutual antagonism between NF $\kappa$ B (nuclear factor  $\kappa$ -light-chain enhancer of activated B cells) and the sirtuin SirT1 [8] is altered in favor of inflammation, with reduced SirT1, in the brains of patients with AD [9]; genomic studies implicate multiple inflammation-associated genes in AD [10]; and phagocytosis of amyloid- $\beta$  peptide is reduced by inflammation in patients with AD [11]. Moreover, a recent integrative analysis of AD susceptibility factors in the context of the signaling networks and molecular mechanisms mediating Alzheimer's disease pathophysiology implicated persistent wound-like microenvironments/pockets as playing a potentially causative role in AD etiology [12]. However, unlike other neuro-inflammatory diseases such as multiple sclerosis and encephalitides, the inflammation in AD involves primarily the innate immune system [6]. The pathology of AD includes inflammatory microglia and activated astroglia, and many but not all patients with AD show evidence of systemic inflammation, as well:

A 65-year-old man presented with a four-year history of progressive memory loss. He had had a superior memory for his entire life, and in fact had been known for his prodigious memory, but in his early 60s he began to have "senior moments" and to feel tentative about his driving directions. Both parents had died with

dementia. Quantitative neuropsychological testing suggested a diagnosis of mild cognitive impairment. He was found to be heterozygous for the  $\epsilon$ 4 allele of Apolipoprotein E (3/4) and for MTHFR (methylene tetrahydrofolate reductase) A1298C. Magnetic resonance imaging was read as "normal, with hippocampal volume at 17<sup>th</sup> percentile for age." Fluorodeoxyglucose PET scan was abnormal, revealing a pattern typical of AD, with temporal and parietal reductions in glucose utilization. Amyloid PET scan was positive.

His high-sensitivity C-reactive protein was 9.9mg/l, albumin:globulin ratio 1.6, fasting insulin 32uIU/ml, fasting serum glucose 96mg/dl, homocysteine 15.1uM, 25-hydroxycholecalciferol 21ng/ml, testosterone 264ng/dl, pregnenolone <5ng/dl, TSH 2.21mIU/l, free T3 2.4pg/ml, free T4 0.8pg/ml, vitamin B12 328pg/ml, serum zinc 98mcg/dl, serum ceruloplasmin 26mg/dl, and serum mercury 19ng/ml. BMI (body mass index) was 25.

#### **Subtype 2: Non-inflammatory**

In addition to inflammatory mechanisms in AD, numerous alternative associations have been described, such as insulin resistance, hypovitaminosis D, hyperhomocysteinemia, and hormonal loss associated with early oophorectomy [2, 13]. The extent to which each of these, beyond being a risk factor, contributes directly to AD pathogenesis is incompletely defined. Nonetheless, for each of these, as well as other metabolic mediators, there are theoretical mechanisms to support contributions to AD pathogenesis. Homocysteine, for example, has been shown to exert multiple effects that may contribute to cognitive decline, such as increasing tau phosphorylation via a post-translational modification-mediated reduction in protein phosphatase 2A (PP2A) function [14], glutamate receptor dysfunction, neuronal apoptosis induction, endoplasmic reticulum stress, DNA methylation, mitochondrial dysfunction, vascular damage, and oxidative stress [15].

A 75-year-old woman had progressive memory loss over one year. She had been otherwise healthy. Her mother had developed dementia in her eighth decade, as well. Her MoCA was 17/30. Her hs-CRP was 0.7mg/l, hemoglobin A1c 5.4%, 25-hydroxycholecalciferol 34ng/ml, homocysteine 24.1uM, MTHFR C677T heterozygous, vitamin B12 338pg/ml, MCV 102fl, pregnenolone 40ng/dl, TSH 3.5mIU/l, free T3 2.7pg/ml, free T4 1.0pg/ml, AM cortisol 21mcg/dl, and serum zinc 82mcg/dl.

### Subtype 3: Cortical

Alzheimer's disease presenting with non-amnestic features such as aphasia, partial Gerstmann's syndrome, alexia, visual agnosia, or apraxias has been well described [16], but metabolic abnormalities distinguishing these atypical presentations have not been reported. These patients represent a group that is distinct from the more typical amnestic presentation in several respects: (1) early symptom onset, typically in the 5<sup>th</sup>-7<sup>th</sup> decades; (2) lack of family history; (3) ApoE4-negative in the majority; (4) MRI showing general cortical atrophy (and in some cases, cerebellar atrophy, as well) rather than hippocampal atrophy out of proportion to the rest of the cerebrum; (5) FDG-PET may show reductions in glucose utilization beyond the typical temporal-parietal distribution. A summary of six patients with this presentation is shown in Table 1.

A 52-year-old scientist presented with a two-year history of cognitive decline, which had started with difficulty with numbers: she was unable to figure a tip, unable to pay bills, and then after several months she asked for help to write a grant proposal. She declined rapidly and developed a simple, childlike affect.

Despite this, she was able to learn and remember the names of all 28 children on the playground at her son's school. Family history was negative. Her MoCA score was 19. Her MRI showed "global cerebral volume loss, advanced for age." There were several areas of FLAIR (fluid-attenuated inversion recovery) hyperintensity in the subcortical and periventricular white matter. In addition, there was atrophy of the superior cerebellar vermis, and to a lesser degree the cerebellar hemispheres. CSF was markedly abnormal, with reduced Aβ42 of 294pg/ml and increased p-tau of 133pg/ml, compatible with a diagnosis of Alzheimer's disease.

BMI was 24.9. She was ApoE 3/3, klotho variant negative (SNP Rs9536314), hs-CRP was 1.4mg/l, albumin:globulin ratio 1.57, IL-6 1.4pg/dl, hemoglobin A1c 5.3%, fasting insulin 4.5mIU/l, TSH 2.14mIU/l, free T3 4.2pg/ml, reverse T3 11ng/dl, free T4 1.0pg/ml, progesterone < 0.21ng/ml, estradiol 3pg/ml, 17-hydroxypregnenolone 14ng/dl, AM cortisol 9mcg/dl, 25-hydroxycholecalciferol 22ng/ml, total cholesterol 264mg/dl, HDL-cholesterol 67mg/dl, LDL-cholesterol 167mg/dl, triglycerides 61mg/dl, cholesterol:HDL ratio 3.7, serum copper 101mcg/dl, serum zinc 56mcg/dl, and Cu:Zn ratio 1.8.

**Table 1.** Patients with the third subtype of Alzheimer's disease described in the text, Alzheimer's-plus with low zinc.

Patient	Age at onset	Initial Symptoms	ApoE4?	Zinc	Other
1M	65	Visual agnosia	- (3/3)	56	MRI:general atrophy, mild FLAIR
2M	59	Dyscalculia, aphasia	- (2/3)	59	MRI:general atrophy, mild FLAIR; FDG PET: frontal, temporal, parietal abnl.
3F	50	Dyscalculia	- (3/3)	56	MRI:general atrophy, mild FLAIR; CSF +
4F	64	Dyscalculia, prosopagnosia, word finding	Declined	59	Cu:Zn=3:1
5M	55	Dyscalculia	- (3/3)	ND	MRI:general atrophy, CSF +
6F	57	Dyscalculia	+ (3/4)	70	MRI:general atrophy, mild FLAIR; amyloid PET +

A 59-year-old man began to have word-finding difficulties, followed by difficulties with arithmetic. He had been a type A personality with a high-powered position, whose symptoms had begun after two years of the most stressful time of his career, and he became very passive and timid. Neuropsychological testing showed profound impairment in semantic fluency, executive functioning, attention, overall mental status, processing, and visual memory. Fluorodeoxyglucose PET scanning showed reduced metabolism in temporal and parietal lobes, L>R precuneus, and left frontal lobe.

His BMI was 24.9, ApoE genotype 2/3, hs-CRP 0.5mg/l, albumin 4.5g/dl, globulin 2.4g/dl, albumin:globulin ratio 1.9, AM cortisol 15.8mcg/dl, total cholesterol 235mg/dl, HDL-cholesterol 70mg/dl, LDL-cholesterol 150mg/dl, triglycerides 75mg/dl, cholesterol:HDL ratio 3.4, DHEA-S 130mcg/dl, progesterone 0.4ng/ml, fasting insulin 6mIU/l, 25-hydroxycholecalciferol 44.5ng/ml, alpha-tocopherol 22.5mg/l, beta-gamma-tocopherol 0.5mg/l, TSH 2.98mIU/l, free T3 2.7ng/ml, free T4 1.2ng/dl, reverse T3 21ng/dl, pregnenolone <5ng/dl, homocysteine 7.3umol/l, folate 16.6ng/ml, RBC Mg 5.5mg/dl, serum iron 135mcg/dl, serum copper 97mcg/dl, serum zinc 59mcg/dl, Cu:Zn ratio 1.6, blood arsenic/lead/mercury all <2mcg/l, TNF 1.2pg/ml, and IL-6 1.7pg/ml.

Sleep study showed mild obstructive sleep apnea, with apnea/hypopnea index of 7 events per hour. No REM behavioral disturbance was noted.

## DISCUSSION

The classification of Alzheimer's disease into subtypes may be useful for therapeutic studies. Since increasing evidence supports an important role for metabolic abnormalities such as insulin resistance in Alzheimer's disease pathophysiology, it is of interest to determine whether metabolic profiling may be useful clinically, both in classification and, ultimately, in therapeutic trials.

Here it is shown that clinical metabolic testing reveals three readily distinguishable subtypes of Alzheimer's disease. The first type, inflammatory, is associated with markers of systemic inflammation, such as high hs-CRP, low albumin:globulin ratio, and high interleukin-6. Additional metabolic abnormalities may also be present, such as insulin resistance, metabolic syndrome, hyperhomocysteinemia, hypovitaminosis D, hypothyroidism, and hypercortisolemia. ApoE4, which exerts pro-inflammatory effects, is associated with this subtype of Alzheimer's disease. The presentation is typically amnesic, and imaging studies are compatible

with such a presentation, showing hippocampal atrophy in the absence of widespread cerebral atrophy.

The second type, non-inflammatory, is associated with other metabolic abnormalities such as insulin resistance, hypovitaminosis D, hyperhomocysteinemia, and reductions in hormonal support. Indicators of systemic inflammation, such as high hs-CRP, reduced albumin:globulin ratio, and high interleukin-6, are by definition absent, but of course this does not exclude the possibility of intra-CNS inflammation. The patients with this second subtype of AD tend to be slightly older than those in the first, often in the eighth instead of seventh decade. Interestingly, Fiala's studies have shown that both inflammatory and non-inflammatory subtypes display phagocytic defects for amyloid- $\beta$  in their peripheral blood mononuclear cells [17]. This second subtype is also associated with ApoE4, and, as for the inflammatory subtype, tends to present with an amnesic syndrome and FDG-PET showing temporal-parietal reductions in glucose utilization.

In contrast to the profiles for the first two subtypes, the profile of the third subtype argues that it is a fundamentally different disease process than the first two: instead of losing the ability to form new memories as the initial presentation, in this subtype there is an initial loss of long-term memory maintenance, resulting in problems such as dyscalculia and aphasia, with an initial retention of new memory formation and retrieval. A recurring feature was the patients' ability to describe recent events in detail, but frequent inability to keep their trains of thought. In some cases, the presentation was associated with a history of depression. However, none had the visual hallucinations, delusions, REM behavioral disturbance, or autonomic disorders that would suggest Lewy body dementia. Some of the patients were also noted to become passive, simple-minded, or childlike, often in marked contrast to their earlier, highly-accomplished, hard-driving personalities. There was widespread cerebral atrophy (sometimes along with cerebellar atrophy), and early symptom onset in the fifth, sixth, or early seventh decades, but no ApoE4-related over-representation and typically no family history of Alzheimer's disease. Surprisingly, all had very low serum zinc, typically 50-60mcg/dl. It should be noted that serum zinc is a relatively insensitive test for zinc deficiency, so that low serum zinc is strongly suggestive of relatively severe zinc deficiency, but a normal serum zinc does not necessarily exclude some degree of zinc deficiency.

Zinc is the second most abundant trace metal in the human body, following only iron. Over 300 enzymes utilize zinc as a co-factor, either for catalysis (in which

it functions as a Lewis acid) or structure, and it typically sits in a distorted tetrahedral structure, coordinated with three or four protein side chains and interacting directly with a cysteine sulfur and/or histidine nitrogen and/or glutamate or aspartate oxygen [18]. Zinc deficiency, which is common in aging individuals, affects many functions that are directly or indirectly related to cognitive performance and Alzheimer's disease. For example, zinc deficiency induces insulin resistance, a known risk factor for AD. Zinc deficiency also increases inflammation, and reduces the finely tuned nature of the immune response, resulting in a reduced specific response (and thus loss of resistance to infectious agents) and a greater autoimmune response. Zinc is also involved in wound healing, DNA repair, and oxidative damage. Zinc deficiency is associated with increased aging, increased susceptibility to toxins, increased susceptibility to infections, increased production of reactive oxygen species, reduced hormonal function, reduced adrenal support, increased susceptibility to copper toxicity, and gastrointestinal hyperpermeability. Furthermore, zinc treatment has been shown to mitigate cognitive decline [19]. Therefore, zinc deficiency is a concern as a potential contributor to cognitive decline.

Zinc deficiency is relatively common, and may be associated with poor absorption due to reduced gastric acidity (e.g., due to *H. pylori* and/or the use of proton pump inhibitors), a zinc-deficient diet (e.g., due to vegetarianism without supplementation), adrenal stress, diabetes, alcohol use, toxic exposure, intestinal parasites, or aging. As noted above, serum zinc represents a relatively insensitive test for zinc; RBC zinc provides a more accurate assessment. Thus by the time that serum zinc is low, the body's zinc deficiency is likely to be quite severe.

The cause(s) of zinc deficiency in the six patients reported here is unknown, as is the potential relationship of the zinc deficiency to the distinctive neurodegenerative process. Given the relationship between zinc deficiency and susceptibility to toxins and infectious agents, historical data were obtained from all patients on potential toxic exposure. Whether or not causally related, all had histories of toxic exposures: one had grown up in Tom's River, New Jersey, a well documented area of extreme chemical toxicity; another had a sibling with childhood leukemia (which may suggest exposure to chemical toxins) and himself had worked for a chemical company for years, describing the difficulty with dealing with the severe chemical odors. Two others had lived in a home heavily contaminated with molds for years, another had worked with sewage for many years, and

another had had unusually extensive dental amalgam work over the years.

In summary, metabolic profiling of patients with cognitive decline, as described previously [5], reveals three readily distinguishable subtypes of Alzheimer's disease: inflammatory, non-inflammatory, and cortical. The distinctive features, presentation, lack of association with ApoE4, and marked hypozincemia, together suggest that the cortical subtype of Alzheimer's disease is a fundamentally different disease than the other two subtypes. This subtype deserves further genetic, epigenetic, and metabolomic studies.

## ACKNOWLEDGEMENTS

I thank Dr. Rammohan Rao, Dr. Aida Lasheen Bredesen, and Dr. Alexei Kurakin for discussions, and Rowena Abulencia for preparing the manuscript.

## Funding

I am grateful for support from the NIH (AG16570, AG034427 and AG036975), the Mary S. Easton Center for Alzheimer's Disease Research at UCLA, the Douglas and Ellen Rosenberg Foundation, the Stephen D. Bechtel, Jr. Foundation, the Joseph Drown Foundation, the Alzheimer's Association, the Accelerate Fund, the Buck Institute and Marin Community Foundation, the Michael and Catherine Podell Fund, Mr. Craig Johnson, Mr. Allan Bortell, and Ms. Michaela Hoag.

## Conflict of interest statement

The author of this manuscript declares no conflict of interest.

## REFERENCES

1. James BD, Leurgans SE, Hebert LE, Scherr PA, Yaffe K and Bennett DA. Contribution of Alzheimer disease to mortality in the United States. *Neurology*. 2014;82:1045-1050.
2. Sasanka Chakrabarti, Vineet Kumar Khemka, Anindita Banerjee, Gargi Chatterjee, Anirban Ganguly, Atanu Biswas. Metabolic Risk Factors of Sporadic Alzheimer's Disease: Implications in the Pathology, Pathogenesis and Treatment. *Aging and Disease*. 2015;6:282-299.
3. Ngandu T, Lehtisalo J, Solomon A, Levalahti E, Ahtiluoto S, Antikainen R, Backman L, Hanninen T, Jula A, Laatikainen T, Lindstrom J, Mangialasche F, Paajanen T, et al. A 2 year multidomain intervention of diet, exercise, cognitive training, and vascular risk monitoring versus control to prevent cognitive decline in at-risk elderly people (FINGER): a randomised controlled trial. *Lancet*. 2015;385:2255-2263.

4. Goetzl EJ, Boxer A, Schwartz JB, Abner EL, Petersen RC, Miller BL and Kapogiannis D. Altered lysosomal proteins in neural-derived plasma exosomes in preclinical Alzheimer disease. *Neurology*. 2015;85:40-47.
5. Bredesen DE. Reversal of cognitive decline: A novel therapeutic program. *Aging Journal*. 2014;6:1-11.
6. Heppner FL, Ransohoff RM and Becher B. Immune attack: the role of inflammation in Alzheimer disease. *Nat Rev Neurosci*. 2015;16:358-372.
7. Wyss-Coray T. Inflammation in Alzheimer disease: driving force, bystander or beneficial response? *Nat Med*. 2006;12:1005-1015.
8. Kauppinen A, Suuronen T, Ojala J, Kaarniranta K and Salminen A. Antagonistic crosstalk between NF-kappaB and SIRT1 in the regulation of inflammation and metabolic disorders. *Cell Signal*. 2013;25:1939-1948.
9. Theendakara V, Patent A, Peters Libeu CA, Philpot B, Flores S, Descamps O, Poksay KS, Zhang Q, Cailing G, Hart M, John V, Rao RV and Bredesen DE. Neuroprotective Sirtuin ratio reversed by ApoE4. *Proc Natl Acad Sci U S A*. 2013;110:18303-18308.
10. Lambert JC, Ibrahim-Verbaas CA, Harold D, Naj AC, Sims R, Bellenguez C, DeStafano AL, Bis JC, Beecham GW, Grenier-Boley B, Russo G, Thornton-Wells TA, Jones N, et al. Meta-analysis of 74,046 individuals identifies 11 new susceptibility loci for Alzheimer's disease. *Nat Genet*. 2013;45:1452-1458.
11. Mizwicki MT, Liu G, Fiala M, Magpantay L, Sayre J, Siani A, Mahanian M, Weitzman R, Hayden EY, Rosenthal MJ, Nemere I, Ringman J and Teplow DB. 1alpha,25-dihydroxyvitamin D3 and resolvin D1 retune the balance between amyloid-beta phagocytosis and inflammation in Alzheimer's disease patients. *J Alzheimers Dis*. 2013;34:155-170.
12. Kurakin A and Bredesen DE. Dynamic self-guiding analysis of Alzheimer's disease. *Oncotarget*. 2015;6:14092-14122.
13. Rocca WA and Henderson VW. Is there a link between gynecologic surgeries and Alzheimer disease? *Neurology*. 2014;82:196-197.
14. Zhang CE, Tian Q, Wei W, Peng JH, Liu GP, Zhou XW, Wang Q, Wang DW and Wang JZ. Homocysteine induces tau phosphorylation by inactivating protein phosphatase 2A in rat hippocampus. *Neurobiol Aging*. 2008;29:1654-1665.
15. Moustafa AA, Hewedi DH, Eissa AM, Frydecka D and Misiak B. Homocysteine levels in schizophrenia and affective disorders-focus on cognition. *Frontiers in behavioral neuroscience*. 2014;8:343.
16. Alladi S, Xuereb J, Bak T, Nestor P, Knibb J, Patterson K and Hodges JR. Focal cortical presentations of Alzheimer's disease. *Brain*. 2007;130:2636-2645.
17. Fiala M, Lin J, Ringman J, Kermani-Arab V, Tsao G, Patel A, Lossinsky AS, Graves MC, Gustavson A, Sayre J, Sofroni E, Suarez T, Chiappelli F, et al. Ineffective phagocytosis of amyloid-beta by macrophages of Alzheimer's disease patients. *J Alzheimers Dis*. 2005;7:221-232; discussion 255-262.
18. McCall KA, Huang CC, Fierke CA. Function and Mechanism of Zinc Metalloenzymes. *The Journal of Nutrition*. 2000;1427S-1446S.
19. Brewer GJ and Kaur S. Zinc deficiency and zinc therapy efficacy with reduction of serum free copper in Alzheimer's disease. *International journal of Alzheimer's disease*. 2013;2013:586365.

## Reversal of cognitive decline: A novel therapeutic program

Dale E. Bredesen<sup>1,2</sup>

<sup>1</sup> Mary S. Easton Center for Alzheimer's Disease Research, Department of Neurology, University of California, Los Angeles, CA 90095;

<sup>2</sup> Buck Institute for Research on Aging, Novato, CA 94945.

**Key words:** Alzheimer's, dementia, mild cognitive impairment, neurobehavioral disorders, neuroinflammation, neurodegeneration, systems biology

**Received:** 9/15/14; **Accepted:** 9/26/14; **Published:** 9/27/14 **doi:** [10.18632/aging.100690](https://doi.org/10.18632/aging.100690)

**Correspondence to:** Dale E. Bredesen, MD; **E-mail:** [dbredesen@mednet.ucla.edu](mailto:dbredesen@mednet.ucla.edu); [dbredesen@buckinstitute.org](mailto:dbredesen@buckinstitute.org)

**Copyright:** Bredesen. This is an open-access article distributed under the terms of the Creative Commons Attribution License, which permits unrestricted use, distribution, and reproduction in any medium, provided the original author and source are credited

**Abstract:** This report describes a novel, comprehensive, and personalized therapeutic program that is based on the underlying pathogenesis of Alzheimer's disease, and which involves multiple modalities designed to achieve metabolic enhancement for neurodegeneration (MEND). The first 10 patients who have utilized this program include patients with memory loss associated with Alzheimer's disease (AD), amnesic mild cognitive impairment (aMCI), or subjective cognitive impairment (SCI). Nine of the 10 displayed subjective or objective improvement in cognition beginning within 3-6 months, with the one failure being a patient with very late stage AD. Six of the patients had had to discontinue working or were struggling with their jobs at the time of presentation, and all were able to return to work or continue working with improved performance. Improvements have been sustained, and at this time the longest patient follow-up is two and one-half years from initial treatment, with sustained and marked improvement. These results suggest that a larger, more extensive trial of this therapeutic program is warranted. The results also suggest that, at least early in the course, cognitive decline may be driven in large part by metabolic processes. Furthermore, given the failure of monotherapeutics in AD to date, the results raise the possibility that such a therapeutic system may be useful as a platform on which drugs that would fail as monotherapeutics may succeed as key components of a therapeutic system.

## INTRODUCTION

### Magnitude of the problem

Cognitive decline is a major concern of the aging population, and Alzheimer's disease is the major cause of age-related cognitive decline, with approximately 5.4 million American patients and 30 million affected globally [1]. In the absence of effective prevention and treatment, the prospects for the future are of great concern, with 13 million Americans and 160 million globally projected for 2050, leading to potential bankruptcy of the Medicare system. Unlike several other chronic illnesses, Alzheimer's disease prevalence is on the rise, which makes the need to develop effective prevention and treatment increasingly pressing. Recent estimates suggest that AD has become the third leading cause of death in the United States [2],

behind cardiovascular disease and cancer. Furthermore, it has been pointed out recently that women are at the epicenter of the Alzheimer's epidemic, with 65% of patients and 60% of caregivers being women [3]. Indeed, a woman's chance of developing AD is now greater than her chance of developing breast cancer [4].

### Failure of monotherapeutics

Neurodegenerative disease therapeutics has been, arguably, the field of greatest failure of biomedical therapeutics development. Patients with acute illnesses such as infectious diseases, or with other chronic illnesses, such as cardiovascular disease, osteoporosis, human immunodeficiency virus infection, and even cancer, have access to more effective therapeutic options than do patients with AD or other neurodegenerative diseases such as Lewy body

dementia, frontotemporal lobar degeneration, and amyotrophic lateral sclerosis. In the case of Alzheimer's disease, there is not a single therapeutic that exerts anything beyond a marginal, unsustainable symptomatic effect, with little or no effect on disease progression. Furthermore, in the past decade alone, hundreds of clinical trials have been conducted for AD, at an aggregate cost of billions of dollars, without success. This has led some to question whether the approach taken to drug development for AD is an optimal one.

Therapeutic success for other chronic illnesses such as cardiovascular disease, cancer, and HIV, has been improved through the use of combination therapies [5]. In the case of AD and its predecessors, mild cognitive impairment (MCI) and subjective cognitive impairment (SCI), comprehensive combination therapies have not been explored. However, the past few decades of genetic and biochemical research have revealed an extensive network of molecular interactions involved in AD pathogenesis, suggesting that a network-based therapeutics approach, rather than a single target-based approach, may be feasible and potentially more effective for the treatment of cognitive decline due to Alzheimer's disease.

### Preclinical studies

Extensive preclinical studies from numerous laboratories have identified multiple pathogenetic targets for potential intervention. These include, in addition to amyloid- $\beta$  ( $A\beta$ ) oligomers and tau, inflammatory mediators, apolipoproteins and lipid metabolism factors, hormonal mediators, trophic factors and their receptors, calcium regulatory pathways, axoplasmic transport machinery, neurotransmitters and their receptors, prion protein, and a host of other potential targets. However, one of the drawbacks of these preclinical studies is that many have implicated single pathways, and shown large effects of targeting one pathway, whereas in human studies, such approaches have not been borne out. There are several possible inferences from such discrepant results: first, it is possible that it will be necessary to target multiple pathways simultaneously in order to effect an improvement in symptoms and pathophysiology. Second, it is possible that targeting a single pathway will be sufficient, but that earlier intervention will be required. Third, it is possible that all of these seemingly disparate pathways will converge on a single critical pathway, so that either a single targeted therapy or a multi-component, multi-targeted approach may be effective. And fourth, of course it is possible that neither of these two types of approaches will be

sufficient. It is worth noting, however, that it is possible that addressing multiple targets within the network underlying AD pathophysiology may be successful even when each target is affected in a relatively modest way; in other words, the effects of the various targets may be additive, multiplicative, or otherwise synergistic.

Based on a combination of in vitro and in vivo studies, we have advanced a model in which AD results from an imbalance in endogenous plasticity signaling (Fig. 1), [5-9], and in which the  $\beta$ -amyloid precursor protein (APP) is a mediator of such plasticity-related signaling. Thus the model suggests that AD is analogous to other chronic illnesses such as cancer, osteoporosis, and atherosclerosis. In the case of osteoporosis, osteoblastic signaling is chronically exceeded by osteoclastic signaling, resulting in an age-associated chronic illness featuring loss of bone. By analogy, in Alzheimer's disease, there is a fundamental, age-associated imbalance between the dynamically opposed physiological processes that mediate plasticity, i.e., between synaptoblastic and synaptoclastic activity. This signaling involves physiological mediators of synaptic development, maintenance, repair, and remodeling, including APP, its derivative peptides, ApoE, and tau, and is modulated by all of the many disparate factors associated with Alzheimer's disease. Furthermore, just as for neoplasia, positive feedback selects and amplifies the disease process; however, whereas in oncogenesis, the positive feedback occurs at the cellular level, in Alzheimer's disease, the positive feedback occurs at the molecular species level, in the form of prionic loops [5, 8, 9].

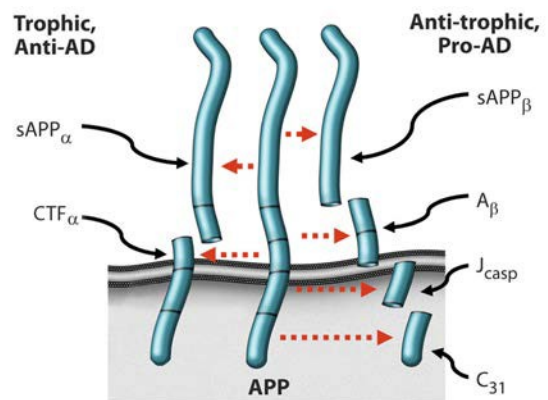


**Figure 1.** Alternative processing of, and signaling by, APP. [5].

In support of this model, the four peptides derived from the amyloidogenic processing of  $\beta$ -amyloid precursor protein (APP)—sAPP $\beta$ , A $\beta$ , Jcasp, and C31—have been shown to mediate neurite retraction, synaptic inhibition, caspase activation, and programmed cell death [6, 10-12]; whereas, in contrast, the two peptides derived from the non-amyloidogenic processing of APP—sAPP $\alpha$  and  $\alpha$ CTF—mediate neurite extension, and inhibit A $\beta$  production, caspase activation, and programmed cell death [13-15]. Thus APP appears to function as a molecular switch, mediating plasticity-related processes, and AD is associated, whether causally or incidentally, with an increase in the ratio of the neurite-retractive peptides to the neurite-extending peptides. Reducing this ratio, whether by affecting BACE ( $\beta$ -site APP cleaving enzyme) or other cleavage of APP, appears to mitigate the AD severity [7, 16, 17].

Of particular interest for the development of a therapeutic program whose goal is to correct the hypothesized chronic synaptoblastic:synaptoclastic imbalance is the feedback mechanism: whereas homeostatic (negative) feedback is utilized by biological systems with single goal outcomes (e.g., serum pH) and no requirement for amplification, prionic loop (positive) feedback is utilized by biological systems with multi-goal outcomes and a requirement for rapid amplification (e.g., thrombus formation or, potentially, synapse modulation), and such systems therefore function as molecular switches [9]. In these latter systems, the positive feedback feature of the systems dictates that the molecular mediators involved, or a subset thereof, beget more of themselves, or enhance their own activities. Thus such amplifying systems are prionic, with the degree of infectivity depending on the stability of the molecular species involved. In the case of APP signaling, binding of a trophic ligand such as netrin-1 increases the production of sAPP $\alpha$  [18], which inhibits BACE cleavage [19], with the complementary fragment,  $\alpha$ CTF, inhibiting  $\gamma$ -secretase cleavage [14]; thus cleavage at the  $\alpha$ -site produces fragments that inhibit cleavage at the  $\beta$ -site and  $\gamma$ -site rather than feeding back to reduce  $\alpha$ -site cleavage. Similarly, cleavage at the  $\beta$ -site and  $\gamma$ -site to produce A $\beta$  feeds back positively to increase APP-C31 production [20], thus favoring the pro-AD, anti-trophic processing of APP. Moreover, A $\beta$  itself has been shown to exhibit prionic properties [21], although the mechanism by which it does so has not been clarified.

Thus APP processing displays positive feedback, and therefore APP and its derivative peptides function as a molecular switch. This has critical implications for therapeutic development, since it offers a mechanism by

which a threshold effect occurs. We have taken advantage of this phenomenon to develop drug candidates that increase the anti-AD, trophic APP signaling, while reducing the pro-AD, anti-trophic APP signaling [22] and enhancing cognition [23].

We have found that the manipulation of the plasticity balance that is mediated or reflected by the APP-derivative peptide balance (Fig. 1), whether genetically or pharmacologically, leads to predictable effects on learning and memory. Mutation of the caspase site at Asp664 inhibits the synaptic loss, memory deficits, and dentate gyrus atrophy that otherwise occurs in the PDAPP transgenic mouse model of AD [7, 17, 24-26]. Furthermore, knock-in studies of a wild type mouse D664A support the notion that APP is indeed involved fundamentally in plasticity. (Kane, et al, unpublished data, 2014)

### Systems biology and systems therapeutics of AD

The transgenic mouse studies suggest that APP signaling can be manipulated to inhibit AD pathophysiology. However, the mouse models feature mutations in APP or other familial AD-related genes such as presenilin-1, whereas the large majority of patients with AD suffer from sporadic AD, without an APP or PS1 mutation (although the majority do express the  $\epsilon$ 4 allele of ApoE). Given the many inputs to the APP signaling balance in humans (e.g., estrogen, netrin-1, A $\beta$ , etc.), and the minimal success with each of many potentially therapeutic agents (e.g., estrogen, melatonin, exercise, vitamin D, curcumin, *Ashwagandha*, etc.), the pathobiology of AD dictates a system or program rather than a single targeted agent. Successes with other chronic illnesses such as cardiovascular disease, neoplasia, and HIV support the efficacy of multiple-component systems. My colleague and I have recently described such a system for AD [5]. The basic tenets for such a comprehensive therapeutic system are the following:

1) Just as for other chronic illnesses such as atherosclerotic cardiovascular disease, the goal is not simply to normalize metabolic parameters, but rather to optimize them. As an example, a serum homocysteine level of 12  $\mu$ mol/l is considered to be within normal limits, but is well documented to be suboptimal [27]. Similar arguments can be made for many other metabolic parameters.

2) Based on the hypothesis that AD results from an imbalance in an extensive plasticity network, the therapy should address as many of the network components as possible, with the idea that a combination may create an effect that is more than the sum of the effects of many monotherapeutics [5].

3) Just as for other chronic illnesses such as osteoporosis, cancer, and cardiovascular disease, the underlying network features a threshold effect, such that, once enough of the network components have been impacted, the pathogenetic process would be halted or reversed. Therefore, even though it is not expected that most patients will be able to follow every single step of the protocol, as long as enough steps are followed to exceed the threshold, that should be sufficient.

4) The approach is personalized, based on the contributory laboratory values affecting the plasticity network; and is computationally intensive, since many physiological data points are analyzed, interdependent network-component status is assessed, and many interventions are prioritized to determine the therapeutic program.

5) The program is iterative, so that there is continued optimization over time.

6) For each network component, the goal is to address it in as physiological a way, and as far upstream, as possible.

## RESULTS

### CASE STUDIES

#### Patient one: history

A 67-year-old woman presented with two years of progressive memory loss. She held a demanding job that involved preparing analytical reports and traveling widely, but found herself no longer able to analyze data or prepare the reports, and therefore was forced to consider quitting her job. She noted that when she would read, by the time she reached the bottom of a page she would have to start at the top once again, since she was unable to remember the material she had just read. She was no longer able to remember numbers, and had to write down even 4-digit numbers to remember them. She also began to have trouble navigating on the road: even on familiar roads, she would become lost trying to figure out where to enter or exit the road. She also noticed that she would mix up the names of her pets, and forget where the light switches were in her home of years.

Her mother had developed similar progressive cognitive decline beginning in her early 60s, had become severely demented, entered a nursing home, and died at approximately 80 years of age. When the patient consulted her physician about her problems, she was told that she had the same problem her mother had had, and that there was nothing he could do about it. He wrote “memory problems” in her chart, and therefore

the patient was turned down in her application for long-term care.

After being informed that she had the same problem as her mother had had, she recalled the many years of her mother’s decline in a nursing home. Knowing that there was still no effective treatment and subsequently losing the ability to purchase long-term care, she decided to commit suicide. She called a friend to commiserate, who suggested that she get on a plane and visit, and then referred her for evaluation.

She began System 1.0 (Table 1), and was able to adhere to some but not all of the protocol components. Nonetheless, after three months she noted that all of her symptoms had abated: she was able to navigate without problems, remember telephone numbers without difficulty, prepare reports and do all of her work without difficulty, read and retain information, and, overall, she became asymptomatic. She noted that her memory was now better than it had been in many years. On one occasion, she developed an acute viral illness, discontinued the program, and noticed a decline, which reversed when she reinstated the program. Two and one-half years later, now age 70, she remains asymptomatic and continues to work full-time.

#### Patient one: therapeutic program

As noted above, and following an extended discussion of the components of the therapeutic program, the patient began on some but not all of the system: (1) she eliminated all simple carbohydrates, leading to a weight loss of 20 pounds; (2) she eliminated gluten and processed food from her diet, and increased vegetables, fruits, and non-farmed fish; (3) in order to reduce stress, she began yoga, and ultimately became a yoga instructor; (4) as a second measure to reduce the stress of her job, she began to meditate for 20 minutes twice per day; (5) she took melatonin 0.5mg po qhs; (6) she increased her sleep from 4-5 hours per night to 7-8 hours per night; (7) she took methylcobalamin 1mg each day; (8) she took vitamin D3 2000IU each day; (9) she took fish oil 2000mg each day; (10) she took CoQ10 200mg each day; (11) she optimized her oral hygiene using an electric flosser and electric toothbrush; (12) following discussion with her primary care provider, she reinstated HRT (hormone replacement therapy) that had been discontinued following the WHI report in 2002; (13) she fasted for a minimum of 12 hours between dinner and breakfast, and for a minimum of three hours between dinner and bedtime; (14) she exercised for a minimum of 30 minutes, 4-6 days per week.

**Table 1. Therapeutic System 1.0**

<b>Goal</b>	<b>Approach</b>	<b>Rationale and References</b>
Optimize diet: minimize simple CHO, minimize inflammation.	Patients given choice of several low glycemic, low inflammatory, low grain diets.	Minimize inflammation, minimize insulin resistance.
Enhance autophagy, ketogenesis	Fast 12 hr each night, including 3 hr prior to bedtime.	Reduce insulin levels, reduce A $\beta$ .
Reduce stress	Personalized—yoga or meditation or music, etc.	Reduction of cortisol, CRF, stress axis.
Optimize sleep	8 hr sleep per night; melatonin 0.5mg po qhs; Trp 500mg po 3x/wk if awakening. Exclude sleep apnea.	[36]
Exercise	30-60' per day, 4-6 days/wk	[37, 38]
Brain stimulation	Posit or related	[39]
Homocysteine <7	Me-B12, MTHF, P5P; TMG if necessary	[40]
Serum B12 >500	Me-B12	[41]
CRP <1.0; A/G >1.5	Anti-inflammatory diet; curcumin; DHA/EPA; optimize hygiene	Critical role of inflammation in AD
Fasting insulin <7; HgbA1c <5.5	Diet as above	Type II diabetes-AD relationship
Hormone balance	Optimize ft3, ft4, E2, T, progesterone, pregnenolone, cortisol	[5, 42]
GI health	Repair if needed; prebiotics and probiotics	Avoid inflammation, autoimmunity
Reduction of A-beta	Curcumin, Ashwagandha	[43-45]
Cognitive enhancement	Bacopa monniera, MgT	[46, 47]
25OH-D3 = 50-100ng/ml	Vitamins D3, K2	[48]
Increase NGF	H. erinaceus or ALCAR	[49, 50]
Provide synaptic structural components	Citicoline, DHA	[51].
Optimize antioxidants	Mixed tocopherols and tocotrienols, Se, blueberries, NAC, ascorbate, $\alpha$ -lipoic acid	[52]
Optimize Zn:fCu ratio	Depends on values obtained	[53]
Ensure nocturnal oxygenation	Exclude or treat sleep apnea	[54]
Optimize mitochondrial function	CoQ or ubiquinol, $\alpha$ -lipoic acid, PQQ, NAC, ALCAR, Se, Zn, resveratrol, ascorbate, thiamine	[55]
Increase focus	Pantothenic acid	Acetylcholine synthesis requirement
Increase SirT1 function	Resveratrol	[32]
Exclude heavy metal toxicity	Evaluate Hg, Pb, Cd; chelate if indicated	CNS effects of heavy metals
MCT effects	Coconut oil or Axona	[56]

CHO, carbohydrates; Hg, mercury; Pb, lead; Cd, cadmium; MCT, medium chain triglycerides; PQQ, polyquinoline quinone; NAC, N-acetyl cysteine; CoQ, coenzyme Q; ALCAR, acetyl-L-carnitine; DHA, docosahexaenoic acid; MgT, magnesium threonate; ft3, free triiodothyronine; ft4, free thyroxine; E2, estradiol; T, testosterone; Me-B12, methylcobalamin; MTHF, methyltetrahydrofolate; P5P, pyridoxal-5-phosphate; TMG, trimethylglycine; Trp, tryptophan

### **Patient two: history**

A 69-year-old entrepreneur and professional man presented with 11 years of slowly progressive memory loss, which had accelerated over the past one or two years. In 2002, at the age of 58, he had been unable to recall the combination of the lock on his locker, and he felt that this was out of the ordinary for him. In 2003, he had FDG-PET (fluoro-deoxyglucose positron emission tomography), which was read as showing a pattern typical for early Alzheimer's disease, with reduced glucose utilization in the parietotemporal cortices bilaterally and left > right temporal lobes, but preserved utilization in the frontal lobes, occipital cortices, and basal ganglia. In 2003, 2007, and 2013, he had quantitative neuropsychological testing, which showed a reduction in CVLT (California Verbal Learning Test) from 84<sup>th</sup> to 1<sup>st</sup> percentile, a Stroop color test at 16<sup>th</sup> percentile, and auditory delayed memory at 13<sup>th</sup> percentile. In 2013, he was found to be heterozygous for ApoE4 (3/4). He noted that he had progressive difficulty recognizing the faces at work (prosopagnosia), and had to have his assistants prompt him with the daily schedule. He also recalled an event during which he was several chapters into a book before he finally realized that it was a book he had read previously. In addition, he lost an ability he had had for most of his life: the ability to add columns of numbers rapidly in his head.

He had a homocysteine of 18  $\mu\text{mol/l}$ , CRP <0.5mg/l, 25-OH cholecalciferol 28ng/ml, hemoglobin A1c 5.4%, serum zinc 78mcg/dl, serum copper 120mcg/dl, ceruloplasmin 25mg/dl, pregnenolone 6ng/dl, testosterone 610ng/dl, albumin:globulin ratio of 1.3, cholesterol 165mg/dl (on Lipitor), HDL 92, LDL 64, triglyceride 47, AM cortisol 14mcg/dl, free T3 3.02pg/ml, free T4 1.27ng/l, TSH 0.58mIU/l, and BMI 24.9.

He began on the therapeutic program, and after six months, his wife, co-workers, and he all noted improvement. He lost 10 pounds. He was able to recognize faces at work unlike before, was able to remember his daily schedule, and was able to function at work without difficulty. He was also noted to be quicker with his responses. His life-long ability to add columns of numbers rapidly in his head, which he had lost during his progressive cognitive decline, returned. His wife pointed out that, although he had clearly shown improvement, the more striking effect was that he had been accelerating in his decline over the prior year or two, and this had been completely halted.

### **Patient two: therapeutic program**

The patient began on the following parts of the overall

therapeutic system: (1) he fasted for a minimum of three hours between dinner and bedtime, and for a minimum of 12 hours between dinner and breakfast; (2) he eliminated simple carbohydrates and processed foods from his diet; (3) he increased consumption of vegetables and fruits, and limited consumption of fish to non-farmed, and meat to occasional grass-fed beef or organic chicken; (4) he took probiotics; (5) he took coconut oil 1 tsp bid; (6) he exercised strenuously, swimming 3-4 times per week, cycling twice per week, and running once per week; (7) he took melatonin 0.5mg po qhs, and tried to sleep as close to 8 hours per night as his schedule would allow; (8) he took herbs *Bacopa monniera* 250mg, *Ashwagandha* 500mg, and turmeric 400mg each day; (9) he took methylcobalamin 1mg, methyltetrahydrofolate 0.8mg, and pyridoxine-5-phosphate 50mg each day; (10) he took citicoline 500mg po bid; (11) he took vitamin C 1g per day, vitamin D3 5000IU per day, vitamin E 400IU per day, CoQ10 200mg per day, Zn picolinate 50mg per day, and  $\alpha$ -lipoic acid 100mg per day; (12) he took DHA (docosahexaenoic acid) 320mg and EPA (eicosapentaenoic acid) 180mg per day.

### **Patient three: history**

A 55-year-old attorney suffered progressively severe memory loss for four years. She accidentally left the stove on when she left her home on multiple occasions, and then returned, horrified to see that she had left it on once again. She would forget meetings, and agree to multiple meetings at the same time. Because of an inability to remember anything after a delay, she would record conversations, and she carried an iPad on which she took copious notes (but then forgot the password to unlock her iPad). She had been trying to learn Spanish as part of her job, but was unable to remember virtually anything new. She was unable to perform her job, and she sat her children down to explain to them that they could no longer take advantage of her poor memory, that instead they must understand that her memory loss was a serious problem. Her children noted that she frequently became lost in mid-sentence, that she was slow with responses, and that she frequently asked if they had followed up on something she thought she had asked them to do, when in fact she had never asked them to do the tasks to which she referred.

Her homocysteine was 9.8 $\mu\text{mol/l}$ , CRP 0.16mg/l, 25-OH cholecalciferol 46ng/ml, hemoglobin A1c 5.3%, pregnenolone 84ng/dl, DHEA 169ng/dl, estradiol 275pg/ml, progesterone 0.4ng/ml, insulin 2.7 $\mu\text{IU/ml}$ , AM cortisol 16.3mcg/dl, free T3 3.02pg/ml, free T4 1.32ng/l, and TSH 2.04mIU/l.

After five months on the therapeutic program, she noted that she no longer needed her iPad for notes, and no longer needed to record conversations. She was able to work once again, was able to learn Spanish, and began to learn a new legal specialty. Her children noted that she no longer became lost in mid-sentence, no longer thought she had asked them to do something that she had not asked, and answered their questions with normal rapidity and memory.

### Patient three: therapeutic program

She began on the following parts of the therapeutic system: (1) she fasted for a minimum of three hours between dinner and bedtime, and for a minimum of 12 hours between dinner and breakfast; (2) she eliminated simple carbohydrates and processed foods from her diet;

(3) she increased consumption of vegetables and fruits, limited consumption of fish to non-farmed, and did not eat meat; (4) she exercised 4-5 times per week; (5) she took melatonin 0.5mg po qhs, and tried to sleep as close to 8 hours per night as her schedule would allow; (6) she tried to reduce stress in her life with meditation and relaxation; (7) she took methylcobalamin 1mg 4x/wk and pyridoxine-5-phosphate 20mg each day; (8) she took citicoline 200mg each day; (9) she took vitamin D3 2000IU per day and CoQ10 200mg per day; (10) she took DHA 700mg and EPA 500mg bid; (11) her primary care provider prescribed bioidentical estradiol with estriol (BIEST), and progesterone; (12) her primary care provider worked with her to reduce her bupropion from 150mg per day to 150mg 3x/wk.

All 10 patients are summarized in Table 2.

**Table 2. Summary of patients treated with the therapeutic system described**

Patient	History, evaluation	Diagnosis	Status
67F 3/3	2yr memory ↓; FH+	aMCI	Normal x 2.5 yrs; working
69M 4/3	12yr memory ↓; FDG-PET+, NPsych+	Early AD	“Clearly improved;” working
70M 4/3	4yr memory ↓; NPsych+, failed MemTrax	AD	Improved; MemTrax passed
75M 3/3	1yr memory ↓	SCI	Improved; working
75F C677T	1yr memory ↓	aMCI/early AD	Improved
55F 3/3	4yr memory ↓	aMCI/early AD	Normal; working
72M 3/3	7yr memory ↓	aMCI	Improved; working
55M 4/3	2yr memory ↓	SCI	Normal; working
63F 4/3	FH dementia, mild memory ↓	SCI	Normal, negative amyloid PET; working
60F 4/3	4yr rapid decline; MoCA 6, amyloid PET+	Late AD	Decline

F, female; M, male; 3/3, ApoE 3/3; 4/3, ApoE 4/3; C677T, the C677T mutation in methylene tetrahydrofolate reductase (MTHFR); FH, family history; aMCI, amnesic mild cognitive impairment; SCI, subjective cognitive impairment; FDG-PET+, fluorodeoxyglucose positron emission tomography interpreted as typical of Alzheimer’s disease; amyloid PET+, amyloid PET scan read as abnormal, indicative of amyloid accumulation; NPsych+, quantitative neuropsychology tests showing abnormalities typical of AD; MoCA, Montreal Cognitive Assessment; MemTrax, an iPhone application that quantitates memory.

## DISCUSSION

Results from the 10 patients reported here suggest that memory loss in patients with subjective cognitive impairment, mild cognitive impairment, and at least the early phase of Alzheimer's disease, may be reversed, and improvement sustained, with the therapeutic program described here. This is the first such demonstration. However, at the current time the results are anecdotal, and therefore a more extensive, controlled clinical trial is warranted.

The results reported here are compatible with the notion that metabolic status represents a crucial, and readily manipulable, determinant of plasticity, and in particular of the abnormal balance of plasticity exhibited in SCI, MCI, and early AD. Furthermore, whereas the normalization of a single metabolic parameter, such as vitamin D3, may exert only a modest effect on pathogenesis, the optimization of a comprehensive set of parameters, which together form a functional network, may have a much more significant effect on pathogenesis and thus on function.

The therapeutic system described in this report derives from basic studies of the role of APP signaling and proteolysis in plasticity, and the imbalance in this receptor proteolysis that reproducibly occurs in Alzheimer's disease. There are numerous physiological parameters that feed into this balance, such as hormones [28, 29], trophic factors [18], glucose metabolism [30], inflammatory mediators [31], ApoE genetic status [32] sleep-related factors [33], exercise-related factors [34], and many others; therefore, the therapeutic system is designed to reverse the self-reinforcing (i.e., prionic) signaling imbalance that we have hypothesized to mediate Alzheimer's disease pathophysiology [8].

One potentially critical result from the study is the impact of the therapeutic program on the ability of the various patients to work effectively. Six of the 10 patients had had to discontinue working or were struggling with their jobs at the time of presentation, and all were able to return to work or continue working with improved performance. One additional patient had not had difficulty at work at the time of presentation, and has continued to work without difficulty. The other three patients had not worked for years, and did not begin again after treatment. The improvement in function that is required to work effectively after struggling due to cognitive decline is an important outcome of any successful therapeutic system, and is ultimately more critical to the patients than biomarker effects or test performance.

It is recognized that the system described here is an initial system, one that is likely to benefit from optimization. The system is designed to address multiple key pathogenetic mechanisms, but most of the key pathogenetic mechanisms are suboptimally affected by this initial system. This highlights multiple potential therapeutic targets, and optimizing the therapeutics for each of these targets is the goal of ongoing research and development.

It is noteworthy that the major side effect of this therapeutic system is improved health and optimal BMI (body mass index), a result in stark contrast to monopharmaceutical treatments. However, the program is not easy to follow, and none of the patients followed the entire protocol. The significant diet and lifestyle changes, and multiple pills required each day, were the two most common complaints of the patients. However, these complaints were mitigated by the fact that all of the patients had previously been made aware, either through their physicians or the media, that their prognosis was poor and their cognitive decline essentially untreatable.

One potentially important application of the therapeutic program described herein is that such a therapeutic system may be useful as a platform on which drugs that would fail as monotherapeutics may succeed as key components of a therapeutic system. Combination therapeutics have proven successful in multiple chronic illnesses, such as HIV and cancer [5].

The positive results reported here are perhaps not surprising given that therapeutic programs have proven more effective than monotherapeutics in multiple chronic illnesses, such as atherosclerotic cardiovascular disease, HIV, and cancer [5, 35]. Indeed, chronic illnesses may be more amenable to therapeutic systems than to monotherapeutics. However, the current, anecdotal results require a larger trial, not only to confirm or refute the results reported here, but also to address key questions raised, such as the degree of improvement that can be achieved routinely, how late in the course of cognitive decline reversal can be effected, whether such an approach may be effective in patients with familial Alzheimer's disease, and how long improvement can be sustained.

### In summary:

- A novel, comprehensive, and personalized therapeutic system is described that is based on the underlying pathogenesis of Alzheimer's disease. The basic tenets for the development of this system are also described.

- Of the first 10 patients who utilized this program, including patients with memory loss associated with Alzheimer's disease (AD), amnesic mild cognitive impairment (aMCI), or subjective cognitive impairment (SCI), nine showed subjective or objective improvement.
- One potentially important outcome is that all six of the patients whose cognitive decline had a major impact on job performance were able to return to work or continue working without difficulty.
- These anecdotal results suggest the need for a controlled clinical trial of the therapeutic program.

## ACKNOWLEDGEMENTS

I am grateful for support from the NIH (AG16570, AG034427 and AG036975), the Mary S. Easton Center for Alzheimer's Disease Research at UCLA, the Douglas and Ellen Rosenberg Foundation, the Stephen D. Bechtel, Jr. Foundation, the Joseph Drown Foundation, the Alzheimer's Association, the Accelerate Fund, the Buck Institute and Marin Community Foundation, the Michael and Catherine Podell Fund, Mr. Craig Johnson, and Ms. Michaela Hoag. I thank Dr. David Jones, Dr. Rammohan Rao, and Dr. Varghese John for discussions, and Rowena Abulencia for preparing the manuscript.

## Conflict of interest statement

The author of this manuscript declares no conflict of interest.

## REFERENCES

1. Prince MA, Emiliano; Guerchet, Maëlen; Prina, Matthew. 2014; World Alzheimer Report 2014 United Kingdom: Alzheimer's Disease International.
2. James BD, Leurgans SE, Hebert LE, Scherr PA, Yaffe K and Bennett DA. Contribution of Alzheimer disease to mortality in the United States. *Neurology*. 2014;82:1045-1050.
3. Shriver M. A Woman's Nation Takes on Alzheimer's. 2010; New York, USA: Alzheimer's Association.
4. 2014 Alzheimer's Disease Facts and Figures. Special Report on Women and Alzheimer's Disease. USA: Alzheimer's Association, 2014; pp. 1-80.
5. Bredesen DE, John, V. Next generation therapeutics for Alzheimer's disease. *EMBO Mol Med*. 2013; 5:795-798.
6. Lu DC, Rabizadeh S, Chandra S, Shayya RF, Ellerby LM, Ye X, Salvesen GS, Koo EH and Bredesen DE. A second cytotoxic proteolytic peptide derived from amyloid beta-protein precursor. *Nat Med*. 2000;6:397-404.
7. Galvan V, Gorostiza OF, Banwait S, Ataie M, Logvinova AV, Sitaraman S, Carlson E, Sagi SA, Chevallier N, Jin K, Greenberg DA and Bredesen DE. Reversal of Alzheimer's-like pathology and behavior in human APP transgenic mice by mutation of Asp664. *Proc Natl Acad Sci U S A*. 2006;103:7130-7135.

8. Bredesen DE. Neurodegeneration in Alzheimer's disease: caspases and synaptic element interdependence. *Mol Neurodegener*. 2009;4:27.
9. Bredesen DE. Prionic Loops, Anti-Prions, and Dependence Receptors in Neurodegeneration. In: Legname GR, Detlev, ed. *Prion Research of Stan Prusiner and his Colleagues*. 2013; (Germany: Dusseldorf University Press), pp. 1-24.
10. Lu DC, Shaked GM, Maslah E, Bredesen DE and Koo EH. Amyloid beta protein toxicity mediated by the formation of amyloid-beta protein precursor complexes. *Ann Neurol*. 2003; 54:781-789.
11. Bertrand E, Brouillet E, Caille I, Bouillot C, Cole GM, Prochiantz A and Allinquant B. A short cytoplasmic domain of the amyloid precursor protein induces apoptosis in vitro and in vivo. *Mol Cell Neurosci*. 2001;18:503-511.
12. Nikolaev A, McLaughlin T, O'Leary DD and Tessier-Lavigne M. APP binds DR6 to trigger axon pruning and neuron death via distinct caspases. *Nature*. 2009;457:981-989.
13. Guo H, Tittle TV, Allen H and Maziarz RT. Brefeldin A-mediated apoptosis requires the activation of caspases and is inhibited by Bcl-2. *Exp Cell Res*. 1998;245:57-68.
14. Tian Y, Crump CJ and Li YM. Dual role of alpha-secretase cleavage in the regulation of gamma-secretase activity for amyloid production. *J Biol Chem*. 2010;285:32549-32556.
15. Deyts C, Vetrivel KS, Das S, Shepherd YM, Dupre DJ, Thinakaran G and Parent AT. Novel GalphaS-Protein Signaling Associated with Membrane-Tethered Amyloid Precursor Protein Intracellular Domain. *J Neurosci*. 2012;32:1714-1729.
16. Jonsson T, Atwal JK, Steinberg S, Snaedal J, Jonsson PV, Bjornsson S, Stefansson H, Sulem P, Gudbjartsson D, Maloney J, Hoyte K, Gustafson A, Liu Y, et al. A mutation in APP protects against Alzheimer's disease and age-related cognitive decline. *Nature*. 2012;488:96-99.
17. Bredesen DE, John, V., Galvan, V. Importance of the caspase cleavage site in amyloid-beta protein precursor. *J Alzheimers Dis*. 2010; 22:57-63.
18. Lourenco FC, Galvan V, Fombonne J, Corset V, Llambi F, Muller U, Bredesen DE and Mehlen P. Netrin-1 interacts with amyloid precursor protein and regulates amyloid-beta production. *Cell Death Differ*. 2009;16:655-663.
19. Obregon D, Hou H, Deng J, Giunta B, Tian J, Darlington D, Shahaduzzaman M, Zhu Y, Mori T, Mattson MP and Tan J. Soluble amyloid precursor protein-alpha modulates beta-secretase activity and amyloid-beta generation. *Nature communications*. 2012;3:777.
20. Lu D, Soriano S, Bredesen D and Koo E. Caspase cleavage of the amyloid precursor protein modulates amyloid beta-protein toxicity. *J Neurochem*. 2003;87:733-741.
21. Meyer-Luehmann M, Coomaraswamy J, Bolmont T, Kaeser S, Schaefer C, Kilger E, Neuenschwander A, Abramowski D, Frey P, Jaton AL, Vigouret JM, Paganetti P, Walsh DM, et al. Exogenous induction of cerebral beta-amyloidogenesis is governed by agent and host. *Science*. 2006;313:1781-1784.
22. Spilman P, Descamps O, Gorostiza O, Peters-Libe C, Poksay KS, Matalis A, Campagna J, Patent A, Rao R, John V and Bredesen DE. The multi-functional drug tropisetron binds APP and normalizes cognition in a murine Alzheimer's model. *Brain Res*. 2014; 1551:25-44.
23. Zhang XY, Liu L, Liu S, Hong X, Chen da C, Xiu MH, Yang FD, Zhang Z, Zhang X, Kosten TA and Kosten TR. Short-term

- tropisetron treatment and cognitive and P50 auditory gating deficits in schizophrenia. *Am J Psychiatry*. 2012; 169:974-981.
24. Saganich MJ, Schroeder BE, Galvan V, Bredesen DE, Koo EH and Heinemann SF. Deficits in synaptic transmission and learning in amyloid precursor protein (APP) transgenic mice require C-terminal cleavage of APP. *J Neurosci*. 2006;26:13428-13436.
25. Banwait S, Galvan V, Zhang J, Gorostiza OF, Ataie M, Huang W, Crippen D, Koo EH and Bredesen DE. C-terminal cleavage of the amyloid-beta protein precursor at Asp664: a switch associated with Alzheimer's disease. *J Alzheimers Dis*. 2008; 13:1-16.
26. Galvan V, Zhang J, Gorostiza OF, Banwait S, Huang W, Ataie M, Tang H and Bredesen DE. Long-term prevention of Alzheimer's disease-like behavioral deficits in PDAPP mice carrying a mutation in Asp664. *Behav Brain Res*. 2008; 191:246-255.
27. Heijer T, Skoog I, Oudkerk M, de Leeuw FE, de Groot JC, Hofman A and Breteler MM. Association between blood pressure levels over time and brain atrophy in the elderly. *Neurobiol Aging*. 2003;24:307-313.
28. Lan YL, Zhao J and Li S. Update on the Neuroprotective Effect of Estrogen Receptor Alpha Against Alzheimer's Disease. *J Alzheimers Dis*. 2014.
29. Shi C, Zhu X, Wang J and Long D. Estrogen receptor alpha promotes non-amyloidogenic processing of platelet amyloid precursor protein via the MAPK/ERK pathway. *J Steroid Biochem Mol Biol*. 2014;144PB:280-285.
30. Yang Y, Wu Y, Zhang S and Song W. High glucose promotes Abeta production by inhibiting APP degradation. *PLoS One*. 2013; 8:e69824.
31. Sutinen EM, Pirttila T, Anderson G, Salminen A and Ojala JO. Pro-inflammatory interleukin-18 increases Alzheimer's disease-associated amyloid-beta production in human neuron-like cells. *Journal of neuroinflammation*. 2012;9:199.
32. Theendakara V, Patent A, Peters Libeu CA, Philpot B, Flores S, Descamps O, Poksay KS, Zhang Q, Cailing G, Hart M, John V, Rao RV and Bredesen DE. Neuroprotective Sirtuin ratio reversed by ApoE4. *Proc Natl Acad Sci U S A*. 2013;110:18303-18308.
33. Wade AG, Farmer M, Harari G, Fund N, Laudon M, Nir T, Frydman-Marom A and Zisapel N. Add-on prolonged-release melatonin for cognitive function and sleep in mild to moderate Alzheimer's disease: a 6-month, randomized, placebo-controlled, multicenter trial. *Clin Interv Aging*. 2014;9:947-961.
34. Cotman CW, Berchtold NC and Christie LA. Exercise builds brain health: key roles of growth factor cascades and inflammation. *Trends Neurosci*. 2007;30:464-472.
35. Silberman A, Banthia R, Estay IS, Kemp C, Studley J, Hareras D and Ornish D. The effectiveness and efficacy of an intensive cardiac rehabilitation program in 24 sites. *Am J Health Promot*. 2010; 24:260-266.
36. Polimeni G, Esposito E, Bevelacqua V, Guarneri C and Cuzzocrea S. Role of melatonin supplementation in neurodegenerative disorders. *Front Biosci (Landmark Ed)*. 2014; 19:429-446.
37. Aguiar P, Monteiro L, Feres A, Gomes I and Melo A. Rivastigmine transdermal patch and physical exercises for Alzheimer's disease: a randomized clinical trial. *Curr Alzheimer Res*. 2014; 11:532-537.
38. Smith JC, Nielson KA, Woodard JL, Seidenberg M, Durgerian S, Hazlett KE, Figueroa CM, Kandah CC, Kay CD, Matthews MA and Rao SM. Physical activity reduces hippocampal atrophy in elders at genetic risk for Alzheimer's disease. *Frontiers in aging neuroscience*. 2014; 6:61.
39. Smith GE, Housen P, Yaffe K, Ruff R, Kennison RF, Mahncke HW and Zelinski EM. A cognitive training program based on principles of brain plasticity: results from the Improvement in Memory with Plasticity-based Adaptive Cognitive Training (IMPACT) study. *J Am Geriatr Soc*. 2009;57:594-603.
40. Hooshmand B, Solomon A, Kareholt I, Leiviska J, Rusanen M, Ahtiluoto S, Winblad B, Laatikainen T, Soininen H and Kivipelto M. Homocysteine and holotranscobalamin and the risk of Alzheimer disease: a longitudinal study. *Neurology*. 2010; 75:1408-1414.
41. Tangney CC, Tang Y, Evans DA and Morris MC. Biochemical indicators of vitamin B12 and folate insufficiency and cognitive decline. *Neurology*. 2009;72:361-367.
42. Yaffe K, Haan M, Byers A, Tangen C and Kuller L. Estrogen use, APOE, and cognitive decline: evidence of gene-environment interaction. *Neurology*. 2000;54:1949-1954.
43. Begum AN, Jones MR, Lim GP, Morihara T, Kim P, Heath DD, Rock CL, Pruitt MA, Yang F, Hudspeth B, Hu S, Faull KF, Teter B, et al. Curcumin structure-function, bioavailability, and efficacy in models of neuroinflammation and Alzheimer's disease. *J Pharmacol Exp Ther*. 2008;326:196-208.
44. Ma QL, Zuo X, Yang F, Ubeda OJ, Gant DJ, Alaverdyan M, Teng E, Hu S, Chen PP, Maiti P, Teter B, Cole GM and Frautschy SA. Curcumin suppresses soluble tau dimers and corrects molecular chaperone, synaptic, and behavioral deficits in aged human tau transgenic mice. *J Biol Chem*. 2013;288:4056-4065.
45. Sehgal N, Gupta A, Valli RK, Joshi SD, Mills JT, Hamel E, Khanna P, Jain SC, Thakur SS and Ravindranath V. Withania somnifera reverses Alzheimer's disease pathology by enhancing low-density lipoprotein receptor-related protein in liver. *Proc Natl Acad Sci U S A*. 2012;109:3510-3515.
46. Zanotta D, Puricelli S and Bonoldi G. Cognitive effects of a dietary supplement made from extract of *Bacopa monnieri*, astaxanthin, phosphatidylserine, and vitamin E in subjects with mild cognitive impairment: a noncomparative, exploratory clinical study. *Neuropsychiatr Dis Treat*. 2014; 10:225-230.
47. Li W, Yu J, Liu Y, Huang X, Abumaria N, Zhu Y, Xiong W, Ren C, Liu XG, Chui D and Liu G. Elevation of brain magnesium prevents and reverses cognitive deficits and synaptic loss in Alzheimer's disease mouse model. *J Neurosci*. 2013; 33:8423-8441.
48. Littlejohns TJ, Henley WE, Lang IA, Annweiler C, Beauchet O, Chaves PH, Fried L, Kestenbaum BR, Kuller LH, Langa KM, Lopez OL, Kos K, Soni M, et al. Vitamin D and the risk of dementia and Alzheimer disease. *Neurology*. 2014.
49. Mori K, Obara Y, Hirota M, Azumi Y, Kinugasa S, Inatomi S and Nakahata N. Nerve growth factor-inducing activity of *Hericium erinaceus* in 1321N1 human astrocytoma cells. *Biol Pharm Bull*. 2008;31:1727-1732.
50. Tagliatalata G, Navarra D, Cruciani R, Ramacci MT, Alema GS and Angelucci L. Acetyl-L-carnitine treatment increases nerve growth factor levels and choline acetyltransferase activity in the central nervous system of aged rats. *Exp Gerontol*. 1994; 29:55-66.
51. Cansev M, Wurtman RJ, Sakamoto T and Ulus IH. Oral administration of circulating precursors for membrane phosphatides can promote the synthesis of new brain synapses. *Alzheimers Dement*. 2008;4:S153-168.
52. Parachikova A, Green KN, Hendrix C and LaFerla FM. Formulation of a medical food cocktail for Alzheimer's disease:

beneficial effects on cognition and neuropathology in a mouse model of the disease. *PLoS One*. 2010; 5:e14015.

**53.** Brewer GJ and Kaur S. Zinc deficiency and zinc therapy efficacy with reduction of serum free copper in Alzheimer's disease. *International journal of Alzheimer's disease*. 2013; 2013:586365.

**54.** Troussiere AC, Monaca Charley C, Salleron J, Richard F, Delbeuck X, Derambure P, Pasquier F and Bombois S. Treatment of sleep apnoea syndrome decreases cognitive decline in patients with Alzheimer's disease. *J Neurol Neurosurg Psychiatry*. 2014.

**55.** Bland J. *The Disease Delusion: Conquering the Causes of Illness for a Healthier, Longer and Happier Life*. 2014; United States: Harper Wave.

**56.** Henderson ST, Vogel JL, Barr LJ, Garvin F, Jones JJ and Costantini LC. Study of the ketogenic agent AC-1202 in mild to moderate Alzheimer's disease: a randomized, double-blind, placebo-controlled, multicenter trial. *Nutr Metab (Lond)*. 2009; 6:31.